

**Design and Synthesis of Novel Ligands for
Serotonin (5-HT₆) Receptor and Inhibitors of
ABCB1 Efflux Pump**

Dissertation
zur Erlangung des Grades
des Doktors der Naturwissenschaften
der Naturwissenschaftlich-Technischen Fakultät
der Universität des Saarlandes

Von
M.Sc.-Pharm. Wesam Ali

Saarbrücken

2020

Tag des Kolloquiums: 17. Februar 2021

Dekan: Prof. Dr. Jörn Erik Walter

Berichterstatter: Prof. Dr. Claus Jacob

Prof. Dr. Cecilia Batistelli

Prof. Dr. Jadwiga Handzlik

Vorsitzende: Prof. Dr. Anna K.H. Hirsch

Akad. Mitarbeiter: Dr. Josef Zapp

Die vorliegende Arbeit wurde von September 2017 bis August 2020 unter Anleitung von Herrn Prof. Dr. Claus Jacob in der Fachrichtung Pharmazie (Bioorganische Chemie) der Naturwissenschaftlich- Technischen Fakultät der Universität des Saarlandes angefertigt.

Dedicated to my
Lovely Family

Table of Contents

Acknowledgments.....	i
Abbreviations.....	iii
Summary.....	v
Zusammenfassung.....	vi
Mol ganz kurz.....	vii
Résumé.....	viii
Publications Included in this thesis.....	ix
1. Introduction.....	1
1.1. 5-HT₆ receptor.....	3
1.2. Designing novel 5-HT₆ receptor Ligands.....	6
1.3. Selenium and CNS:.....	7
1.4. Selenium and natural nitrogen heterocycles.....	9
1.5. Multidrug resistance and cancer.....	10
1.6. ABC transporters.....	11
1.7. ABC and multidrug resistance.....	12
1.8. MDR modulators.....	13
1.9. Recent advance in cancer therapy.....	15
2. Aims of the thesis.....	17
3. Results.....	18
3.1. Publication 1.....	18
3.2. Publication 2.....	45
3.3. Publication 3.....	58
4. Discussion.....	76
4.1. Synthetic strategies for the designing of novel 5HT₆ Serotonin Receptor Ligands.....	76
4.2. Biological evaluation of the 5-HT₆ ligands.....	78
4.3. Design and synthesis of ABCB1 efflux pump modulating agents.....	80
4.4. Biological evaluation of phenylselenoether-hydantoin hybrids.....	81
5. Conclusions.....	84
6. References.....	85
7. Supplementary Material.....	92
7.1. Supplementary material for Publication 1: Computer-Aided Studies for Novel Arylhydantoin 1,3,5-Triazine Derivatives as 5-HT₆ Serotonin Receptor Ligands with Antidepressive-Like, Anxiolytic and Antiobesity Action In Vivo.....	92
7.2. Supplementary material for Publication 2: Synthesis and computer-aided SAR studies for derivatives of phenoxyalkyl-1,3,5-triazine as the new potent ligands for serotonin receptors 5-HT₆.	

7.3. Supplementary material for Publication 3: Discovery of phenylselenoether-hydantoin hybrids as ABCB1 efflux pump modulating agents with cytotoxic and antiproliferative actions in resistant T-lymphoma.	186
8. List of conferences and workshop:.....	249

Acknowledgments

It is with immense gratitude that I acknowledge the support and help of my Prof. Dr. Claus Jacob, as he was always available for giving help, support, and providing me with an excellent atmosphere to achieve the research. I would like to thank Prof. Dr. Claus Jacob for providing me the opportunity to learn under his supervision.

I am very grateful to my second supervisor Dr. Cecilia Battistelli, for her valuable advice and suggestions during my research.

I would also like to thank Prof. Dr. Anna K. H. Hirsch for the time and discussion during my Ph.D. study. Her excellent knowledge and experience in the field of medicinal chemistry, humble yet energetic personality, extensively contributed to my technical training.

I would like to thank Prof. Dr. Jadwiga Handzlik, especially, and Prof. Dr. Lama Youssef for the time and efforts, besides the excellent support on moral and scientific grounds during my work. This thesis would not have been possible without their work and support.

Special thanks to Dr. Clemens Zwergel, Sapienza University, for the support and advice during my Ph.D. study. I would also like to thank Dr. Dorota Łazewska, Jagiellonian University, Dr. Gabriella Spengler, the University of Szeged for the nice and productive collaboration.

Special thanks to Dr. Muhammad Jawad Nasim for the help and support during my study. I would like to express my respect for the time, guidance, and advice he gave to my work.

I would also like to thank Dr. Adel Al-Marby and Yannick Ney for guidance and advice. I would also like to thank all the members of the “Academiacs International Network” for the useful discussions and maintaining the ever-encouraging environment.

I would especially like to thank my family for their constant support through my study in Germany. Their love and moral support have seen me through many difficulties; my Mom, my Father, my brothers: Gayath, Ali, Moyaser, and Gevara. My sisters: Hiba, Nahwand, Shahinaz, Ola, and Liza.

Our lovely new generation: Gaith, Maya, Anna, Lea, Sam, and Adam, to all of you, thanks a lot. You are always giving me hope.

Finally, this thesis would not have been possible without the financial support from Saarland University, “Landesforschungsförderungsprogramm” (Grant No. WT/2 – LFFP 16/01) and the spiritual support of my family. I am also thankful for the Erasmus+ program, National Science Centre, Poland grants: No UMO-2015/17/B/NZ7/02973, UMO-2016/21/N/NZ7/03265 and all the members of the Department of Technology and Biotechnology of Drugs, Faculty of Pharmacy, Jagiellonian University, Medical College, Krakow, Poland.

Abbreviations

ABBREVIATION	DEFINITION
EU	European Union
NCDS	Noncommunicable diseases
ARDS	Age-related diseases
WHO	World Health Organization
USA	United States of America
PTSD	Posttraumatic stress disorder
5-HT	5-hydroxytryptamine
CNS	Central nervous system
MDR	Multidrug resistance
PGP	P-glycoprotein
GPCR	G-protein-coupled receptors
GI TRACT	Gastrointestinal tract
ADMET	Absorption, distribution, metabolism, elimination, toxicity
HYD	Hydrophobic area
PI	Positive ionizable nitrogen
HBA	Hydrogen bond acceptor
GPX	Glutathione peroxidases
TRXR	Thioredoxin reductases
MSRS	Methionine-sulfoxide-reductase
FST	Forced swimming test
TST	Tail suspension test
ROS	Reactive oxygen species
ACE	Angiotensin-converting enzyme
ATP	Adenosine triphosphate
NBD	Nucleotide-binding domains
TMDS	Transmembrane domains

AR	Aromatic region
NMR	Nuclear magnetic resonance
MS	Mass spectra
RP-TL	Reversed-phase thin-layer chromatography
SAR	Structure-activity relationship
PAR	Parental
BBB	Blood-brain-barrier
FAR	Fluorescence activity ratio

Summary

Selenium and Biology have a unique relationship. Selenium is an element which exists in several amino acids, including selenocysteine and selenomethionine. It plays several vital roles in the human body and is essential for several physiological processes.

The last few years have witnessed the development of a new generation of biologically active and pharmaceutically relevant organo-selenium compounds, ranging from effective anticancer agents to novel ligands for serotonin 5-HT₆ receptors and ABCB1 efflux pump modulators.

This study describes the role of phenylselenoether-hydantoin hybrids as ABCB1 efflux pump modulating agents. Moreover, this work aims to synthesize novel and highly (re)active agents employing triazine-methyl piperazine hybrids for therapeutic applications in the treatment of current civilization central nervous system disorder.

In summary, a library of 50 active novel compounds has been prepared to serve as efflux pump modulators or 5-HT₆ ligands.

Melting point, mass spectroscopy (MS), and nuclear magnetic resonance spectroscopy (NMR) evaluation have been employed to establish and confirm the structure of the compounds. The biological assays have been performed to evaluate their affinity towards 5HT₆ receptor or efflux pump modulating ability. Finally, structure-activity relationship analysis has been performed to review and suggest modifications for the pharmacophore features.

Zusammenfassung

Selen ist ein Element, das in mehreren Aminosäuren, einschließlich Selenocystein und Selenomethionin, vorkommt. Es spielt verschiedene lebenswichtige Rollen im menschlichen Körper und ist für zahlreiche physiologische Prozesse unerlässlich.

In den letzten Jahren wurde eine neue Generation biologisch aktiver und pharmazeutisch relevanter Organo-Selen-Verbindungen entwickelt, die von wirksamen Krebsbekämpfungsmitteln bis hin zu neuartigen Liganden für Serotonin-5-HT₆-Rezeptoren und ABCB1-Effluxpumpenmodulatoren reichen.

Diese Studie beschreibt die Rolle von Phenylselenoether-Hydantoin-Hybriden als ABCB1-Effluxpumpenmodulatoren sowie die Synthese von neuartigen und hoch (re)aktiven Wirkstoffen unter Verwendung von Triazin-Methylpiperazin-Hybriden für therapeutische Anwendungen bei der Behandlung von Störungen des Zentralnervensystems der modernen Gesellschaft Zivilisation.

Zusammenfassend lässt sich sagen, dass eine Bibliothek von 50 aktiven neuartigen Verbindungen vorbereitet wurde, die als Effluxpumpenmodulatoren oder 5-HT₆-Liganden dienen sollen.

Die Verbindungen wurden durch Schmelzpunkt-, Massenspektroskopie- (MS) und Kernresonanzspektroskopie- (NMR) charakterisiert. Biologische Assays wurden durchgeführt, um die Fähigkeit der synthetisierten Verbindungen zur Modulation des 5HT₆-Rezeptors oder der Effluxpumpe zu bestimmen. Schließlich wurde eine Struktur-Aktivitäts Beziehungsanalyse durchgeführt, um die pharmakophoren Eigenschaften zu überprüfen und Änderungen vorzuschlagen.



Mol ganz kurz

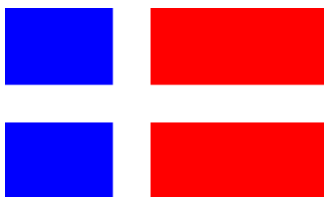
Selen iss e Element unn kommt in a paar Aminosäure vor, inklusive Selenocystein unn Selenomethionin. Es hat verschiedene lebenswichtige Rolle im menschliche Kerper unn is vor zahlreiche physiologische Prozesse notwendig.

In de ledschde Johre is e neijie Generation vun biologisch aktive unn pharmazeutisch relevante Organ-Selen-Verbindunge entwickelt wor, die vun wirksame Mittel vor die Bekämpfung vun Krebs bis hin zu neijartiche Ligande vor die Serotonin-5-HT₆-Rezeptore und Modulare vun de ABCB1-Effluxpumpe reiche.

Die do Studie beschreibt die Roll vun Phenylselenoether-Hydantoin-Hybride als Modulare vun de ABCB1-Effluxpumpenmodulatore unn die Synthese vun neijartiche unn hoch(re)aktive Wirkstoffe. Das Zeich soll dann bei de Behandlung vun Sterunge vum Zentralnervesystem angewend werre. Dodebei werre Triazin-Methylpiperazin-Hybride verwennend.

Zusamme genommt lässt sich sahn, dass e Haufe vun 50 aktive neijartiche Verbindunge hergestellt wor is, die als Modulare vun Effluxpumpe odder als 5-HT₆-Ligande ehr Ding mache solle.

Die Verbindunge sinn dorch Schmelzpunkt-, Massespektroskopie (MS) unn Kernresonanzspektroskopie- (NMR) beschrieb wor. Biologische Knebb sinn dorchgefiehrd wor, um die Affinität vun de synthetische Verbindunge als Modulare vor die 5HT₆-Rezeptore oder vor die Effluxpumpe se bestimme. Unn dann sinn noch a paar Analyse vor die Beziehung zwische de Struktur unn de Aktivität gemacht wor, um sich dodemedd die pharmakophore Eigenschafte anzugucke unn Ännerunge vorzuschlahn.



Résumé

Le sélénium est un élément qui existe dans plusieurs acides aminés, dont la sélénocystéine et la sélénométhionine. Il joue plusieurs rôles vitaux dans le corps humain et est essentiel à plusieurs processus physiologiques.

Ces dernières années ont vu le développement d'une nouvelle génération de composés organoséléniés biologiquement actifs et pharmaceutiquement pertinents, allant d'agents anticancéreux efficaces à de nouveaux ligands pour les récepteurs de la sérotonine 5-HT₆ et les modulateurs de la pompe à efflux ABCB1.

Cette étude décrit le rôle des hybrides de phénylsélénioéther-hydantoïne en tant qu'agents modulateurs de la pompe à efflux ABCB1. En outre, ces travaux visent à synthétiser de nouveaux agents hautement (ré)actifs utilisant des hybrides de triazine-méthyl-pipérazine pour des applications thérapeutiques dans le traitement des troubles du système nerveux central de la civilisation actuelle.

En résumé, une bibliothèque de 50 nouveaux composés actifs a été préparée pour servir de modulateurs de la pompe à efflux ou de ligands 5-HT₆.

Le point de fusion, la spectroscopie de masse (MS) et l'évaluation par spectroscopie par résonance magnétique nucléaire (RMN) ont été utilisés pour établir et confirmer la structure des composés. Les essais biologiques ont été réalisés pour évaluer leur affinité avec le récepteur 5-HT₆ ou la capacité de modulation de la pompe à efflux. Enfin, une analyse de la relation structure-activité a été réalisée pour examiner et suggérer des modifications des caractéristiques des pharmacophores.



Publications Included in this thesis

The following publications have been selected for this cumulative thesis:

1. Computer-Aided Studies for Novel Arylhydantoin 1,3,5-Triazine Derivatives as 5-HT₆ Serotonin Receptor Ligands with Antidepressive-Like, Anxiolytic and Antiobesity Action In Vivo.

Rafał Kurczab, **Wesam Ali**, Dorota Łażewska, Magdalena Kotanska, Magdalena Jastrzębska-Więsek, Grzegorz Satała, Małgorzata Więcek, Annamaria Lubelska, Gniewomir Latacz, Anna Partyka, Małgorzata Starek, Monika Dąbrowska, Anna Wesołowska, Claus Jacob, Katarzyna Kieć-Kononowicz and Jadwiga Handzlik.

Molecules **2018**, 23, 2529; doi:10.3390/molecules23102529

2. Synthesis and computer-aided SAR studies for derivatives of phenoxyalkyl-1,3,5-triazine as the new potent ligands for serotonin receptors 5-HT₆.

Wesam Ali, Małgorzata Więcek a, Dorota Łażewska, Rafał Kurczab, Magdalena Jastrzębska-Więsek, Grzegorz Satała, Katarzyna Kucwaj-Brysz, Annamaria Lubelska, Monika Głuch-Lutwin, Barbara Mordyl, Agata Siwek, Muhammad Jawad Nasim, Anna Partyka, Sylwia Sudoł, Gniewomir Latacz, Anna Wesołowska d, Katarzyna Kieć-Kononowicz and Jadwiga Handzlik.

European Journal of Medicinal Chemistry **2019**, 178, 740-751.

3. Discovery of phenylselenoether-hydantoin hybrids as ABCB1 efflux pump modulating agents with cytotoxic and antiproliferative actions in resistant T-lymphoma.

Wesam Ali, Gabriella Spengler, Annamaria Kincses, Marta Nove, Cecilia Battistelli, Gniewomir Latacz, Małgorzata Starek, Monika Dąbrowska, Ewelina Honkisz-Orzechowska, Annalisa Romanelli, Manuela Monica Rasile, Ewa Szymanska, Claus Jacob, Clemens Zwergel and Jadwiga Handzlik.

European Journal of Medicinal Chemistry **2020**, 200, 112435.

1. Introduction

Europe's population is getting older as life expectancy, and the percentage of the European population that is surviving at older ages has increased dramatically over the last century. In 2018, the share of the population aged 65 years or over reached 18.2% of the European Union (EU) population, and this percentage is predicted to increase to 30% by 2050 (1). Globally, the elderly people aged 60 years or older represent approximately 10% of the world population, and this percentage is also expected to double by 2050 (2).

Population aging will be accompanied by more illness, disability, and dependency. People of all age groups, regions, and countries are affected by noncommunicable diseases (NCDs), also known as chronic diseases, such as atherosclerosis and cardiovascular disease, cancer, osteoarthritis and osteoporosis, cataracts, type 2 diabetes, hypertension, and Alzheimer's disease. However, these conditions are often associated with older age groups. Elderly people are also prone to develop "comorbidities" (i.e., more than one disease/condition or multiple inter-related health problems), which severely impact their health and quality of life.

The mortality rates of age-related diseases (ARDs) increase with age (3). According to the World Health Organization (WHO), NCDs kill 41 million people each year, equivalent to 71% of all deaths (56.9 million) globally. Of these, an estimated 1.7 million (4% of NCD deaths) occurred in people younger than 30 years of age, 15.2 million (38%) in people aged between 30 years and 70 years, and 23.6 million (58%) in people aged 70 years and older (4).

NCDs are estimated to account for 91% of all deaths in Germany (5). Therefore, the prevalence of the major NCDs (diabetes, cardiovascular diseases, cancer, chronic respiratory diseases, and mental disorders) is expected to rise worldwide and particularly in the developed countries, such as the United States of America (USA) and Western Europe, at least in part due to their growing populations of elderly. However, the highest risk of dying from NCDs is currently observed in low-income and middle-income countries, especially in sub-Saharan Africa, the Middle East, and, for men, in central Asia and Eastern Europe.

We can summarize the most common functions change and corresponding age-related diseases in the following table (6).

Table 1: The most common functions change and corresponding age-related diseases.

Type of function	Disease
Sensory Changes related diseases	<ul style="list-style-type: none"> ❖ Hearing Loss ❖ Visual Acuity ❖ Dizziness
Immunosenescence	<ul style="list-style-type: none"> ❖ Inflammatory diseases ❖ Viral infections
Urologic changes	<ul style="list-style-type: none"> ❖ antimicrobial resistance.
Somatic disease and multiple chronic conditions	<ul style="list-style-type: none"> ❖ Cardiovascular Disease ❖ Hypertension ❖ Cancer ❖ Osteoarthritis ❖ Diabetes Mellitus ❖ Osteoporosis ❖ Multiple Chronic Conditions
Psychological and cognitive	<ul style="list-style-type: none"> ❖ Cognitive Aging ❖ Dementia ❖ Depression
<p>Among all of them, somatic disease and multiple chronic conditions, psychological and cognitive attract more attention in the last few years in the attempt to prepare an effective and selective treatment.</p>	

Population aging is a powerful and transforming demographic force that will inevitably affect health care and social costs. The remarkable increases in life expectancy and projected growth of the older population will impact the society and pose new and additional special needs and services, such as the need for services at home, interactions with health care providers, assistance with the daily life duties, specialized care in clinics and hospitals, and advance care planning (7).

According to Statistisches Bundesamt (Destatis), of 954.874 death cases, the percentage of fatalities by chapters of the International Statistical Classification of Diseases and Related Health Problems 2018 were: 24.9% by neoplasms, 6% due to mental and behavioural disorders, and 3.6% by diseases of the nervous system (8).

Among several psychological and cognitive diseases, depression and anxiety are common within the aged population. In general, older adults present higher vulnerability towards risk factors and worse symptoms of depression or anxiety than younger adults (9-11). In Germany, the mean health care

costs were estimated to be around 5,243 € per six months for people with posttraumatic stress disorder (PTSD). The health-related quality of life was also observed to be lower due to anxiety/depression (12).

In this context, the 5-hydroxytryptamine (5-HT: serotonin) subtype 6 receptor (5-HT₆R), one of the latest cloned receptors among the known 5-HT receptors, has gained considerable attention as an attractive target for drug development against psychological and cognitive diseases. The expression profile of 5-HT₆R in the central nervous system (CNS), especially in the striatum, hippocampus, and cortex (13), and its high affinity for antipsychotic and antidepressant drugs have suggested significant implications for 5-HT₆R modulators in a broad spectrum of CNS disorders, including depression, cognitive dysfunction associated with Alzheimer's disease, anxiety, and schizophrenia (14, 15).

Cancer can be considered an age-related disease because the incidence and prevalence of most cancers increase with age, peaking in men and women in their 80s. Almost 70% of all cancer cases and cancer-related deaths were reported in patients aged 65 years or older (16). Older people exhibit worse prognosis of cancer because of delayed diagnosis. Different methods are required for the diagnosis and treatment of cancer in older people, such as new chemotherapy agents (17).

The emergence of multidrug resistance (MDR) in cancer cells is one of the biggest challenges face by physicians and scientists across the globe. One of the essential mechanisms in MDR action involves adenosine triphosphate-binding cassette (ABC) transporters, such as the P-glycoprotein (Pgp, ABCB1), which are involved in crucial processes in cancer cells' defense. Designing compounds which target these transporter proteins provides an interesting strategy to overcome drug resistance (18).

1.1. 5-HT₆ receptor

Serotonin mediates diverse behavioral and physiological actions in both the peripheral and central nervous systems. Based on structural, biochemical, and pharmacological differences, 5-HT receptors (5-HTRs) are classified into seven distinct receptor families: 5-HT₁, 5-HT₂, 5-HT₃, 5-HT₄, 5-HT₅, 5-HT₆, and 5-HT₇ receptors. Except for the 5-HT₃ receptors, which are ligand-gated ion channels, all 5-HT receptors are G-protein-coupled receptors (GPCR), transmitting their signals via G-proteins (19).

Table 2 summarizes types, distributions, and the functions of serotonin receptors (20-22).

Table 2: 5-HT distributions and functions in the CNS, which could be imperative for selective and more effective drug design.

Receptor	Distribution	Functions
5-HT ₁	CNS GI Tract Blood vessels	Addiction, aggression, anxiety, appetite, autoreceptor, blood pressure, cardiovascular function, emesis, heart rate, impulsivity, memory, mood, nausea, nociception, penile erection, pupil dilation, respiration, sexual behavior, sleep, sociability, thermoregulation, vasoconstriction, learning, locomotion, migraine
5-HT ₂	CNS, Blood vessels GI Tract Platelets Peripheral nervous system Smooth Muscle	Addiction, anxiety, appetite, cognition, imagination, learning, memory, mood, perception, sexual behavior, sleep, thermoregulation, vasoconstriction, cardiovascular function, GI motility, locomotion, mood, penile erection
5-HT ₃	CNS GI Tract Peripheral nervous system	Addiction, anxiety, emesis, GI motility, learning, memory, nausea
5-HT ₄	CNS GI Tract Peripheral nervous system	Anxiety, appetite, GI motility, learning, memory, mood, respiration
5-HT ₅	CNS	Autoreceptor, locomotion, sleep
5-HT₆	CNS	Anxiety, cognition, learning, memory, mood
5-HT ₇	CNS, Blood vessels GI Tract	Anxiety, autoreceptor, memory, mood, respiration, sleep, thermoregulation, vasoconstriction
Gastrointestinal tract (GI tract).		

The 5-hydroxytryptamine (5-HT: serotonin) subtype 6 receptor (5-HT₆R) is one of the most recent additions to the family of mammalian 5-HT receptors. It belongs to (GPCRs) which transmit their signals via G-proteins (23). 5-HT₆R was first identified by Kohen *et al.* in 1996 (24) and since then

has gained considerable interest as an attractive target for designing novel drugs targeting Alzheimer's disease, schizophrenia, depression, and Parkinson's disease (25).

The growing interest of this receptor stem, at least in part, from its predominant expression in the central nervous system (CNS). Therefore, the potential therapeutic indications of the 5-HT₆R ligands encompass a spectrum of diseases, including depression (26), cognitive dysfunction associated with Alzheimer's disease (27), anxiety, dementia (28), schizophrenia, and reducing food intake and body weight (29). Moreover, due to the 5-HT₆ receptor unique distribution, predictions have been made that these new agents will have quite a few side-effects (30).

The results of preclinical studies are rather confusing since they reveal that activation and inhibition of 5-HT₆ receptor evoke the same pharmacological responses, *e.g.*, in the animal behavioral model of depression, both agonists and antagonists presented antidepressant- or anti-anxiety-like effects (23). Nevertheless, despite the abundance (>20) of selective 5-HT₆R antagonists (*i.e.*, Ro 04-6790 **1**, Ro 63-0563 **2** (**31**), SB-258585 **3**, the novel and highly selective pyrazole-conjugated aryl sulfonamides **4** and 1-sulfonyl-6-piperazinyl-7-azaindoles **5**), there are only a limited number of 5-HT₆R agonists that have exhibited high selectivity and have reached Phase I clinical trials such as Wyeth agonist WAY-181187 **6** (25, 30) (Figure 1).

Within 20 years, from 1995 to 2015, more than 3000 active 5-HT₆R ligands have been successfully prepared and studied. Still, their structural diversity is limited, with 80% of sulfone-containing structures and more than 40% of indole-containing ones (32, 33).

Recently, a new group of non-indole and non-sulfone hydantoin-triazine 5-HT₆R ligands were synthesized by Lubelska *et al.* and evaluated for their pro-cognitive and antiobesity activities. The compounds presented significant anxiolytic, precognitive, and some antiobesity properties in *in vivo* models. Moreover, these compounds also met the criteria established for "drug-likeness" (33). Nevertheless, no 5-HT₆R agent has reached the pharmaceutical market. The most innovative 5-HT₆R agents, such as Idalopirdine **7** and Intepirdine **8**, failed at phase III of clinical trials, while SUVN-502 **9** (34) still provides an exceptional hope since it has been successfully accepted in phase II trials. Most of these ligands exhibit an insufficient "drug-ability" profiles, such as "ADMET (absorption, distribution, metabolism, elimination, toxicity). Moreover, most of these ligands are unable to cross the blood-brain barrier (23, 33).

To sum up, the serotonin 5-HT₆ receptor is an interesting target for drug developers because of:

- ❖ Unique distribution, exclusive to CNS
- ❖ Multiple cellular signaling pathways activated by the receptor in CNS
- ❖ The potential utility of ligands in the treatment of critical diseases (*e.g.*, Alzheimer's diseases, depression)

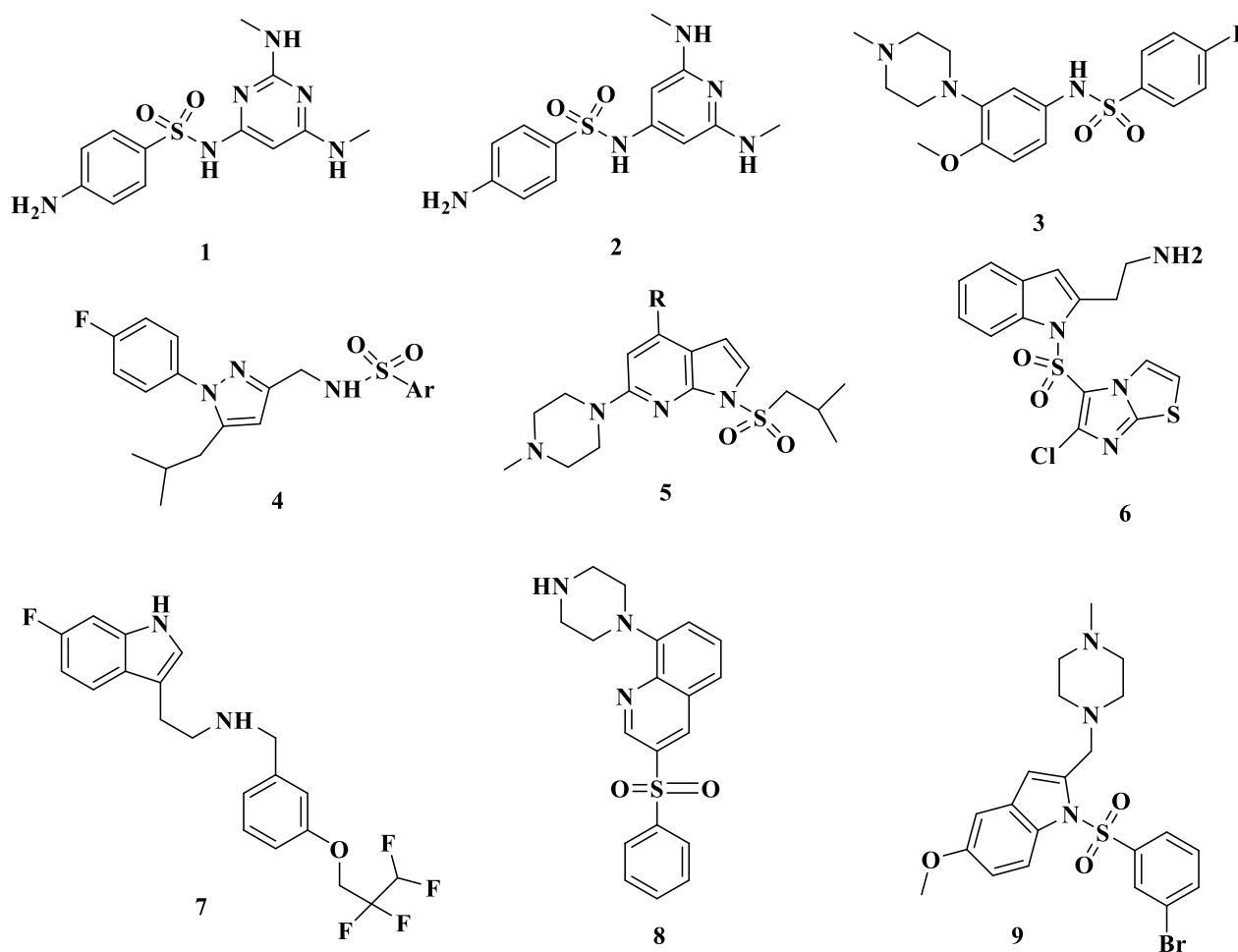


Figure 1: Some 5-HT₆R agonist and antagonist

1.2. Designing novel 5-HT₆ receptor Ligands

Lines of evidence have indicated several families of chemical compounds that display significant affinities for the serotonin receptors 5-HT₆. The most active compounds with affinities in nano- or sub-nanomolar ranges belong to the families of amine derivatives, including nitrogen heterocycles of pyridino-sulfonamide, indole, benzothiofene, benzimidazole, or aza-analogs of ergoline (33).

In 2005, Rodríguez *et al.* suggested a pharmacophore model for the 5-HT₆R antagonists. The pharmacophore model comprises four distinct features: large hydrophobic area (HYD), positive ionizable nitrogen (PI), a hydrogen bond acceptor (HBA), and a central aromatic fragment (35).

The HYD is commonly personified by fused aromatic rings of naphthalene or halogen-substituted benzene, an indole, or a benzothiofene. The nitrogen heterocycle, (un)substituted piperazine is a suitable moiety containing the PI. The HBA frequently occurs in several sulfonyl ligands and the

carbonyl moieties. Interestingly, the HYD linked to aromatic heterocyclic groups, such as pyridine, benzimidazole, quinolone, or triazine, provides an aromatic feature (36).

In 2017, D. Łażewska *et al.* demonstrated the roles of piperazine linked to 1,3,5-triazine (compounds **10-12**) for the 5-HT₆R affinity. The HYD is fragment determined by both a kind of aromatic moieties linked by the methylene group to the 1,3,5-triazine ring and substituents at the aromatic moieties. It is confirmed that more hydrophobic substituents are more favorable.

For HBA, the results proved that the sulfonyl group is not required for a strong affinity to the 5-HT₆R. Instead, a one-atom spacer which can be embodied by the sulfonyl, methylene group, or an ether-chalcogen atom, such as oxygen or sulfur, seems to be crucial, and lack of this motif caused an enormous decrease of the affinity (Figure 2) (36).

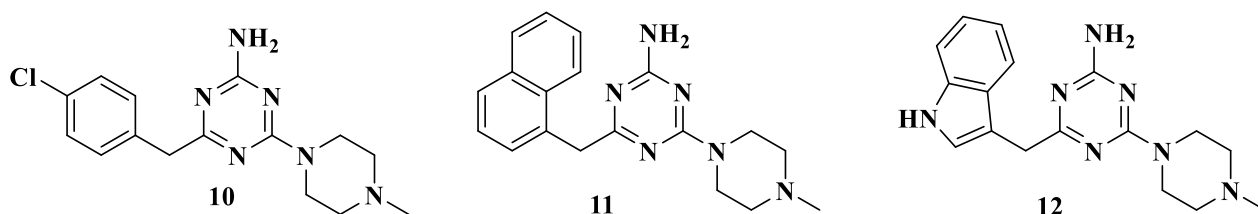


Figure 2: Examples of some of the 1st generation of 5-HT₆R triazine-piperazine agents

1.3. Selenium and CNS

Selenium-containing organic molecules exhibit promising pharmacological properties. The oxidative stress is proposed as a mechanism in neurodegenerative diseases. Selenium and selenium-dependent enzymes, such as glutathione peroxidases (GPx), thioredoxin reductases (TrxR), and methionine-sulfoxide-reductase (Msrs), are involved in antioxidant defense, intracellular redox regulation, and modulation and thereby exhibit neuroprotective actions. Selenium-dependent enzymes have a significant influence on proper brain function (37, 38). The brain receives a priority supply of selenium uptakes (39-41). Selenoenzyme GPx4 controls the interneuron function. Cerebral selenium deficiency may cause reduced GPx4 expression and, consequently, increased/reduced interneuron development (42).

Elemental selenium intakes have important roles for cell death, prevention of lipid peroxidation, and plasma membrane protection (43). A few examples of compounds which have central nervous system pharmacological properties are presented in Figure 3.

Organoselenium compounds, such as compound **13** (methyl phenyl selenide, CH₃SePh) exhibited an antidepressant- action in the mouse models, reduced the immobility time in the mouse forced swimming test FST and the tail suspension test TST (44). Compound **14** (*m*-trifluoromethyl-diphenyl

diselenide (*m*-CF₃-PhSe)₂) displayed antioxidant, anxiolytic activities and presented antidepressant effect in the mouse FST (45).

3-(4-fluorophenylselenyl)-2,5-diphenylselenophene (F-DPS) **15** blocked behavioural changes induced by neuropathic pain. In addition, sub-chronic treatment inverted depression-like behavior (FST) test and (TST) test and formed a noteworthy anxiolytic-like action in mice (46, 47).

Compound **16** ((*Z*)-2,3-Bis(4-chlorophenylselenyl)prop-2-en-1-ol, also exhibited anti-depressant effect in the mouse TST and FST (48). Moreover compound **17** (4-phenyl-1-(phenylselenylmethyl)-1,2,3-triazole) was identified as an antidepressant agent (49).

Diphenyl diselenide (PhSe)₂ **18** exhibited a neuroprotective activity by reducing neuropathic and acute thermal hyperalgesia in mice (50). Moreover, compound **18** exhibited antidepressant-like and anxiolytic-like activity in mice (51, 52). Compound **18** also provided a neuroprotective effect against the toxic impact of MeHg on mitochondrial activities in mice. Compound **18** reduced oxidative stress and MeHg deposition in the brain (53).

The elemental selenium proved to play several imperative roles in CNS. Oral supplementation of dietary selenium may considerably slow down the process of neurodegeneration. Selenium exhibits a protective effect against the neurotoxicity caused by the multiple-dose administration of methamphetamine. Se uptakes significantly increase the glutathione peroxidase (GPx) activity and modulates the oxidative damages mediated by increased production of hydrogen peroxide or other reactive oxygen species (ROS) in the dopaminergic system (54, 55).

Inadequate uptake of selenium may also contribute to Alzheimer's disease pathophysiology. Selenium supplementation resulted in reduced intractable epileptic seizures in children. Moreover, low plasma selenium concentrations in the elderly were linked to faster cognitive failure. In contrast, high dietary selenium uptake significantly improved mood, reduced anxiety, depression, and tiredness compared to people with lower selenium intake (39).

Sodium selenate (**19**) supplementation at a high dose encouraged an increase in selenium uptake into the CNS, which increased the expression and incorporation of selenium into biomolecules (56). Sodium selenite **20** administered to mice reduced the immobility time in the FST, exerting antidepressant and anxiolytic effects (57).

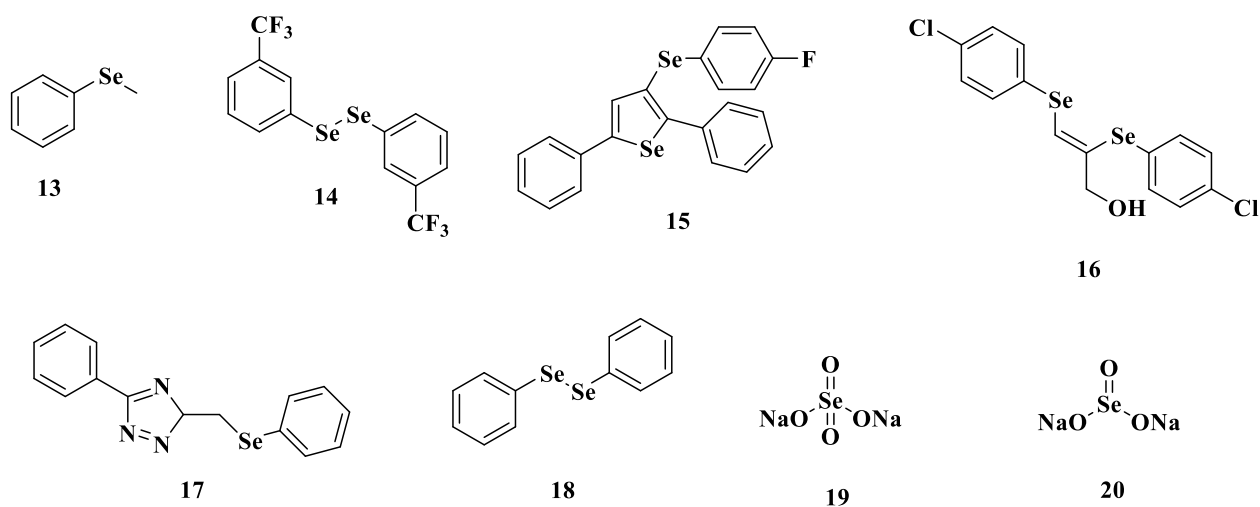


Figure 3: Selenium containing compounds with CNS pharmacological properties

1.4. Selenium and nitrogen heterocycles

The chemistry of selenium and nitrogen heterocycles is attracting considerable attention in the attempt to obtain organoselenium compounds with high GPx like activity. Several pyridyl and pyrimidinyl based diselenide compounds, such as **21**, **22**, have been prepared, which presented good antioxidant activity (58).

A series of compounds comprising selenium analogues of captopril (**23**) was also synthesized, which inhibited the angiotensin-converting enzyme (ACE) (59). Moreover, dipeptide-based selenium compounds (**24**, **25**) were also prepared by Bhaskar *et al.* and evaluated for ACE inhibition. Intriguingly, selenocysteine containing peptides demonstrated better antioxidant activity than cysteine-containing peptides (60). Furthermore, selenium-containing naphthylamide (**26**, **27**) and 3-allyl seleno-6-alkyl thiopyridazine (**28**) exhibited moderate to good anticancer activities (61, 62).

Recently, the click chemistry provides the advantage of preparing multifunctional compounds containing selenium and triazole moiety (**29**). The synthesis and antitumor activity of selenium-containing triazoles combined with diphenyl diselenide and *a*-Lapachone motifs have been reported. The compounds presented excellent antitumor activity against several cancer cell lines (63).

Organoselenium compounds containing nitrogen heterocycles were also employed as antiviral agents. Selenoacyclovir (**30**) exhibited promising anti-herpes simplex virus-1 and -2 activities whilst selenoganciclovir (**31**) revealed moderate anti-human cytomegalovirus activity (64).

Another class of selenium-nitrogen heterocycle includes nucleic acids. The replacement of oxygen by selenium in nucleobases opens the window for a new application of the selenium in DNA and RNA (65, 66).

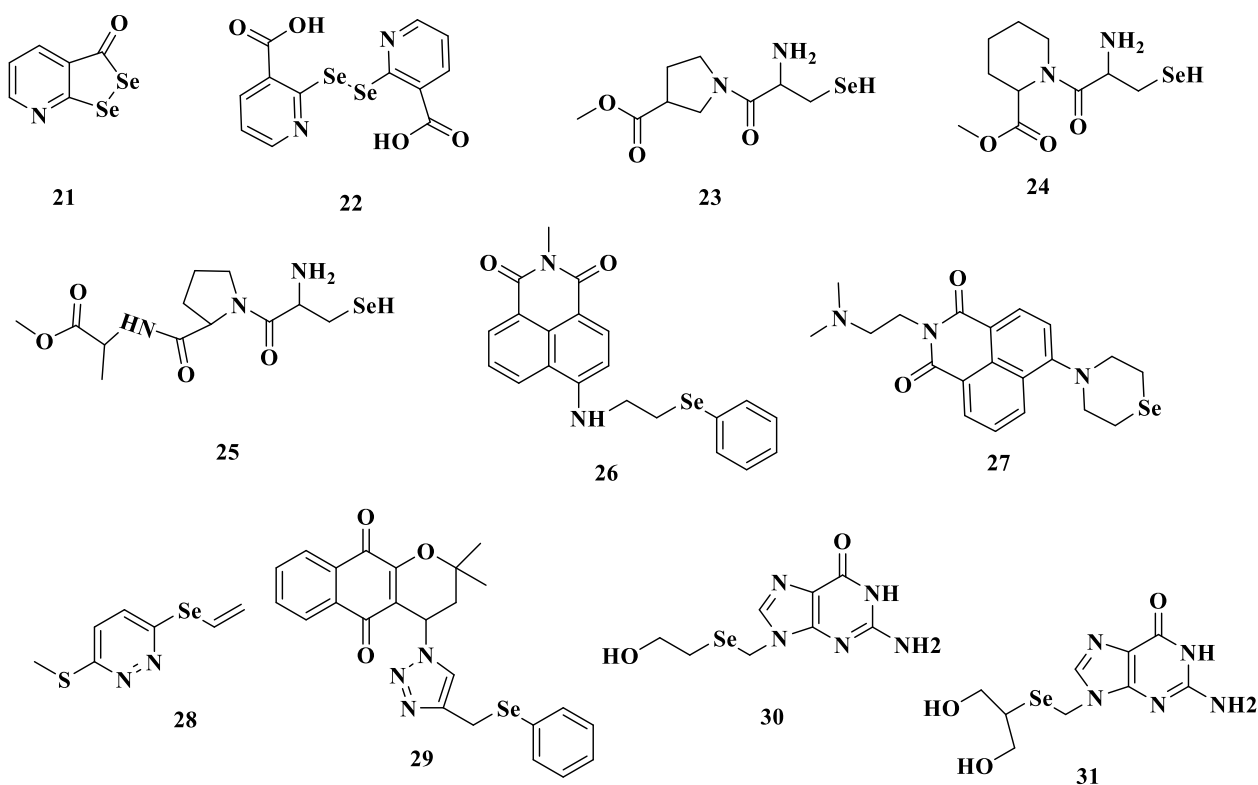


Figure 4: Selenium and nitrogen heterocycles compounds

1.5. Multidrug resistance and cancer

The emergence of multidrug resistance (MDR) in cancer cells is a critical problem requiring special attention for more efficient cancer therapy. MDR are mechanisms that cancer cells developed to confront the cytotoxic effect of anticancer drugs (67).

MDR is responsible for increased death rate to over 90% in cancer patients receiving traditional chemotherapeutics or new drugs. Different mechanisms of resistance in cancer cells are summarized in Table 3

Table 3: Different mechanisms of resistance in cancer cells

Mechanisms	Types of action
Upregulation actions	<ul style="list-style-type: none"> • Increasing drug efflux • Improving cell growth, and in the term, survival signaling. • An increase in DNA repairing and overexpression of plasma membranes.
Down-regulation	<ul style="list-style-type: none"> • Downregulation of apoptosis signals • Decrease drug uptakes

P-glycoprotein (Pgp) transporters play an important role in the MDR mechanism, namely by increasing drug efflux. They are expressed widely in cancer cells, recognize and catalyse the efflux of various anticancer drugs from cells (68-71).

1.6. ABC transporters

Cells contain transporters to sustain an equilibrium condition. There are two kinds of transporters, namely primary transporters and secondary ones. These transporters play a central role in the transportation of organic and inorganic molecules across cellular membranes. The primary transporters work against gradients employing adenosine triphosphate (ATP) hydrolysis as a source of energy. Whilst in secondary transporters, the energy is consequent from the electrochemical gradient generated by active transport (72).

ABC belongs to the ATP Binding Cassette transporters. ABC proteins are present in the cytoplasmic (inner) membrane of bacteria, and both the plasma membrane and organelle membranes in eukaryotes. ABC are found in bacteria and eukaryotes (73, 74). They are characterized by two pairs of domains: two nucleotide-binding domains (NBD), which comprise of a phosphate-binding loop, and two transmembrane domains (TMDs). ATP hydrolysis at NBD leads to change of TMDs and activate the transportation across the membrane (72).

In bacteria, NBD and TMSs exist as two or four separate polypeptides, whereas in eukaryotes, the four domains are often fused into a single abundant protein with an internal duplication (75). Most ABC transporters on eukaryotes are exporting while serving as an exporting and importing in Bacteria (75). There are 48 ABC transporters in humans, which are subdivided into seven sub-families: A-G. Many of these sub-families are involved in diseases, including cystic fibrosis (76), Tangier disease (77), adrenoleukodystrophy, and cancer (78-80).

ABC transports a range of inorganic and organic molecules, such as metal ions, amino acids, vitamins, sugars, peptides, lipids, oligonucleotides, and polysaccharides across the membrane. (75).

ABC transporters are present in the liver, placenta, and blood-brain barrier in humans. They serve as an intermediate in the detoxification of hydrophobic organic molecules and, therefore, result in the multidrug resistance of some anticancer drugs (81).

1.7. ABC and multidrug resistance

Three sub-families are belonging to the ABC superfamily, which serves as a multidrug efflux pump and hence are responsible for drug resistance. These families include P-glycoprotein (ABCB1), MRP1 (ABCC1), and breast cancer resistance protein (ABCG2) and are located in the plasma membrane. These proteins are also overexpressed in tumor cells, resulting in increased expulsion of the toxic materials (82). Efflux pump modulators have recently received considerable attention in cancer therapy (83).

Pgp and ABCG2 export unmodified drugs whilst MRP1 export both conjugated drugs with glutathione and unconjugated ones together with free glutathione (75, 83).

Pgp (ABCB1) is the first human ABC transporter cloned and characterized for its ability to confer multidrug resistance on cancer cells. ABCB1 transports a wide range of amphipathic molecules, including anticancer drugs, HIV protease inhibitors, analgesics, antihistamines, H₂-receptor antagonists, immunosuppressive agents, cardiac glycosides, calcium channel blockers, calmodulin antagonists, anti-emetics, anthelmintic, antibiotics, and steroids (83). Pgp is abundantly found in the apical membranes of epithelial cells lining the colon, small intestine, pancreatic, bile ductulus, proximal kidney tubule (84), endothelial cells lining capillaries in the brain, testis, and inner ear. Since Pgp is also found in pregnant endometrium, the placenta, and the adrenal gland (85), it protects the fetus and sensitive organs from toxic substances (86-88).

Moreover, Pgp is also highly expressed in the mitochondrial membrane and cell nucleus. It pumps out anticancer drugs from mitochondria or nuclei into the cytosol, thereby causing multidrug resistance in the cancer cells (89, 90). A recent study proved that ABCB1 is involved in the uptake of the antidepressant vortioxetine into mice's brains (91).

ABCB4 is closely related to Pgp, with 78% genetic sequence homology. It is found in the intestine, kidney, placenta, brain endothelial cells, and hematopoietic stem cells. It transports both positively and negatively charged drugs, such as sulfate conjugates. It exports phosphatidylcholine (PC) from the liver canalicular cells into the bile (92). Moreover, ABCB4 plays an essential physiological role by secreting riboflavin (vitamin B₂) into milk (93).

ABC multidrug transporters play several other physiological roles. They can change the absorption and deposition of many drugs. Pgp and ABCG2, for instance, can reduce the uptake of drugs in the intestine and hence reduce or their therapeutic activity. On the other hand, they can also limit the accumulation of drugs in the brain by pumping them back to the blood (94, 95).

MRP1 is expressed at the basolateral membrane of polarized epithelial cells and protects tissues such as the bone marrow, kidney collecting tubules, and oropharyngeal and intestinal mucosa from xenobiotics. It is also involved in drug clearance from the cerebrospinal fluid, testicular tubules, and peritoneum. MRP1 provides resistance against a variety of anticancer agents. It prefers anionic substrates, and as mentioned before, drugs are either exported as anionic glutathione, glucuronate, or sulfate conjugates or co-transported with free glutathione. MRP1 also transports heavy metal oxyanions, such as arsenite and trivalent antimonite (83, 95).

1.8. MDR modulators

MDR modulators have received growing interest in the last few decades due to their ability to reversibly block the efflux pump-action and hence recover the effects exerted by the anticancer drugs (96). Such agents may either disrupt the hydrolysis of ATP or compete with the substrates for the drug-binding pocket of the transporter. In this way, the modulators will help to sustain an active concentration of drug inside the cell or lowering the cytotoxic concentration of the drug (83).

Even though the fact that numerous Pgp modulators have been prepared and investigated (96), fewer numbers of MRP1 and ANCG2 modulators have been designed. Recently, some multifunctional, such as Elacridar (GF120918) **32**, agents have been developed, which inhibited Pgp and ABCG2. Some other agents like Biricodar (VX710) **33** inhibited the activity of Pgp, MRP1, and ABCG2 at low doses (97, 98).

Verapamil **34**, cyclosporine A **35**, tamoxifen **36**, and vincristine **37** represent the first generation of modulators. These agents were already employed in clinical uses to treat other medical conditions, such as blood pressure, immunosuppression, and estrogen receptor modulator. These agents, however, presented low efficacy at tolerable doses. Furthermore, these compounds caused severe side effects on patients. The second-generation agents, such as valspodar and VX-710, presented better efficiency at low doses, but these agents provided poor pharmacokinetics. The third-generation modulators include zosuquidar **38** and tariquidar **39**, which exhibited low toxicity and high selectivity and potency against Pgp (83).

It is essential to understand that MDR modulators may interact with some of the functions of ABC receptors and cause positive or negative consequences (94, 99). Since all of the inhibitors, including

the third-generation agents, failed to reach the market, there is an urgent need for new, effective, and nontoxic inhibitors (100).

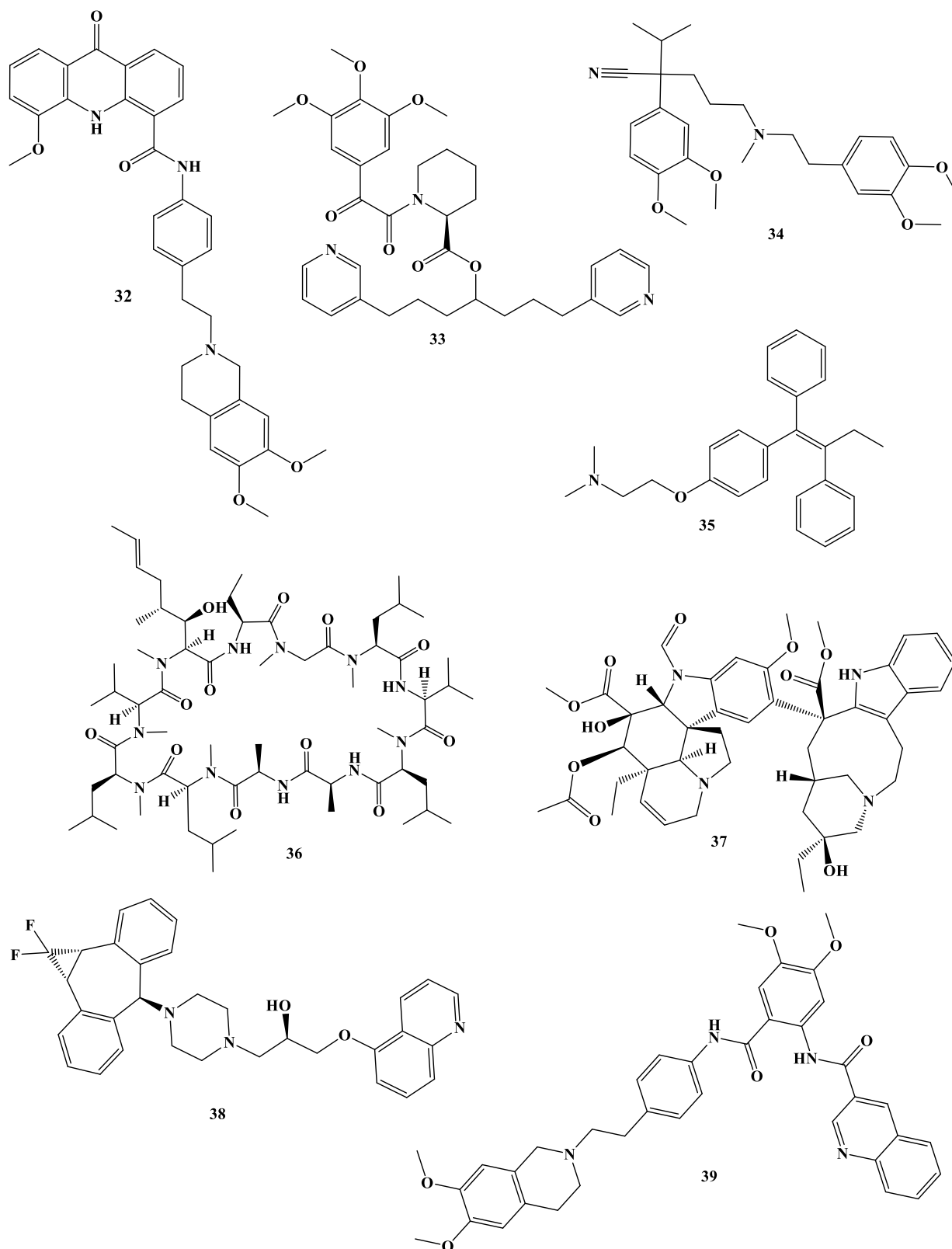


Figure 5: Structures of different MDR modulators

1.9. Recent advance in cancer therapy

ABCB1 (Pgp) is the most studied member of the ATP-binding cassette (ABC) transport proteins. It is encoded by the MDR1 gene and export various cytotoxic agents out of cells by depending on energy mechanism, (ATP) hydrolysis. This action reduces the concentrations inside the cell. Up to date, no ABCB1 modulator has reached the market due to a lack of clinical efficacy, pharmacokinetic interaction, or other side effects related to toxicity. As a result, there is an urgent need to develop novel, selective, and effective ABCB1 inhibitors to reverse drug resistance (101).

Multifunctional compounds serve as the source of lead structures in designing efficient molecules that could act as anticancer and efflux pump modulators. Moreover, combining two or more multifunctional motifs in one molecule provides an interesting strategy from the perspective of drug design. Nitrogen heterocycles and chalcogens (in general and selenium in particular) attract considerable attention due to their diverse biological activities.

The literature reveals that the presence of an aromatic ring is vital for the MDR modulation effect. The addition of another aromatic ring, mostly a benzene or nitrogen heterocycle, increases the modulation effect. The presence of a positive ionizable centre and hydrogen bond acceptor is also beneficial but not essential for the efflux pump modulation activity (102).

Triazole-N-ethyl-tetrahydroisoquinoline based compounds, for instance, compound **40**, presented more potency than the classical Pgp inhibitor verapamil (103). Moreover, 1,2,3-triazole-pyrimidine sulfide hybrid compound **41** was reported to act as a potential reversal agent against ABCB1-mediated multidrug resistance. Compound **41** exhibited good ABCB1 inhibition activity and was suggested as a lead structure for further synthesis of ABCB1 modulators agents (101). Aryl piperazine derivatives of hydantoin (**42**) and aryl-piperazine derivatives of hydantoin-3-acetate (**43**) significantly inhibited the ABCB1 (102, 104).

Intriguingly, an indole derivative (**44**) served as an adjuvant and inhibited ABCB1 and ANCG2. This adjuvant activity enhanced the chemotherapeutic activity and increased the intracellular concentration of doxorubicin and mitoxantrone in MDR cells(105).

It is possible to design novel agents based on suitable pharmacophore moiety, which exerts the biological activities *via* multiple biochemical pathways. Nitrogen heterocycles, such as piperazine, could be considered good candidate for building up such novel compounds. Piperazine derivatives presented excellent cytotoxic and antiproliferative activities. They act *via* different biochemical pathways, such as inhibition of cancer signaling (100) and mitotic arrest (106).

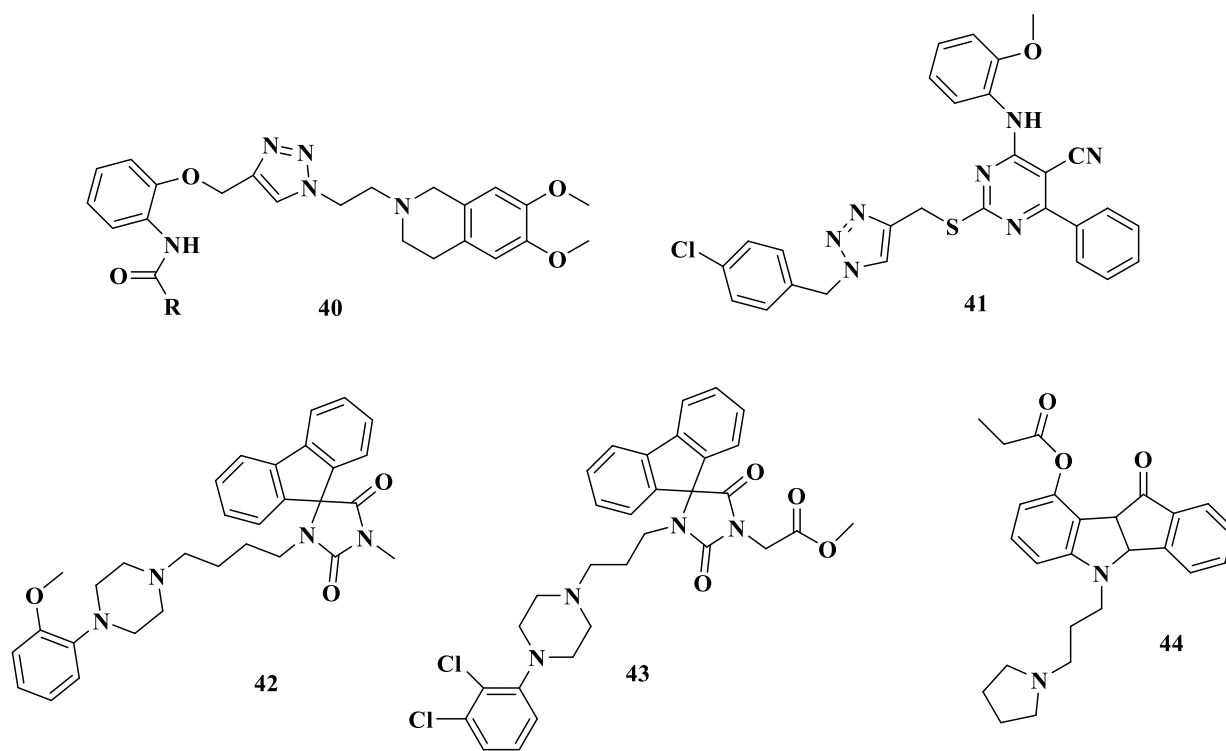


Figure 6: Examples of the newest ABCB1 modulators

2. Aims of the thesis

Following the study of Rodríguez *et al.* and D. Łażewska *et al.* (36), the main goal of the work is to obtain a new and active chemical group of ligands for the 5-HT₆ receptors. This study will give a proper perspective for future therapeutic usage in treating current civilization CNS diseases, i.e., a group of compounds with an antidepressant, pro-cognitive, anxiolytic, or antiobesity action. Also, following the study of Źesławska *et al.* (102), the second part of this work will discuss the design, synthesis, and biological evaluation of novel ABCB1 modulators.

There is a real need for more active compounds with satisfying “drug-ability” properties, which can be a good source of new drug candidates. The work may also give indications for further modifications to improve ligand binding affinity and bioavailability.

3. Results

3.1. Publication 1

Computer-Aided Studies for Novel Arylhydantoin 1,3,5-Triazine Derivatives as 5-HT₆ Serotonin Receptor Ligands with Antidepressive-Like, Anxiolytic and Antiobesity Action *In Vivo*.

Rafał Kurczab, Wesam Ali, Dorota Łażewska, Magdalena Kotanska, Magdalena Jastrzębska-Więsek, Grzegorz Satała, Małgorzata Więcek, Annamaria Lubelska, Gniewomir Latacz, Anna Partyka, Małgorzata Starek, Monika Dąbrowska, Anna Wesołowska, Claus Jacob, Katarzyna Kieć-Kononowicz and Jadwiga Handzlik.

Molecules 2018, 23, 2529; doi:10.3390/molecules23102529

Article

Computer-Aided Studies for Novel Arylhydantoin 1,3,5-Triazine Derivatives as 5-HT₆ Serotonin Receptor Ligands with Antidepressive-Like, Anxiolytic and Antiobesity Action In Vivo

Rafał Kurczab ^{1,†}, Wesam Ali ^{2,3,†}, Dorota Łazewska ², Magdalena Kotańska ⁴,
Magdalena Jastrzębska-Więsek ⁵, Grzegorz Satała ¹, Małgorzata Więcek ², Annamaria Lubelska ²,
Gniewomir Latacz ², Anna Partyka ⁵, Małgorzata Starek ⁶, Monika Dąbrowska ⁶, Anna Wesolowska ⁵,
Claus Jacob ³, Katarzyna Kieć-Kononowicz ² and Jadwiga Handzlik ^{2,*}

¹ Department of Medicinal Chemistry, Institute of Pharmacology, Polish Academy of Sciences, Smętna 12, PL 31-343 Cracow, Poland; kurczab@if-pan.krakow.pl (R.K.); satala@if-pan.krakow.pl (G.S.)

² Department of Technology and Biotechnology of Drugs, Jagiellonian University, Medical College, Medyczna 9, PL 30-688 Cracow, Poland; s8wealii@stud.uni-saarland.de (W.A.); dlazewska@cm-uj.krakow.pl (D.Ł.); mwiecek@cm-uj.krakow.pl (M.W.); annamaria.lubelska@doctoral.uj.edu.pl (A.L.); glatacz@cm-uj.krakow.pl (G.L.); mfkono@cyf-kr.edu.pl (K.K.-K.)

³ Division of Bioorganic Chemistry, School of Pharmacy, University of Saarland, Campus B2 1, D-66123 Saarbruecken, D-66123 Saarland, Germany; c.jacob@mx.uni-saarland.de

⁴ Department of Pharmacodynamics, Jagiellonian University, Medical College, Medyczna 9, PL 30-688 Cracow, Poland; magda.dudek@uj.edu.pl

⁵ Department of Clinical Pharmacy, Jagiellonian University, Medical College, Medyczna 9, PL 30-688 Cracow, Poland; mj.wiesek@gmail.com (M.J.-W.); annairena.partyka@uj.edu.pl (A.P.); awesolowska@cm-uj.krakow.pl (A.W.)

⁶ Department of Inorganic Chemistry, Jagiellonian University, Medical College, Medyczna 9, PL 30-688 Cracow, Poland; m.starek@uj.edu.pl (M.S.); monika.1.dabrowska@uj.edu.pl (M.D.)

* Correspondence: j.handzlik@uj.edu.pl; Tel.: +48-12-620-55-84

† These authors contributed equally to this work.

Received: 1 September 2018; Accepted: 24 September 2018; Published: 3 October 2018



Abstract: This study focuses on the design, synthesis, biological evaluation, and computer-aided structure-activity relationship (SAR) analysis for a novel group of aromatic triazine-methylpiperazines, with an hydantoin spacer between 1,3,5-triazine and the aromatic fragment. New compounds were synthesized and their affinities for serotonin 5-HT₆, 5-HT_{1A}, 5-HT_{2A}, 5-HT₇, and dopamine D₂ receptors were evaluated. The induced-fit docking (IFD) procedure was performed to explore the 5-HT₆ receptor conformation space employing two lead structures. It resulted in a consistent binding mode with the activity data. For the most active compounds found in each modification line, anti-obesity and anti-depressive-like activity in vivo, as well as “druglikeness” in vitro, were examined. Two 2-naphthyl compounds (**18** and **26**) were identified as the most active 5-HT₆R agents within each lead modification line, respectively. The 5-(2-naphthyl)hydantoin derivative **26**, the most active one in the series (5-HT₆R: K_i = 87 nM), displayed also significant selectivity towards competitive G-protein coupled receptors (6–197-fold). Docking studies indicated that the hydantoin ring is stabilized by hydrogen bonding, but due to its different orientation, the hydrogen bonds form with S5.44 and N6.55 or Q6.58 for **18** and **26**, respectively. Compound **26** exerted anxiolytic-like and antidepressant-like activities. Importantly, it demonstrated anti-obesity properties in animals fed palatable feed, and did not show toxic effects in vitro.

Keywords: serotonin receptors; 5-HT₆ ligands; 1,3,5-triazine; hydantoin; docking; obesity; antidepressive; ADMET in vitro

1. Introduction

The serotonin receptor 5-HT₆ is one of the recently discovered members of the 5-HTRs family [1]. It is quite unique, since it includes a short third cytoplasmatic loop in parallel, with a long C-terminal tail, and one introne located in the middle of the third cytoplasmatic loop [2,3]. The localization of 5-HT₆R is limited to the central nervous system, especially as it is located in the brain areas involved in learning and memory processes. Relatively limited, but intensive, research efforts in this area led to several families of potent 5-HT₆R ligands [4,5], which have been proposed for potential treatment in the cognitive dysfunction associated with Alzheimer's disease, anxiety or depression [5–7]. Over 20 compounds have qualified for clinical trials, most of which in studies following a cure for Alzheimer's disease [5]. Nonetheless, none has reached the pharmaceutical market yet. Recent lines of evidence also point towards promising properties of some 5-HT₆R ligands in the battle against obesity [8,9]. Therefore, the search for new ligands for the 5-HT₆R, in particular, those with an action directed against obesity, seems to be a challenge for current medicinal chemistry.

Lines of evidence have identified several groups of chemical compounds, which displayed significant affinities for the serotonin receptors 5-HT₆ [4,10,11]. The structure-activity relationship (SAR) analysis performed for the 5-HT₆ ligands obtained previously enabled to identify pharmacophore features, including a triangle topology with tops of: A bulky hydrophobic area (HYD), positive ionizable nitrogen (PI), and hydrogen bond acceptor (HBA), as well as a central aromatic fragment (AR) (Figure 1) [12].

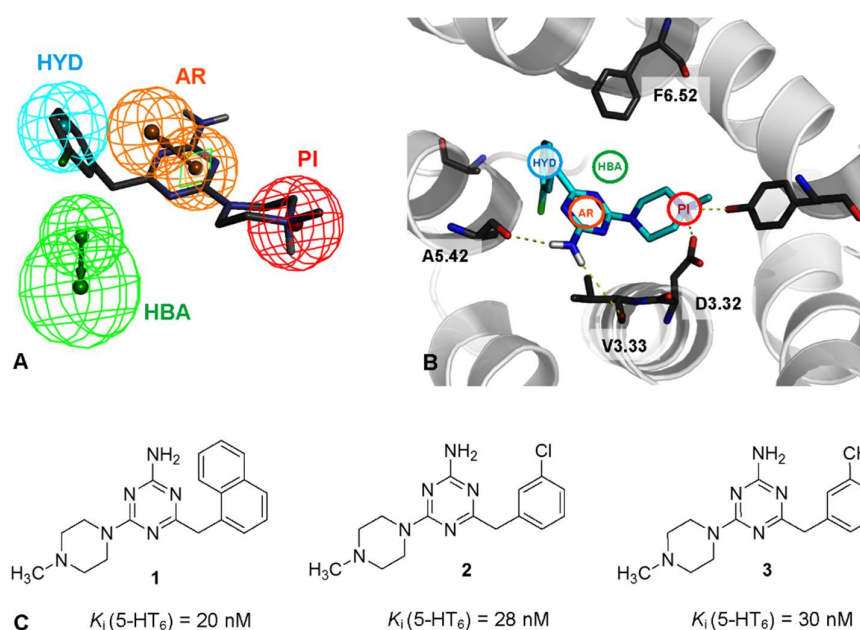


Figure 1. Modified pharmacophore model based of the 1,3,5-triazine with mapped compound **2**, including four key pharmacophore features, namely: A positive ionizable group (PI, red), an aromatic ring (AR, orange), a hydrogen bond acceptor group (HBA, green) and hydrophobic group (HYD, blue) (A). The lead compound **2** mapped onto the binding site of 5-HT₆R (B). Examples of the most active 1,3,5-triazine 5-HT₆ ligands found recently **1–3** (C).

Taking into consideration the pharmacophore features, our previous studies have successfully found a new group of potent 5-HT₆R agents among methylpiperazine derivatives of benzyl 2-amino-1,3,5-triazines which fit 3 out of 4 pharmacophore features. Two closed HBAs were the missing feature [13]. The computer-aided SAR analysis allowed us to modify the previous pharmacophore features and it has underlined the notable importance of aromatic substituents separated by a short linker from the 1,3,5-triazine. Thus, a bulky aromatic moiety, represented by the naphthyl (**1**) or

m-chloro- (2) or *m*-methyl- (3) substituted phenyl ring (Figure 1) was beneficial for the kind of 5-HT₆R affinity evaluated experimentally [13].

Taking into account both, the need to search for the 5-HT₆R agents with new pharmacological possibilities and the results of previous SAR studies, we decided to explore a novel group of triazine-methylpiperazine derivatives (Figure 2), in which the spacer between 1,3,5-triazine and aromatic fragment is represented by a differently positioned hydantoin system containing both, two closed HBAs and HYD/AR features. In the first step, five pilot compounds (4–8) were synthesized and evaluated with regard to their affinity for the 5-HT₆R. These initial studies resulted in two parallel lead structures 5 and 7 (Figure 2). Chemical modifications of the lead structures subsequently provided a series of compounds 9–27 (Table 1). Therefore, these studies are focused on the design, synthesis and biological evaluation, including affinity and selectivity for the 5-HT₆R, as well as computer-aided SAR discussion for an entire series of hydantoin-triazines (4–27). For representative compounds, anti-obesity and anti-depressive activity *in vivo*, as well as their “drugability” properties, were also examined.

2. Results

2.1. Identification of Lead Structures

In the first step, a nonaromatic 5,5-dimethylhydantoin 1,3,5-triazine derivative 4 was found as a moderate 5-HT₆R ligand after the radioligand binding assay and was therefore selected as an initial lead structure (Figure 2). Then, four different hydantoin moieties were taken into consideration as lead modifications, including: two *N*-substituted *p*-chlorobenzyl derivatives 5 and 6, with respect to position 3-*N* (5) and 1-*N* (6), the 5-(4-chlorophenyl)-5-methyl derivative 7 and 5,5-*bis*(4-chlorophenyl)hydantoin 8 (Figure 2).

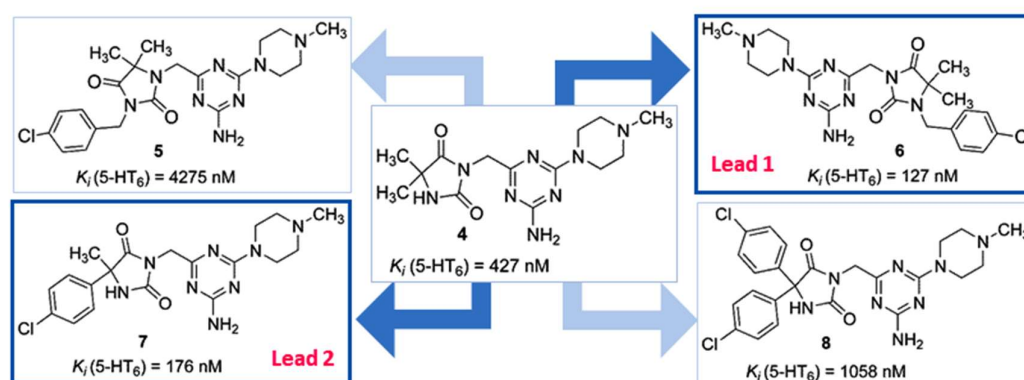
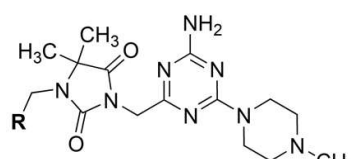


Figure 2. The rationale for the design of novel lead structures of the 5-HT₆R ligand among hydantoin 1,3,5-triazine derivatives.

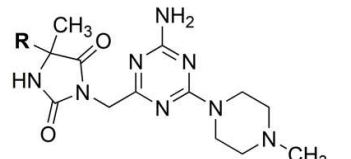
Table 1. Structures and affinities for serotonin/dopamine receptors of hydantoin-triazine compounds 4–26.

Group A



6, 9-18

Group B



4, 7, 19-26

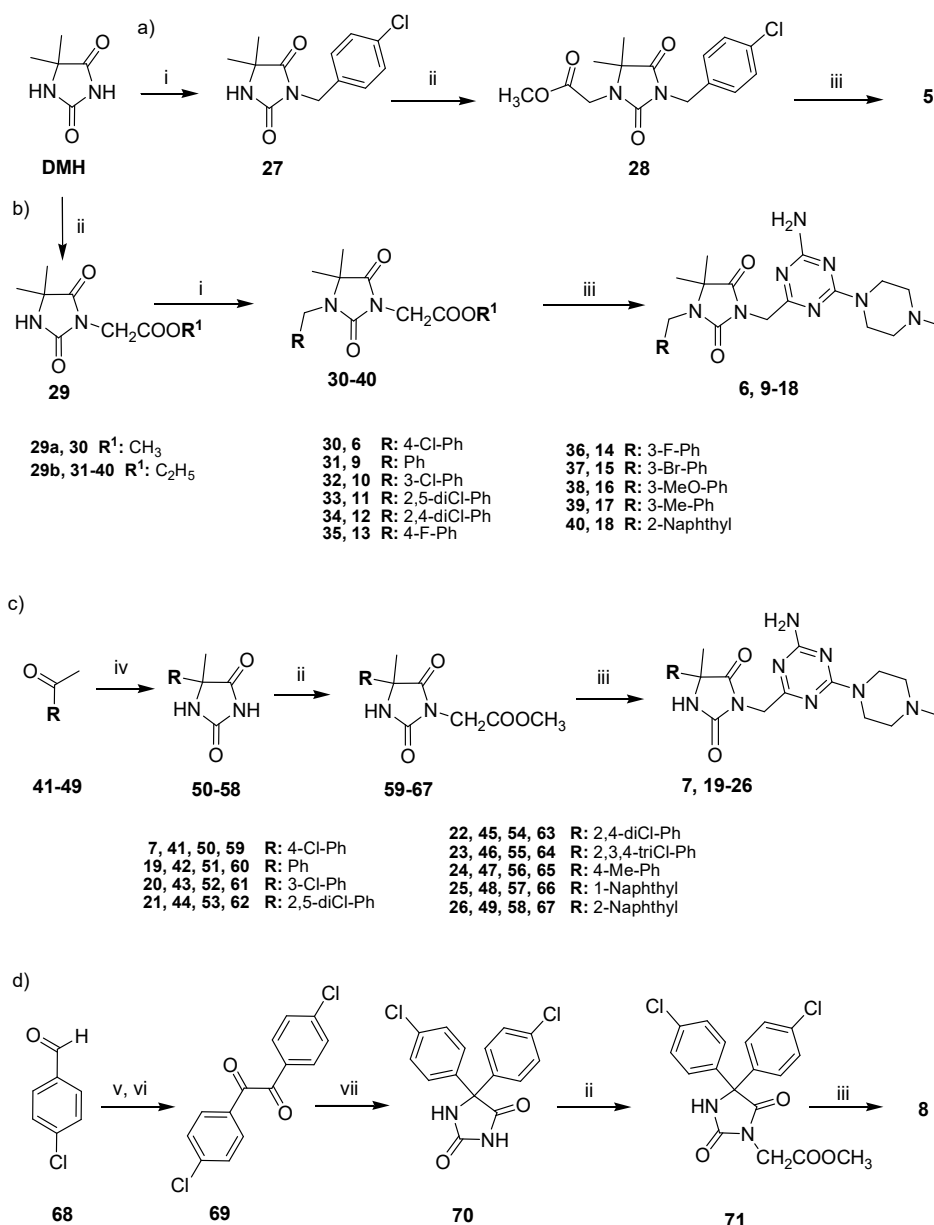
Cpd	Gr	R	K_i (nM) ^a				
			5-HT ₆ [³ H]-LSD	D ₂ [³ H]-Raclopride	5-HT _{1A} [³ H]-8-OH-DPAT	5-HT _{2A} [³ H]-Ketanserin	5-HT ₇ [³ H]-5-CT
4	B	Methyl	427	22,330	9.99×10^6	nt	35,790
5	-	-	4275	5007	15,430	nt	1620
6	A	4-Chlorophenyl	127	4098	23,300	nt	3711
7	B	4-Chlorophenyl	176	31,240	28,070	nt	938
8	-	-	1058	6855	3052	nt	594
9	A	Phenyl	592	8783	42,630	1596	350
10	A	3-Chlorophenyl	271	4631	13,570	328	159
11	A	2,5-dichlorophenyl	597	2867	4155	809	279
12	A	2,4-dichlorophenyl	205	681	7693	3589	1116
13	A	4-Fluorophenyl	663	6557	48,360	3548	953
14	A	3-Fluorophenyl	447	6577	37,090	239	88
15	A	3-Bromophenyl	570	6677	12,930	1327	571
16	A	3-Methoxyphenyl	692	15,490	23,910	2036	3587
17	A	3-Methylphenyl	895	5207	16,990	817	420
18	A	2-Naphthyl	182	888	5718	1907	1525
19	B	Phenyl	726	41,040	31,620	12,150	1096
20	B	3-Chlorophenyl	418	16,780	4101	7396	791
21	B	2,5-dichlorophenyl	403	11,550	26,190	11,050	1565
22	B	2,4-dichlorophenyl	457	15,090	13,980	10,770	10,130
23	B	2,3,4-trichlorophenyl	195	4738	6028	3433	8905
24	B	4-Methylphenyl	667	23,300	22,320	24,410	564
25	B	1-Naphthyl	121	7811	7146	8080	3367
26	B	2-Naphthyl	87	4247	14,160	17,170	514
Ref.			7 ^b	9 ^b	20 ^c	-	18 ^d

^a Tested experimentally in the radioligand binding assay, binding affinity, K_i , expressed as the average of at least two independent experiments; nt—not tested. ^{b-d} Reference ligands for GPCRs investigated, ^b olanzapine, ^c buspirone, ^d clozapine.

Compounds 5–8 were synthesized and their affinity for the 5-HT₆R was evaluated in the radioligand binding assays. Results displayed an increase of the 5-HT₆R affinity in the case of compounds 6 and 7, whereas both 5 and 8 were much less active than the initial lead 4. Interestingly, the structure-activity relationship indicated a crucial role for the position of the 1,3,5-triazine substitution at hydantoin ring. Thus, 1,3,5-triazine linked by a methylene group at position 3 of hydantoin seems to be profitable (6), whilst that fragment situated at position 1 of hydantoin caused a huge decrease in activity (5). Taking into account these results, both 1-(4-chlorobenzyl)-3-((4-amino-6-(4-methylpiperazin-1-yl)-1,3,5-triazin-2-yl)methyl)-5,5-hydantoin (6), and the 3-((4-amino-6-(4-methylpiperazin-1-yl)-1,3,5-triazin-2-yl)methyl)-5-(4-chlorophenyl)-5-methylhydantoin (7) were selected in parallel as two particularly promising lead structures (Lead 1 and Lead 2, Figure 2). These two leads were subsequently modified within their aromatic area to generate a library of two distinct series of derivatives, i.e., compounds 9–18 and compounds 19–26, respectively (Table 1).

2.2. Chemical Synthesis of Compounds 5–26

The final compounds 5–26 were obtained using four different synthesis pathways (Scheme 1a–d). The synthesis of 5,5-dimethylhydantoin triazine derivative 4 was described earlier [14]. As for the syntheses of the 3-benzyl derivative (5) and the 1-arylmethyl ones (6, 9–18), the commercial 5,5-dimethylhydantoin (DMH) was a starting material, which was substituted with an appropriate arylmethyl halide and methyl bromoacetate in a different order, respectively (a and b, Scheme 1). The reactions were performed as basic two-phase alkylations in acetone in the presence of a catalytic amount of benzyltriethylammonium chloride (TEBA). In case of 5, an alkylation with 4-chlorobenzyl at position 3 was the first step (27) [15], followed by the introduction of the methyl acetate fragment at position 1 (28, Scheme 1a). In contrast, the methyl ester 29a for the synthesis of 6 and the ethyl ester 29b, i.e., the common first intermediate for the synthesis of 9–18, were obtained by an alkylation of 5,5-dimethylhydantoin with a suitable alkyl bromoacetate at position 3. The ester 29 was substituted using commercial arylmethyl halides to give compounds 30–40. Although a variety of purification methods was applied, including extraction, crystallization with charcoal and chromatography, only compounds 33, 34 and 40 gave precipitates (purity > 90%). Compounds 30–32 and 35–39 were obtained as glue-like residues with varying contents of the target product (44–81%) and were used for final cyclization in the crude form. In the case of 5-aryl-5-methylhydantoin derivatives (7, 19–26), standard Bucherer-Bergs cyclic condensation of suitable commercial ketones (41–49) was the first synthetic step providing 5-aryl-5-methylhydantoins 50–58. Next, esters 59–67 were synthesized via *N*-alkylation of 50–58 in the hydantoin position 3 with methyl bromoacetate, under similar conditions to those for 29 and purification methods as those for 30–40 (Scheme 1c). Among the esters (59–67), compounds 60 and 66 were obtained in glue forms (purity 76–85%) with the remaining compounds (59, 61–65 and 67) yielding white crystals (purity 95–100%). The ester intermediate for compound 8 was obtained within a 3-step synthesis, starting from the acyloin condensation of commercial 4-chlorobenzaldehyde (68), followed by oxidation to benzyl compound 69. The benzyl intermediate was used to perform a cyclic condensation with urea providing 5,5-bis(4-chlorophenyl)hydantoin (70), followed by an alkylation with methyl bromoacetate in position 3 of the hydantoin, in the aforementioned conditions of two-phase alkylation, to produce ester 71 (Scheme 1d). All ester hydantoin intermediates (28, 30–40, 59–67, and 71) were converted into the 1,3,5-triazine final products (5–26) via cyclic condensation with 1-(imino(4-methylpiperazin-1-yl)methyl)guanidine, which proceeded in sodium methanolate under the conditions corresponding to those for a series of benzyl-1,3,5-triazines described previously [13,14].



Scheme 1. Synthesis of compounds 5–26 (Table 1); (a) 3-arylmethylhydantoin product 5; (b) 1-arylmethylhydantoin derivatives (6, 9–18); (c) 5-aryl-5-methylhydantoin derivatives (7, 19–26); (d) 5,5-diarylmethylhydantoin derivative and triazines (8). Reagents and conditions: (i) RCH₂Cl, K₂CO₃, TEBA, acetone, 3–5 h reflux; (ii) BrCH₂COOMe, K₂CO₃, TEBA, acetone, 5–7 h reflux; (iii) 1-(imino(4-methylpiperazin-1-yl)methyl)guanidine hydrochloride, MeONa, reflux for 3–5 h, then rt, 10–20 h; (iv) KCN, (NH₄)₂CO₃, 50% EtOH, 55 °C; (v) KCN, EtOH, 1 h reflux; (vi) HNO₃ conc., 3 h reflux; (vii) EtONa, urea, 2 h reflux, HCl.

2.3. Molecular Modeling

Molecular docking was performed to gain an insight into the binding mode of the library of compounds synthesized (5–26) to the recently developed 5-HT₆R homology models [13] built on the β₂ adrenergic receptor template and optimized for the structures of Lead 1 and 2. The molecular docking indicated that newly synthesized compounds, generally, exhibited a very consistent binding mode with recently reported 5-HT₆ ligands [16–18]. An influence of the topology of aromatic substituents and the position of the 1,3,5-triazine substitution at the hydantoin ring on the binding has been observed (Figure 2) and was in good agreement with results of the radioligand binding assay (see below).

2.4. Pharmacology

2.4.1. Radioligand Binding Assay

Compounds **5–26** were evaluated with respect to their affinity and selectivity for the target 5-HT₆R in radioligand binding assays based on the human serotonin receptors 5-HT₆, 5-HT_{1A}, 5-HT_{2A}, 5-HT_{7b}R and dopaminergic D_{2L}R, all of whom were expressed stably in HEK-293 cells. Five selective radioligands were employed (Table 1). Results expressed as K_i indicate that all derivatives of both leads displayed submicromolar affinities for the target 5-HT₆R. More active agents (**6**, **7**, **18**, **23**, **25** and **26**) exerted K_i (5-HT₆R) values lower than 200 nM. Compound **26** was the most active one ($K_i = 87$ nM) and also highly selective over 5-HT_{1A}R, 5-HT_{2A}R, and D_{2L}R, with some selectivity over 5-HT_{7R} (6-fold). Furthermore, a slightly less active 5-HT₆R agent, compound **25**, was highly selective with respect to all competitive GPCRs tested (Table 1). Most of the compounds displayed much weaker affinities for 5-HT_{1A}, 5-HT_{2A} and D_{2L}R receptors than for 5-HT₆R. Notably, compounds **8–11**, **14**, **17** and **24** were more potent for 5-HT_{7R} than for the target 5-HT₆R, in particular, compound **14** (5-HT_{7R}; $K_i = 88$ nM), which was also selective toward 5-HT_{7R} (Table 1).

2.4.2. Behavioral Tests In Vivo

The most potent 5-HT₆R agent identified in the radioligand binding assays, i.e., compound **26**, was selected for behavioral assays to determine its antidepressant- and anxiolytic-like properties in vivo in male Wistar rats.

Antidepressant-Like Activity of Compound 26

In the forced swim test (FST), compound **26** significantly decreased immobility time about 20% (ANOVA: $F(3,28) = 3.7674$, $p < 0.05$) vs. vehicle treated group. A U-shaped dose-response in the FST test for compound **26** was observed (Figure 3).

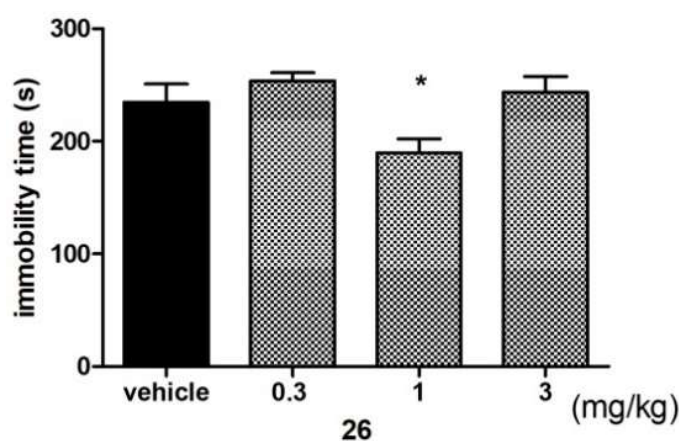


Figure 3. Influence of compound **26** on the immobility time of rats in the forced swim test. Compound **26** was administered i.p. 60 min before the test. The animals were observed for 5 min. The data are presented as the mean \pm SEM of 6–8 rats. The data were statistically evaluated by one-way ANOVA followed by Bonferroni's post-hoc test, * $p < 0.05$ vs. vehicle group.

This effect seems to be typical for some antidepressants with different mechanisms of action also producing U-shaped dose-response curves in some animal models and evaluated for antidepressant-like activity [19,20]. Moreover, this effect was also observed for other 5-HT₆ ligands (i.e., SB258585) [21].

Anxiolytic-Like Activity of Compound 26

Anxiolytic-like activity was assessed using a Vogel conflict drinking test. As demonstrated in Figure 4, compound 26, administered at a dose of just 3 mg/kg, has significantly increased (by 76%) the number of accepted shocks (ANOVA: $F(3,22) = 3.4967$, $p < 0.05$) during the 5 min experimental session. Thus, compound 26 (at a dose of 3 mg/kg) exerted anxiolytic-like activity in this behavioral test.

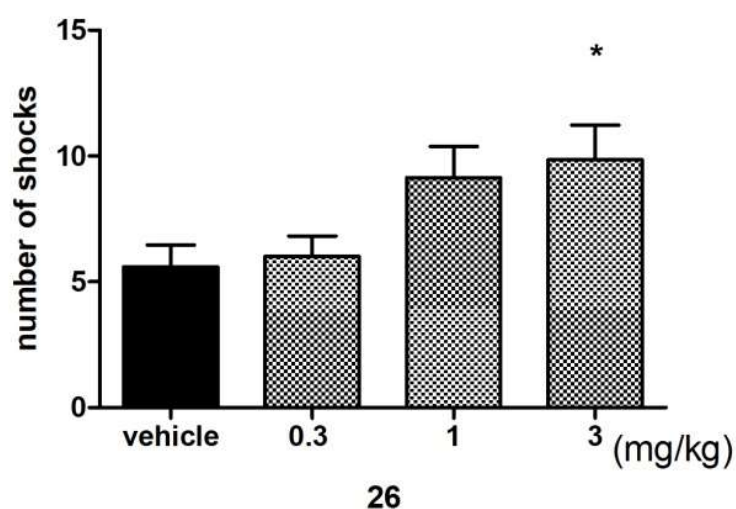


Figure 4. Compound 26 increases the number of shocks accepted in the Vogel conflict test in rats. Compound 26 was administered i.p. 60 min before the test. The animals were monitored for 5 min. The data are presented as the mean \pm SEM of 6–8 rats. The data were statistically evaluated by one-way ANOVA followed by Bonferroni's post-hoc test, * $p < 0.05$ vs. vehicle group.

2.4.3. Metabolic Assays In Vivo

Compounds 6 and 26, representing the most potent 5-HT₆R agents of both groups, A (6) and B (26), were evaluated with regard to their influence on the body weight of male Wistar rats within metabolic assays in vivo (Figure 5). Animals that were fed palatable feed, and treated with 6, exhibited significantly less weight gain when compared to animals in the control group consuming a standard feed. From day 16 of the experiment, there was a significant difference between the groups. The body weight of rats treated with 6 having access to preferential feed differed significantly from the weight of control animals fed standard feed. Results are shown in Figure 3A,B.

Similarly, animals fed palatable feed and treated with 26 showed significantly less weight gain than animals in the control group consuming a preferential feed (Figure 5C,D), but there was a significant difference between the groups from day 12 of the experiment,. Additionally, the body weight of rats treated with 26 and having access to preferential feed did not differ significantly from the weight of control animals fed standard feed. No effects on body weight were noted in animals treated either with 6 or with 26 and consuming standard feed.

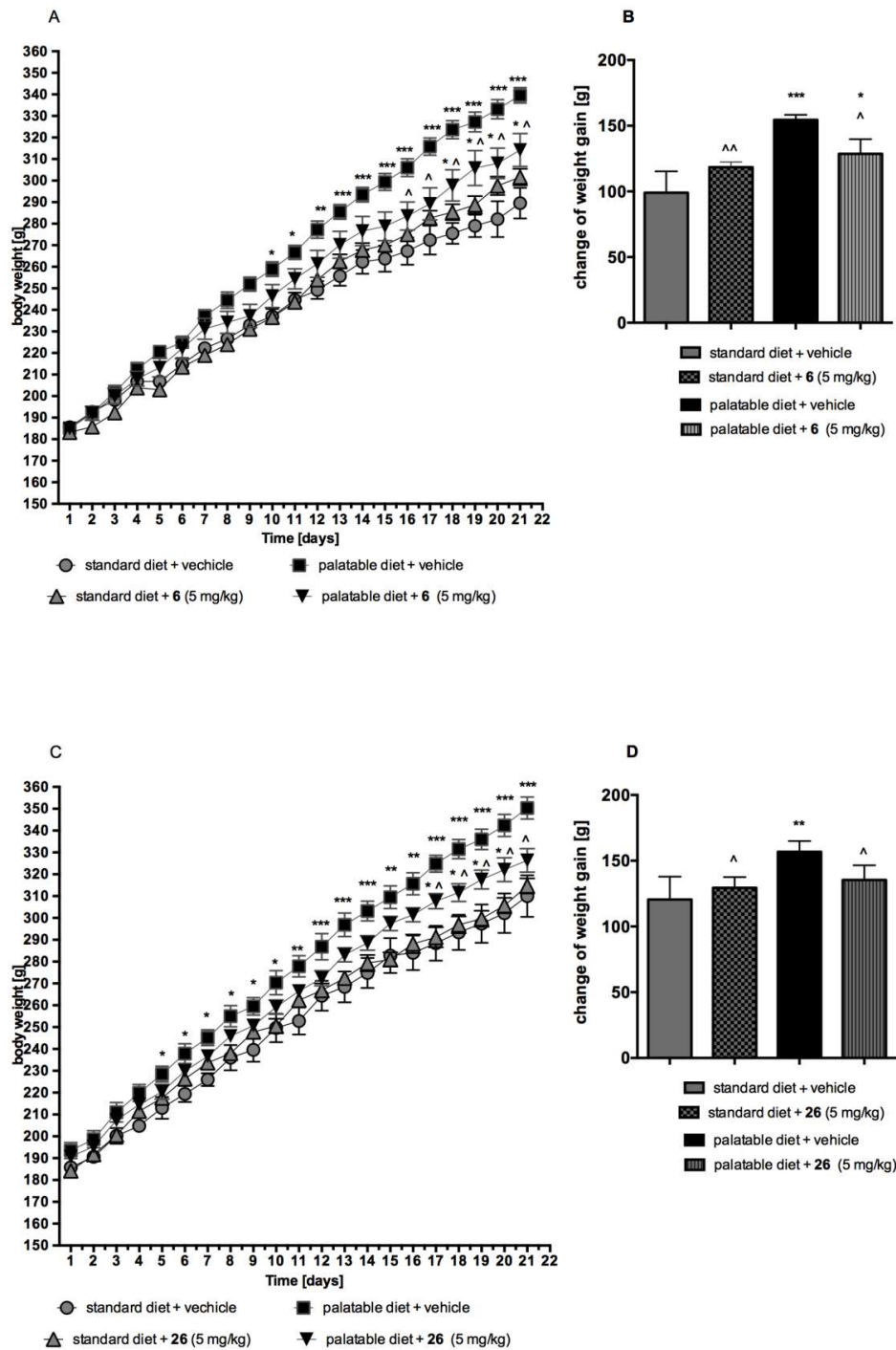


Figure 5. Influence of long-term administration of 6 or 26 on the body weight in male Wistar rats. The change in body weight in Wistar rats fed palatable diet or standard diet and in Wistar rats fed palatable diet or standard diet treated for 21 days with 6 (A,B) or 26 (C,D). Results are means \pm SEM, $n = 6$. Multiple comparisons were performed by two-way ANOVA, Sidak post-hoc (A,C) or by one-way ANOVA, Sidak post-hoc (B,D); * $p < 0.05$, ** $p < 0.01$, *** $p < 0.001$ significant vs. control rats fed standard diet; $\wedge p < 0.05$, $\wedge\wedge p < 0.01$ significant vs. control rats fed palatable diet.

2.5. “Drug-Like” Properties

2.5.1. Lipophilicity

The lipophilicity for compounds considered in the search for lead structures (5–8) in particular for the most active compounds found as derivatives of both lead modifications (18, 23, 25 and 26) was determined with the standard RP-TLC method [22]. For comparison, the active arylmethyl-triazine compounds previously found (1–3) were also examined. Stationary phase RP-18 and mixtures of water/methanol (1:9, *v/v*) as a mobile phase were employed. R_M values were calculated from the R_F data obtained. It was found that the R_M parameters decreased linearly with increasing amounts of the organic modifier (methanol) in the mobile phases tested. The regression coefficients (r^2) determined for all compounds were higher than 0.95. On the basis of the linear relationship between R_M values and the volume fraction of methanol, values of R_{M0} in the systems analyzed corresponding to 100% of water were obtained by extrapolation. R_{M0} values received for the compounds tested ranged from 3.14 to 4.49 (Figure 6).

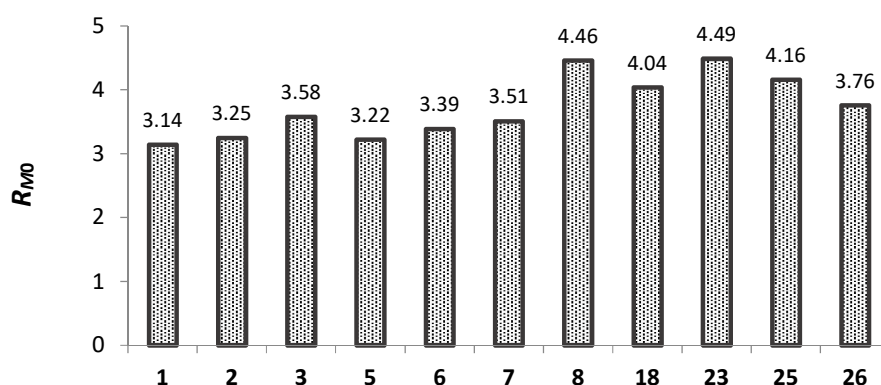


Figure 6. Lipophilicity parameters evaluated using R-TLC: R_{M0} values for compounds 1–3, 5–8, 18, 23, 25 and 26.

The most lipophilic character is associated with compound 23 ($R_{M0} = 4.49$), while the least lipophilic hydantoin compound is a weak 5-HT₆R agent 5 ($R_{M0} = 3.22$). The arylmethyl derivatives previously investigated (1–3) displayed slightly less lipophilic properties than those of the most active hydantoin agents (18–26). Overall, these results indicate a good “drug-like” lipophilicity for the entire series of compounds investigated, taking into consideration either classical rules (Rules of Five, Ghose or Pfizer) or the latest CNS MPO approach [23].

2.5.2. Toxicity In Vitro

The preliminary evaluation of the safety profile for the most promising 5-HT₆R ligands 6 and 26 was performed in vitro with the HEK-293 eukaryotic cell line. The compounds examined were dissolved in culture growth media and incubated with cells for 72 h. Next, the MTS test was applied to determine the viability of the cells. As shown in Figure 7, a statistically significant decrease of viability (***) $p < 0.001$ was observed only for compound 6 and only at the highest concentration used, i.e., 100 μ M. The reference cytostatic drug doxorubicin (DX) at the very low concentration 1 μ M was also cytotoxic. Thus, the results obtained confirm a low or no significant toxicity for compounds 6 and 26, respectively.

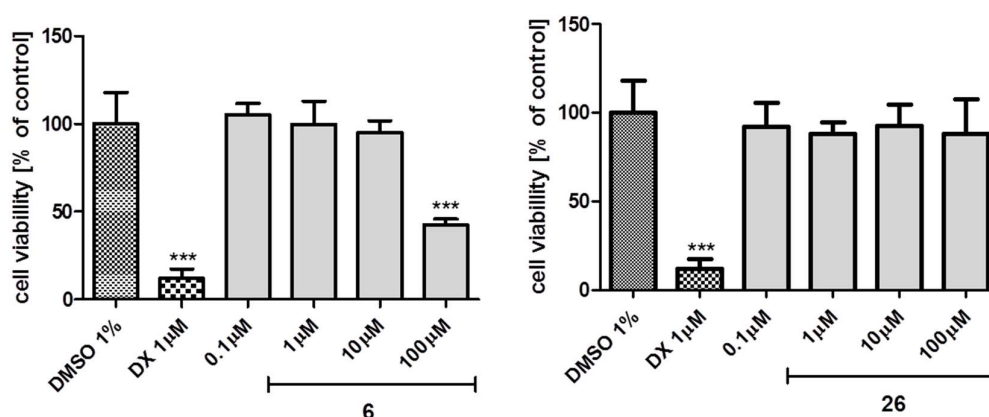


Figure 7. The influence of doxorubicin (DX) and 5-HT₆R ligands on the viability of cultured HEK-293 cells. Statistical significance was evaluated by one-way ANOVA, followed by Bonferroni's comparison test (***) $p < 0.001$ compared with the negative control).

2.5.3. Blood-Brain Barrier Permeability

In order to estimate an ability of the library synthesized (4–26) to penetrate the blood-brain barrier (BBB), the permeability QPlogBB parameter was calculated (Table 2) using QikProp from Schrodinger Suite 2017 [24]. QikProp predictions are for orally delivered drugs, and thus some natural neurotransmitters, e.g., dopamine and serotonin, are CNS negative, because they are extremely polar to cross the blood-brain barrier. Recommended values range for compounds that penetrate BBB is from -3.0 to 1.2 . All the hydantoin-triazines investigated (4–26) are predicted as BBB-permeable (Table 2) with QPlogBB values from -0.98 (25) to -0.33 (12).

Table 2. The blood-brain barrier permeability parameter (QPlogBB) for compounds 4–26.

Cpd	QPlogBB	Cpd	QPlogBB	Cpd	QPlogBB
4	−0.97	12	−0.33	20	−0.63
5	−0.60	13	−0.73	21	−0.46
6	−0.60	14	−0.46	22	−0.47
7	−0.89	15	−0.65	23	−0.38
8	−0.62	16	−0.92	24	−0.84
9	−0.84	17	−0.54	25	−0.98
10	−0.40	18	−0.63	26	−0.92
11	−0.37	19	−0.75		

3. Computer-Aided SAR Analysis

In order to expand the current knowledge about structural properties responsible for 5-HT₆R activity in the group of recently discovered aryl derivatives of 1,3,5-triazine, this study took into account the crucial role of the linker, which was found by comparative SAR analysis for the previously active arylmethyl- and inactive aryl-triazine molecules [13]. The new series of hydantoin-triazines (5–26) were designed as an extension of the methylene linker of the most active 2-arylmethyl-1,3,5-triazines, via an introduction of the inflexible, cyclic hydantoin insert, containing also hydrogen bond acceptors, and occurring in two topological variants found to be profitable in the preliminary lead identification (4–8). Both leads (6 and 7) and their derivatives (9–18 and 19–26, respectively) displayed significant submicromolar affinities for the target 5-HT₆ receptors, much more potent than those of previously investigated linker-free aryl-triazines [13], but slightly less potent if compared to the arylmethyl ones (1–3, Figure 1). Interestingly, the influence of the topology of the aromatic moieties in the group of 1,3,5-triazine derivatives seems to be distinctly linker-dependent. Although the bulky aromatic area of the naphthalene was beneficial for all the groups considered, it was distinctly predominant in the case of the 5-arylmethyl (25, 26 vs. 7 and 19–24; Table 1), comparable with

the 3-methylphenyl and 3-chlorophenyl compounds in the group arylmethyl triazines (1–3, Figure 1), and slightly less favourable than the 4-chlorophenyl substituent within the 5,5-dimethylhydantoin group (18 vs. 6, Table 1). Furthermore, the preferable *m*-substitution within the phenyl ring, found for the benzyl 1,3,5-triazine 5-HT₆R agents earlier [13], has not been confirmed in this study, either for the 5,5-dimethyl-1-benzylhydantoin- (6 vs. 10) or for the 5-phenyl-5-methylhydantoin triazine compounds (7 vs. 20). Consequently, an influence of both variants of the hydantoin linkers (1,3,5-substitution, group A or 3,5-substitution, group B) on the 5-HT₆R activity was dependent on the properties of the aromatic moiety. Thus, both variants appear to be comparable, although the most active compound (26) is a member of the 5-aryl-5-methylhydantoin derivatives (group B).

Results of our docking studies have provided data useful to explain SAR on the molecular level (Figure 8).

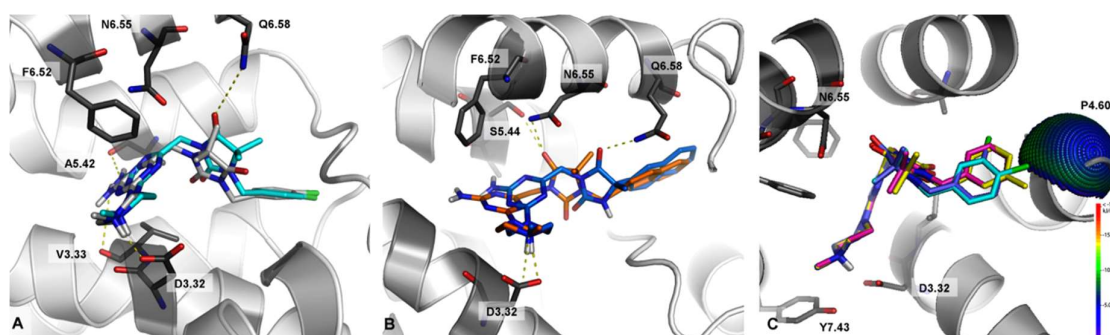


Figure 8. Molecular docking results of the representative library members for the 5-HT₆ receptor. (A) Comparison of the binding mode of compounds 6 (cyan) and 7 (gray). (B) Binding mode of 18 (orange) and 26 (blue). (C) A superposition of the poses of compounds 9 (magenta), 17 (yellow), 6 (cyan), and 10 (violet) against the putative halogen binding pocket interaction spheres for the 5-HT₆ receptor. The chlorine-oxygen theoretical interaction spheres illustrate the projected qualities of the formed ligand-receptor halogen bonds. Key residues in the binding site are presented as thick dark-grey sticks. The dotted yellow lines represent hydrogen bonds with polar residues.

In general, all of the newly synthesized derivatives of Lead 1 and Lead 2 exhibited a binding mode to 5-HT₆R, which was very consistent with derivatives of 1,3,5-triazines studied previously [13]. In addition to the crucial salt bridge interaction with D3.32, all of the docked ligands formed CH– π aromatic interactions with F6.52, and partially with F6.51. Additionally, the –NH₂ group of the 1,3,5-triazine fragment was, usually, hydrogen-bonded with the carbonyl oxygen of A5.42 and V3.33 (Figure 8A). The methylene linker connecting 1,3,5-triazine and hydantoin rings, due to its tetrahedral conformation, forced the terminal aromatic group into a hydrophobic cavity formed by transmembrane helices 3–5 and extracellular loop 2. Thus, the structure-activity relationship in this series is determined by the different substituents at the terminal aromatic ring, and by the different orientation of hydantoin ring induced by its different positioning within the compound's structure. A comparison of the analogues with different positions of the 1,3,5-triazine substitution at the hydantoin ring indicated that linking by the methylene group at position 3 of hydantoin is profitable (6, $K_i = 127$ nM), whereas a significant decrease of activity was noted for the derivative where the 1,3,5-triazine was linked with hydantoin via position 1 (5, $K_i = 4275$ nM). The analysis of the binding mode showed that a differently positioned hydantoin ring induces its different spatial orientation in the binding site (Figure 8A), and only the complex of 6 with the receptor is stabilized additionally by a hydrogen bond with a Q6.58 side chain.

Interestingly, within the group A and B, the best activity showed 2-naphthyl derivatives (18 and 26, respectively; Figure 8B). It should be noted, that apart from the length of the linker and the positioning of the hydantoin ring, the difference of activity between 18 and 26 is negligible—a comparison of its binding modes indicated that the most significant difference is noted for the hydantoin ring interaction.

In both derivatives, the hydantoin ring is stabilized by hydrogen bonding, but due to its different orientation, the hydrogen bonds form with S5.44 and N6.55 or Q6.58 for **18** and **26**, respectively. It is worth to note that the shift of the chlorine atom from 3- to 4-position resulted in a 4- (for modification B) to 5-fold (for modification A) increase of affinity for 5-HT₆R compared to its unsubstituted analogues. This relationship was confirmed by molecular docking (Figure 8C) revealing that only the presence of chlorine atom in 4-position stabilized the L–R complex through the formation of halogen bond with the carbonyl oxygen of P4.60 residue (Cl...O distance = 3.31 Å, σ-hole angle = 151.47°). As the halogen bond appeared to possess a highly directional nature, to explain the decrease in activity by shifting the chlorine atom from position 3 to 4 in the phenyl ring, the interaction sphere [25,26] was plotted onto the relevant backbone carbonyl oxygens (Figure 8C). The 4-chloro substituent was positioned within the energetically favorable areas of the sphere, whereas the 3-chloro substituent pointed outside of the sphere, indicating no ability to form halogen bond.

4. Experimental Section

4.1. Chemistry

Reagents were purchased from Alfa Aesar (Karlsruhe, Germany) or Sigma Aldrich (Darmstadt, Germany). Methanol was dried over calcium oxide. Reaction progress was verified using thin layer chromatography (TLC), which was carried out on 0.2 mm Merck silica gel 60 F254 plates. Spots were visualized by UV light or treatment with Dragendorff reagent. Melting points (m.p.) were determined using MEL-TEMP II apparatus (LD Inc., Long Beach, CA, USA) and are uncorrected. The ¹H-NMR and ¹³C-NMR spectra were obtained on a Mercury-VX 300 Mz spectrometer (Varian, Palo Alto, CA, USA) in DMSO-*d*₆ or CDCl₃. Chemical shifts in ¹H-NMR spectra were reported in parts per million (ppm) on the δ scale using the solvent signal as an internal standard. Data are reported as follows: Chemical shift, multiplicity (s, singlet; br.s., broad singlet; d, doublet; t, triplet; m, multiplet), coupling constant *J* in Hertz (Hz), number of protons, proton's position (Ind—indole, Naph—naphthalene, Ph—phenyl, Pp—piperazine). LC-MS were carried out on a system Water TQ Detector (Water Corporation, Milford, CT, USA) consisting of a Waters Acquity UPLC, coupled to a Waters TQD mass spectrometer. Retention times (t_R) are given in minutes. The UPLC/MS purity of all final compounds was determined (%).

Synthesis of compounds **27**, **29**, **50–58**, **63**, **65** and **68–70** was obtained by our [15,27] or other research groups [28–32] earlier and are reported in Chemical Abstract Database (see Supplementary Information).

4.1.1. Synthesis of Methyl 2-(3-(4-chlorobenzyl)-5,5-dimethyl-2,4-dioximidazolidin-1-yl)acetate (**28**)

A mixture of 3-(4-chlorobenzyl)-5,5-dimethylimidazolidine-2,4-dione **27** (20 mmol, 5.05 g), TEBA (2.60 mmol, 0.60 g), K₂CO₃ (58 mmol, 8 g) in acetone (100 mL) was heated under reflux for 30 min. Methyl bromoacetate (20 mmol, 3.06 g) in acetone (20 mL) was added. The mixture was heated under reflux for 5 h and stirred at room temperature overnight. The inorganic precipitate was separated by filtration. The filtrate was evaporated, and the residue was crystallized with methanol. White solid, m.p. 78–80 °C, yield: 58% (11.60 mmol, 3.77 g), C₁₅H₁₇ClN₂O₄ (MW 324.76). ¹H-NMR (300 MHz, DMSO-*d*₆) δ = 7.38–7.41 (d def., 2H, Ar-3,5-H), 7.22–7.25 (d def., 2H, Ar-2,6-H), 4.57 (s, 2H, Ar-CH₂), 4.18 (s, 2H, CH₂COO), 3.68 (s, 3H, OCH₃), 1.30 (s, 6H, 2 × 5-CH₃) ppm. LC/MS⁺: Purity: 98.40%, t_R = 6.14, (ESI) *m/z* [M + H]⁺ 325.11.

4.1.2. General Procedure for the Synthesis of Alkyl 2-(1-arylmethyl-5,5-dimethyl-2,4-dioximidazolidin-3-yl)acetate (**30–40**)

A mixture of alkyl 2-(5,5-dimethyl-2,4-dioximidazolidin-3-yl)acetate **29** (12 mmol, **29a**: 2.40 g or **29b**: 2.58 g), TEBA (1.20 mmol, 0.36 g), K₂CO₃ (12 mmol, 4.80 g) in acetone (60 mL) was heated under reflux for 30 min. The appropriate arylmethyl halide (12 mmol) in acetone (15 mL) was added. The mixture was heated under reflux for 5–7 h and stirred at room temperature for further 24–48 h.

The inorganic precipitate was separated by filtration. The filtrate was collected, the solvent then evaporated and the residue was dissolved in 30 mL of DCM and washed with 1% NaOH (2 × 30 mL) and H₂O (2 × 30 mL). The organic phase was dried on anhydrous Na₂SO₄ overnight, separated from the drying agent and the solvent was evaporated. Then, Methods A or B were applied for purification. Method A: The residue was crystallized with EtOH and charcoal to give crystals of the intermediates. Method B: If Method A was applied, but no crystal appeared, the ethanolic solution was concentrated to give crude ester intermediates in glue form. No ester intermediate (**30–40**) was isolated in pure form (purity < 80%). The purity and identity of crude intermediates were evaluated using LC-MS. Taking into consideration the results of LC-MS a desirable ester was used for the synthesis of the final product in the amount suitable to its concentration in the crude product obtained (40–80%)

Ethyl 2-(1-(4-chlorobenzyl)-5,5-dimethyl-2,4-dioximidazolidin-3-yl)acetate (30). 1-Chloro-4-(chloromethyl) benzene (1.93 g) and **29a** were used. Method A. White crystals, m.p. 88–90 °C, yield: 68% (8.16 mmol, 2.65 g), C₁₅H₁₇ClN₂O₄ (MW 324.76). ¹H-NMR (300 MHz, DMSO-*d*₆) δ = 7.36–7.37 (d def., 4H, Ar), 4.52 (s, 2H, Ar-CH₂), 4.25 (s, 2H, CH₂COO), 3.70 (s, 3H, OCH₃), 1.25 (s, 6H, 2 × CH₃) ppm. LC/MS⁺: Purity: 81%, t_R = 6.31, (ESI) *m/z* [M + H]⁺ 325.18.

Ethyl 2-(1-benzyl-5,5-dimethyl-2,4-dioximidazolidin-3-yl)acetate (31). Benzyl chloride (1.52 g) and **29a** were used. Method B. Glue mixture containing 44% of **31**, yield: 61.37%, C₁₅H₁₈N₂O₄ (MW 304.15). LC/MS⁺: Purity: 44%, t_R = 6.09, (ESI) *m/z* [M + H]⁺ 304.14.

Ethyl 2-(1-(3-chlorobenzyl)-5,5-dimethyl-2,4-dioximidazolidin-3-yl)acetate (32). 1-Chloro-3-(chloromethyl) benzene (1.93 g) and **29a** were used. Method B. Sticky liquid, yield: 85.22%, C₁₅H₁₉ClN₂O₄ (MW 338.59). ¹H-NMR (300 MHz, DMSO-*d*₆) δ = 7.41–7.33 (m, 1H, Ph-5-H), 7.31–7.28 (m, 3H, Ph-2,4,6-H), 4.54 (s, 2H, Ph-CH₂), 4.23 (s, 2H, CH₂COO), 4.10 (q, *J* = 7.05 Hz, 2H, CH₃–CH₂), 1.26 (s, 6H, 2 × CH₃), 1.16 (t, *J* = 7.35 Hz, 3H, CH₃–CH₂) ppm. LC/MS⁺: Purity: 67.03%, t_R = 6.73, (ESI) *m/z* [M + H]⁺ 339.59.

Ethyl 2-(1-(2,5-dichlorobenzyl)-5,5-dimethyl-2,4-dioximidazolidin-3-yl) acetate (33). 1-Bromo-2,5-(di-chloro methyl) benzene (3.60 g) and **29a** were used. Method A. yellowish Solid, m.p. 98 °C, yield: 98.21%, C₁₆H₁₈Cl₂N₂O₄ (MW 373.04). ¹H-NMR (300 MHz, DMSO-*d*₆) δ = 7.52–7.41 (m, 1H, Ph-6-H), 7.39–7.40 (m, 2H, Ph-3,4-H), 4.58 (s, 2H, Ph-CH₂), 4.24 (s, 2H, CH₂COO), 4.10 (q, *J* = 7.00 Hz, 2H, CH₃–CH₂), 1.29 (s, 6H, 2 × CH₃), 1.17 (d, *J* = 7.00 Hz, 3H, CH₃–CH₂) ppm. LC/MS⁺: Purity: 93.90%, t_R = 7.28, (ESI) *m/z* [M + H]⁺ 373.03.

Ethyl 2-(1-(2,4-dichlorobenzyl)-5,5-dimethyl-2,4-dioximidazolidin-3-yl)acetate (34). 1-Chloro-2,4-(di-chloro methyl) benzene (2.34 g) and **29a** were used. Method B. White Solid, m.p. 105 °C, yield: 91.52%, C₁₆H₁₈Cl₂N₂O₄ (MW 373.04). ¹H-NMR (300 MHz, DMSO-*d*₆) δ = 7.66 (d, *J* = 2.0 Hz, 1H, Ph-3-H), 7.47–7.37 (m, 2H-Ph-5,6-H), 4.60 (s, 2H-Ph-CH₂), 4.26 (s, 2H, CH₂COO), 4.16 (q, *J* = 7.1 Hz, 2H-CH₃–CH₂), 1.29 (s, 6H, 2 × CH₃), 1.21 (t, *J* = 7.1 Hz, 3H, CH₃) ppm. ¹³C-NMR (75 MHz, DMSO-*d*₆) δ = 175.83, 167.53, 154.84, 134.60, 133.22, 133.18, 130.71, 129.32, 127.98, 62.51, 61.83, 22.68, 14.38 ppm. LC/MS⁺: Purity: 91.74%, t_R = 7.52, (ESI) *m/z* [M + H]⁺ 374.04.

Ethyl 2-(1-(4-fluorobenzyl)-5,5-dimethyl-2,4-dioximidazolidin-3-yl)acetate (35). 4-Flouro benzyl chloride (2.17 g) and **29a** were used. Method B. Sticky liquid, yield: 90.72%, C₁₆H₁₉FN₂O₄ (MW 322.99). LC/MS⁺: Purity: 69.51%, t_R = 7.52, (ESI) *m/z* [M + H]⁺ 323.99.

Ethyl 2-(1-(3-fluorobenzyl)-5,5-dimethyl-2,4-dioximidazolidin-3-yl)acetate (36). 3-Flouro benzyl chloride (1.74 g) and **29a** were used. Method A. Sticky liquid, yield: 77.06%, C₁₆H₁₉FN₂O₄ (MW 322.99). ¹H-NMR (300 MHz, DMSO-*d*₆) δ = 7.41–7.36 (m, 1H, Ph-5-H), 7.19–7.13 (m, 3H, Ph-2,4,6-H), 4.55 (s, 2H, Ph-CH₂), 4.23 (s, 2H, CH₂COO), 4.10 (q, *J* = 7.05 Hz, 2H, CH₃–CH₂), 1.26 (s, 6H, 2 × CH₃), 1.16 (t, *J* = 7.05 Hz, 3H, CH₃–CH₂) ppm. LC/MS⁺: Purity: 69.43%, t_R = 6.23, (ESI) *m/z* [M + H]⁺ 323.99.

Ethyl 2-(1-(3-bromobenzyl)-5,5-dimethyl-2,4-dioximidazolidin-3-yl)acetate (37). 3-Bromo benzyl chloride (3.75 g) and **29a** were used. Method B. Sticky liquid, yield: 60%, C₁₆H₁₉BrN₂O₄ (MW 383.24). LC/MS⁺: Purity: 78.26%, t_R = 6.85, (ESI) *m/z* [M + H]⁺ 384.24.

Ethyl 2-(1-(3-methoxybenzyl)-5,5-dimethyl-2,4-dioxoimidazolidin-3-yl)acetate (38). 3-Methoxy benzyl chloride (1.88 g) and **29a** were used. Method B. Sticky liquid, yield: 68.94%, C₁₇H₂₂N₂O₅ (MW 334.38). LC/MS⁺: Purity: 88.03%, t_R = 6.65, (ESI) *m/z* [M + H]⁺ 335.38.

Ethyl 2-(1-(3-methylbenzyl)-5,5-dimethyl-2,4-dioxoimidazolidin-3-yl)acetate (39). 3-Methyl benzyl chloride (1.69 g) and **29a** were used. Method B. Sticky liquid, yield: 61.05%, C₁₇H₂₂N₂O₄ (MW 318.38). LC/MS⁺: Purity: 81.94%, t_R = 6.12, (ESI) *m/z* [M + H]⁺ 319.38.

Ethyl 2-(1-(2-naphthyl)-5,5-dimethyl-2,4-dioxoimidazolidin-3-yl)acetate (40). 2-(Chloromethyl)naphthalene (2.65 g) and **29a** were used. Method B. White solid, m.p. 95 °C, yield: 81.47%, C₂₀H₂₂N₂O₄ (MW 354.19). ¹H-NMR (300 MHz, DMSO-*d*₆) δ = 7.90–7.84 (m, 4H, naft-1,4,5,8-H), 7.52–7.45 (m, 3H, naft-3,6,7-H), 4.71 (s, 2H, Ph-CH₂), 4.26 (s, 2H, CH₂COO), 4.16–4.11 (q, *J* = 7.35 Hz, 2H, CH₃–CH₂), 1.26 (s, 6H, 2 × CH₃), 1.17 (d, *J* = 7.00 Hz, 3H, CH₃–CH₂) ppm. LC/MS⁺: Purity: 90.56%, t_R = 7.08, (ESI) *m/z* [M + H]⁺ 355.15.

4.1.3. General Procedures for the Synthesis of Methyl 2-(5-arylhydantoin-3-yl)acetates (**60–67** and **71**)

A mixture of a suitable arylhydantoin **50–58** (Scheme 1) or **70** (15–20 mmol) with K₂CO₃ (6–8 g), TEBA (0.45–0.60 g) in acetone (75–100 mL) was stirred and refluxed for 30 min. Then, the solution of methyl bromoacetate (15–20 mmol, 2.30–3.06 g) in acetone (15–20 mL) was added. The mixture was stirred and refluxed for 3–6 h, then, stirred at room temperature overnight. The inorganic components were separated by filtration. The filtrate was concentrated, and the residue was purified using the similar methods as those for compounds 30–40, but MeOH in place of EtOH was used for crystallization.

Methyl 2-(5-methyl-2,4-dioxo-5-phenylimidazolidin-3-yl)acetate (60). Compound **51** (2.85 g) and methyl bromoacetate (2.30 g) were used. Sticky liquid, yield: 48.6%, C₁₃H₁₄N₂O₄ (MW 262.26). ¹H-NMR (300 MHz, DMSO-*d*₆) δ = 9.06 (s, 1H, N1-H), 7.47–7.50 (d, *J* = 7.00 Hz, 2H, Ph-2,6-H), 7.33–7.42 (m, 3H Ph-3,4,5-H), 4.19 (s, 2H, N3-CH₂), 3.67 (s, 3H, O-CH₃), 1.70 (s, 3H, CH₃) ppm. LC/MS⁺: Purity: 85.92%, t_R = 4.43, (ESI) *m/z* [M + H]⁺ 263.11.

Methyl 2-(5-(3-chlorophenyl)-5-methyl-2,4-dioxoimidazolidin-3-yl)acetate (61). Compound **52** (4.49 g) and methyl bromoacetate (3.06 g) were used. White Crystal, m.p. 102 °C, yield: 51.10%, C₁₃H₁₃ClN₂O₄ (MW 296.71). ¹H-NMR (300 MHz, DMSO-*d*₆) δ = 9.13 (s, 1H, N1-H), 7.51 (s, 1H, Ph-6-H), 7.43–7.47 (m, 3H, Ph-2,4,5-H), 4.20 (s, 2H, N3-CH₂), 3.66 (s, 3H, O-CH₃), 1.70 (s, 3H, CH₃) ppm. LC/MS⁺: Purity: 100%, t_R = 5.25, (ESI) *m/z* [M + H]⁺ 297.07.

Methyl 2-(5-(2,5-dichlorophenyl)-5-methyl-2,4-dioxoimidazolidin-3-yl)acetate (62). Compound **53** (4.14 g) and methyl bromoacetate (2.45 g) were used. White solid, m.p. 214 °C, yield: 83.19%, C₁₃H₁₂Cl₂N₂O₄ (MW 331.15). ¹H-NMR (300 MHz, DMSO-*d*₆) δ = 8.75 (s, 1H, N1-H), 7.69 (s, 2H, Ph-4-H), 7.52 (s, 2H, Ph-3,6-H), 4.25 (s, 2H, N3-CH₂), 3.68 (s, 3H, O-CH₃), 1.80 (s, 3H, CH₃) ppm. LC/MS⁺: Purity: 99.10%, t_R = 5.41, (ESI) *m/z* [M + H]⁺ 330.69.

Methyl 2-(5-(2,3,4-trichlorophenyl)-5-methyl-2,4-dioxoimidazolidin-3-yl)acetate (64). Compound **54** (5.18 g) and methyl bromoacetate (3.06 g) were used. White solid, m.p. 172 °C, yield: 37.76%, C₁₃H₁₂Cl₃N₂O₄ (MW 331.15). ¹H-NMR (300 MHz, DMSO-*d*₆) δ = 8.75 (s, 1H, N1-H), 7.68–7.71 (d, *J* = 8.8 Hz, 1H, Ph-3-H), 7.65–7.66 (s, 1H, Ph-5-H), 7.48–7.52 (m, 1H, Ph-6-H), 4.25 (s, 2H, N3-CH₂), 3.68 (s, 3H, O-CH₃), 1.78 (s, 3H, CH₃) ppm. LC/MS⁺: Purity: 96.70%, t_R = 5.49, (ESI) *m/z* [M + H]⁺ 330.76.

Methyl 2-(5-methyl-5-(naphthalen-1-yl)-2,4-dioxoimidazolidin-3-yl)acetate (66). 5-Methyl-5-(naphthalen-1-yl)imidazolidine-2,4-dione **57** (20 mmol, 4.80 g), K₂CO₃ (8 g), TEBA (0.60 g) in acetone (100 mL) and methyl bromoacetate (20 mmol, 3.06 g) in acetone (20 mL) were stirred and refluxed for 6 h. Method B. White glue-crystals, m.p. 105–109 °C, yield: 78% (15.60 mmol, 4.86 g), C₁₇H₁₆N₂O₄ (MW 312.11). ¹H-NMR (300 MHz, DMSO-*d*₆) δ = 8.98 (s, 1H, NH), 7.94–8.01 (m, 3H, Ar-4,5,8), 7.75 (d, *J* = 7.44 Hz, 1H, Ar-2), 7.48–7.57 (m, 3H, Ar-3,6,7), 4.33–4.39 (m, 2H, –CH₂CO), 3.73 (s, 3H, –OCH₃), 1.94 (s, 3H, 5-CH₃) ppm. LC/MS⁺: Purity: 65.46%, t_R = 5.47, (ESI) *m/z* [M + H]⁺ 312.95.

Methyl 2-(5-methyl-5-(naphthalen-2-yl)-2,4-dioxoimidazolidin-3-yl)acetate (67). 5-Methyl-5-(naphthalen-2-yl)imidazolidine-2,4-dione **58** (15 mmol, 3.60 g), K₂CO₃ (6 g), TEBA (0.45 g) in acetone (75 mL) and methyl bromoacetate (15 mmol, 2.30 g) in acetone (15 mL) were stirred and refluxed for 5 h. Method A. White crystals, m.p. 134–138 °C, yield: 58% (8.7 mmol, 2.72 g), C₁₇H₁₆N₂O₄ (MW 312.11). ¹H-NMR (300 MHz, DMSO-*d*₆) δ = 9.15 (s, 1H, NH), 8.02 (s, 1H, Ar-1-H), 7.60 (dd, *J*₁ = 8.72 Hz, *J*₂ = 1.80 Hz, 2H, Ar-6,7-H), 7.87–7.99 (m, 3H, Ar-4,5,8-H), 7.51–7.57 (m, 1H, Ar-3), 4.23 (s, 2H, –CH₂CO), 3.66 (s, 3H, –OCH₃), 1.81 (s, 3H, 5-CH₃) ppm. LC/MS⁺: Purity: 76.61%, t_R = 5.63, (ESI) *m/z* [M + H]⁺ 312.82.

Methyl 2-(5,5-bis(4-chlorophenyl)-2,4-dioxoimidazolidin-3-yl)acetate (71). 5,5-bis(4-Chlorophenyl)imidazolidin-2,4-dione **70** (15 mmol, 4.80 g), K₂CO₃ (6 g), TEBA (0.45 g) in acetone (75 mL) and methyl bromoacetate (15 mmol, 2.30 g) in acetone (15 mL) were stirred and refluxed for 4 h. Method A. Creamy crystals, m.p. 120–121 °C, yield: 62%, C₁₈H₁₄C₁₂N₂O₄ (MW 392.03). ¹H-NMR (300 MHz, DMSO-*d*₆) δ = 7.53 (d, *J* = 8.7 Hz, 4H-ph), 7.37 (d, *J* = 8.7 Hz, 4H-ph), 4.31 (s, 2H–CH₂), 3.70 (s, 3H–CH₃), 1.04 (d, *J* = 6.1 Hz, 1H–NH) ppm. LC/MS⁺: Purity: 91.91%, t_R = 7.26, (ESI) *m/z* [M + H]⁺ 393.10.

4.1.4. General Procedure for the Synthesis of 1,3,5-Triazine Final Products (5–26)

Sodium (8–10 mmol) was dissolved in 10 mL of absolute methanol, then 4-methylpiperazin-1-yl biguanidine × 2HCl (4–5 mmol) and an appropriate ester **28**, **30–40**, **59–67** or **71** (4–5 mmol) were added. The reaction mixture was refluxed for 15–30 h. After cooling to room temperature, water (10 mL) was added and the mixture was stirred for 0.5 h. The triazine product precipitated (**5–26**) was separated and purified using Methods C, D or E. Method C: Crystallization with methanol. Method D: crystallization with methanol and charcoal. Method E: crystallization with ethanol.

3-(4-Chlorobenzyl)-1-((4-amino-6-(4-methylpiperazin-1-yl)-1,3,5-triazin-2-yl)methyl)-5,5-dimethylimidazolidine-2,4-dione (5). Ester **28** (4.30 mmol, 1.40 g) and 4-methylpiperazin-1-yl biguanidine × 2HCl (4.30 mmol, 1.11 g) were used (48 h refluxed). Method C. White solid, m.p. 166–169 °C, yield: 34% (0.67 g), C₂₁H₂₇N₈O₂Cl (MW 458.95). ¹H-NMR (300 MHz, DMSO-*d*₆) δ 7.34–7.52 (m, 2H, Ph-3,5-H), 7.21–7.32 (m, 2H, Ph-2,6-H), 6.82 (br. s., 2H, NH₂), 4.55 (s, 2H, Ph-CH₂), 4.19 (s, 2H, TR-CH₂), 3.72–3.37 (br s, 4H, Pp-2,6-H), 2.15 (s, 7H, Pp-3,5-H + Pp-CH₃), 1.31 (s, 6H, 2 × CH₃) ppm. ¹³C-NMR (75 MHz, DMSO-*d*₆) δ = 176.83, 173.77, 167.04, 164.65, 154.86, 136.23, 132.52, 129.73, 129.03, 62.11, 54.67, 46.19, 44.19, 42.75, 41.08, 22.84 ppm. LC/MS⁺: Purity: 99.46%, t_R = 3.75, (ESI) *m/z* [M + H]⁺ 459.23.

1-(4-Chlorobenzyl)-3-((4-amino-6-(4-methylpiperazin-1-yl)-1,3,5-triazin-2-yl)methyl)-5,5-dimethylimidazolidine-2,4-dione (6). Ester **30** (4.30 mmol, 1.40 g) and 4-methylpiperazin-1-yl biguanidine × 2HCl (4.30 mmol, 1.11 g) were used (50 h refluxed). Method C. White solid, m.p. 204–205 °C, yield: 19% (0.38 g), C₂₁H₂₇N₈O₂Cl (MW 458.95). ¹H-NMR (300 MHz, DMSO-*d*₆) δ = 7.38 (s, 4H, Ph-2,3,5,6-H), 6.87 (br. s., 2H, NH₂), 4.51 (s, 2H, Ph-CH₂), 4.27 (s, 2H, TR-CH₂), 3.55 (br. s., 4H, Pp-2,6-H), 2.15 (s, 7H, Pp-3,5-H + Pp-CH₃), 1.26 (s, 6H, 2 × CH₃) ppm. LC/MS⁺: Purity: 100%, t_R = 3.94, (ESI) *m/z* [M + H]⁺ 459.23.

3-((4-Amino-6-(4-methylpiperazin-1-yl)-1,3,5-triazin-2-yl)methyl)-5-(4-chlorophenyl)-5-methylimidazolidine-2,4-dione (7). Ester **59** (5 mmol, 1.48 g) and 4-methylpiperazin-1-yl biguanidine × 2HCl (4.30 mmol, 1.11 g) were used (13.5 h refluxed). Method C. White solid, m.p. 218–220 °C, yield: 23% (0.42 g), C₁₉H₂₃N₈O₂Cl (MW 430.89). ¹H-NMR (300 MHz, DMSO-*d*₆) δ = 9.02 (s, 1H, Hyd-1-H), 7.51–7.69 (m, 2H, Ph-3,5-H), 7.36–7.51 (m, 2H, Ph-2,6-H), 6.83 (br. s., 2H, NH₂), 4.21 (s, 2H, TR-CH₂), 3.53 (br. s., 2H, Pp-2,6-He), 3.27–3.32 (m, 2H, Pp-2,6-Ha), 2.13 (s, 7H, Pp-3,5-H + Pp-CH₃), 1.68 (s, 3H, Hyd-CH₃) ppm. ¹³C-NMR (75 MHz, DMSO-*d*₆) δ = 175.25, 171.94, 166.94, 164.54, 155.78, 139.22, 133.15, 128.87, 127.93, 62.99, 54.57, 46.16, 42.63, 42.45, 25.92 ppm. LC/MS⁺: Purity: 100%, t_R = 3.23, (ESI) *m/z* [M + H]⁺ 431.19.

3-((4-Amino-6-(4-methylpiperazin-1-yl)-1,3,5-triazin-2-yl)methyl)-5,5-bis(4-chlorophenyl)imidazolidine-2,4-dione (8). Ester **71** (4.80 mmol, 1.90 g) and 4-methylpiperazin-1-yl biguanidine × 2HCl (4 mmol, 1.03 g) were used (30 h refluxed). Method C. White solid, m.p. 266–268 °C, yield: 40% (0.83 g), C₂₄H₂₄N₈O₂Cl₂ (MW 526.14). ¹H-NMR (300 MHz, DMSO-*d*₆) δ = 9.79 (s, 1H, Hyd-1-H), 7.34–7.59 (m, 8H, 2 × Ph-2,3,5,6-H), 6.85 (br. s, 2H, NH₂), 4.30 (s, 2H, TR-CH₂), 3.55 (br. s, 2H, Pp-2,6-He), 3.09 (br. s, 2H, Pp-2,6-Ha), 1.76–2.35 (m,

7H, Pp-3,5-H + Pp-CH₃) ppm. ¹³C-NMR (75 MHz, DMSO-*d*₆) δ = 173.01, 171.74, 166.92, 164.52, 155.38, 138.75, 133.57, 129.12, 129.01, 68.59, 54.58, 46.16, 42.77, 42.53 ppm. LC/MS⁺: Purity: 100%, t_R = 3.23, (ESI) *m/z* [M]⁺ 527.16.

3-((4-Amino-6-(4-methylpiperazin-1-yl)-1,3,5-triazin-2-yl)methyl)-1-benzyl-5,5-dimethylimidazolidine-2,4-dione (**9**). Ester **31** (3 mmol, 2.03 g) and 4-methylpiperazin-1-yl biguanidine × 2HCl (3 mmol, 0.77 g) were used (36 h refluxed). Method D. White solid, m.p. 206 °C, yield: 3.94%, C₂₁H₂₈N₈O₂ (MW 424.23). ¹H-NMR (300 MHz, DMSO-*d*₆) δ = 7.36–7.25 (m, 5H-Ph), 6.87 (s, 2H, NH₂), 4.52 (s, 2H, CH₂), 4.28 (s, 2H, TR-CH₂), 3.62 (s, 4H, Pp-2,6-H), 2.15–2.23 (m, 7H, Pp-3,5-H, Pp-CH₃), 1.25 (m, 6H, 2 × CH₃) ppm. LC/MS⁺: Purity: 98.30%, t_R = 3.50, (ESI) *m/z* [M]⁺ 425.20.

1-(3-Chlorobenzyl)-3-((4-amino-6-(4-methylpiperazin-1-yl)-1,3,5-triazin-2-yl)methyl)-5,5-dimethylimidazolidine-2,4-dione (**10**). Ester **32** (5 mmol, 2.52 g) and 4-methylpiperazin-1-yl biguanidine × 2HCl (5 mmol, 0.92 g) were used (6 h refluxed), and stirred for another 24 h in a room temperature. Method D. White solid, m.p. 168 °C, yield: 24.81%, C₂₁H₂₈N₈O₂ (MW 458.19). ¹H-NMR (300 MHz, DMSO-*d*₆) δ = 7.42 (s, 1H, Ph-6-H), 7.33 (m, 3H, Ph-2,4,5-H), 6.86 (s, 2H, NH₂), 4.52 (s, 2H-CH₂), 4.27 (s, 2H, TR-CH₂), 3.58 (s, 4H, Pp-2,6-H), 2.13 (m, 7H, Pp-3,5-H, Pp-CH₃), 1.27 (s, 6H, 2 × CH₃) ppm. LC/MS⁺: Purity: 96.12%, t_R = 5.34, (ESI) *m/z* [M]⁺ 459.23.

1-(2,5-Dichlorobenzyl)-3-((4-amino-6-(4-methylpiperazin-1-yl)-1,3,5-triazin-2-yl)methyl)-5,5-dimethylimidazolidine-2,4-dione (**11**). Ester **33** (5 mmol, 2.01 g) and 4-methylpiperazin-1-yl biguanidine × 2HCl (5 mmol, 0.92 g) were used (6 h refluxed), and stirred for another 144 h in room a temperature. Method D. White solid, m.p. 163 °C, yield: 27.32%, C₂₁H₂₆Cl₂N₈O (MW 492.16). ¹H-NMR (300 MHz, DMSO-*d*₆) δ = 7.53–7.50 (s, 1H, Ph-4-H), 7.41–7.38 (m, 2H, Ph-3,6-H), 6.84 (s, 2H, NH₂), 4.58 (s, 2H, CH₂), 4.29 (s, 2H, TR-CH₂), 3.63 (s, 4H, Pp-2,6-H), 2.23–2.15 (m, 7H, Pp-3,5-H, Pp-CH₃), 1.30 (s, 6H, 2 × CH₃) ppm. LC/MS⁺: Purity: 100%, t_R = 4.40, (ESI) *m/z* [M]⁺ 493.13.

1-(2,4-Dichlorobenzyl)-3-((4-amino-6-(4-methylpiperazin-1-yl)-1,3,5-triazin-2-yl)methyl)-5,5-dimethylimidazolidine-2,4-dione (**12**). Ester **34** (5 mmol, 2.03 g) and 4-methylpiperazin-1-yl biguanidine × 2HCl (5 mmol, 0.92 g) were used (3 h refluxed), and stirred for another 24 h in room a temperature. Method D. White solid, m.p. 123 °C, yield: 23.98%, C₂₁H₂₆Cl₂N₈O (MW 492.16). ¹H-NMR (300 MHz, DMSO-*d*₆) δ = 7.65–7.64 (s, 1H, Ph-6-H), 7.40–7.41 (m, 2H, Ph-3,5-H), 6.88 (s, 2H, NH₂), 4.58 (s, 2H, CH₂), 4.28 (s, 2H, TR-CH₂), 3.62 (s, 4H, Pp-2,6-H), 2.52–2.26 (m, 7H, Pp-3,5-H, Pp-CH₃), 1.29 (s, 6H, 2 × CH₃) ppm. LC/MS⁺: Purity: 100%, t_R = 4.56, (ESI) *m/z* [M]⁺ 493.13.

1-(4-Fluorobenzyl)-3-((4-amino-6-(4-methylpiperazin-1-yl)-1,3,5-triazin-2-yl)methyl)-5,5-dimethylimidazolidine-2,4-dione (**13**). Ester **35** (5 mmol, 2.32 g) and 4-methylpiperazin-1-yl biguanidine × 2HCl (5 mmol, 0.92 g) were used (10 h refluxed), and stirred for another 24 h in room a temperature. Method D. White solid, m.p. 180 °C, yield: 9.23%, C₂₁H₂₇FN₈O₂ (MW 442.22). ¹H-NMR (300 MHz, DMSO-*d*₆) δ = 7.38–7.43 (m, 2H, Ph-2,6-H), 7.11–7.17 (m, 2H, Ph-3,5-H), 6.86 (s, 2H, NH₂), 4.51 (s, 2H, CH₂), 4.27 (s, 2H, TR-CH₂), 3.57 (s, 4H, Pp-2,6-H), 2.14–2.23 (m, 7H, Pp-3,5-H, Pp-CH₃), 1.26 (m, 6H, 2 × CH₃) ppm. LC/MS⁺: Purity: 100%, t_R = 3.68, (ESI) *m/z* [M]⁺ 443.28.

1-(3-Fluorobenzyl)-3-((4-amino-6-(4-methylpiperazin-1-yl)-1,3,5-triazin-2-yl)methyl)-5,5-dimethylimidazolidine-2,4-dione (**14**). Ester **36** (5 mmol, 2.34 g) and 4-methylpiperazin-1-yl biguanidine × 2HCl (5 mmol, 0.92 g) were used (10 h refluxed), and stirred for another 24 h in room a temperature. Method D. White solid, m.p. 207 °C, yield: 9.32%, C₂₁H₂₇FN₈O₂ (MW 442.22). ¹H-NMR (300 MHz, DMSO-*d*₆) δ = 7.34 (m, 1H, Ph-6-H), 7.13 (m, 3H, Ph-2,4,5-H), 6.86 (s, 2H, NH₂), 4.53 (s, 2H, CH₂), 4.27 (s, 2H, TR-CH₂), 3.58 (s, 4H, Pp-2,6-H), 2.14 (m, 7H, Pp-3,5-H, Pp-CH₃), 1.27 (s, 6H, 2 × CH₃) ppm. LC/MS⁺: Purity: 100%, t_R = 3.59, (ESI) *m/z* [M]⁺ 443.22.

1-(3-Bromobenzyl)-3-((4-amino-6-(4-methylpiperazin-1-yl)-1,3,5-triazin-2-yl)methyl)-5,5-dimethylimidazolidine-2,4-dione (**15**). Ester **37** (5 mmol, 2.51 g) and 4-methylpiperazin-1-yl biguanidine × 2HCl (5 mmol, 0.92 g) were used (4 h refluxed), and stirred for another 24 h in room a temperature. Method D. White powder,

m.p. 125 °C, yield: 56%, C₂₁H₂₇BrN₈O₂ (MW 502.14). ¹H-NMR (300 MHz, DMSO-*d*₆) δ = 7.59 (s, 1H, Ph-4-H), 7.51–7.44 (m, 1H, Ph-2-H), 7.38 (d, *J* = 7.8 Hz, 1H, Ph-6-H), 7.30 (t, *J* = 7.7 Hz, 1H, Ph-5-H), 6.88 (s, 2H, NH₂), 4.54 (s, 2H, CH₂), 4.29 (s, 2H, TR-CH₂), 3.77–3.44 (m, 4H, Pp-2,6-H), 2.16 (m, 7H, Pp-3,5-H, Pp-CH₃), 1.29 (s, 6H, 2 × CH₃) ppm. LC/MS⁺: Purity: 97.66%, t_R = 4.07, (ESI) *m/z* [M]⁺ 505.16.

1-(3-Methoxybenzyl)-3-((4-amino-6-(4-methylpiperazin-1-yl)-1,3,5-triazin-2-yl)methyl)-5,5-dimethylimidazolidine-2,4-dione (**16**). Ester **38** (5 mmol, 2.42 g) and 4-methylpiperazin-1-yl biguanidine × 2HCl (5 mmol, 0.92 g) were used (10 h refluxed), and stirred for another 24 h in room a temperature. Method D. White solid, m.p. 111 °C, yield: 13.79%, C₂₂H₃₀N₈O₃ (MW 454.24). ¹H-NMR (300 MHz, DMSO-*d*₆) δ = 7.25–7.20 (m, 1H, Ph-3-H), 6.93 (m, 2H, Ph-2,4-H), 6.84–6.82 (m, 1H, Ph-6-H, 2H, NH₂), 4.49 (s, 2H, CH₂), 4.28 (s, 2H, TR-CH₂), 3.71 (s, 3H, CH₃), 3.59 (s, 4H, Pp-2,6-H), 2.15 (m, 7H, Pp-3,5-H, Pp-CH₃), 1.25 (m, 6H, 2 × CH₃) ppm. LC/MS⁺: Purity: 97.60%, t_R = 3.55, (ESI) *m/z* [M]⁺ 455.24.

1-(3-Methylbenzyl)-3-((4-amino-6-(4-methylpiperazin-1-yl)-1,3,5-triazin-2-yl)methyl)-5,5-dimethylimidazolidine-2,4-dione (**17**). Ester **39** (5 mmol, 2.61 g) and 4-methylpiperazin-1-yl biguanidine × 2HCl (5 mmol, 0.92 g) were used (5 h refluxed) and stirred for another 24 h in room a temperature. Method D. White solid, m.p. 154 °C, yield: 13.79%, C₂₂H₃₀N₈O (MW 438.25). ¹H-NMR (300 MHz, DMSO-*d*₆) δ = 7.22–7.07 (m, 4H, Ph), 6.86 (s, 2H, NH₂), 4.48 (s, 2H, CH₂), 4.27 (s, 2H, TR-CH₂), 3.59 (s, 4H, Pp-2,6-H), 2.27–2.15 (m, 10H, Pp-3,5-H, Pp-CH₃, Ph-CH₃), 1.25 (s, 6H, 2 × CH₃) ppm. LC/MS⁺: Purity: 98.88%, t_R = 3.94, (ESI) *m/z* [M]⁺ 439.23.

3-((4-Amino-6-(4-methylpiperazin-1-yl)-1,3,5-triazin-2-yl)methyl)-5,5-dimethyl-1-(naphthalen-1-ylmethyl)imidazolidine-2,4-dione (**18**). Ester **40** (5 mmol, 1.96 g) and 4-methylpiperazin-1-yl biguanidine × 2HCl (5 mmol, 0.92 g) were used (5 h refluxed) and stirred for another 24 h in room a temperature. Method D. White powder, m.p. 116 °C, yield: 13.79%, C₂₅H₃₀N₈O₂ (MW 474.25). ¹H-NMR (300 MHz, DMSO-*d*₆) δ = 7.88–7.84 (m, 4H, naft-1,4,5,8-H), 7.50–7.48 (m, 3H, naft-3,6,7-H), 6.86 (s, 2H, NH₂), 4.70 (s, 2H, CH₂), 4.30 (s, 2H, TR-CH₂), 3.55 (s, 4H, Pp-2,6-H), 2.22–2.02 (m, 7H, Pp-3,5-H, Pp-CH₃), 1.29 (s, 6H, 2 × CH₃) ppm. LC/MS⁺: Purity: 100%, t_R = 4.31, (ESI) *m/z* [M]⁺ 475.25.

3-((4-Amino-6-(4-methylpiperazin-1-yl)-1,3,5-triazin-2-yl)methyl)-5-methyl-5-phenylimidazolidine-2,4-dione (**19**). Ester **60** (5 mmol, 1.31 g) and 4-methylpiperazin-1-yl biguanidine × 2HCl (5 mmol, 0.92 g) were used (4.5 h refluxed) and stirred for another 24 h in room a temperature. Method C. White solid, m.p. 270 °C, yield: 50%, C₁₉H₂₄N₈O₂ (MW 396.45). ¹H-NMR (300 MHz, DMSO-*d*₆) δ = 9.00 (s, 1H, N1-H), 7.54–7.56 (d, *J* = 7.5 Hz, 2H, Ph-2,6-H), 7.39–7.43 (t, *J* = 7.25 Hz, Ph-3,5-H), 7.33–7.36 (d, *J* = 7.5 Hz, 1H, Ph-4-H), 6.85 (s, 2H, NH₂), 4.24 (s, 2H, N3-CH₂), 3.61 (s, 2H, Pp-2,6-Hb), 3.40–3.50 (m, 2H, Pp-2,6-Ha), 2.16–2.24 (s, 4H, Pp-3,5-H), 2.16 (s, 3H, N-CH₃), 1.73 (s, 3H, 5-CH₃) ppm. ¹³C-NMR (75 MHz, DMSO-*d*₆) δ = 175.62, 172.08, 166.96, 164.61, 155.92, 140.14, 128.88, 128.31, 125.98, 63.40, 54.64, 46.20, 42.72, 42.47, 25.82 ppm. LC/MS⁺: Purity: 96.38%, t_R = 2.62, (ESI) *m/z* [M]⁺ 397.22.

3-((4-Amino-6-(4-methylpiperazin-1-yl)-1,3,5-triazin-2-yl)methyl)-5-(3-chlorophenyl)-5-methylimidazolidine-2,4-dione (**20**). Ester **61** (5 mmol, 1.49 g) and 4-methylpiperazin-1-yl biguanidine × 2HCl (5 mmol, 0.92 g) were used (5 h refluxed). Method C. White solid, m.p. 234 °C, yield: 56.80%, C₁₉H₂₃ClN₈O₂ (MW 430.89). ¹H-NMR (300 MHz, DMSO-*d*₆) δ = 9.00 (s, 1H, N-H), 7.54–7.58 (m, 2H, Ph-2,6-H), 7.45–7.49 (m, 2H, Ph-4,5-H), 6.85 (s, 2H, NH₂), 4.25 (s, 2H, N3-CH₂), 3.60 (s, 2H, Pp-2,6-Hb), 3.30 (s, 2H, Pp-2,6-Ha), 2.26 (s, 2H, Pp-3,5-Hb), 2.16 (s, 3H, N-CH₃), 2.09 (s, 2H, Pp-3,5-Ha), 1.72 (s, 3H, 5-CH₃) ppm. ¹³C-NMR (75 MHz, DMSO-*d*₆) δ = 175.08, 171.94, 166.96, 164.55, 155.74, 142.65, 133.63, 130.92, 128.38, 125.80, 124.85, 63.11, 54.60, 46.19, 42.67, 42.50, 26.21 ppm. LC/MS⁺: Purity: 100%, t_R = 3.23, (ESI) *m/z* [M]⁺ 431.12.

3-((4-Amino-6-(4-methylpiperazin-1-yl)-1,3,5-triazin-2-yl)methyl)-5-(2,5-dichlorophenyl)-5-methylimidazolidine-2,4-dione (**21**). Ester **62** (5 mmol, 1.65 g) and 4-methylpiperazin-1-yl biguanidine × 2HCl (5 mmol, 0.92 g) were used (3.5 h refluxed). Method C. White solid, m.p. 166 °C, yield: 79.10%, C₁₉H₂₂Cl₂N₈O₂ (MW 465.34). ¹H-NMR (300 MHz, DMSO-*d*₆) δ = 8.66 (s, 1H, N1-H), 7.72 (s, 1H, Ph-4-H), 7.54 (s, 2H, Ph-3,6-H), 6.89 (s, 2H, NH₂), 4.30 (s, 2H, N3-CH₂), 3.67 (m, 4H, Pp-2,6-H), 2.29 (s, 4H, Pp-3,5-H), 2.19 (s, 3H, N-CH₃), 1.87 (s, 3H, 5-CH₃) ppm. ¹³C-NMR (75 MHz, DMSO-*d*₆) δ = 174.90, 172.31, 167.02, 164.70, 156.23, 137.56,

133.13, 132.49, 132.26, 130.68, 130.05, 62.65, 54.71, 46.21, 42.90, 42.49, 25.18 ppm. LC/MS⁺: Purity: 99.11%, t_R = 3.53, (ESI) *m/z* [M]⁺ 465.15.

3-((4-Amino-6-(4-methylpiperazin-1-yl)-1,3,5-triazin-2-yl)methyl)-5-(2,4-dichlorophenyl)-5-methylimidazolidine-2,4-dione (**22**). Ester **63** (5 mmol, 1.66 g) and 4-methylpiperazin-1-yl biguanidine × 2HCl (5 mmol, 0.92 g) were used (4.5 h refluxed). Method C. White solid, m.p. 228 °C, yield: 76.56%, C₁₉H₂₂C₁₂N₈O₂ (MW 465.34). ¹H-NMR (300 MHz, DMSO-*d*₆) δ = 8.65 (s, 1H, N1-H), 7.71–7.73 (d, 1H, Ph-3-H), 7.67–7.68 (s, 1H, Ph-5-H), 7.50–7.53 (d, 1H, Ph-6-H), 6.89 (s, 2H, NH₂), 4.30 (s, 2H, N3-CH₂), 3.67 (s, 4H, Pp-2,6-H), 2.29 (s, 4H, Pp-3,5-H), 2.19 (s, 3H, N-CH₃), 1.86 (s, 3H, 5-CH₃) ppm. ¹³C-NMR (75 MHz, DMSO-*d*₆) δ = 175.12, 172.34, 167.02, 164.70, 156.25, 134.70, 134.66, 134.57, 131.70, 130.83, 127.80, 62.49, 54.71, 46.21, 42.88, 42.47, 25.29 ppm. LC/MS⁺: Purity: 100%, t_R = 3.66, (ESI) *m/z* [M]⁺ 465.08.

3-((4-Amino-6-(4-methylpiperazin-1-yl)-1,3,5-triazin-2-yl)methyl)-5-(2,3,4-trichlorophenyl)-5-methylimidazolidine-2,4-dione (**23**). Ester **64** (5 mmol, 1.83 g) and 4-methylpiperazin-1-yl biguanidine × 2HCl (5 mmol, 0.92 g) were used (4 h refluxed). Method C. White crystal, m.p. 256 °C, yield: 83.68%, C₁₉H₂₁C₁₃N₈O₂ (MW 499.78). ¹H-NMR (300 MHz, DMSO-*d*₆) δ = 7.74 (s, 2H, Ph-5,6-H), 6.89 (s, 2H, NH₂), 4.32 (s, 2H, N3-CH₂), 3.67 (s, 4H, Pp-2,6-H), 2.29 (s, 4H, Pp-3,5-H), 2.19 (s, 3H, N-CH₃), 1.88 (s, 3H, 5-CH₃) ppm. ¹³C-NMR (75 MHz, DMSO-*d*₆) δ = 175.94, 172.32, 167.01, 164.70, 156.33, 136.85, 133.94, 133.58, 132.24, 129.48, 129.09, 63.11, 54.71, 46.21, 42.90, 42.59, 25.56 ppm. LC/MS⁺: Purity: 98.93%, t_R = 4.07, (ESI) *m/z* [M]⁺ 499.05.

3-((4-Amino-6-(4-methylpiperazin-1-yl)-1,3,5-triazin-2-yl)methyl)-5-(4-methylphenyl)-5-methylimidazolidine-2,4-dione (**24**). Ester **65** (5 mmol, 1.38 g) and 4-methylpiperazin-1-yl biguanidine × 2HCl (5 mmol, 0.92 g) were used (4.5 h refluxed). Method C. White solid, m.p. 240 °C, yield: 49.27%, C₂₀H₂₆N₈O₂ (MW 410.47). ¹H-NMR (300 MHz, DMSO-*d*₆) δ = 7.41–7.43 (d, *J* = 8.3 Hz, 2H, Ph-2,6), 7.20–7.22 (d, *J* = 7.9 Hz, 2H, Ph-3,5-H), 6.84 (s, 2H, NH₂), 4.23 (s, 2H, N3-CH₂), 3.59 (s, 4H, Pp-2,6-H), 2.30 (s, 3H, Ph-CH₃), 2.16 (s, 4H, Pp-3,5-H), 2.10 (s, 3H, N-CH₃), 1.69 (s, 3H, 5-CH₃) ppm. ¹³C-NMR (75 MHz, DMSO-*d*₆) δ = 175.74, 172.10, 166.96, 164.61, 155.91, 137.49, 137.29, 129.39, 125.87, 63.21, 54.65, 46.20, 42.70, 42.44, 25.83, 21.03 ppm. LC/MS⁺: Purity: 98.31%, t_R = 3.10, (ESI) *m/z* [M]⁺ 411.18.

3-((4-Amino-6-(4-methylpiperazin-1-yl)-1,3,5-triazin-2-yl)methyl)-5-methyl-5-(naphthalen-1-yl)imidazolidine-2,4-dione (**25**). Ester **66** (5 mmol, 1.56 g) and 4-methylpiperazin-1-yl biguanidine × 2HCl (5 mmol, 0.92 g) were used (5 h refluxed). Method E. White solid, m.p. 208 °C, yield: 32.87%, C₂₃H₂₆N₈O₂ (MW 446.50). ¹H-NMR (300 MHz, DMSO-*d*₆) δ = 8.95 (s, 1H, N1-H), 8.05–8.07 (m, 1H, Naft-8-H), 7.96–8.00 (t, 2H, Naft-4,5-H), 7.76–7.78 (d, *J* = 7.5 Hz; 1H, Naft-2-H), 7.51–7.55 (t, *J* = 7.7 Hz, 3H, Naft-3,6,7-H), 6.90 (s, 2H, NH₂), 4.40 (s, 2H, N3-CH₂), 3.63 (s, 4H, Pp-2,6-H), 2.17 (s, 4H, Pp-3,5-H), 2.07 (s, 3H, N-CH₃), 2.02 (s, 3H, 5-CH₃) ppm. ¹³C-NMR (75 MHz, DMSO-*d*₆) δ = 176.31, 172.32, 167.07, 164.73, 156.03, 134.61, 134.21, 130.87, 130.22, 129.62, 126.92, 126.43, 126.10, 125.43, 125.11, 64.18, 54.66, 46.20, 42.88, 42.71, 26.74 ppm. LC/MS⁺: Purity: 99.06%, t_R = 3.55, (ESI) *m/z* [M]⁺ 447.20.

3-((4-Amino-6-(4-methylpiperazin-1-yl)-1,3,5-triazin-2-yl)methyl)-5-methyl-5-(naphthalen-2-yl)imidazolidine-2,4-dione (**26**). Ester **67** (5 mmol, 1.56 g) and 4-methylpiperazin-1-yl biguanidine × 2HCl (5 mmol, 0.92 g) were used (3 h refluxed). Method E. White solid, m.p. 144 °C, yield: 34.57%, C₂₃H₂₆N₈O₂ (MW 446.50). ¹H-NMR (300 MHz, DMSO-*d*₆) δ = 9.12 (s, 1H, N1-H), 8.07 (s, 1H, Naft-1-H), 7.93–7.99 (m, 3H, Naft-4,5,8-H), 7.72–7.74 (d def., 1H, Naft-3-H), 7.54–7.57 (m, 2H, Naft-6,7-H), 6.85 (s, 2H, NH₂), 4.27 (s, 2H, N3-CH₂), 3.40–3.60 (m, 2H, Pp-2,6-Hb), 3.05–3.20 (m, 2H, Pp-2,6-Ha), 2.09 (s, 4H, Pp-3,5-H), 2.00 (s, 3H, N-CH₃), 1.83 (s, 3H, 5-CH₃) ppm. ¹³C-NMR (75 MHz, DMSO-*d*₆) δ = 175.56, 172.01, 166.95, 164.53, 155.92, 137.75, 132.96, 132.81, 128.62, 128.57, 127.89, 126.95, 126.90, 124.51, 124.33, 63.56, 53.90, 46.00, 42.56, 42.47, 25.94 ppm. LC/MS⁺: Purity: 99.11%, t_R = 3.49, (ESI) *m/z* [M]⁺ 447.20.

4.2. Molecular Modeling

4.2.1. Optimization of the 5-HT₆R Binding Site Using Induced-Fit Docking Procedure

The 5-HT₆R homology model (build on β_2 adrenergic template) was optimized using the induced-fit docking (IFD) [33] protocol from Schrödinger. The IFD combines flexible ligand docking, using the Glide algorithm [34], with receptor structure prediction and side chain refinement in Prime. The structures of Lead 1 and Lead 2 were used as inputs to IFD. In each case, the centroid of the grid box was anchored on D3.32 and allowed on residues refinement within 12 Å of ligand poses. The ten top-scored L–R complexes were inspected visually to select those showing the closest compliance with the common binding mode for monoaminergic receptor ligands [35]. The final validation of the receptor conformations selected was performed by docking (Glide SP mode) the synthesized library, retaining only those with a coherent binding mode for the whole set.

4.2.2. Molecular Docking

The 5-HT₆R models selected in IFD procedure were used to study the binding mode of the library synthesized. 3-dimensional structures of the ligands were prepared using LigPrep v3.6 (Schrödinger, New York, NY, USA) [36], and the appropriate ionization states at pH = 7.4 ± 1.0 were assigned using Epik v3.4 (Schrödinger, New York, NY, USA) [37]. Compounds with unknown absolute configuration were docked in all configurations. The Protein Preparation Wizard was used to assign the bond orders, appropriate amino acid ionization states and to check for steric clashes. The receptor grid was generated (OPLS3 force field [38]) by centering the grid box with a size of 12 Å on the D3.32 side chain. Automated flexible docking was performed using Glide at SP level [39].

4.2.3. Plotting Interaction Spheres for Halogen Bonding

The halogen bonding web server was used (accessed on 22 February 2018, <http://www.halogenbonding.com/>) to visualize (plotting interaction spheres) the potential contribution of halogen bonding to ligand–receptor complexes.

4.3. Lipophilicity Study

4.3.1. Thin-Layer Chromatography

The mobile phases were prepared by mixing the respective amounts of water and organic modifier (methanol) in a range from 40 to 90% (v/v) in 5% increments. TLC was performed on Silica gel 60RP-18 F₂₅₄ plates (7 × 10 cm) plates (Merck, Darmstadt, Germany). Methanol was used to prepare the solutions of the substances. Solutions (10 µL) of the analyzed compounds were applied to the plates as 5 mm bands, 10 mm apart and 10 mm from the lower edge and sides of the plates, by using Linomat V applicator (Camag, Basel, Switzerland). The vertical chamber (Sigma–Aldrich, St. Louis, MI, USA), 20 × 10 × 18 cm in size, was saturated with mobile phase for 20 min. Development was carried out over 9 cm from the starting line at a temperature of 20 °C. Next, the plates were dried at room temperature, and the spots were observed under ultraviolet light at 254 nm and/or 366 nm (UV lamp, Camag, Basel, Switzerland). In each case, sharp and symmetric spots without a tendency for tailing were obtained. Each experiment was run in triplicate and mean R_F (retardation factor) values were calculated.

Starting from the R_F values, the R_M parameters were computed as described in the formula:

$$R_M = \log(1/R_F - 1)$$

The linear correlations between the R_M values of the substances and the concentration of methanol in mobile phases were calculated for each compound with the Soczewiński-Wachtmeister equation [22]:

$$R_M = R_{M0} + aC$$

where C is the concentration of the organic modifier (in %) in the mobile phase, a is the slope, and R_{M0} is the concentration of organic modifier extrapolated to zero.

4.3.2. Statistical Methods

Statistical analysis was performed using Statistica v10 software (StatSoft, Tulsa, OK, USA). The correlation coefficients (r , r^2), and the standard errors of the slope, interception, and estimate (S_a , S_b , S_e) were used as the basis for testing the linearity of regression plots.

4.4. Studies In Vitro

4.4.1. Radioligand Binding Assay

Radioligand binding assays were used to determine the affinity of the synthesized compounds for human serotonin 5-HT₆R, which were stably expressed in HEK-293 cells. This procedure was accomplished via the displacement of [3H]-LSD (85.2 Ci mmol⁻¹) for 5-HT₆R. Each compound was tested in triplicate at 7 to 8 different concentrations (10⁻¹¹ to 10⁻⁴ M). The inhibition constants (K_i) were calculated using the Cheng–Prusoff equation [40], and the results are expressed as the mean of at least two independent experiments.

4.4.2. Toxicity In Vitro Test

The ATCC CRL 1573 HEK-293 cells were seeded in 96-well plates (Nunc™) at a concentration of 1×10^4 cells/well in 200 μ L in Dulbecco's Modified Eagle's Medium (Gibco®) supplemented with 10% fetal bovine serum (Gibco®), and cultured at 37 °C in an atmosphere containing 5% of CO₂ for 24 h to reach 60% confluence. The 10 mM stock solutions of 5-HT₆R ligands 6 and 26 in DMSO were diluted into fresh growth medium and added into the microplates at the final concentrations 0.1 μ M–100 μ M. Total DMSO concentration did not exceed 1% in growth media. The cytostatic drug doxorubicin (Sigma-Aldrich) at the concentration 1 μ M was used as a reference. After 72 h of incubation 20 μ L of CellTiter 96® Aqueous Non-Radioactive Cell Proliferation Assay (MTS) (Promega®) was added to each well and the cells were incubated under the same conditions for 2 h. The absorbance of the samples was measured using a microplate reader EnSpire (PerkinElmer, Waltham, MA, USA) at 490 nm. Statistical significance was analyzed by GraphPad Prism™ software v. 5.01 (GraphPad Software, La Jolla, CA, USA) using One-way ANOVA and Bonferroni's Multiple Comparison Post Test.

4.5. Studies In Vivo

4.5.1. Animals

The experiments were performed on male Wistar rats (200–220 g—behavioural test or 170–190 g—metabolic assay) obtained from an accredited animal facility at the Jagiellonian University Medical College, Poland. The animals were housed in a group of four in a controlled environment (ambient temperature 21 ± 2 °C; relative humidity 50–60%; 12 h light/dark cycles (lights on at 8:00). Standard laboratory food (LSM-B) and filtered water were freely available (behavioral tests). Animals were assigned randomly to treatment groups. All the experiments were performed by two observers unaware of the treatment applied between 9:00 and 14:00 on separate groups of animals. All animals were used only once.

The experimental protocols and procedures described in this manuscript were approved by the I Local Ethics Commission in Cracow (no 293/2015) and complied with the European Communities Council Directive of 24 November 1986 (86/609/EEC) and were in accordance with the 1996 NIH Guide for the Care and Use of Laboratory Animals.

4.5.2. Drugs

Compounds were suspended in 1% Tween 80 immediately before administration in a volume of 2 mL/kg—behavioral tests or 1 mL/kg—body weight measures. Compounds were administered intraperitoneally (i.p.) 60 min before testing—behavioral tests. Control animals received vehicle (1% Tween 80) according to the same schedule.

4.5.3. Behavioral Procedures in Rats

Forced Swim Test (FST Test)

The experiment was carried out according to the method of Porsolt et al. [41]. On the first day of an experiment, the animals were gently individually placed in Plexiglas cylinders (40 cm high, 18 cm in diameter) containing 15 cm of water maintained at 23–25 °C for 15 min. On removal from water, the rats were placed for 30 min in a Plexiglas box under 60-W bulb to dry. On the following day (24 h later), the rats were replaced in the cylinder and the total duration of immobility was recorded during the whole 5-min test period. The immobility was assigned when no additional activity was observed other than that necessary to keep the rat's head above the water. Fresh water was used for each animal.

Vogel Conflict Drinking Test

The testing procedure was based on a method of Vogel et al. [42] and used the Anxiety Monitoring System “Vogel test” produced by TSE Systems (Germany). It was consisted of polycarbonate cages (dimensions 26.5 × 15 × 42 cm), equipped with a grid floor made from stainless steel bars and drinking bottles containing tap water. Experimental chambers were connected to PC software by control chassis and on electric shocks' generator. On the first day of the experiment, the rats were adapted to the test chambers and drink water from the bottle spout for 10 min. Afterward, the rats were returned to their home cages and were given 30 min free access to water followed by a 24 h water deprivation period. The adaptation session and water deprivation protocols were repeated on the second day of the experiment. On the third day, the rats were placed again in the test chambers 60 min after compound **26** and diazepam administration and were given free access to the drinking tube. Recording data started immediately after the first lick and rats were punished with an electric shock (0.5 mA, lasting 1 s) delivered to the metal drinking tube every 20 licks. The number of licks and the number of shocks received during a 5 min experimental session were recorded automatically.

4.5.4. Metabolic Assays In Vivo

The Effect of compound **6** or **26** on Body Weight by Non-Obese Rats Fed Palatable Diet (Model of Excessive Eating)

In order to determine the anorectic activity of **6** or **26**, the model of excessive eating was used [43,44]. Male Wistar rats (170–190 g) were housed in a pair in plastic cages in constant temperature facilities exposed to a light-dark cycle. Water and food were available ad libitum. Two groups of 6 rats were fed with diets consisting of milk chocolate with nuts, cheese, salted peanuts, and 7% condensed milk and also had access to standard feed (Labofeed B, Morawski Manufacturer Feed, Kcynia, Poland) and water ad libitum for 3 weeks. Palatable control group (palatable diet + vehicle) received vehicle (1% Tween 80, intraperitoneally), while palatable test group (palatable diet + **6** or palatable + **26**) was injected (intraperitoneally) with **6** or **26** at the dose of 5 mg/kg b.w. dissolved in 1% Tween 80 (1 mL/kg). Body weights were measured daily, immediately prior to administration of drugs.

The palatable diet contained: 100 g peanuts—614 kcal; 100 mL condensed milk—131 kcal; 100 g milk chocolate—529 kcal; 100g cheese (Greek type)—270 kcal. The standard diet contained 100 g feed—280 kcal.

The Effect of compound **6** or **26** on Body Weight by Non-Obese Rats Fed Only with Standard Diet

Male Wistar rats (170–190 g) were housed in a pair in plastic cages in constant temperature facilities exposed to a light-dark cycle. Control group (standard diet + vehicle) received vehicle (1% Tween 80, intraperitoneally), while the test group (standard diet + **6** or standard diet + **26**) was injected (intraperitoneally) with **6** or **26** at the dose of 5 mg/kg b.w. dissolved in 1% Tween 80 (1 mL/kg). Body weights were measured daily immediately prior to administration of drugs.

4.6. Statistical Analysis

4.6.1. Lipophilicity

Statistical analysis was performed using Statistica v10 software (StatSoft, Tulsa, OK, USA). The correlation coefficients (r , r^2), and the standard errors of the slope, interception, and estimate (S_a , S_b , S_e) served as the basis for testing the linearity of regression plots.

4.6.2. Studies In Vitro and In Vivo

Statistical calculations were performed using GraphPad Prism 6 software (GraphPad Software, La Jolla, CA, USA). Results are provided as arithmetic means with a standard error of the mean. The data of behavioral studies were evaluated by an analysis of variance one-way ANOVA followed by Bonferroni's post hoc test (statistical significance set at $p < 0.05$). Statistical significance of body weight was calculated using one-way ANOVA with Sidak's multiple comparison test post-hoc or two-way ANOVA with Sidak's multiple comparison test post-hoc. Differences were considered statistically significant at: $p \leq 0.05$, $p \leq 0.01$, $p \leq 0.001$.

5. Conclusions

These comprehensive studies, including: Computer-aided design, synthesis, pharmacological screening in vitro and in vivo, "drugability" experiments and an extensive docking-based SAR analysis, have provided an insight into chemical properties, ligand–receptor interactions and potential therapeutic perspectives for the new group of 1,3,5-triazine molecules. Lead structures with two topological variants of the hydantoin linker have been identified, followed by the synthesis of numerous lead modifications. As result, a new series of 18 active 5-HT₆ agents, with submicromolar affinities confirmed in the radioligand binding assays, has been obtained (groups A and B). Computer-aided SAR analysis indicates the significance of both, linker and aromatic moiety properties, and their mutual dependences, for the 5-HT₆R affinity of the 1,3,5-triazine derived compounds. Thus, the combination of 1-unsubstituted hydantoin (group B) with the β -naphthyl moiety at position 5 (**26**) was found as the most profitable, followed by either the corresponding α -naphthyl analogue (**25**) and the tri-substituted combination of 1-(4-chlorobenzyl)-3-((4-amino-6-(4-methylpiperazin-1-yl)-1,3,5-triazin-2-yl)methyl)-5,5-dimethylimidazolidine-2,4-dione (**6**, group A). The most active agent (**26**) displayed also antidepressant-like and anxiolytic-like activities in vivo, whereas the best members of both groups (**6** and **26**) demonstrated anti-obesity properties in animals fed palatable feed, as well as lipophilicity favorable for CNS drugs with a low risk of toxicity in vitro.

The interesting pharmacological properties together with a promising "drugability" designate this group of chemical molecules as a good starting point for further consideration in order to explore molecular mechanisms of the 5-HT₆R–ligand interaction, and even to search of new drug candidates for the treatment of depression and obesity. In this context, 3-((4-Amino-6-(4-methylpiperazin-1-yl)-1,3,5-triazin-2-yl)methyl)-5-methyl-5-(naphthalen-2-yl)imidazolidine-2,4-dione (**26**) can be selected as a new lead structure.

Supplementary Materials: The supplementary materials are available online.

Author Contributions: R.K. and J.H. conceived and designed the article; W.A., D.L., M.W. and J.H. performed syntheses; J.H. and K.K.-K. supervised synthesis works; W.A. elaborated synthesis description (paragraph 4.1); R.K. performed molecular modeling studies, G.S. performed radioligand binding assays; M.K. performed metabolic tests in vivo; M.J.W., A.P., and A.W. performed behavioral tests in vivo, A.L. and, G.L. performed toxicity in vitro test; M.S. and M.D. performed lipophilicity experiments, R.K., J.H., W.A., and C.J. wrote the paper.

Funding: This study was financially supported by Polish National Science Centre (NCN) grants: No UMO-2015/17/B/NZ7/02973, UMO-2016/21/N/NZ7/03265 (Toxicity in vitro) and UMO-2014/15/D/NZ7/01782. Authors thank also to the University of Saarland and the Erasmus Plus scheme for financial support of Wesam Ali.

Acknowledgments: Authors thank Andrzej J. Bojarski for the opportunity to conduct RBA and MM studies in his Department. Thanks to our excellent technician, Maria Kaleta and to students: Kinga Pólichłopek, Angelika Nowakowska and Raluca Mihaela Şişu, for their contribution in the synthesis work.

Conflicts of Interest: The authors declare no conflict of interest.

References

1. Barnes, N.M.; Sharp, T. A review of central 5-HT receptors and their function. *Neuropharmacology* **1999**, *38*, 1083–1152. [[CrossRef](#)]
2. Ruat, M.; Traiffort, E.; Arrang, J.M.; Tardivellacombe, J.; Diaz, J.; Leurs, R.; Schwartz, J.C. A Novel Rat Serotonin (5-HT₆) Receptor: Molecular Cloning, Localization and Stimulation of cAMP Accumulation. *Biochem. Biophys. Res. Commun.* **1993**, *193*, 268–276. [[CrossRef](#)] [[PubMed](#)]
3. Kohen, R.; Metcalf, M.A.; Khan, N.; Druck, T.; Huebner, K.; Lachowicz, J.E.; Meltzer, H.Y.; Sibley, D.R.; Roth, B.L.; Hamblin, M.W. Cloning, Characterization, and Chromosomal Localization of a Human 5-HT₆ Serotonin Receptor. *J. Neurochem.* **2002**, *66*, 47–56. [[CrossRef](#)]
4. Liu, K.G.; Robichaud, A.J. 5-HT₆ Medicinal Chemistry. *Int. Rev. Neurobiol.* **2010**, *94*, 1–34. [[PubMed](#)]
5. Benhamú, B.; Martín-Fontecha, M.; Vázquez-Villa, H.; Pardo, L.; López-Rodríguez, M.L. Serotonin 5-HT₆ Receptor Antagonists for the Treatment of Cognitive Deficiency in Alzheimer's Disease. *J. Med. Chem.* **2014**, *57*, 7160–7181. [[CrossRef](#)] [[PubMed](#)]
6. Wesolowska, A. Potential role of the 5-HT₆ receptor in depression and anxiety: An overview of preclinical data. *Pharmacol. Rep.* **2010**, *62*, 564–577. [[CrossRef](#)]
7. Heal, D.; Gosden, J.; Smith, S. The 5-HT₆ Receptor as a Target for Developing Novel Antiobesity Drugs. *Int. Rev. Neurobiol.* **2011**, *96*, 73–109. [[PubMed](#)]
8. Frassetto, A.; Zhang, J.; Lao, J.Z.; White, A.; Metzger, J.M.; Fong, T.M.; Chen, R.Z. Reduced sensitivity to diet-induced obesity in mice carrying a mutant 5-HT₆ receptor. *Brain Res.* **2008**, *1236*, 140–144. [[CrossRef](#)] [[PubMed](#)]
9. Dudek, M.; Marcinkowska, M.; Bucki, A.; Olczyk, A.; Kołaczkowski, M. Idalopirdine—A small molecule antagonist of 5-HT₆ with therapeutic potential against obesity. *Metab. Brain Dis.* **2015**, *30*, 1487–1494. [[CrossRef](#)] [[PubMed](#)]
10. Krogsgaard-Larsen, N.; Jensen, A.A.; Schröder, T.J.; Christoffersen, C.T.; Kehler, J. Novel Aza-analogous Ergoline Derived Scaffolds as Potent Serotonin 5-HT₆ and Dopamine D₂ Receptor Ligands. *J. Med. Chem.* **2014**, *57*, 5823–5828. [[CrossRef](#)] [[PubMed](#)]
11. De la Fuente, T.; Martín-Fontecha, M.; Sallander, J.; Benhamú, B.; Campillo, M.; Medina, R.A.; Pellissier, L.P.; Claeysen, S.; Dumuis, A.; Pardo, L.; et al. Benzimidazole Derivatives as New Serotonin 5-HT₆ Receptor Antagonists. Molecular Mechanisms of Receptor Inactivation. *J. Med. Chem.* **2010**, *53*, 1357–1369. [[CrossRef](#)] [[PubMed](#)]
12. Bojarski, A. Pharmacophore Models for Metabotropic 5-HT Receptor Ligands. *Curr. Top. Med. Chem.* **2006**, *6*, 2005–2026. [[CrossRef](#)] [[PubMed](#)]
13. Łażewska, D.; Kurczab, R.; Więcek, M.; Kamińska, K.; Satała, G.; Jastrzębska-Więsek, M.; Partyka, A.; Bojarski, A.J.; Wesolowska, A.; Kieć-Kononowicz, K.; et al. The computer-aided discovery of novel family of the 5-HT₆ serotonin receptor ligands among derivatives of 4-benzyl-1,3,5-triazine. *Eur. J. Med. Chem.* **2017**, *135*, 117–124. [[CrossRef](#)] [[PubMed](#)]

14. Latacz, G.; Kechagioglou, P.; Papi, R.; Łażewska, D.; Więcek, M.; Kamińska, K.; Wencel, P.; Karcz, T.; Schwed, J.S.; Stark, H.; et al. The Synthesis of 1,3,5-triazine Derivatives and JNJ7777120 Analogues with Histamine H₄ Receptor Affinity and Their Interaction with PTEN Promoter. *Chem. Biol. Drug Des.* **2016**, *88*, 254–263. [[CrossRef](#)] [[PubMed](#)]
15. Handzlik, J.; Bojarski, A.J.; Satała, G.; Kubacka, M.; Sadek, B.; Ashoor, A.; Siwek, A.; Więcek, M.; Kucwaj, K.; Filipek, B.; et al. SAR-studies on the importance of aromatic ring topologies in search for selective 5-HT₇ receptor ligands among phenylpiperazine hydantoin derivatives. *Eur. J. Med. Chem.* **2014**, *78*, 324–339. [[CrossRef](#)] [[PubMed](#)]
16. Łażewska, D.; Więcek, M.; Ner, J.; Kamińska, K.; Kottke, T.; Schwed, J.S.; Zygmunt, M.; Karcz, T.; Olejarz, A.; Kuder, K.; et al. Aryl-1,3,5-triazine derivatives as histamine H₄ receptor ligands. *Eur. J. Med. Chem.* **2014**, *83*, 534–546. [[CrossRef](#)] [[PubMed](#)]
17. Grychowska, K.; Kurczab, R.; Śliwa, P.; Satała, G.; Dubiel, K.; Matłoka, M.; Moszczyński-Pętkowski, R.; Pieczykolan, J.; Bojarski, A.J.; Zajdel, P. Pyrroloquinoline scaffold-based 5-HT₆R ligands: Synthesis, quantum chemical and molecular dynamic studies, and influence of nitrogen atom position in the scaffold on affinity. *Bioorg. Med. Chem.* **2018**, *26*, 3588–3595. [[CrossRef](#)] [[PubMed](#)]
18. González-Vera, J.A.; Medina, R.A.; Martín-Fontecha, M.; Gonzalez, A.; de la Fuente, T.; Vázquez-Villa, H.; García-Cárceles, J.; Botta, J.; McCormick, P.J.; Benhamú, B.; et al. A new serotonin 5-HT₆ receptor antagonist with procognitive activity—Importance of a halogen bond interaction to stabilize the binding. *Sci. Rep.* **2017**, *7*, 41293. [[CrossRef](#)] [[PubMed](#)]
19. Borsini, F.; Meli, A. Is the forced swimming test a suitable model for revealing antidepressant activity? *Psychopharmacology (Berlin)* **1988**, *94*, 147–160. [[CrossRef](#)]
20. Borsini, F. Role of the serotonergic system in the forced swimming test. *Neurosci. Biobehav. Rev.* **1995**, *19*, 377–395. [[CrossRef](#)]
21. Wesołowska, A.; Nikiforuk, A.; Stachowicz, K. Anxiolytic-like and antidepressant-like effects produced by the selective 5-HT₆ receptor antagonist SB-258585 after intrahippocampal administration to rats. *Behav. Pharmacol.* **2007**, *18*, 439–446. [[CrossRef](#)] [[PubMed](#)]
22. Soczewiński, E.; Wachtmeister, C.A. The relation between the composition of certain ternary two-phase solvent systems and RM values. *J. Chromatogr. A* **1962**, *7*, 311–320. [[CrossRef](#)]
23. Wager, T.T.; Hou, X.; Verhoest, P.R.; Villalobos, A. Moving beyond rules: The development of a central nervous system multiparameter optimization (CNS MPO) approach to enable alignment of druglike properties. *ACS Chem. Neurosci.* **2010**, *1*, 435–449. [[CrossRef](#)] [[PubMed](#)]
24. *Schrödinger Release 2017-3: QikProp*; Schrödinger LLC: New York, NY, USA, 2017.
25. Wilcken, R.; Zimmermann, M.O.; Lange, A.; Zahn, S.; Boeckler, F.M. Using halogen bonds to address the protein backbone: A systematic evaluation. *J. Comput. Aided Mol. Des.* **2012**, *26*, 935–945. [[CrossRef](#)] [[PubMed](#)]
26. Wilcken, R.; Zimmermann, M.O.; Lange, A.; Joerger, A.C.; Boeckler, F.M. Principles and Applications of Halogen Bonding in Medicinal Chemistry and Chemical Biology. *J. Med. Chem.* **2013**, *56*, 1363–1388. [[CrossRef](#)] [[PubMed](#)]
27. Matys, A.; Podlewska, S.; Witek, K.; Witek, J.; Bojarski, A.J.; Schabikowski, J.; Otrębska-Machaj, E.; Latacz, G.; Szymańska, E.; Kieć-Kononowicz, K.; et al. Imidazolidine-4-one derivatives in the search for novel chemosensitizers of Staphylococcus aureus MRSA: Synthesis, biological evaluation and molecular modeling studies. *Eur. J. Med. Chem.* **2015**, *101*, 313–325. [[CrossRef](#)] [[PubMed](#)]
28. Safari, J.; Naeimi, H.; Ghanbari, M.M.; Sabzi Fini, O. Preparation of phenytoin derivatives under solvent-free conditions using microwave irradiation. *Russ. J. Org. Chem.* **2009**, *45*, 477–479. [[CrossRef](#)]
29. Werbel, L.M.; Elslager, E.F.; Islip, P.J.; Closier, M.D. Antischistosomal effects of 5-(2,4,5-trichlorophenyl)hydantoin and related compounds. *J. Med. Chem.* **1977**, *20*, 1569–1572. [[CrossRef](#)] [[PubMed](#)]
30. Linol, J.; Coquerel, G. Influence of high energy milling on the kinetics of the polymorphic transition from the monoclinic form to the orthorhombic form of (±)5-methyl-5-(4'-methylphenyl)hydantoin. *J. Therm. Anal. Calorim.* **2007**, *90*, 367–370. [[CrossRef](#)]
31. Keshtov, M.L.; Rusanov, A.L.; Belomoina, N.M.; Mikitaev, A.K. Improved synthesis of bis[p-(phenylethynyl)phenyl]hetarylenes. *Russ. Chem. Bull.* **1997**, *46*, 1794–1796. [[CrossRef](#)]

32. Safari, J.; Javadian, L. Montmorillonite k-10 as a catalyst in the synthesis of 5,5-disubstituted hydantoins under ultrasound irradiation. *J. Chem. Sci.* **2013**, *125*, 981–987. [[CrossRef](#)]
33. Sherman, W.; Day, T.; Jacobson, M.P.; Friesner, R.A.; Farid, R. Novel Procedure for Modeling Ligand/Receptor Induced Fit Effects. *J. Med. Chem.* **2006**, *49*, 534–553. [[CrossRef](#)] [[PubMed](#)]
34. Friesner, R.A.; Banks, J.L.; Murphy, R.B.; Halgren, T.A.; Klicic, J.J.; Mainz, D.T.; Repasky, M.P.; Knoll, E.H.; Shelley, M.; Perry, J.K.; et al. Glide: A New Approach for Rapid, Accurate Docking and Scoring. 1. Method and Assessment of Docking Accuracy. *J. Med. Chem.* **2004**, *47*, 1739–1749. [[CrossRef](#)] [[PubMed](#)]
35. Kooistra, A.J.; Kuhne, S.; De Esch, I.J.P.; Leurs, R.; De Graaf, C. A structural chemogenomics analysis of aminergic GPCRs: Lessons for histamine receptor ligand design. *Br. J. Pharmacol.* **2013**, *170*, 101–126. [[CrossRef](#)] [[PubMed](#)]
36. *Schrödinger Release 2017-3: LigPrep*; Schrödinger LLC: New York, NY, USA, 2017.
37. *Schrödinger Release 2017-3: Epik*; Schrödinger LLC: New York, NY, USA, 2017.
38. Harder, E.; Damm, W.; Maple, J.; Wu, C.; Reboul, M.; Xiang, J.Y.; Wang, L.; Lupyran, D.; Dahlgren, M.K.; Knight, J.L.; et al. OPLS3: A Force Field Providing Broad Coverage of Drug-like Small Molecules and Proteins. *J. Chem. Theory Comput.* **2016**, *12*, 281–296. [[CrossRef](#)] [[PubMed](#)]
39. *Schrödinger Release 2017-3: Glide*; Schrödinger LLC: New York, NY, USA, 2017.
40. Cheng, Y.-C.; Prusoff, W.H. Relationship between the inhibition constant (KI) and the concentration of inhibitor which causes 50 per cent inhibition (I50) of an enzymatic reaction. *Biochem. Pharmacol.* **1973**, *22*, 3099–3108. [[PubMed](#)]
41. Porsolt, R.D.; Bertin, A.; Jalfre, M. “Behavioural despair” in rats and mice: Strain differences and the effects of imipramine. *Eur. J. Pharmacol.* **1978**, *51*, 291–294. [[CrossRef](#)]
42. Vogel, J.R.; Beer, B.; Clody, D.E. A simple and reliable conflict procedure for testing anti-anxiety agents. *Psychopharmacologia* **1971**, *21*, 1–7. [[CrossRef](#)] [[PubMed](#)]
43. Kotańska, M.; Lustyk, K.; Bucki, A.; Marcinkowska, M.; Śniecikowska, J.; Kołaczkowski, M. Idalopirdine, a selective 5-HT₆ receptor antagonist, reduces food intake and body weight in a model of excessive eating. *Metab. Brain Dis.* **2018**, *33*, 733–740. [[CrossRef](#)] [[PubMed](#)]
44. Kotańska, M.; Śniecikowska, J.; Jastrzębska-Więsek, M.; Kołaczkowski, M.; Pytko, K. Metabolic and Cardiovascular Benefits and Risks of EMD386088—A 5-HT₆ Receptor Partial Agonist and Dopamine Transporter Inhibitor. *Front. Neurosci.* **2017**, *11*, 50. [[CrossRef](#)] [[PubMed](#)]

Sample Availability: Not available.



© 2018 by the authors. Licensee MDPI, Basel, Switzerland. This article is an open access article distributed under the terms and conditions of the Creative Commons Attribution (CC BY) license (<http://creativecommons.org/licenses/by/4.0/>).

3.2. Publication 2

Synthesis and computer-aided SAR studies for derivatives of phenoxyalkyl-1,3,5-triazine as the new potent ligands for serotonin receptors 5-HT₆.

Wesam Ali, Małgorzata Więcek a, Dorota Łażewska, Rafał Kurczab, Magdalena Jastrzębska-Więsek, Grzegorz Satała, Katarzyna Kucwaj-Brysz, Annamaria Lubelska, Monika Głuch-Lutwin, Barbara Mordyl, Agata Siwek, Muhammad Jawad Nasim, Anna Partyka, Sylwia Sudoł, Gniewomir Latacz, Anna Wesółowska d, Katarzyna Kieć-Kononowicz and Jadwiga Handzlik.

European Journal of Medicinal Chemistry 2019, 178, 740-751.



Contents lists available at ScienceDirect

European Journal of Medicinal Chemistry

journal homepage: <http://www.elsevier.com/locate/ejmech>

Research paper

Synthesis and computer-aided SAR studies for derivatives of phenoxyalkyl-1,3,5-triazine as the new potent ligands for serotonin receptors 5-HT₆



Wesam Ali ^{a, b}, Małgorzata Więcek ^a, Dorota Łażewska ^a, Rafał Kurczab ^c, Magdalena Jastrzębska-Więsek ^d, Grzegorz Satała ^c, Katarzyna Kucwaj-Brysz ^a, Annamaria Lubelska ^a, Monika Głuch-Lutwin ^e, Barbara Mordyl ^e, Agata Siwek ^e, Muhammad Jawad Nasim ^{a, b}, Anna Partyka ^d, Sylwia Sudoł ^a, Gniewomir Latacz ^a, Anna Wesołowska ^d, Katarzyna Kieć-Kononowicz ^a, Jadwiga Handzlik ^{a, *}

^a Department of Technology and Biotechnology of Drugs, Faculty of Pharmacy, Jagiellonian University, Medical College, Medyczna 9, PL, 30-688, Kraków, Poland

^b Division of Bioorganic Chemistry, School of Pharmacy, University of Saarland, Campus B2 1, D-66123, Saarbruecken, Germany

^c Department of Medicinal Chemistry Institute of Pharmacology, Polish Academy of Sciences, Smętna 12, PL, 31-343, Kraków, Poland

^d Department of Clinical Pharmacy, Faculty of Pharmacy, Jagiellonian University, Medical College, Medyczna 9, PL, 30-688, Kraków, Poland

^e Department of Pharmacobiology, Faculty of Pharmacy, Jagiellonian University, Medical College, Medyczna 9, PL, 30-688, Kraków, Poland

ARTICLE INFO

Article history:

Received 28 February 2019

Received in revised form

31 May 2019

Accepted 7 June 2019

Available online 10 June 2019

Keywords:

Serotonin receptors

5-HT₆R ligands

1,3,5-Triazine

Thioether

Selenoether

Antidepressive

ABSTRACT

This research has provided the most active 5-HT₆R agents among 1,3,5-triazine derivatives investigated to date and has also identified the world's first selenium-containing 5-HT₆R ligands. The studies are focused on design, synthesis, biological evaluation and docking-supported SAR analysis for novel 5-HT₆R agents as derivatives of lead structure 4-(4-methylpiperazin-1-yl)-6-(phenoxyethyl)-1,3,5-triazin-2-amine (**7**). The lead modifications included an introduction of: (i) various small substituents at benzene ring, (ii) a branched ether linker or (iii) the ether oxygen replacement with other chalcogen (S, Se) or sulfonyl moiety. Hence, a series of new compounds (**7–24**) was synthesized and examined on their affinities for 5-HT₆R and selectivity, in respect to the 5-HT_{1A}R, 5-HT_{2A}R, 5-HT₇R and dopamine D₂ receptor, in the radioligand binding assays. For representative most active compounds functional bioassays and toxicity profile *in vitro* and antidepressant-like activity *in vivo* were examined. The 2-isopropyl-5-methylphenyl derivative (**10**) was found as the most active triazine 5-HT₆R antagonist ($K_i = 11$ nM). SAR analysis indicated, that an exchange of oxygen to selenium (**7** vs. **22**), and especially, to sulfur (**7** vs. **19**) was beneficial to increase both affinity and antagonistic action for 5-HT₆R. Surprisingly, an introduction of SO₂ caused a drastic decrease of the 5-HT₆R affinity, which was explained at a molecular level based on docking studies. All *in vivo* tested compounds (**10**, **18** and **21**) did not show any risk of toxicity in the safety studies *in vitro*.

© 2019 Elsevier Masson SAS. All rights reserved.

1. Introduction

The 5-hydroxytryptamine (5-HT: serotonin) subtype 6 receptor (5-HT₆R) has gained a great interest as an attractive target for drug discovery [1]. The growing appeal of this receptor stems, at least in part, from its almost exclusive expression in the central nervous

system (CNS), and the potential therapeutical indications of the 5-HT₆R ligands which encompass a spectrum of diseases; including depression, cognitive dysfunction associated with Alzheimer's disease, anxiety, schizophrenia, and obesity [2–8]. Intriguingly, both 5-HT₆R agonists and antagonists may paradoxically evoke pro-cognitive, antidepressant-like, or anti-anxiety-like effects [8]. Lines of evidence indicated several selective 5-HT₆R agonists (e.g. **WAY-181187**), partial agonists (e.g. **EMDT 386088**) and antagonists (e.g. **SB-271046**, **SB-399885**) [9–11], intensively explored in pre-clinical and clinical trials but none of them has reached the

* Corresponding author.

E-mail address: j.handzlik@uj.edu.pl (J. Handzlik).

pharmaceutical market as an accepted drug (Fig. 1a). Recent years have provided new groups of 5-HT₆R antagonists, based on pyrrolo [2,3-b]pyridine- (1) [12], pyrrolo [3,2-c]quinoline- (2) [13] or non-sulfonyl imidazo [4,5-b]pyridine (3) [14] derivatives (Fig. 1b). The compounds (1–3) displayed potent nanomolar affinities, nonetheless their structures resemble known ligands (Fig. 1a vs. Fig. 1b) due to the presence of an indole-like core and/or sulfonyl moieties. Thus, more efforts of medicinal chemists are needed to search for 5-HT₆R agents in more diverse chemical groups which could provide both potent and selective action on 5-HT₆R and satisfying CNS-drugability properties. In this context, we started to explore a new group of piperazine 1,3,5-triazine derivatives as potent and linker-dependent 5-HT₆R agents [15]. Hence, compounds with methylene linker (4 and 5, Fig. 1c) displayed significant affinities, whereas those with direct aromatic substituents (6) were very weak 5-HT₆-agents. The decrease in activity was also observed for triazine compounds with stiffened linker, i.e. incorporating vinyl- [16] or hydantoin [17] moieties. Wider investigations of the role of linkers have provided an ether compound (7) with a moderate activity towards 5-HT₆R. The unsubstituted phenyl ring of 7 provides various possibilities for substitutions in order to improve pharmacophoric properties of the hydrophobic feature. Thus, compound 7 was selected as a new lead structure for further modifications which were performed within this study.

Apart from pharmacomodulation focused on benzene substituents, the lead structure allows for variety of linker modifications, such as branching the ether linker or a heteroatom exchange. Based on interesting pro- or/and antioxidant properties of

chalcogen compounds [18,19], the significance of sulfur in previous 5-HT₆R ligands [12,13] and growing interest of selenium-compounds as neuroprotective agents with therapeutic potential [20–22], especially confirmed for selenides [23,24], we sought to explore the potency of S and Se-containing 1,3,5-triazine derivatives of the lead 7 as 5-HT₆R ligands with pharmacological activity *in vivo*.

In this context, the design and synthesis of new derivatives of lead 7 with (un)branched linker and a different substitution at phenyl ring as well as their respective S- or Se analogs (8–24, Table 1), including one sulfone analogue (24), were performed. The 5-HT₆R affinity and selectivity for the series were tested in the radioligand binding assay. For selected compounds intrinsic activity in functional bioassays, toxicity profile *in vitro* and antidepressant-like activity *in vivo* were examined.

2. Results

2.1. Synthesis

The synthesis of the compounds (8–24) investigated followed several chemical approaches due to different availability of starting materials (Scheme 1). The common step for compounds 8–23 (Scheme 1a) was the formation of the triazine ring *via* cyclic condensation of 4-methyl piperazine-1-yl biguanide dihydrochloride (25) with an appropriate ester (26–41), according to a method already described [15–17,25,26]. In the case of synthesis of sulfone 24, selective oxidation of the thioether sulfur atom of 20

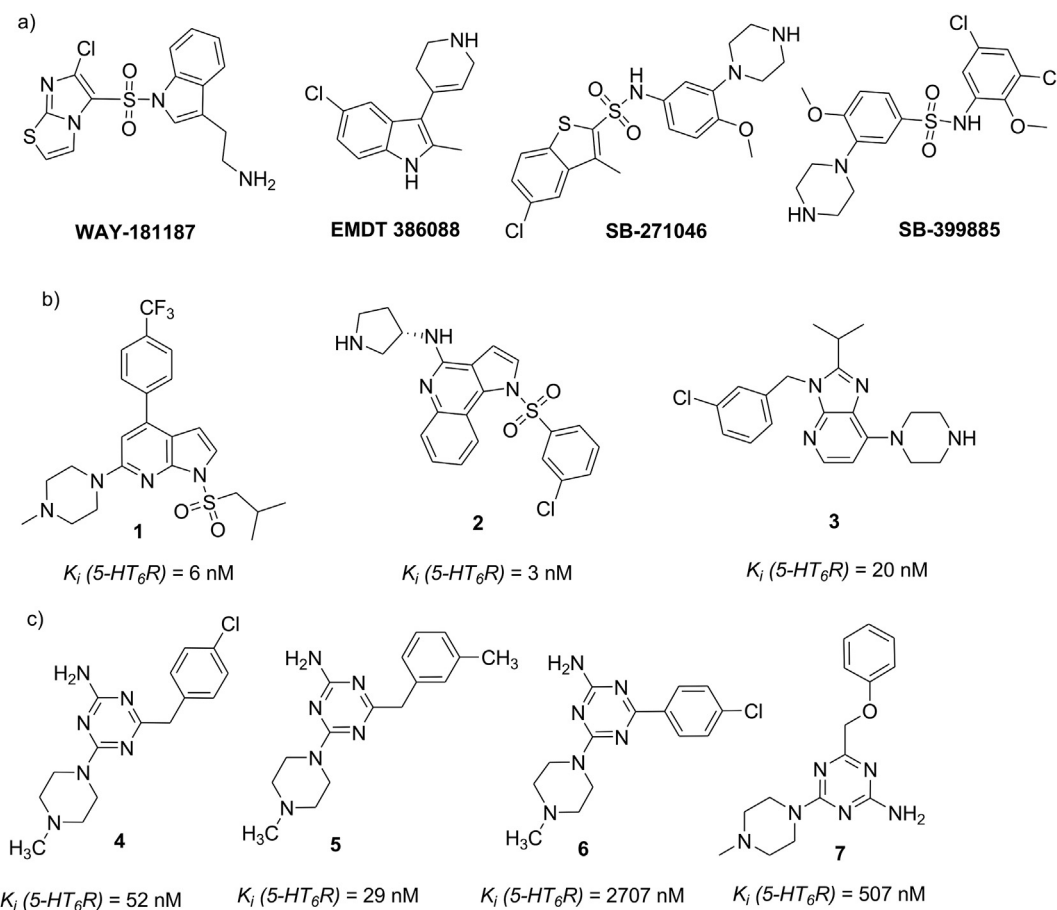
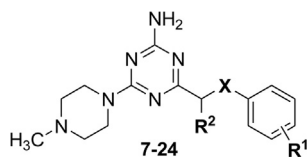


Fig. 1. Structures of the 5-HT₆R ligands found within previous studies; a) explored in preclinical or clinical trials [9–11]; b) found by other research teams in 2016–2017 [12–14]; c) 1,3,5-triazine derivatives [15,16].

Table 1
Structure of the compounds investigated.

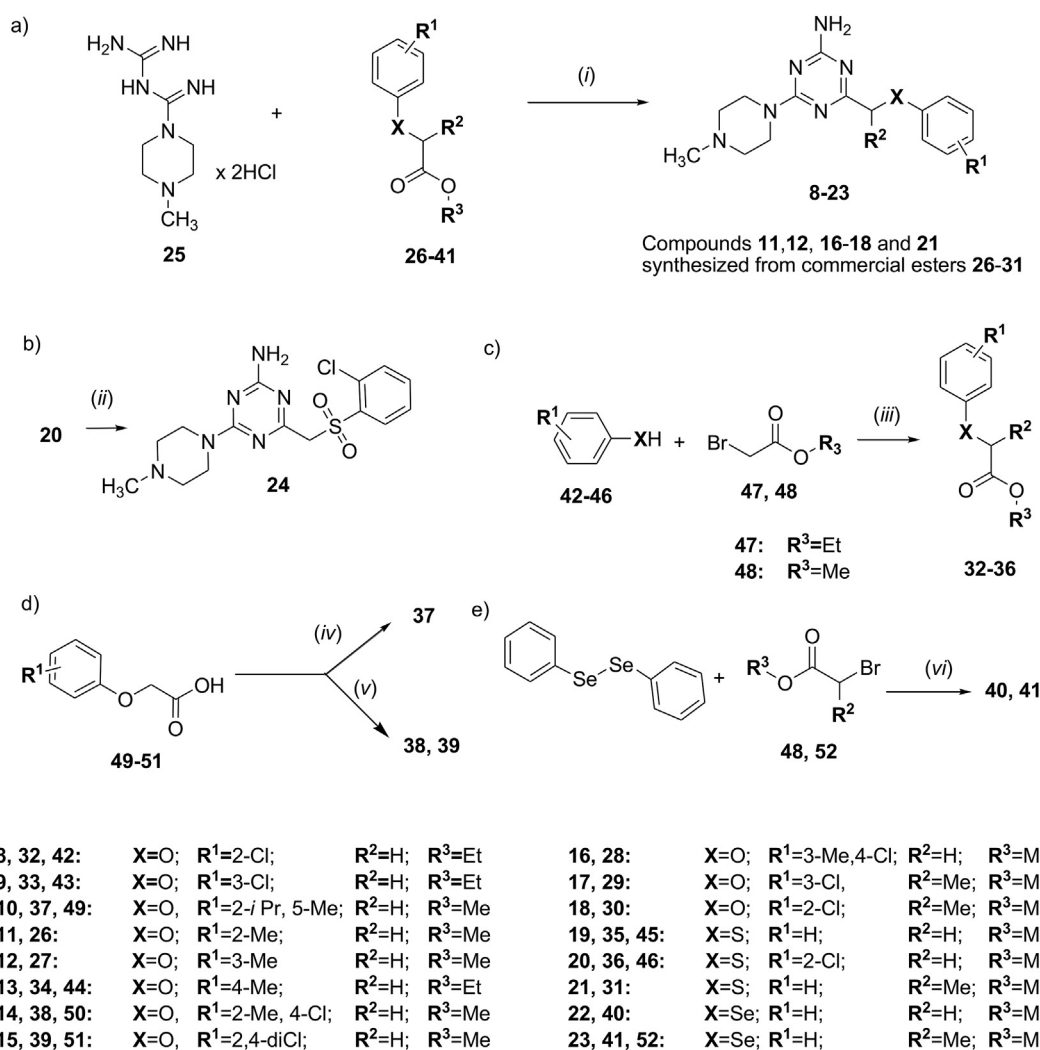


Cpd	R ¹	R ²	X	Cpd	R ¹	R ²	X
7	H	H	O	16	3-Me, 4-Cl	H	O
8	2-Cl	H	O	17	3-Cl	Me	O
9	3-Cl	H	O	18	2-Cl	Me	O
10	2- <i>i</i> -Pr, 5-Me	H	O	19	H	H	S
11	2-Me	H	O	20	2-Cl	H	S
12	3-Me	H	O	21	2-Cl	Me	S
13	4-Me	H	O	22	H	H	Se
14	2-Me, 4-Cl	H	O	23	H	Me	Se
15	2,4-diCl	H	O	24	2-Cl	H	SO ₂

was performed according to [Scheme 1b](#). The ester intermediates necessary for synthesis of **8–28** were obtained *via* five different routes. For preparation of compounds **11**, **12**, **16–18** and **21**, commercially available (thio)ether derivatives of methyl esters (**26–31**) were purchased. For the compounds **8**, **9**, **13**, **19** and **20**, related (thio)ether derivatives of methyl- or ethyl esters (**32–36**, [Scheme 1c](#)) were obtained during *O*- or *S*-alkylation of adequate (thio)phenols (**42–46**) with suitable alkyl bromoacetates (**47**, **48**). Moreover, methyl ester **37** was obtained *via* acid-catalyzed esterification of corresponding commercial phenylacetic acid (**49**), whereas reactions of suitable carboxylic acids (**50**, **51**) with iodomethane in the presence of DBU were carried out for esters **38** and **39** [[15](#)] ([Scheme 1d](#)). The synthesis of Se-containing esters **40** and **41** was performed starting from diphenyl diselenides, and commercial bromoesters (**48**, **52**) were employed as alkylation agents ([Scheme 1e](#)).

2.2. Molecular modelling

Molecular docking was employed to study the mechanism of action of a newly synthesized library of compounds with the 5-



Scheme 1. Synthesis route for final compounds **8–24** (a, b) and intermediates **32–36**, **40** and **41** (c–e). a) The cyclic condensation for **8–23**; (i) absolute methanol, Na, reflux 15–30 h. b) The selective oxidation for **24**; (ii) ethanol, Na₂WO₄·2H₂O, H₂O₂, rt. c) *O*- or *S*-alkylation for **32–36**; (iii) acetonitrile, K₂CO₃, reflux. d) Esterification for **37–39**; (iv) dried methanol, concentrated H₂SO₄, reflux; (v) dried toluene, DBU, iodomethane, rt. e) Synthesis of Se-intermediates **40** and **41**; (vi) THF/water, NaBH₄, N₂, rt.

HT₆R. Since this receptor has not been crystallized so far, its homology models used for studying the interaction of other 1,3,5-triazine derivatives [15,16] have been applied. In general, results revealed that newly synthesized compounds (7–24) had a very consistent binding mode with the previously reported 1,3,5-triazine derivatives [15,16]. Small structural modifications introduced in the obtained library, and their influence on 5-HT₆R activity was reflected in the ligand-receptor complexes obtained. Emphasis was placed on: (i) the influence of the oxygen replacement in the linker on the sulfur and sulfone group, (ii) the influence of different substituents in the phenyl ring, and (iii) the role of the branching in the linker (Fig. 2).

2.3. Radioligand binding assays

Radioligand binding assays were applied to determine the affinity and selectivity profiles of the newly synthesized compounds for human serotonin 5-HT₆R in comparison to 5-HT₇, 5-HT_{1A}, 5-HT_{2A} and dopaminergic D₂ receptors. All derivatives tested, except **14** and **24**, displayed higher affinity towards 5-HT₆R ($K_i < 400$ nM) than that of lead **7** (Table 2). Compounds **10**, **11**, **18**, **19**, **21** demonstrated high affinities for 5-HT₆R ($K_i < 100$ nM), particularly potent in the case of **10**, **18**, **19** and **21** ($K_i \leq 30$ nM). Each of the active compounds featured predominant affinity toward 5-HT₆R in comparison to both 5-HT_{1A}R and D₂R. Compounds **10**, **11**, **18**, **19** and **21** exhibited the highest selectivity to 5-HT₆R over D₂, 5-HT_{1A}, 5-HT_{2A} and 5-HT₇ receptors. Compound **10** was identified as the most active one with an affinity for 5-HT₆R in the range of the standard 5-HT₆R antagonist olanzapine. In parallel, compound **10** was much more selective with respect to the D₂-dopamine receptor when compared to the dual target reference olanzapine.

2.4. Functional assays

For selected active 5-HT₆R ligands (**10**, **18**, **21**), their intrinsic activity was investigated *in vitro* by the cellular aequorin-based functional assay with recombinant CHO–K1 cells expressing mitochondrially targeted aequorin, human GPCR and the promiscuous G protein $\alpha 16$ for 5-HT₆R. Compound **SB-742457** served as the highly potent antagonist, mianserin as moderate one, and serotonin as reference agonist (Table 3). The results obtained indicated a lack of agonistic activity, and rather pointed towards a potent antagonist action for the triazines tested, with K_b values in the nanomolar range ($K_b = 2.9$ – 4.6 nM).

Table 2
Radioligand binding assays results for the investigated compounds (7–24).

Cpd	K_i [nM] ^a				
	5-HT ₆ R	D ₂ R	5-HT _{1A} R	5-HT _{2A} R	5-HT ₇ R
7	507	1348	8726	2628	9531
8	129	2362	5467	nt	9247
9	148	674	7505	nt	5818
10	11	1094	12530	430	11950
11	87	4247	14160	17170	514
12	207	740	15070	2274	10660
13	235	2916	28510	nt	16050
14	911	4369	7688	nt	15180
15	128	1234	1610	nt	3804
16	355	1224	3584	197	5840
17	118	566	3438	590	8361
18	23	1001	4540	1830	38730
19	26	734	4389	197	2871
20	126	329	1680	nt	614
21	19	520	3384	407	4570
22	242	506	3176	406	2329
23	111	656	5311	376	4247
24	3574	50140	>10 ⁶	11590	98430
Ref ^{b-d}	7 ^b	9 ^b	20 ^c	-	18 ^d

^{b-d} Reference ligands for GPCRs investigated.

^a Tested experimentally in the radioligand binding assay; binding affinity, K_i , expressed as the average of at least two independent experiments. Radioligands used: [³H]-8-OH-DPAT (5-HT_{1A}), [³H]-Ketanserin (5-HT_{2A}), [³H]-LSD (5-HT₆), [³H]-5-CT (5-HT₇) and [³H]-Raclopride (D₂). Results for 5-HT₆R bolded.

^b Olanzapine.

^c Buspirone.

^d Clozapine.

2.5. In vivo studies

2.5.1. Antidepressant-like activity of compounds investigated

Compounds **10**, **18** and **21** were selected for behavioral studies *in vivo* in male Wistar rats. Their potential antidepressant-like properties were assessed in the forced swim test (FST) [27]. These compounds exhibited different activity in the FST (Fig. 3). Compound **10**, for instance, decreased about 20% immobility at the doses of 0.3–3 mg/kg (but not at 0.1 mg/kg) compared to the vehicle group (one-way ANOVA, $F(4,35) = 4.5546$; $p < 0.01$). Compound **18** showed antidepressant-like activity only in one medium (1 mg/kg) dose; it decreased the immobility time about 22% vs the respective vehicle treated group (one-way ANOVA $F(3,24) = 4.0751$; $p < 0.05$) (Fig. 3). Compound **21** was not active in the FST (one-way ANOVA $F(3,24) = 2.4252$; NS; Fig. 3). reference 5-

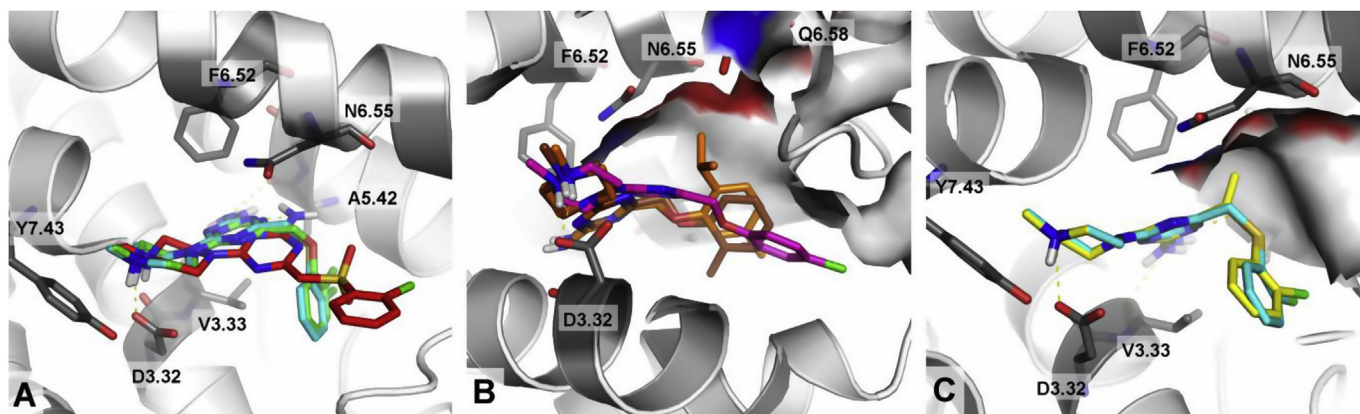


Fig. 2. The interactions of selected 1,3,5-triazine analogs with 5-HT₆R. (A) A difference of the binding modes of derivatives with O (**8**–green), S (**20**–cyan), and sulfonyl (**24**–red) in the linker. (B) A comparison of the binding modes of selected analogs with different substituents in the phenyl ring (**10**–orange, **14**–magenta, **11**–brown). (C) Illustration of the binding modes for analogs with hydrogen (**20**–cyan) and methyl (**21**–yellow) linker substituent. (For interpretation of the references to colour in this figure legend, the reader is referred to the Web version of this article.)

Table 3
Functional-vs. Radioligand binding assays results for **10**, **18** and **21**.

Compound	5-HT ₆ R		
	Binding affinity (RBA) K_i [nM]	Antagonist mode ^a K_b [nM]	Agonist mode ^b E_{max} [%]
10	11	4.60	1
18	23	3.00	1
21	19	2.90	1
Serotonin	—	nc	100
SB-742457	—	0.67	2
Mianserin	—	30.0	1

^a Results were normalized as percentage of maximal response in the absence of antagonist.

^b Results were normalized as percentage of maximal agonist response (serotonin 10-6 M). E_{max} is the maximum possible effect; nc - not calculable.

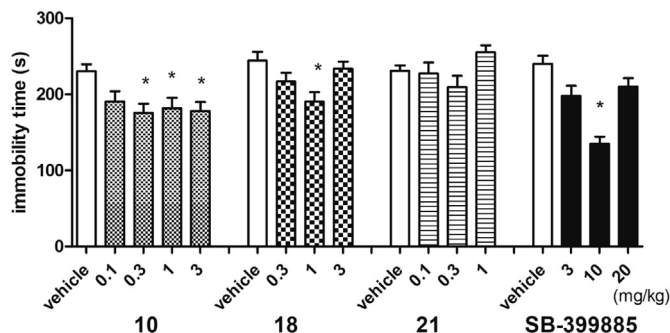


Fig. 3. Effects of compounds **10**, **18**, **21** and **SB-399885** on the immobility time of rats in the forced swim test. Compounds **10**, **18**, and **21** were administered *i. p.* 60 min, whilst **SB-399885** was given 30 min before the test. The animals were observed for 5 min. The data are presented as the mean \pm SEM of 6–8 rats. The data were statistically evaluated by one-way ANOVA followed by Bonferroni's post-hoc test, * $p < 0.05$, vs. respective vehicle group.

HT₆ receptor antagonist, compound **SB-399885**, was active in the FST only at the dose of 10 mg/kg ($F(3,28) = 9.7153$; $p < 0.0001$; Fig. 3) [28]. An U-shaped dose-response in the FST test for compounds **18** and **SB-399885** was observed. This effect seems to be typical for some antidepressants with different mechanisms of action also producing U-shaped dose-response effects in some animal models and tests for antidepressant-like activity [29,30]. Moreover this effect was also observed for other 5-HT₆ ligands, such as standard potent 5-HT₆R antagonist **SB-258585** [31].

2.5.2. Locomotor activity

For compounds **10** and **18**, locomotor activity assays in rats were also performed. These triazine derivatives, especially compound **10** at the doses active in the FST, slightly increased locomotor activity measured in the open field (OF) test (Table 4).

These results indicate that the antidepressant-like effects in the FST observed may not be specific ones. Compound **SB-399885** did not change the rats' locomotor activity under identical experimental settings [31].

Table 4
Effects of compounds **10** and **18** on the rat locomotor activity measured in the OF test.

Treatment	Dose (mg/kg)	Total distance (cm)	AmbulationX	AmbulationY	Rearings
Vehicle	0	2165 \pm 119	190 \pm 12	187 \pm 15	57 \pm 6
10	0.3	2833 \pm 157 *** $F(1,10) = 11.502$; $p < 0.01$	307 \pm 19 *** $F(1,10) = 27.956$; $p < 0.001$	290 \pm 19 ** $F(1,10) = 18.645$; $p < 0.01$	56 \pm 3 $F(1,10) = 0.0157$; NS
Vehicle	0	929 \pm 36	213 \pm 13	187 \pm 14	68 \pm 7
18	1	1005 \pm 68 $F(1,10) = 0.9711$; NS	269 \pm 8 ** $F(1,10) = 14.308$; $p < 0.01$	227 \pm 14 $F(1,10) = 4.5275$; NS	46 \pm 4 * $F(1,10) = 6.4150$; $p < 0.05$

Compounds were administered *i. p.* 60 min before the test. The animals were observed for 5 min. The data are presented as the mean \pm SEM of 5–6 rats. The data were statistically evaluated by one-way ANOVA followed by Bonferroni's post-hoc test, * $p < 0.05$, ** $p < 0.01$, *** $p < 0.001$ vs vehicle group, NS = not significant.

2.6. Drug-likeness

The safety profile of the most active triazine 5-HT₆R agents (**10**, **18** and **21**) was estimated in, both neurotoxicity and mutagenicity assays *in vitro*.

Neurotoxicity was examined in the SH-SY5Y eukaryotic cell line. The colorimetric MTS assay allowed the determination of SH-SY5Y cell viability after 72 h of incubation with **10**, **18** and **21**, respectively. A statistically significant decrease in cell viability was observed only for the highest dose for each of the 5-HT₆R agents tested (100 μ M, Fig. 4).

The mutagenicity of **10**, **18** and **21** was determined following the Ames microplate fluctuation protocol (MPF) with *Salmonella typhimurium* strain TA100, which enabled the detection of base-pair mutations [32]. The results were compared to the reference mutagen nonyl-4-hydroxyquinoline-*N*-oxide (NQNO) at 0.5 μ M. The numbers of revertants were estimated colourimetrically and the mutagenicity potential was evaluated according to the procedure provided by the manufacturer [32]. The medium control baseline (MCB) was calculated first, as a number of revertants observed in the growth medium with 1% DMSO as negative control plus standard deviation. A compound was considered as mutagenic one if data point with fold increase ≥ 2 of MCB, and Binomial B-value ≥ 0.99 (Table 5). The results of the study did not indicate any risk of mutagenicity for the triazine derivatives **10**, **18** and **21** tested.

In summary, compounds **10**, **18** and **21** displayed statistically significant neurotoxicity only at > 4000 -fold higher concentrations than the one required for 5-HT₆R activity ($K_i = 11$ – 23 nM, Table 1) and 100-fold higher concentrations than the one for the positive control doxorubicin. Furthermore, none of the compounds investigated caused any mutagenic effects. Thus, results of the study using models *in vitro* indicated high pharmaceutical safety for these active 5-HT₆R antagonists.

3. Discussion

The modifications performed on the lead **7** were addressed in order to analyse an influence on the affinity for 5-HT₆R of three following structural factors: (i) the substituents at phenyl ring,

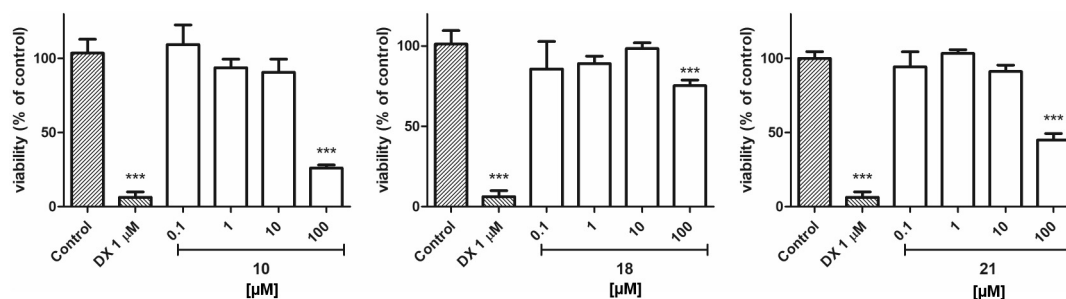


Fig. 4. The impact of doxorubicin (DX), **10**, **18** and **21** on the viability of the *neuroblastoma* SH-SY5Y cell line after 72 h of incubation. Statistical significance was evaluated by one-way ANOVA, followed by Bonferroni's comparison test (***) $p < 0.001$ compared with the negative control).

Table 5

The mutagenicity potential of **10**, **18** and **21**.

Conc.[μ M]	Cpd	Fold increase over MCB	Binomial <i>B</i> -value ^a	Number of revertants \pm SD
0.5	NQNO	5.41	1.0000	46.00 \pm 2.29
1	10	0.55	0.0570	4.67 \pm 1.53
	18	0.73	0.1755	8.00 \pm 2.65
	21	0.94	0.7035	10.33 \pm 1.53
10	10	0.47	0.0172	4.00 \pm 1.00
	18	1.00	0.8259	11.00 \pm 2.65
	21	0.76	0.2366	8.33 \pm 3.06

^a Binomial *B*-value indicates the probability that spontaneous mutation events alone. The result ≥ 0.99 indicates that chances of spontaneous mutation are $\leq 1\%$.

including kind, number and position; (ii) the methyl (un)branched linker and (iii) different chalcogen-ether linker with respect to the S-oxidized form (SO₂) that is an indispensable structural feature of more than 80% 5-HT₆R agents found within the 20-year global studies on this receptor [33]. The results obtained within this study allow to perform comprehensive structure-activity relationship discussion.

The first subseries of 11 unbranched ether derivatives (7–16, Table 1) enabled to estimate SAR for substituents at the phenyl ring. On the basis of previous results, we took into consideration a variety of alkyl- and chlorine substituents only, since they were found as beneficial, in contrast to alkoxy moieties [15]. Thus, the following order of the 5-HT₆R affinity decrease can be observed: 2-*i*Pr-5-Me \gg 2-Me > 2-Cl > 2,4-diCl > 3-Cl > 3-Me > 4-Cl > 4-Me > 3-Me-4-Cl > H > 2-Me-4-Cl (Table 2) [16]. This order confirmed the general preference of electrodonating and hydrophobic substituents at the phenyl ring that was also observed for previous methylene- [15] and hydantoin-linked aromatic triazine 5-HT₆R agents [17]. The isopropyl derivative (**10**) seems to be a special example of optimal electrodonating-hydrophobic balance for the substituent that, as more hydrophobic than methyl- (**10** vs. **11**, Table 1), and stronger electro-donating than the hydrophobic chlorine substituent (**10** vs. **8**), provided an outstanding 5-HT₆ affinity, not only in the considered series but also among all 1,3,5-triazines 5-HT₆R agents investigated so far [15–17]. As position of substituents at phenyl ring, the previous studies indicated the preferable *meta*-position in the case of benzyltriazine derivatives [15], while *para* one was emphatically beneficial for the 5-HT₆R affinity of the hydantoin-linked series [17]. In contrast, the presently considered ether-linked 1,3,5-triazines distinctly favour *ortho*-position in the binding with 5-HT₆R in comparison to both *meta* and *para*. Furthermore, the following trend of the 5-HT₆R affinity increase: *para* < *meta* < *ortho*, can be observed, either for Cl- (5-HT₆R *K*_i: 226 nM > 148 nM > 129 nM) [16] or for Me- (5-HT₆R *K*_i: 235 nM > 207 nM > 87 nM) substituents. Otherwise, an impact of di-substitution is not so clear and seems to be rather unprofitable (**16**, **14**) or at best indifferent (**15**), and also responsible for selectivity decrease (**16** vs. **12**).

In concordance to previous studies [15–17], results of this work underline the linker-dependent influence of Ph-substituents on the activity towards 5-HT₆R. In the case of S- and Se-ether linked triazines (**19**–**23**), the impact of substituents at the phenyl ring seems to be less meaningful than that observed for O-ether compounds (**7**–**16**), and significantly dominated by the impact of methyl-branching. It is particularly evident during analysis of results for S-ether compounds **19**–**21**, where the methyl-branched *o*-Cl-phenyl- (**21**) and the unbranched phenyl-unsubstituted (**19**) derivatives displayed comparable affinities for 5-HT₆R, and significantly more potent than that of the *o*-Cl-phenyl-, but linker-unbranched, derivative **20** (Table 1). The similar trend is also observed for selenoethers (**22** and **23**) demonstrating in 2-fold increase of the 5-HT₆R affinity with the appearance of methyl-branching within the linker.

Two parallel comparative analyses of the linker-activity relationship, performed for *o*-Cl- (**8**, **18**, **20**, **21** and **24**) and (un) substituted phenyl (**7**, **19**, **22** and **23**) derivatives, respectively, allow to assess the role of hetero-atom within the linker, connecting phenyl moiety with 1,3,5-triazine. In the case of *o*-chlorophenyl derivatives, the following activity order was found: S (Me-branched) \geq O (Me-branched) > S (unbranched) \geq O (unbranched) \gg SO₂, while the 5-HT₆R affinity decrease for the phenyl derivatives was as follows: S (unbranched) > Se (Me-branched) > Se (unbranched) > O (unbranched). Both sequences distinctly indicate the beneficial impact of the sulphide linker, whereas the selenoether seems to be slightly more profitable than the simple O-ether. It is worth to emphasize that presence of SO₂ drastically decreased the desirable pharmacological activity. This is a breakthrough observation against the majority of world's lines of evidence [33]. Thus, we have carried out computer-aided analysis to explain this and other SAR-observations in the molecular level.

The docked compounds showed very consistent binding mode, i.e. they formed the salt bridge interaction with D3.32, an aromatic interaction (CH- π or π - π stacking) with F6.52, and a hydrogen bond between NH₂ group of 1,3,5-triazine ring and carbonyl oxygen of V3.33 and/or A5.42 (Fig. 2). These contacts were crucial for recognition the active scaffolds by the 5-HT₆ receptor, however, the

substituted aromatic moiety linked with the triazine ring was found to have a significant influence on the activity modulation [15,16]. This fragment interacted with the hydrophobic cavity formed by transmembrane domains (TM) 3–5 and extracellular loop 2 (ECL2), and the positioned into this cavity was resulted by the tetrahedral conformation of the linker.

Two used modifications of the linker, namely: (1) changing the oxygen on the chalcogen atoms (S and Se) or a sulfone group and (2) branching the linker by adding the methyl group, were also explored within this simulation *in silico*. The derivatives with oxygen, sulfur and selenium atom in the linker showed high-to-medium activity to 5-HT₆R (11–911 nM). Analysis of the docking results (Fig. 2A) indicated that these compounds had a very similar binding mode, and the potential role of the atoms mentioned above is to bend the conformation of the molecule and further directing the aryl fragment into the hydrophobic pocket formed by TM3–5 and ECL2. However, a significant decrease in the activity was found for derivative with sulfonyl group **24** ($K_i = 3574$ nM). The analysis of binding mode revealed that it may be caused by forcing a straightened conformation (in which the phenyl and triazine rings are in one plane and do not form an angle of 90°), and thus no interaction with the hydrophobic pocket is probable. In order to confirm this hypothesis, the geometry optimization for compound **24** was additionally performed using quantum-mechanical methods (DFT: B3LYP/6–31++G**, PCM model with water as a solvent). The calculations confirmed that the most energetically stable conformation is straightened and the repulsion interaction between free electron pairs of one of the triazine nitrogen atoms and oxygen of the sulfone group was responsible for inducing such conformation.

A comparison of the binding modes for analogs having different substituents at phenyl fragment (Fig. 2B) showed that modulation of the activity can be related with the position and the size of the substituents. The most active compound **10** ($K_i = 11$ nM) was very well fitted to the hydrophobic sub-pocket formed by helices 3–5 and extracellular loop 2. However, the less active **14** ($K_i = 911$ nM) showed that improper configuration of substituents at the phenyl ring may even lead to destabilization of the complex and breaking some key interactions (the NH₂ group does not form hydrogen bonds, Fig. 2B).

The branching of the linker by a methyl group increased the affinity for each of the compared pairs, *i.e.*: **8** vs. **18**; **20** vs. **21**; **22** vs. **23**. Molecular docking indicated (Fig. 2C) that in each case the methyl group was located in a small binding cavity formed by helices 5 and 6 which increased the stability of the resulting ligand–receptor complexes.

Our comprehensive studies allowed also to examine the selectivity of series (**7–24**) towards the target 5-HT₆R as well as the intrinsic activity, the primary antidepressant-like action *in vivo* and safety properties *in vitro* for the most active compounds elected (**10**, **18** and **21**). Although some of the assays were performed for a few members only, different results are noteworthy for an initial qualitative SAR analysis. Results of the receptor screening have indicated a favourable 5-HT₆R-selectivity, in respect to 5-HT₇, 5-HT_{1A}, 5-HT_{2A} and dopaminergic D₂L receptors, for almost whole investigated ether 1,3,5-triazine derivatives (**7–24**), with one exception of the 3-methyl-4-chlorophenyl derivative **16** that acted almost 2-fold stronger towards 5-HT_{2A} (Table 1). However, the affinity of **16** for either 5-HT₆R or 5-HT_{2A}R was rather moderate ($K_i > 100$ nM). Hence, the results for the whole series indicate that this chemical family, consisting the skeleton of 2-amine-1,3,5-triazine core with methyl piperazine at position 4 and ether-linked phenyl at position 6, tend to selective action towards desirable 5-HT₆R over other GPCR-competitors.

The functional assays have confirmed a strong antagonistic

action for the tested compounds (**10**, **18** and **21**), the most potent in the case of the thioether **21** ($K_b = 2.8$ nM). However, this potent antagonist did not demonstrate antidepressant-like activity in the behavioral tests *in vivo*, while both the 2-isopropylphenyl (**10**) and 2-chlorophenyl (**18**) O-ether derivatives were active in the FST assay with probable non-specific action, estimated on the basis of the open field test results. Taking into account, still not enough recognized mechanisms of physiological actions mediated by 5-HT₆R receptor and lines of evidence indicating wider pharmacological abilities of its ligands, including: pro-cognitive, anxiolytic and anti-obesity properties, the obtained lack of anti-depressive potency *in vivo* for the potent sulfide antagonist **21** does not exclude other possible pharmacological directions for this agent, and even suggests some selectivity in comparison to the O-analogs (**10** and **18**). Furthermore, results of both, the neurotoxicity (MTS-test) and the mutagenicity AMES screening, confirmed profitable CNS-drug-likeness properties for all the investigated compounds (**10**, **18** and **21**).

Results obtained for the two “pilot” selenoethers (**22** and **23**) are worth emphasizing since both **22** and **23** displayed significant affinities, although they do not possess any beneficial substituents at the phenyl moiety. The unbranched Se-ether **22** was two-fold more active than corresponding O-ether derivative **7**.

4. Conclusions

The studies reported here are concerned with the design, synthesis, molecular modelling and biological screening, including: (i) RBA-evaluated affinity and selectivity towards 5-HT₆R in respect to 5-HT_{1A}R, 5-HT_{2A}R, 5-HT₇R and dopamine D₂ receptor, (ii) functional assays, (iii) behavioral assays *in vivo* and (iv) safety screening *in vitro* for a new series of phenoxyalkyl derivatives of 1,3,5-triazine. On the basis of the data obtained, an insightful SAR-analysis was performed. In the course of the study, a new family of active and selective 5-HT₆R antagonists was obtained, which may serve as a tool for deeper insight into the mechanisms of action of this most intriguing member of the serotonin GPCRs. Although this series was not such SAR-regular as the aryl-methyl-1,3,5-triazines described previously, it has provided the most active 1,3,5-triazine 5-HT₆R agents to date, *i.e.* 4-((2-isopropyl-5-methylphenoxy)methyl)-6-(4-methylpiperazin-1-yl)-1,3,5-triazin-2-amine (**10**) and 4-(1-((2-chlorophenyl)thio)ethyl)-6-(4-methylpiperazin-1-yl)-1,3,5-triazin-2-amine (**21**), with $K_i < 20$ nM. Furthermore, the world's first selenium-containing 5-HT₆R agents (**22** and **23**, $K_i < 250$ nM) were identified within these studies. SAR-analysis indicated that presence of sulphide is especially beneficial, while the SO₂-containing derivative (**24**) investigated proved to be distinctly less active than the other members of the series ($K_i > 3$ μM). This result, contrary to a majority of lines of evidence, was justified in the molecular level by our docking studies. Taking into account lines of evidence indicating antidepressant, procognitive and neuroprotective roles of selenides, in addition to a wide range of pharmacomodulation possibilities for these unsubstituted-phenyl derivatives, the selenocompounds **22** and **23** seem to represent an excellent starting point for new chemical modifications in search for successful CNS-selenoagents acting *via* 5-HT₆ receptor.

The most active agents **10** and **21** require wider pharmacological evaluation with a prospect to produce new CNS-drug candidate. Compounds **10** and **21** and the most active selenocompound **23** can be considered as suitable new lead structures for further chemical modifications in search for highly potent and selective 5-HT₆R antagonists.

The series of phenoxyalkyl-1,3,5-triazine derivatives presented seems to be a new promising alternative in search for 5-HT₆R

agents which, as distinctly structurally differing from the world's dominating derivatives of sulfone and indole, may form a basis for a breakthrough in the search for new therapies of the civilization CNS diseases related to this exceptional serotonin GPCR.

5. Experimental

5.1. Chemical synthesis

Melting points (mp) were determined using MEL-TEMP II apparatus and are uncorrected.

^1H NMR and ^{13}C NMR spectra were recorded on a Varian Mercury-VX 300 MHz PFG instrument or FT-NMR JEOL (JNM-ECZR500 RS1 v. ECZR) 500 MHz instrument (^{13}C NMR for **8–10**, **12–16** and **21**) in DMSO- d_6 (for most compounds) or MeOD (^{13}C NMR for **19** and **24**) at ambient temperature using the solvent signal as an internal standard: the values of the chemical shifts expressed as δ values in (ppm) and the coupling constants (J) in Hz. Data are reported as follows: chemical shift, multiplicity (s, singlet; br. s, broad singlet; d, doublet; t, triplet; dd, doublet of doublet, q, quintet, td triplet of doublet, m, multiplet), coupling constant J , number of protons, proton's position (Ph-phenyl, Pp-piperazine). Mass spectra recorded on a UPLC–MS/MS system consisted of a Waters ACQUITY[®] UPLC[®] (Waters Corporation, Milford, MA, USA) coupled to a Waters TQD mass spectrometer (electrospray ionization mode ESI-tandem quadrupole). The UPLC/MS purity of all the final compounds was confirmed to be higher than 95% (except **24**). Retention time values (t_R) are given in minutes. Elemental analyses (C, H, N) were performed on an Elemental Analyser Vario El III (Hanau, Germany) and agreed with theoretical values within $\pm 0.4\%$. Thin-layer chromatography (TLC) was performed on pre-coated Merck silica gel 60 F254 aluminum sheets. The reactions at fixed temperature were carried out using a magnetic stirrer with a contact thermometer Heidolph MR 2001. Esters **32–41** have been synthesized due to their high commercial costs. However, all of them are already described in Chemical Abstract Database, thus, their CAS numbers and ^1H NMR or LC/MS⁺ are indicated in Supplementary Information.

5.1.1. General procedure for the synthesis of final 1,3,5-triazine derivatives (**8–23**)

Sodium (10 mmol) was dissolved in 10 ml of absolute methanol, then 4-methylpiperazine-1-yl biguanide HCl (5 mmol) and a suitable carboxylic acid ester containing O- S- or Se-ether, respectively, (**26–41**, 5 mmol) was added. The reaction mixture was refluxed for 15–30 h. After cooling to room temperature, the solvent was evaporated, and the residue was dissolved in water (10 ml), stirred for 30 min at room temperature and kept overnight at the fridge. The precipitated triazine product was isolated by filtration and crystallized from methanol to give the desired final products as solids in basic form (method A). In case of lack of desirable precipitate, the methanol solution was saturated with gaseous HCl to give pure final product in hydrochloric salt form (method B)

5.1.1.1. 4-((2-Chlorophenoxy)methyl)-6-(4-methylpiperazin-1-yl)-1,3,5-triazin-2-amine (8). Method A. White solid, Yield 23%, mp 141–142 °C. $\text{C}_{15}\text{H}_{19}\text{ClN}_6\text{O}$ (MW 334.80). LC/MS⁺: purity: 100%, $t_R = 3.25$, (ESI) m/z $[\text{M}+\text{H}]^+$ 335.31. ^1H NMR δ : 7.41–7.37 (dd, $J_1 = 7.8$ Hz, $J_2 = 1.67$ Hz, 1H, Ph), 7.27–7.24 (m, 1H, Ph), 7.05–6.98 (m, 4H, Ph-2,6-H, NH₂), 4.88 (s, 2H, CH₂), 3.62 (s, 4H, Pp-2,6-H), 2.23 (s, 4H, Pp-3,5-H), 2.15 (s, 3H, CH₃). ^{13}C NMR (125 MHz, DMSO- d_6) δ : 173.01; 167.28; 164.75; 154.46; 130.44; 128.61; 122.04; 121.78; 114.73; 70.53; 54.79; 46.27. Anal. calcd. for $\text{C}_{15}\text{H}_{19}\text{ClN}_6\text{O}$: C 53.81%, H 5.72%, N 25.10%. Found: C 53.86%, H 5.86%, N 25.19%

5.1.1.2. 4-((3-Chlorophenoxy)methyl)-6-(4-methylpiperazin-1-yl)-1,3,5-triazin-2-amine (9). Method A. Pale yellow solid. Yield 30%, mp 140–141 °C. $\text{C}_{15}\text{H}_{19}\text{ClN}_6\text{O}$ (MW 334.80). LC/MS⁺: purity: 100%, $t_R = 3.45$, (ESI) m/z $[\text{M}+\text{H}]^+$ 335.31. ^1H NMR δ : 7.26 (t, $J = 8.1$ Hz, 1H-Ph), 7.00–6.86 (m, 2H, NH₂), 7.00 (m, 1H, Ph), 6.98–6.94 (m, 1H, Ph), 4.80 (s, 2H, CH₂), 3.65–3.62 (m, 4H, Pp-2,6-H), 2.24 (s, 4H, Pp-3,5-H), 2.15 (s, 3H, CH₃). ^{13}C NMR (125 MHz, DMSO- d_6) δ : 173.03; 167.29; 164.76; 159.95; 134.06; 131.27; 121.12; 115.38; 114.33; 70.25; 54.80; 46.28. Anal. calcd. for $\text{C}_{15}\text{H}_{19}\text{ClN}_6\text{O}$: C 53.81%, H 5.72%, N 25.10%. Found: C 53.80%, H 5.72%, N 25.20%

5.1.1.3. 4-((2-Isopropyl-5-methylphenoxy)methyl)-6-(4-methylpiperazin-1-yl)-1,3,5-triazin-2-amine (10). Method A. White solid. Yield 23%, mp 92–93 °C. $\text{C}_{19}\text{H}_{28}\text{N}_6\text{O}$ (MW 356.47). LC/MS⁺: purity: 100%, $t_R = 4.57$, (ESI) m/z $[\text{M}+\text{H}]^+$ 357.38. ^1H NMR δ : 7.02 (d, $J = 7.7$ Hz, 1H, Ph), 6.87 (br. s, 2H, NH₂), 6.71 (s, 1H, Ph), 6.67 (d, $J = 7.9$ Hz, 1H, Ph), 4.74 (s, 2H, CH₂), 3.65 (t, $J = 4.7$ Hz, 4H, Pp-2,6-H), 3.30–3.22 (m, 1H, CH), 2.25 (s, 4H, Pp-3,5-H), 2.20 (s, 3H, CH₃), 2.15 (s, 3H, CH₃), 1.14 (d, $J = 6.9$ Hz, 6H, 2x-CH₃). ^{13}C NMR (125 MHz, DMSO- d_6) δ : 173.70; 167.31; 164.93; 156.03; 136.14; 133.82; 126.09; 121.67; 113.31; 70.30; 54.80; 46.27; 26.76; 23.12; 21.52. Anal. calcd. for $\text{C}_{19}\text{H}_{28}\text{N}_6\text{O}$: C 60.88%, H 8.01%, N 22.43%. Found: C 60.60%, H 7.90%, N 22.39%

5.1.1.4. 4-(4-Methylpiperazin-1-yl)-6-(o-tolylloxymethyl)-1,3,5-triazin-2-amine (11). Method A. White solid. Yield 45%, mp 252–254 °C. $\text{C}_{16}\text{H}_{22}\text{N}_6\text{O}$ (MW 314.39). LC/MS⁺: purity: 100%, $t_R = 3.19$, (ESI) m/z $[\text{M}+\text{H}]^+$ 315.14. ^1H NMR δ : 7.12–7.04 (m, 2H, Ph-3,5-H), 6.83–6.77 (m, 4H, 2H, Ph-2,6-H, NH₂), 4.78 (s, 2H-CH₂), 3.65 (s, 4H, Pp-2,6-H), 2.25 (s, 4H, Pp-3,5-H), 2.18 (s, 3H, CH₃), 2.15 (s, 3H, CH₃). ^{13}C NMR (DMSO- d_6) δ : 173.62, 167.23, 164.78, 157.06, 130.83, 127.21, 126.33, 120.75, 112.18, 70.22, 54.72, 46.20, 16.60.

5.1.1.5. 4-(4-Methylpiperazin-1-yl)-6-(m-tolylloxymethyl)-1,3,5-triazin-2-amine (12). Method A. White solid. Yield 10%, mp 132–135 °C. $\text{C}_{16}\text{H}_{22}\text{N}_6\text{O}$ (MW 314.39). LC/MS⁺: purity: 100%, $t_R = 3.11$, (ESI) m/z $[\text{M}+\text{H}]^+$ 315.21. ^1H NMR δ : 7.11 (t, $J = 7.6$ Hz, 1H, Ph), 7.05–6.78 (br. s, 2H, NH₂), 6.78–6.61 (m, 3H, Ph), 4.72 (s, 2H, CH₂), 3.65 (s, 4H, Pp-2,6-H), 2.34–2.19 (m, 7H, 4H, Pp-3,5-H, Pp-CH₃), 2.16 (s, 3H, CH₃). ^{13}C NMR (125 MHz, DMSO- d_6) δ : 173.52, 167.34, 164.84, 159.00, 139.34, 129.64, 121.91, 115.91, 112.09, 70.12, 54.83, 46.29, 42.99, 21.65.

5.1.1.6. 4-(4-Methylpiperazin-1-yl)-6-(p-tolylloxymethyl)-1,3,5-triazin-2-amine (13). Method A. White solid. Yield 21%, mp 144–145 °C. $\text{C}_{16}\text{H}_{22}\text{N}_6\text{O}$ (MW 314.39). LC/MS⁺: purity: 96.95%, $t_R = 3.18$, (ESI) m/z $[\text{M}+\text{H}]^+$ 315.30. ^1H NMR δ : 7.03 (d, $J = 8.7$ Hz, 2H, Ph), 6.96–6.84 (m, 2H, NH₂), 6.78 (dd, $J_1 = 6.41$ Hz, $J_2 = 2.05$ Hz, 2H, Ph), 4.69 (s, 2H, CH₂), 3.64 (s, 4H, Pp-2,6-H), 2.25 (s, 4H, Pp-3,5-H), 2.20 (s, 3H, CH₃), 2.16 (s, 3H, CH₃). ^{13}C NMR (125 MHz, DMSO- d_6) δ : 173.60; 167.34; 164.85; 156.87; 130.23; 129.75; 114.98; 70.25; 54.83; 46.29; 20.59. Anal. calcd. for $\text{C}_{16}\text{H}_{22}\text{N}_6\text{O}$: C 61.13%, H 7.05%, N 26.73%. Found: C 61.10%, H 7.09%, N 26.69%

5.1.1.7. 4-((4-Chloro-2-methylphenoxy)methyl)-6-(4-methylpiperazin-1-yl)-1,3,5-triazin-2-amine (14). Method A. White solid. Yield 44%, mp 132–133 °C. $\text{C}_{16}\text{H}_{21}\text{ClN}_6\text{O}$ (MW 348.83). LC/MS^{+/−}: purity: 99.71%, $t_R = 4.05$, (ESI) m/z $[\text{M}+\text{H}]^+$ 349.33. ^1H NMR δ : 7.19 (d, $J = 2.6$ Hz, 1H, Ph), 7.11 (dd, $J_1 = 8.71$ Hz, $J_2 = 2.82$ Hz, 1H, Ph), 6.90 (br. s, 2H, NH₂), 6.83 (d, $J = 8.7$ Hz, 1H, Ph), 4.79 (s, 2H, CH₂), 3.63 (s, 4H, Pp-2,6-H), 2.24 (br. s, 4H, Pp-3,5-H), 2.17 (s, 3H, Ph-CH₃), 2.15 (s, 3H, CH₃). ^{13}C NMR (125 MHz, DMSO- d_6) δ : 173.46; 167.33; 164.84; 154.42; 148.32; 141.70; 108.46; 106.48; 101.51; 98.51; 71.06; 54.83; 46.29. Anal. calcd. for $\text{C}_{16}\text{H}_{21}\text{ClN}_6\text{O}$: C 55.09%, H 6.07%, N 24.09%. Found: C 55.31%, H 6.10%, N 24.19%

5.1.1.8. 4-((2,4-Dichlorophenoxy)methyl)-6-(4-methylpiperazin-1-yl)-1,3,5-triazin-2-amine (**15**). Method A. White solid. Yield 35%, mp 104–105 °C. C₁₅H₁₈Cl₂N₆O (MW 369.25). LC/MS⁺: purity: 100%, t_R = 4.06, (ESI) *m/z* [M]⁺ 369.28. ¹H NMR δ: 7.53 (d, *J* = 2.6 Hz, 1H, Ph), 7.29 (dd, *J*₁ = 8.86 Hz, *J*₂ = 2.56 Hz, 1H, Ph), 7.02 (d, *J* = 8.9 Hz, 1H-Ph), 6.95–6.88 (br s, 2H, NH₂), 4.91 (s, 2H, CH₂), 3.61 (s, 4H, Pp-2,6-H), 2.22 (br s, 4H, Pp-3,5-H), 2.15 (s, 3H, CH₃). ¹³C NMR (125 MHz, DMSO-*d*₆) δ: 172.69; 167.23; 164.68; 153.64; 129.72; 128.39; 124.94; 116.02; 70.58; 54.77; 46.27. Anal. calcd. for C₁₅H₁₈Cl₂N₆O: C 48.79%, H 4.91%, N 22.76. Found: C 49.1%, H 5.08%, N 22.63%

5.1.1.9. 4-((4-Chloro-3-methylphenoxy)methyl)-6-(4-methylpiperazin-1-yl)-1,3,5-triazin-2-amine (**16**). Method A. White solid. Yield 19%, mp 131–134 °C. C₁₆H₂₁N₆OCl (MW 348.83). LC/MS⁺: purity: 100%, t_R = 3.85, (ESI) *m/z* [M+H]⁺ 349.10. ¹H NMR δ: 7.24 (d, *J* = 8.7 Hz, 1H, Ph), 7.03–6.79 (m, 3H, Ph-5-H, NH₂), 6.74 (dd, *J*₁ = 3.1 Hz, *J*₂ = 9.0 Hz, 1H, Ph), 4.74 (s, 2H, CH₂), 3.64 (t, *J* = 4.5 Hz, 4H, Pp-2,6-H), 2.30–2.20 (m, 7H, Pp-3,5-H, CH₃), 2.16 (s, 3H, CH₃). ¹³C NMR (125 MHz, DMSO-*d*₆) δ: 173.20, 167.30, 164.78, 157.75, 136.82, 129.88, 125.17, 118.08, 117.65, 114.28, 70.27, 68.56, 54.81, 46.29, 42.95, 20.33.

5.1.1.10. 4-(1-(3-Chlorophenoxy)ethyl)-6-(4-methylpiperazin-1-yl)-1,3,5-triazin-2-amine (**17**). Method A. Brown solid. Yield 16%, mp 138 °C. C₁₆H₂₁N₆OCl (MW 348.83). LC/MS⁺: purity: 100%, t_R = 3.60, (ESI) *m/z* [M+H]⁺ 349.17. ¹H NMR δ: 7.25 (t, *J* = 8.1 Hz, 1H, Ph), 7.07–6.92 (m, 3H, Ph), 6.91–6.77 (m, 2H, NH₂), 4.95 (q, *J* = 6.5 Hz, 1H, CH), 3.66 (s, 4H, Pp-2,6-H), 2.27 (s, 4H, Pp-3,5-H), 2.18 (s, 3H, CH₃), 1.53 (d, *J* = 6.5 Hz, 3H, CH₃). ¹³C NMR (DMSO-*d*₆) δ: 176.59, 167.46, 164.89, 159.41, 133.90, 131.17, 120.85, 115.72, 114.61, 76.56, 54.69, 46.20, 20.59.

5.1.1.11. 11.4-(1-(2-Chlorophenoxy)ethyl)-6-(4-methylpiperazin-1-yl)-1,3,5-triazin-2-amine (**18**). Method A. White solid. Yield 30%, mp 156 °C. C₁₆H₂₁N₆OCl (MW 348.83). LC/MS⁺: purity: 100%, t_R = 3.57, (ESI) *m/z* [M+H]⁺ 349.17. ¹H NMR δ: 7.40 (dd, *J*₁ = 7.9 Hz, *J*₂ = 1.6 Hz, 1H, Ph), 7.30–6.93 (m, 3H-Ph), 7.00–6.80 (m, 2H, NH₂), 4.98 (q, *J* = 6.5 Hz, 1H, CH), 3.67 (s, 4H, Pp-2,6-H), 2.38–2.19 (m, 4H, Pp-3,5-H), 2.17 (s, 3H, CH₃), 1.57 (d, *J* = 6.5 Hz, 3H, CH₃). ¹³C NMR (DMSO-*d*₆) δ: 176.56, 167.44, 164.88, 154.01, 130.41, 128.46, 122.03, 121.87, 115.37, 77.20, 54.68, 46.21, 20.74.

5.1.1.12. 4-(4-Methylpiperazin-1-yl)-6-((phenylthio)methyl)-1,3,5-triazin-2-amine hydrochloride (**19**). Method B. White solid. Yield 33%; mp 250 °C. C₁₅H₂₁ClN₆S (MW 352.89, MW 316.15- basic form). LC/MS⁺: purity: 100%, t_R = 2.92, (ESI) *m/z* [M+H]⁺ 317.14. ¹H NMR δ: 11.95 (br. s, 1H, NH⁺), 8.40–7.87 (br, 2H, NH₂), 7.49–7.46 (m, 2H, Ph), 7.36–7.33 (m, 2H, Ph), 7.27–7.23 (m, 1H, Ph), 4.13 (s, 2H, CH₂), 3.45 (s, 4H, Pp-2,6-H), 3.16–2.72 (m, 7H, Pp-3,5-H, CH₃). ¹³C NMR (MeOD-*d*₄) δ: 166.58, 161.54, 157.07, 132.88, 131.30, 128.97, 127.72, 52.30, 52.03, 42.08, 40.73, 40.55, 36.62.

5.1.1.13. 13-((2-Chlorophenyl)thio)methyl)-6-(4-methylpiperazin-1-yl)-1,3,5-triazin-2-amine (**20**). Method A. White solid. Yield 37%, mp 170 °C. C₁₅H₁₉ClN₆S (MW 350.11). LC/MS⁺: purity: 98.94%, t_R = 3.40, (ESI) *m/z* [M+H]⁺ 351.36. ¹H NMR δ: 7.58 (dd, *J*₁ = 8.0 Hz, *J*₂ = 1.4 Hz, 1H, Ph-3-H), 7.41 (dd, *J*₁ = 7.9 Hz, *J*₂ = 1.4 Hz, 1H, Ph-6H), 7.27 (td, *J*₁ = 7.7 Hz, *J*₂ = 1.4 Hz, 1H, Ph-5-H), 7.18–7.11 (m, 1H, Ph-4-H), 6.97–6.87 (br, 2H, NH₂), 3.94 (s, 2H, CH₂), 3.67–3.60 (m, 4H, Pp-2,6-H), 2.24 (s, 4H, Pp-3,5-H), 2.15 (s, 3H-CH₃). ¹³C NMR (DMSO-*d*₆) δ: 173.78, 167.24, 164.67, 136.51, 131.00, 129.67, 128.15, 128.01, 126.76, 54.72, 49.00, 46.20.

5.1.1.14. 4-(1-((2-Chlorophenyl)thio)ethyl)-6-(4-methylpiperazin-1-yl)-1,3,5-triazin-2-amine hydrochloride (**21**). Method B. White solid. Yield 65%, mp 271 °C. C₁₆H₂₂Cl₂N₆S (MW 401.36, MW 364.12 – basic form). LC/MS⁺: purity: 99.49%, t_R = 3.90, (ESI) *m/z* [M+H]⁺ 365.12. ¹H NMR δ: 11.87 (br. s, 1H, NH⁺), 8.05 (br, 2H, NH₂), 7.66 (dd, *J*₁ = 7.5 Hz, *J*₂ = 1.7 Hz, 1H, Ph), 7.53 (m, 1H, Ph), 7.39–7.29 (m, 2H, Ph), 4.39 (q, *J* = 7.0 Hz, 1H, CH), 3.46 (d, *J* = 10.5 Hz, 4H, Pp-2,6-H), 2.92 (m, 7H, Pp-3,5-H, Pp-CH₃), 1.60 (d, *J* = 7.0 Hz, 3H, CH₃). ¹³C NMR (DMSO-*d*₆) δ: 171.21, 162.27, 160.33, 135.37, 133.83, 132.24, 130.34, 130.32, 128.40, 51.92, 45.03, 42.42, 18.04.

5.1.1.15. 4-(4-Methylpiperazin-1-yl)-6-((phenylselenenyl)methyl)-1,3,5-triazin-2-amine hydrochloride (**22**). Method A. White solid. Yield 39%; mp 249 °C. C₁₅H₂₀N₆Se (MW 364.09). LC/MS⁺: purity: 100%, t_R = 2.82, (ESI) *m/z* [M+H]⁺ 365.12. ¹H NMR δ: 7.60–7.47 (m, 2H, Ph), 7.31–7.15 (m, 3H, Ph), 6.85 (s, 2H, NH₂), 3.82 (d, *J* = 5.4 Hz, 2H, CH₂), 3.60 (s, 4H, Pp-2,6-H), 2.23 (s, 4H, Pp-3,5-H), 2.15 (s, 3H, CH₃). ¹³C NMR (DMSO-*d*₆) δ: 175.48, 171.16, 167.35, 164.82, 134.10, 131.78, 131.40, 130.45, 129.49, 129.25, 127.03, 125.59, 54.77, 46.23, 42.84, 34.62, 33.19.

5.1.1.16. 4-(4-Methylpiperazin-1-yl)-6-(1-(phenylselenenyl)ethyl)-1,3,5-triazin-2-amine hydrochloride (**23**). White solid. Yield 12%; mp 238 °C. C₁₆H₂₃ClN₆Se (MW 413.81, MW 378.11- basic form). LC/MS⁺: purity: 100%, t_R = 3.23, (ESI) *m/z* [M+H]⁺ 379.08. ¹H NMR δ: 11.88 (br. s, 1H, NH⁺), 8.16 (br, 2H, NH₂), 7.56 (d, *J* = 6.7 Hz, 2H, Ph), 7.38 (m, 3H, Ph), 4.32 (q, *J* = 7.1 Hz, 1H, CH), 3.45 (s, 4H, Pp-2,6-H), 2.75 (s, 7H, Pp-3,5-H, Pp-CH₃), 1.61 (s, 3H, CH₃). ¹³C NMR δ: 162.14, 136.07, 131.31, 129.97, 129.62, 129.20, 128.32, 51.75, 42.45, 42.37, 22.49, 18.24.

5.1.2. Synthesis of 4-(((2-chlorophenyl)sulfonyl)methyl)-6-(4-methylpiperazin-1-yl)-1,3,5-triazin-2-amine (**24**)

A solution of **20** (2 mmol, 701 mg) in ethanol (4 ml) was cooled to 0 °C and sodium tungstate dehydrate (Na₂WO₄·2H₂O) (0.23 mmol, 303 mg) was added. After 5 min at 0 °C, 35% aqueous solution of H₂O₂ (4.5 ml) was added dropwise. The resulting mixture was stirred at 0 °C for 30 min. Subsequently, the reaction mixture was stirred at room temperature for 24 h. Saturated aqueous sodium thiosulfate anhydrous Na₂S₂O₃ (15 mL) was added and resulting layers were separated. The aqueous layer was extracted with ethyl acetate three times and the combined organic layers was washed with brine, dried over MgSO₄ anhydrous, filtered and the solvents was removed under reduced pressure. The pure product was obtained by recrystallization from methanol to give beige crystals of desired product.

White solid. Yield 37%, mp 170 °C. C₁₅H₁₉ClN₆O₂S (MW 382.10). LC/MS⁺: purity: 93.49%, t_R = 2.77, (ESI) *m/z* [M+H]⁺ 383.20. ¹H NMR δ: 7.80 (d, *J* = 7.1 Hz, 1H, Ph-3-H), 7.66–7.55 (m, 3H, Ph-4,5,6-H), 7.13–7.00 (m, 2H, NH₂), 4.06 (m, 2H, CH₂), 3.68 (m, 8H, Pp), 1.11 (s, 3H, CH₃). ¹³C NMR (125 MHz, MeOD-*d*₄) δ: 170.24, 168.40, 165.75, 134.02, 131.79, 131.14, 129.45, 127.22, 65.82, 59.93, 38.69.

5.2. Molecular modelling procedures

The procedure of 5-HT₆R homology models generation based on the β₂ adrenergic receptor template and these further validation for the support of structure-activity relationship analyses of our earlier 1,3,5-triazine derivatives was described previously [15,16]. In order to select the best subset of the receptor conformations, all the newly synthesized derivatives (**7–24**) were docked. Only models showing coherent binding mode to the previously described triazine derivatives and explained the main structure-activity relationships were used.

The LigPrep [34] and Epik [35] were used to prepare the 3-

dimensional structures and to assigned appropriate ionization states at $\text{pH} = 7.4 \pm 1.0$ of the ligands, respectively. If not specified, the all possible R/S or Z/E isomers were generated and used in the docking. The Protein Preparation Wizard was used to assign the bond orders, appropriate amino acid ionization states and to check for steric clashes. The receptor grid was generated (OPLS3 force field [36]) by centering the grid box with a size of 12 Å on the D3.32 side chain. Automated flexible docking was performed using Glide at SP level [37]. All of the used programs are a part of Schrödinger Suite.

5.3. Radioligand binding assay

Radioligand binding assays to determine affinities of the tested compounds towards 5-HT₆R and competitive GPCRs were carried out, using [³H]-8-OH-DPAT (135.2 Ci/mmol), [³H]-Ketanserin (53.4 Ci/mmol), [³H]-LSD (83.6 Ci/mmol), [³H]-5-CT (80.1 Ci/mmol) and [³H]-Raclopride (76.0 Ci/mmol) for 5-HT_{1A}, 5-HT_{2A}, 5-HT₆, 5-HT₇ and D₂, respectively. Non-specific binding is defined with 10 mM of 5-HT in 5-HT_{1A}R and 5-HT₇R binding experiments, whereas 10 mM of chlorpromazine, 10 mM of methiothepine or 10 mM of haloperidol were used in 5-HT_{2A}R, 5-HT₆R and D₂L assays, respectively. Each compound was tested in triplicate at 7–8 concentrations (10^{-11} – 10^{-4} M). The inhibition constants (K_i) were calculated from the Cheng-Prusoff equation [38]. HEK293 cells with stable expression of human serotonin 5-HT_{1A}R, 5-HT₆R, 5-HT_{7b}R or dopamine D_{2L}R as well as CHO–K1 cells with stable expression of human serotonin 5-HT_{2A}R purchased from PerkinElmer BioSignal Inc were used in the assays, according to the procedures described previously [14–17].

5.4. Functional assays for 5-HT₆ receptor

Test and reference compounds were dissolved in dimethyl sulfoxide (DMSO) at a concentration of 1 mM. Serial dilutions were prepared in 96-well microplate in assay buffer and 8 to 10 concentrations were tested. A cellular aequorin-based functional assay was performed with recombinant CHO–K1 cells expressing mitochondrially targeted aequorin, human GPCR and the promiscuous G protein $\alpha 16$ for 5-HT₆R. Assay was executed according to previously described protocol [39]. After thawing, cells were transferred to assay buffer (DMEM/HAM's F12 with 0.1% protease free BSA) and centrifuged. The cell pellet was resuspended in assay buffer and coelenterazine h was added at final concentrations of 5 μM . The cells suspension was incubated at 16 °C, protected from light with constant agitation for 16 h and then diluted with assay buffer to the concentration of 100,000 cells/ml. After 1 h of incubation, 50 μl of the cell's suspension was dispensed using automatic injectors built into the radiometric and luminescence plate counter MicroBeta2 LumijET (PerkinElmer, USA) into white opaque 96-well microplates preloaded with test compounds. Immediate light emission generated following calcium mobilization was recorded for 60 s. In antagonist mode, after 30 min of incubation the reference agonist was added to the above assay mix and light emission was recorded again. Final concentration of the reference agonist was equal to EC80 (40 nM serotonin).

5.5. Safety in vitro

SH-SY5Y (ATCC[®] CRL-2266[™]) cell line was purchased from American Type Culture Collection ATCC (Manassas, VA, USA). The CellTiter 96[®] AQueous Non-Radioactive Cell Proliferation Assay (MTS) was purchased from Promega (Madison, WI, USA). The cells were cultured in Dulbecco's Modified Eagle's Medium (DMEM/F12) with 10% fetal bovine serum (FBS) (Gibco, Carlsbad, CA, USA) at

37 °C in an atmosphere containing 5% of CO₂. The cells were seeded in 96-well plates at a concentration of 1.5×10^4 cells/well in 100 μl culture medium and cultured for 24 h to reach 60% confluence. The 10 mM stock solutions of 5-HT₆R ligands in DMSO were diluted into fresh growth medium and added into the microplates at the final concentrations 0.1–100 μM (DMSO concentration did not exceed 1%). After 72 h of incubation, the MTS labeling mixture was added to the each well, and the cells were incubated under the same conditions for 5 h. The absorbance of the samples was measured using a microplate reader EnSpire (PerkinElmer, Waltham, MA USA) at 490 nm. Each compound was tested in at least three repetitions. GraphPad Prism[™] software (version 5.01, San Diego, CA, USA) was used to calculate statistical significances.

The *Salmonella typhimurium* TA100 strain with base pair substitution (hisG46 mutation, which target is GGG) was purchased from Xenometrix, Allschwil, Switzerland. The reference mutagen nonyl-4-hydroxyquinoline-N-oxide (NQNO) was purchased from Sigma-Aldrich, (St. Louis, MO, USA). All experiments were performed as described before [40,41]. The mutagenic potential was calculated according to the procedure provided by Xenometrix [32]. Each compound was tested in triplicate.

5.6. In vivo studies

5.6.1. Animals

The experiments were performed on male Wistar rats (200–250 g) obtained from an accredited animal facility at the Jagiellonian University Medical College, Poland. The animals were housed in group of four in controlled environment (ambient temperature 21 ± 2 °C; relative humidity 50–60%; 12-h light/dark cycles (lights on at 8:00). Standard laboratory food (LSM-B) and filtered water were freely available. Animals were assigned randomly to treatment groups. All the experiments were performed by two observers unaware of the treatment applied between 9:00 and 14:00 on separate groups of animals. All animals were used only once. Procedures involving animals and their care were conducted in accordance with current European Community and Polish legislation on animal experimentation. Additionally, all efforts were made to minimize animal suffering and to use only the number of animals necessary to produce reliable scientific data. Animal testing was limited to the study only for compounds that have previously demonstrated enough interest in *in vitro* experiments. The experimental protocols and procedures described in this manuscript were approved by the I Local Ethics Commission in Cracow (no 293/2015) and complied with the EU Directive 2010/63/EU for animal experiments, and were in accordance with the National Institutes of Health guide for the care and use of Laboratory animals (NIH Publications No. 8023, revised 1978).

5.6.2. Drugs

The following drugs were administered: **SB-399885** (N-[3,5-dichloro-2-(methoxy)-phenyl]-4-(methoxy)-1-(piperazinyl)benzenesulfonamide; GlaxoSmithKline, UK).

All the compounds were suspended in 1% Tween 80 immediately before administration in a volume of 2 ml/kg. Compounds investigated were administered intraperitoneally (*i.p.*) 60 min, while **SB-399885** *i.p.* 30 min before testing. Control animals received vehicle (1% Tween 80) according to the same schedule.

5.6.3. Behavioral procedures in rats

5.6.3.1. Forced swim test (FST test). The experiment was carried out according to the method of Borsini and Meli [30]. On the first day of an experiment, the animals were gently individually placed in Plexiglas cylinders (40 cm high, 18 cm in diameter) containing 15 cm of water maintained at 23–25 °C for 15 min. On removal

from water, the rats were placed for 30 min in a Plexiglas box under 60-W bulb to dry. On the following day (24 h later), the rats were re-placed in the cylinder and the total duration of immobility was recorded during the whole 5-min test period. The immobility was assigned when no additional activity was observed other than that necessary to keep the rat's head above the water. Fresh water was used for each animal.

5.6.3.2. Open field (OF) test. The experiment was performed employing a Motor Monitor System (Campden Instruments, Ltd., UK) consisting of two SmartFrame Open Field stations (40 x 40 x 38 cm) with 16 x 16 beams, located in sound attenuating chambers and connected to PC software by control chassis. Individual vehicle- or drug-injected animals were gently placed in the center of the station. An automated Motor Monitor System recorded ambulation (in X and Y axis), the number of rearing episodes, and total distance covered by a rat for 5 min.

5.6.4. Statistical analysis

The data of behavioral studies were evaluated by an analysis of variance one-way ANOVA followed by Bonferroni's post hoc test (statistical significance set at $p < 0.05$).

Acknowledgements

Authors thank Prof. Andrzej J. Bojarski for the opportunity to conduct RBA and MM studies in his Department. Authors thank Prof. Claus Jacob, the tutor of PhD-students Wesam Ali and Jawad Nasim, for his contribution in chemical, not biological, part of this study (supervision of Se-intermediates synthesis). This study was financially supported by National Science Centre, Poland grants: No UMO-2015/17/B/NZ7/02973, UMO-2016/21/N/NZ7/03265 (Safety studies *in vitro*) and DEC-2011/02/A/NZ4/00031 (synthesis of 7–11). Wesam Ali was financed by Saarland University, "Landesforschungsförderungsprogramm" (Grant No. WT/2 – LFFP 16/01).

Appendix A. Supplementary data

Supplementary data to this article can be found online at <https://doi.org/10.1016/j.ejmech.2019.06.022>.

References

- [1] M.L. Woolley, C.A. Marsden, K.C. Fone, 5-HT₆ receptors, *Curr. Drug Targets - CNS Neurol. Disord.* 3 (2004) 59–79.
- [2] K. Wicke, A. Haupt, A. Bespalov, Investigational drugs targeting 5-HT₆ receptors for the treatment of Alzheimer's disease, *Expert Opin. Investig. Drugs* 24 (2015) 1515–1528.
- [3] M. Kołaczkowski, M. Marcinkowska, A. Bucki, J. Śniecikowska, M. Pawłowski, G. Kazek, A. Siwek, M. Jastrzębska-Więsek, A. Partyka, A. Wasik, A. Wesolowska, P. Mierzejewski, P. Bienkowski, Novel 5-HT₆ receptor antagonists/D₂ receptor partial agonists targeting behavioral and psychological symptoms of dementia, *Eur. J. Med. Chem.* 92 (2015) 221–235.
- [4] C. Mattsson, P. Svensson, H. Boettcher, C. Sonesson, Structure activity relationship of 5-chloro-2-methyl-3-(1,2,3,6-tetrahydropyridin-4-yl)-1H-indole analogues as 5-HT₆ receptor agonists, *Eur. J. Med. Chem.* 63 (2013) 578–588.
- [5] M. Kotańska, K. Lustyk, A. Bucki, M. Marcinkowska, J. Śniecikowska, M. Kołaczkowski, Idalopirdine, a selective 5-HT₆ receptor antagonist, reduces food intake and body weight in a model of excessive eating, *Metab. Brain Dis.* 33 (2018) 733–740.
- [6] S.E. Shortall, O. Negm, M. Fowler, L.C. Fairclough, P.J. Tighe, P.M. Wigmore, M.V. King, Characterization of behavioral, signaling and cytokine alterations in a rat neurodevelopmental model for schizophrenia, and their reversal by the 5-HT₆ receptor antagonist SB-399885, *Mol. Neurobiol.* 55 (2018) 7413–7430.
- [7] A. Więckowska, T. Wichur, J. Godyń, A. Bucki, M. Marcinkowska, A. Siwek, K. Więckowski, P. Zaręba, D. Knez, M. Giuch-Lutwin, G. Kazek, G. Latacz, K. Mika, M. Kołaczkowski, J. Korabecny, O. Soukup, M. Benkova, K. Kieć-Kononowicz, S. Gobec, B. Malawska, Novel multitarget-directed ligands aiming at symptoms and causes of Alzheimer's disease, *ACS Chem. Neurosci.* 9 (2018) 1195–1214.
- [8] J.R. Hong, H. Choo, G. Nam, Neuropathic pain-alleviating effects of pyrazole-conjugated arylsulfonamides as 5-HT₆ receptor antagonists, *Bioorg. Med. Chem. Lett* 27 (2017) 4146–4149.
- [9] A. Wesolowska, Potential role of the 5-HT₆ receptor in depression and anxiety: an overview of preclinical data, *Pharmacol. Rep.* 62 (2010) 564–577.
- [10] H.M. Yun, H. Rhim, The serotonin-6 receptor as a novel therapeutic target, *Exp. Neurobiol.* 20 (2011) 159–168.
- [11] M. Jastrzębska-Więsek, A. Siwek, A. Partyka, M. Kołaczkowski, M. Walczak, M. Smolik, G. Latacz, K. Kieć-Kononowicz, A. Wesolowska, Study on the effect of EMD386088, a 5-HT₆ receptor partial agonist, in enhancing the anti-immobility action of some antidepressants in rats, *Naunyn-Schmiedeberg's Arch. Pharmacol.* 391 (2018) 37–49.
- [12] C.H. Fabritius, U. Pesonen, J. Messenger, R. Horvath, H. Salo, M. Gałęzowski, M. Galek, K. Stefanska, J. Szeremeta-Spisak, M. Olszak-Plachta, A. Buda, J. Adamczyk, M. Król, P. Prusis, M. Sieprawska-Lupa, M. Mikulski, K. Kuokkanen, H. Chapman, R. Obuchowicz, T. Korjamo, N. Jalava, M. Nowak, 1-Sulfonyl-6-Piperazinyl-7-Azaindoles as potent and pseudoselective 5-HT₆ receptor antagonists, *Bioorg. Med. Chem. Lett* 26 (2016) 2610–2615.
- [13] K. Grychowska, G. Satała, T. Kos, A. Partyka, E. Colacino, S. Chaumont-Dubel, X. Bantreil, A. Wesolowska, M. Pawłowski, J. Martinez, P. Marin, G. Subra, A.J. Bojarski, F. Lamaty, P. Popik, P. Zajdel, Novel 1H-Pyrrolo[3,2-c]quinoline based 5-HT₆ receptor antagonists with potential application for the treatment of cognitive disorders associated with Alzheimer's disease, *ACS Chem. Neurosci.* 7 (2016) 972–983.
- [14] D. Vanda, M. Soural, V. Canale, S. Chaumont-Dubel, G. Satała, T. Kos, P. Funk, V. Fülöpová, B. Lemrová, P. Koczurkiewicz, E. Pękala, A.J. Bojarski, P. Popik, P. Marin, P. Zajdel, Novel non-sulfonamide 5-HT₆ receptor partial inverse agonist in a group of imidazo[4,5-b]pyridines with cognition enhancing properties, *Eur. J. Med. Chem.* 144 (2017) 716–729.
- [15] D. Łażewska, R. Kurczab, M. Więcek, K. Kamińska, G. Satała, M. Jastrzębska-Więsek, A. Partyka, A.J. Bojarski, A. Wesolowska, K. Kieć-Kononowicz, J. Handzlik, The computer-aided discovery of novel family of the 5-HT₆ serotonin receptor ligands among derivatives of 4-benzyl-1,3,5-triazine, *Eur. J. Med. Chem.* 28 (2017) 117–124.
- [16] D. Łażewska, R. Kurczab, M. Więcek, G. Satała, K. Kieć-Kononowicz, J. Handzlik, Synthesis and computer-aided analysis of the role of linker for novel ligands of the 5-HT₆ serotonin receptor among substituted 1,3,5-triazinylpiperazines, *Bioorg. Chem.* 26 (2018) 319–325.
- [17] R. Kurczab, W. Ali, D. Łażewska, M. Kotańska, M. Jastrzębska-Więsek, G. Satała, M. Więcek, A. Lubelska, G. Latacz, A. Partyka, M. Starek, M. Dąbrowska, A. Wesolowska, C. Jacob, K. Kieć-Kononowicz, J. Handzlik, Computer-aided studies for novel arylhydantoin 1,3,5-triazine derivatives as 5-HT₆ serotonin receptor ligands with antidepressant-like, anxiolytic and antiobesity action *in vivo*, *Molecules* 23 (2018) 1–26, 2529.
- [18] G.I. Giles, M.J. Nasim, W. Ali, C. Jacob, The reactive sulfur species concept: 15 Years on, *Antioxidants* 6 (2017) 1–29, 38.
- [19] M.J. Nasim, W. Ali, E. Domínguez-Álvarez, E. Júnior, R. Saleem, C. Jacob, Reactive selenium species, in: V.K. Jain, K.I. Priyadarini (Eds.), *Organoselenium Compounds in Biology and Medicine: Synthesis, Biological and Therapeutic Treatments*, Royal Society of Chemistry, 2017, pp. 277–302.
- [20] J.T.D. Rocha, B.M. Gai, S. Pinton, T.B. Sampaio, C.W. Nogueira, G. Zeni, Effects of diphenyl diselenide on depressive-like behavior in ovariectomized mice submitted to subchronic stress: involvement of the serotonergic system, *Psychopharmacology* 222 (2012) 709–719.
- [21] G.R. Dias, T.M.D. Almeida, J.H. Sudati, F. Dobrachinski, S. Pavin, F.A. Soares, C.W. Nogueira, N.B. Barbosa, Diphenyl diselenide supplemented diet reduces depressive-like behavior in hypothyroid female rats, *Physiol. Behav.* 124 (2014) 116–122.
- [22] M.P. Pinz, A.S.D. Reis, A.G. Vogt, R. Krüger, D. Alves, C.R. Jesse, S.S. Roman, M.P. Soares, E.A. Wilhelm, C. Luchese, Current advances of pharmacological properties of 7-chloro-4-(phenylselenanyl) quinoline: prevention of cognitive deficit and anxiety in Alzheimer's disease model, *Biomed. Pharmacother.* 105 (2018) 1006–1014.
- [23] C.E.S. Oliveira, B.M. Gai, B. Godoi, G. Zeni, C.W. Nogueira, The antidepressant-like action of a simple selenium-containing molecule, methyl phenyl selenide, in mice, *Eur. J. Pharmacol.* 690 (2012) 119–223.
- [24] V. Glaser, B. Moritz, A. Schmitz, A.L. Dafré, E.M. Nazari, Y.M.R. Müller, L. Felksa, M.R. Straliootta, A.F.D. Bem, M. Farina, J.B.T. da Rocha, A. Latini, Protective effects of diphenyl diselenide in a mouse model of brain toxicity, *Chem. Biol. Interact.* 206 (2013) 18–26.
- [25] R. Moszczyński-Pętkowski, J. Majer, M. Borkowska, L. Bojarski, S. Janowska, M. Matłoka, F. Stefaniak, D. Smuga, K. Bazydio, K. Dubiel, M. Wiecezorek, Synthesis and characterization of novel classes of PDE10A inhibitors - 1H-1,3-benzodiazoles and imidazo[1,2-a]pyrimidines, *Eur. J. Med. Chem.* 15 (2018) 96–116.
- [26] D. Łażewska, M. Więcek, J. Ner, K. Kaminska, T. Kottke, J.S. Schwed, M. Zygmunt, T. Karcz, A. Olejarz, K. Kuder, G. Latacz, M. Grosicki, J. Sapa, J. Karolak-Wojciechowska, H. Stark, K. Kieć-Kononowicz, Aryl-1,3,5-triazine derivatives as histamine H₄ receptor ligands, *Eur. J. Med. Chem.* 83 (2014) 534–546.
- [27] R.D. Porsolt, A. Bertin, M. Jalfre, Behavioural despair" in rats and mice: strain differences and the effects of imipramine, *Eur. J. Pharmacol.* 51 (1978) 291–294.
- [28] A. Wesolowska, A. Nikiforuk, Effects of the brain-penetrant and selective 5-HT₆ receptor antagonist SB-399885 in animal models of anxiety and depression, *Neuropharmacology* 52 (2007) 274–283.

- [29] F. Borsini, Role of the serotonergic system in the forced swimming test, *Neurosci. Biobehav. Rev.* 19 (1995) 377–395.
- [30] F. Borsini, A. Meli, Is the forced swimming test a suitable model for revealing antidepressant activity? *Psychopharmacology* 94 (1988) 147–160.
- [31] A. Wesolowska, A. Nikiforuk, K. Stachowicz, Anxiolytic-like and antidepressant-like effects produced by the selective 5-HT₆ receptor antagonist SB-258585 after intrahippocampal administration to rats, *Behav. Pharmacol.* 18 (2007) 439–446.
- [32] S. Fluckiger-Isler, A. Baumeister, K. Braun, V. Gervais, N. Hasler-Nguyen, R. Reimann, J. Van Gompel, H.G. Wunderlich, G. Engelhardt, Assessment of the performance of the Ames II (TM) assay: a collaborative study with 19 coded compounds, *Mutat. Res.* 558 (2004) 181–197.
- [33] Y.A. Ivanenkov, A.G. Majouga, M.S. Veselov, N.V. Chufarova, S.S. Baranovsky, G.I. Filkov, Computational approaches to the design of novel 5-HT₆ R ligands, *Rev. Neurosci.* 25 (2014) 451–467.
- [34] Schrödinger Release 2018-4, LigPrep, Schrödinger, LLC, New York, NY, 2018.
- [35] Schrödinger Release 2018-4, Epik, Schrödinger, LLC, New York, NY, 2018.
- [36] E. Harder, W. Damm, J. Maple, C. Wu, M. Reboul, J.Y. Xiang, L. Wang, D. Lupyán, M.K. Dahlgren, J.L. Knight, J.W. Kaus, D.S. Cerutti, G. Krilov, W.L. Jorgensen, R. Abel, R.A. Friesner, OPLS3: a force field providing broad coverage of drug-like small molecules and proteins, *J. Chem. Theory Comput.* 12 (2016) 281–296.
- [37] Schrödinger Release 2018-4: Glide, Schrödinger, LLC, New York, NY, 2018.
- [38] Y. Cheng, W.H. Prusoff, Relationship between the inhibition constant (K_i) and the concentration of inhibitor which causes 50 per cent inhibition (I₅₀) of an enzymatic reaction, *Biochem. Pharmacol.* 22 (1973) 3099–3108.
- [39] M. Kołaczkowski, M. Marcinkowska, A. Bucki, M. Pawłowski, K. Mitka, J. Jaśkowska, P. Kowalski, G. Kazeł, A. Siwek, A. Wasik, A. Wesolowska, P. Mierzejewski, P. Bienkowski, Novel arylsulfonamide derivatives with 5-HT₆/5-HT₇ receptor antagonism targeting behavioral and psychological symptoms of dementia, *J. Med. Chem.* 57 (2014) 4543–4557.
- [40] G. Latacz, A. Lubelska, M. Jastrzebska-Wiesek, A. Partyka, A. Sobito, A. Olejarz, K. Kucwaj-Brysz, G. Satala, A.J. Bojarski, A. Wesolowska, K. Kiec-Kononowicz, J. Handzlik, In the search for a lead structure among series of potent and selective hydantoin 5-HT₇R agents: the drug-likeness *in vitro* study, *Chem. Biol. Drug Des.* 90 (2017) 1295–1306.
- [41] G. Latacz, A. Lubelska, M. Jastrzebska-Więsek, A. Partyka, K. Kucwaj-Brysz, A. Wesolowska, J. Handzlik, K. Kieć-Kononowicz, MF-8, a novel promising arylpiperazine-hydantoin based 5-HT₇ receptor antagonist: *in vitro* drug-likeness studies and *in vivo* pharmacological evaluation, *Bioorg. Med. Chem. Lett* 28 (2018) 878–883.

3.3. Publication 3

Discovery of phenylselenoether-hydantoin hybrids as ABCB1 efflux pump modulating agents with cytotoxic and antiproliferative actions in resistant T-lymphoma.

Wesam Ali, Gabriella Spengler, Annamaria Kincses, Marta Nove, Cecilia Battistelli, Gniewomir Latacz, Małgorzata Starek, Monika Dąbrowska, Ewelina Honkisz-Orzechowska, Annalisa Romanelli, Manuela Monica Rasile, Ewa Szymanska, Claus Jacob, Clemens Zwergel and Jadwiga Handzlik.

European Journal of Medicinal Chemistry 2020, 200, 112435.



Contents lists available at ScienceDirect

European Journal of Medicinal Chemistry

journal homepage: <http://www.elsevier.com/locate/ejmech>

Research paper

Discovery of phenylselenoether-hydantoin hybrids as ABCB1 efflux pump modulating agents with cytotoxic and antiproliferative actions in resistant T-lymphoma

Wesam Ali ^{a,b}, Gabriella Spengler ^c, Annamária Kincses ^c, Márta Nové ^c, Cecilia Battistelli ^d, Gniewomir Latacz ^a, Małgorzata Starek ^e, Monika Dąbrowska ^e, Ewelina Honkisz-Orzechowska ^a, Annalisa Romanelli ^f, Manuela Monica Rasile ^f, Ewa Szymańska ^a, Claus Jacob ^{b,**}, Clemens Zwergel ^{b,f,g,***}, Jadwiga Handzlik ^{a,*}

^a Department of Technology and Biotechnology of Drugs, Jagiellonian University, Medical College, Medyczna 9, PL 30-688, Kraków, Poland

^b Division of Bioorganic Chemistry, School of Pharmacy, Saarland University, Campus B 2.1, D-66123, Saarbruecken, Germany

^c Institute of Medical Microbiology and Immunobiology, Faculty of Medicine, University of Szeged, Dóm tér 10, H-6720, Szeged, Hungary

^d Istituto Pasteur Italia, Fondazione Cenci-Bolognetti, Department of Molecular Medicine, "Department of Excellence 2018-2022", Sapienza University of Rome, Viale Regina Elena 324, 00161, Rome, Italy

^e Department of Inorganic Chemistry, Jagiellonian University, Medical College, Medyczna 9, PL 30-688, Cracow, Poland

^f Department of Drug Chemistry and Technologies, "Department of Excellence 2018-2022", Sapienza University of Rome, Piazzale Aldo Moro 5, 00185 Rome, Italy

^g Department of Precision Medicine, "Luigi Vanvitelli" University of Campania, Via L. De Crecchio 7, 80138 Naples, Italy

ARTICLE INFO

Article history:

Received 11 February 2020

Received in revised form

23 April 2020

Accepted 6 May 2020

Available online 15 May 2020

Keywords:

MDR

Selenoether

ABCB1

P-glycoprotein inhibitor

T-lymphoma

JURKAT

ABSTRACT

Multidrug resistance (MDR) in cancer cells is a crucial aspect to consider for a successful cancer therapy. P-gp/ABCB1, a member of ABC transporters, is involved in the main tumour MDR mechanism, responsible for the efflux of drugs and cytotoxic substances. Herein, we describe a discovery of potent selenium-containing ABCB1 MDR efflux pump modulators with promising anticancer activity. On three groups of selenoethers comprehensive studies in terms of design, synthesis, and biological assays, including an insight into cellular mechanisms of anticancer action as well as an ADMET-screening *in vitro* were performed, followed by in-depth SAR analysis. Among the investigated new phenylselenoether hybrids, four compounds showed significant cytotoxic and anti-proliferative effects, in particular, in resistant cancer cells. Hydantoin derivatives (**5–7**) were significantly more effective than the reference inhibitor verapamil (up to 2.6-fold at a 10-fold lower concentration) modulating ABCB1-efflux pump, also possessing a good drug-drug interaction profile. The best compound (**6**) was further evaluated in human JURKAT T-lymphocytic cancer cells for its impact on cell proliferation rate. Mechanistically, the expression of cyclin D1, an enhancer of the cell cycle, decreases, while p53, an inhibitor of cell proliferation, was up-regulated upon the treatment with compound **6** alone or in combination with the chemotherapeutic agent doxorubicin. In summary, a new chemical space of highly active selenium-containing anticancer agents has been discovered, with a new lead compound **6** that warrants more in-depth biological evaluation and further pharmacomodulation.

© 2020 Elsevier Masson SAS. All rights reserved.

1. Introduction

During the last decades, numerous new classes of anti-cancer drugs emerged, which usually support the natural body defence. At the same time, the cancer cells developed different mechanisms to face the cytotoxic effect of these drugs. In this field, the term of multidrug resistance (MDR) is defined as the low sensitivity for

* Corresponding author affiliated with a

** Corresponding author affiliated with b

*** Corresponding author affiliated with b,f,g

E-mail addresses: c.jacob@mx.uni-saarland.de (C. Jacob), clemens.zwergel@uniroma1.it (C. Zwergel), j.handzlik@uj.edu.pl (J. Handzlik).

certain cells against drugs, often found in cancer for tumour therapy [1–5]. MDR is now a deeply investigated issue in the field of chemotherapy. It can result in the upregulation of drug efflux/drug efflux pumps, cell growth, and survival signalling. MDR can also be related to the down-regulation of apoptosis signals or drug uptakes.

Nevertheless, key players of the MDR action are ATP-binding cassette (ABC) transporters, such as the P-glycoprotein (Pgp, ABCB1), MRP1 (ABCC1) and BCRP (ABCG2) ones [6], which are involved in essential processes in cancer cells' defence. Moreover, the inhibition of these transporters could be beneficial to overcome drug resistance [7]. In more detail, P-glycoprotein/ABCB1 (P-gp/ABCB1) is a member of the ABC transporter family, which is encoded by the *MDR1* (*ABCB1*) gene, found in a plethora of healthy and cancerous cells. In the latter ones, they are often overexpressed and work as a self-defence against cytotoxic substances [8,9] by acting as an efflux pump for various drugs, including anticancer agents.

One critical key in the battle against cancer is to overcome drug resistance thus to resume the activity of current or well-known anti-cancer drugs, e.g. topotecan, doxorubicin, vincristine, cisplatin, cyclophosphamide, methotrexate or 5-fluorouracil. A successful and well-accepted method in this field is the inhibition of P-gp function during chemotherapy [10]. The co-administration of efflux pump inhibitors (EPIs), which are specific compounds able to modulate the efflux action of MDR drug transporters, has been reported and well-reviewed [1–5]. Due to the complexity of cancer aetiology, a combined approach targeting these MDR proteins as well as hitting known antitumoral pathways such as p53 is more and more considered to be a successful strategy to fight cancer.

Recently, plenty of compounds that modulate P-gp in various assays conditions were synthesized and studied. Mainly, three generations of reversal MDR agents, e.g. verapamil (**I**), dexniguldipine (**II**) and zosuquidar (**III**) (Fig. 1A) have been widely investigated [1,3,7,11]. Furthermore, a group of inhibitors for other ABC family members involved in cancer MDR, i.e. MRP1 (MK571, LY171883 and BAYu9773, Fig. 1B) and BCRP (Ko143 and FTC, Fig. 1C), have been evaluated [6]. However, their therapeutic usage is restricted by insufficient pharmaceutical profile, in particular, in the field of safety. Thus, further search for EPIs among new chemical groups is in great medical importance, but it is worth to emphasize that rational design of new EPIs is a high challenge. Although recent scientific achievements provided crystal structures of some MDR ABC transporters, the computer aided structure-based design is significantly limited in this protein family due to a variety of key-points that could be targeted by inhibitors, and thus providing various structurally different "binding pockets". For instance, some structures can inactivate pump as energy users acting on ATP, while different structures can act via a competition with a drug-substrate to one of the binding sites.

On the other hand, the structure-activity relationship analysis (SAR) in the vast group of Pgp-modulators allowed to indicate a beneficial role for hydrophobic/aromatic ending within their structures and also some flexibility in the middle (Fig. 1A). Although the number of modulators found for either MRP1 or BCRP is much smaller, SAR for their several agents shows that both groups differ from the Pgp pharmacophores. In contrast to bulky aromatic ends of members of the three generations of Pgp-inhibitors (Fig. 1A), the inhibitors MRP1 (MK571, LY171883, BAY u9773, Fig. 1B) tend to have an amphiphilic structure with the clear hydrophilic moiety at the end opposite to the aromatic/hydrophobic one, while BCRP inhibitors (Ko143, FTC, Fig. 1C) seem to prefer 4- or 5-fused ring structures. Thus, the ligand-based design is still a predominant approach in the rational design of cancer EPIs,

in particular in the case of ABCB1, thanks to the rich library of modulators identified so far.

In the last decade, our research team described numerous compounds targeting ABCB1 inhibitors in cancer cell lines belonging to the types of inhibitors shown in Fig. 1A [12–16]. In more detail, we were able to show highly potent ABCB1-inhibitory properties for aryl-piperazine hydantoin compounds [12,14,15]. The 5-aromatic substituted hydantoins were particularly potent [12,15], while the potency decreased when the aromatic moiety was moved into position 3 [13]. Among the most active hydantoin-compounds found so far, the 5,5-diphenylhydantoin derivative **1** and spirofluorene derivative **2** (Fig. 2) were 4–7-fold more potent than the reference P-gp inhibitor verapamil, but they did not display either cytotoxic or antiproliferative activity towards cancer cell lines, i.e., T-lymphoma [15] and NCI60 cell line panel (https://dtp.cancer.gov/discovery_development/nci-60/, data not published). In contrast, recent evidence indicates an increasing role of the triazine scaffold in potent hybrid anticancer agents [16], including 1,3,5-triazine-2,4-diamines [17,18], especially, piperazine and morpholine derivatives displayed strong cytotoxic effects *in vitro* against NCI60 cancer cell lines [18].

Furthermore, our recent follow-up study was focused on aromatic selenoesters and seleno-anhydrides, possessing both anticancer and P-gp inhibitory properties [10]. The most active compounds **3** and **4** (Fig. 2), were tested in MDR mouse T-lymphoma cells overexpressing P-gp, displaying at the same time up to 3.4-fold more potent P-gp modulatory effect compared to the reference verapamil [19]. The main drawback of those selenoesters and seleno-anhydride lies in their low chemical stability and their very unpleasant intensive smell, limiting their further evaluation and potential therapeutic application.

Taking into consideration the conclusions of previous studies [10,12–19], and the fact that selenium in the form of ethers is chemically much more stable and devoid of any unpleasant smell, we decided to design and investigate a series of new phenylselenoethers with different aromatic/heterocyclic termination. In this study, a new series of compounds was designed as hybrid structures of both selenoethers and moieties found in the previous active P-gp inhibitors. We designed phenylselenoether derivatives, which can be divided into three main groups: (i) aryl-hydantoins and their bioisosteres with variable alkyl chain lengths (**5–7**, group A), (ii) (aryl)piperazines with various substituents at N-piperazine, including aromatic, alkyl and ester moieties (**8–13**, group B), as well as (iii) the 1,3,5-triazine scaffold with small C1-linker branches (**5–17**, group C, Table 2). The new hybrid compounds were synthesized and tested against P-gp in mouse T-lymphoma cells, then, their possible ability to regulate the cell proliferation rate and their cytotoxic effects were evaluated, as well. The best compounds **5–7** were further studied regarding the mechanism of ABCB1 modulation. For the most active compound (**6**), we extended our studies from the mouse cells to a cellular model of human T-lymphocytic cancer (JURKAT) [20], in order to evaluate its effects alone or in combination with the reference chemotherapeutic agent doxorubicin, as well as potential molecular mechanisms of action for the selenoether at a cellular level. Selected compounds, active in lymphocytic cancer cells, were also examined on their antiproliferative action in neuroblastoma cancer cell lines. Furthermore, we evaluated their drug-like properties, including lipophilicity, possible metabolic pathways, and potential drug-drug interactions (DDI) risks. Finally, qualitative SAR were discussed.

Thus, the goal of this work was a comprehensive study regarding differently substituted seleno-ethers (**5–17**, Table 1), in

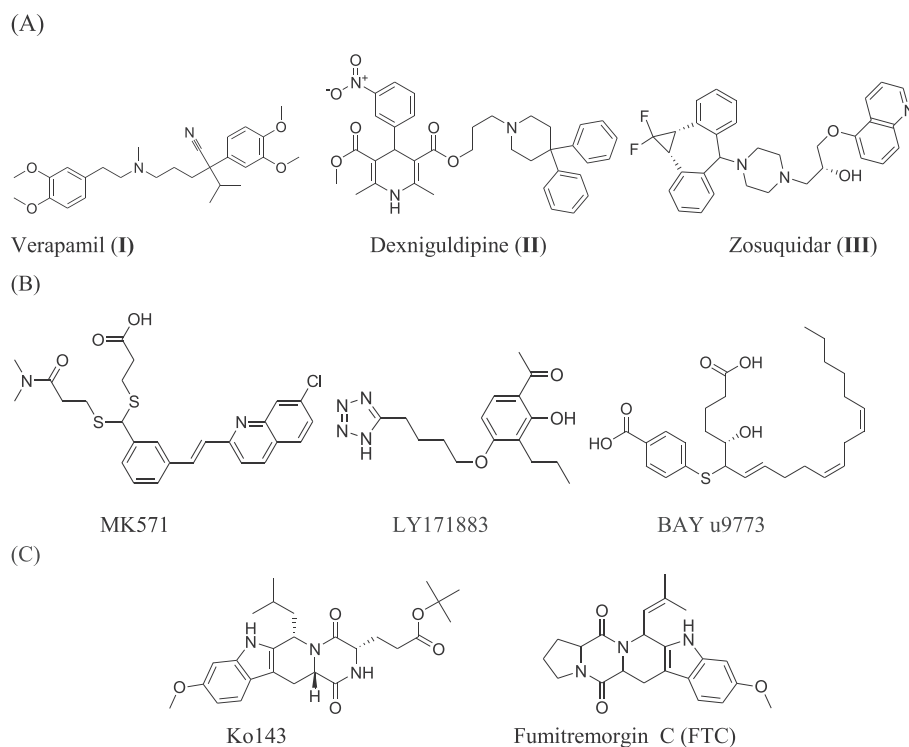


Fig. 1. Selected structures of cancer efflux ABC efflux pump inhibitors; (A) three generations (I–III) of ABCB1 inhibitors; (B) inhibitors of MRP1: MK571, LY171883 and BAYu9773; (C) inhibitors of BCRP: Ko143 and FTC [6].

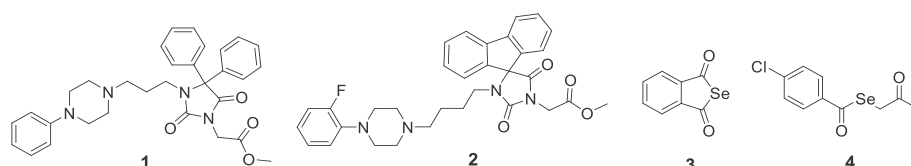


Fig. 2. Hydantoin Pgp-modulators, **1** and **2**, and seleno-compounds (**3** and **4**) with both anticancer and Pgp-modulatory properties found previously.

order to find new lead structure(s) in search of innovative anti-cancer drugs to overcome cancer MDR mechanisms.

2. Results and discussion

2.1. Chemical synthesis

Compounds **5–17** (Table 1) were obtained according to the synthesis route shown in Scheme 1. The hydantoin derivatives **5–7** (group A) were prepared applying a one-pot synthesis method, including Se-alkylation of previously described hydantoin intermediates **18–20** [14,21–23]. In more detail, a reduction of the diphenyl diselenide to produce sodium selenolate was performed using sodium borohydride in water/tetrahydrofuran mixture (THF) 1/1 under a nitrogen atmosphere [23]. Upon decolorization of the solution, a suitably substituted hydantoin in dichloromethane (DCM) was injected without any need of a deprotonation salt to produce the corresponding phenyl selenium hydantoin **5–7** in moderate yields and with excellent purity, within 3–4 days. (Scheme 1A).

In the case of the phenyl selenium piperazine derivatives (**8–13**), the appropriate commercially available piperazines were alkylated using 1-bromo-3-chloropropane in the presence of anhydrous potassium carbonate in acetone as solvent at room temperature [24]. The so obtained crude intermediates were used

applying the Se-alkylation method described for **5–7** (Scheme 1B).

1,3,5-Triazine selenium derivatives (**14–17**) were obtained as follows: firstly, the preparation of the sodium selenolate was carried out in a similar way as described for group A. The subsequent Se-alkylation was performed within 3–4 h, without any need to use higher temperatures or deprotonation salt. The next step involved cyclic condensations in basic conditions with methyl piperazine biguanide, as previously described [23,24].

Spectral and chromatographic analytical methods confirmed the structures and purity of the final compounds **5–17**. The intermediates (**21–30**) were either bought (**22** and **24**) or synthesized in the case of compounds **21**, **23**, and **25–30** according to the previous methods [24–29]. The compounds **9–17** have been transformed into the corresponding crystalline hydrochloric salts for the relative biological studies.

2.2. Pharmacology

2.2.1. Efflux modulating effects

Compounds **5–17** (Table 1) were evaluated for their efflux modulating effects in mouse T-lymphoma cell line transfected with the human *MDR1* gene that codes for the ABC transporter ABCB1 measuring the accumulation of rhodamine 123, which is a substrate for ABCB1 [12,30–32]. The percentage of mean fluorescence

Table 1
Chemical structures of compounds 5–17.

Cpd	Gr.	A		B		C		n
		5-7	Ar	8-13	R	14-17		
5	A				-CH ₂ COOCH ₃	4		
6	A				-CH ₂ COOCH ₃	6		
7	A				-CH ₃	4		
8	B		—		Ph	—		
9	B		—		2-MeO-Ph	—		
10	B		—		4-F-Ph	—		
11	B		—		3,4-diCl-Ph	—		
12	B		—		-CH ₃	—		
13	B		—			—		
14	C		—		-H	—		
15	C		—		-CH ₃	—		
16	C		—		C ₂ H ₅	—		
17	C		—		diCH ₃	—		

Table 2
Effects of compounds 5–17 on rhodamine 123 retention by human *MDR1* (*ABCB1*) gene-transfected mouse lymphoma cells.

FAR (Control)			
DMSO (2 v/v%)	0.84		
Compounds	FAR (0.2 μM)	FAR (2 μM)	FAR (20 μM)
Verapamil	—	—	17.59
5	2.47	42.91	—
6	2.77	24.20	—
7	1.09	45.05	—
8	—	1.07	1.57
9	—	0.92	1.02
10	—	1.07	4.25
11	1.07	2.27	—
12	—	0.97	0.85
13	—	0.75	0.96
14	—	0.82	0.87
15	—	0.83	0.95
16	—	0.93	1.13
17	—	1.11	1.40

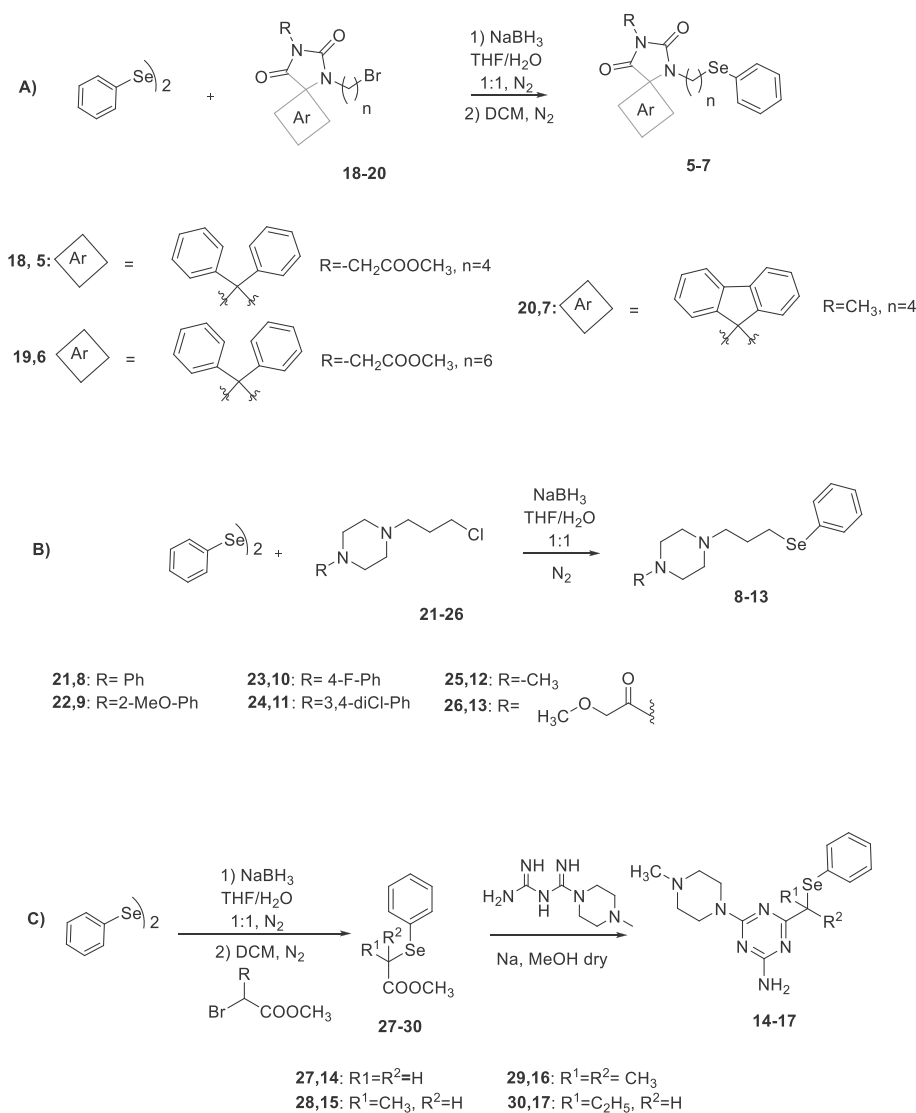
intensity was calculated for the treated MDR cells compared to the untreated cells, and then a fluorescence activity ratio (FAR) was determined. Verapamil was tested at the commonly used concentration (20 μM). All compounds (5–17) were investigated at the 10-fold lower concentration (2 μM) while weakly-active ones (8–10, 12–17) also at the concentration of verapamil. In the case of the active modulators at 2 μM (FAR>2, 5–7, 11), the FAR values were determined at a low concentration of 0.2 μM, as well. Results are presented in Table 2.

FAR, Fluorescence activity ratio was calculated using the following equation.

$$FAR = \frac{MDR \text{ treated} / MDR \text{ control}}{parental \text{ treated} / parental \text{ control}}$$

The inhibition of ABCB1 transporter is evident when FAR >1 [32]. Since the treatment had no effect on the parental cells (PAR) lacking the overexpressed ABCB1 system, the intensity of fluorescence did not change in the treated cells compared to the control ones, for this reason, the denominator was considered as 1.

Among the evaluated derivatives, the compounds 5–7 (tested at 2 μM) displayed strong inhibitory potency, being up to 2.6-fold



Scheme 1. Synthesis pathways of the final compound 5–17 and the relative intermediates 18–30.

more effective than the reference inhibitor verapamil (at 20 μ M). Other compounds (**10**, **11**), had significantly lower inhibitory activities (FAR 2.27 at 2 μ M or 4.25 at 20 μ M), while compounds **8**, **9** and **12–17** were inactive (Table 2).

2.2.1.1. Studies on ABCB1 modulating mechanisms of compounds 5–7.

The most active compounds found in the rhodamine 123 accumulation assay (**5–7**) were tested at 100 μ M on their influence on ATPase activity of Pgp pump in the luminescence Pgp-Glo™ Assay, according to previously described methods and protocols [33–35] (Fig. 3). In this assay, the Pgp-dependent decreases in luminescence are measured to reflect its increased ATP consumption. The ABCB1 basal ATP consumption (basal activity) is considered as a difference between the luminescent signal of samples treated with sodium orthovanadate, the selective and potent Pgp inhibitor (100% inhibition observed), and the luminescence of untreated Pgp samples. Thus, inhibitors give lower values (<100% of the basal activity), while the pump stimulators/substrates cause a statistically significant increase of the basal activity. Verapamil at 200 μ M was used as a reference modulator with the substrate/ATPase stimulatory mode of action, and caffeine as a reference inactive towards ABCB1 transporter to give negative control.

The obtained results showed that all compounds **5–7** significantly increased ($p < 0.001$, $p < 0.0001$) the Pgp basal activity in a similar way, but stronger, than verapamil (Fig. 3). These results are in line with those from the rhodamine 123 efflux assay, where stronger effects for **5–7** in respect verapamil were also found.

Summing up, compounds **5–7** did not inhibit the work of Pgp pump in this assay but displayed a substrate property. Thus, the putative mechanism of the dye-substrate efflux inhibition caused by **5–7** (Table 2) was the most probably associated with a competitive displacement in the substrate-binding site of this MDR transporter.

2.2.2. Cytotoxic and anti-proliferative effects

The whole series (**5–17**) was also examined on their cytotoxic and anti-proliferative activity in both sensitive (PAR) and resistant (MDR) mouse T-lymphoma cell lines (Table 3).

The tested compounds **5–7** and **11** showed very high cytotoxic effects in both MDR and PAR cell lines ($IC_{50} < 5 \mu$ M), with compound **6** presenting the highest activity among the tested seloneoethers. Most compounds of the series displayed lower cytotoxic concentrations for PAR T-lymphoma cells in comparison to MDR ones. This difference is particularly evident in the case of compound

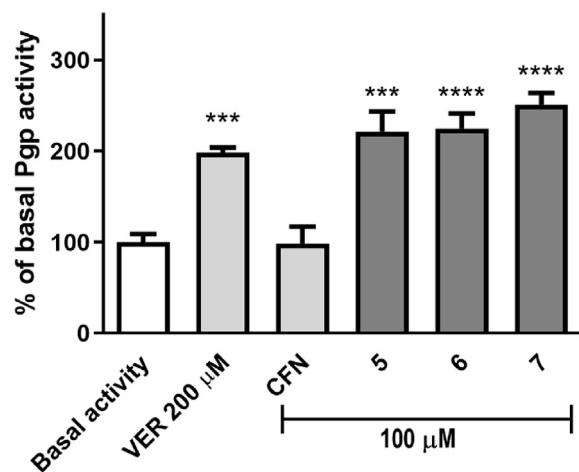


Fig. 3. The effect of the ABCB1 substrate verapamil (VER) (200 μM), ABCB1-negative compound caffeine (CFN) (100 μM) and compounds **5**, **6** and **7** (100 μM) on ABCB1 basal activity. The compounds are recognized as an ABCB1 substrate if they stimulate their basal activity (>100%). Data are presented as the mean \pm SD. Statistical significance was evaluated by one-way ANOVA, followed by Bonferroni's comparison test (*** p < 0.001, **** p < 0.0001 compared with the basal activity).

10 (>4-fold) and **8** (>2-fold), and only slight in the case of the most cytotoxic compounds (**5–7** and **11**). Compounds **12**, **13** with low cytotoxic effects in PAR cell lines were less potent in MDR cells too, while compounds **9** and **14–17** displayed no cytotoxicity in both PAR and MDR cell lines, even at a concentration of 100 μM (84 μM for **16** tested in PAR).

The series demonstrated unexpectedly interesting anti-proliferative properties in MDR mouse T-lymphoma cells, as each member caused more potent anti-proliferative effects in MDR than in PAR cells. Almost the whole series displayed IC_{50} (MDR) lower than 100 μM , while **5–7**, **10**, **11**, and **17** lower than 10 μM . Similar to the cytotoxicity test results, compound **6** also displayed the most potent anti-proliferative action for both PAR (IC_{50} = 3.83 μM) and MDR (IC_{50} = 1.33 μM) cells, being the only member with IC_{50} < 10 μM in PAR cells. To sum up, most of the compounds showed moderate anti-proliferative properties in PAR cells, with IC_{50} in the range of 12–65 μM , excluding **9** and **14**, which were inactive up to a concentration of 100 μM .

2.2.3. Anticancer properties in JURKAT human T-lymphoblastic leukaemia cell line

2.2.3.1. Effects of compound **6** on proliferation rate in JURKAT cells.

Compound **6** was the best compound of our series so far in terms of

anti-proliferative and cytotoxic activities, as well endowed with significant efflux pump inhibitory properties in mouse T-lymphoma. In order to extend the analysis to a human cell context, representing an immortalized T lymphocyte cell line used as a model for acute lymphoblastic leukaemia (ALL) [36], we decided to explore the effect of compound **6** on proliferating JURKAT leukaemia cells. This cellular system represents a useful model for testing the effects of different compounds on cell metabolism [37] and proliferation rate [38]. The effects of compound **6** on either proliferation rate or cell cycle-related gene expression were examined alone or in combination with doxorubicin (a chemotherapeutic agent able to block tumour growth *in vivo*) in order to find whether the co-treatment should enhance the effect of doxorubicin [38–40]. Doxorubicin is a well-known and successful antineoplastic drug commonly used as a chemotherapeutic agent in various cancers, including ALL, but, at present, drug resistance is common [41,42].

For these reasons, we performed proliferation assays in JURKAT cells treated with compound **6** at 0.1–0.5 and 2 μM concentrations, alone or in combination with doxorubicin, tested at 50 and 250 nM at two distinct time points (24 and 72 h).

While at early time compound **6** did not significantly affect cell proliferation rate, doxorubicin alone was able to block proliferation, especially at higher concentrations (Fig. 4A). Notably, at 72 h post-treatment, a significant reduction in proliferation was observed in cells treated with compound **6** alone and with doxorubicin alone, but a more significant effect was detected in cells co-treated with both compound **6** and doxorubicin. These data highlighted a synergistic effect of compound **6** with doxorubicin, especially when compound **6** was added to cell cultures at a higher dose (2 μM) (Fig. 4B). In summary, these results indicate that the co-treatments with compound **6** and doxorubicin counteracted cell proliferation in JURKAT cells and that the co-treatment with compound **6** enhances the effect of doxorubicin.

2.2.3.2. Effects of compound **6** on cell cycle-related gene expression in JURKAT.

In order to estimate a potential molecular mechanism for the anticancer activity found for **6**, we focused on the expression levels of cyclin D1, a well-known gene related to cell cycle progression contributing to uncontrolled proliferation and found to be negatively regulated in a previous study by the treatment with a selenium-containing compound in gastric cancer [20]. In addition, we analysed the expression level of p53 involved in apoptotic response, cell cycle arrest, and senescence [43].

In order to understand whether compound **6** was able to limit cell proliferation through gene expression regulation of cyclin D1 and p53, we treated JURKAT cells with compound **6** at three

Table 3

Cytotoxic and anti-proliferative effect of the compounds **5–17** on sensitive parental (PAR) and resistant (MDR) mouse T-lymphoma cells.

Compound	Cytotoxic effects		Anti-proliferative effects	
	PAR mean IC_{50} (μM) \pm SD	MDR mean IC_{50} (μM) \pm SD	PAR mean IC_{50} (μM) \pm SD	MDR mean IC_{50} (μM) \pm SD
5	2.91 \pm 0.18	3.39 \pm 0.09	16.75 \pm 1.37	7.82 \pm 0.57
6	0.67 \pm 0.03	0.90 \pm 0.07	3.84 \pm 0.05	1.34 \pm 0.05
7	3.25 \pm 0.11	4.21 \pm 0.40	12.53 \pm 0.95	4.67 \pm 0.38
8	21.50 \pm 0.24	44.35 \pm 2.88	28.96 \pm 2.30	13.07 \pm 0.97
9	>100	>100	>100	71.94 \pm 4.30
10	6.55 \pm 0.53	29.09 \pm 0.97	13.92 \pm 0.07	7.67 \pm 0.84
11	2.27 \pm 0.26	3.50 \pm 0.29	17.04 \pm 2.22	3.66 \pm 1.23
12	60.59 \pm 0.98	98.56 \pm 0.64	62.91 \pm 3.03	23.40 \pm 1.22
13	51.56 \pm 1.30	75.70 \pm 3.31	53.72 \pm 1.71	37.67 \pm 1.95
14	>100	>100	>100	>100
15	>100	>100	38.12 \pm 1.74	28.93 \pm 1.89
16	84.93 \pm 1.36	>100	65.16 \pm 1.36	48.47 \pm 2.56
17	>100	>100	35.29 \pm 1.07	8.28 \pm 1.47

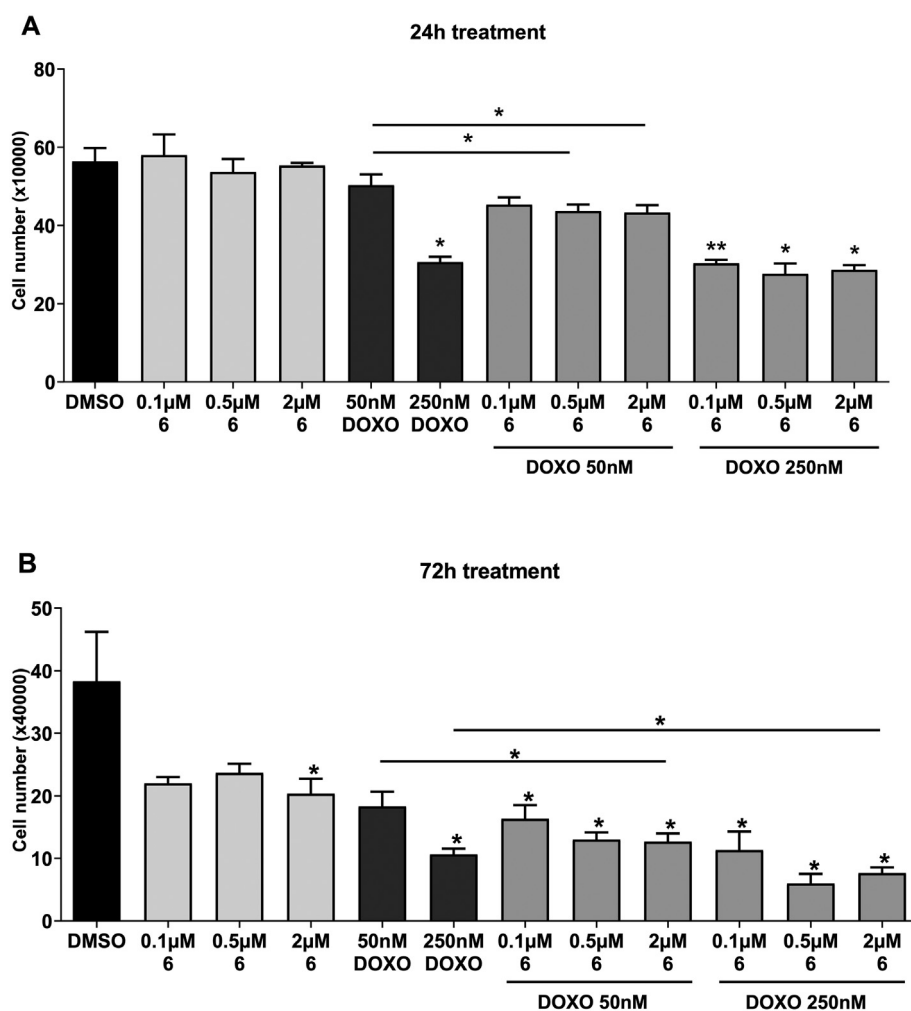


Fig. 4. Dose-response curves for anti-proliferation activity of compound **6** and doxorubicin in a dose range (0.1, 0.5, and 2 μ M for compound **6** and 50 and 250 nM for doxorubicin) on JURKAT cells after 24 h (A) and 72 h (B) of treatment. The results represent the average cell number \pm SEM of three independent experiments. Significance is represented as * p < 0.05 and ** p < 0.01 related to control groups.

concentrations (0.1, 0.5 and 2 μ M) and doxorubicin (50 nM), analysing with RT-PCR the mRNA transcripts levels of cyclin D1 and p53 (Fig. 5A), already after 24 h of treatment. Moreover, the co-treatment with both compound **6** and doxorubicin enhanced the effect of the single treatments on gene expression.

The results depicted in Fig. 5 show that compound **6** was able to significantly reduce cyclin D1 expression and increase the level of p53 (Fig. 5A), already after 24 h of treatment. Moreover, the co-treatment with both compound **6** and doxorubicin enhanced the effect of the single treatments on gene expression.

To sum up, these results indicate that compound **6** inhibited cell cycle progression through the reduction of the expression of cyclin D1 and inhibited cell proliferation by inducing p53 expression.

2.2.4. Anticancer action against neuroblastoma cancer cells

In order to estimate a broader range of anti-cancer potency, including also non-lymphocytic cancer cells, an influence of the most active selenoethers **5–7** on neuroblastoma cancer proliferation was investigated in SH-SY5Y cells affecting their viability (Fig. 6). The results show that all tested compounds at a concentration of 10 μ M significantly inhibited cell proliferation up to 60%. Compounds **6** and **7** were the most active ones, inhibiting cell growth by 12% and 8%, respectively, already at a concentration of 0.5 μ M, while the compound **5** was active only at 10 μ M.

2.3. Drug-likeness in vitro

2.3.1. Lipophilicity

In the presented work, the lipophilicity of the selenoethers was estimated using standard RP-TLC method. Retention parameters for the compounds were designated and analysed to give R_{M0} values that reflect the lipophilic properties of the tested compounds (details in Table S1, Supplementary).

The R_{M0} values of the tested compounds ranged from 0.79 to 6.05 (Fig. 7) and were corresponding to structural differences of the compounds. Thus, group A of hydantoin derivatives (**5–7**) was more lipophilic than both, group B of phenylpiperazine selenoethers (**9–13**) and C of 1,3,5-triazine derivatives (**14–17**). In the case of group B, the significant internal diversity of lipophilic properties between aromatic- (**9–11**) and non-aromatic piperazine (**12, 13**) compounds was seen in good accordance with the piperazine substituent properties. In contrast, most of the members of group C (**14, 15** and **17**) demonstrated almost identical lipophilic character. Taking into consideration the results, lipophilic-dependent trends can be observed for the ABCB1 modulatory action examined (Table 2). Thus the most lipophilic hydantoin derivatives (**6–7**) displayed significantly stronger action than either piperazine (**9–13**) or triazine (**14–17**) ones. Furthermore,

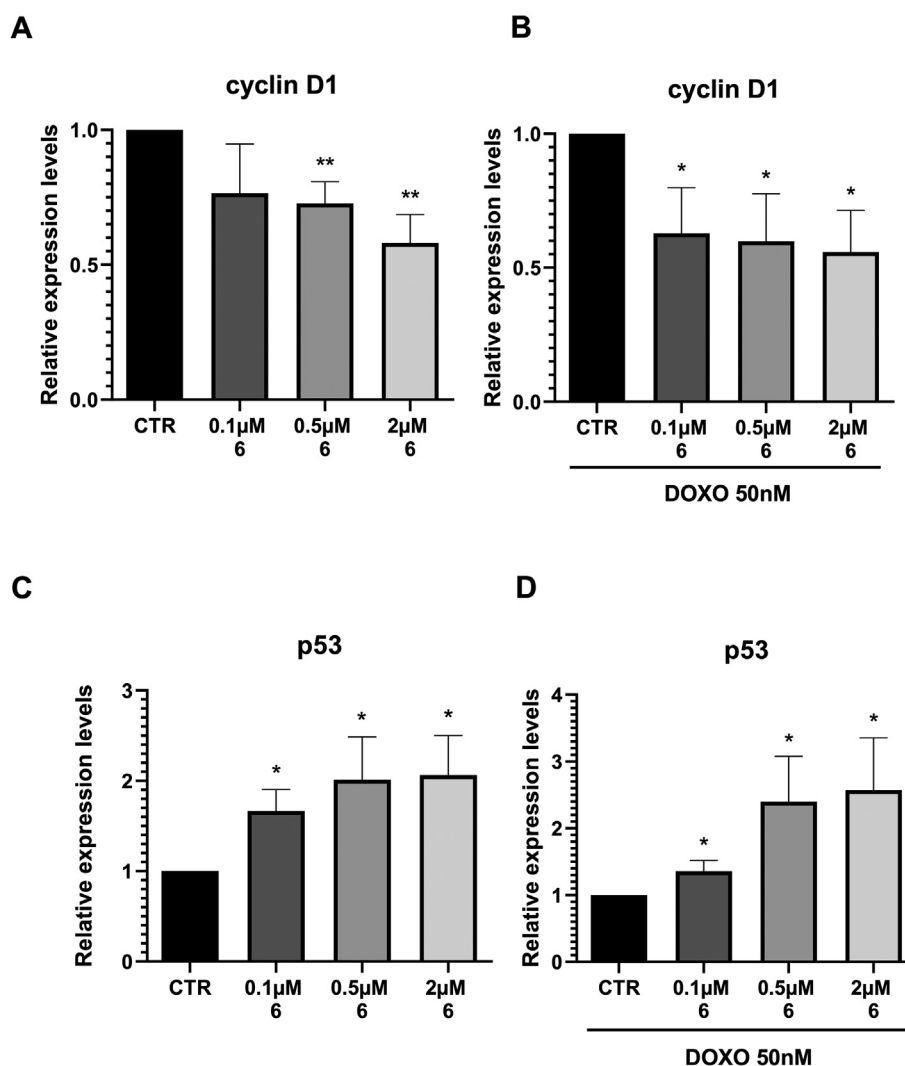


Fig. 5. (A–C) JURKAT cells were treated with compound **6** (0.1–0.5 or 2 μM) alone or (B–D) in combination with doxorubicin (50 nM) or with DMSO (CTR), as a control, for 24 h. Expression of *cyclinD1* (A–B) and *p53* (C–D) mRNAs were evaluated on total RNA by qRT-PCR. Bars represent means ± SEM of 6 experiments.

compound **6**, the outstanding one in terms of cytotoxicity and antiproliferative properties in the cancer cells, was also the most lipophilic within the series.

2.3.2. Metabolic stability *in vitro*

The metabolic stability of selenoorganic compounds **5–7** was investigated using mouse liver microsomes (MLMs). The UPLC spectra of the reaction mixtures after 120 min incubation with MLMs showed that all examined compounds were metabolically unstable (Fig. 8).

Compound **5** was metabolized completely into four metabolites M1–M4, as no parent compound was observed at UPLC spectra (Fig. 8A). Only a slight amount (4.5%) of compound **6** remained in the reaction mixture. This compound was biotransformed mainly into metabolite M1 and small amounts of three more metabolites M2–M4 (Fig. 8B). Compound **7** was metabolized mainly into metabolite M1 and four more metabolites M2–M5 (Fig. 8C).

According to UPLC spectra, compound **7** was determined as the most stable among the tested series, as around 30% of this compound remained in the reaction mixture. The performed next MS and precise ion fragment analyses of the parent compounds and their metabolites allowed for a determination of the metabolic

pathways and the most probable structures of metabolites among tested series. Generally, the most common metabolic pathways of **5** and **6** were ester hydrolysis and hydroxylation (Figs. S1A–C and S2A–D, Supplementary information). Compound **7** was mostly hydroxylated and decomposed at Se atom (Figs. S3A–E, Supplementary information). A similar to **7** decomposition pattern for Se was also observed for compound **5** (Figs. S1D and S3B, Supplementary information). All metabolic pathways of the tested selenoethers were summarized in Table 4.

2.3.3. Drug–drug interactions prediction

The potential drug–drug interactions (DDI) of selenoethers **5–7** were predicted by *in vitro* assessment of their effect on CYP3A4 isoform being the most involved in drug metabolism. The compounds **5–7** were screened at 10 μM, and the results were compared to the reference selective CYP3A4 inhibitor ketoconazole. All examined compounds in a statistically significant manner (**** $p < 0.0001$) reduced CYP3A4 activity (Fig. 9).

The weakest inhibition was shown for compound **6**, which reduced CYP3A4 activity up to ~53% of untreated control, whereas **5** and **7** decreased its activity up to 28 and 20%, respectively. However, the observed effects of **5–7** were much weaker than that for

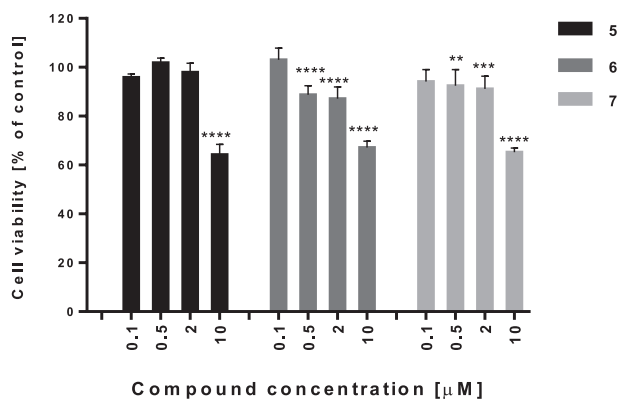


Fig. 6. Effect of selenoethers 5–7 on neuroblastoma cell viability. SH-SY5Y cells were incubated for 72 h in the presence of the compounds 5–7 at a concentration of 0.1, 0.5, 2, 10 [μM]. Cell viability was measured by MTS assay. Each point (mean \pm SEM of two independent experiments, each of which consisted of six replicates per treatment group) represents absorbance units and is expressed as a percentage of control compared to 0.1% DMSO control cells (set as 100%). Statistical analysis by one-way ANOVA showed significant differences between the groups ($p < 0.05$) and was followed by the Bonferroni multiple comparison test. Data indicated with **** $p < 0.0001$, *** $p < 0.001$, ** $p < 0.01$ reflects statistically significant differences between control and experimental groups.

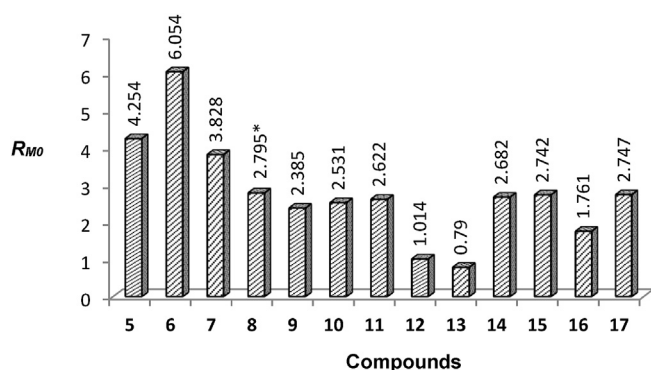


Fig. 7. Lipophilicity data for compounds 5–17. * Lipophilicity tested for the basic form (8), unlike the hydrochloric salts of the rest of group B (9–17). This relatively overstated lipophilicity of 8, as not comparable, was excluded from the discussion on results.

the reference drug ketoconazole, which reduced almost entirely CYP3A4 activity at 1 μM (Fig. 9).

2.4. General and SAR discussion

In order to find new anticancer hybrids able to overcome MDR mechanisms, we explored the chemical space of moieties that were useful to join the phenylselenoether fragment as a fixed scaffold, including selenoether linkers. Our rational design of suitable moieties based on results coming from recent literature evidence [16–18] or our previous experiences in searching anticancer and anti-MDR agents [10–15]. In this context, our present modifications divided the chemical space of the phenylselenoether derivatives into three main groups, *i.e.*, 5-arylhydantoin derived compounds (5–7, group A), aryl- (8–11), alkyl- (12) or ester- (13) piperazine derivatives (group B) and 1,3,5-triazine derivatives with different alkyl branches within the Se-ether linker (14–17, group C). The comprehensive biological screening, including cancer efflux pump inhibitory-, cytotoxic and antiproliferative properties for whole series (5–17) on the one hand, and ADMET *in vitro* studies for selected compounds 5–7, on the other hand, has provided exciting

and even unexpected qualitative structure-activity relationship (Fig. 10).

Among the three considered groups, hydantoin derivatives (group A, 5–7) were found to be the most promising structural moiety, being up to 2.6-fold more effective MDR EPI (at a 10-fold lower concentration) than the reference ABCB1-inhibitor verapamil. These compounds possessed also significant ABCB1 substrate potency in Pgp ATPase test, significantly higher than that of reference verapamil. Both assays indicated the relatively strongest effect for the compound with the rigid spirofluorene moiety (7), if comparing to 5 and 6 containing roteable 5,5-diphenyl moiety (marked in green, Fig. 10). Furthermore, all three members (5–7) displayed significant cytotoxic and antiproliferative properties in the MDR cancer cells of T-lymphoma. The length of the linker seems to be of considerable importance, as 5,5-diphenylhydantoin compound 6 ($\text{IC}_{50} < 1.5 \mu\text{M}$ in both cases, Table 3) with the longest (C6) linker was the best one of the present study. Taking into account our previous results, both 5,5-diphenylhydantoin and 5-spirofluorenehydantoin moieties, appeared in the structures of highly potent arylpiperazine ABCB1-inhibitors [14]. Their combination with a phenylpiperazine moiety gave even stronger inhibitory effects than those observed in this study, more than 20-fold stronger than verapamil [32]. However, those compounds displayed neither cytotoxic nor antiproliferative actions on cancer cells (T-lymphoma).

Furthermore, a too potent ABCB1-inhibitory property can be considered as risky for host organisms, taking into consideration the role of ABC-transporters in healthy human cells, which protect them from toxic substances or drugs. From a therapeutic point of view, the identified pharmacological properties of seleno-diphenylhydantoin 6 seem to be much more promising, and thus provides a new therapeutic direction for structural derivatives of anticonvulsant drug phenytoin (5,5-diphenylhydantoin). It should be noted that the hydantoin scaffold is a common motive in other anticancer drugs, *e.g.*, the 5,5-dimethylhydantoin derivative, nilutamide. However, our previous studies on the series of 5,5-dimethylhydantoin derivatives indicated a weaker (usually negligible) ABCB1-inhibitory properties in T-lymphoma in comparison to their 5,5-diphenyl analogues [13,14,32].

Comparing the piperazine phenylselenoethers (8–13, group B) to hydantoins (5–7), the phenylpiperazine subgroup demonstrated generally lower pharmacological effects but with notable mutual differences, almost regular and highly corresponding to their structural traits. The structural difference of compounds 8–13 concerns substituents at N-piperazine, including aromatic, alkyl and ester moieties, which influence the hydrophobic properties of the subseries, in the following order: 3,4-diClPh (11) > 4-FPh (10) > Ph (8) > 2-MeOPh (9) > Me (12) > EtOCO (13). Almost an identical order can be observed for both ABCB1-inhibitory and anticancer properties, including cytotoxic and antiproliferative actions (Tables 2 and 3). The biggest and most hydrophobic 3,4-dichlorophenyl substituted compound (11) was outstanding in the field of the efflux pump modulatory action ($\text{FAR} = 2.27$ at 2 μM), also exceeding the rest of group B in cytotoxic ($\text{IC}_{50} = 3.50 \mu\text{M}$) and antiproliferative action ($\text{IC}_{50} = 3.66 \mu\text{M}$). The 4-fluorophenyl derivative (10), the next in the hydrophobicity order, displayed some EPI properties at the high concentration ($\text{FAR} = 4.25$ at 20 μM), but was especially potent in terms of antiproliferative action in the MDR T-lymphoma ($\text{IC}_{50} = 3.50 \mu\text{M}$). It is worth to underline that both, 11 and 10, displayed corresponding or even slightly stronger antiproliferative properties than those of hydantoin derivatives 5 and 7, respectively (Table 3).

The last subseries of the triazine phenylselenoethers (14–17, group C) was surprisingly inactive, taking into consideration increasing literature evidence indicating a beneficial role of the

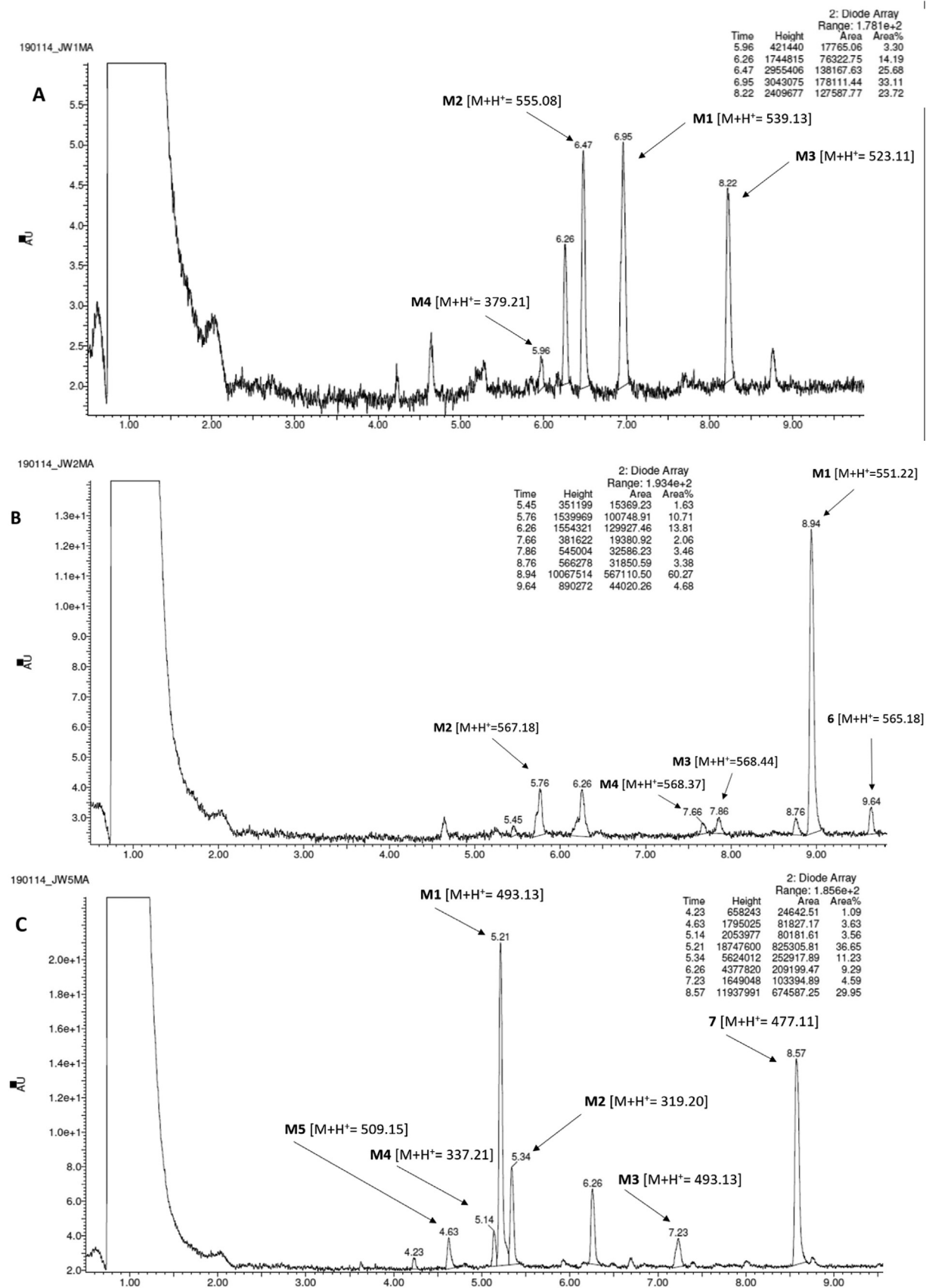


Fig. 8. UPLC spectra of the reaction mixtures after 120 min incubation of selenoethers **5** (A), **6** (B) and **7** (C) with MLMs. The peak at the retention time 6.26 min was identified as the contamination.

Table 4

The molecular masses and metabolic pathways of compounds 5–7.

Substrate	Molecular mass (m/z)	Number of identified metabolites	Molecular mass of the metabolite (m/z)	Metabolic pathway
5	537.14	4	539.13 (M1)	ester bond hydrolysis, hydroxylation
			555.08 (M2)	ester bond hydrolysis, double hydroxylation
			523.11 (M3)	ester bond hydrolysis
			379.21 (M4)	decomposition at the Se atom
6	565.18	4	551.22 (M1)	ester bond hydrolysis,
			567.18 (M2)	ester bond hydrolysis, hydroxylation
			568.44 (M3)	ester bond hydrolysis, ketone reduction, hydroxylation
			568.37 (M4)	ester bond hydrolysis, ketone reduction, hydroxylation
7	477.11	5	493.13 (M1)	hydroxylation
			319.20 (M2)	decomposition at the Se atom
			493.13 (M3)	hydroxylation
			337.21 (M4)	decomposition at the Se atom, hydroxylation
			509.15 (M5)	double hydroxylation

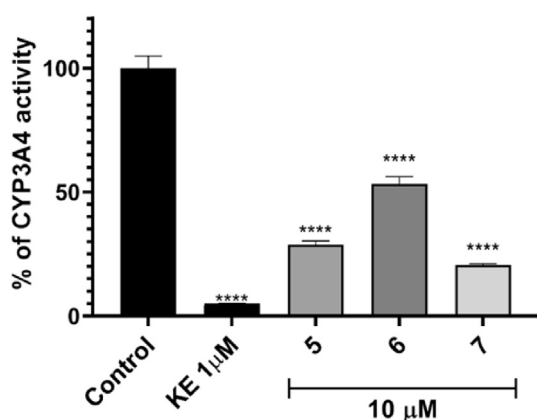


Fig. 9. The influence of selenoethers 5–7, and the reference inhibitor ketoconazole (KE) on CYP3A4 activity. The statistical significance was evaluated by a one-way ANOVA, followed by Bonferroni's Multiple Comparison Test (*****p* < 0.0001 compared with untreated control).

1,3,5-triazine scaffold in various cancers [16–18]. This small sub-series differs only in the field of the C1-linker branches, which undoubtedly influence slightly hydrophobicity and the steric hindrance/flexibility due to the variety of the spacer. In this group, only the dimethyl-branched derivative **17** displayed notable anti-proliferative property in MDR T-lymphoma (IC₅₀ = 8.28 μM). It should be noted that the antiproliferative action of compound **17** is almost 4-fold more potent in the MDR-than in the PAR cells.

The trends of more potent antiproliferative activity in the resistant T-lymphoma (MDR), than that in sensitive (PAR) cells, was noted for all three series A–C (Table 3). It suggests that the phenylselenoether moiety, as the characteristic common feature, is responsible for this favourable behaviour (marked in red, Fig. 10), while changeable moieties could modulate the intensity of this effect. The strongest result was observed for the 3,4-dichlorophenylpiperazine derivative **11** and the aforementioned triazine derivative **17**.

Comparing the lack of anticancer action in previous studies for the hydantoin-phenylpiperazines [14,32] to the significant effects found in this study (groups A and B), it is not hard to recognize that the selenoether linker is the most probable structural factor, responsible for an introduction of both, the cytotoxic and anti-proliferative, properties into the considered chemical families of hydantoin and phenylpiperazines. Likewise, the length of the linker seems to be crucial. It catches the eye that the most active hydantoin derivative **6**, distinctly predominant in the whole series is only

one that contains the longest C6-linker, while the anticancer action is decreasing with C4-linker (**5** and **7**) and C3-linker of phenylpiperazine derivatives (**8–13**, group B), to be the weakest in the case of short and rather stiff C1-linkers of 1,3,5-triazine derivatives **14–17** (group C). This is especially noticeable in the results of cytotoxic properties in both MDR and PAR T-lymphoma cells (Table 3).

Analysing the present results for the new Se-ether compounds (**5–17**) in comparison to those for the previous selenoesters (**4**) and selenoanhydride (**3**, Fig. 1) [15], corresponding efflux pump inhibitory and cytotoxic effects in MDR T-lymphoma can be observed. In more detail, the ABCB1-inhibitory properties of the most active hydantoin-selenoethers (**5–7**) were in the range of 1.38–2.56 of the action of verapamil (at a 10-fold higher concentration), while they were 1.57 and 3.43, tested in the same conditions for the selenoanhydride **3** and selenoester **4**, respectively. In the case of cytotoxic action in MDR T-lymphoma, the IC₅₀ values were 4.65 μM (**3**) and 1.03 μM (**4**) vs 0.90–4.21 μM for the best selenoethers found in this study. Interestingly the most active compounds (**5–7**) were also active in neuroblastoma SH-SY5Y cells.

On the other hand, an undeniable advantage of these newly discovered hydantoin selenoethers, referring to previous Se-esters, is the lack of any unpleasant smell and their higher chemical stability observed in the test conditions. Furthermore, the results of the assays using an *in vitro* CYP3A4 model for most active compounds (**5–7**) demonstrated their low DDI risk in comparison to ketoconazole (Fig. 9). However, their metabolic stability tested in mouse microsomes was rather low; the highest stability was observed in the case of the spirofluorene derivative (**7**). These results require further scientific considerations, *i.e.*, more comprehensive studies on biotransformation of **5–7** and their potential metabolites, also using human metabolism models, as well as an estimation of the intrinsic anticancer/MDR EPI properties of the most probable metabolites. On the other hand, further rational pharmacomodulations to improve metabolic stability and general “drugability” within this interesting new group of hydantoin-selenoethers is needed.

This study also provided an insight into potential molecular mechanisms of actions for the hydantoin-selenoether compounds. In order to explore the biological effects of the best compound determined from the mouse T-lymphoma assays, the longest-linker hydantoin derivative **6**, was evaluated in JURKAT human lymphoblastoid cells since these cells represent a good system to study drug resistance, cell death and proliferation in response to drugs treatment [38]. It has been reported in colon cancer cells that selenium shows chemotherapeutic potential against cancer cells by inactivating AKT and leading to suppression of cyclin D1 while

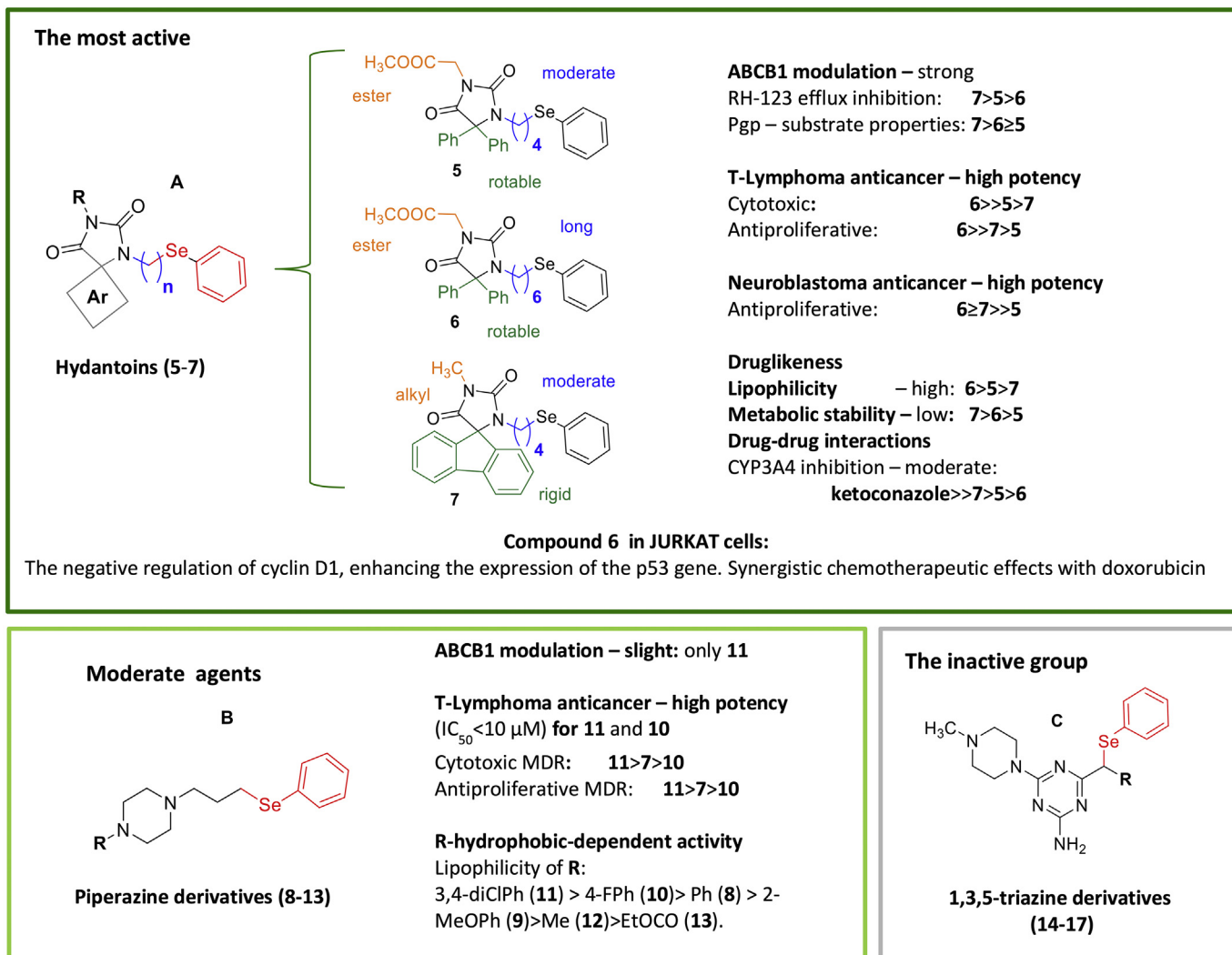


Fig. 10. SAR overview of compounds 5–17. The common phenylselenoether (red) moiety is probably responsible for the trend of more potent antiproliferative activity in the resistant T-lymphoma (MDR), than that in sensitive (PAR) cells in all three series A-C. Advantage of these new-discovered hydantoin selenoethers (red), referring to previous Se-esters, is the lack of any unpleasant smell and their higher chemical stability. (For interpretation of the references to colour in this figure legend, the reader is referred to the Web version of this article.)

triggering apoptosis [39]. Notably, methylselenol exposure changed the expression of genes related to the regulation of cell cycle and apoptosis, among which the tumour suppressor gene *p53* [40]. Thus, we focused on the regulation of proliferation rate and on cyclinD1 and p53 expression. We were pleased to observe that the selenium-containing compound **6** inhibited cell proliferation through the negative regulation of cyclin D1, while enhanced the expression of the p53 gene. Furthermore, the co-treatment of JURKAT cells with doxorubicin and our compound enhances the chemotherapeutic effect of this drug, suggesting a synergistic activity warranting further studies. This effect is evident and statistically significant especially after 72 h of treatment and when compound **6** is used at the higher dose tested (2 μM). At the present this data indicate the effectiveness of strategies based on different compound combinations to enhance the activity of commonly used antineoplastic drugs.

3. Conclusions

In the present work, we have discussed a new chemical family of potent selenium-containing compounds as hybrids of

phenylselenoethers with either arylhydantoin or phenylpiperazine moieties. Comprehensive studies, *i.e.*, design, synthesis and both, biological and ADMET-screening *in vitro*, including an insight into cellular mechanisms of anticancer action and followed by in-depth SAR analysis, have been performed, yielding promising results.

Among the new hybrids (5–17), the hydantoin derivatives (5, 6, and 7) were significantly more effective than the reference inhibitor verapamil (up to 2.6-fold at a 10-fold lower concentration) in order to inhibit the crucial tumour MDR mechanism of ABCB1-efflux pump. The very high stimulation of Pgp efflux pump (>200% of Pgp basal activity) at the presence of 5–7 confirmed their substrate potency and the probable competitive action with 123 rhodamine to the binding site in ABCB1-efflux modulating assay. Next, the cytotoxic and anti-proliferative action in both, sensitive (PAR) and resistant (MDR), mouse T-lymphoma cell lines revealed that both hydantoin- (5–7) and phenylpiperazine-selenoethers (10 and 11) possessed a good activity profile, being the 5,5-diphenylhydantoin compound (6) the best one out of the complete series. The promising antiproliferative action of the hydantoin compounds **6** and **7** were confirmed additionally in non-lymphocytic cancer cells, *i.e.* neuroblastoma, suggesting a therapeutically-promising broader

spectrum of anticancer potency for this chemical family, also with an accent on the longer-linker compound **6**. The mechanistic study results indicate that compound **6** inhibits cell cycle progression through the reduction of the expression of cyclin D1 and cell proliferation by inducing p53 expression, thus giving a first insight into the mechanism of action. Furthermore, the SAR analysis proved that the lipophilic properties, together with a longer selenoether spacer, are the likely factors affecting all, cancer EPI-, antiproliferative- and cytotoxic effects, in the tested cancer models for the new family of selenocompounds.

Overall, this study discovered a new chemical space of highly active selenium-containing anticancer agents, worthy of being studied more in-depth in order to improve drug-likeness and to reveal the precise mode of action. In this context, compound **6**, as the most active agent found in this study, will serve as a new lead structure for further pharmacomodulations and extended mechanistic studies as well as a medicinal chemistry optimization.

4. Experimental

4.1. Chemistry

Reagents were bought from Alfa Aesar (Karlsruhe, Germany) or Sigma Aldrich (Darmstadt, Germany). Solvents were dried over calcium hydrochloride (toluene) or calcium oxide (methanol). Reaction progress was verified using Thin Layer Chromatography (TLC), which was carried out on 0.2 mm Merck silica gel 60 F254 plates. Spots were visualized by UV light or treatment with Dragendorff reagent. Melting points (mp) were determined using a MEL-TEMP II apparatus and are uncorrected. The ^1H NMR and ^{13}C NMR spectra were obtained on a Varian Mercury-VX 300 MHz spectrometer and for the ^{77}Se NMR on a Bruker Variance 500 MHz spectrometer in DMSO- d_6 , CDCl_3 - d , MeOD- d_4 , or Acetone- d_6 . Chemical shifts in the relative NMR spectra were reported in parts per million (ppm) on the δ scale using the solvent signal as an internal standard. Data are reported as follows: chemical shift, multiplicity (s, singlet; br. s, broad singlet; d, doublet; t, triplet; dd, doublet of doublet, q, quintet, td triplet of doublet, m, multiplet), coupling constant J in Hertz (Hz), number of protons, proton's position (Ph-phenyl, Flou-Fluorine, Pp-piperazine). LC-MS were carried out on a system consisting of a Waters Acquity UPLC, coupled to a Waters TQD mass spectrometer. Retention times (t_{R}) are given in minutes. The UPLC/MS purity of all final compounds was determined (%). The intermediates **18–20** are described in our previous works [14,21,22]. While the intermediates **21, 23, 25–30** were obtained according to the procedure described earlier [21] and are known in the literature [24,26–29,44,45] (for details see Supporting Information).

4.1.1. General procedure for the Se-alkylation (5–14)

As part of this general procedure, the appropriate diphenyl diselenide (9.5 mmol) was dissolved in a 1:1 mixture of water and THF (50 mL) under protective nitrogen gas. Then, sodium borohydride (47.5 mmol) was added, and the mixture was stirred for approximately 35 min, with a decolorization of the solution observed already after 1–3 min. Next, a solution of hydantoin substitutions or piperazine derivatives (19.37 mmol) in THF or DCM (5 mL) was slowly added, and the reaction mixture was stirred at room temperature and monitored *via* TLC until the complete consumption of the starting material which occurred after 24–48 h. Upon completion, the reaction was quenched with 50 mL of a saturated aqueous solution of ammonium chloride and extracted with diethyl ether. The combined organic layers were dried over sodium sulphate and evaporated under reduced pressure to yield the desired products **5–14**.

4.1.1.1. *Methyl 2-(2,5-dioxo-4,4-diphenyl-3-(4-(phenylselanyl)butyl)imidazolidin-1-yl)acetate (5)*. Compound **18** (10 mmol) was used. White solid, mp 128 °C. Yield 23.59%. LC/MS $^{+}$: purity: 100%, $t_{\text{R}} = 8.97$, (ESI) m/z $[\text{M}+\text{H}]^{+}$ 537.33. $\text{C}_{28}\text{H}_{28}\text{O}_4\text{N}_2\text{Se}$ (MW 536.12). ^1H NMR (DMSO) δ 7.47–7.43 (m, 5H-Ph), 7.29 (s, 10H-2Ph), 4.34 (s, 2H- CH_2), 3.71 (s, 3H- CH_3), 3.33–3.28 (m, 2H- CH_2), 2.62 (t, $J = 7.3$ Hz, 2H- CH_2), 1.37–1.17 (m, 2H- CH_2), 0.88 (dt, $J = 15.3, 7.7$ Hz, 2H- CH_2). ^{13}C NMR (DMSO) δ 172.80, 167.95, 136.69, 131.32, 129.15, 128.93, 128.79, 128.15, 128.07, 126.44, 74.51, 73.31, 52.55, 27.61, 26.47, 26.01. ^{77}Se NMR (CDCl_3) δ 294.61.

4.1.1.2. *Methyl 2-(2,5-dioxo-4,4-diphenyl-3-(6-(phenylselanyl)hexyl)imidazolidin-1-yl)acetate (6)*. Compound **19**, Cas Number (1350707-01-5) (10 mmol) was used. Yellowish solid, mp 80 °C. Yield 23.20%. $\text{C}_{30}\text{H}_{32}\text{O}_4\text{N}_2\text{Se}$ (MW 564.15). LC/MS $^{+}$: purity: 92.76%, $t_{\text{R}} = 9.65$, (ESI) m/z $[\text{M}+\text{H}]^{+}$ 565.25. ^1H NMR (CDCl_3) δ 7.31–7.27 (m, 2H-Ph), 7.26–7.18 (m, 10H-2Ph), 7.12–7.04 (m, 3H-Ph), 4.17 (s, 2H- CH_2), 3.64 (s, 3H- CH_3), 3.20–3.14 (m, 2H- CH_2), 2.62 (t, $J = 7.5$ Hz, 2H- CH_2), 1.44 (s, 2H- CH_2), 1.36–1.28 (m, 2H- CH_2), 0.97 (dt, $J = 14.9, 7.5$ Hz, 2H- CH_2), 0.83 (dt, $J = 14.6, 7.3$ Hz, 2H- CH_2), 0.72 (dt, $J = 15.0, 7.5$ Hz, 2H- CH_2). ^{13}C NMR (CDCl_3) δ 173.57, 167.70, 154.88, 136.93, 132.30, 130.56, 128.99, 128.96, 128.79, 128.46, 126.59, 77.26, 77.01, 76.75, 75.25, 52.70, 42.13, 39.84, 33.59, 32.25, 29.69, 28.96, 27.60, 27.57, 26.03. ^{77}Se NMR (CDCl_3) δ 290.63.

4.1.1.3. *1'-Methyl-3'-(4-(phenylselanyl)butyl)spiro[fluorene-9,4'-imidazolidine]-2',5'-dione (7)*. Compound **20** (10 mmol) was used. White solid, mp 132 °C. Yield 15.20%. $\text{C}_{26}\text{H}_{24}\text{O}_2\text{N}_2\text{Se}$ (MW 476.10). LC/MS $^{+}$: purity: 95.87%, $t_{\text{R}} = 8.56$, (ESI) m/z $[\text{M}+\text{H}]^{+}$ 477.18. ^1H NMR (CDCl_3) δ 7.72 (d, $J = 7.6$ Hz, 2H-Flu), 7.45 (td, $J = 7.5, 1.1$ Hz, 2H-Flu), 7.36–7.31 (m, 2H-Flu), 7.28 (td, $J = 7.5, 1.0$ Hz, 2H-Flu), 7.21 (d, $J = 7.5$ Hz, 2H-Ph), 7.20–7.17 (m, 3H-Ph), 3.17 (s, 3H- CH_3), 2.96 (t, $J = 7.4$ Hz, 2H- CH_2), 2.66–2.55 (m, 2H- CH_2), 1.44 (dt, $J = 15.1, 7.5$ Hz, 2H- CH_2), 1.20 (dt, $J = 15.0, 7.5$ Hz, 2H- CH_2). ^{13}C NMR (CDCl_3) δ 171.89, 157.27, 141.52, 140.17, 132.64, 130.31, 129.85, 128.83, 128.24, 126.71, 123.57, 120.89, 77.16, 76.91, 76.65, 75.01, 40.63, 28.83, 26.87, 26.83, 25.61. ^{77}Se NMR (CDCl_3) δ 292.63.

4.1.1.4. *1-Phenyl-4-(3-(phenylselanyl)propyl)piperazine (8)*. Compound **21** (10 mmol), CAS Number (10,599-17-4), was used. White solid, mp 248 °C. Yield 20.11%. $\text{C}_{19}\text{H}_{24}\text{N}_2\text{Se}$ (MW 360.11). LC/MS $^{+}$: purity: 100%, $t_{\text{R}} = 4.82$, (ESI) m/z $[\text{M}+\text{H}]^{+}$ 361.07. ^1H NMR (MeOD) δ 7.61–7.58 (m, 2H-Ph), 7.34–7.28 (m, 5H-Ph), 7.05–7.02 (m, 2H-Ph), 6.94 (ddd, $J = 8.3, 2.0, 1.0$ Hz, 1H-Ph), 3.79–3.37 (m, 8H-Pp-2,6-H + Pp-3,5-H), 3.36 (s, 2H- CH_2), 3.05 (t, $J = 7.1$ Hz, 2H- CH_2), 2.24–2.16 (m, 2H- CH_2). ^{13}C NMR (DMSO) δ 149.57, 131.56, 129.57, 129.32, 129.07, 126.75, 119.88, 115.87, 55.10, 50.65, 45.21, 42.46, 23.74, 23.32. ^{77}Se NMR (DMSO): 283.99.

4.1.1.5. *1-(2-Methoxyphenyl)-4-(3-(phenylselanyl)propyl)piperazine hydrochloride (9)*. Commercial 1-(3-chloropropyl)-4-(2-methoxyphenyl)piperazine (10 mmol), CAS Number (21,279-77-6), was used. White solid, mp 287 °C. Yield 8.6%. Basic form $\text{C}_{20}\text{H}_{26}\text{ON}_2\text{Se}$ (MW 390.12), $\text{C}_{20}\text{H}_{27}\text{ClON}_2\text{Se}$ (MW 426.10). LC/MS $^{+}$: purity: 100%, $t_{\text{R}} = 4.97$, (ESI) m/z $[\text{M}+\text{H}]^{+}$ 391.17. ^1H NMR (DMSO) δ 11.36 (s, 1H, NH^+), 7.23–7.15 (m, 6H-Ph), 6.91 (d, $J = 8.4$ Hz, 2H-Ph), 6.78 (t, $J = 7.3$ Hz, 1H-Ph), 3.69 (dd, $J = 11.7, 5.3$ Hz, 2H- CH_2), 3.43 (d, $J = 10.3$ Hz, 2H- CH_2), 3.16–2.96 (m, 8H-Pp-2,6-H + Pp-3,5-H), 2.10–2.02 (m, 2H- CH_2). ^{13}C NMR (126 MHz, DMSO) δ 131.58, 129.59, 129.41, 129.31, 129.08, 126.76, 115.86, 50.58, 45.19, 23.74, 23.31, 0.10. ^{77}Se NMR (DMSO): 481.64.

4.1.1.6. *1-(4-Fluorophenyl)-4-(3-(phenylselanyl)propyl)piperazine hydrochloride (10)*. Compound **21** (10 mmol), was used. White solid, mp 204 °C. Yield 37.68%. Basic form $\text{C}_{19}\text{H}_{23}\text{FN}_2\text{Se}$ (MW

378.10), C₁₉H₂₄ClFN₂Se (MW 414.08). LC/MS⁺: purity: 100%, t_R = 4.83, (ESI) *m/z* [M+H]⁺ 379.14. ¹H NMR (DMSO) δ 11.10 (s, 1H, NH⁺), 7.50–7.46 (m, 2H-Ph), 7.31–7.21 (m, 3H-Ph), 7.08–7.02 (m, 2H-Ph), 6.99–6.94 (m, 2H-Ph), 3.65 (d, *J* = 10.3 Hz, 2H-CH₂), 3.47 (d, *J* = 9.8 Hz, 2H-CH₂), 3.20–2.96 (m, 8H-Pp-2,6-H + Pp-3,5-H), 2.08 (dt, *J* = 15.2, 7.5 Hz, 2H-CH₂). ¹³C NMR (DMSO) δ 164.50, 157.51, 155.63, 146.41, 131.63, 129.55, 129.34, 126.82, 117.84, 117.78, 115.58, 115.40, 55.17, 50.72, 46.06, 23.85, 23.22. ⁷⁷Se NMR (DMSO): 285.00.

4.1.1.7. 1-(3,4-Dichlorophenyl)-4-(3-(phenylselanyl)propyl)piperazine hydrochloride (11). Commercial 1-(3-chloropropyl)-4-(3,4-dichlorophenyl)piperazine (10 mmol), CAS Number (101,364-27-6), was used. White solid, mp 170 °C. Yield 15.09%. Basic form C₁₉H₂₂Cl₂N₂Se (MW 428.03), C₁₉H₂₃Cl₃N₂Se (MW 464.01). LC/MS⁺: purity: 99.22%, t_R = 5.84, (ESI) *m/z* [M+H]⁺ 429.12. ¹H NMR (DMSO) δ 11.31 (s, 1H, NH⁺), 7.55–7.48 (m, 2H, Ph), 7.44 (d, *J* = 9.0 Hz, 1H, Ph), 7.35–7.20 (m, 4H, Ph), 6.99 (dd, *J* = 9.0, 2.9 Hz, 1H, Ph), 3.86 (d, *J* = 13.2 Hz, 2H, CH₂), 3.48 (d, *J* = 11.7 Hz, 2H, CH₂), 3.28–3.16 (m, 4H, Pp-2,6-H), 3.12–2.98 (m, 4H, Pp-3,5-H), 2.11 (p, *J* = 7.5 Hz, 2H, CH₂). ¹³C NMR (DMSO) δ 149.28, 131.65, 131.61, 131.57, 130.63, 129.59, 129.33, 126.79, 120.75, 116.96, 115.79, 55.15, 50.22, 44.65, 23.75, 23.30. ⁷⁷Se NMR (DMSO): 284.24.

4.1.1.8. 1-Methyl-4-(3-(phenylselanyl)propyl)piperazine hydrochloride (12). Commercial 1-(3-chloropropyl)-4-methylpiperazine (10 mmol), CAS Number (104-16-5), was used. White solid, mp 132 °C. Basic form C₁₄H₂₂N₂Se (MW 298.09), C₁₄H₂₂ClN₂Se (MW 333.59). Yield 11.97%. LC/MS⁺: purity: 97.97%, t_R = 2.89, (ESI) *m/z* [M+H]⁺ 299.13. ¹H NMR (DMSO) δ 12.01 (s, 1H, NH⁺), 7.52–7.46 (m, 2H, Ph), 7.33–7.22 (m, 3H, Ph), 3.50–3.13 (m, 10H, 8H-Pp-2,6-H + Pp-3,5-H + 2H-CH₂), 3.01 (t, *J* = 7.4 Hz, 2H, CH₂), 2.81 (s, 3H, CH₃), 2.07 (p, *J* = 7.6 Hz, 2H). ¹³C NMR (DMSO) δ 131.47, 129.59, 129.34, 129.25, 126.74, 55.29, 49.39, 47.99, 23.89, 23.31, 23.05, 22.80. ⁷⁷Se NMR (DMSO): 284.41.

4.1.1.9. Ethyl 4-(3-(phenylselanyl)propyl)piperazine-1-carboxylate hydrochloride (13). Synthesis from 10 mmol of ester **26**. White solid, mp 83 °C. Yield 23.59%. Basic form C₁₆H₂₄N₂O₂Se (MW 356.10), C₁₆H₂₄ClN₂O₂Se (MW 391.60). LC/MS⁺: purity: 98.59%, t_R = 3.82, (ESI) *m/z* [M+H]⁺ 357.21. ¹H NMR (DMSO) δ 11.62 (s, 1H, NH⁺), 7.53–7.48 (br, 2H), 7.33–7.23 (m, 3H, Ph), 4.06 (m, 2H, Ph), 4.00 (d, *J* = 13.4 Hz, 2H, CH₂), 3.39 (d, *J* = 9.8 Hz, 4H, Pp-2,6-H), 3.18–3.11 (m, 2H, CH₂), 3.04–2.91 (m, 4H, Pp-3,5-H), 2.08 (p, *J* = 7.5 Hz, 2H), 1.18 (t, *J* = 7.1 Hz, 3H). ¹³C NMR (DMSO) δ 154.27, 131.65, 131.60, 131.56, 129.57, 129.31, 126.76, 61.31, 55.27, 50.31, 23.66, 23.29, 14.47. ⁷⁷Se NMR (DMSO) δ 283.96.

4.1.2. General procedure of synthesis of 1,3,5-triazines (14–17)

Sodium (10 mmol) was dissolved in 10 mL of absolute methanol, then 4-methylpiperazin-1-yl biguanidine x 2HCl (5 mmol) and the appropriate carboxylic acid ester (5 mmol) were added. The reaction mixture was refluxed for 15–30 h. After cooling to room temperature, water (10 mL) was added and the mixture was stirred for 0.5 h. The precipitated triazine product was separated and crystallized from methanol.

4.1.2.1. 4-(4-Methylpiperazin-1-yl)-6-((phenylselanyl)methyl)-1,3,5-triazin-2-amine hydrochloride (14). Synthesis from 10 mmol of ester **27**. White solid. Yield 26%, mp 249 °C. Basic form C₁₅H₂₀N₆Se (MW 364.09), C₁₅H₂₀ClN₆Se (MW 400.07). LC/MS⁺: purity: 100%, t_R = 2.82, (ESI) *m/z* [M+H]⁺ 365.12. ¹H NMR (DMSO) δ 11.50 (s, 1H, NH⁺), 7.87 (br.s, 2H-NH₂), 7.61–7.56 (m, 2H Ph), 7.37–7.25 (m, 3H Ph), 3.96 (d, *J* = 5.4 Hz, 2H-CH₂), 3.50–2.78 (m, 8H, 4H-Pp-2,6-H+4H-Pp-3,5-H), 2.73 (d, *J* = 4.0 Hz, 3H-CH₃). ¹³C NMR (DMSO) δ 175.48, 171.16, 167.35, 164.82, 134.10, 131.78, 131.40, 130.45, 129.49,

129.25, 127.03, 125.59, 54.77, 46.23, 42.84, 34.62, 33.19.

4.1.2.2. 4-(4-Methylpiperazin-1-yl)-6-(1-(phenylselanyl)ethyl)-1,3,5-triazin-2-amine hydrochloride (15). Synthesis from 10 mmol of ester **28**. White solid. Yield 12.19%, mp 238 °C. Basic form C₁₆H₂₂N₆Se (MW 378.11), C₁₆H₂₃ClN₆Se (MW 413.81). LC/MS⁺: purity: 100%, t_R = 3.23, (ESI) *m/z* [M+H]⁺ 379.08. ¹H NMR (DMSO) δ 11.93 (s, 1H-NH⁺), 8.33 (br.s, 2H-NH₂), 7.54 (dt, *J* = 7.0, 1.4 Hz, 2H-Ph), 7.45–7.29 (m, 3H-Ph), 4.34 (q, *J* = 7.0 Hz, 1H-CH), 4.11–2.55 (m, 11H, 4H-Pp-2,6-H + 4H-Pp-3,5-H + 3H-Pp-CH₃), 1.59 (s, 3H-CH₃). ¹³C NMR (DMSO) δ 162.20, 136.14, 131.33, 129.98, 129.64, 129.22, 128.34, 51.62, 42.38, 18.15. ⁷⁷Se NMR (DMSO) δ 492.76.

4.1.2.3. 4-(4-Methylpiperazin-1-yl)-6-(1-(phenylselanyl)propyl)-1,3,5-triazin-2-amine hydrochloride (16). Synthesis from 10 mmol of ester **29**. White solid. Yield 29.78%, mp 231 °C. Basic form C₁₇H₂₄N₆Se (MW 392.12), C₁₇H₂₅ClN₆Se (MW 428.10). LC/MS⁺: purity: 100%, t_R = 3.67, (ESI) *m/z* [M+H]⁺ 393.17. ¹H NMR (DMSO) δ 11.87 (s, 1H, NH⁺), 9.02–7.87 (br, 2H, NH₂), 7.56–7.50 (m, 2H, Ph), 7.42–7.30 (m, 3H, Ph), 4.07 (t, *J* = 7.6 Hz, 1H, CH), 3.54–2.93 (m, 8H, Pp-2,6-H + Pp-3,5-H), 2.75 (s, 3H, CH₃), 1.94 (d, *J* = 76.0 Hz, 2H, CH₂), 0.95 (t, *J* = 7.2 Hz, 3H, CH₃). ¹³C NMR (DMSO) δ 167.12, 164.46, 162.05, 135.95, 131.30, 130.45, 129.97, 129.64, 129.19, 128.32, 51.89, 42.44, 42.37, 28.93, 25.05, 21.87, 13.76, 12.82, 11.32. ⁷⁷Se NMR (DMSO) δ 454.52.

4.1.2.4. 4-(4-Methylpiperazin-1-yl)-6-(2-(phenylselanyl)propan-2-yl)-1,3,5-triazin-2-amine hydrochloride (17). Synthesis from 10 mmol of ester **30**. Light yellow solid. Yield 12.19%, mp 252 °C. Basic form C₁₇H₂₄N₆Se (MW 392.12), C₁₇H₂₅ClN₆Se (MW 428.10). LC/MS⁺: purity: 96.21%, t_R = 3.72, (ESI) *m/z* [M+H]⁺ 393.10. ¹H NMR (DMSO) δ 11.45 (br, 1H, NH⁺), 8.83–7.75 (br, 2H, NH₂), 7.61–7.41 (m, 3H, Ph), 7.39–7.33 (m, 2H, Ph), 3.36–2.86 (m, 8H, Pp-2,6-H + Pp-3,5-H), 2.76 (s, 3H, CH₃), 1.69 (s, 6H, 2CH₃). ¹³C NMR (DMSO) δ 174.94, 162.37, 162.09, 157.22, 132.42, 131.30, 130.45, 129.96, 128.31, 71.57, 51.88, 51.54, 42.41, 42.36, 28.81, 27.59, 18.71. ⁷⁷Se NMR (DMSO) δ 447.73.

4.2. Biological assays

4.2.1. Assays in mouse T-lymphoma

4.2.1.1. Cell lines. The L5178Y mouse T-cell lymphoma cells (ECACC Cat. No. 87111908, obtained from FDA, Silver Spring, MD, USA) were transfected with pHa MDR1/A retrovirus. The ABCB1-expressing cell line (MDR) was selected by culturing the infected cells with colchicine. L5178Y (parental, PAR) mouse T-cell lymphoma cells and the L5178Y human ABCB1-transfected subline were cultured in McCoy's 5A medium supplemented with 10% heat-inactivated horse serum, 200 mM L-glutamine, and penicillin-streptomycin mixture in 100 U/l and 10 mg/l concentration, respectively.

4.2.1.2. Assay for cytotoxic effect in mouse lymphoma cells.

Stock solutions of compounds were 10 mM in DMSO. The effects of increasing concentrations of the drugs alone on cell growth were tested in 96-well flat-bottomed microtiter plates. The compounds were diluted in 100 μL of McCoy's 5A medium. 1 × 10⁴ mouse T-cell lymphoma cells (PAR or MDR) in 100 μL of medium were then added to each well, with the exception of the medium control wells. The culture plates were further incubated at 37 °C for 24 h; at the end of the incubation period, 20 μL of MTT solution (from a 5 mg/mL stock) was added to each well. After incubation at 37 °C for 4 h, 100 μL of SDS solution (10% in 0.01 M HCl) was added to each well, and the plates were further incubated at 37 °C overnight. The cell growth was determined by measuring the OD at 540 nm (ref. 630 nm) with a Multiscan EX ELISA reader (Thermo Labsystems,

Cheshire, WA, USA). IC₅₀ values were calculated via the following equation:

4.2.1.3. Assay for antiproliferative effect in mouse lymphoma cells.

The effects of increasing concentrations of the drugs alone on cell growth were tested in 96-well flat-bottomed microtiter plates. The compounds were diluted in 100 µL of McCoy's 5A medium. 6×10^3 mouse T-cell lymphoma cells (PAR or MDR) in 100 µL of medium were then added to each well, with the exception of the medium control wells. The culture plates were further incubated at 37 °C for 72 h in a CO₂ incubator; at the end of the incubation period, 20 µL of MTT solution (from a 5 mg/mL stock) was added to each well. After incubation at 37 °C for 4 h, 100 µL of SDS solution (10% in 0.01 M HCl) was added to each well, and the plates were further incubated at 37 °C overnight. The cell growth was determined by measuring the OD at 540 nm (ref. 630 nm) with a Multiscan EX ELISA reader (Thermo LabSystems, Cheshire, WA, USA). IC₅₀ values were calculated via the following equation:

4.2.1.4. Fluorescence uptake assay.

The cell numbers of the L5178Y PAR and MDR cell lines were adjusted to 2×10^6 cells/mL, resuspended in serum-free McCoy's 5A medium, and distributed in 0.5 mL aliquots into Eppendorf centrifuge tubes. The tested compounds were added at a final concentration of 0.2, 2, or 20 µM, and the samples were incubated for 10 min at room temperature. Verapamil was applied as a positive control at 20 µM. DMSO was added to the negative control tubes in the same volume as had been used for the tested compounds. No activity of DMSO was observed. Next, 10 µL (5.2 µM final concentration) of the fluorochrome and ABCB1 substrate rhodamine 123 was added to the samples, and the cells were incubated for a further 20 min at 37 °C, washed twice and resuspended in 1 mL PBS for analysis. The fluorescence of the cell population was measured with a PartecCyFlow® flow cytometer (Partec, Münster, Germany). The percentage of mean fluorescence intensity was calculated for the treated MDR cells as compared with the untreated cells. A fluorescence activity ratio (FAR) was calculated based on the measured fluorescence values via the following equation:

$$FAR = \frac{MDR \text{ treated} / MDR \text{ control}}{\text{parental treated} / \text{parental control}}$$

4.2.2. Assays with JURKAT human T-lymphocytes

4.2.2.1. Cell culture and treatments.

JURKAT human T lymphocyte cells (ATCC, VA, USA) were propagated in RPMI 1640 medium (Gibco, Monza, Italy) with 10% fetal bovine serum (FBS; Gibco, Monza, Italy), 2 mM L-glutamine (Euroclone, Pero (MI), Italy), and antibiotics (100 U/mL penicillin, 100 g/mL streptomycin) (Euroclone, Pero (MI), Italy).

For the treatments with compound **6**, doxorubicin and DMSO as a negative control, cells were seeded and treated once with compound **6** at the final concentration of 0.1 µM, 0.5 µM and 2 µM, alone or in combination with doxorubicin at the final concentration of 50 nM and 250 nM. Cells were collected after 24 and/or 72 h from the treatment and analysed for proliferation rate and gene expression.

4.2.2.2. RNA extraction, reverse transcription, and quantitative PCR in JURKAT cells.

RNAs were extracted by ReliaPrep™ RNA Tissue Miniprep (Promega, Madison, WI, USA) and reverse-transcribed with PrimeScript RT Master Mix (Takara, Kusatsu, Shiga, Japan). cDNAs were amplified by a qPCR reaction using GoTaq qPCR Master Mix (Promega) and analysed with the oligonucleotide pairs specific

for the target genes. Relative amounts, determined with the 2(-ΔCt) method, were normalized with respect to the human housekeeping gene L32.

The primers used are as follows: L32 (forward: 5'-GGAGC-GACTGCTACGGAAG-3', reverse: 5'-GATACTGTCCAAAAGCTGGAA-3'), *CyclinD1* (forward: 5'-CCTCTAAGATGAAGGAGACCA-3', reverse: 5'-CACTTGAGCTTGTTACCA-3'), and *p53* (forward: 5'-GGCCACTTCACCGTACTAA-3', reverse: 5'-GTGGTTCAAGGCCA-GATGT-3').

4.2.2.3. Cell proliferation assay.

Cell viability was measured using a CellTiter 96® Aqueous One Solution Cell Proliferation Assay (MTS) (Promega) following the manufacturer's instructions, as reported in Stazi et al., 2019 [46]. Briefly, JURKAT cells were seeded in 96 well tissue culture plates. After 24 h or 72 h of treatment with compound **6**, doxorubicin, or DMSO as a negative control at the reported concentrations, 20 µL of Aqueous One Solution Reagent was added to each well and absorbance was recorded at 490 nm. Three independent experiments were performed.

4.2.2.4. Statistical methods.

Statistical analysis was performed using Statistica v10 software (StatSoft, USA). The correlation coefficients (r , r^2), and the standard errors of the slope, interception, and estimate (S_a , S_b , S_e) were used as the basis for testing the linearity of regression plots.

Statistical significance for gene expression analysis and proliferation assays was determined with a *t*-test with GraphPad Prism version 5.0 (La Jolla, CA, USA). Differences were considered significant at $p < 0.05$ (* $p < 0.05$; ** $p < 0.01$; *** $p < 0.001$).

4.2.3. Assays with human neuroblastoma cell line SH-SY5Y

4.2.3.1. Cell culture and treatment conditions.

Human neuroblastoma cell line SH-SY5Y (ATCC® no. CRL-2266™) was grown in Dulbecco's Modified Eagle's Medium/Nutrient Mixture F-12 (DMEM/F12, Life Technologies) with 10% (v/v) fetal bovine serum (FBS, South America, Life Technologies) at 37 °C in a humidified atmosphere of 5% CO₂/95% air. Cells were routinely passaged at 70% confluence by trypsinization (0.05% Trypsin-EDTA, Invitrogen) and re-seeded at 5×10^3 cells/cm². To make experiments comparable, cells at passages 10–17 were evaluated. In every experiment, cells were seeded in 100 µL (96-well plates) of complete growth medium and initially cultured for 24 h. Subsequently, the medium was changed to medium containing tested compounds diluted to the desired concentrations. After 72 h, the given assay was performed as described below. All tested compounds were dissolved in DMSO to generate 10 mM stock. Directly before analysis, each stock solution of tested compounds was made in DMSO as a 1000-fold stock solution and then diluted in culture medium to a final desired concentration.

4.2.3.2. Cell viability assay.

SH-SY5Y cells (2.5×10^4 cells/well) were cultured in transparent 96-well plates (Nunc) in DMEM/F12 supplemented with 10% FBS in the presence of dimethylsulfoxide (DMSO < 0.1%, vehicle control) or increasing concentration of compounds **5**, **6** and **7** (0.1, 0.5, 2, 10 [µM]). Treatment with compounds was performed for 72 h. After the incubation time, cell viability was examined using an MTS-based [3-(4,5-dimethylthiazol-2-yl)-5-(3-carboxymethoxyphenyl)-2-(4-sulfophenyl)-2 H tetrazolium] CellTiter96® Aqueous One Solution Cell Proliferation Assay (Promega, Madison, USA) following the manufacturer's protocol. Briefly, 20 µL of MTS solution was pipetted into each well containing 100 µL of culture or culture medium (negative control) and incubated at 37 °C for 4 h. After incubation time, formazan product turnover absorbance was measured at 490 nm using the microplate reader EnSpire (PerkinElmer, Massachusetts, USA).

4.2.3.3. Statistical analysis. Data are presented as the mean \pm SEM of two independent experiments. Each treatment point was repeated (six times) in two technical and independent replicates. All statistical analyses were carried out using GraphPad Prism 7 with significance determined by One-way ANOVA followed by Bonferroni's post-hoc comparisons tests as detailed in the figure legends.

4.2.4. Intrinsic activity towards Pgp in vitro

The luminescent Pgp-Glo™ Assay System used for determination of 1,3,5-Triazine selenium derivatives influence on P-gp activity was purchased from Promega (Madison, WI, USA). The assay was performed in triplicate, as described previously [33–35]. Compounds 5–7 (100 μ M) were incubated with Pgp membranes for 40 min at 37 °C. The references: Pgp-stimulator verapamil (VER) and Pgp-negative compound caffeine (CFN) were incubated at 200 and 100 μ M, respectively. For basal P-gp activity calculation, the membranes were incubated with 100 μ M of sodium orthovanadate (Na_2VO_4). The luminescence signal was measured by microplate reader EnSpire PerkinElmer (Waltham, MA, USA). The statistical significances were calculated using GraphPad Prism 8.0.1 software.

4.3. Lipophilicity study

4.3.1. Thin-Layer Chromatography

The mobile phases were prepared by mixing the respective amounts of water and organic modifier (methanol) in a range from 40 to 90% (v/v) in 5% increments. TLC was carried out on Silica gel 60 RP-18 F₂₅₄ plates (7 × 10 cm) plates (Merck, Darmstadt, Germany). Methanol was used to prepare the solutions of the substances. Solutions (10 μ L) of the analysed compounds were applied to the plates as 5 mm bands, 10 mm apart, and 10 mm from the lower edge and sides of the plates, by using a Linomat V applicator (Camag, Basel, Switzerland). The vertical chamber (Sigma–Aldrich, St. Louis, USA), 20 × 10 × 18 cm in size, was saturated with the mobile phase for 20 min. The development was carried out over 9 cm from the starting line at a temperature of 20 °C. Next, the plates were dried at room temperature, and the spots were observed in ultraviolet light at 254 and/or 366 nm (UV lamp, Camag, Basel, Switzerland). In each case, sharp and symmetric spots without a tendency for tailing were obtained. Each experiment was run in triplicate, and mean R_F (retardation factor) values were calculated.

Starting from the R_F values, the R_M parameters were computed as described in the formula:

$$R_M = \log(1/R_F - 1) \quad (1)$$

Linear correlations between the R_M values of the substances and the concentration of organic modifier in mobile phases were calculated for each compound with the Soczewiński-Wachtmeister equation [47].

$R_M = R_{M0} + aC$ where C is the concentration of the organic solvent (in %) in the mobile phase, a is the slope, and R_{M0} is the concentration of organic modifier extrapolated to zero.

4.4. Metabolic stability assay

The *in vitro* evaluation of metabolic pathways was performed by 120 min incubation of compounds 5–7 at 37 °C with mouse liver microsomes (MLMs) obtained from Sigma–Aldrich (St. Louis, MO, USA), according to the described previously protocols [48,49]. The LC/MS analyses with additional MS ion fragmentation of the products and substrates were performed to determine the most probable structures of metabolites.

4.5. Drug-drug interaction prediction

The used CYP3A4 P450-Glo™ commercial assay was purchased from Promega (Madison, WI, USA). The influence of compounds on CYP3A4 activity was tested according to the manufacturer protocol and as described previously [48,49]. The bioluminescence signal was measured with a microplate reader EnSpire (PerkinElmer, Waltham, MA, USA) in luminescence mode.

Supporting Information

In the supporting information available online at XXX, we provide the detailed procedures for the preparation of the compounds 21–30, copies of the NMR spectra ¹H, ¹³C, ⁷⁷Se and LCMS data for 5–17, lipophilicity data for compounds 5–17 by RP-TLC and the ion fragment analyses and the most probable structures of compounds 5, 6, 7 during our metabolic stability tests.

Declaration of competing interest

The authors declare that they have no known competing financial interests or personal relationships that could have appeared to influence the work reported in this paper.

Acknowledgements

This study was financially supported by Polish National Science Centre (NCN) grants: No UMO-2018/31/B/NZ7/02160 (synthesis of compounds 14–17) and N42/DBS/000027 (synthesis of 5–13). Wesam Ali was financed by Saarland University, “Landesforschungsförderungsprogramm” (Grant No.WT/2 e LFFP 16/01) and he is thankful to the Erasmus+ program co-financing his research stay in Poland. C.Z is thankful for the generous financial support of the KOHR GmbH and the Sapienza Ateneo Project funding scheme.

Appendix A. Supplementary data

Supplementary data to this article can be found online at <https://doi.org/10.1016/j.ejmech.2020.112435>.

References

- [1] S. Nobili, I. Landini, B. Giglioli, E. Mini, Pharmacological strategies for overcoming multidrug resistance, *Curr. Drug Targets* 7 (2006) 861–879.
- [2] A.A. Stavrovskaya, T.P. Stromskaya, Transport proteins of the ABC family and multidrug resistance of tumor cells, *Biochemistry (Mosc.)* 73 (2008) 592–604.
- [3] E. Teodori, S. Dei, S. Scapecchi, F. Gualtieri, The medicinal chemistry of multidrug resistance (MDR) reversing drugs, *Farmacologia* 57 (2002) 385–415.
- [4] R. Ernst, P. Kueppers, J. Stindt, K. Kuchler, L. Schmitt, Multidrug efflux pumps: substrate selection in ATP-binding cassette multidrug efflux pumps—first come, first served? *FEBS J.* 277 (2010) 540–549.
- [5] M.D. Hall, M.D. Handley, M.M. Gottesman, Is resistance useless? Multidrug resistance and collateral sensitivity, *Trends Pharmacol. Sci.* 30 (2009) 546–556.
- [6] X. Liu, ABC family transporters, *Adv. Exp. Med. Biol.* 1141 (2019) 13–100.
- [7] I. Genovese, A. Ilari, Y.G. Assaraf, F. Fazi, G. Colotti, Not only P-glycoprotein: amplification of the ABCB1-containing chromosome region 7q21 confers multidrug resistance upon cancer cells by coordinated overexpression of an assortment of resistance-related proteins, *Drug Resist. Updates* 32 (2017) 23–46.
- [8] H. Hamada, T. Tsuruo, Functional role for the 170- to 180-kDa glycoprotein specific to drug-resistant tumor cells as revealed by monoclonal antibodies, *Proc. Natl. Acad. Sci. U. S. A.* 83 (1986) 7785–7789.
- [9] Y. Tanigawara, N. Okamura, M. Hirai, M. Yasuhara, K. Ueda, N. Kioka, T. Komano, R. Hori, Transport of digoxin by human P-glycoprotein expressed in a porcine kidney epithelial cell line (LLC-PK1), *J. Pharmacol. Exp. Therapeut.* 263 (1992) 840–845.
- [10] G. Spengler, M. Gajdacs, M.A. Marc, E. Dominguez-Alvarez, C. Sanmartin, Organoselenium compounds as novel adjuvants of chemotherapy drugs—A promising approach to fight cancer drug resistance, *Molecules* 24 (2) (2019)

- 336.
- [11] K. Katayama, K. Noguchi, Y. Sugimoto, Regulations of P-glycoprotein/ABCB1/MDR1 in human cancer cells, *N. J. Sci.* (2014) 119–128.
 - [12] G. Spengler, J. Handzlik, I. Ocsovszki, M. Viveiros, K. Kiec-Kononowicz, J. Molnar, L. Amaral, Modulation of multidrug efflux pump activity by new hydantoin derivatives on colon adenocarcinoma cells without inducing apoptosis, *Anticancer Res.* 31 (2011) 3285–3288.
 - [13] A. Martins, A. Dymek, J. Handzlik, G. Spengler, A. Armada, J. Molnar, K. Kiec-Kononowicz, L. Amaral, Activity of fourteen new hydantoin compounds on the human ABCB1 efflux pump, *Vivo* 26 (2012) 293–297.
 - [14] E. Zeslowska, A. Kincses, G. Spengler, W. Nitek, K. Wyrzuc, K. Kiec-Kononowicz, J. Handzlik, The 5-aromatic hydantoin-3-acetate derivatives as inhibitors of the tumour multidrug resistance efflux pump P-glycoprotein (ABCB1): synthesis, crystallographic and biological studies, *Bioorg. Med. Chem.* 24 (2016) 2815–2822.
 - [15] E. Dominguez-Alvarez, M. Gajdacs, G. Spengler, J.A. Palop, M.A. Marc, K. Kiec-Kononowicz, L. Amaral, J. Molnar, C. Jacob, J. Handzlik, C. Sanmartin, Identification of selenocompounds with promising properties to reverse cancer multidrug resistance, *Bioorg. Med. Chem. Lett* 26 (2016) 2821–2824.
 - [16] N. Kerru, P. Singh, N. Koorbanally, R. Raj, V. Kumar, Recent advances (2015–2016) in anticancer hybrids, *Eur. J. Med. Chem.* 142 (2017) 179–212.
 - [17] A. Makowska, F. Saczewski, P.J. Bednarski, J. Saczewski, L. Balewski, Hybrid molecules composed of 2,4-Diamino-1,3,5-triazines and 2-imino-coumarins and coumarins. Synthesis and Cytotoxic Properties, *Molecules* 23 (7) (2018) 1616.
 - [18] P. Singla, V. Luxami, K. Paul, Synthesis and in vitro evaluation of novel triazine analogues as anticancer agents and their interaction studies with bovine serum albumin, *Eur. J. Med. Chem.* 117 (2016) 59–69.
 - [19] M. Gajdacs, G. Spengler, C. Sanmartin, M.A. Marc, J. Handzlik, E. Dominguez-Alvarez, Selenoesters and selenoanhydrides as novel multidrug resistance reversing agents: a confirmation study in a colon cancer MDR cell line, *Bioorg. Med. Chem. Lett* 27 (2017) 797–802.
 - [20] B. Wu, J. Ge, Z. Zhang, C. Huang, X. Li, Z. Tan, X. Fang, J. Sun, Combination of sodium selenite and doxorubicin prodrug Ac-Phe-Lys-PABC-ADM affects gastric cancer cell apoptosis in xenografted mice, *BioMed Res. Int.* 2019 (2019) 2486783.
 - [21] J. Handzlik, M. Bajda, M. Zygmunt, D. Maciag, M. Dybala, M. Bednarski, B. Filipek, B. Malawska, K. Kiec-Kononowicz, Antiarrhythmic properties of phenylpiperazine derivatives of phenytoin with alpha(1)-adrenoceptor affinities, *Bioorg. Med. Chem.* 20 (2012) 2290–2303.
 - [22] J. Handzlik, E. Szymanska, J. Chevalier, E. Otrebska, K. Kiec-Kononowicz, J.M. Pages, S. Alibert, Amine-alkyl derivatives of hydantoin: new tool to combat resistant bacteria, *Eur. J. Med. Chem.* 46 (2011) 5807–5816.
 - [23] W. Ali, M. Wiecek, D. Lazewska, R. Kurczab, M. Jastrzebska-Wiesek, G. Satala, K. Kucwaj-Brysz, A. Lubelska, M. Gluch-Lutwin, B. Mordyl, A. Siwek, M.J. Nasim, A. Partyka, S. Sudol, G. Latacz, A. Wesolowska, K. Kiec-Kononowicz, J. Handzlik, Synthesis and computer-aided SAR studies for derivatives of phenoxyalkyl-1,3,5-triazine as the new potent ligands for serotonin receptors 5-HT6, *Eur. J. Med. Chem.* 178 (2019) 740–751.
 - [24] S.-J. Zhu, H.-Z. Ying, Y. Wu, N. Qiu, T. Liu, B. Yang, X.-W. Dong, Y.-Z. Hu, Design, synthesis and biological evaluation of novel podophyllotoxin derivatives bearing 4β-disulfide/trisulfide bond as cytotoxic agents, *RSC Adv.* 5 (2015) 103172–103183.
 - [25] D. Lazewska, R. Kurczab, M. Wiecek, K. Kaminska, G. Satala, M. Jastrzebska-Wiesek, A. Partyka, A.J. Bojarski, A. Wesolowska, K. Kiec-Kononowicz, J. Handzlik, The computer-aided discovery of novel family of the 5-HT6 serotonin receptor ligands among derivatives of 4-benzyl-1,3,5-triazine, *Eur. J. Med. Chem.* 135 (2017) 117–124.
 - [26] S. Paudel, S. Acharya, K.M. Kim, S.H. Cheon, Design, synthesis, and biological evaluation of arylpiperazine-benzylpiperidines with dual serotonin and norepinephrine reuptake inhibitory activities, *Bioorg. Med. Chem.* 24 (2016) 2137–2145.
 - [27] P. Bernardelli, A. Denis, E. Lorthiois, H. Jacobelli, F. Vergne, D. Serradeil, F. Rousseau, A. Cronin, M. Kemp, Preparation of substituted phenols as histamine H3 ligands, Warner-Lambert Company LLC, USA, 2005, p. 126.
 - [28] S. Torii, T. Inokuchi, G. Asanuma, N. Sayo, H. Tanaka, A direct phenyl-selenenylation of alkyl halides, alkenyl sulfonates, and epoxides by an electroreduction of diphenyl diselenide, *Chem. Lett.* 9 (1980) 867–868.
 - [29] F. Malihi, D.L. Clive, C.C. Chang, Minaruzzaman, Synthetic studies on CP-225,917 and CP-263,114: access to advanced tetracyclic systems by intramolecular conjugate displacement and [2,3]-Wittig rearrangement, *J. Org. Chem.* 78 (2013) 996–1013.
 - [30] M.M. Cornwell, I. Pastan, M.M. Gottesman, Certain calcium channel blockers bind specifically to multidrug-resistant human KB carcinoma membrane vesicles and inhibit drug binding to P-glycoprotein, *J. Biol. Chem.* 262 (1987) 2166–2170.
 - [31] G. Spengler, M. Viveiros, M. Martins, L. Rodrigues, A. Martins, J. Molnar, I. Couto, L. Amaral, Demonstration of the activity of P-glycoprotein by a semi-automated fluorometric method, *Anticancer Res.* 29 (2009) 2173–2177.
 - [32] G. Spengler, M. Evaristo, J. Handzlik, J. Serly, J. Molnar, M. Viveiros, K. Kiec-Kononowicz, L. Amaral, Biological activity of hydantoin derivatives on P-glycoprotein (ABCB1) of mouse lymphoma cells, *Anticancer Res.* 30 (2010) 4867–4871.
 - [33] G. Latacz, A. Lubelska, M. Jastrzebska-Wiesek, A. Partyka, A. Sobilo, A. Olejarz, K. Kucwaj-Brysz, G. Satala, A.J. Bojarski, A. Wesolowska, K. Kiec-Kononowicz, J. Handzlik, The search for a lead structure among series of potent and selective hydantoin 5-HT7 R agents: the drug-likeness in vitro study, *Chem. Biol. Drug Des.* 90 (2017) 1295–1306.
 - [34] G. Latacz, A. Lubelska, M. Jastrzebska-Wiesek, A. Partyka, K. Kucwaj-Brysz, A. Wesolowska, K. Kiec-Kononowicz, J. Handzlik, MF-8, a novel promising arylpiperazine-hydantoin based 5-HT7 receptor antagonist: in vitro drug-likeness studies and in vivo pharmacological evaluation, *Bioorg. Med. Chem. Lett* 28 (2018) 878–883.
 - [35] G. Latacz, A.S. Hogendorf, A. Hogendorf, A. Lubelska, J.M. Wieronska, M. Wozniak, P. Cieslik, K. Kiec-Kononowicz, J. Handzlik, A.J. Bojarski, Search for a 5-CT alternative. In vitro and in vivo evaluation of novel pharmacological tools: 3-(1-alkyl-1H-imidazole-5-yl)-1H-indole-5-carboxamides, low-basicity 5-HT7 receptor agonists, *Medchemcomm* 9 (2018) 1882–1890.
 - [36] A.A. Mahbub, C.L. Le Maitre, S.L. Haywood-Small, N.A. Cross, N. Jordan-Mahy, Polyphenols act synergistically with doxorubicin and etoposide in leukaemia cell lines, *Cell Death Dis.* 1 (2015) 15043.
 - [37] A.A. Fernandez-Ramos, C. Marchetti-Laurent, V. Poindessous, S. Antonio, C. Petitgas, I. Ceballos-Picot, P. Laurent-Puig, S. Bortoli, M.A. Lorient, N. Pallet, A comprehensive characterization of the impact of mycophenolic acid on the metabolism of Jurkat T cells, *Sci. Rep.* 7 (2017) 10550.
 - [38] A. Zuryń, A. Litwiniec, L. Gackowska, A. Pawlik, A.A. Grzanka, A. Grzanka, Expression of cyclin A, B1 and D1 after induction of cell cycle arrest in the Jurkat cell line exposed to doxorubicin, *Cell Biol. Int.* 36 (2012) 1129–1135.
 - [39] H. Luo, Y. Yang, F. Huang, F. Li, Q. Jiang, K. Shi, C. Xu, Selenite induces apoptosis in colorectal cancer cells via AKT-mediated inhibition of beta-catenin survival axis, *Canc. Lett.* 315 (2012) 78–85.
 - [40] H. Zeng, W.H. Cheng, L.K. Johnson, Methylselenol, a selenium metabolite, modulates p53 pathway and inhibits the growth of colon cancer xenografts in Balb/c mice, *J. Nutr. Biochem.* 24 (2013) 776–780.
 - [41] D.S. Thakur, Topoisomerase II inhibitors in cancer treatment, *Int J Pharm Sci Nanotechnol* 3 (2011) 1173–1181.
 - [42] O. Tacar, C.R. Dass, Doxorubicin-induced death in tumour cells and cardiomyocytes: is autophagy the key to improving future clinical outcomes? *J. Pharm. Pharmacol.* 65 (2013) 1577–1589.
 - [43] B.J. Aubrey, G.L. Kelly, A. Janic, M.J. Herold, A. Strasser, How does p53 induce apoptosis and how does this relate to p53-mediated tumour suppression? *Cell Death Differ.* 25 (2018) 104–113.
 - [44] D.L. Clive, Z. Li, M. Yu, Intramolecular conjugate displacement: a general route to hexahydroquinolizines, hexahydroindolizines, and related [m,n,0]-bicyclic structures with nitrogen at a bridgehead, *J. Org. Chem.* 72 (2007) 5608–5617.
 - [45] Z. Janousek, S. Piettre, F. Gorissen-Hervens, H.G. Viehe, Capto-dative substituent effects, *J. Organomet. Chem.* 250 (1983) 197–202.
 - [46] G. Stazi, C. Battistelli, V. Piano, R. Mazzone, B. Marrocco, S. Marchese, S.M. Louie, C. Zwergel, L. Antonini, A. Patsilinakos, R. Ragno, M. Viviano, G. Sbardella, A. Ciogli, G. Fabrizi, R. Cirilli, R. Strippoli, A. Marchetti, M. Tripodi, D.K. Nomura, A. Mattevi, A. Mai, S. Valente, Development of alkyl glycerone phosphate synthase inhibitors: structure-activity relationship and effects on ether lipids and epithelial-mesenchymal transition in cancer cells, *Eur. J. Med. Chem.* 163 (2019) 722–735.
 - [47] E. Soczewiński, C.A. Wachtmeister, The relation between the composition of certain ternary two-phase solvent systems and RM values, *J. Chromatogr. A* 7 (1962) 311–320.
 - [48] A. Lubelska, G. Latacz, M. Jastrzebska-Wiesek, M. Kotanska, R. Kurczab, A. Partyka, M.A. Marc, D. Wilczynska, A. Doroz-Plonka, D. Lazewska, A. Wesolowska, K. Kiec-Kononowicz, J. Handzlik, Are the hydantoin-1,3,5-triazine 5-HT6R ligands a hope to a find new procognitive and anti-obesity drug? Considerations based on primary in vivo assays and ADME-tox profile in vitro, *Molecules* 24 (24) (2019) 4472.
 - [49] G. Latacz, A. Lubelska, M. Jastrzebska-Wiesek, A. Partyka, M.A. Marc, G. Satala, D. Wilczynska, M. Kotanska, M. Wiecek, K. Kaminska, A. Wesolowska, K. Kiec-Kononowicz, J. Handzlik, The 1,3,5-triazine derivatives as innovative chemical family of 5-HT6 serotonin receptor agents with therapeutic perspectives for cognitive impairment, *Int. J. Mol. Sci.* 20 (14) (2019) 3420.

4. Discussion

4.1. Synthetic strategies for the designing of novel 5-HT₆ Serotonin

Receptor Ligands

The project has been focused on introducing two ways of chemical modifications on the 1,3,5-triazine motif by involving hydantoin and chalcogens (oxygen, sulfur, and selenium) ether- moieties. This study reports the synthesis of the first novel organo-selenium compound to serve as a ligand for 5-HT₆ receptors. From the perspective of drug design, the *N*-methyl piperazine fragment contains the positive ionizable nitrogen PI-feature. The hydantoin (imidazolidine-2,4-dione) moiety has two carbonyl functional groups, which serve as hydrogen bond acceptor (HBA-feature). Interestingly, the chalcogen atoms also can serve as hydrogen bond acceptor. The heterocyclic 1,3,5-triazine moiety provides the central aromatic region (AR) of the pharmacophore. The substituents at the hydantoin fragment represent the hydrophobic area (HYD), which were replaced by benzene or benzene substituted functional groups in the new chalcogen molecules.

Thus, the following research tasks have been performed:

- ❖ Computer aided-rational design of new derivatives of 1,3,5-triazine.
- ❖ The synthesis of the derivatives of the lead structure.
- ❖ Studies *in vitro* on the affinity and selectivity of the compounds for the 5-HT₆ receptor. Radioligand binding assays have been employed for determining both the affinity and the selectivity profile of the synthesized compounds.
- ❖ *In vitro* functional studies on intrinsic mechanisms of action for selected active compounds found in the affinity studies *in vitro*.
- ❖ Drug-ability – ADMET studies *in vitro* for selected active compounds found in the affinity studies *in vitro*
- ❖ Structure-activity relationship analysis to review and modify pharmacophore features for the ligand-receptor interactions in the case of ligands for the 5-HT₆ receptor that belongs to the derivatives of 1,3,5-triazine.
- ❖ Analysis and elaboration of the obtained results.

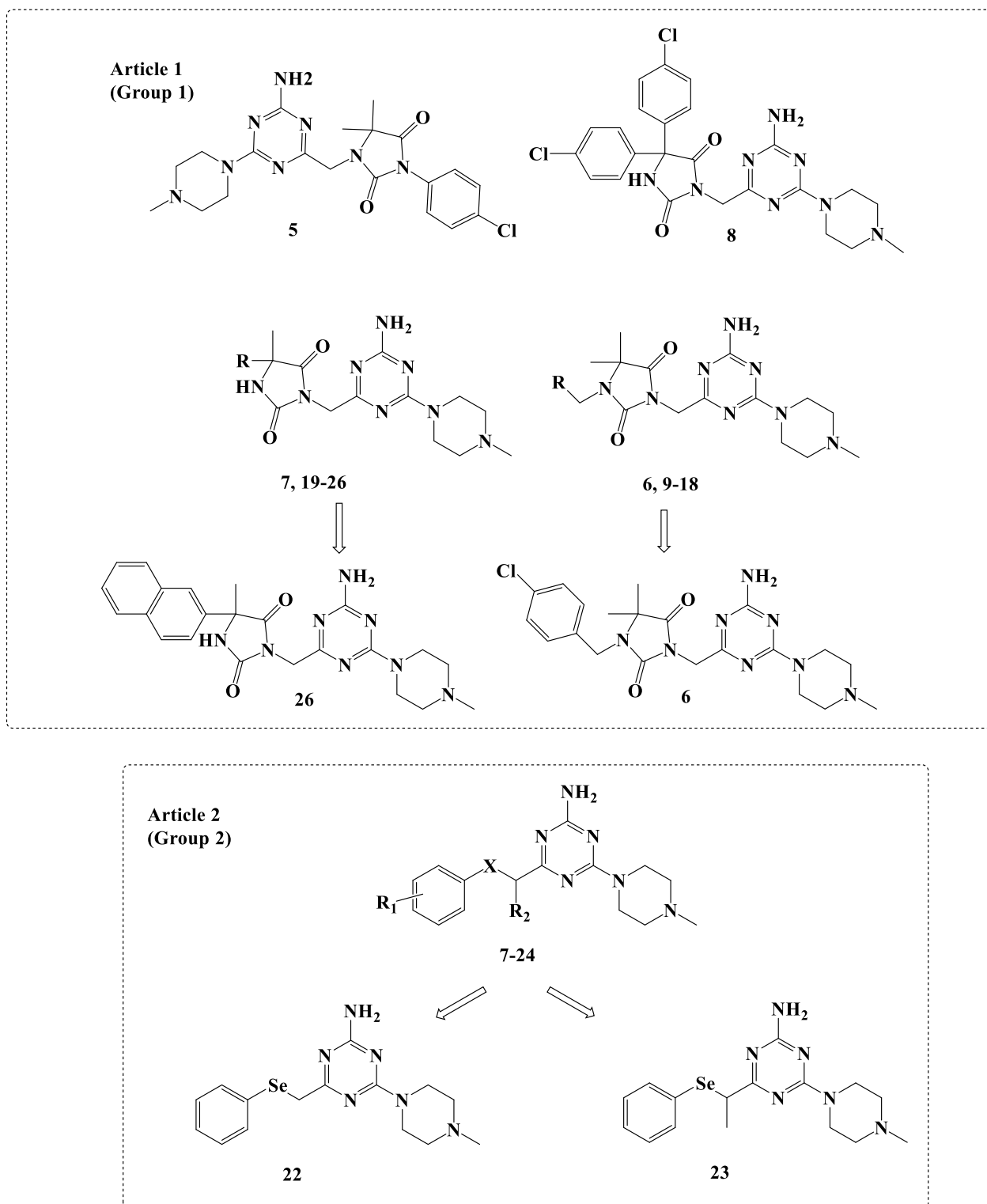


Figure 7: General structures for the 5-HT₆ serotonin receptor ligands

Two novel groups of serotonin receptors 5-HT₆ ligands have been prepared, *i.e.*, aromatic triazine-methyl piperazine, coupled with a hydantoin spacer between 1,3,5-triazine (Group 1) and the aromatic fragment, and phenoxy alkyl-, phenyl thioether- or phenyl selenoether-1,3,5-triazine derivatives with a carbon spacer (Group 2). Figure 7

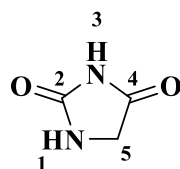
22 new compounds have been synthesized for Group 1, employing four different synthetic pathways (107). Nuclear magnetic resonance (NMR), Mass spectra (MS), and chromatographic analytical methods confirm the structures and purity of the obtained compounds. Melting point, percentage yield, physical state, $^1\text{H-NMR}$, $^{13}\text{C-NMR}$, molecular weight, and purity have been reported for the final compounds. In general, the compounds have been obtained in good yield and purity. No specific conditions are needed as the compounds are stable, and no unpleasant smell has been recorded. The compounds are prepared following the procedures described in Article 1 and stored at room temperature.

17 new compounds have been synthesized for Group 2 (108). Since all the obtained compounds are solid, hence melting point, percentage yield, physical state, $^1\text{H-NMR}$, $^{13}\text{C-NMR}$, molecular weight, and purity have been reported for the final compounds. The compounds have been obtained in good yield and have been purified by recrystallization. All the compounds are stable, and no unpleasant smell has been recorded. The selenium compounds have been prepared in an inert nitrogen atmosphere at room temperature.

4.2. Biological evaluation of the 5-HT₆ ligands

Considering Lipinski's rule of five, the data obtained show good lipophilicity (3.14-4.49) determined with the standard reversed-phase thin-layer chromatography RP-TL. All the hydantoin-triazines derivatives (**4–26**) are predicted as blood-brain-barrier BBB-permeable.

Because of its unique structure, hydantoin is considered as a versatile motif in medicinal chemistry comprising of five potential substituent sites, including two hydrogen bond acceptors and two hydrogen bond donors. Moreover, the delocalization of the negative charge at the imidic nitrogen atom provides hydantoin a weak acid property, making N-3H more prone to ionization than at N-1H. As a result, the N-3H position is more reactive toward electrophiles in a basic medium than N-1H, Figure 8.



imidazolidine-2,4-dione

Figure 8: Hydantoin structure with atom numbers.

Computer-aided SAR (structure-activity relationship) analysis reveals a significant influence of linker and aromatic moiety to enhance the affinity of the hydantoin ring for the 5-HT₆R. Besides, the substitution at the hydantoin ring shows that the methylene group at position 3 of hydantoin is profitable. In contrast, a significant decrease in the radioligand binding assay activity is noted for substitution by the methylene group at position 1 (**5**). The combination of hydantoin substituted at position 5 with the β -naphthyl moiety provides the compound **26** with desired features. Compound **26** presents good drug-like features, such as the lipophilicity (3.76) and molecular weight (446.50). Compound (**26**) displays antidepressant-like activity *in vivo* in forced swim test (FST) and anxiolytic-like activities employing the Vogel conflict drinking test. Compounds **6** and **26** also exhibit antiobesity properties.

Still, the hydantoin series provides several hints to improve the design of the compounds. As observed, the hydantoin ring doesn't prove to be critical for 5-HT₆R affinity. The highest affinity is obtained with the compound with the largest hydrophobic area **26**, which follows Rodríguez *et al.* suggestion for the pharmacophore model (35). Furthermore, a higher affinity for HT₆R affinity has also been observed for compounds containing more electron-donating functional groups at the phenyl ring at *para* position (compound **6**). In general, the most potent 5-HT₆R agents (**6** and **26**) display lower toxicity in the HEK-293 eukaryotic cell line.

These hints provide us with the idea to further modify the structure and replace the hydantoin ring with other hydrogen bond acceptor (HBA). For this purpose, we chose to employ the chalcogen elements (oxygen, sulfur, and selenium) to produce new compounds with better affinity and selectivity.

The combination of nitrogen heterocycles and chalcogens appears to be unique. And it is still following the model pharmacophore suggested by Rodríguez *et al.* and Łażewska *et al.* (35, 36).

Several modifications have been performed to enhance the affinity of compounds for 5-HT₆R. These modifications include: (a) the substituents at phenyl ring, including type, number, and position; (b) the methyl (un)branched linker; and (c) different chalcogen-ether linker concerning the *S*-oxidized form (SO₂), which is an indispensable structural feature of more than 80% 5-HT₆R agents (33, 109). Interestingly the results obtained confirm our previous findings regarding the substituents at phenyl ring, *i.e.*, a higher affinity towards 5-HT₆R receptors has been observed for compounds containing more electron-donating and hydrophobic substituents at the phenyl ring. In contrast to previous results, substitution at *ortho*-position turns out to be more favorable than substitution at *meta*- and *para*- positions for the binding of compounds with 5-HT₆R.

Similarly, mono substitution is more desirable than di-substitution. Replacing oxygen with sulfur and selenium, the impact of substituents at the phenyl ring has been less significant. In contrast, the methyl branching proves to be more critical and significantly improves the affinity. In general, the biological results obtained indicate that this chemical family, consisting of the skeleton of 2-amine-1,3,5-triazine core combined with methyl piperazine at position 4 and ether-linked phenyl at position 6, tends to target 5-HT₆R rather selectively. Besides, the compounds investigated display excellent antidepressant-like activity *in vivo* in forced swim test (FST).

Regarding the selenium compounds, two "representative" selenoethers (**22** and **23**) show affinities towards 5-HT₆R, although they are deprived of any particular substituents at the phenyl moiety. The unbranched Se-ether (**22**) exhibits radioligand binding affinity two-fold higher as compared to the corresponding oxygen derivative. This affinity increases with the branched Se-ether (**23**) and provides the maximum 5-HT₆R affinity with butyl branched (data is not published yet). The selenium atom with a larger atomic radius size and more electron density seems to be important from the perspective of affinity towards the receptor. On the other hand, the tellurium analogous is not stable and is not possible to obtain.

As the metabolic test is performed for the most active compounds, it could be essential to investigate the redox behavior for different analogous to get a better idea about the role of chalcogens on 5-HT₆R affinity.

4.3. Design and synthesis of ABCB1 efflux pump modulating agents

Three different groups of organoselenium compounds have been employed to evaluate their efficacy as ABCB1 efflux pump modulating agents. These groups include 5-arylhydantoin derivatives (Group A), piperazine derivatives (Group B), and 1,3,5-triazine derivatives (Group C). As a result, 13 new compounds have been synthesized. The biological screening included the evaluation of the efflux pump inhibition effect, cytotoxicity, and antiproliferative properties, have been performed. The *in vitro* ADMET (absorption, distribution, metabolism, elimination, and toxicity) studies for selected compounds **5-7** have also been performed (18).

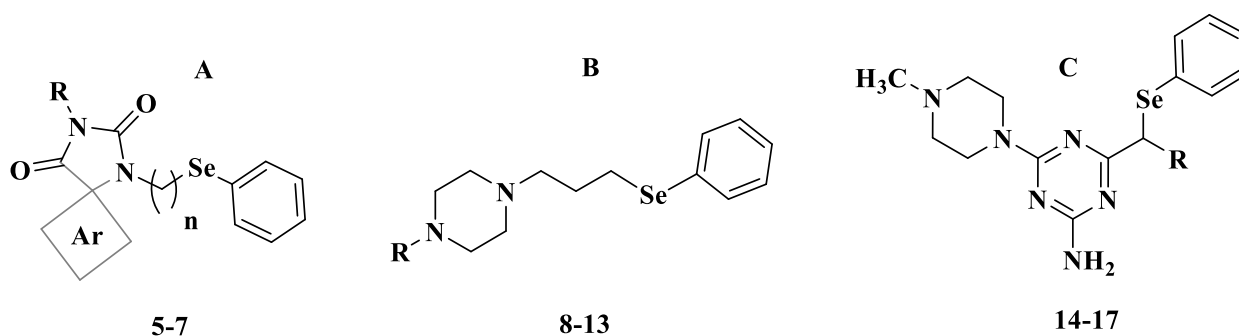


Figure 9: General structures of the ABCB1 efflux pump modulating agents

4.4. Biological evaluation of phenylselenoether-hydantoin hybrids

As discussed before, the hydantoin ring has a unique structure with two reactive nitrogen centres toward electrophiles. N-3H position is more reactive toward electrophiles. After the alkylation of N-3H, the Se-alkylation on N-1H is possible with high yield and purity. From a biological point of view, hydantoin-containing compounds display a spectrum of biological activities, *i.e.*, anticancer (110, 111), antimicrobial (112), antibiotic (113), androgen receptor modulators(114), P-glycoprotein efflux pump inhibitors (102), and 5-HT₆ serotonin receptor ligands with anti-depressive-like, anxiolytic and antiobesity action *in vivo* (107).

Regarding our work, the hydantoin derivatives (Group A) exhibit the highest ABCB1 inhibitory activity, which is up to 2.6-fold more than the reference drug verapamil. They also display significant ABCB1 substrate potency, which has been significantly higher than that of reference drug verapamil in Pgp ATPase assay. Moreover, this group demonstrates significant cytotoxic and antiproliferative properties in the MDR cancer cells of T-lymphoma.

Interestingly, the length of the linker and the substitution at the hydantoin ring is of considerable importance. The hydantoin derivatives represent the highest lipophilicity values (3.82-6.05). The data has been gained employing the standard RP-TLC method, proving the importance of the lipophilicity on the ABCB1 inhibition effect. The highest activity has been observed for 5,5-diphenylhydantoin (compound **6**) with the most extended carbon linker (C6), log(p)= 6.05.

Remarkably, Spengler *et al.* (115) and Źesławska *et al.* (102) have already reported that both 5,5-diphenylhydantoin and 5-spirofluorenehydantoin moieties combined with aryl piperazine inhibit ABCB1. Nevertheless, this combination did not exhibit any cytotoxic or antiproliferative activity against cancer cells (T-lymphoma) pump modulation activity (102, 115, 116). Replacing aryl piperazine with phenylselenoether, however, enhanced the cytotoxic and antiproliferative activities.

Piperazine is an imperative nitrogen heterocycle which has been found in three families of pharmaceuticals: fluoroquinolone family of antibiotics, antihistamine drugs containing cyclizine cores, and the homologous blood pressure medications, prazosin, terazosin, and doxazosin.

In general, piperazine and its derivatives display numerous biological activities, including anticancer properties (117), antituberculosis effect (118), serotonergic receptors affinity (119), and antiarrhythmic properties (120). Furthermore, they can be considered as excellent replacements for other nucleophiles to improve the overall pharmacological and drug-ability of the molecules. Since 2010, about 50 patents containing piperazine moiety have been presented. Piperazine core provides two secondary nitrogen atoms, which increase their solubility in water and hence bioavailability. As a result, the piperazine core can be employed as a subunit in drug design (121, 122). In our work, we employed these properties to produce hydrochloride form of the piperazine compounds to increase water solubility.

Piperazine phenylseleno-ethers (Group B) provide less efflux pump inhibition than Group A. The structure-activity relationship reveals a variation in both ABCB1-inhibitory and anticancer properties correlated to the changing of the substitutions at the *N*-piperazine. These substitutions include aromatic, alkyl, and ester moieties, which in turn influence the hydrophobic properties of the resulting compounds, in the following order: 3,4-diCl-Ph (**11**) > 4-F-Ph (**10**) > Ph (**8**) > 2-MeO-Ph (**9**) > Me (**12**) > EtOCO (**13**). The most hydrophobic 3,4-dichlorophenyl substituted compound (**11**) exhibits the highest efflux pump modulatory (fluorescence activity ratio FAR = 2.27 at 2 mM), cytotoxic (The half-maximal inhibitory concentration IC₅₀ = 3.50 mM) and anti-proliferative (IC₅₀ = 3.66 mM) activities.

Our results confirm that the aromatic ring, combined with positive ionizable nitrogen of piperazine, conforms with the structural requirements of binding pockets found in various protein targets, which play essential roles in mammal tissues. Recent evidence indicates their anticancer properties (117). More electron-donating substitutions on the aromatic ring provide more cytotoxic and antiproliferative effects in sensitive parental (PAR) and resistant (MDR) mouse T-lymphoma cell lines. Compound **11** exhibits corresponding or even slightly stronger antiproliferative properties than those of hydantoin derivatives **5** and **7**.

Finally, the compounds belonging to the group of triazine phenylseleno-ethers (**14-17**, group C) are inactive. In this group, only dimethyl-branched derivative **17** displays notable antiproliferative potential in MDR T-lymphoma (IC₅₀ = 8.28 mM). These results show clearly that the triazine ring is not a suitable candidate for ABCB1 efflux pump inhibition. It is also confirming the selectivity of this moiety for the application for new 5-HT₆R ligands, which is proved in Article 2.

Overall, the selenoether linker is vital for the cytotoxic and antiproliferative properties of hydantoin and piperazine. Furthermore, the length of the carbon linker also plays a significant role in biological activities. The activity decreases significantly, moving from the most active hydantoin derivative **6**, with C6-linker, to the compounds with C4-linker (**5** and **7**) and C3-linker of phenylpiperazine derivatives. The same pattern has also been observed for group C. Yet, the exact role of selenium in this activity is still not clear and needs more investigations. Moreover, the role of chalcogens (oxygen, sulfur, and selenium) and their related anti- or pro-oxidant activity should be studied to clarify the role of selenium in the cytotoxic and the antiproliferative activities.

5. Conclusions

The present study has described the synthesis and biological evaluation of three families of new potent compounds, arylhydantoin derivatives, phenyl piperazine selenoether, and 1,3,5-triazine derivatives. Comprehensive studies, i.e., design, synthesis, *in vitro* ADMET-screening, and biological evaluation, including detailed insight into cellular mechanisms of anticancer activity and in-depth SAR analysis, have been performed.

Among the various series of compounds that have been prepared as a part of this study, the hydantoin selenoether derivatives represent the most promising group of compounds. Hydantoin selenoether significantly inhibited the crucial tumor MDR mechanism of ABCB1-efflux pump in mouse T-lymphoma cell line transfected with the human MDR1 gene, which codes for the ABC transporter ABCB, even better than the reference inhibitor verapamil. Besides, hydantoin and phenylpiperazine-selenoethers exhibited excellent cytotoxic and antiproliferative activities in both sensitive (PAR) and resistant (MDR) mouse T-lymphoma cell lines. The promising antiproliferative activity of the hydantoins has also been confirmed in non-lymphocytic cancer cells, *i.e.*, neuroblastoma, suggesting a therapeutically promising broader spectrum of anticancer potency for this family.

On the other hand, the seleniumether- triazine moiety has been employed to synthesize the first novel organo-selenium compound for 5-HT₆ receptors.

Considering lines of evidence indicating antidepressive, precognitive, and neuroprotective roles of selenides, the organic selenium compounds **22** and **23** (Article 2) represent an excellent starting point for new chemical modifications in the search for successful CNS-seleno agents acting *via* the 5-HT₆ receptor.

In addition to a wide range of pharmacomodulation possibilities are also possible. These compounds can be considered suitable novel lead structures for further chemical modifications in the hunt for highly potent and selective 5-HT₆R antagonists. Moreover, phenyl chalcogen-nitrogen heterocyclic derivatives may serve as new promising alternatives in search of 5-HT₆R agents. This unique structure differs remarkably from the conventional sulfone and indole motifs. It may form a basis for advancement in searching for new therapies of the CNS diseases related to this exceptional serotonin GPCR.

In conclusion, this study describes the synthesis of novel 5-HT₆R ligands and ABCB1 efflux pump modulating agents. These compounds may serve as new lead structures for further pharmacomodulations and extended mechanistic studies as well as a medicinal chemistry optimization.

6. References

1. Guillaume Maroisa ABaWL. Population aging, migration, and productivity in Europe. *Proceedings of the National Academy of Sciences* 2020;117(14):7690–5.
2. Bonomo SAaRA. Taking stock of infections and antibiotic resistance in the elderly and long-term care facilities: a survey of existing and upcoming challenges. *European Journal of Microbiology and Immunology* 2011;1(3):190-7.
3. V.Belikov Aloop. Age-related diseases as vicious cycles. *Ageing Research Reviews*. 2019;49:11-26.
4. collaborators NC. NCD Countdown 2030: worldwide trends in noncommunicable disease mortality and progress towards Sustainable Development Goal target 3.4. *THE LANCET*. 2018;392(10152):1072-88.
5. Noncommunicable diseases country profiles 2018 [database on the Internet]. 2018 [cited September 2020]. Available from: <https://www.who.int/nmh/publications/ncd-profiles-2018/en/>.
6. Barron EJ. Age-Related Diseases and Clinical and Public Health implications for the 85 Years Old and Over Population. *Frontiers in Public Health*. 2017;5:1-7.
7. Jennifer E. DeVoe LSW, and George E. Fryer Jr. Patient Age Influences Perceptions About Health Care Communication. *Family medicine*. 2009;41(2):126-33.
8. Causes of death by chapters of the ICD-10 and gender. Wiesbaden, Germany: Statistisches Bundesamt (Federal Statistical Office); 2020 [updated 18 May 2020; cited 2020 18 May 2020]; Available from: <https://www.destatis.de/EN/Themes/Society-Environment/Health/Causes-Death/Tables/number-of-death.html;jsessionid=671FAFF1226AE73156041C767F1C90A8.internet8712>.
9. Orden JLaKAV. Sadness and Worry in Older Adults: Differentiating Psychiatric Illness from Normative Distress. *The Medical clinics of North America*. 2020;104(5):843-54.
10. Ryan D McMahan DEB, Christine S Ritchie, Chengshi Jin, Ying Shi, Daniel David, Evan J Walker, Victoria L Tang and Rebecca L Sudore. Anxious, Depressed, and Planning for the Future: Advance Care Planning in Diverse Older Adults. *Journal of the American Geriatrics Society*. 2020:1-5.
11. Pshuk OOBaNG. Age and gender features of depressive and anxiety symptoms of depressive disorders. *Wiadomości lekarskie* 2020;73(7):1476-9.
12. Judith Dams ER, Regina Steil, Babette Renneberg, Rita Rosner and Hans-Helmut König. Health-Related Quality of Life and Costs of Posttraumatic Stress Disorder in Adolescents and Young Adults in Germany. *Frontiers in psychiatry*. 2020;11(697):1-8.
13. Hyung-Mun Yun K-RP, Eun-Cheol Kim, Sanghyeon Kim and Jin Tae Hong. Serotonin 6 receptor controls alzheimer's disease and depression. *Oncotarget*. 2015;6:26716-28.
14. Anna Więckowska TW, Justyna Godyń, Adam Bucki, Monika Marcinkowska, Agata Siwek, Krzysztof Więckowski, Paula Zaręba, Damijan Knez, Monika Głuch-Lutwin, Grzegorz Kazek, Gniewomir Latacz, Kamil Mika, Marcin Kołaczkowski, Jan Korabecny, Ondrej Soukup, Marketa Benkova, Katarzyna Kieć-Kononowicz, Stanislav Gobec and Barbara Malawska. Novel Multitarget-Directed Ligands Aiming at Symptoms and Causes of Alzheimer's Disease. *ACS Chemical Neuroscience*. 2018;9(5):1195-214.
15. Magdalena Kotańska KL, Adam Bucki, Monika Marcinkowska, Joanna Śniecikowska and Marcin Kołaczkowski. Idalopirdine, a selective 5-HT 6 receptor antagonist, reduces food intake and body weight in a model of excessive eating. *Metabolic brain disease*. 2018;33(3):733-40.
16. Tas DCaD. Cancer in the elderly. *North Clin Istanbul* 2015;2(1):73-80.
17. Estapé T. Cancer in the Elderly: Challenges and Barriers. *Asia-Pacific Journal of Oncology Nursing*. 2015;5(1):40-2.
18. Wesam Ali GS, Annamaria Kincses, Marta Nove, Cecilia Battistelli, Gniewomir Latacz, Małgorzata Starek, Monika Dabrowska, Ewelina Honkisz-Orzechowska, Annalisa Romanelli, Manuela Monica Rasile, Ewa Szymanska, Claus Jacob, Clemens Zwergel and Jadwiga Handzlik. Discovery of phenylselenoether-hydantoin hybrids as ABCB1 efflux pump modulating agents with cytotoxic and antiproliferative actions in resistant T-lymphoma. *European Journal of Medicinal Chemistry*. 2020;200:1-17.
19. Nicholas M.Barnes TS. A review of central 5-HT receptors and their function. *Neuropharmacology*. 1999;38(8):1083-152.
20. Sara Fidalgo DKiaSHW. Serotonin: from top to bottom. *Biogerontology*. 2013;14(1):21-45.
21. Lorke GAPaDE. The Role of Serotonin in Singultus: A Review. *Frontiers in Neuroscience*. 2020;14(629):1-11.
22. 5-HT receptor. Wikipedia 2020 [updated 14 June 2020; cited 2020 25 August]; Available from: https://en.wikipedia.org/wiki/5-HT_receptor.

23. Hyung-Mun Yun HR. The Serotonin-6 Receptor as a Novel Therapeutic Target. *Experimental Neurobiology*. 2011;20(4):159-68.
24. Ruth Kohen MAM, Naseem Khan, Teresa Druck, Kay Huebner, Jean E. Lachowicz, Herbert Y. Meltzer, David R. Sibley, Bryan L. Roth, Mark W. Hamblin. Cloning, Characterization, and Chromosomal Localization of a Human 5-HT₆ Serotonin Receptor. *Journal of neurochemistry*. 1996;66(1):47-56.
25. Marie L. Woolley CAM, Kevin Fone. 5-HT₆ receptors. *Current drug targets CNS and neurological disorders*. 2004;3(1):59-79.
26. Magdalena Jastrzębska-Więsek AS, Anna Partyka, Marcin Kołaczkowski, Maria Walczak, Magdalena Smolik, Gniewomir Latacz, Katarzyna Kieć-Kononowicz, Anna Wesołowska. Study on the effect of EMD386088, a 5-HT₆ receptor partial agonist, in enhancing the anti-immobility action of some antidepressants in rats. *Naunyn-Schmiedeberg's Arch Pharmacol*. 2018;391:37-49.
27. Lili Hu BW, Yan Zhang. Serotonin 5-HT₆ receptors affect cognition in a mouse model of Alzheimer's disease by regulating cilia function. *Alzheimer's Research & Therapy*. 2017;9(76):1-17.
28. Marcin Kołaczkowski MM, Adam Bucki, Joanna Śniecikowska, Maciej Pawłowski, Grzegorz Kazek, Agata Siwek, Magdalena Jastrzebska-Wiesek, Anna Partyka, Anna Wasik, Anna Wesołowska,, Paweł Mierzejewski PB. Novel 5-HT₆ receptor antagonists/D₂ receptor partial agonists targeting behavioral and psychological symptoms of dementia. *European Journal of Medicinal Chemistry*. 2015;92:221-35.
29. Magdalena Kotańska KL, Adam Bucki, Monika Marcinkowska, Joanna Śniecikowska, Marcin Kołaczkowski. Idalopirdine, a selective 5-HT₆ receptor antagonist, reduces food intake and body weight in a model of excessive eating. *Metabolic Brain Disease*. 2018:1-8.
30. Jörg Holenz PJP, Jose' Luis Di'az, Ramon Merce, Xavier Codony, Helmut Buschmann. Medicinal chemistry strategies to 5-HT₆ receptor ligands as potential cognitive enhancers and antiobesity agents. *Drug Discovery Today*. 2006;11(7-8):283-99.
31. Andrew J Sleight FGB, Michael Bös, Bernard Levet-Trafit, Claus Riemer, Anne Bourson. Characterization of Ro 04-6790 and Ro 63-0563: potent and selective antagonists at human and rat 5-HT₆ receptors. *British journal of pharmacology*. 1998;124(3):556-62.
32. Charles-Henry Fabritius UP, Josef Messinger, Raymond Horvath, Harri Salo, Michał Gałęzowski, Mariusz Galek, Klaudia Stefan'ska, Joanna Szeremeta-Spisak, Marta Olszak-Płachta, Anna Buda, Justyna Adamczyk, Marcin Król, Peteris Prusis, Magdalena Sieprawska-Lupa, Maciej Mikulski, Katja Kuokkanen, Hugh Chapman, Radosław Obuchowicz, Timo Korjamo, Niina Jalava, Mateusz Nowak 1-Sulfonyl-6-Piperazinyl-7-Azaindoles as potent and pseudoselective 5-HT₆ receptor antagonists. *Bioorganic & Medicinal Chemistry Letters*. 2016;26:2610-5.
33. Annamaria Lubelska GL, Magdalena Jastrzebska-Wiesek, Magdalena Kotanska, Rafał Kurczab, Anna Partyka, Małgorzata Anna Mar'c , Daria Wilczy ska, Agata Doroz-Płonka, Dorota Ła'zewsk , Anna Wesołowska, Katarzyna Kie'c-Kononowicz, Jadwiga Handzlik. Are the Hydantoin-1,3,5-triazine 5-HT₆R Ligands a Hope to a Find New Procognitive and Anti-Obesity Drug? Considerations Based on Primary In Vivo Assays and ADME-Tox Profile In Vitro. *Molecules*. 2019;24(4472):1-24.
34. Ramakrishna Nirogi RA, Vijay Benade, Rajesh Medapati, Pradeep Jayarajan, Gopinadh Bhyrapuneni, NageswaraRao Muddana, Venkat Mekala, Ramkumar Subramanian, Anil Shinde, Ramasastry Kambhampati, Venkat Jasti. SUVN-502, a novel, potent, pure, and orally active 5-HT₆ receptor antagonist: pharmacological, behavioral, and neurochemical characterization. *Behavioural pharmacology*. 2019 30(1):16-35.
35. María L. López-Rodríguez BB, Tania de la Fuente, Arantxa Sanz, Leonardo Pardo, Mercedes Campillo. A Three-Dimensional Pharmacophore Model for 5-Hydroxytryptamine₆ (5-HT₆) Receptor Antagonists. *Journal of Medicinal Chemistry*. 2005;48(13):4216-9.
36. Dorota Ła'zewska RK, Małgorzata Wiecek, Katarzyna Kaminska, Grzegorz Satała, Magdalena Jastrzebska-Wiesek, Anna Partyka, Andrzej J. Bojarski, Anna Wesołowska, Katarzyna Kieć-Kononowicz, Jadwiga Handzlik. The computer-aided discovery of novel family of the 5-HT₆ serotonin receptor ligands among derivatives of 4-benzyl-1,3,5-triazine. *European Journal of Medicinal Chemistry*. 2017;135:117-24.
37. David Benton RC. Selenium supplementation improves mood in a double-blind crossover trial. *Psychopharmacology*. 1990;102:549-50.
38. Wayne Chris Hawkes LH. Effects of Dietary Selenium on Mood in Healthy Men Living in a Metabolic Research Unit. *Society of Biological Psychiatry*. 1996;39:121-8.
39. Rayman MP. The importance of selenium to human health. *THE LANCET*. 2000;356:233-41.
40. Ulrich Schweizer AUB, Josef Kohrle, Robert Nitsch, Nicolai E. Savaskan. Selenium and brain function: a poorly recognized liaison. *Brain Research Reviews* 45. 2004;45:164- 78.

41. Solovyev ND. Importance of selenium and selenoprotein for brain function: from antioxidant protection to neuronal signalling. *Journal of Inorganic Biochemistry*. 2015;153:1-12.
42. Eva K. Wirth MC, Jochen Winterer, Christian Wozny, Bradley A. Carlson, Stephan Roth, Dietmar Schmitz, Georg W. Bornkamm, Vincenzo Coppola, Lino Tessarollo, Lutz Schomburg, Josef Kohrle, Dolph L. Hatfield, Ulrich Schweizer. Neuronal selenoprotein expression is required for interneuron development and prevents seizures and neurodegeneration. *The FASEB Journal*. 2010;24(3):844-52.
43. Anja Bräuer NS. Molecular Actions of Selenium in the Brain: Neuroprotective Mechanisms of an Essential Trace Element. *Reviews in the neurosciences*. 2004;15(1):19-32.
44. Carla Elena Sartori Oliveira BMG, Benhur Godoi, Gilson Zenin, Cristina Wayne Nogueira. The antidepressant-like action of a simple selenium-containing molecule, methyl phenylselenide, in mice. *European Journal of Pharmacology*. 2012;690:119-23.
45. César Augusto Brüning ACGS, Bibiana Mozzaquatro Gai, Gilson Zeni, Cristina Wayne Nogueira. Antidepressant-like effect of m-trifluoromethyl-diphenyl diselenide in the mouse forced swimming test involves opioid and serotonergic systems. *European Journal of Pharmacology*. 2011;658:145-9.
46. Bibiana Mozzaquatro Gai CFB, César Augusto Brüning, Vanessa Angonesi Zborowski, André Luiz Stein, Gilson Zeni, Cristina Wayne Nogueira. Depression-related behavior and mechanical allodynia are blocked by 3-(4-fluorophenylselenyl)-2,5-diphenylselenophene in a mouse model of neuropathic pain induced by partial sciatic nerve ligation. *Neuropharmacology*. 2014;79:580-9.
47. Bibiana M. Gay MP, André L. Stein, Cristina W. Nogueira. Antidepressant-like pharmacological profile of 3-(4-fluorophenylselenyl)-2,5-diphenylselenophene: Involvement of serotonergic system. *Neuropharmacology*. 2010;59:172-9.
48. Cristiano R. Jesse EAW, Cristiani F. Bortolato, Cristina W. Nogueira. Evidence for the involvement of the serotonergic 5-HT_{2A/C} and 5-HT₃ receptors in the antidepressant-like effect caused by oral administration of bis selenide in mice. *Progress in Neuro-Psychopharmacology & Biological Psychiatry*. 2010;34:294-302.
49. Franciele Donato MGDG, André Tiago Rossito Goes, Natália Seus, Diego Alves, Cristiano Ricardo Jesse, Lucielli Savegnago, more S. Involvement of the dopaminergic and serotonergic systems in the antidepressant-like effect caused by 4-phenyl-1-(phenylselanyl)methyl-1,2,3-triazole. *Life sciences*. 2013;93(9-11):393-400.
50. Lucielli Savegnago CRJ, Larissa G. Pinto, Joao B.T. Rocha, Cristina W. Nogueira. Diphenyl diselenide attenuates acute thermal hyperalgesia and persistent inflammatory and neuropathic pain behavior in mice. *B R A I N R E S E A R C H*. 2007;1175:54-9.
51. Lucielli Savegnago CRJ, Larissa Garcia Pinto, Joao Batista Teixeira Rocha, Daniela Aline Barancelli, Cristina Wayne Nogueira, Gilson Zeni. Diphenyl diselenide exerts antidepressant-like and anxiolytic-like effects in mice: Involvement of L-arginine-nitric oxide-soluble guanylate cyclase pathway in its antidepressant-like action. *Pharmacology, Biochemistry and Behavior*. 2008;88:418-26.
52. Lucielli Savegnago CRJ, Larissa G. Pinto, Joao B.T. Rocha, Cristina W. Nogueira, Gilson Zeni. Monoaminergic agents modulate antidepressant-like effect caused by diphenyl diselenide in rats. *Progress in Neuro-Psychopharmacology & Biological Psychiatry*. 2007;31:1261-9.
53. Viviane Glaser BM, Ariana Schmitz, Alcir Luiz Dafré, Evelise Maria Nazari, Yara Maria Rauh Müller, Luciane Feksa, Marcos Raniel Straliotho, Andreza Fabro de Bem, Marcelo Farina, João Batista Teixeira da Rocha, Alexandra Latini. Protective effects of diphenyl diselenide in a mouse model of brain toxicity. *Chemico-Biological Interactions*. 2013;206:18-26.
54. Hyoung-Chun Kim W-KJ, Dong-Young Choi, Doo-Hyun Im, Eun-Joo Shin, Jeong-Hye Suh, Robert A. Floyd, Guoying Bing. Protection of methamphetamine nigrostriatal toxicity by dietary selenium. *Brain Research*. 1999;851:76-86.
55. Hyoung-Chun Kim W-KJ, Eun-Joo Shin, Guoying Bing. Selenium deficiency potentiates methamphetamine-induced nigral neuronal loss; comparison with MPTP model. *Brain Research* 862. 2000;862:247-52.
56. Barbara R. Cardoso BRR, Charles B. Malpas, Lucy Vivash, Sila Genc, Michael M. Saling, Patricia Desmond, Christopher Steward, Rodney J. Hicks, Jason Callahan, Amy Brodtmann, Steven Collins, Stephen Macfarlane, Niall M Corcoran, Christopher M. Hovens, Dennis Velakoulis, Terence J. O'Brien, Dominic J. Hare, Ashley I. Bush. Supranutritional Sodium Selenate Supplementation Delivers Selenium to the Central Nervous System: Results from a Randomized Controlled Pilot Trial in Alzheimer's Disease. *Neurotherapeutics*. 2019;16:192-202.

57. Ewa Kędzierska JD, Ewa Poleszak, Jolanta H. Kotlińska. Antidepressant and anxiolytic-like activity of sodium selenite after acute treatment in mice. *Pharmacological reports*. 2017;69(2):276-80.
58. Jamal Rafique SS, Rômulo Faria Santos Canto, Tiago Elias Allievi Frizon, Waseem Hassan, Emily Pansera Waczuk, Maryam Jan, Davi Fernando Back, João Batista Teixeira Da Rocha, Antonio Luiz Braga. Synthesis and Biological Evaluation of 2-Picolylamide-Based Diselenides with Non-Bonded Interactions. *Molecules*. 2015;20(6):10095-109.
59. Bhaskar J. Bhuyana GM. Synthesis, characterization and antioxidant activity of angiotensin converting enzyme inhibitor. *Organic & Biomolecular Chemistry*. 2011;9(5):1356-65.
60. Bhaskar J. Bhuyana GM. Antioxidant activity of peptide-based angiotensin converting enzyme inhibitors. *Organic & Biomolecular Chemistry*. 2012;10(11):2237-47.
61. Liwei Zhao JL, Yiquan Li, Jianwen Liu, Thomas Wirth, Zhong Li. Selenium-containing naphthalimides as anticancer agents: design, synthesis and bioactivity. *Bioorganic & Medicinal Chemistry*. 2012;20(8):2558-63.
62. Kim C LJ, Park MS. Synthesis of new diorganodiselenides from organic halides: their antiproliferative effects against human breast cancer MCF-7 cells. *Archives of Pharmacol Research*. 2015 38(5):659-65.
63. Eduardo H. G. da Cruz MAS, Guilherme A. M. Jardim, Jarbas M. Resende, Bruno C. Cavalcanti, Igor S. Bomfim, Claudia Pessoa, Carlos A. de Simone, Giancarlo V. Botteselle, Antonio L. Braga, Divya K. Nair, Irishi N. N. Namboothiri, David A. Boothman, Eufrânio N. da Silva Júnior. Synthesis and antitumor activity of selenium-containing quinone-based triazoles possessing two redox centres, and their mechanistic insights. *European Journal of Medicinal Chemistry*. 2016;122:1-16.
64. Pramod K. Sahu TU, Jinha Yu, Akshata Nayak, Gyudong Kim, Minsoo Noh, Jae-Young Lee, Dae-Duk Kim, Lak Shin Jeong. Selenoacyclovir and Selenoganciclovir: Discovery of a New Template for Antiviral Agents. *Journal of Medicinal Chemistry*. 2015;58(21):8734-8.
65. Jozef Salon JJ, Jia Sheng, Oksana O. Gerlits, and Zhen Huang. Derivatization of DNAs with selenium at 6-position of guanine for function and crystal structure studies. *Nucleic acids research*. 2008;36(22):7009–18.
66. Huiyan Sun JS, Abdalla E. A. Hassan, Sibao Jiang, Jianhua Gan, Zhen Huang. Novel RNA base pair with higher specificity using single selenium atom. *Nucleic acids research*. 2012;40(11):5171-9.
67. Stefania Nobili IL, Barbara Giglioni and Enrico Mini. Pharmacological strategies for overcoming multidrug resistance. *Current Drug Targets*. 2006;7(7):861-79.
68. Baguley BC. Multiple Drug Resistance Mechanisms in Cancer. *Molecular Biotechnology*. 2010;43:308–16.
69. Stavrovskaya AA. Cellular mechanisms of multidrug resistance of tumor cells. *Biochemistry (Mosc)*. 2000;65(1):95-106.
70. Wanjiru Muriithi LWM, Carlos Pilotto Heming, Juliana Lima Echevarria, Atunga Nyachieo, Paulo Niemeyer Filho and Vivaldo Moura Neto. ABC transporters and the hallmarks of cancer: roles in cancer aggressiveness beyond multidrug resistance. *Cancer biology & medicine*. 2020;17(2):253-69.
71. Karol Bukowski MKaRK. Mechanisms of Multidrug Resistance in Cancer Chemotherapy. *International Journal of Molecular Sciences*. 2020;21(9):1-24.
72. Christopher F. Higgins IDH, George P. C. Salmond, Deborah R. Gill, J. Allan Downie, Ian J. Evans, I. Barry Holland, Lindsay Gray, Scott D. Buckel, Alexander W. Bell, Mark A. Hermodson A family of related ATP-binding subunits coupled to many distinct biological processes in bacteria. *Nature*. 1986;323(6087):448-50.
73. Pedersen PL. Transport ATPases into the year 2008: a brief overview related to types, structures, functions and roles in health and disease. *Journal of bioenergetics and biomembranes*. 2007;39(5-6):349-55.
74. Kentaro Tomii MK. A Comparative Analysis of ABC Transporters in Complete Microbial Genomes. *Genome research*. 1998;8:1048-59.
75. Wilkens S. Structure and mechanism of ABC transporters. *F1000Prime Reports*. 2015;7(14):1-9.
76. NatashaCant NP, Robert C.Ford. CFTR structure and cystic fibrosis. *The International Journal of Biochemistry & Cell Biology*. 2014;52:15-25.
77. Cédric Orelle FJDA, Michael L. Oldham, Arnaud Orelle, Theodore E. Wiley, Jue Chen, Amy L. Davidson. Dynamics of alpha-helical subdomain rotation in the intact maltose ATP-binding cassette transporter. *Proceedings of the National Academy of Sciences of the United States of America*. 2010 107(47):20293-8.
78. Frederick R. Blattner GP, Craig A. Bloch, Nicole T. Perna, Valerie Burland, Monica Riley, Julio Collado-Vides, Jeremy D. Glasner, Christopher K. Rode, George F. Mayhew, Jason Gregor, Nelson Wayne

- Davis, Heather A. Kirkpatrick, Michael A. Goeden, Debra J. Rose, Bob Mau, Ying Shao. The complete genome sequence of *Escherichia coli* K-12. *Science*. 1997;277(5331):1453-62.
79. Vasilis Vasiliou KV, Daniel W Neber. Human ATP-binding cassette (ABC) transporter family. *Human genomics*. 2009;3(3):281-90.
80. I.Barry Holland MB. ABC-ATPases, adaptable energy generators fuelling transmembrane movement of a variety of molecules in organisms from bacteria to humans. *Journal of Molecular Biology*. 1999;293(2):381-99.
81. Michael M. Gottesman TF, Susan E. Bates. Multidrug resistance in cancer: role of ATP-dependent transporters. *Nature Reviews Cancer*. 2002;2(1):48-58.
82. Kazuhiro Katayama KN, Yoshikazu Sugimoto. Regulations of P-Glycoprotein/ABCB1/MDR1 in Human Cancer Cells. *New Journal of Science*. 2014:1-10.
83. Sharom FJ. ABC multidrug transporters: structure, function and role in chemoresistance. *PHARMACOGENOMICS*. 2008;9(1):105-27.
84. Frank Thévenod JMF, Alice D. Katsen, Ingeborg A. Hause. Up-regulation of multidrug resistance P-glycoprotein via nuclear factor-kappaB activation protects kidney proximal tubule cells from cadmium- and reactive oxygen species-induced apoptosis. *The Journal of biological chemistry*. 2000;275(3):1887-96.
85. Lyrialle W. Han CG, Qingcheng Mao. An update on expression and function of p-gp/abcb1 and bcrp/abcg2 in the placenta and fetus. *Expert Opinion on Drug Metabolism & Toxicology*. 2018;14(8):817-29.
86. Fromm MF. Importance of P-glycoprotein at blood-tissue barriers. *Trends in pharmacological sciences*. 2004;25(8):423-9.
87. Angela Doran RSO, Bill J. Smith, Natilie A. Hosea, Stacey Becker, Ernesto Callegari, Cuiping Chen, Xi Chen, Edna Choo, Julie Cianfrogna, Loretta M. Cox, John P. Gibbs, Megan A. Gibbs, Heather Hatch, Cornelis E.C.A. Hop, Ilana N. Kasman, Jennifer LaPerle, JianHua Liu, Xingrong Liu, Michael Logman, Debra Maclin, Frank M. Nedza, Frederick Nelson, Emily Olson, Sandhya Rahematpura, David Raunig, Sabrinia Rogers, Kari Schmidt, Douglas K. Spracklin, Mark Szewc, Matthew Troutman, Elaine Tseng, Meihua Tu, Jeffrey W. Van Deusen, Karthik Venkatakrishnan, Gary Walens, Ellen Q. Wang, Diane Wong, Adam S. Yasgar, Chenghong Zhang. The impact of P-glycoprotein on the disposition of drugs targeted for indications of the central nervous system: evaluation using the MDR1A/1B knockout mouse model. *Drug metabolism and disposition: the biological fate of chemicals*. 2005;33(1):165-74.
88. Edmund Capparelli NR, Mark Mirochnick. Pharmacotherapy of perinatal HIV. *Seminars in fetal & neonatal medicine*. 2005;10(2):161-75.
89. Jingwei Zhang FZ, Xiaolan Wu, Xiaoxuan Zhang, Yuancheng Chen, Beth S Zha, Fang Niu, Meng Lu, Gang Hao, Yuan Sun, Jianguo Sun, Ying Peng, Guangji Wang. Cellular pharmacokinetic mechanisms of adriamycin resistance and its modulation by 20(S)-ginsenoside Rh2 in MCF-7/Adr cells. *British journal of pharmacology*. 2012;165(1):120-34.
90. Sen Yu YY, Li Liu, Xinting Wang, Shousi Lu, Yan Liang, Xiaodong Liu, Lin Xie, Guangji Wang. Increased plasma exposures of five protoberberine alkaloids from *Coptidis Rhizoma* in streptozotocin-induced diabetic rats: is P-GP involved? *Planta medica*. 2010;76(9):876-81.
91. Derek Spieler CN, Tamara Namendorf, Manfred Uhr. abcb1 ab p-glycoprotein is involved in the uptake of the novel antidepressant vortioxetine into the brain of mice. *Journal of Psychiatric Research*. 2019; 109:48-51.
92. Stephan Ruetz PG. Phosphatidylcholine translocase: a physiological role for the *mdr2* gene. *Cell*. 1994;77(7):1071-81.
93. Antonius E. van Herwaarden EW, Gracia Merino, Johan W. Jonker, Hilde Rosing, Jos H. Beijnen, Alfred H. Schinke. Multidrug transporter ABCG2/breast cancer resistance protein secretes riboflavin (vitamin B2) into milk. *Molecular and cellular biology*. 2007;27(4):1247-53.
94. Dirk M. Hermann CLB. Implications of ATP-binding cassette transporters for brain pharmacotherapies. *Trends in pharmacological sciences*. 2007;28(3):128-34.
95. Elaine M. Leslie RGD, Susan P.C. Cole. Multidrug resistance proteins: role of P-glycoprotein, MRP1, MRP2, and BCRP (ABCG2) in tissue defense. *Toxicology and applied pharmacology*. 2005;204(3):216-37.
96. Jacques Robert CJ. Multidrug Resistance Reversal Agents. *Journal of Medicinal Chemistry*. 2003;46(23):4805-17.
97. Ahcène Boumendjel HB, Cortay Doriane Trompier, Thomas Perrotton, Attilio Di Pietro. Anticancer multidrug resistance mediated by MRP1: recent advances in the discovery of reversal agents. *Medicinal research reviews*. 2005;25(4):453-72.

98. Yoshikazu Sugimoto ST, Etsuko Ishikawa, Junko Mitsuhashi. Breast cancer resistance protein: molecular target for anticancer drug resistance and pharmacokinetics/pharmacodynamics. *Cancer science*. 2005;96(8):457-65.
99. Yilin Fan XL. Alterations in Expression and Function of ABC Family Transporters at Blood-Brain Barrier under Liver Failure and Their Clinical Significances. *Pharmaceutics*. 2018;10(3):1-14.
100. Edward X She ZH. A novel piperazine derivative potently induces caspase-dependent apoptosis of cancer cells via inhibition of multiple cancer signaling pathways. *American journal of translational research*. 2013;5(6):622-33.
101. Bo Wang BZ, Zhe-Sheng Chen, Lu-Ping Pang, Yuan-Di Zhao, Qian Guo, Xin-Hui Zhang, Ying Liu, Guang-Yao Liu, Hao-Zhang, Xin-Yuan Zhang, Li-Ying Ma, Hong-Min Liu. Exploration of 1,2,3-triazole-pyrimidine hybrids as potent reversal agents against ABCB1-mediated multidrug resistance. *European Journal of Medicinal Chemistry*. 2018;143:1535-42.
102. Ewa Żesławska AK, Gabriella Spengler, Wojciech Nitek, Waldemar Tejchmana, Jadwiga Handzlik. Pharmacophoric features for a very potent 5-spirofluorenehydantoin inhibitor of cancer efflux pump ABCB1, based on X-ray analysis. *Chemical biology & drug design*. 2019;93(5):844-53.
103. Lei Jiao QQ, Baomin Liu, Tianxiao Zhao, Wenlong Huang, Hai Qian. Design, synthesis and evaluation of novel triazole core based P-glycoprotein-mediated multidrug resistance reversal agents. *Bioorganic & Medicinal Chemistry*. 2014;22:6857-66.
104. Ewa Żesławska AK, Gabriella Spengler, Wojciech Nitek, Karolina Wyrzuc, Katarzyna Kieć-Kononowicz, Jadwiga Handzlik. The 5-aromatic hydantoin-3-acetate derivatives as inhibitors of the tumour multidrug resistance efflux pump P-glycoprotein (ABCB1): Synthesis, crystallographic and biological studies. *Bioorganic & Medicinal Chemistry*. 2016;24:2815-22.
105. Chao Guo FL, Jie Qi, Jiahui Ma, Shiqi Lin, Caiyun Zhang, Qian Zhang, Hangyu Zhang, Rong Lu, and Xia Li. A Novel Synthetic Dihydroindeno[1,2-b] Indole Derivative (LS-2-3j) Reverses ABCB1- and ABCG2-Mediated Multidrug Resistance in Cancer Cells. *Molecules*. 2018;23(3264):1-14.
106. Avijeet Chopra AA, and Charles Giardina. Novel piperazine-based compounds inhibit microtubule dynamics and sensitize colon cancer cells to tumor necrosis factor-induced apoptosis. *The Journal of biological chemistry*. 2013;289(5):2978-91.
107. Rafał Kurczab WA, Dorota Łazewska, Magdalena Kotańska, Magdalena Jastrzębska-Więsek, Grzegorz Satała, Małgorzata Więcek, Annamaria Lubelska, Gniewomir Latacz, Anna Partyka, Małgorzata Starek, Monika Dąbrowska, Anna Wesołowska, Claus Jacob, Katarzyna Kieć-Kononowicz, Jadwiga Handzlik. Computer-Aided Studies for Novel Arylhydantoin 1,3,5-Triazine Derivatives as 5-HT₆ Serotonin Receptor Ligands with Antidepressive-Like, Anxiolytic and Antiobesity Action In Vivo. *Molecules*. 2018;23(10):1-26.
108. Wesam Ali MW, Dorota Łazewska, Rafał Kurczab, Magdalena Jastrzebska-Wiesek, Grzegorz Satała, Katarzyna Kucwaj-Brysz, Annamaria Lubelska, Monika Głuch-Lutwin, Barbara Mordyl, Agata Siwek,, Muhammad Jawad Nasim AP, Sylwia Sudoł, Gniewomir Latacz, Anna Wesołowska, Katarzyna Kieć-Kononowicz, Jadwiga Handzlik. Synthesis and computer-aided SAR studies for derivatives of phenoxyalkyl-1,3,5-triazine as the new potent ligands for serotonin receptors 5-HT₆. *European Journal of Medicinal Chemistry*. 2019;178:740-51.
109. Yan A Ivanenkov AGM, Mark S Veselov, Nina V Chufarova, Sergey S Baranovsky and Gleb I Filkov. Computational Approaches to the Design of Novel 5-HT₆ R Ligands. *Reviews in the neurosciences*. 2014;25(3):451-67.
110. Dana E. Rathkopf HIS. Apalutamide for the treatment of prostate cancer. *Expert Review of Anticancer Therapy*. 2018; 18(9):823-36.
111. MaoZhang Y-R, HuanLiMing-MingLiu, YangWang. Design, synthesis, and biological evaluation of hydantoin bridged analogues of combretastatin A-4 as potential anticancer agents. *Bioorganic & Medicinal Chemistry*. 2017;25(24):6623-34.
112. Shady Farah OA, Natalia Laout, Stanislav Ratner, Abraham J.Domb. Antimicrobial N-brominated hydantoin and uracil grafted polystyrene beads. *Journal of Controlled Release*. 2015;216:18-29.
113. Ma Su DX, Peng Teng, Alekhya Nimmagadda, Chao Zhang, Timothy Odom, Annie Cao, Yong Hu, Jianfeng Cai. Membrane-Active Hydantoin Derivatives as Antibiotic Agents. *Journal of Medicinal Chemistry*. 2017;60(20):8456-65.
114. Xin Wang WH, Jiazhong Li. QSAR Analysis of a Series of Hydantoin-based Androgen Receptor Modulators and Corresponding Binding Affinities. *Molecular informatics*. 2019;38(8-9):1-20.

115. Gabriella Spengler ME, Jadwiga Handzlik, Julianna Serly, Joseph Molnár, Miguel Viveiros, Katarzyna Kieć-Kononowicz and Leonard Amaral. Biological Activity of Hydantoin Derivatives on P-glycoprotein (ABCB1) of Mouse Lymphoma Cells. *Anticancer research*. 2010;30(12):4867-71.
116. Ewa Żesławska AK, Gabriella Spengler, Wojciech Nitek, Karolina Wyrzuc, Katarzyna Kieć-Kononowicz and Jadwiga Handzlik. The 5-aromatic hydantoin-3-acetate Derivatives as Inhibitors of the Tumour Multidrug Resistance Efflux Pump P-glycoprotein (ABCB1): Synthesis, Crystallographic and Biological Studies. *Bioorganic & medicinal chemistry*. 2016;24(12):2815-22.
117. Lee YB GY, Kim DJ, Ahn CH, Kong JY, Nam-Sook Kang. Synthesis, anticancer activity and pharmacokinetic analysis of 1-[(substituted 2-alkoxyquinoxalin-3-yl)aminocarbonyl]-4-(hetero)arylpiperazine derivatives. *Bioorganic & Medicinal Chemistry*. 2011;20(3):1303-9.
118. Adrian Blaser BDP, Hamish S. Sutherland, Iveta Kmentova, Scott G. Franzblau, Baojie Wan, Yuehong Wang, Zhenkun Ma, Andrew M. Thompson, William A. Denny. Structure-activity relationships for amide-, carbamate-, and urea-linked analogues of the tuberculosis drug (6S)-2-nitro-6-{[4-(trifluoromethoxy)benzyl]oxy}-6,7-dihydro-5H-imidazo[2,1-b][1,3]oxazine (PA-824). *Journal of Medicinal Chemistry*. 2011;55(1):312-26.
119. Jadwiga Handzlik AJB, Grzegorz Satala, Monika Kubacka, Bassem Sadek, Abrar Ashoor, Agata Siwek, Magorzata Wiecek, Katarzyna Kucwaj, Barbara Filipek, Katarzyna Kieć-Kononowicz. SAR-studies on the importance of aromatic ring topologies in search for selective 5-HT₇ receptor ligands among phenylpiperazine hydantoin derivatives. *European Journal of Medicinal Chemistry*. 2014;78:324-39.
120. Jadwiga Handzlik MB, Małgorzata Zygmunt, Dorota Macia, Małgorzata Dybała, Marek Bednarski, Barbara Filipek, Barbara Malawska, Katarzyna Kieć-Kononowicz. Antiarrhythmic properties of phenylpiperazine derivatives of phenytoin with α₁-adrenoceptor affinities. *Bioorganic & Medicinal Chemistry*. 2012;20:2290-303.
121. Anuj K. Rathi RS, Han-Seung Shin, Rahul V. Patel. Piperazine derivatives for therapeutic use: a patent review (2010-present). *Expert Opinion on Therapeutic Patents*. 2016;26(7):777-97.
122. Edon Vitaku DTS, and Jon T. Njardarson. Analysis of the Structural Diversity, Substitution Patterns, and Frequency of Nitrogen Heterocycles among U.S. FDA Approved Pharmaceuticals. *Journal of Medicinal Chemistry*. 2014;57(24):10257-74.

7. Supplementary Material

7.1. Supplementary material for Publication 1: Computer-Aided Studies for Novel Arylhydantoin 1,3,5-Triazine Derivatives as 5-HT₆ Serotonin Receptor Ligands with Antidepressive-Like, Anxiolytic and Antiobesity Action *In Vivo*.

Supplementary

Computer-aided studies for novel arylhydantoin 1,3,5-triazine derivatives as 5-HT₆ serotonin receptor ligands with antidepressive-like, anxiolytic and antiobesity action *in vivo*

Rafał Kurczab^{1†}, Wesam Ali^{2,6†}, Dorota Łażewska², Magdalena Kotańska³, Magdalena Jastrzębska-Więsek⁴, Grzegorz Satała¹, Małgorzata Więcek², Annamaria Lubelska², Gniewomir Latacz², Anna Partyka⁴, Małgorzata Starek⁵, Monika Dąbrowska⁵, Anna Wesołowska⁴, Claus Jacob⁶, Katarzyna Kieć-Kononowicz², Jadwiga Handzlik^{2,*}

Characteristics of intermediates obtained before 27, 29, 50-58, 63, 65 and 68-70

Cpd	Cas number	Article
27	860787-34-4 3-(4-chlorobenzyl)-5,5-dimethyl-1H-imidazole-2,4(3H,5H)-dione	SAR-studies on the importance of aromatic ring topologies in search for selective 5-HT ₇ receptor ligands among phenylpiperazine hydantoin derivatives. By Handzlik, Jadwiga et al From European Journal of Medicinal Chemistry, 78, 324-339; 2014
29	179409-69-9, Aldlab Chemicals Building Blocks United States methyl 2-(4,4-dimethyl-2,5-dioximidazolidin-1-yl)acetate	Preparation of substituted β -keto esters as intermediates for photographic yellow couplers Yamakawa, Kazuyoshi; Sato, Tadahisa Assignee Fuji Photo Film Co Ltd, Japan 1996
50	5397-13-7 5-(4-Chloro-phenyl)-5-methyl-imidazolidine-2,4-dione	Safari J. and Javadian L., Montmorillonite K-10 as a catalyst in the synthesis of 5, 5- disubstituted hydantoins under ultrasound irradiation, J. Chem. Sci. 125 (2013) 981– 987.
51	6843-49-8 5-Methyl-5-phenylhydantoin	Safari J. and Javadian L., Montmorillonite K-10 as a catalyst in the synthesis of 5, 5- disubstituted hydantoins under ultrasound irradiation, J. Chem. Sci. 125 (2013) 981– 987.
52	6946-01-6 5-(3-chlorophenyl)-5-methyl-2,4-imidazolidinedione	Safari J. and Javadian L., Montmorillonite K-10 as a catalyst in the synthesis of 5, 5- disubstituted hydantoins under ultrasound irradiation, J. Chem. Sci. 125 (2013) 981– 987.
53	795314-76-0 5-(2,5-dichlorophenyl)-5-methylimidazolidine-2,4-dione	Werbel LM, Elslager EF, Islip PJ and Closier MD, Antischistosomal effects of 5-(2,4,5-trichlorophenyl)hydantoin and related compounds, J Med Chem. 20 (1977):1569-1572.
54	64464-19-3 5-(2,4-dichlorophenyl)-5-methyl-2,4-imidazolidinedione	Werbel LM, Elslager EF, Islip PJ and Closier MD, Antischistosomal effects of 5-(2,4,5-trichlorophenyl)hydantoin and related compounds, J Med Chem. 20 (1977):1569-1572.
55	no	(Patent) Preparation of imidazolidinedione compounds containing substituted carbinol moiety as LXR modulators for treatment and prevention of arteriosclerosis, inflammation, diabetes, etc. Matsuda, Takayuki; Okuda, Ayumu; Koura, Minoru; Yamaguchi, Yuki; Kurobuchi, Sayaka; Watanabe, Yuuichirou; Shibuya, Kimiyuki Assignee: Kowa Company, Ltd., Japan 2008

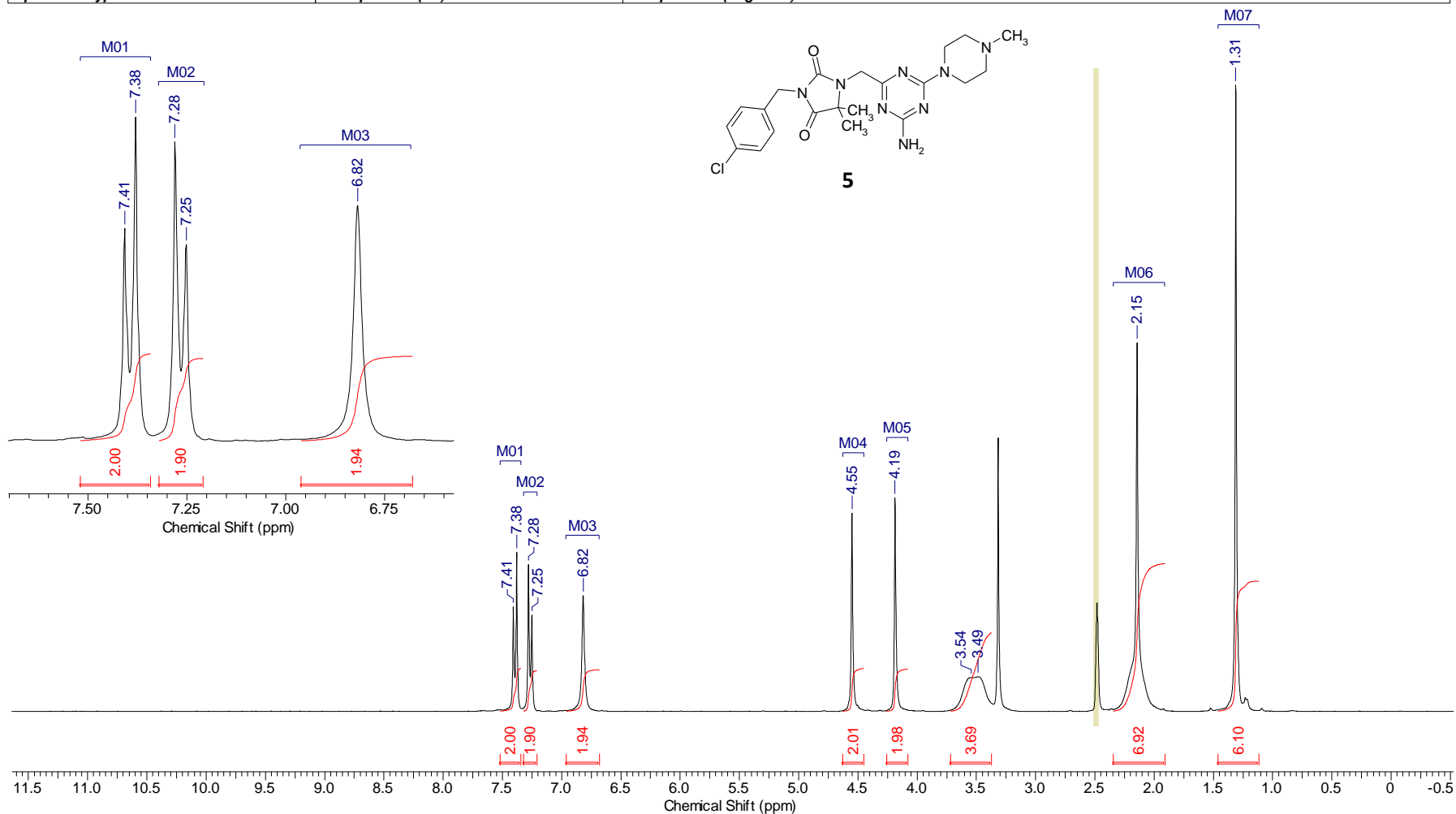
56	23186-96-1 5-methyl-5-(4-methylphenyl)-2,4-imidazolidinedione	J. Linol and G. Coquerel, Influence of high energy milling on the kinetics of the polymorphic transition from the monoclinic form to the orthorhombic form of (\pm)5-methyl-5-(4'-methylphenyl)hydantoin. J Therm Anal Calorim 90 (2007) 367-370.
57	82752-67-8 5-methyl-5-(1-naphthyl)-2,4-imidazolidinedione	M. L. KeshtovA. L. RusanovN. M. Belomoina and A. K. Mikitaev, Improved synthesis of bis[<i>p</i> -(phenylethynyl)phenyl]hetarylenes, Russ Chem Bull. 46 (1997) 1794-1796
58	78772-74-4 5-Methyl-5-(2-naphthyl)-2,4-imidazolidinedione	M. L. KeshtovA. L. RusanovN. M. Belomoina and A. K. Mikitaev, Improved synthesis of bis[<i>p</i> -(phenylethynyl)phenyl]hetarylenes, Russ Chem Bull. 46 (1997) 1794-1796
63	1372008-89-3, Aurora Building Blocks, United States Methyl 2-(4-(2,4-dichlorophenyl)-4-methyl-2,5-dioxoimidazolidin-1-yl)acetate	Aurora Building Blocks
65	1371767-82-6, Aurora Building Blocks, United States Methyl 2-(4-methyl-2,5-dioxo-4-p-tolylimidazolidin-1-yl)acetate	Aurora Building Blocks
68	104-88-1, 4-Chlorobenzaldehyde	sigma
69	88372-92-3 china 1,2-bis(4-chlorophenyl)ethane-1,2-dione	88372-92-3 China
70	23186-92-7, Atomax Chemicals Product List China 5,5-bis(4-chlorophenyl)imidazolidine-2,4-dione	Electrochemical characterization of phenytoin and its derivatives on bare gold electrode. Trisovic, Nemanja P.; Bozic, Bojan Dj.; Lovic, Jelena D.; Vitnik, Vesna D.; Vitnik, Zeljko J.; Petrovic, Slobodan D.; Ivic, Milka L. Avramov. Electrochimica Acta Volume 161 Pages 378-387 Journal; Online Computer File. 2015

$^1\text{H-NMR}$, $^{13}\text{C-N-NMR}$
for final products 5-27

This report was created by ACD/NMR Processor Academic Edition. For more information go to www.acdlabs.com/nmrproc/

1H-NMR

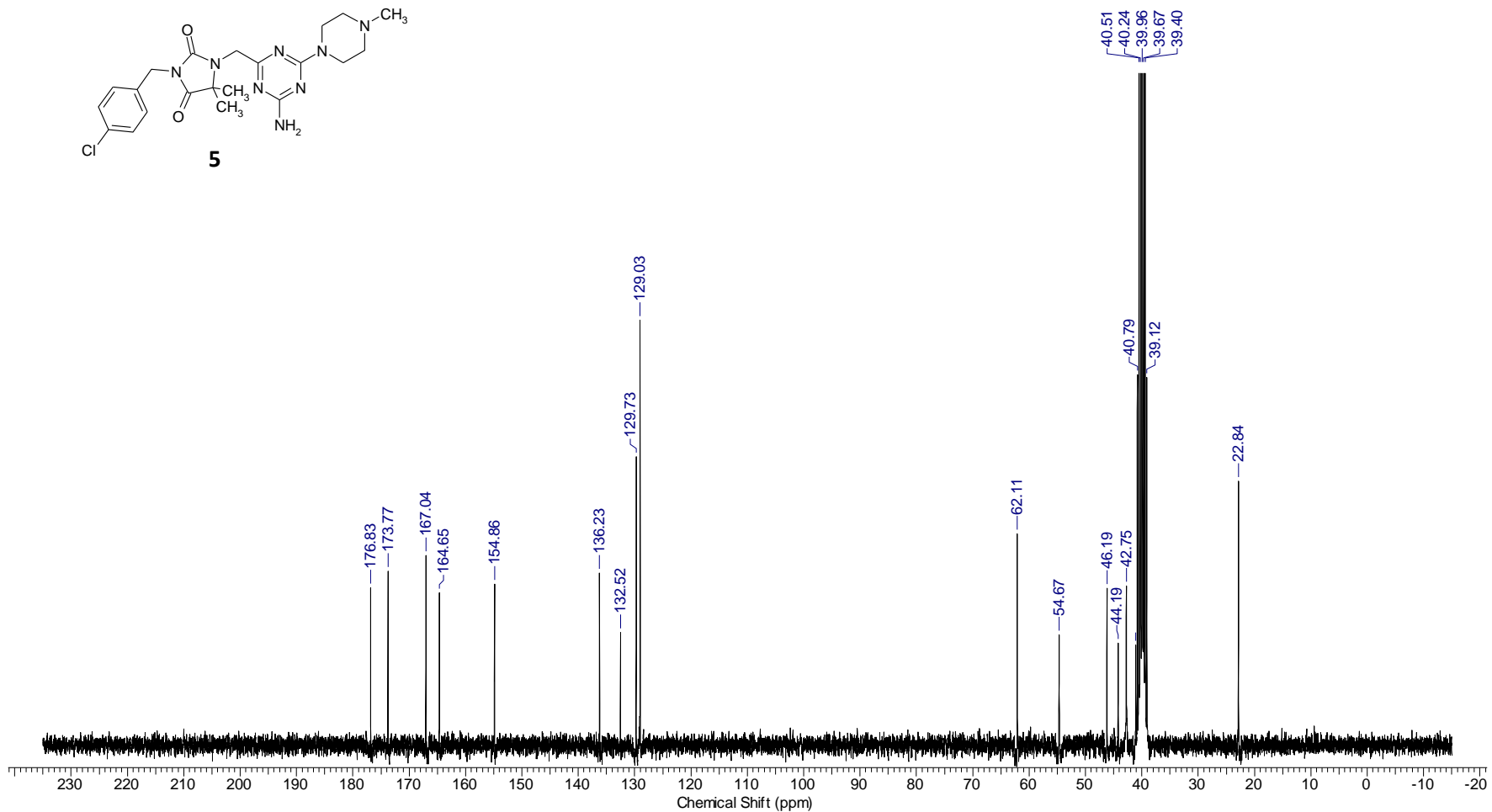
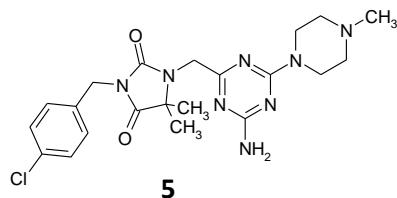
Acquisition Time (sec)	1.7064	Date	Oct 10 2017	Date Stamp	Oct 10 2017		2017-10-10 19:24:29
File Name	C:\Users\Dorota\Desktop\ANALIZY\NMR\2017\17-10-10_DJ24_dlaz\17-10-10_DJ24_dlaz_PROTON_01.fid\fid			Frequency (MHz)	300.08		
Nucleus	1H	Number of Transients	32	Original Points Count	8192	Points Count	8192
Pulse Sequence	s2pul	Receiver Gain	34.00	Solvent	DMSO-d6	Spectrum Offset (Hz)	1800.4814
Spectrum Type	STANDARD	Sweep Width (Hz)	4800.77	Temperature (degree C)	AMBIENT TEMPERATURE		



This report was created by ACD/NMR Processor Academic Edition. For more information go to www.acdlabs.com/nmrproc/

C13-NMR

Acquisition Time (sec)	0.8684	Date	Oct 17 2017	Date Stamp	Oct 17 2017	2017-10-18 11:39:50	
File Name	C:\Users\Dorota\Desktop\ANALIZYNMR\2017\17-10-17_DJ24_dlaz\17-10-17_DJ24_dlaz_CARBON_01.fid\fid						
Frequency (MHz)	75.46	Nucleus	13C	Number of Transients	3000	Original Points Count	16384
Points Count	16384	Pulse Sequence	s2pul	Receiver Gain	34.00	Solvent	DMSO-d6
Spectrum Offset (Hz)	8300.0879	Spectrum Type	STANDARD	Sweep Width (Hz)	18867.92	Temperature (degree C)	23.000

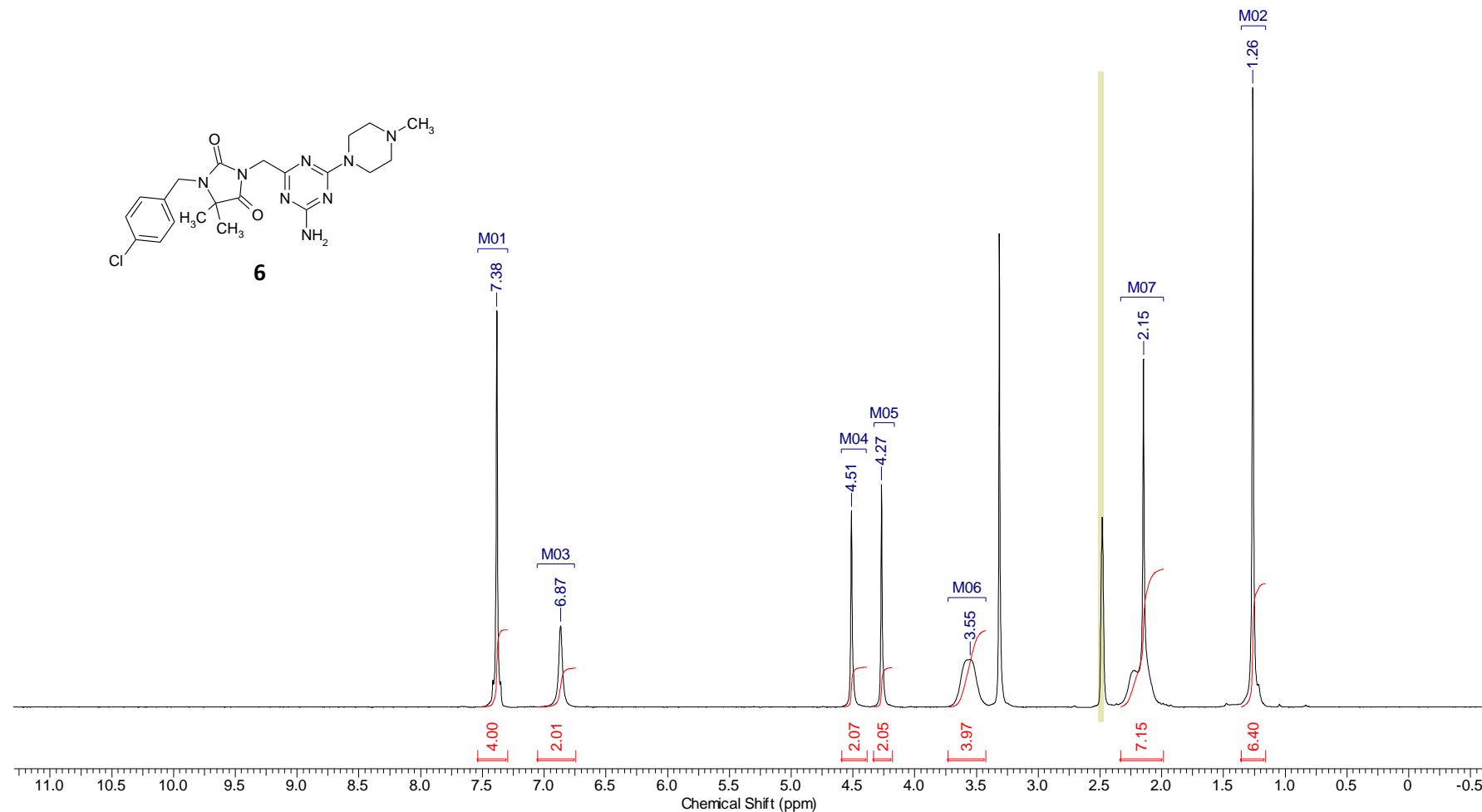


This report was created by ACD/NMR Processor Academic Edition. For more information go to www.acdlabs.com/nmrproc/

1H-NMR

2017-10-10 18:46:57

Acquisition Time (sec)	1.7064	Date	Oct 10 2017	Date Stamp	Oct 10 2017
File Name	C:\Users\Dorota\Desktop\ANALIZY\NMR\2017\17-10-10_DJ18_dlaz\17-10-10_DJ18_dlaz_PROTON_01.fid\fid			Frequency (MHz)	300.08
Nucleus	1H	Number of Transients	32	Original Points Count	8192
Pulse Sequence	s2pul	Receiver Gain	38.00	Solvent	DMSO-d6
Spectrum Type	STANDARD	Sweep Width (Hz)	4800.77	Spectrum Offset (Hz)	1800.4814
		Temperature (degree C)	AMBIENT TEMPERATURE		

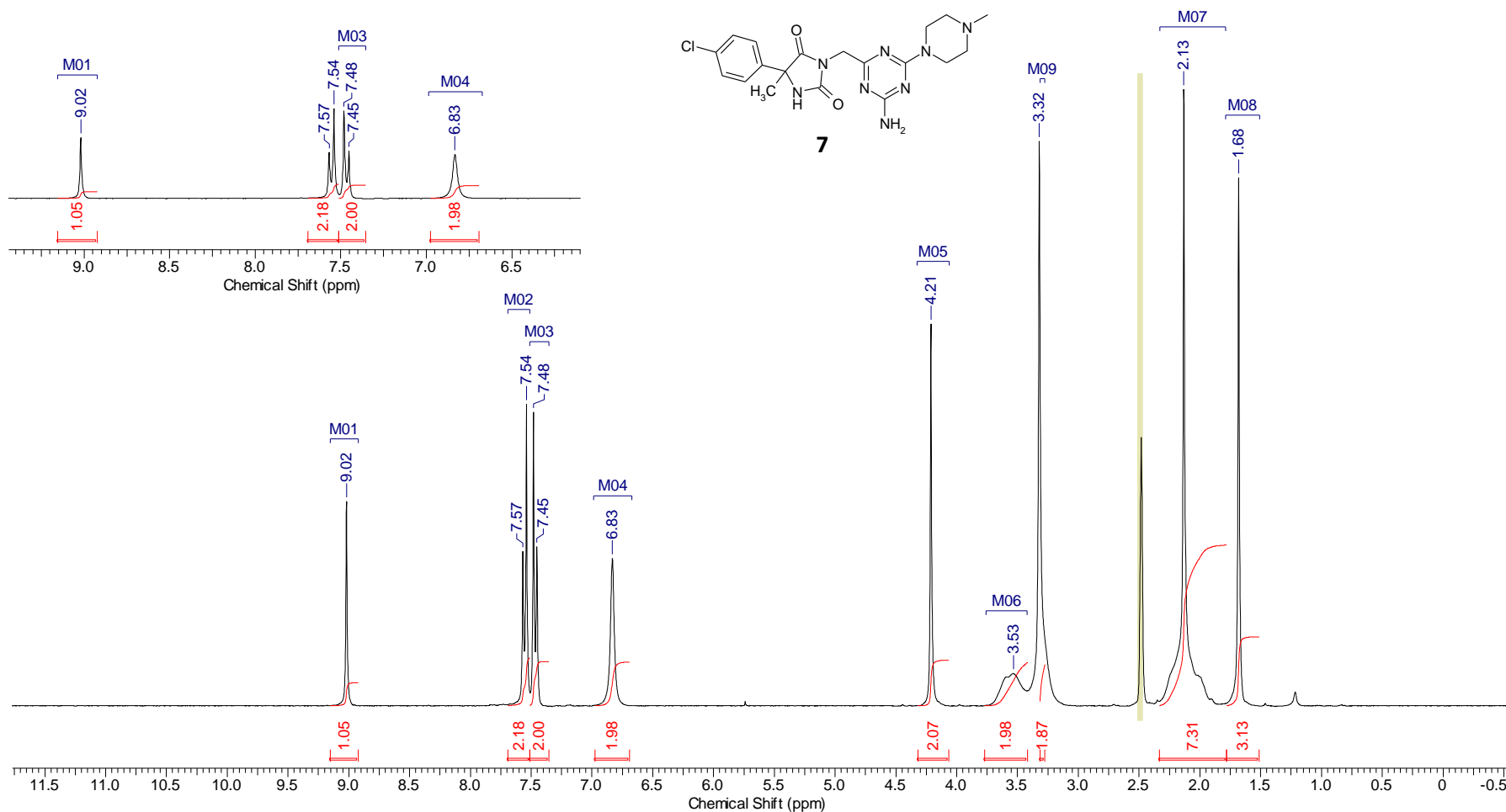


This report was created by ACD/NMR Processor Academic Edition. For more information go to www.acdlabs.com/nmrproc/

1H-NMR

2017-10-10 13:03:40

Acquisition Time (sec)	1.7064	Date	Oct 10 2017	Date Stamp	Oct 10 2017
File Name	C:\Users\Dorota\Desktop\ANALIZY\NMR\2017\17-10-10_DJ2_dlaz\17-10-10_DJ2_dlaz_PROTON_01.fid\fid			Frequency (MHz)	300.08
Nucleus	1H	Number of Transients	32	Original Points Count	8192
Pulse Sequence	s2pul	Receiver Gain	38.00	Solvent	DMSO-d6
Spectrum Type	STANDARD	Sweep Width (Hz)	4800.77	Temperature (degree C)	AMBIENT TEMPERATURE

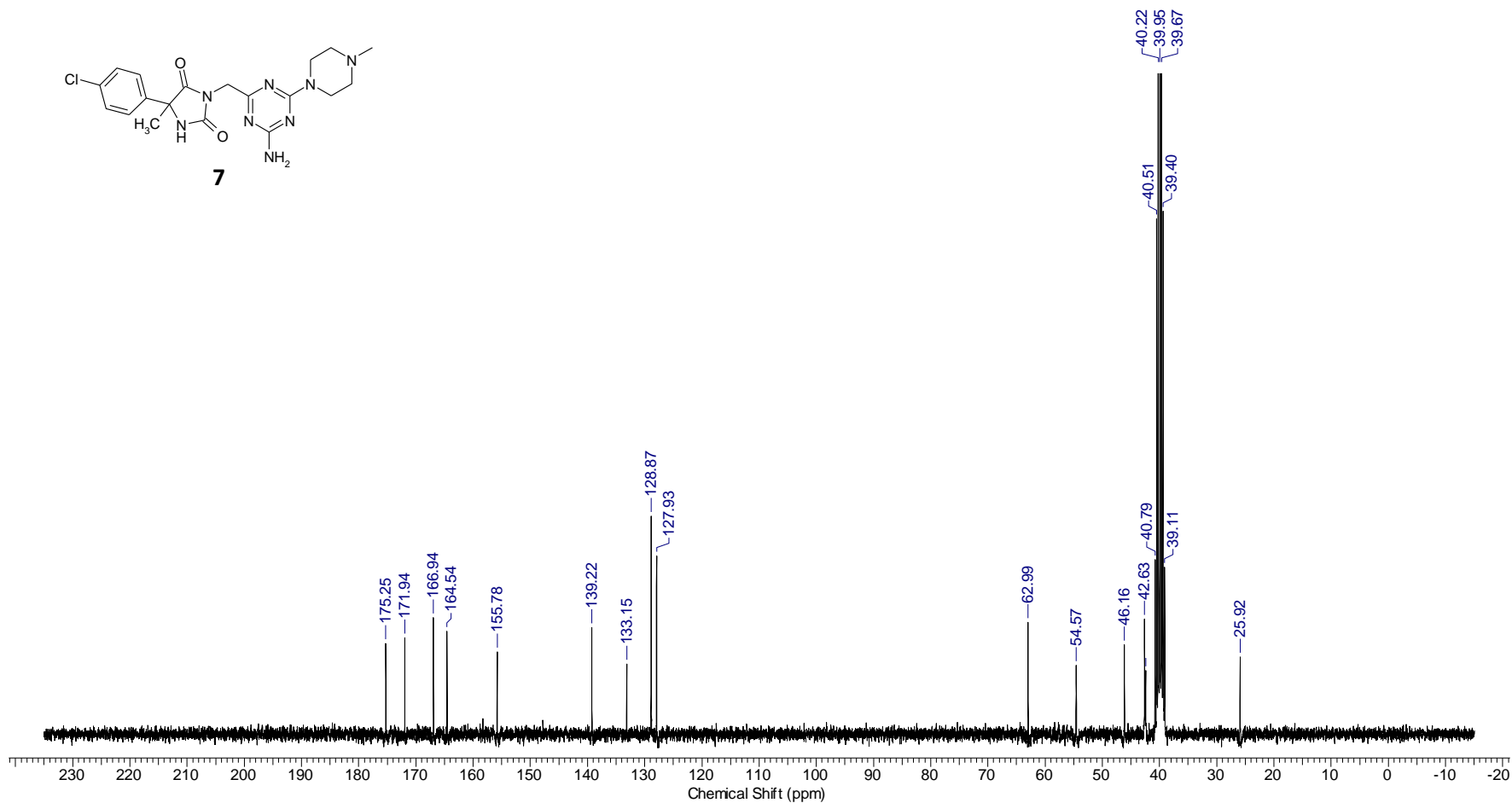
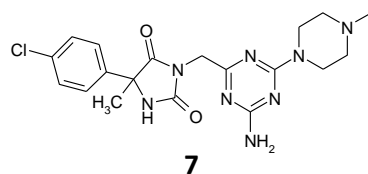


This report was created by ACD/NMR Processor Academic Edition. For more information go to www.acdlabs.com/nmrproc/

C13-NMR

2017-10-18 11:19:51

Acquisition Time (sec)	0.8684	Date	Oct 17 2017	Date Stamp	Oct 17 2017
File Name	C:\Users\Dorota\Desktop\ANALIZYNMR\2017\17-10-17_DJ2_dlaz\17-10-17_DJ2_dlaz_CARBON_01.fid\fid			Frequency (MHz)	75.46
Nucleus	13C	Number of Transients	1536	Original Points Count	16384
Pulse Sequence	s2pul	Receiver Gain	34.00	Solvent	DMSO-d6
Spectrum Type	STANDARD	Sweep Width (Hz)	18867.92	Temperature (degree C)	23.000
				Points Count	16384
				Spectrum Offset (Hz)	8300.0879

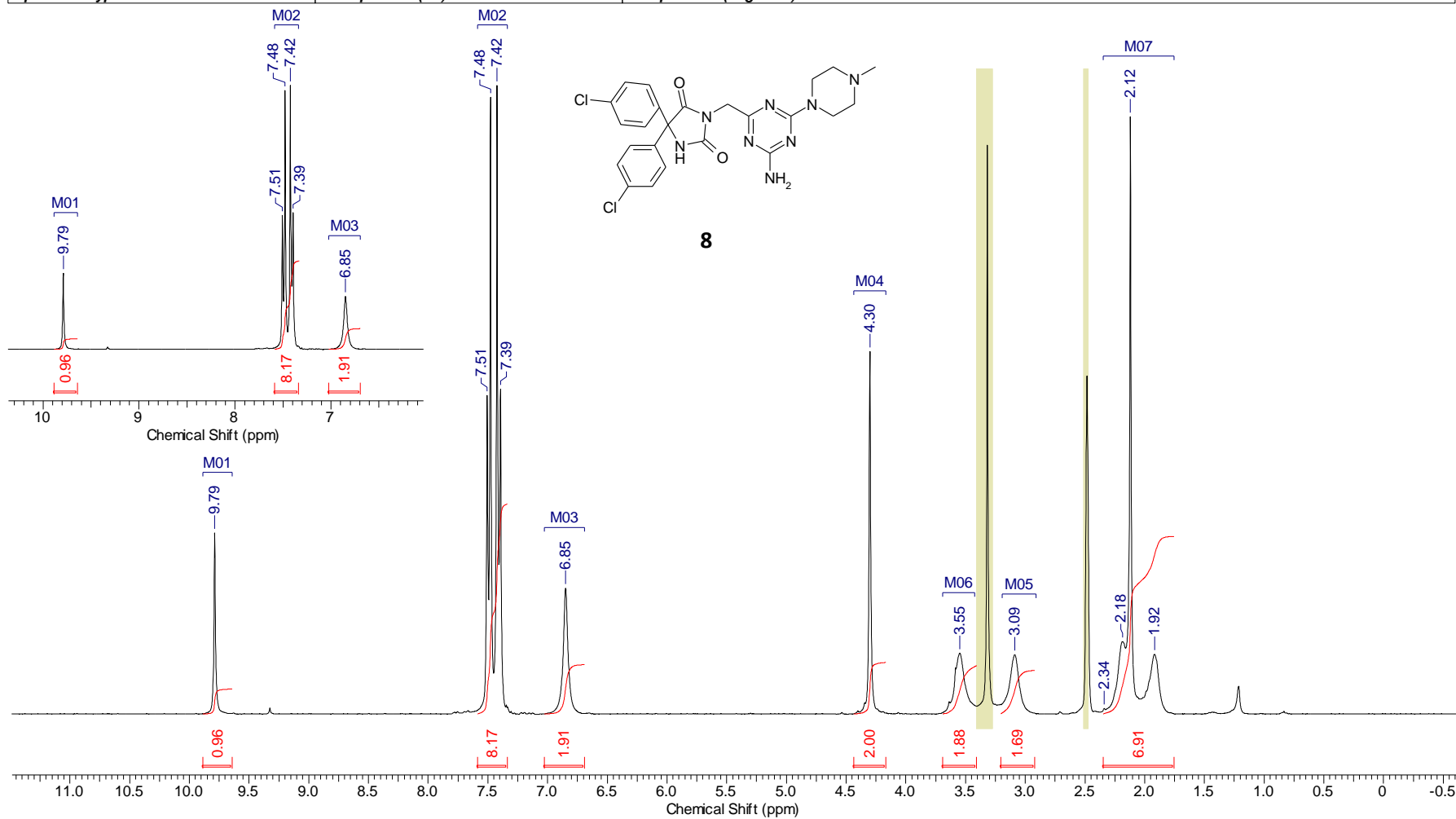


This report was created by ACD/NMR Processor Academic Edition. For more information go to www.acdlabs.com/nmrproc/

1H-NMR

2017-10-10 13:19:36

Acquisition Time (sec)	1.7064	Date	Oct 10 2017	Date Stamp	Oct 10 2017		
File Name	C:\Users\Dorota\Desktop\ANALIZY\NMR\2017-10-10_DJ6_dlaz\17-10-10_DJ6_dlaz_PROTON_01.fid\fid			Frequency (MHz)	300.08		
Nucleus	1H	Number of Transients	32	Original Points Count	8192	Points Count	8192
Pulse Sequence	s2pul	Receiver Gain	38.00	Solvent	DMSO-d6	Spectrum Offset (Hz)	1800.4814
Spectrum Type	STANDARD	Sweep Width (Hz)	4800.77	Temperature (degree C)	AMBIENT TEMPERATURE		

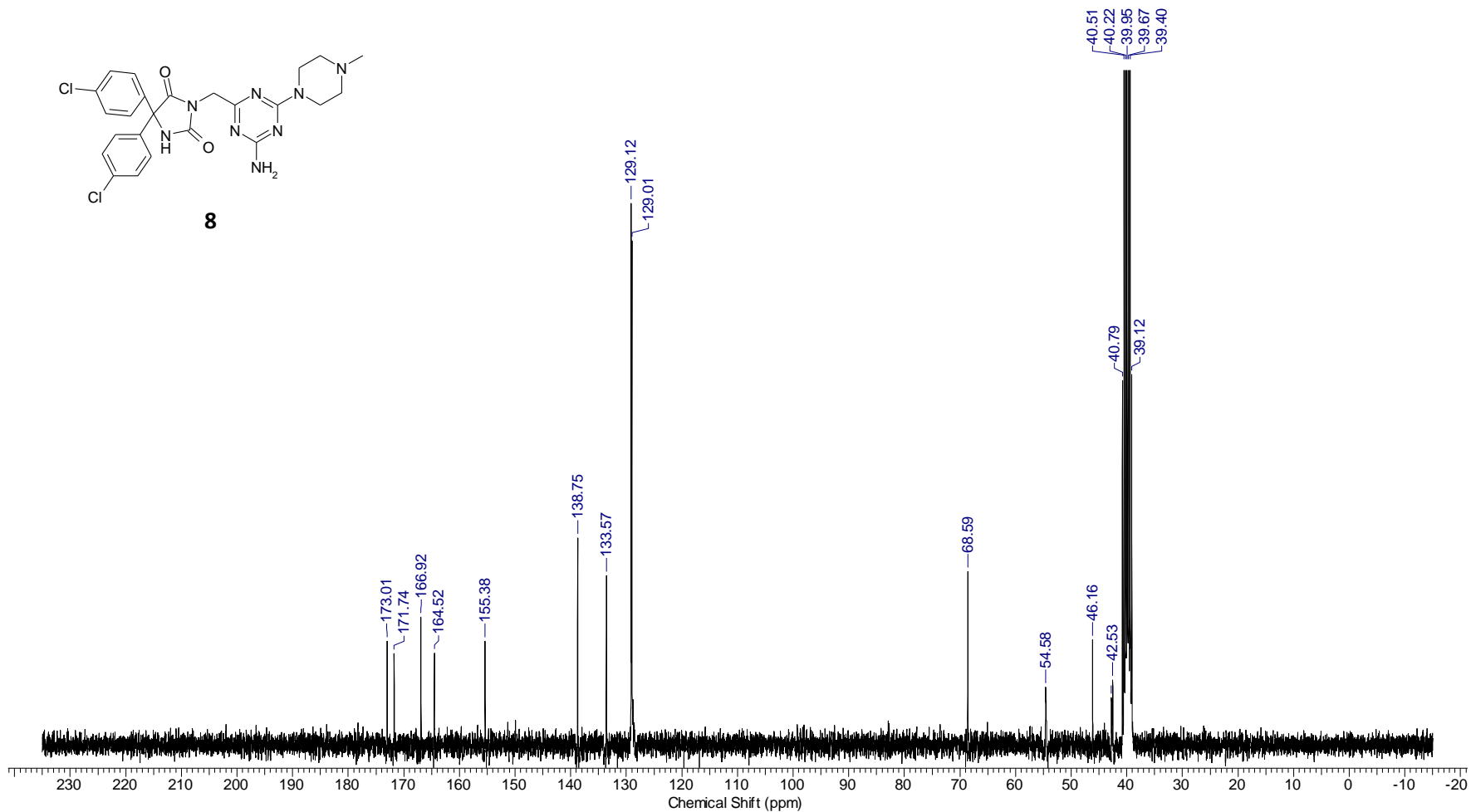
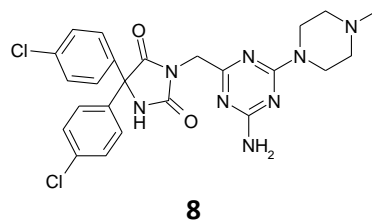


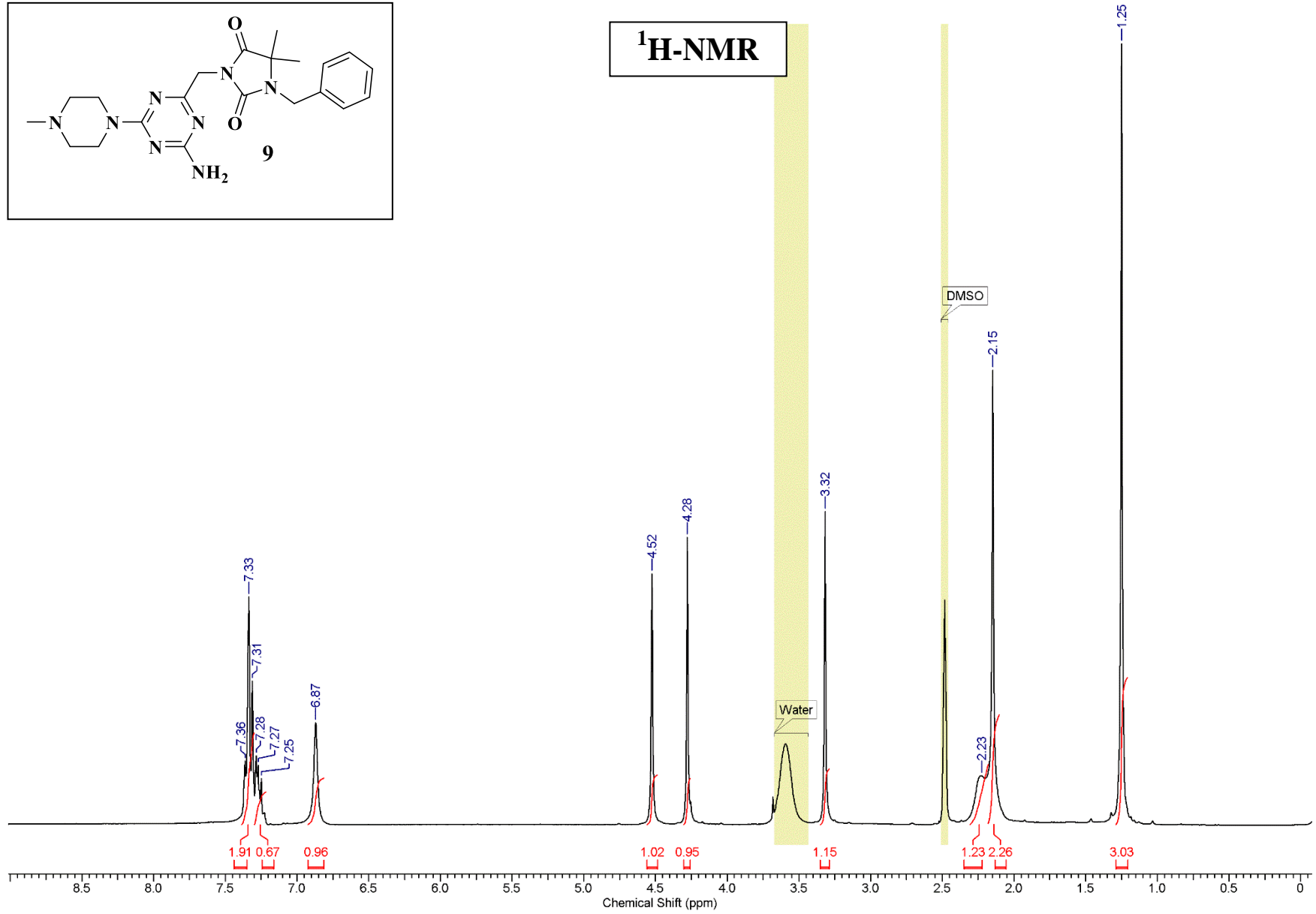
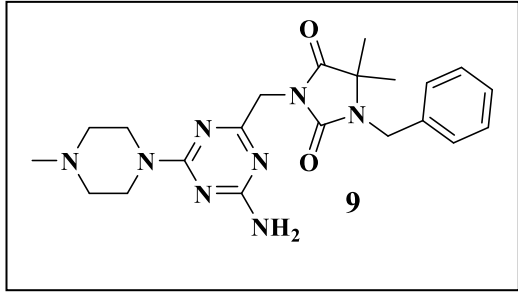
This report was created by ACD/NMR Processor Academic Edition. For more information go to www.acdlabs.com/nmrproc/

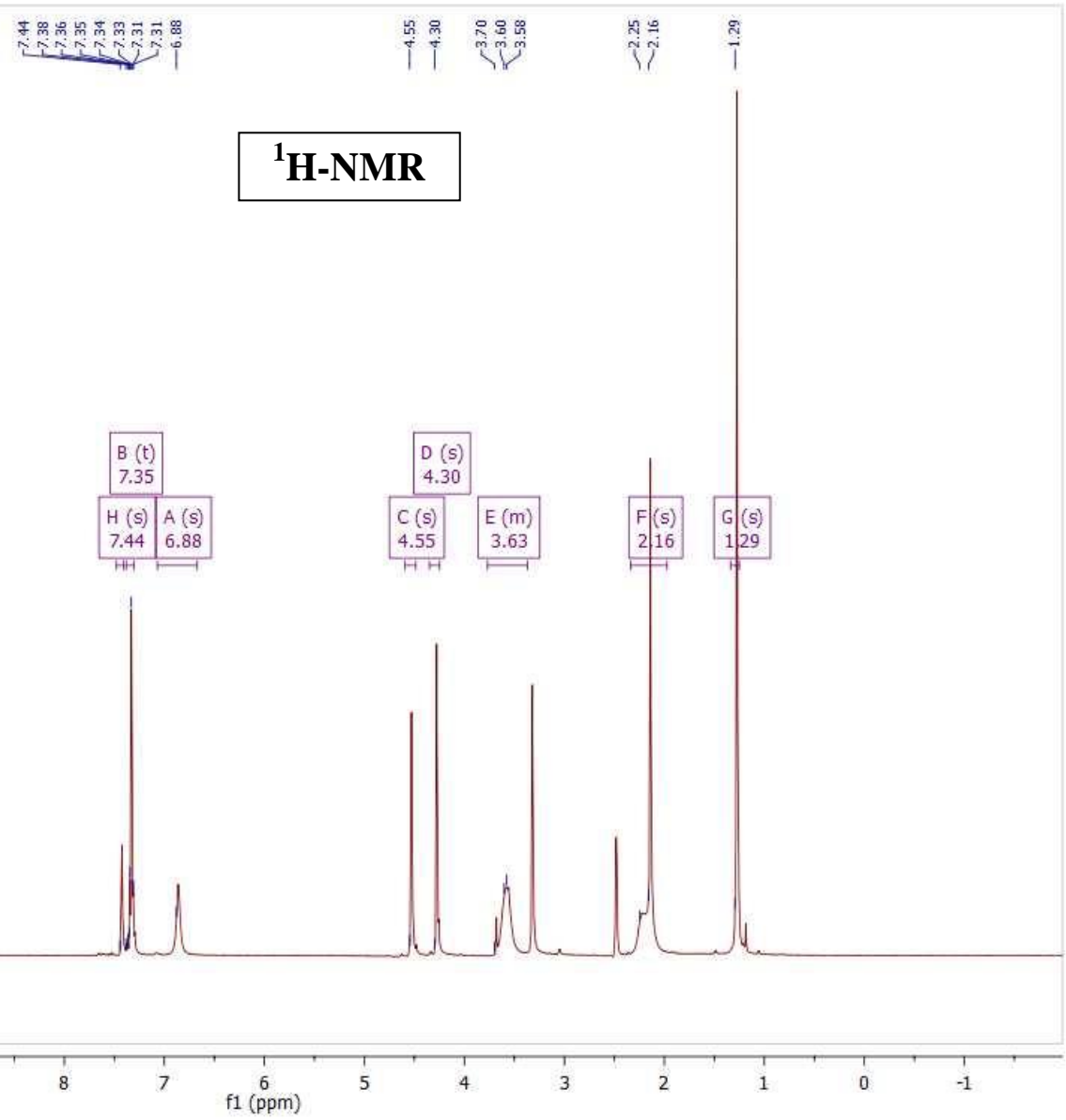
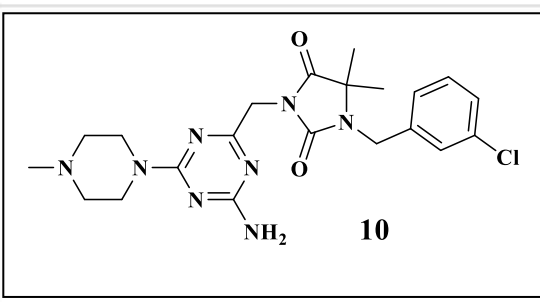
C13-NMR

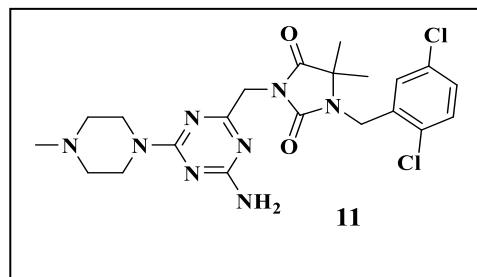
2017-10-18 11:33:03

Acquisition Time (sec)	0.8684	Date	Oct 16 2017	Date Stamp	Oct 16 2017
File Name	C:\Users\Dorota\Desktop\ANALIZYNMR\2017\17-10-16_DJ6_dlaz\17-10-16_DJ6_dlaz_CARBO_01.fid\fid			Frequency (MHz)	75.46
Nucleus	13C	Number of Transients	2224	Original Points Count	16384
Pulse Sequence	s2pul	Receiver Gain	34.00	Solvent	DMSO-d6
Spectrum Type	STANDARD	Sweep Width (Hz)	18867.92	Temperature (degree C)	23.000
				Points Count	16384
				Spectrum Offset (Hz)	8300.0879

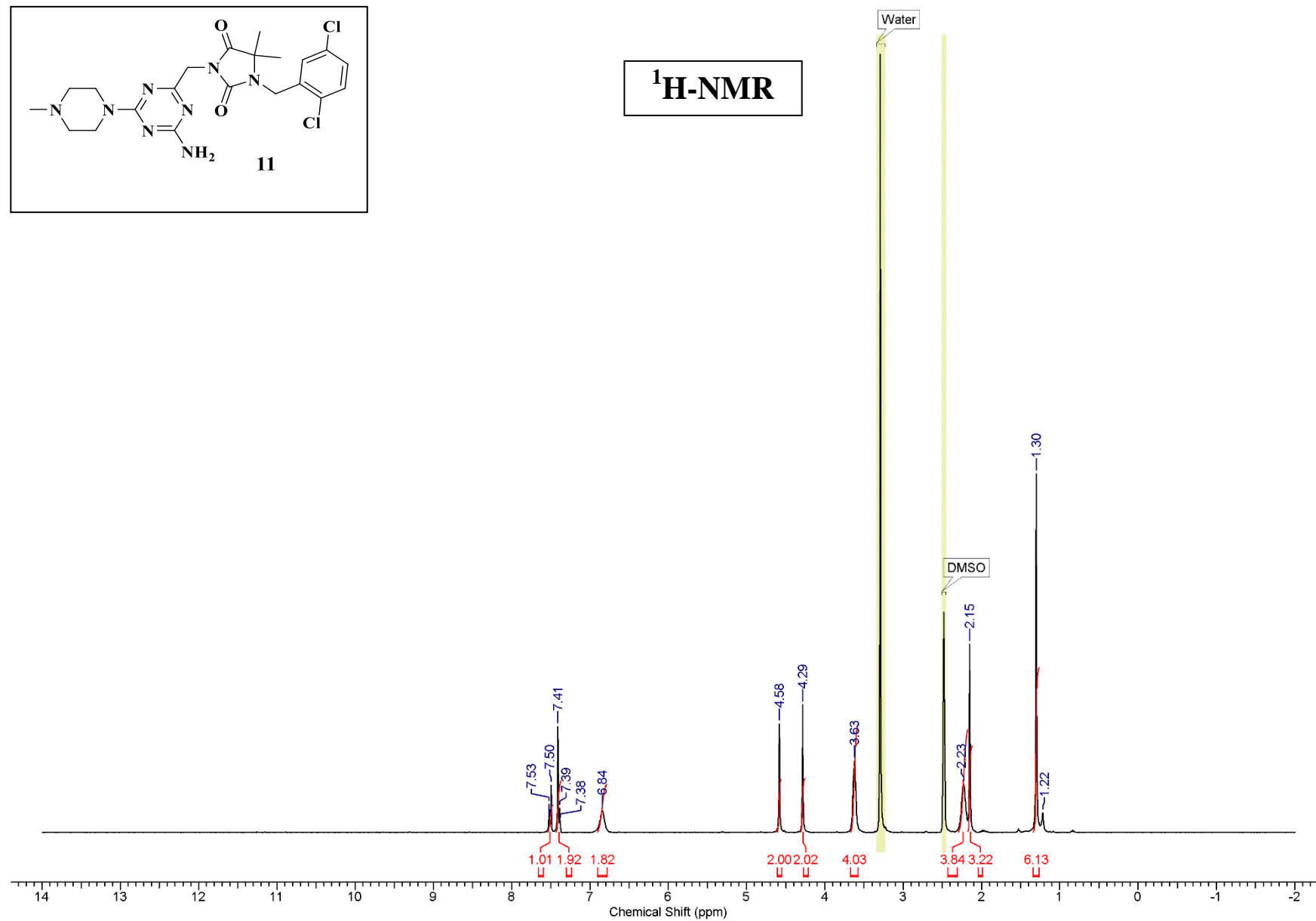


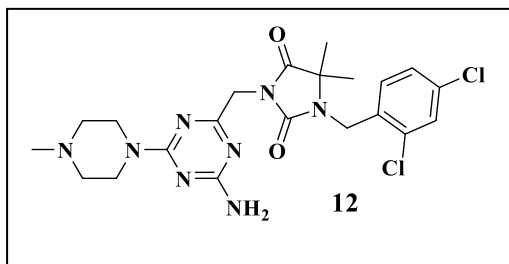




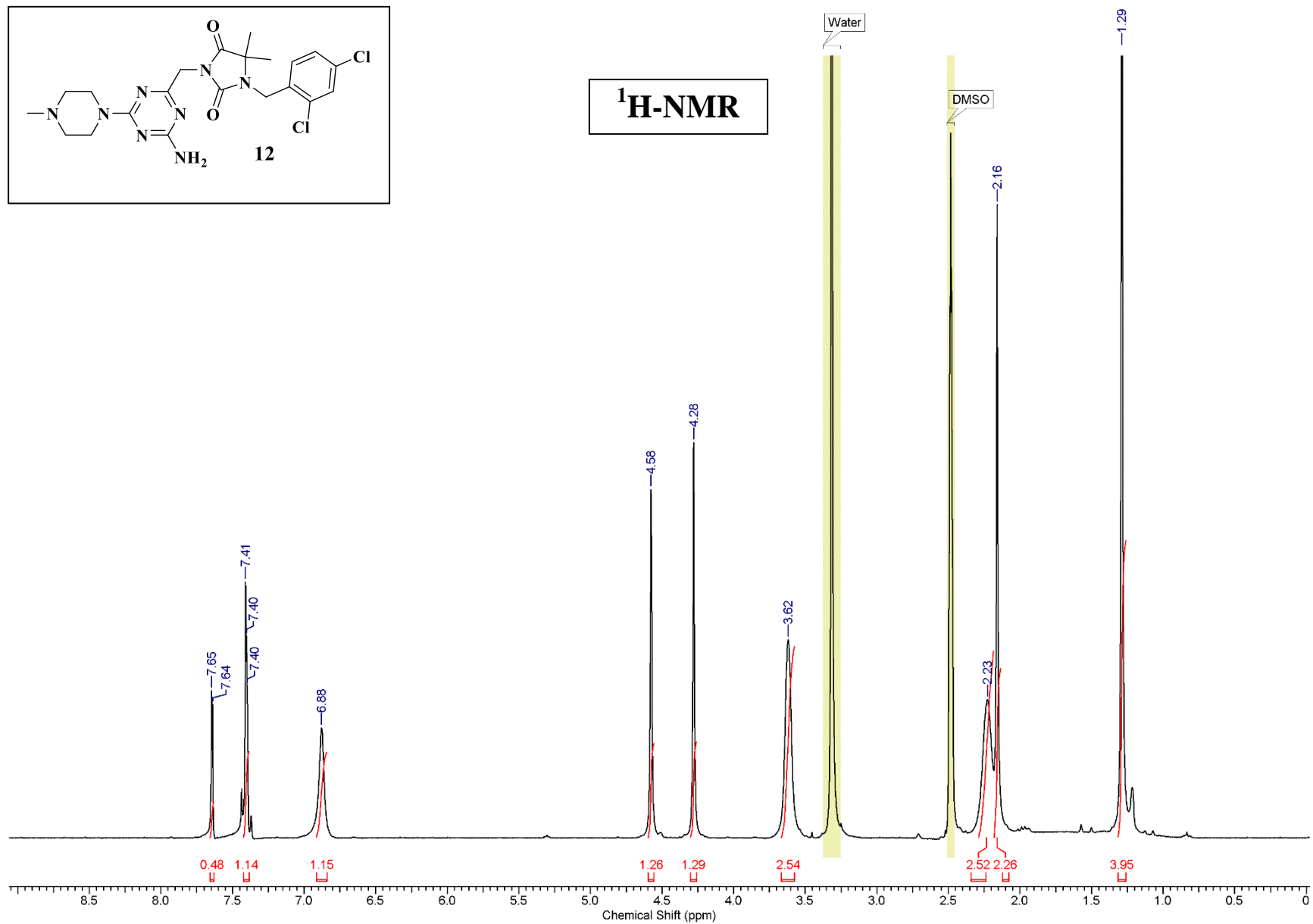


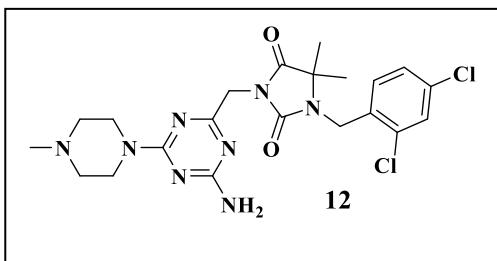
¹H-NMR



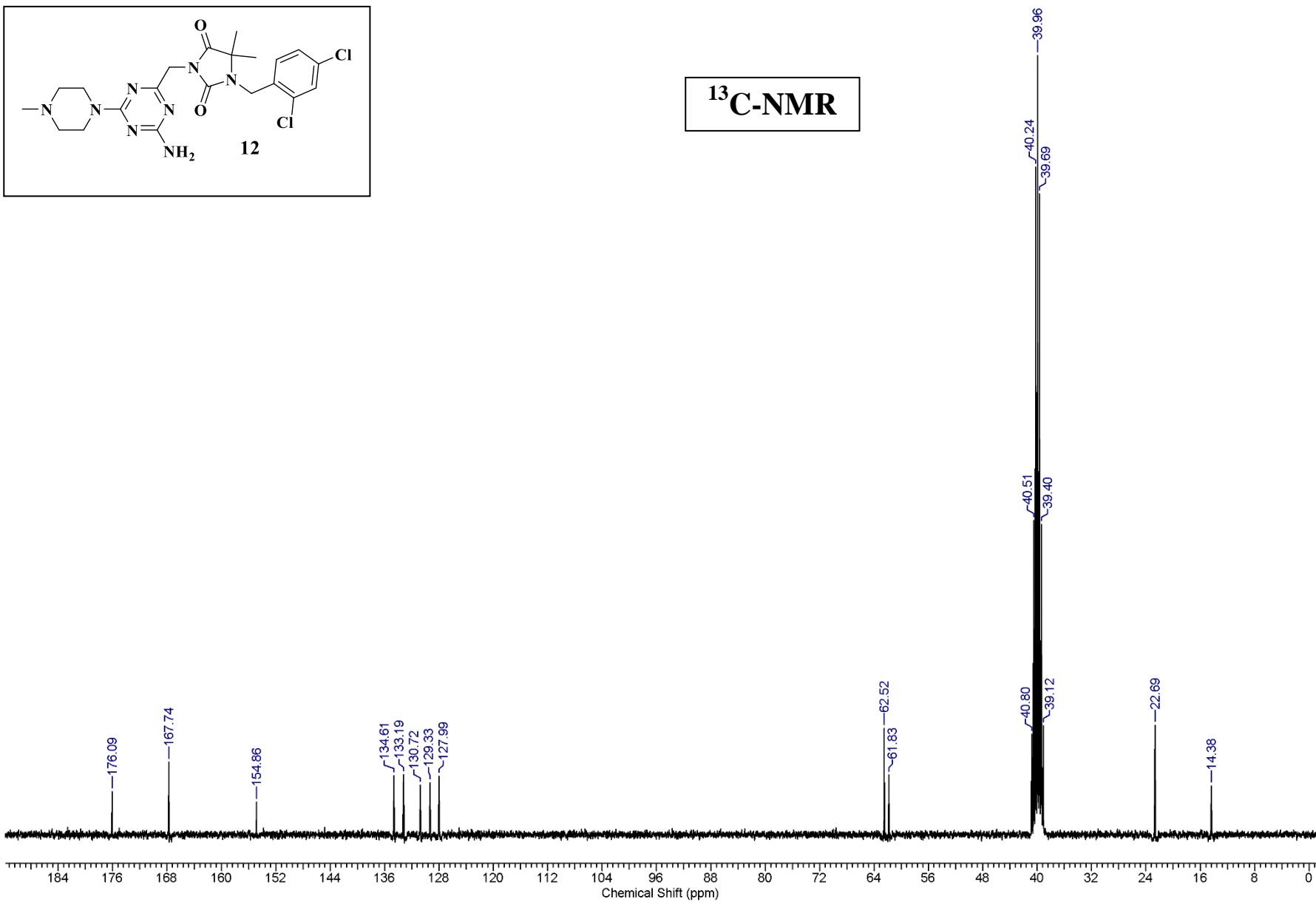


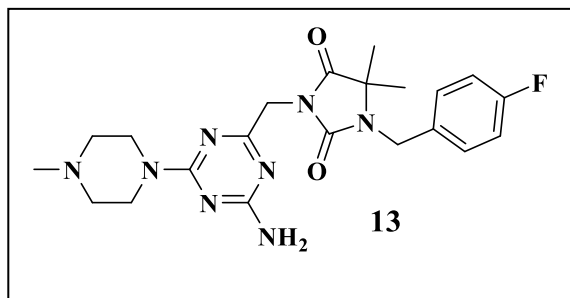
¹H-NMR



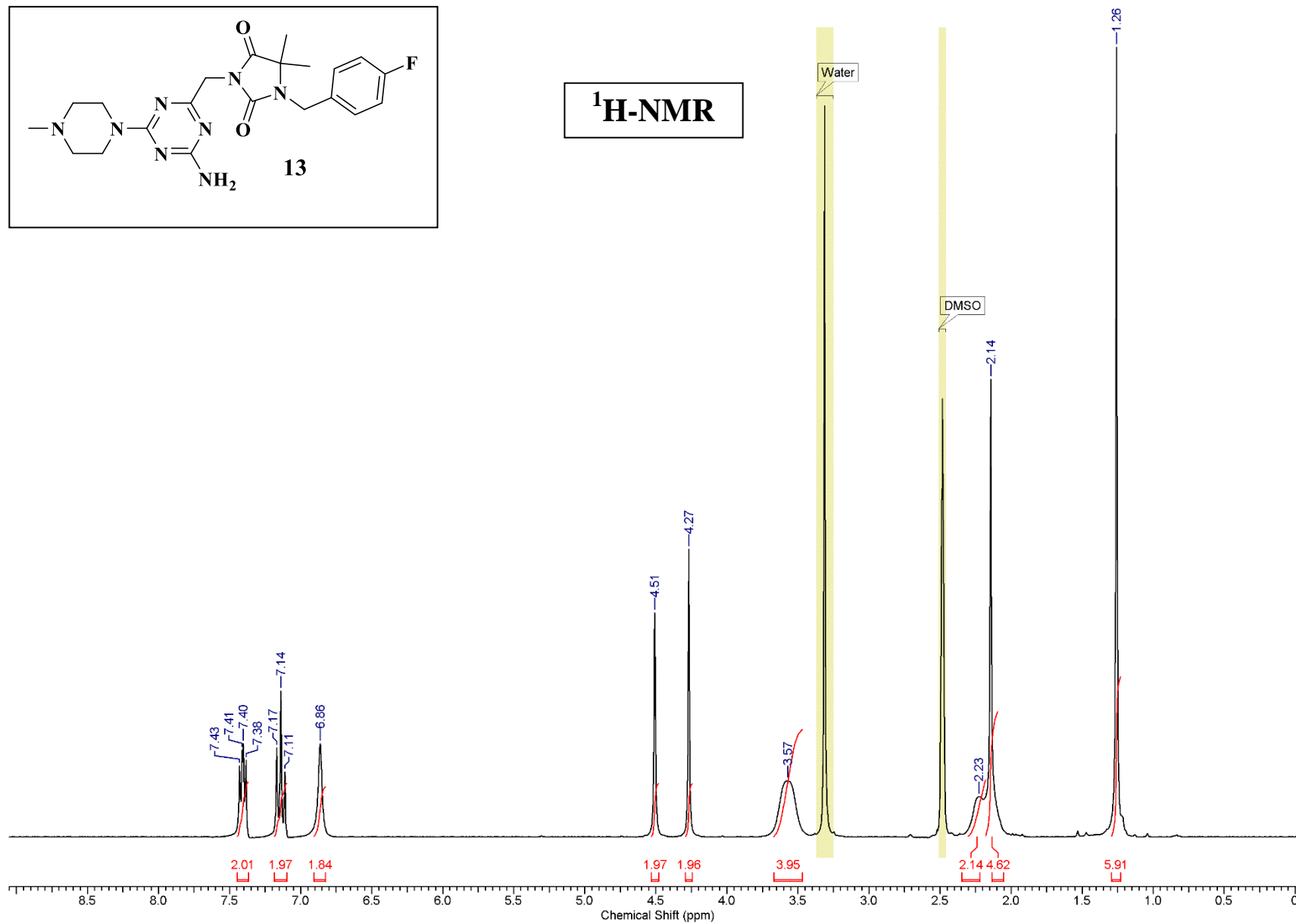


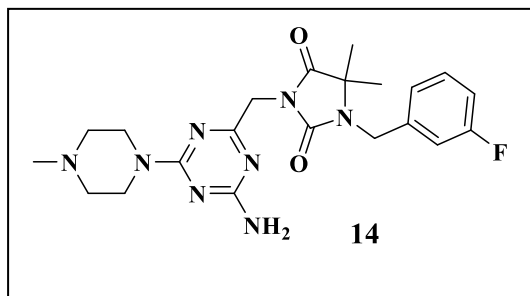
¹³C-NMR





¹H-NMR





7.41
7.39
7.39
7.37
7.36
7.34
7.23
7.20
7.19
7.17
7.16
7.15
7.14
7.13
7.11
7.10
7.08
7.07
6.88

¹H-NMR

4.56
4.30

3.61

2.16

1.29

B (m)
7.16

A (s)
6.88

C (td)
7.38

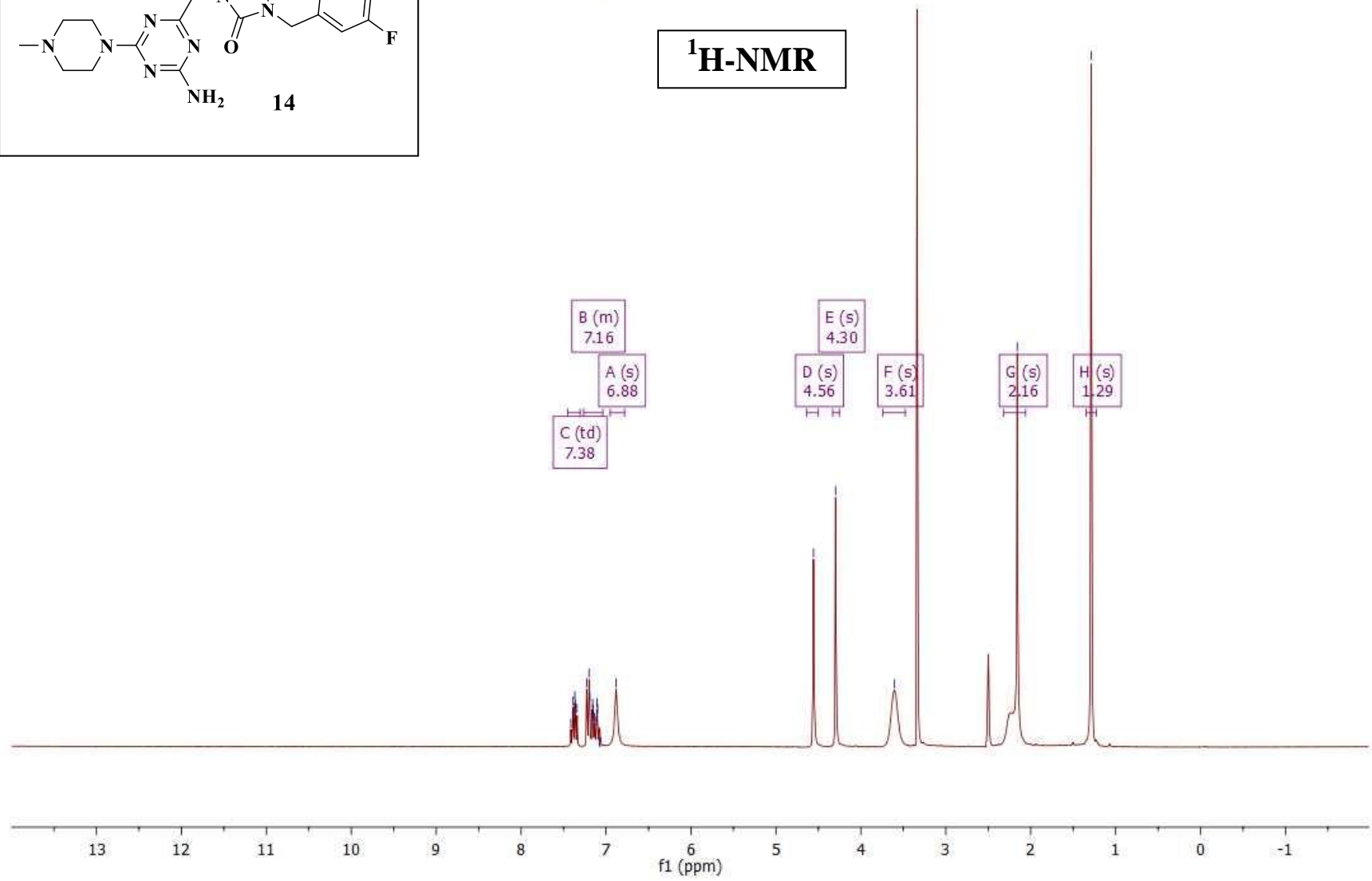
E (s)
4.30

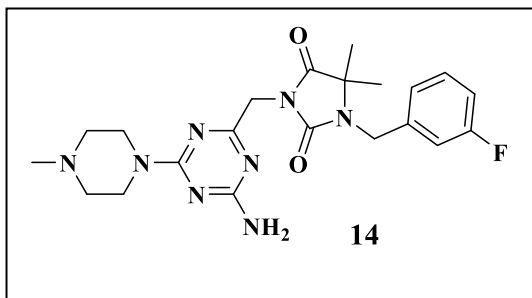
D (s)
4.56

F (s)
3.61

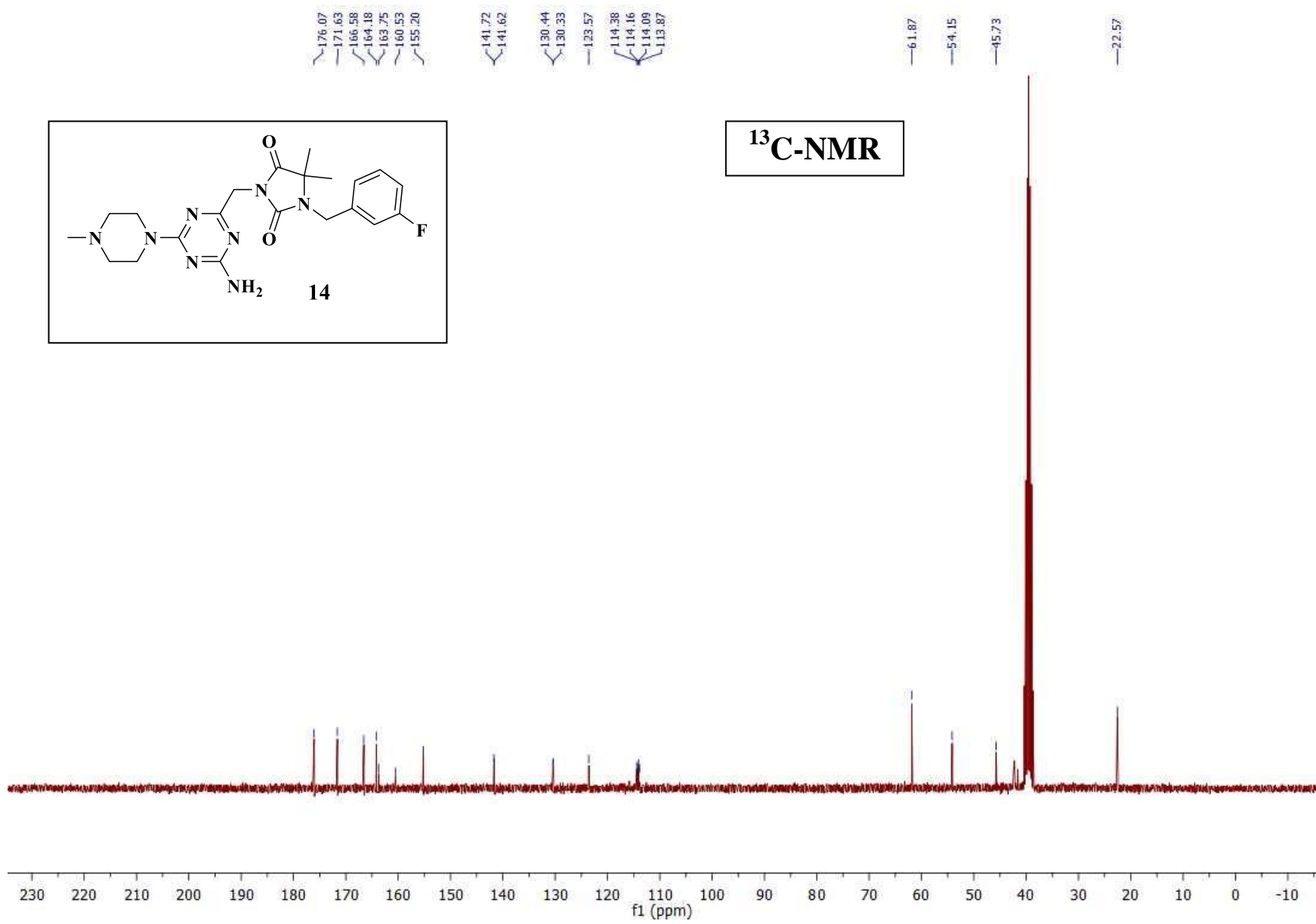
G (s)
2.16

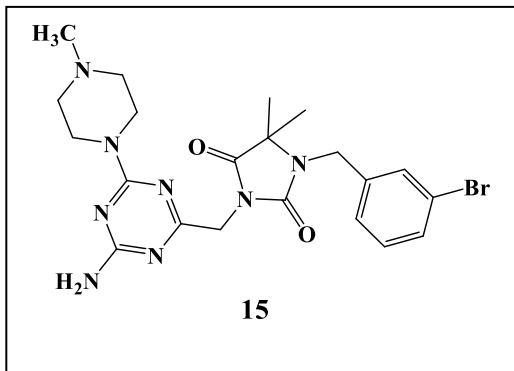
H (s)
1.29





¹³C-NMR





176.05
171.60
166.58
164.15
155.20

141.52

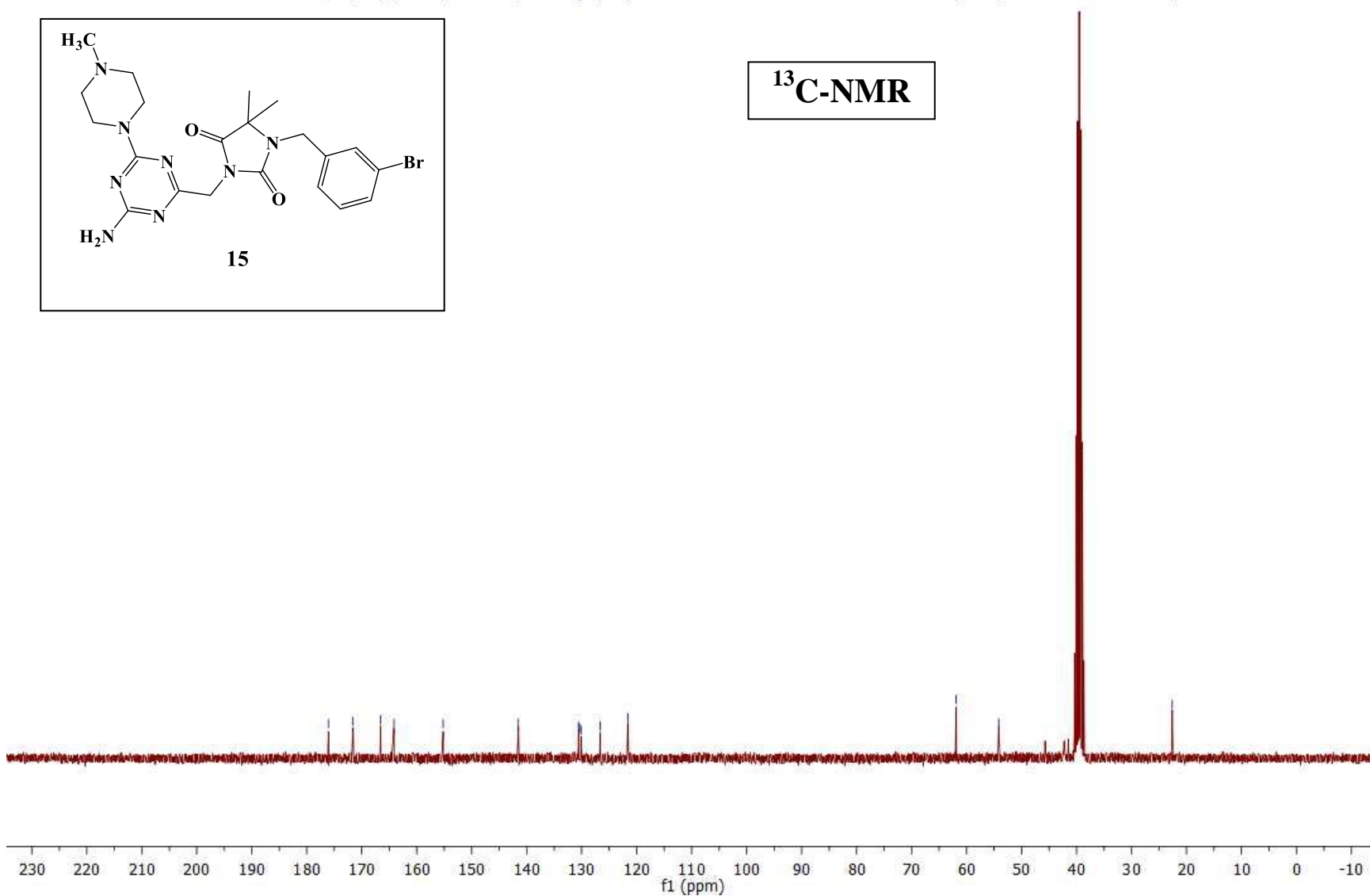
130.59
130.41
130.13
126.67
121.63

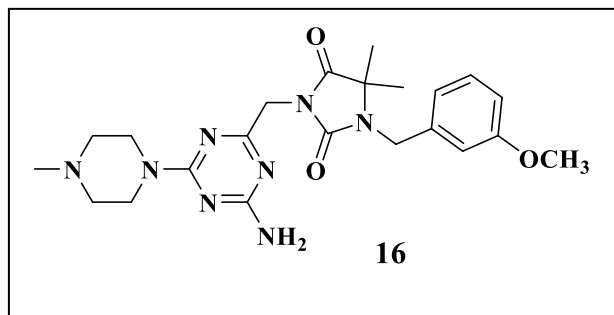
61.90

54.16

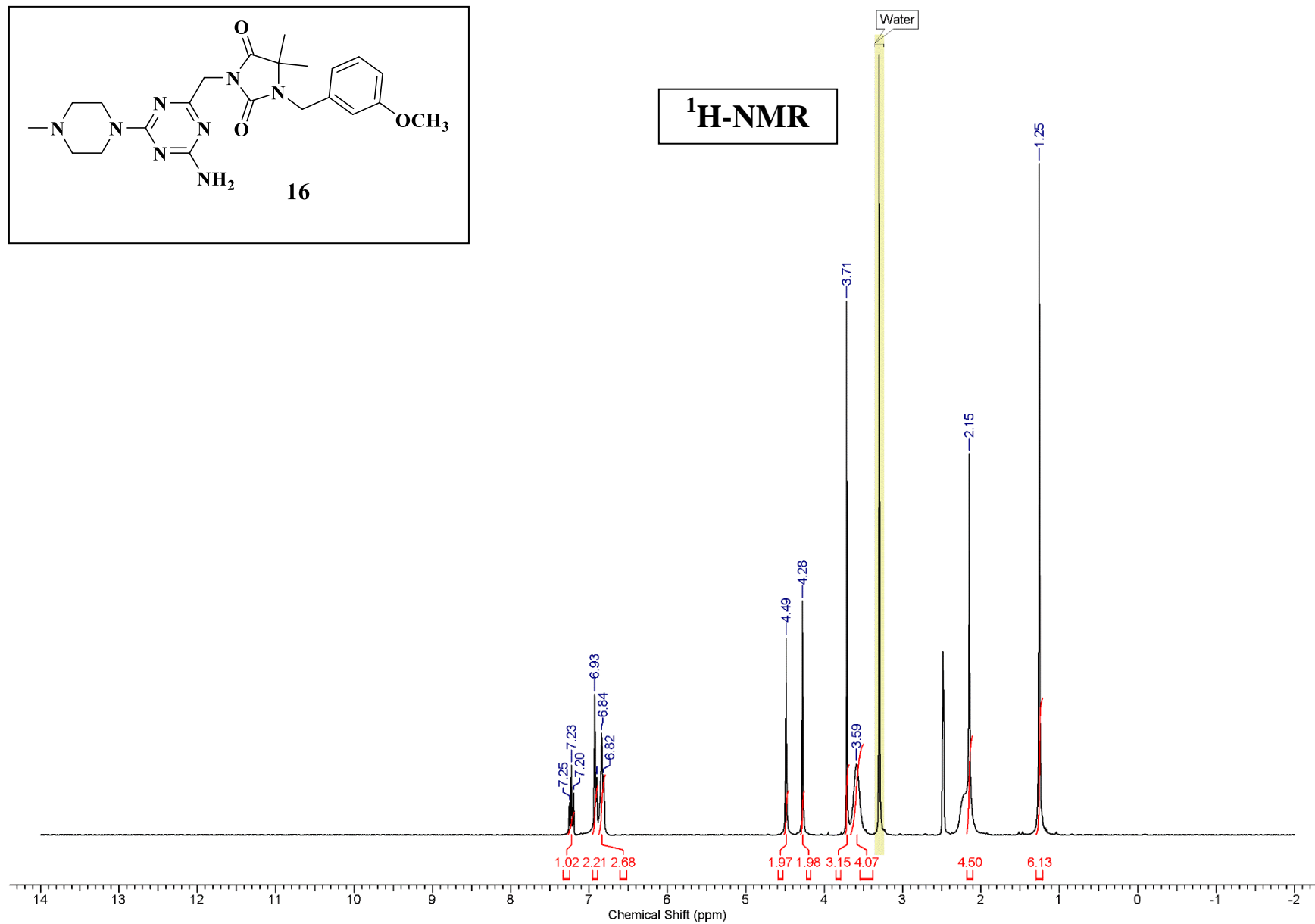
22.60

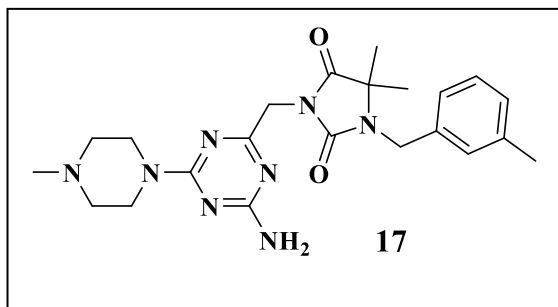
¹³C-NMR



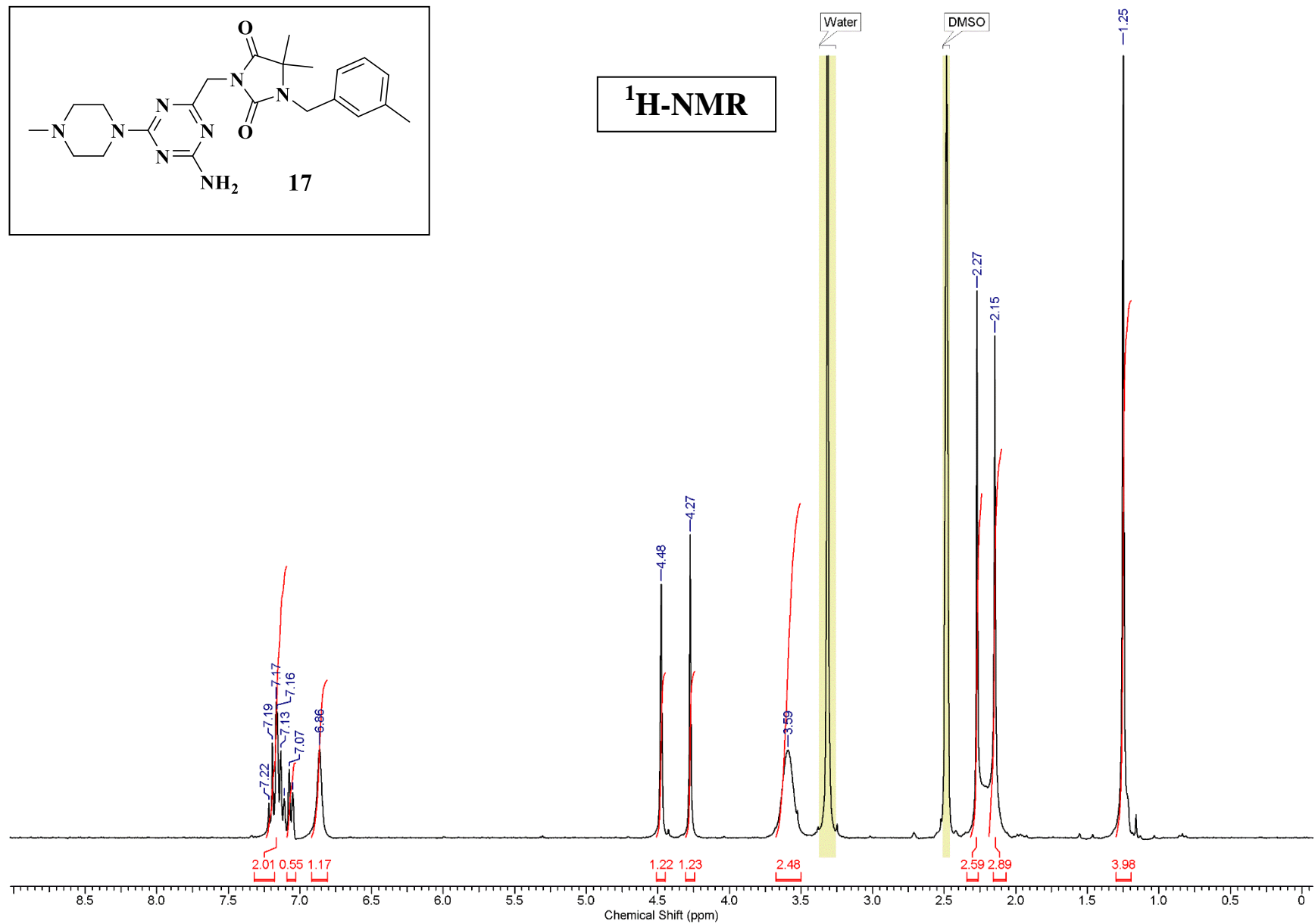


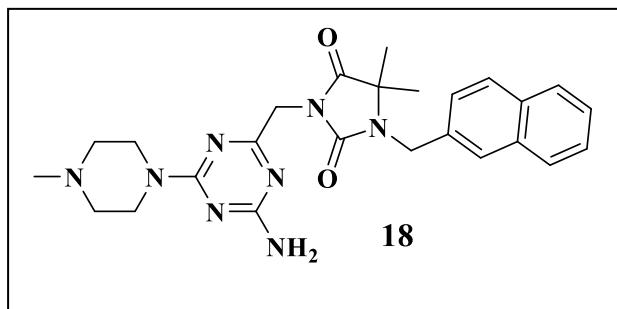
¹H-NMR



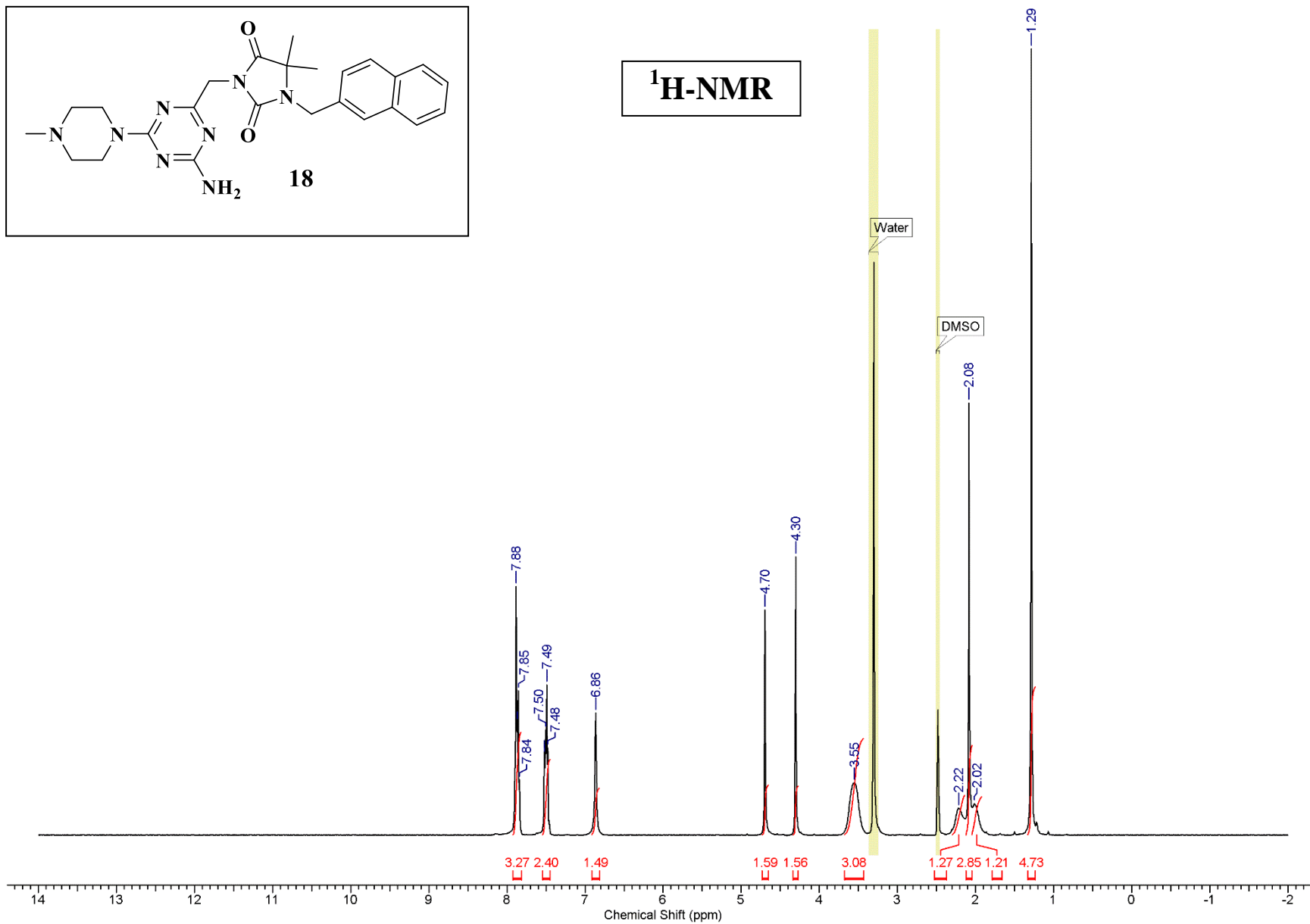


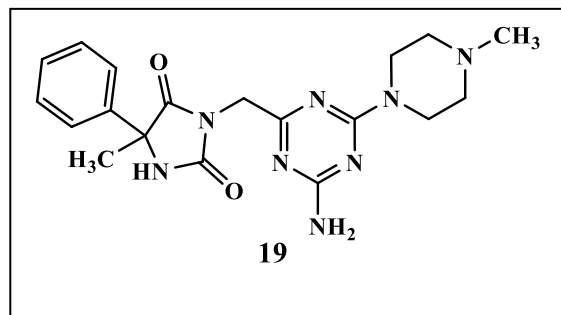
¹H-NMR



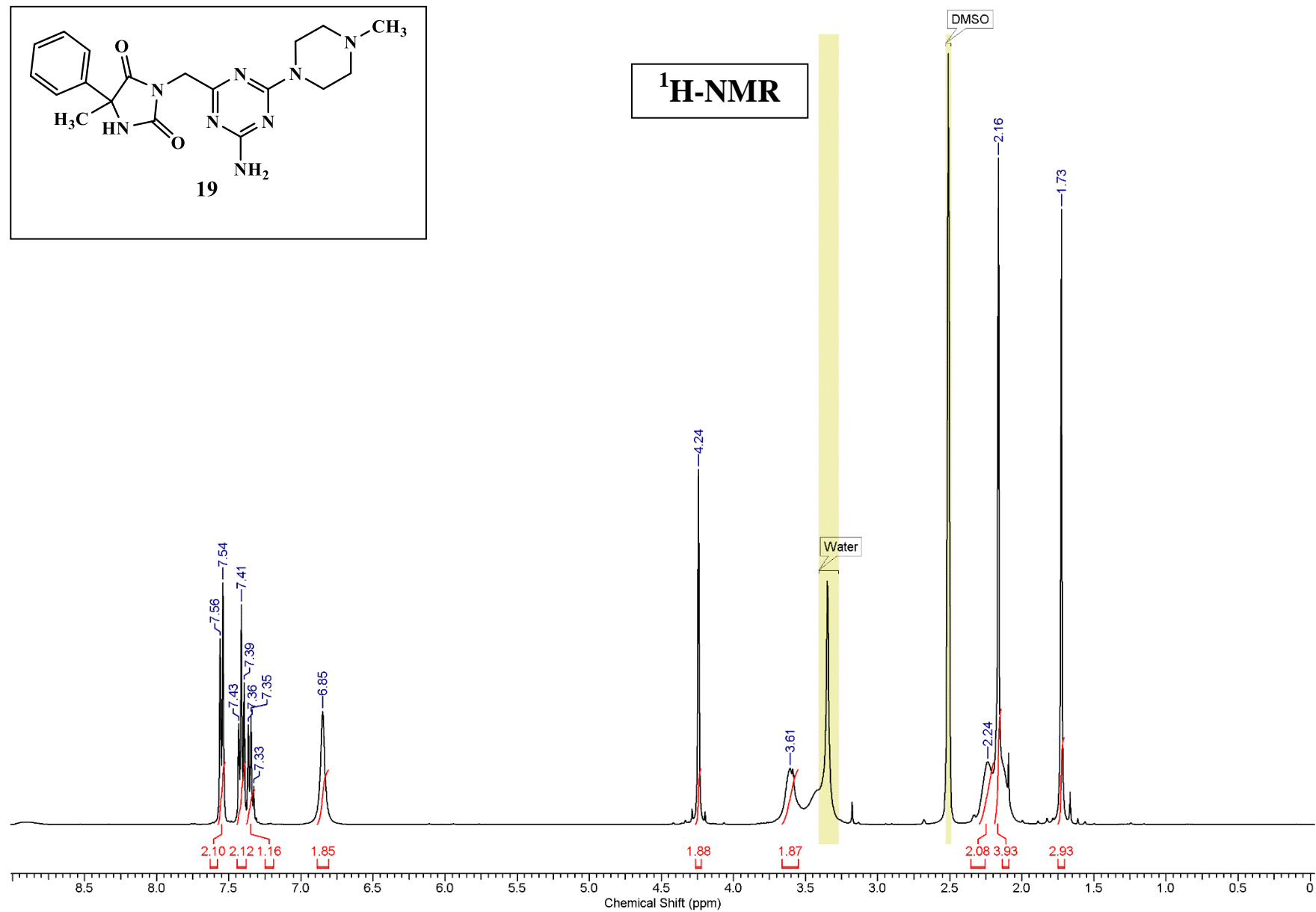


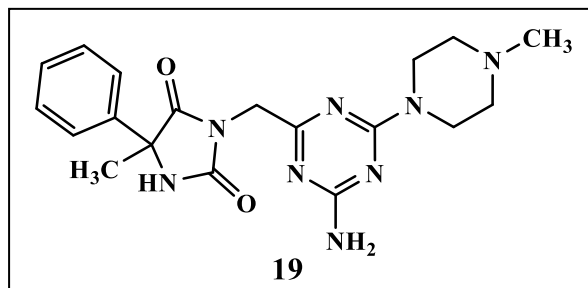
¹H-NMR



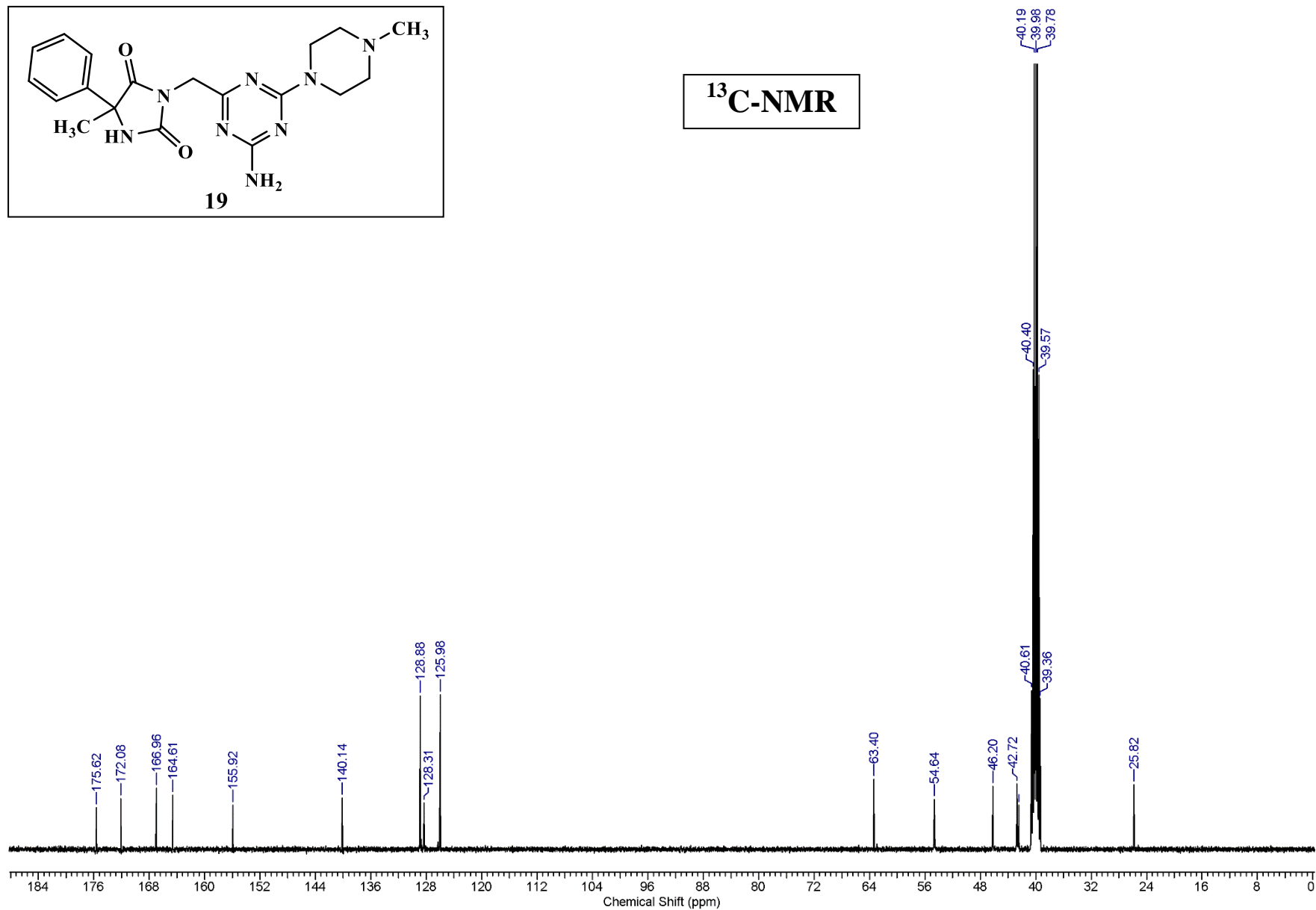


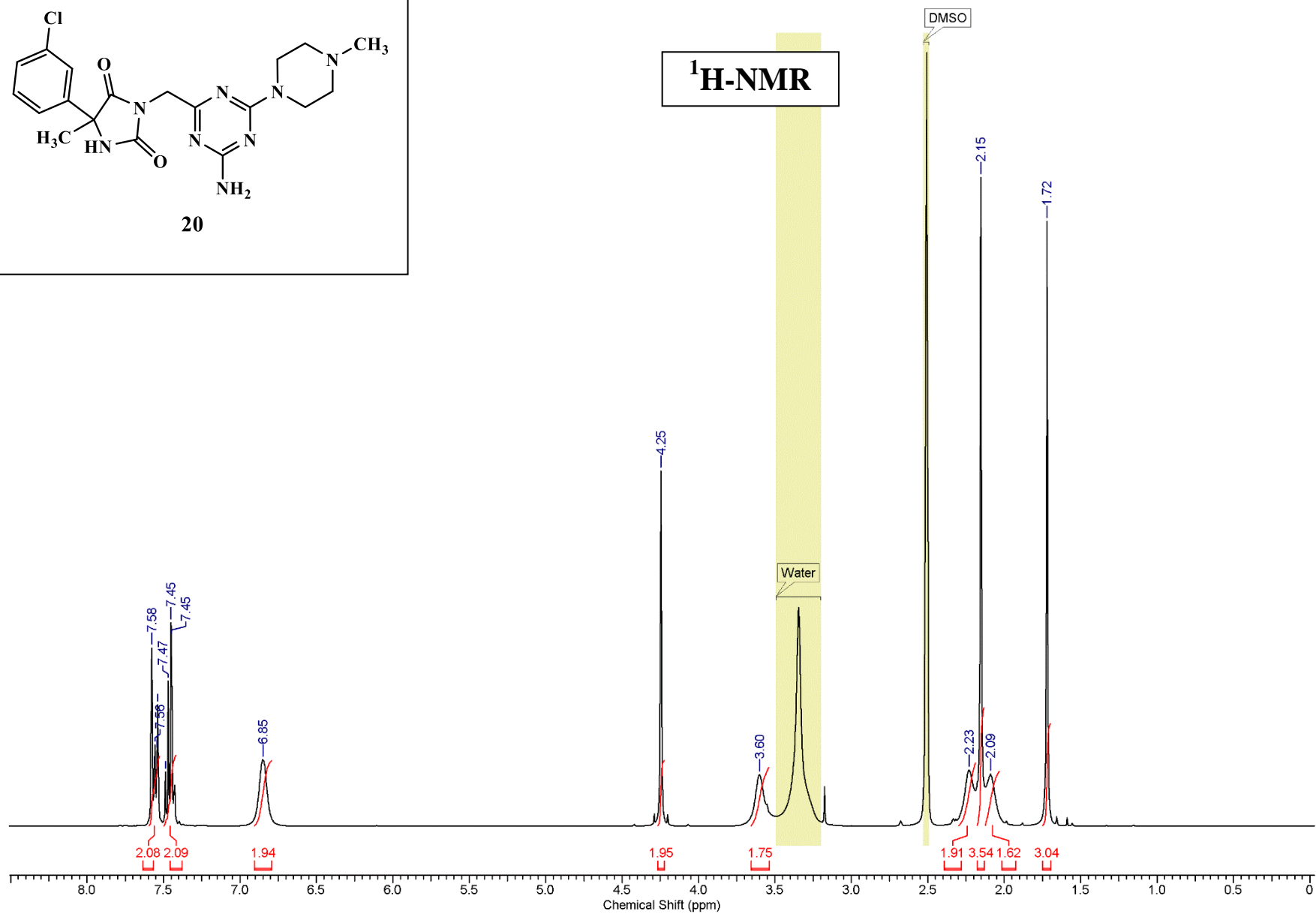
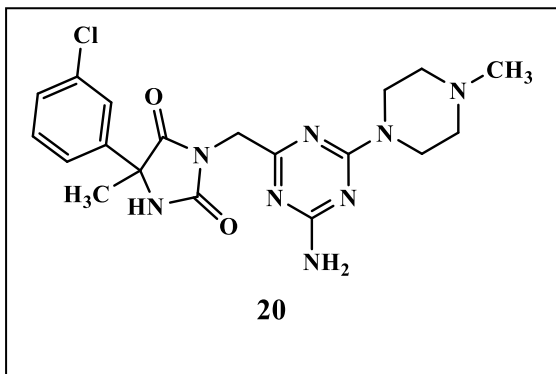
¹H-NMR

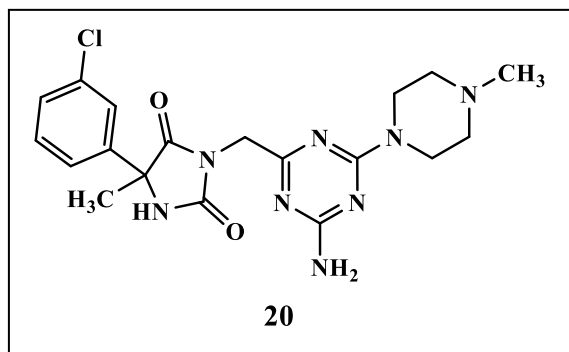




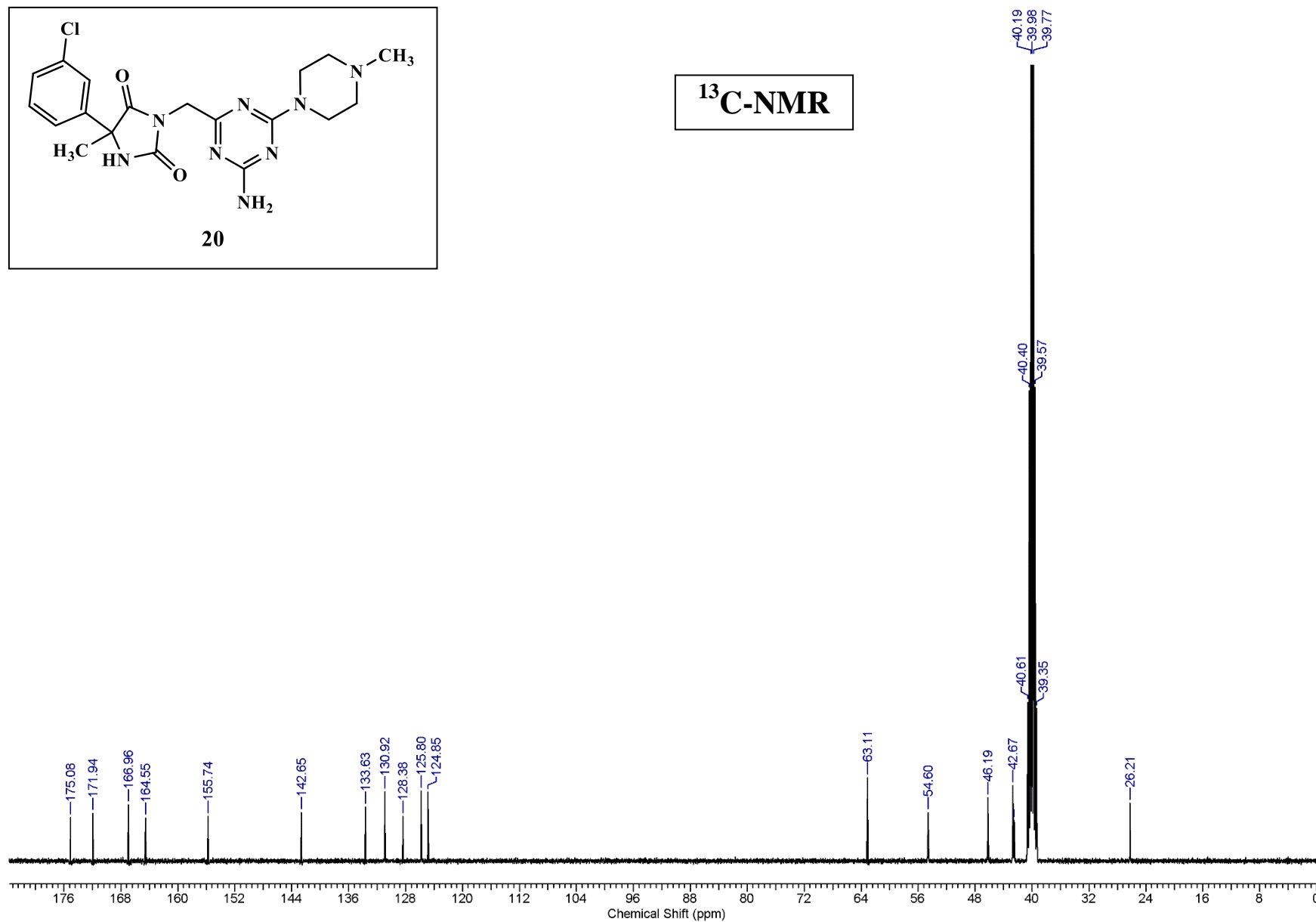
¹³C-NMR

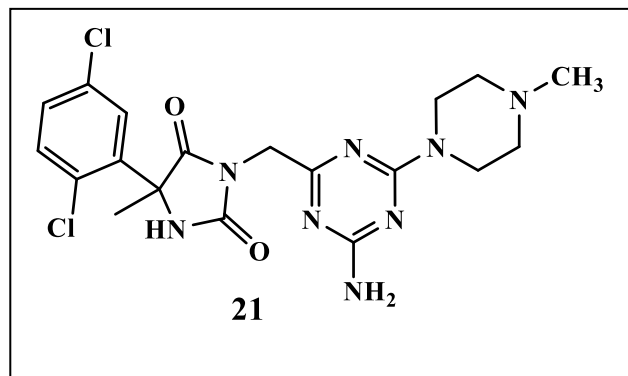




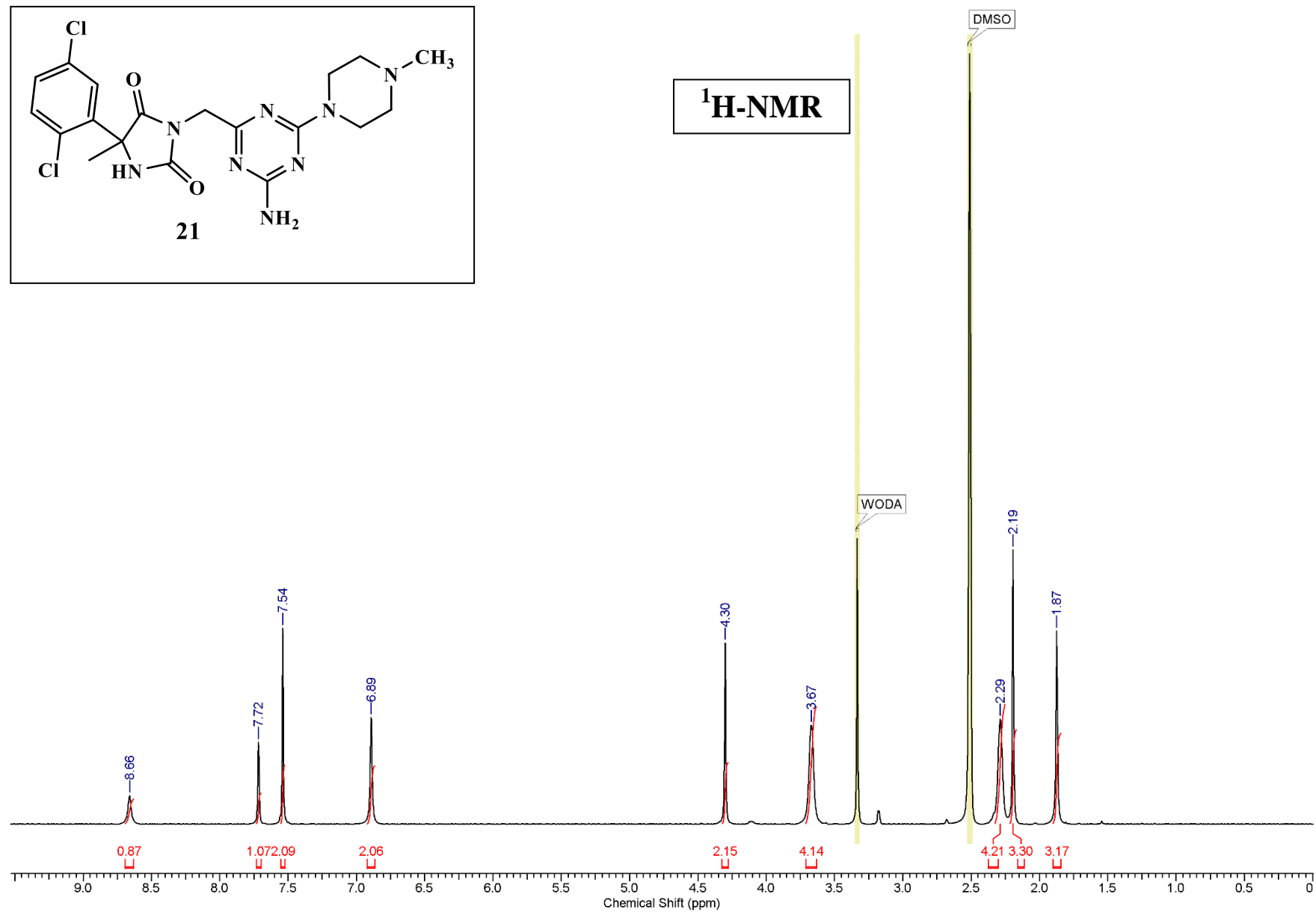


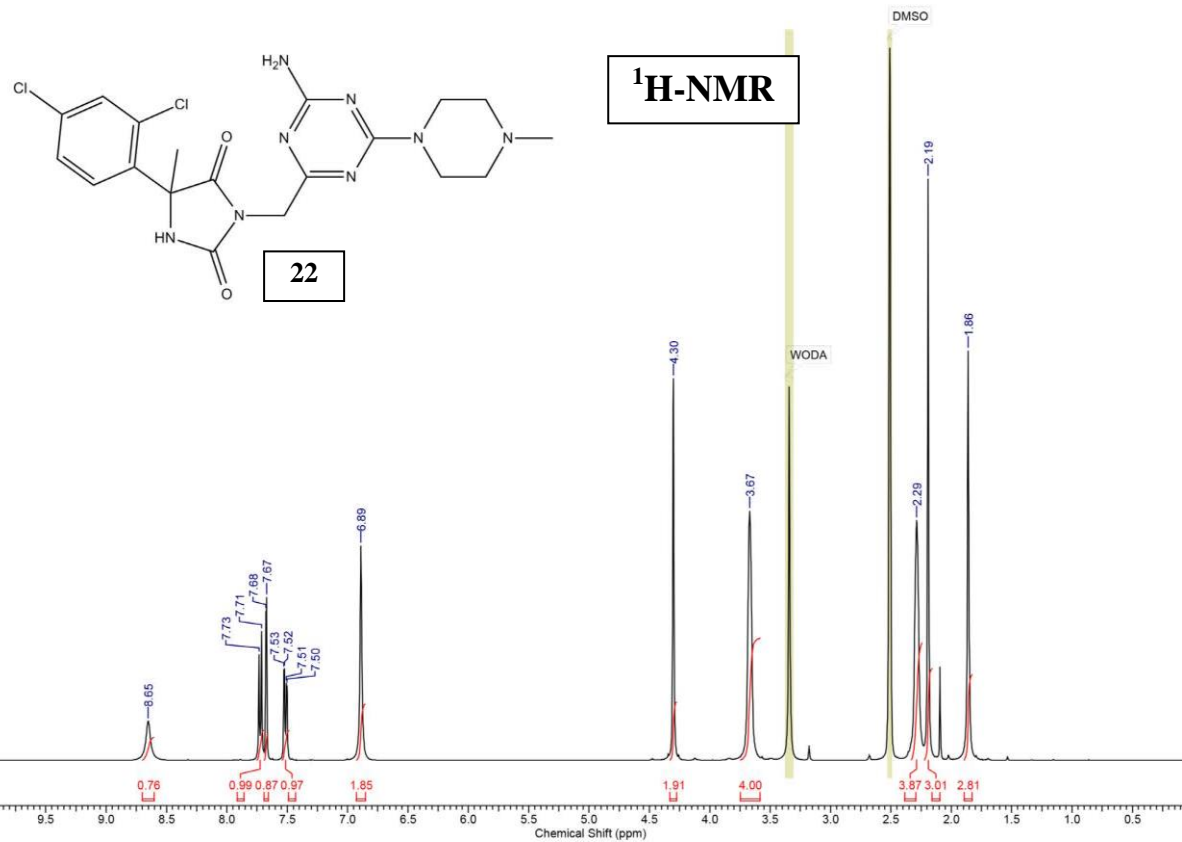
¹³C-NMR

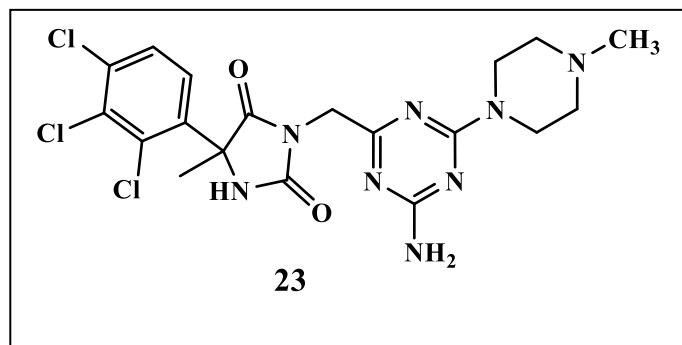




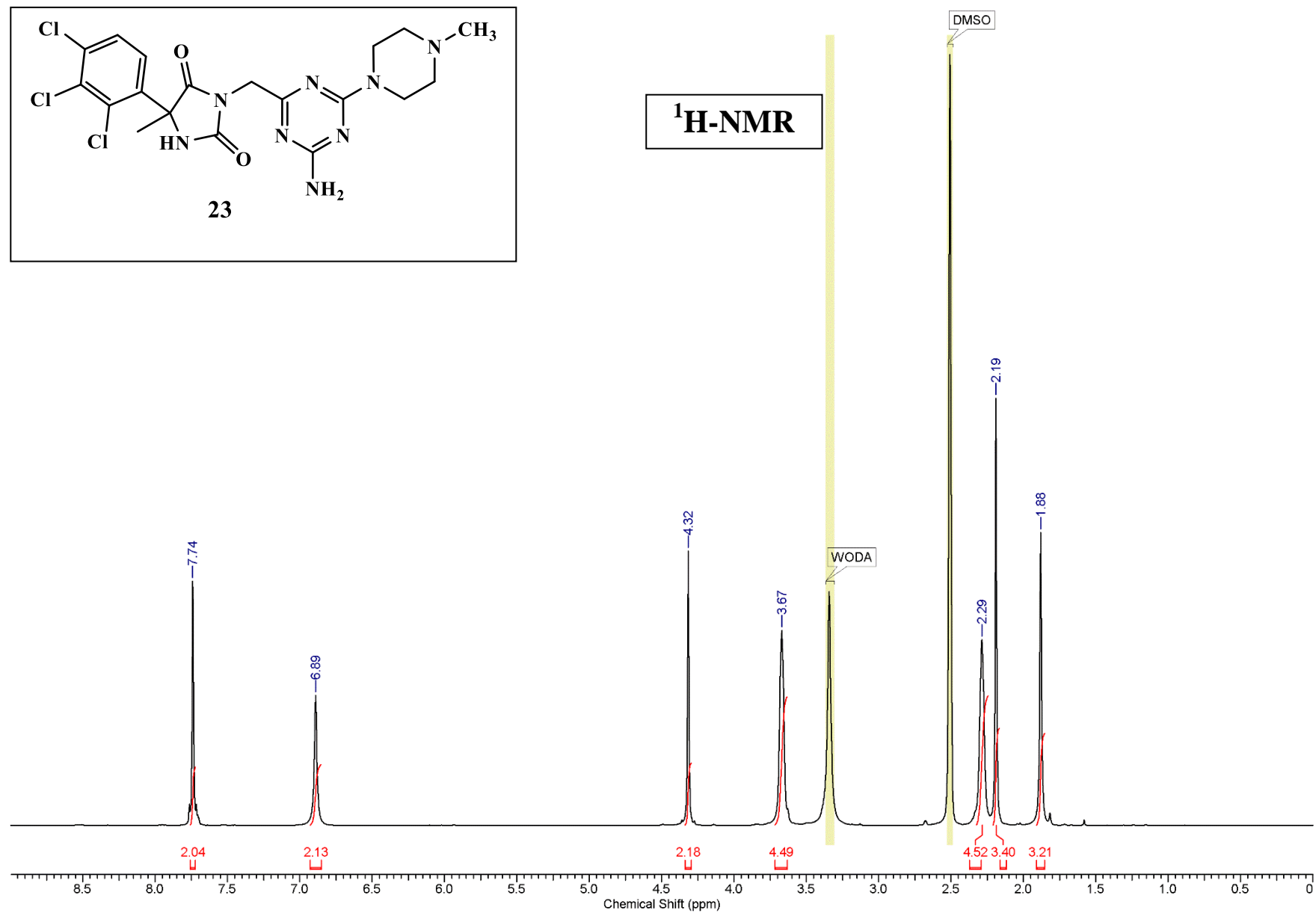
¹H-NMR

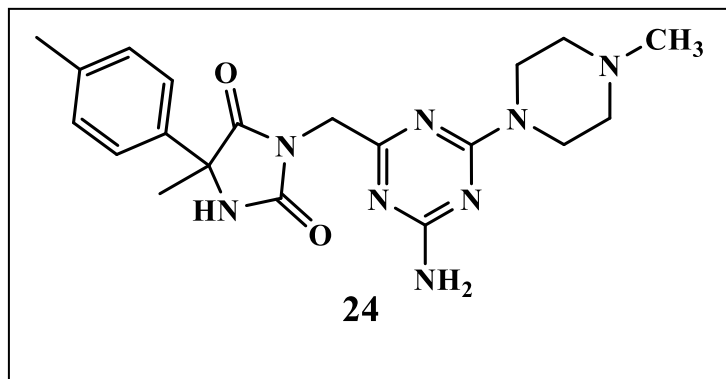




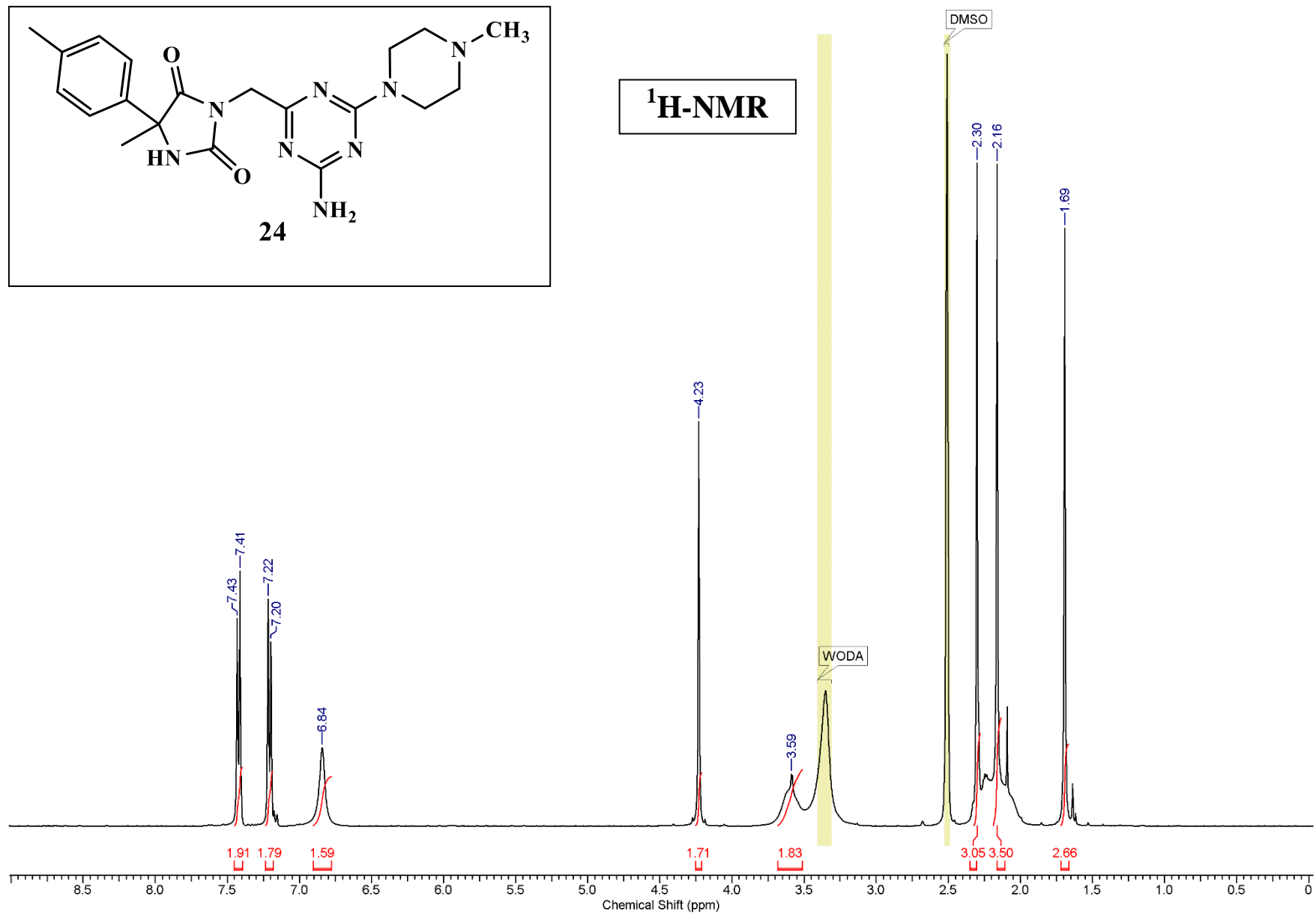


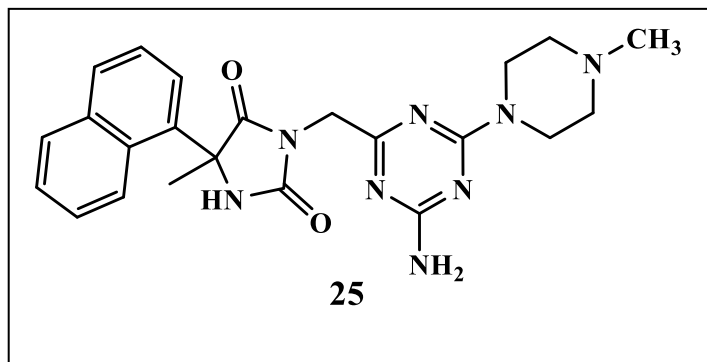
¹H-NMR



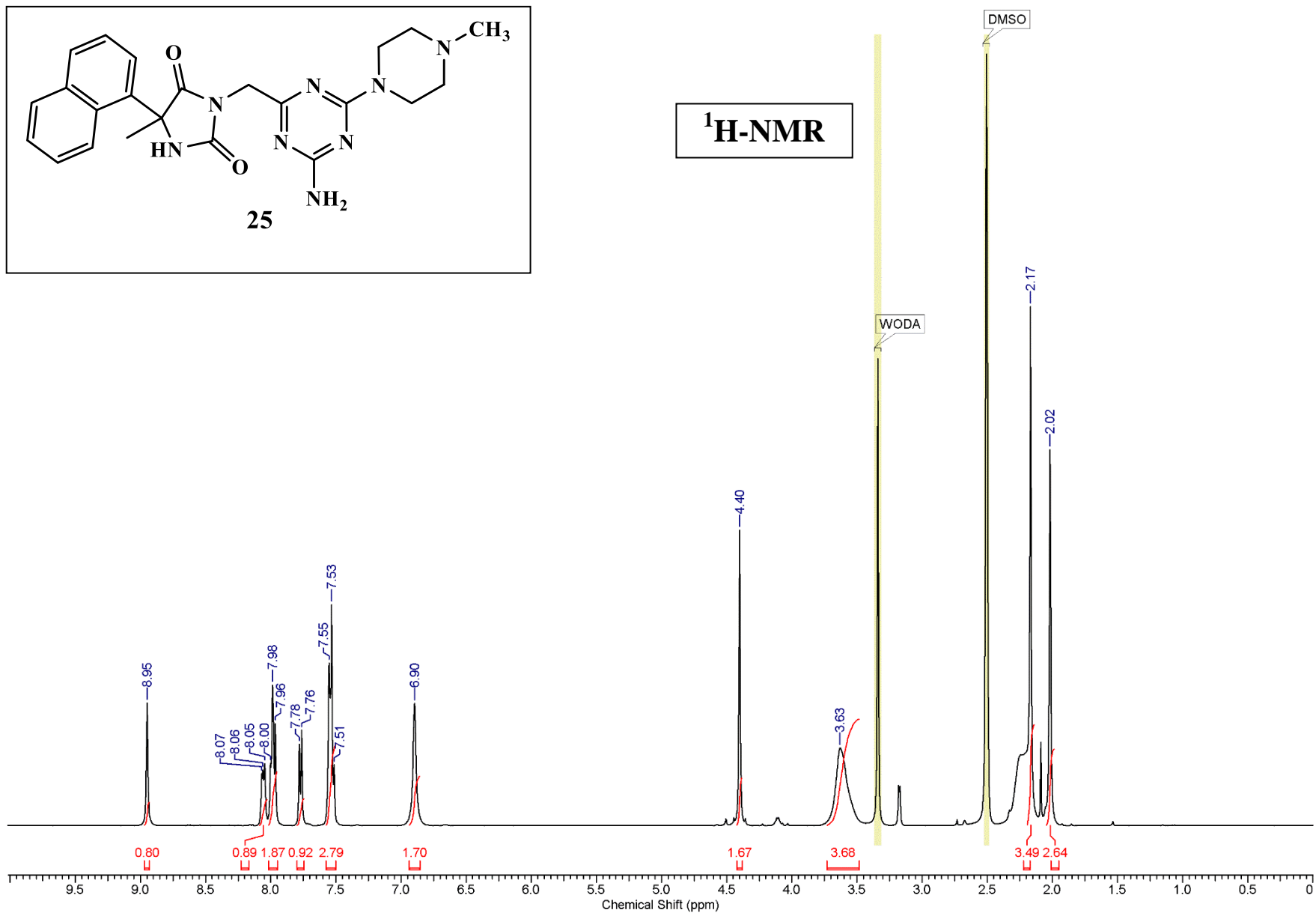


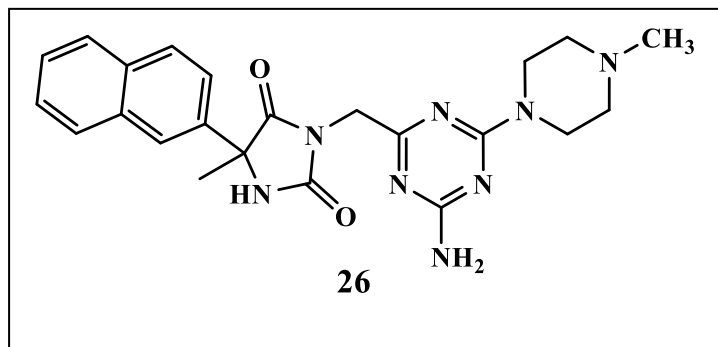
¹H-NMR



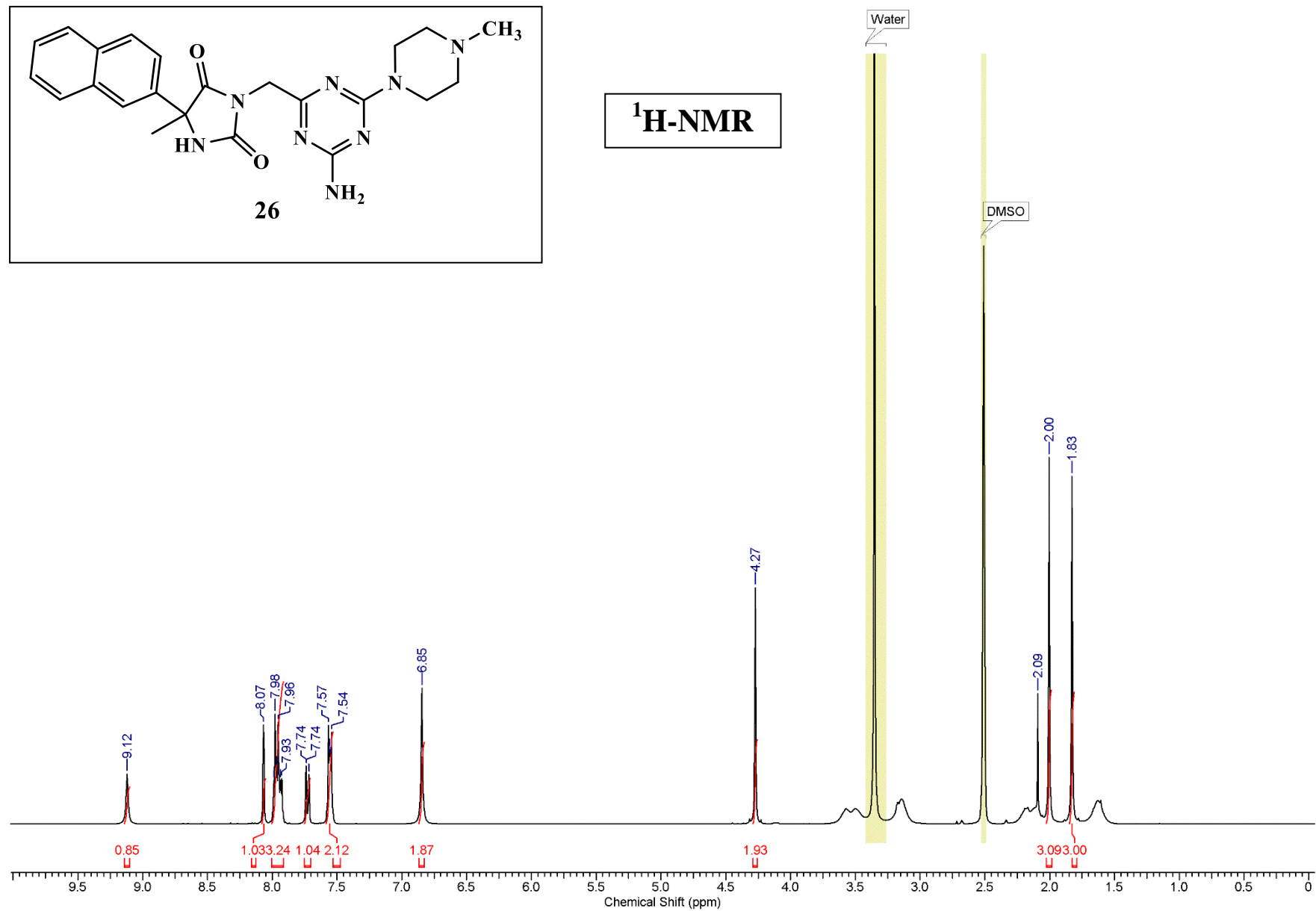


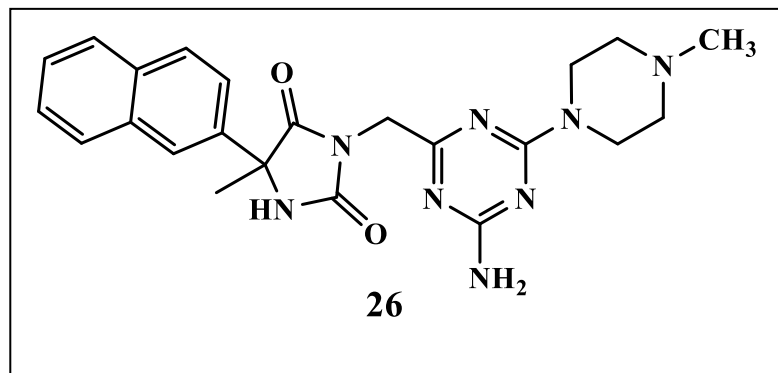
¹H-NMR



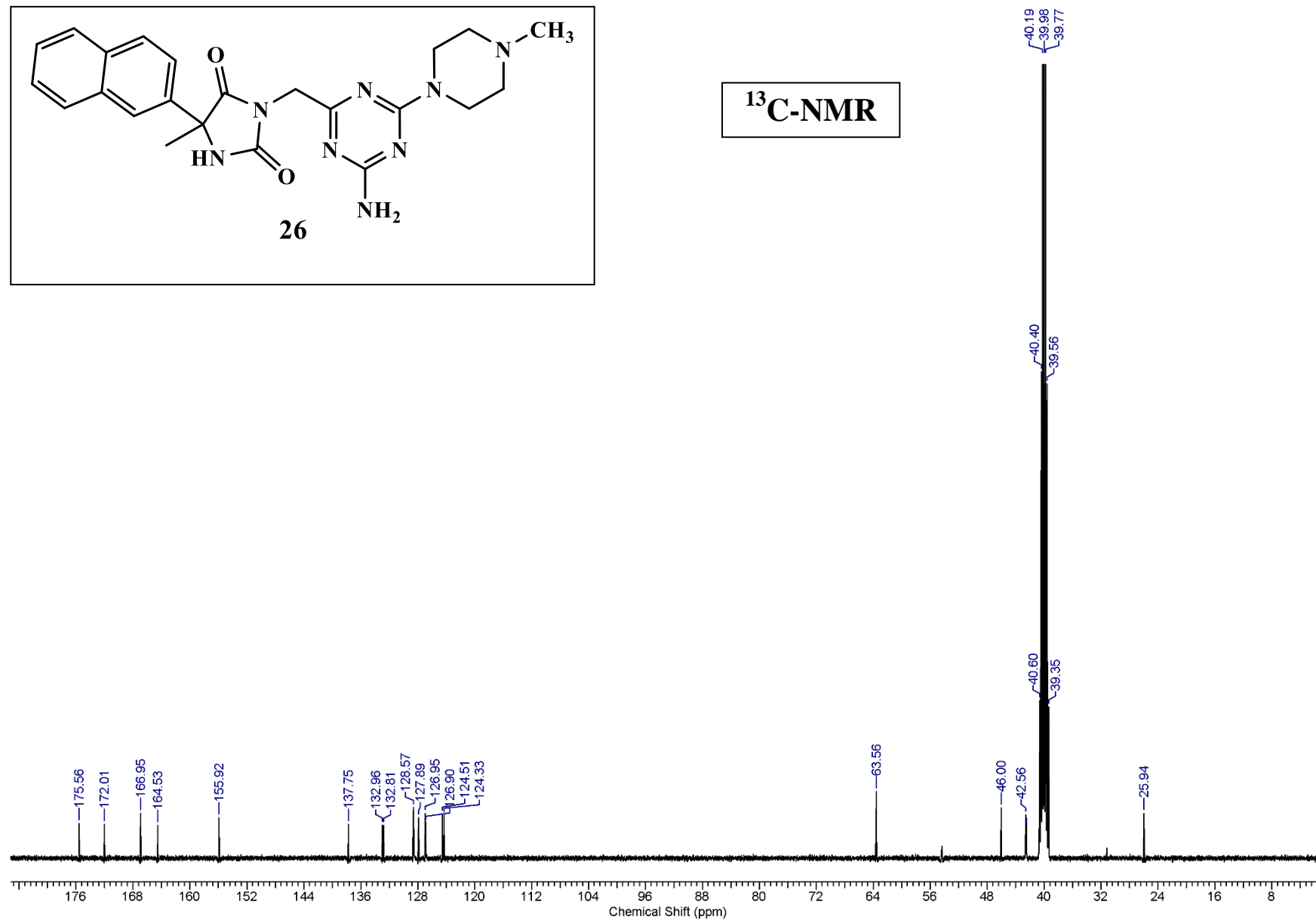


¹H-NMR





¹³C-NMR



7.2. Supplementary material for Publication 2: Synthesis and computer-aided SAR studies for derivatives of phenoxyalkyl-1,3,5-triazine as the new potent ligands for serotonin receptors 5-HT₆.

Supplementary

Synthesis and computer-aided SAR studies for phenoxyalkyl derivatives of 1,3,5-triazine as the new potent ligands for serotonin receptors 5-HT₆.

Wesam Ali^{a,b}, Małgorzata Więcek^a, Dorota Łażewska^a, Rafał Kurczab^c, Magdalena Jastrzębska-Więsek^d, Grzegorz Satała^c, Katarzyna Kucwaj-Brysz^a, Annamaria Lubelska^a, Monika Głuch-Lutwin^e, Barbara Mordyl^e, Agata Siwek^e, Muhammad Jawad Nasim^{a,b}, Anna Partyka^d, Sylwia Sudol^a, Gniewomir Latacz^a, Anna Wesołowska^d, Katarzyna Kieć-Kononowicz^a, and Jadwiga Handzlik^{a*}

1. Synthesis of intermediates

2. Spectral analysis for final products

1. Procedures for synthesis of the ester intermediates

1.1. General procedure for the synthesis of aryl(thio)ether esters (32-36)

The mixture of suitable phenol or thiophenol (15 mmol), potassium carbonate (30 mmol) and alkyl 2-bromoacetate (16.5 mmol) in acetonitrile (40 ml) was heated at reflux for 24 hours. The resulted mixture was filtered to remove inorganic salt. The filtrate was washed with 40 ml of ethyl acetate. The organic phase was collected in a separatory funnel and washed with 40 ml of NaOH 1%, 40 mL of distilled water and 40 ml of brine. The organic layer was dried overnight over MgSO₄, then filtered and evaporated to provide the crude product which was used without further purification for the next step.

1.1.1. Ethyl 2-(2-chlorophenoxy)acetate (32)

CAS Number (6956-85-0). Brown liquid. Yield 54%, C₁₀H₁₁ClO₃ (MW 214.65). ¹H-NMR: (CDCl₃-d) δ [ppm]: 7.38 (dd, *J*=7.82 Hz, *J*=1.67 Hz, 1H, Ph-3H), 7.16-7.22 (m, 1H, Ph), 6.92-6.98 (dt, *J*=7.63 Hz, *J*=1.45 Hz, 1H, Ph), 6.84 (dd, *J*=8.2 Hz, *J*=1.53 Hz, 1H, Ph), 4.70 (s, 2H, CH₂), 4.23-4.30 (q, *J*=7.18 Hz, 2H, CH₂), 1.29 (t, *J*=7.18 Hz, 3H, CH₃).

1.1.2. Ethyl 2-(3-chlorophenoxy)acetate (33)

CAS Number (111304-01-9). White solid. Yield 82%, mp 33-35 °C, C₁₀H₁₁ClO₃ (MW 214.65). ¹H-NMR: (CDCl₃-d) δ [ppm]: 7.18-7.24 (t, *J*=8.21 Hz, 1H, Ph), 6.96-7.00 (m, 1H, Ph), 6.91 (m, 1H, Ph), 6.78-6.82 (m, 1H, Ph), 4.60 (s, 2H, CH₂), 4.23-4.31 (q, *J*=7.18 Hz, 2H, CH₂), 1.30 (t, *J*=7.05 Hz, 3H, CH₃).

1.1.3. Ethyl 2-(p-tolyloxy)acetate (34)

CAS Number (38768-63-7). Colorless liquid. Yield 38%, C₁₀H₁₄O₃ (MW 194.23). ¹H-NMR: (CDCl₃-*d*) δ [ppm]: 7.06-7.10 (m, 2H, Ph), 6.81 (dd, *J*=6,41 Hz, *J*=2,05 Hz, 2H, Ph), 4.59 (s, 2H, CH₂), 4.27 (q, *J*=7,12 Hz, 2H, CH₂), 2.29 (s, 3H, CH₃), 1.29 (t, *J*=7,18 Hz, 3H, CH₃).

1.1.4. Methyl 2-(phenylthio)acetate (**35**)

CAS Number (6956-85-0). Yellow liquid. Yield 95%, C₉H₁₀O₂S (MW= 182.24). ¹H-NMR (DMSO-*d*₆) δ [ppm]: 7.38–7.32 (m, 4H, Ph), 7.25–7.21 (m, 1H, Ph), 4.09 (dd, *J* = 14.3, 7.1 Hz, 2H, CH₂), 3.88 (s, 2H, CH₂), 1.14 (t, *J* = 7.1 Hz, 3H, CH₃).

1.1.5. Methyl 2-((2-chlorophenyl)thio)acetate (**36**)

CAS Number (178213-94-0). Yellow liquid. Yield 96%, C₉H₉ClO₂S (MW 216.68). LC/MS⁺: purity: 87.40%, t_R=6.49, (ESI) *m/z* [M+H]⁺ 216.99.

1.2. Synthesis of methyl 2-(2-isopropyl-5-methylphenoxy)acetate (**37**)

2-(2-Isopropyl-5-methylphenoxy)acetic acid (10 mmol) was dissolved in 50 mL of dried methanol, and a few drops of concentrated sulfuric acid were added. The mixture was refluxed 8 hours. Next, the solvent was evaporated, and the residue dissolved in 40 mL of ethyl acetate, washed with 0.5% NaOH and brine. The organic layer dried over anhydrous Na₂SO₄ and filtered. The solvent was evaporated to give the product **37**.

CAS Number (111304-01-9). Light yellow liquid. Yield 65%, C₁₃H₁₈O₃ (MW 222.28). ¹H-NMR: (CDCl₃-*d*) δ [ppm]: 7.14 (d, *J*=7.69 Hz, 1H, Ph), 6.80 (d, *J*=7.95 Hz, 1H, Ph), 6.55 (d, *J*=0.77 Hz, 1H, Ph), 4.65 (s, 2H, CH₂), 3.82 (s, 3H, CH₃), 3.38(m, 1H, CH), 2.32 (s, 3H, CH₃), 1.24 (d, *J*=6.9 Hz, 6H, 2x-CH₃).

1.3. General procedure of synthesis of esters **38** and **39**

To the solution of 15 mmol of appropriate phenylacetic acid in 45 mL of anhydrous toluene, 15 mmol of DBU was added and the reaction mixture was stirred at room temperature for 1 hour. Afterwards, 15 mmol of iodomethane was added and stirring was continued for 2 days. Then, the solvent was evaporated under reduced pressure. The resulted residue was dissolved in ethyl acetate and washed with 0.5% NaOH and brine. The organic layer was dried over anhydrous Na₂SO₄, filtered off and evaporated under reduced pressure to provide light yellow liquid.

1.3.1. *Methyl 2-(4-chloro-2-methylphenoxy)acetate (38)*

CAS Number (2436-73-9). Obtained from commercial 2-(4-chloro-2-methylphenoxy) acetic acid with iodomethane in the presence of DBU. Light yellow liquid. Yield 56 %, C₁₀H₁₁O₃ (MW 214.65). ¹H-NMR: (CDCl₃-*d*) δ [ppm]: 7.12 (m, 1H, Ph), 7.05-7.09 (dd, *J*=8.85 Hz, *J*=3.08 Hz, 1H, Ph), 6.60 (d, *J*=8.46 Hz, 1H, Ph), 4.62 (s, 2H, CH₂), 3.79 (s, 3H, CH₃), 2.25 (s, 3H, CH₃).

1.3.2. *Methyl 2-(2,4-dichlorophenoxy)acetate (39)*

CAS Number (1928-38-7). Obtained from commercial 2-(2,4-Dichlorophenoxy) acetic acid with iodomethane in the presence of DBU. Light yellow liquid. Yield 65 %, C₉H₈Cl₂O₃ (MW 235.06). ¹H-NMR: (CDCl₃-*d*) δ [ppm]: 7.55 (d, *J*=2.56 Hz, 1H, Ph), 7.30-7.34 (dd, *J*=8.85 Hz, *J*=2.69 Hz, 1H, Ph), 7.09 (d, *J*=8.97 Hz, 1H, Ph), 4.93 (s, 2H, CH₂), 3.69 (s, 3H, CH₃).

1.4. *General procedure for the synthesis of methyl 2-(phenylselenenyl)acetate (40 and 41)*

An appropriate diphenyl diselenide (2.96g, 9.5 mmol) was dissolved in a 1:1 mixture of water and THF (50 mL) under nitrogen gas. NaBH₄ (1.79g, 47.5 mmol) was added. The reaction mixture was stirred until the solution turned colorless (1-3 minutes). The reaction mixture was stirred for a further 30 minutes. A solution of a methyl -2-bromoacetate (2.96g, 19.37 mmol) in THF (5 mL) was added through the rubber septum without opening the reaction apparatus. The reaction mixture was stirred at room temperature and monitored *via* TLC (~4 hours).

Subsequently, the solution was stirred for a further 30 minutes on air, then the reaction mixture was diluted with 50 mL of saturated aqueous solution of NH_4Cl and extracted with diethyl ether. The combined organic phases were dried over Na_2SO_4 , filtered and the solvent was evaporated under reduced pressure to get the product.

1.5.1. Methyl 2-(phenylselenyl)acetate (40)

CAS Number (68872-84-4). Colorless liquid. Yield 85%, $\text{C}_9\text{H}_{10}\text{O}_2\text{Se}$ (MW 229.98). LC/MS[±]: purity: 99.29%, $t_{\text{R}}=6.20$, (ESI) m/z $[\text{M}+\text{H}]^+$ 230.87.

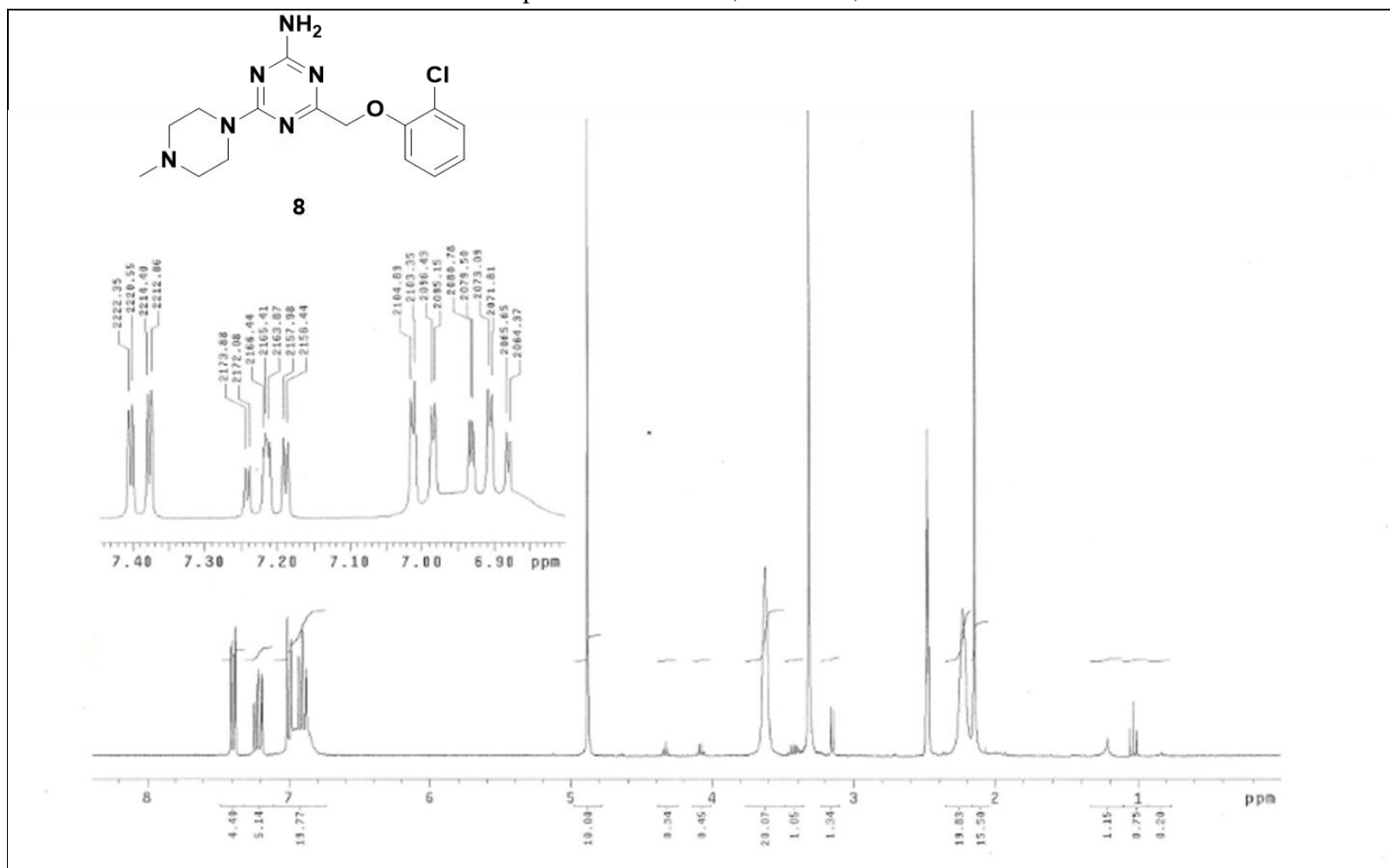
4.1.5.2. Methyl 2-(phenylselanyl)propanoate (41)

CAS Number (65275-66-3). Light yellow liquid. Yield 87%, $\text{C}_{10}\text{H}_{12}\text{O}_2\text{Se}$ (MW= 243.18). $^1\text{H-NMR}$ (Acetone- d_6) δ [ppm]: 7.62–7.59 (m, 2H-Ph), 7.40–7.32 (m, 3H-Ph), 3.88 (q, $J = 7.1$ Hz, 1H-CH), 3.60 (s, 3H- CH_3), 1.50 (d, $J = 7.1$ Hz, 3H- CH_3).

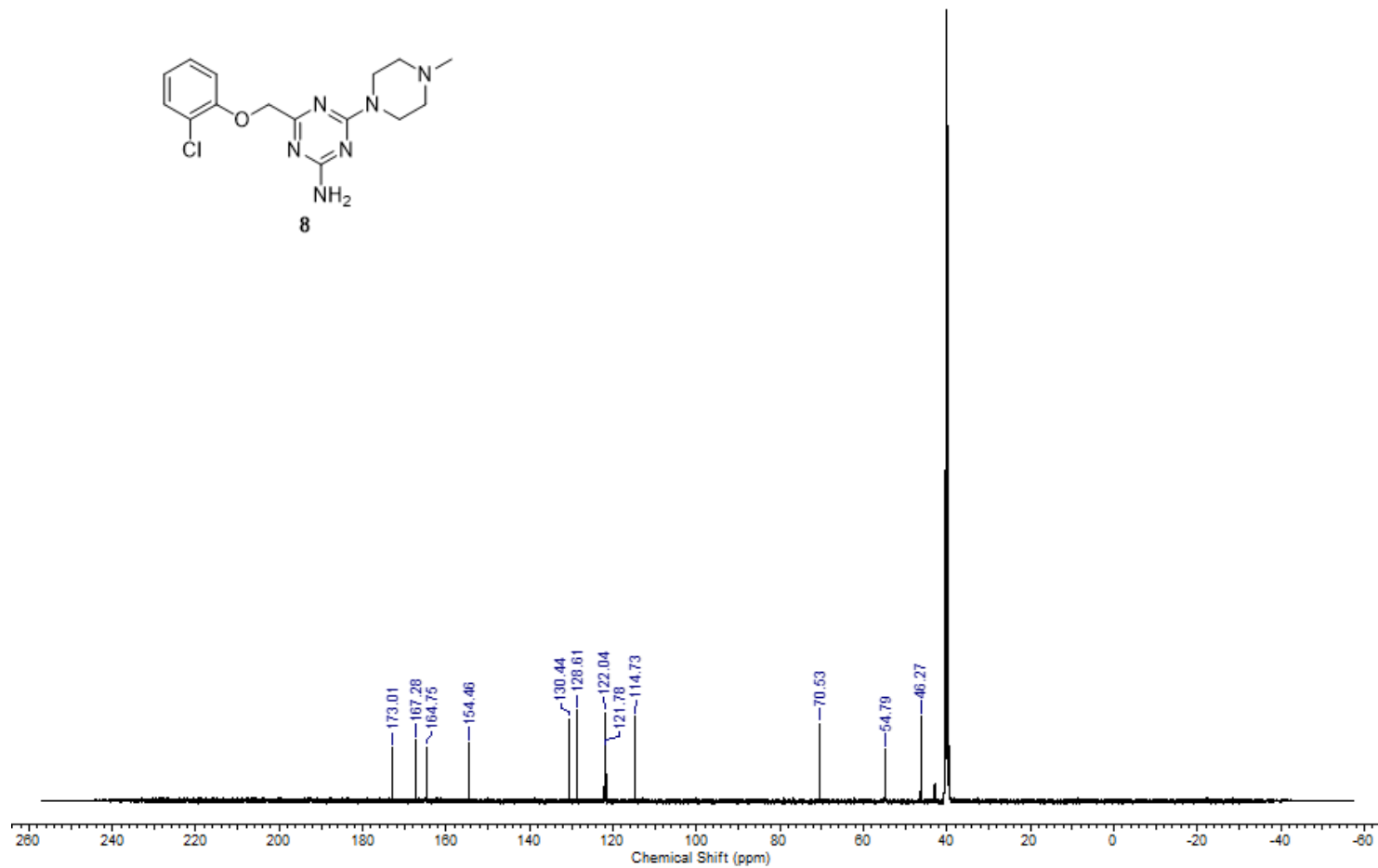
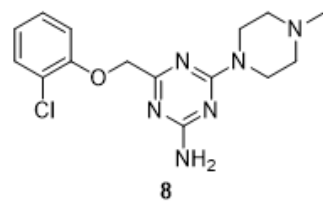
2. Spectral analysis for the final compounds

4-((2-Chlorophenoxy)methyl)-6-(4-methylpiperazin-1-yl)-1,3,5-triazin-2-amine (**8**)

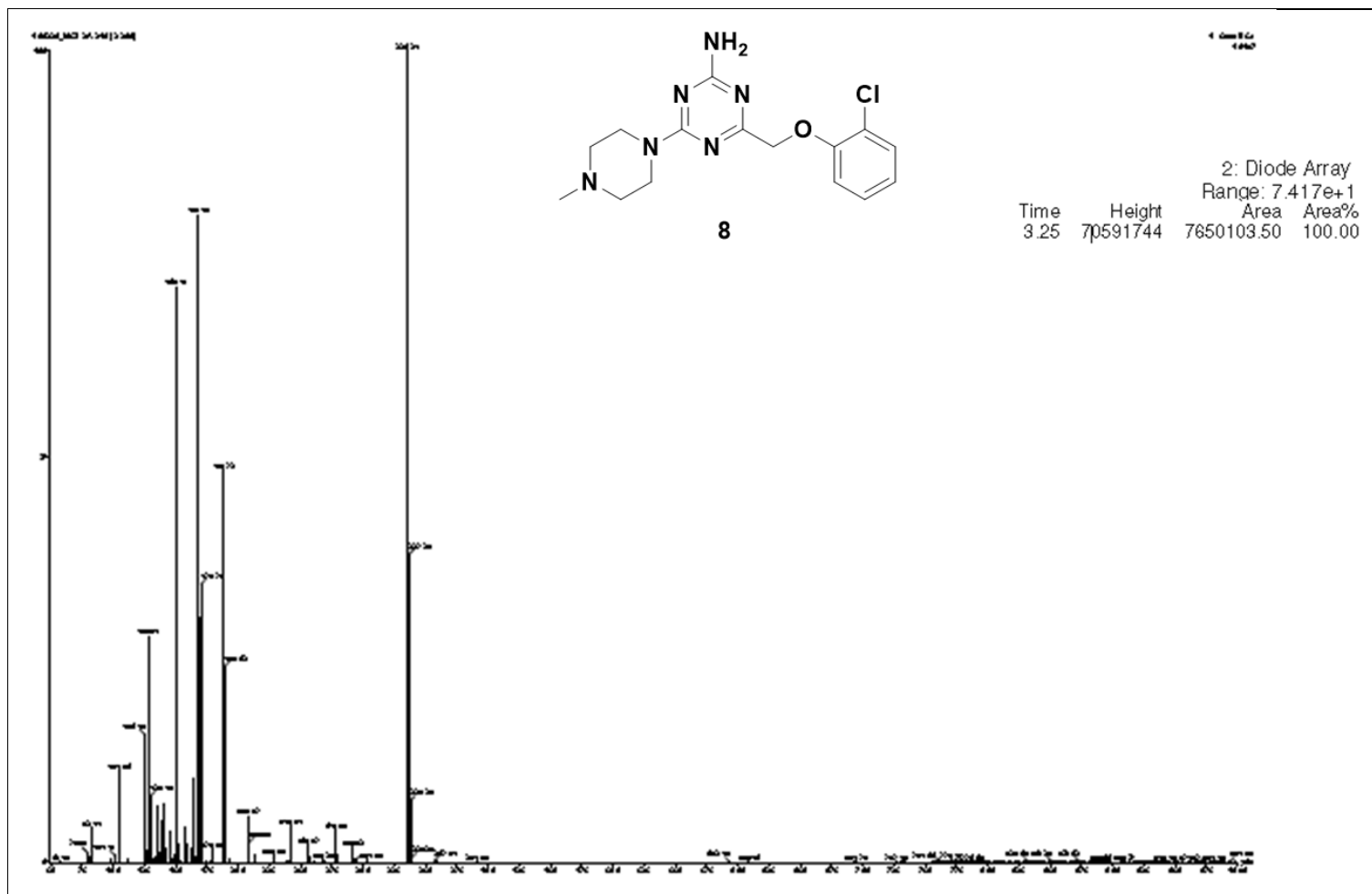
Compound **8** - ^1H NMR, 300 MHz, DMSO



Compound **8** – ^{13}C NMR, 125 MHz, DMSO

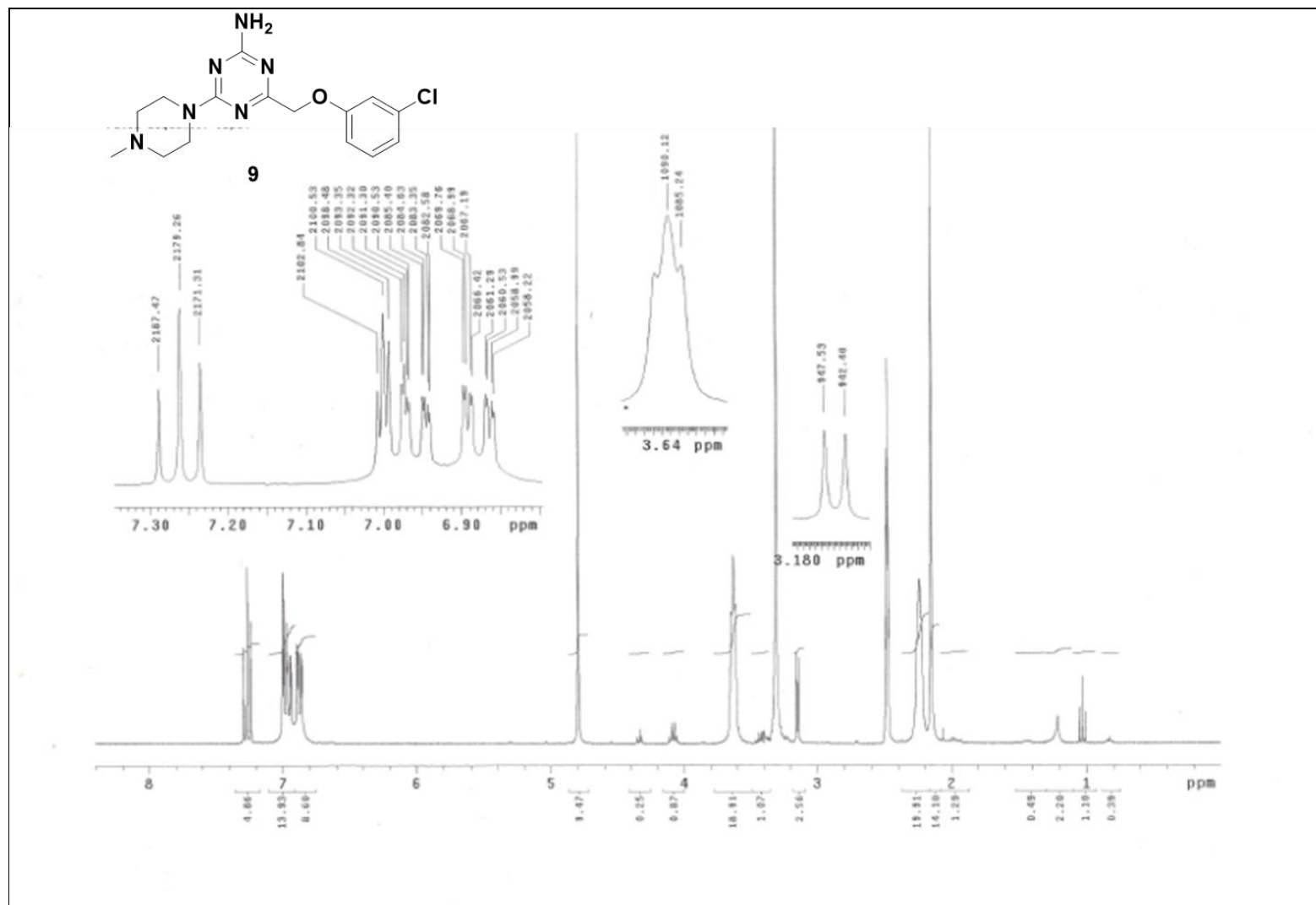


Compound 8 - LC/MS⁺

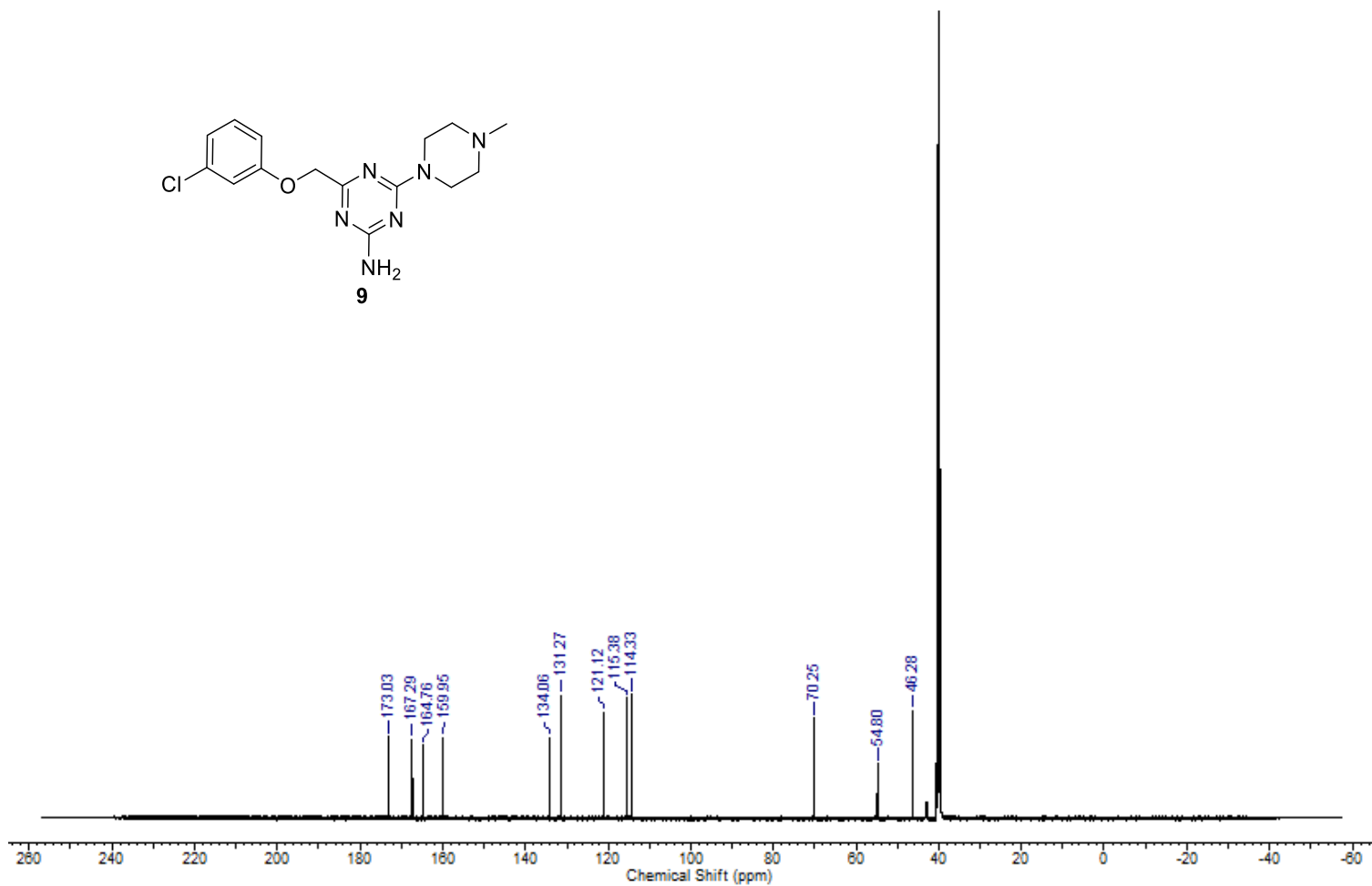
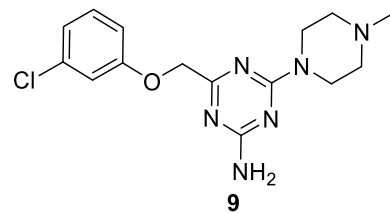


4-((3-Chlorophenoxy)methyl)-6-(4-methylpiperazin-1-yl)-1,3,5-triazin-2-amine (**9**)

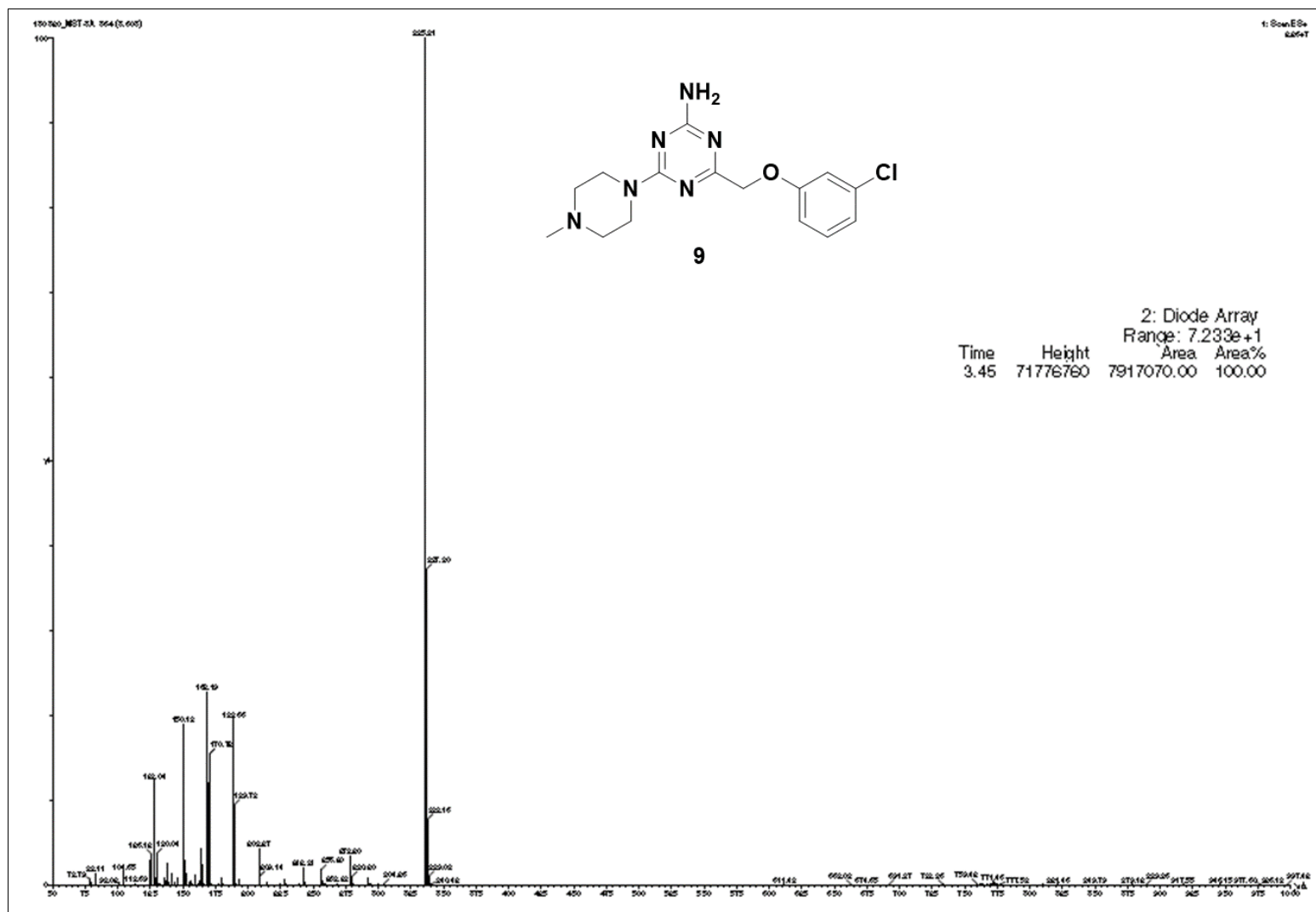
Compound **9** - ^1H NMR, 300 MHz, DMSO



Compound **9** – ^{13}C NMR, 125 MHz, DMSO

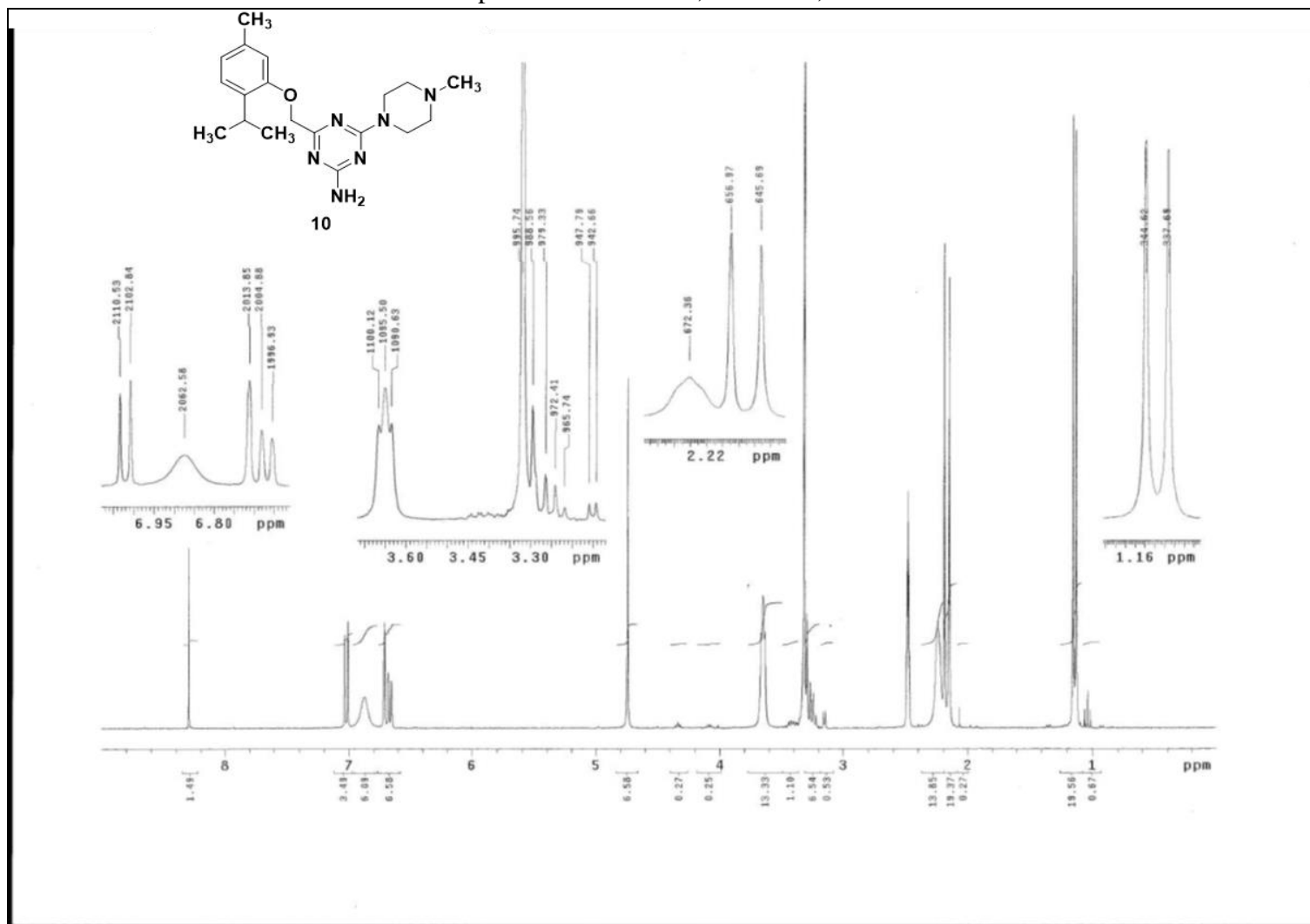


Compound 9 - LC/MS⁺

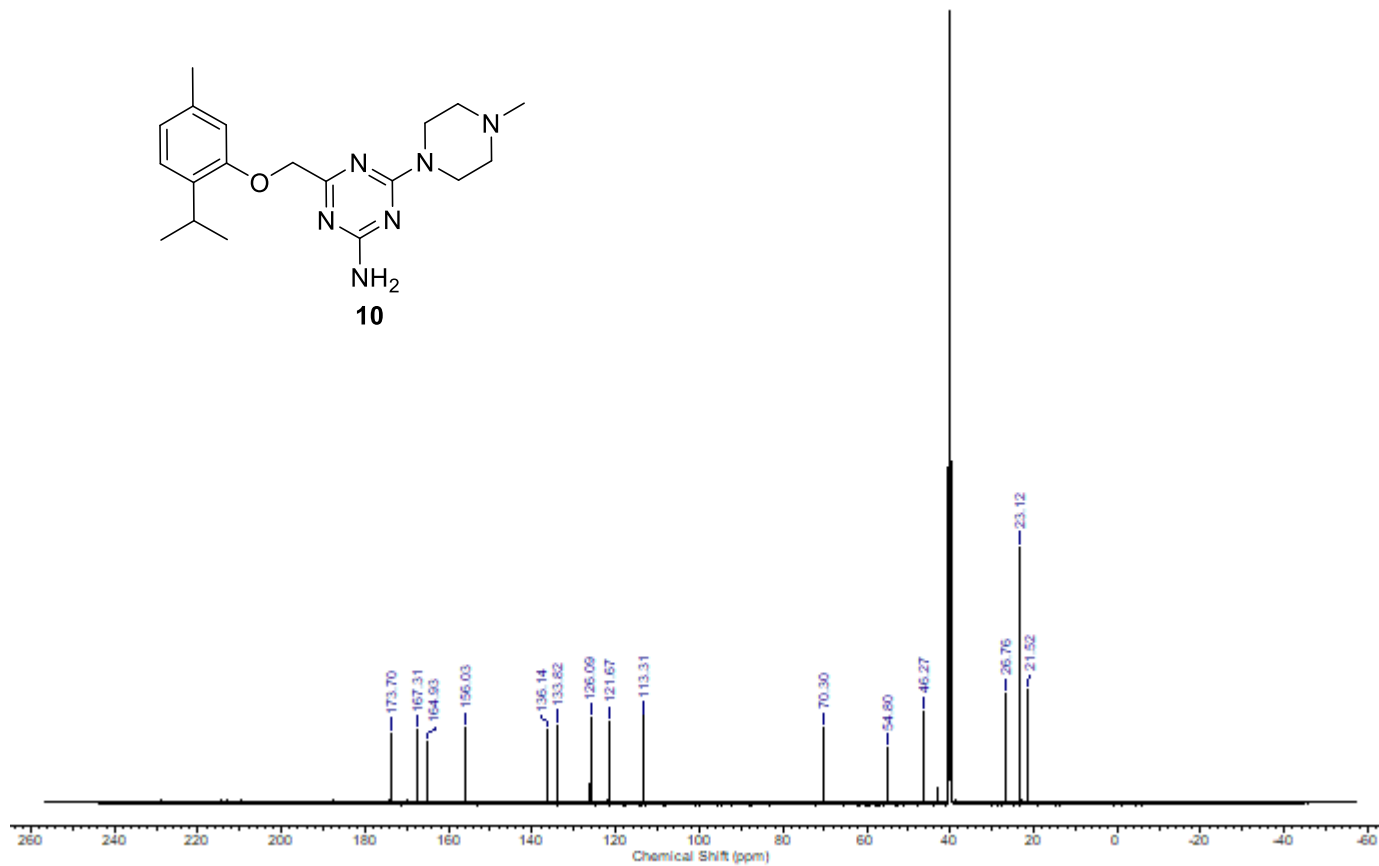
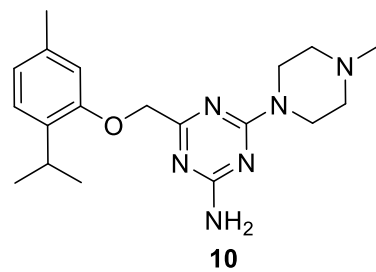


4-((2-Isopropyl-5-methylphenoxy)methyl)-6-(4-methylpiperazin-1-yl)-1,3,5-triazin-2-amine (**10**)

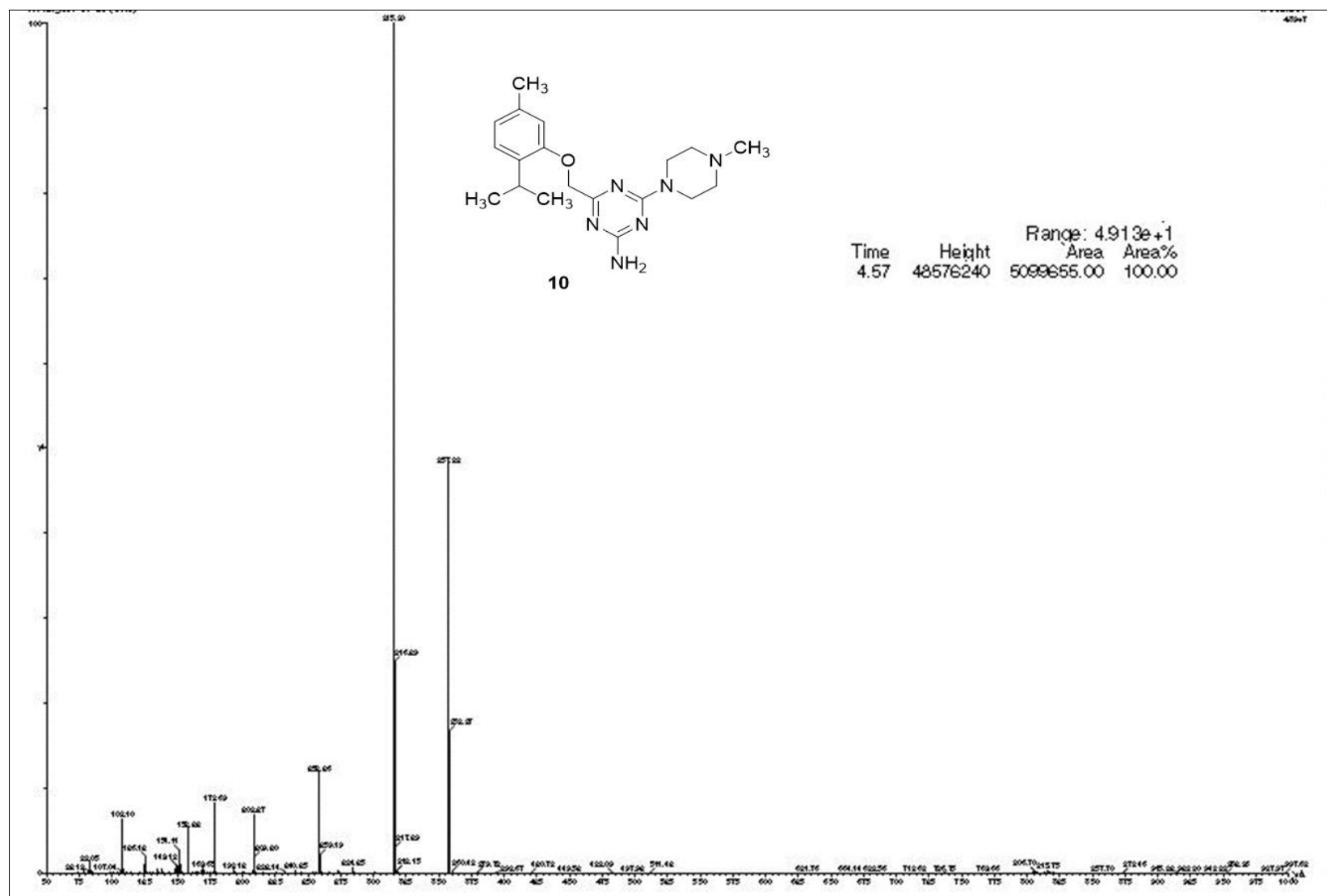
Compound **10**- ^1H NMR, 300 MHz, DMSO



Compound 10- ^{13}C NMR, 125 MHz, DMSO

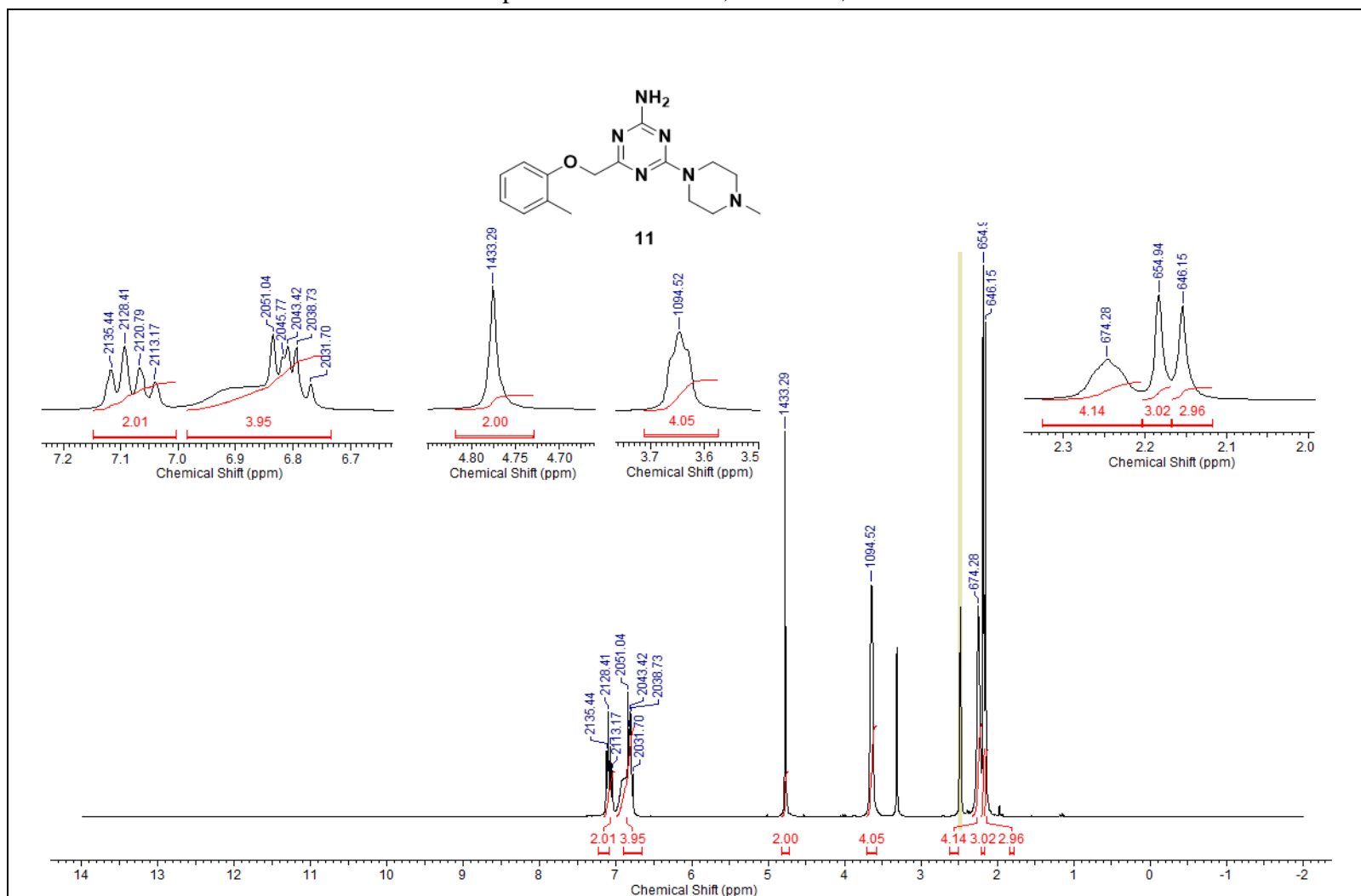


Compound 10 - LC/MS⁺

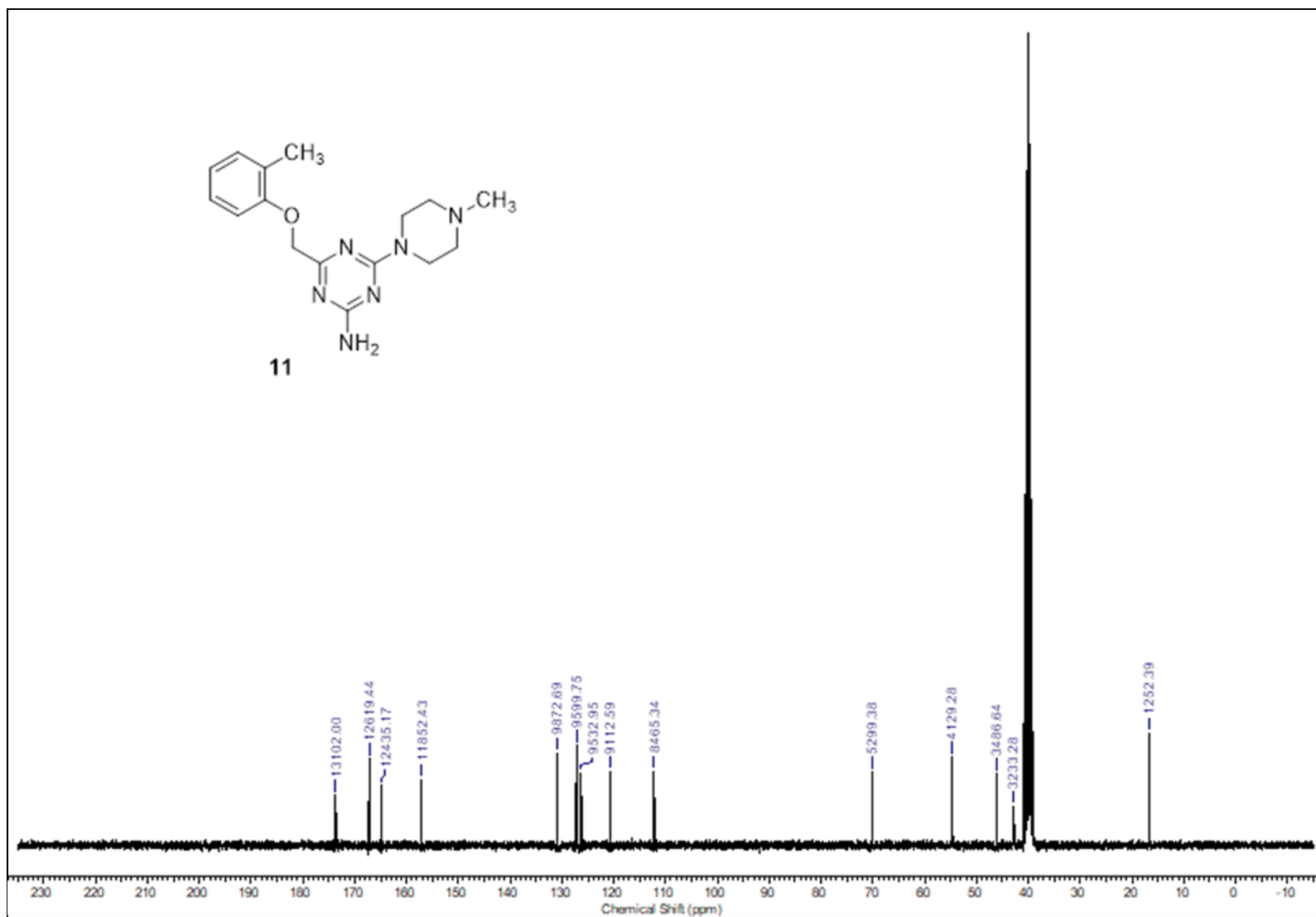


4-(4-Methylpiperazin-1-yl)-6-(o-tolylloxymethyl)-1,3,5-triazin-2-amine (**11**)

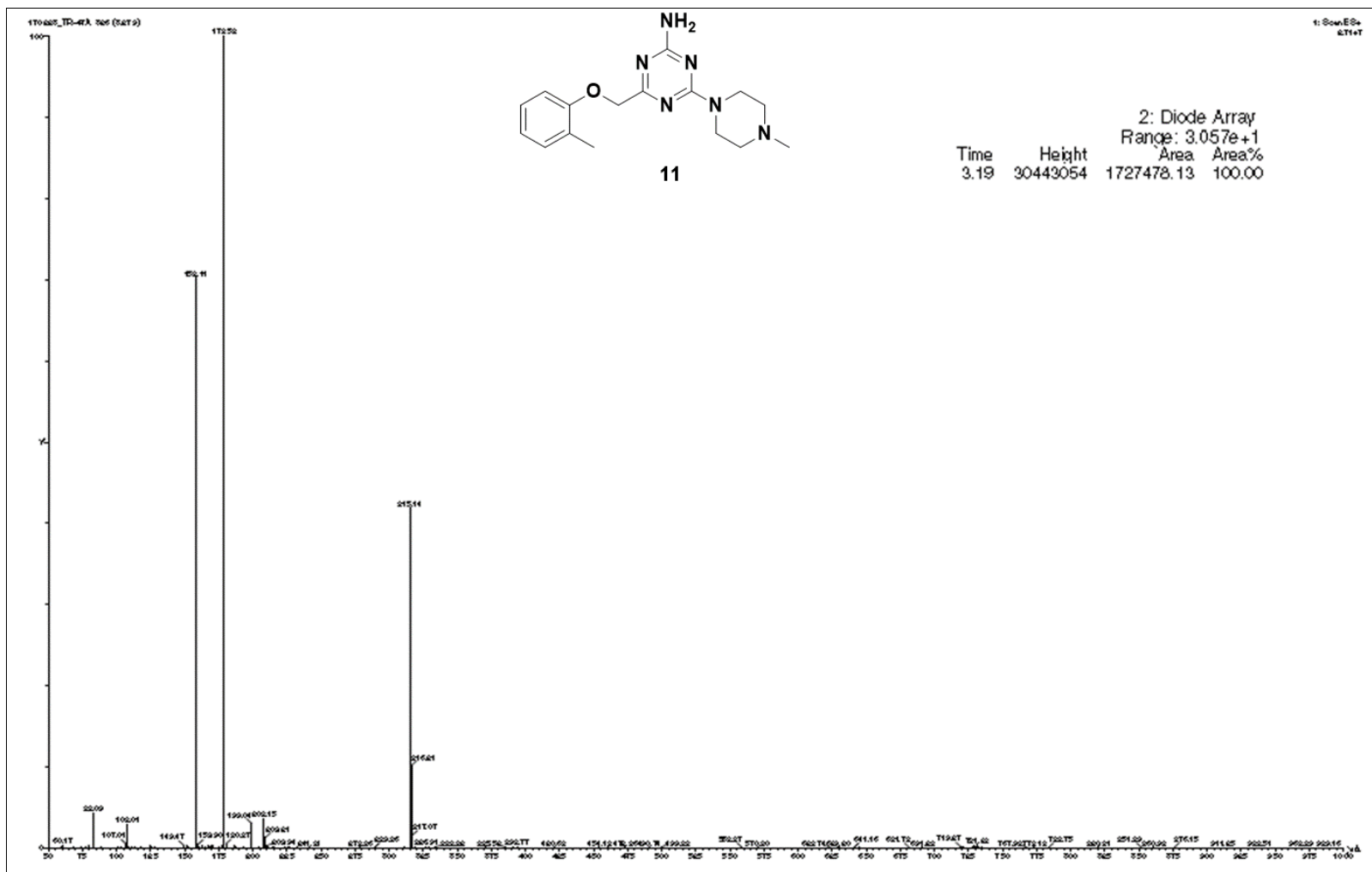
Compound **11** - ^1H NMR, 300 MHz, DMSO



Compound **11** - ^{13}C NMR, 300 MHz, DMSO

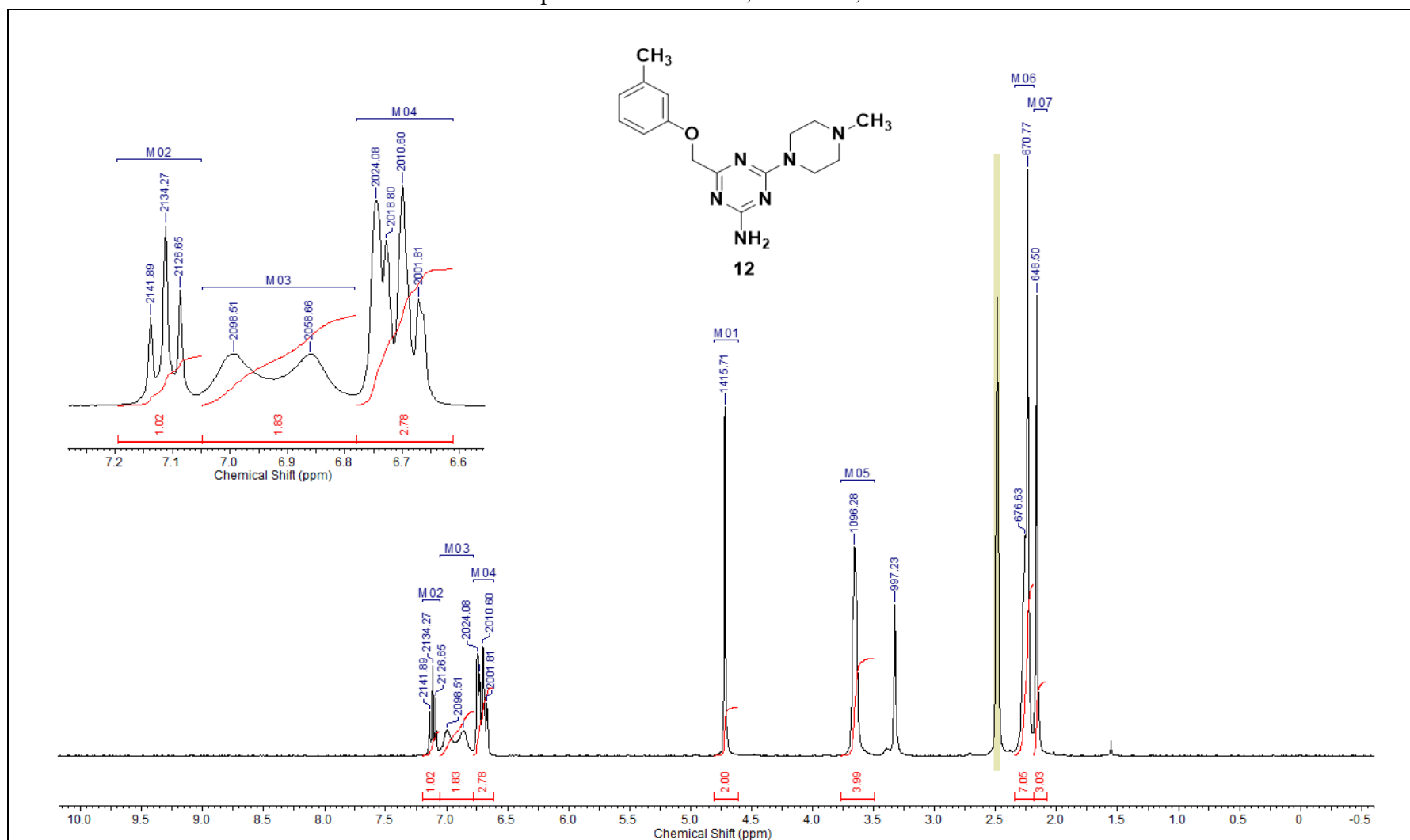


Compound 11 - LC/MS⁺

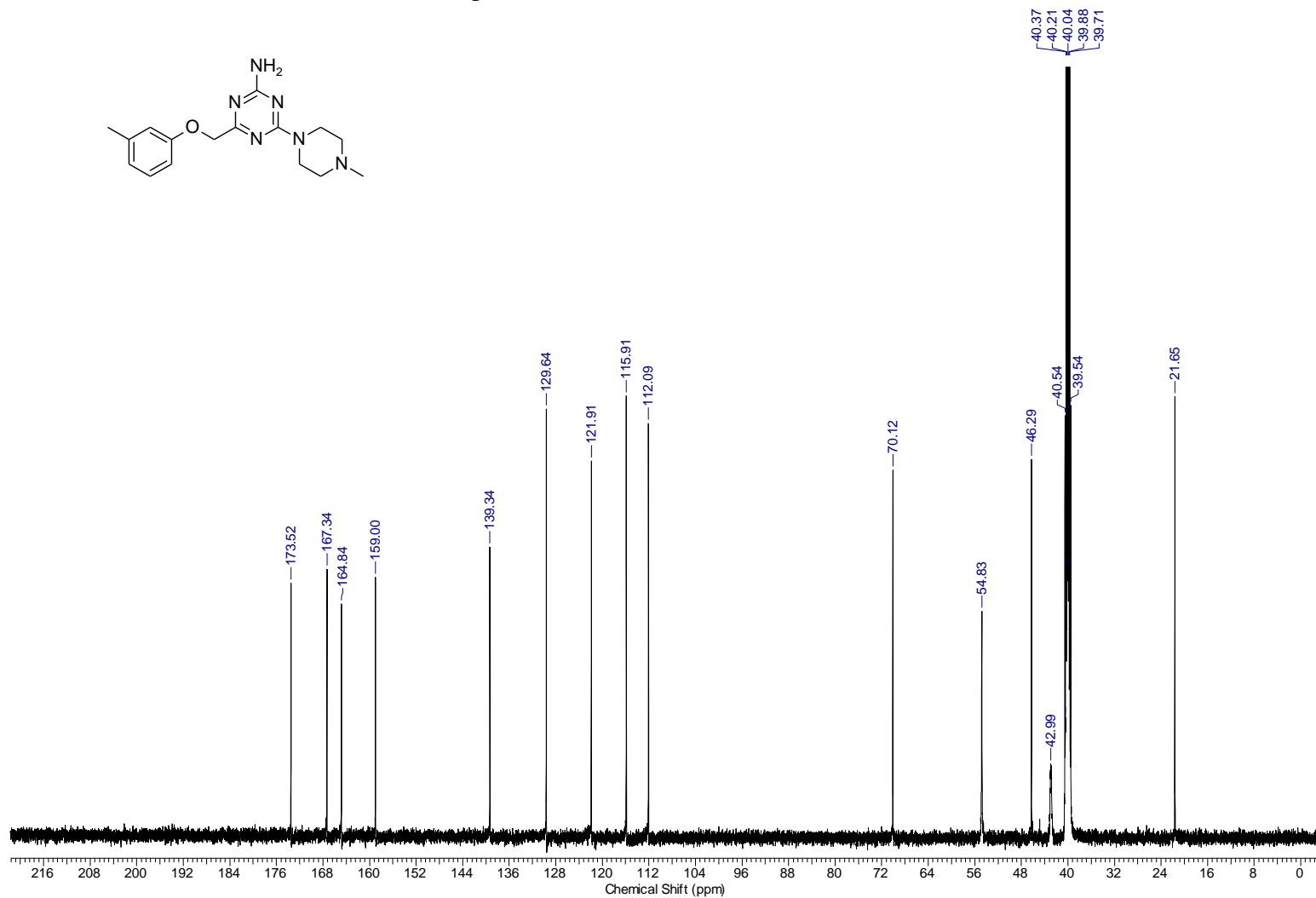
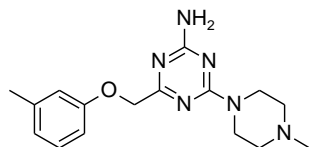


4-(4-Methylpiperazin-1-yl)-6-(m-toloxymethyl)-1,3,5-triazin-2-amine (**12**)

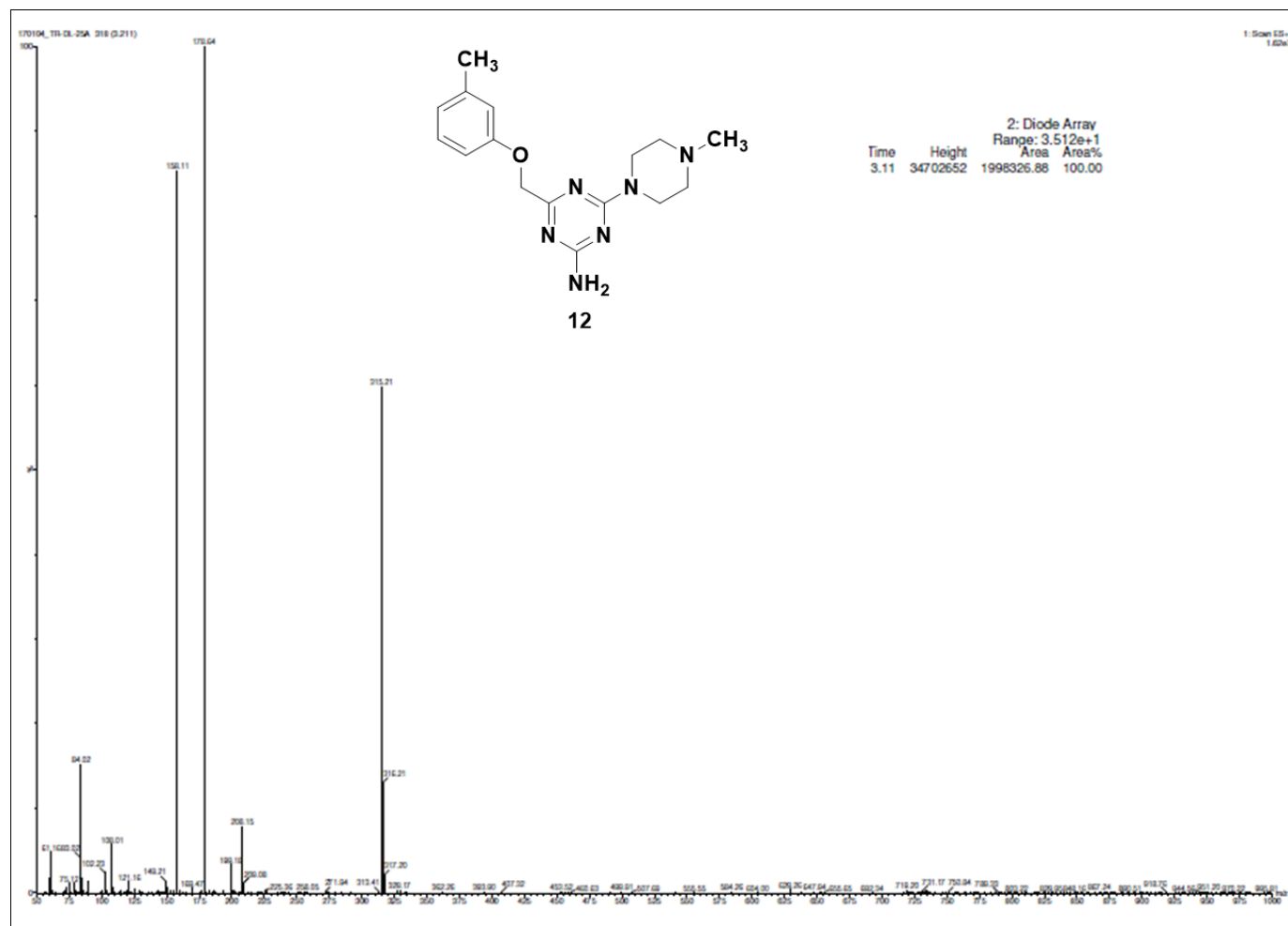
Compound **12** - ^1H NMR, 300 MHz, DMSO



Compound **12** – ^{13}C NMR, 125 MHz, DMSO

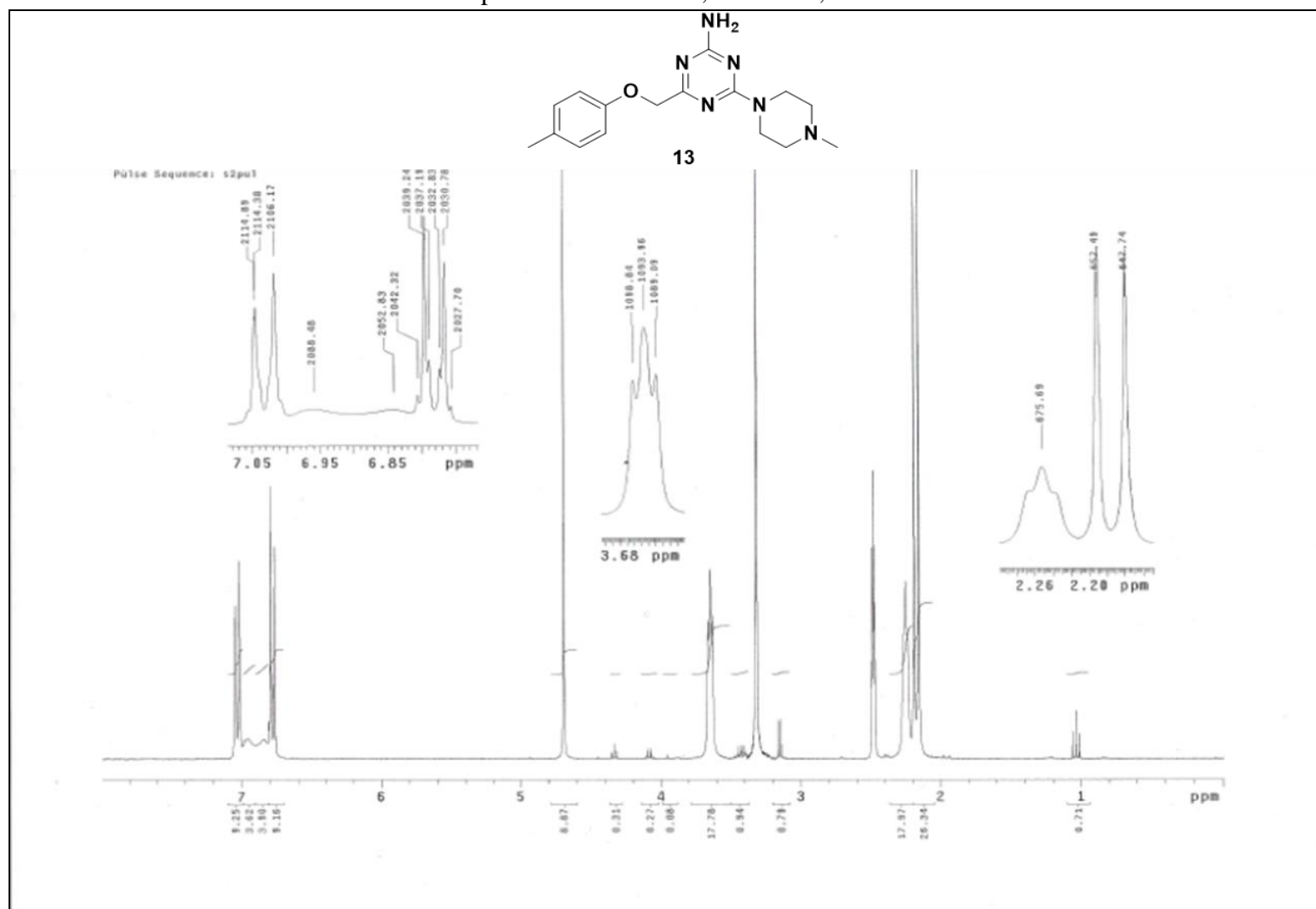


Compound 12 - LC/MS⁺

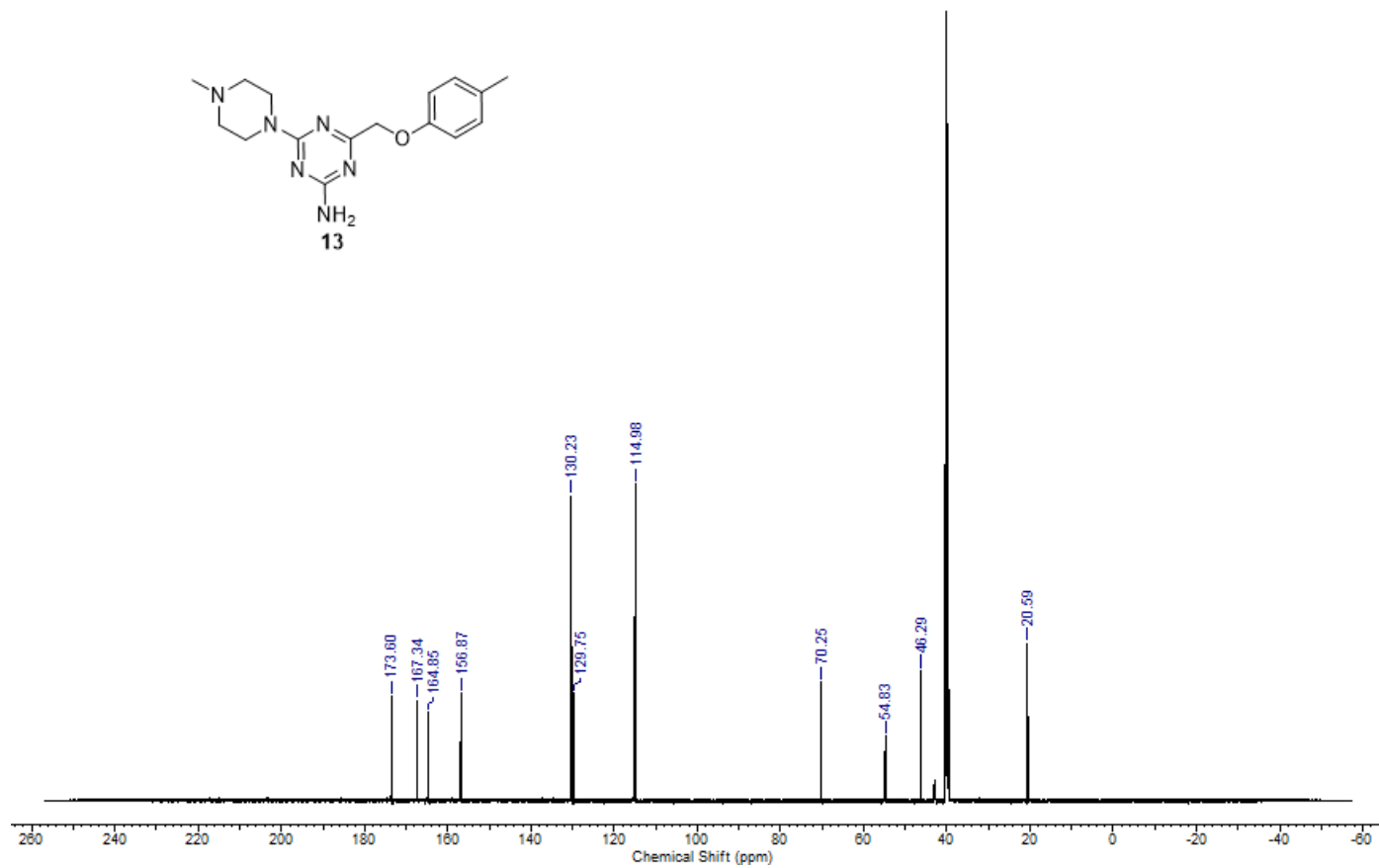
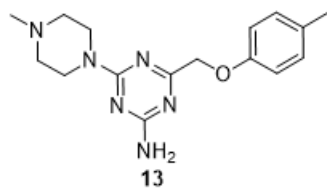


4-(4-Methylpiperazin-1-yl)-6-(p-toloxymethyl)-1,3,5-triazin-2-amine (**13**)

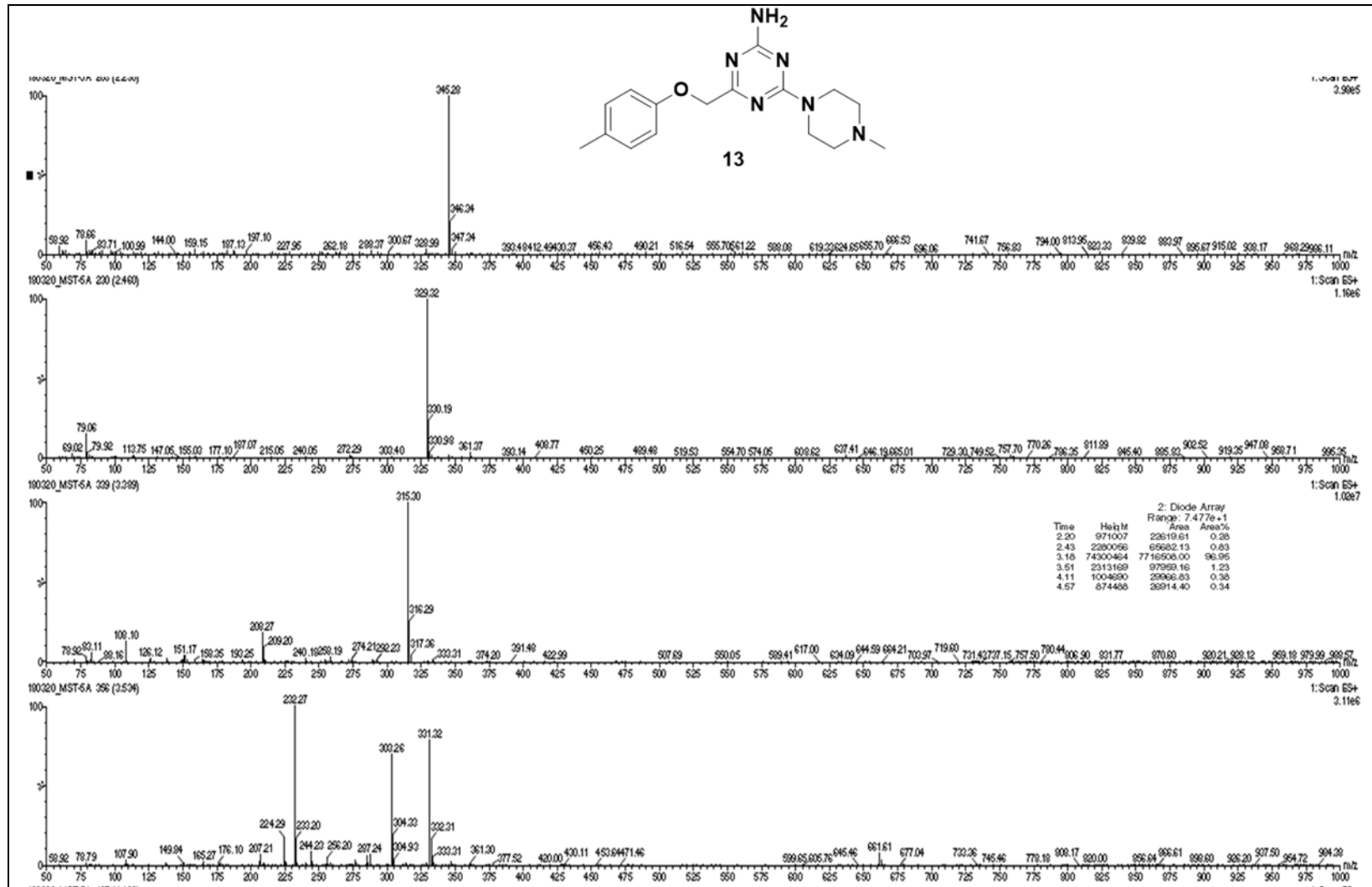
Compound **13** - ^1H NMR, 300 MHz, DMSO



Compound **13** – ^{13}C NMR, 125 MHz, DMSO

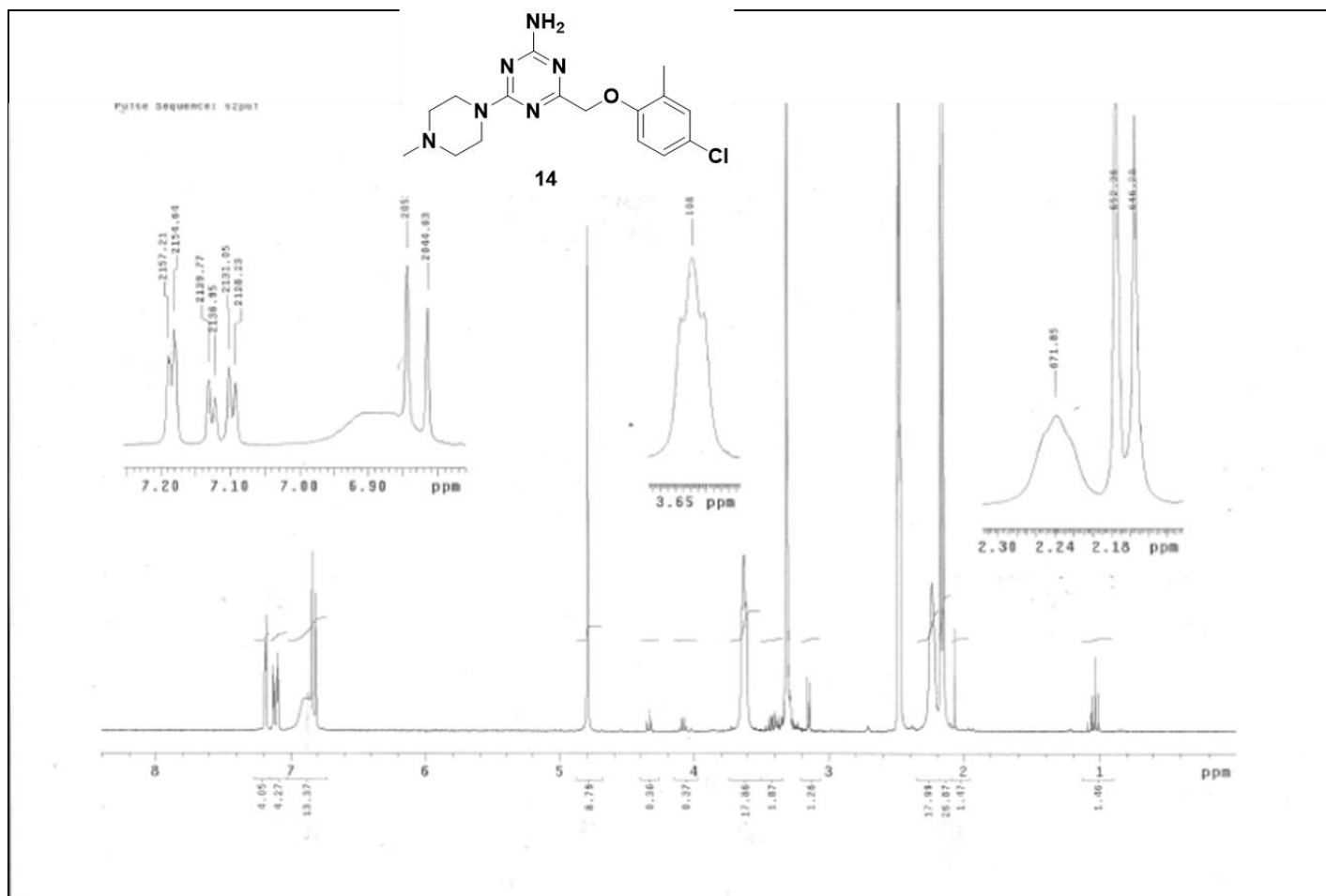


Compound 13 - LC/MS⁺

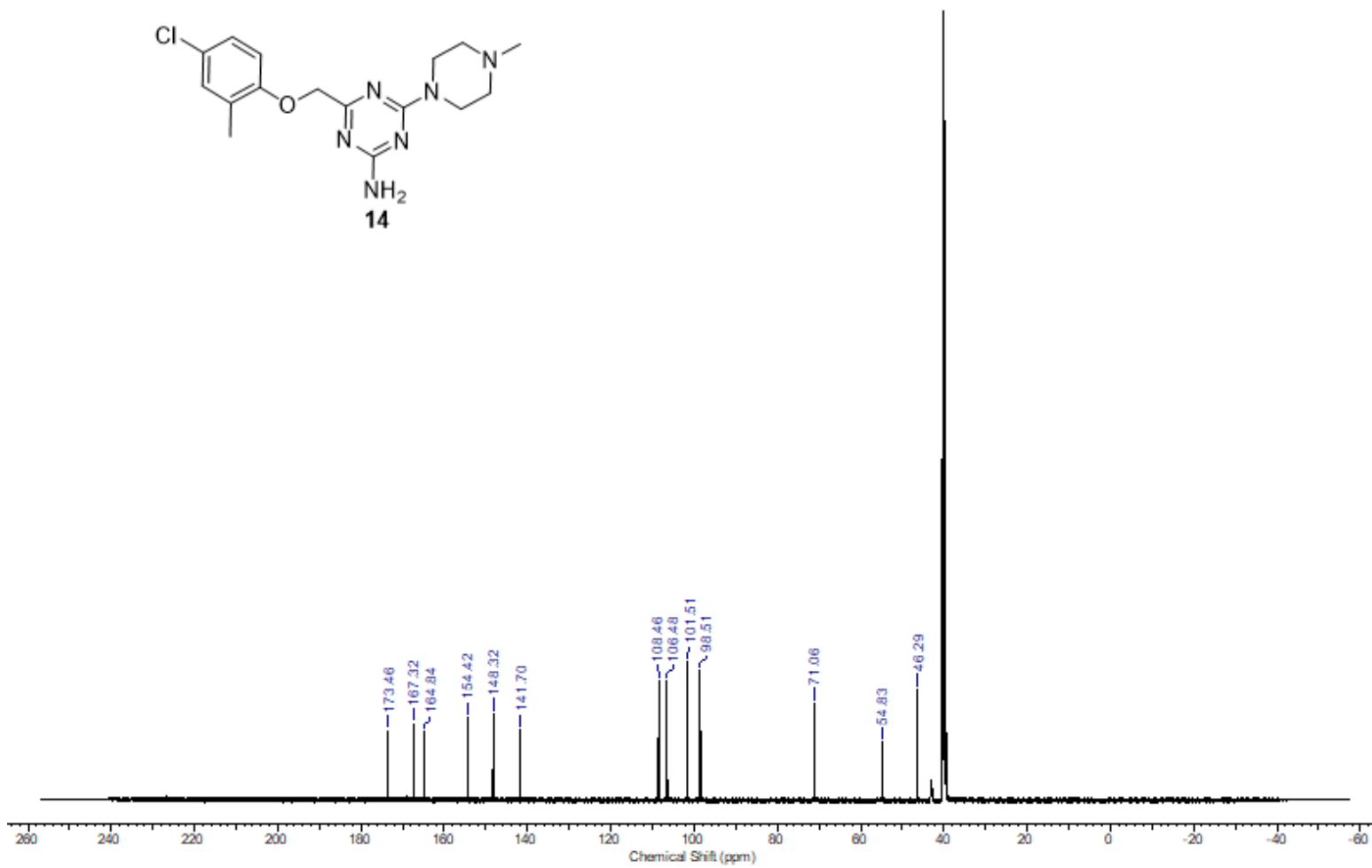
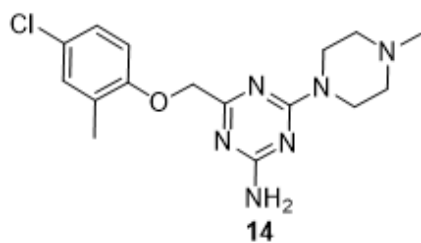


4-((4-Chloro-2-methylphenoxy)methyl)-6-(4-methylpiperazin-1-yl)-1,3,5-triazin-2-amine (**14**)

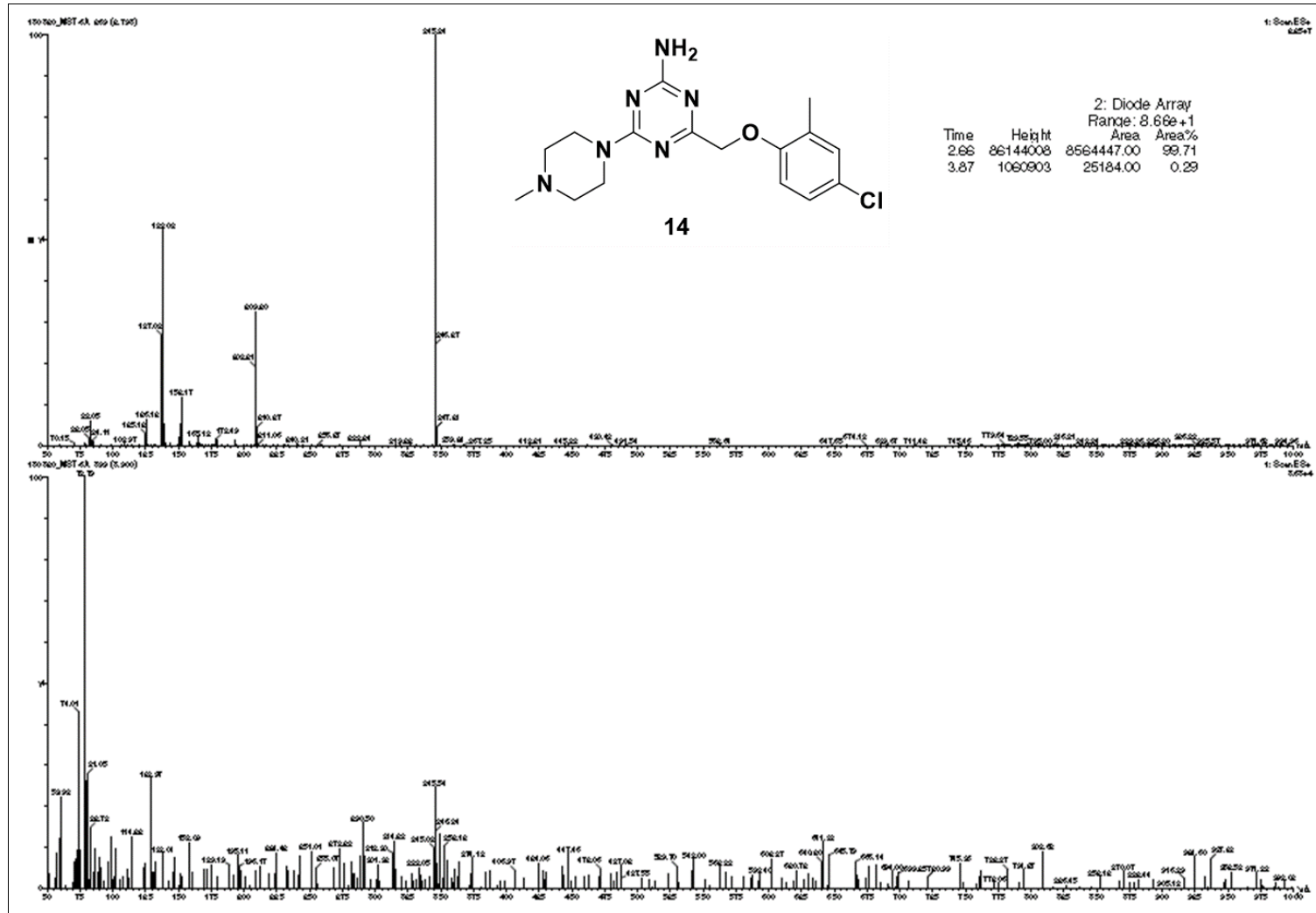
Compound **14** - ^1H NMR, 300 MHz, DMSO



Compound **14** – ^{13}C NMR, 125 MHz, DMSO

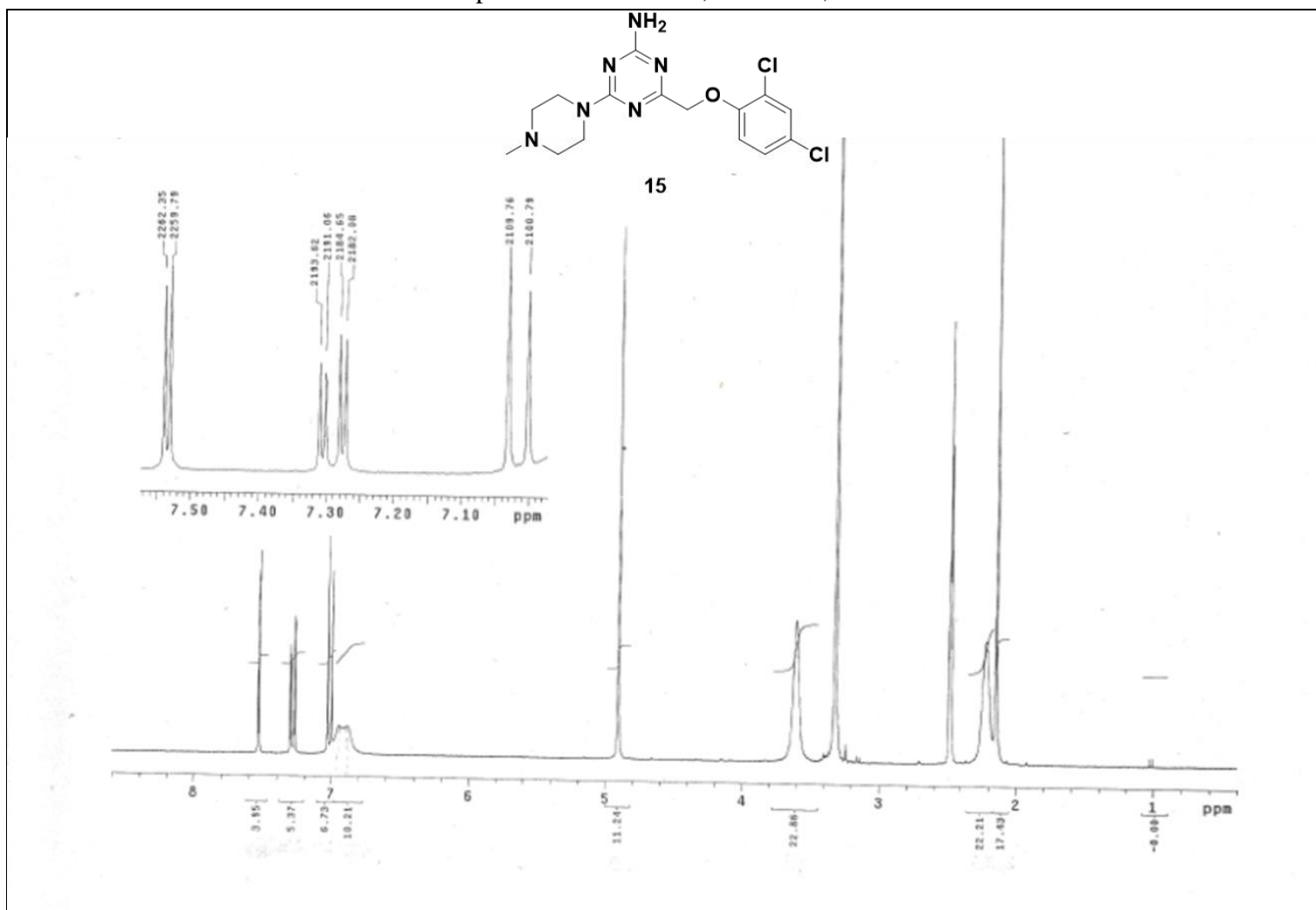


Compound 14 - LC/MS⁺

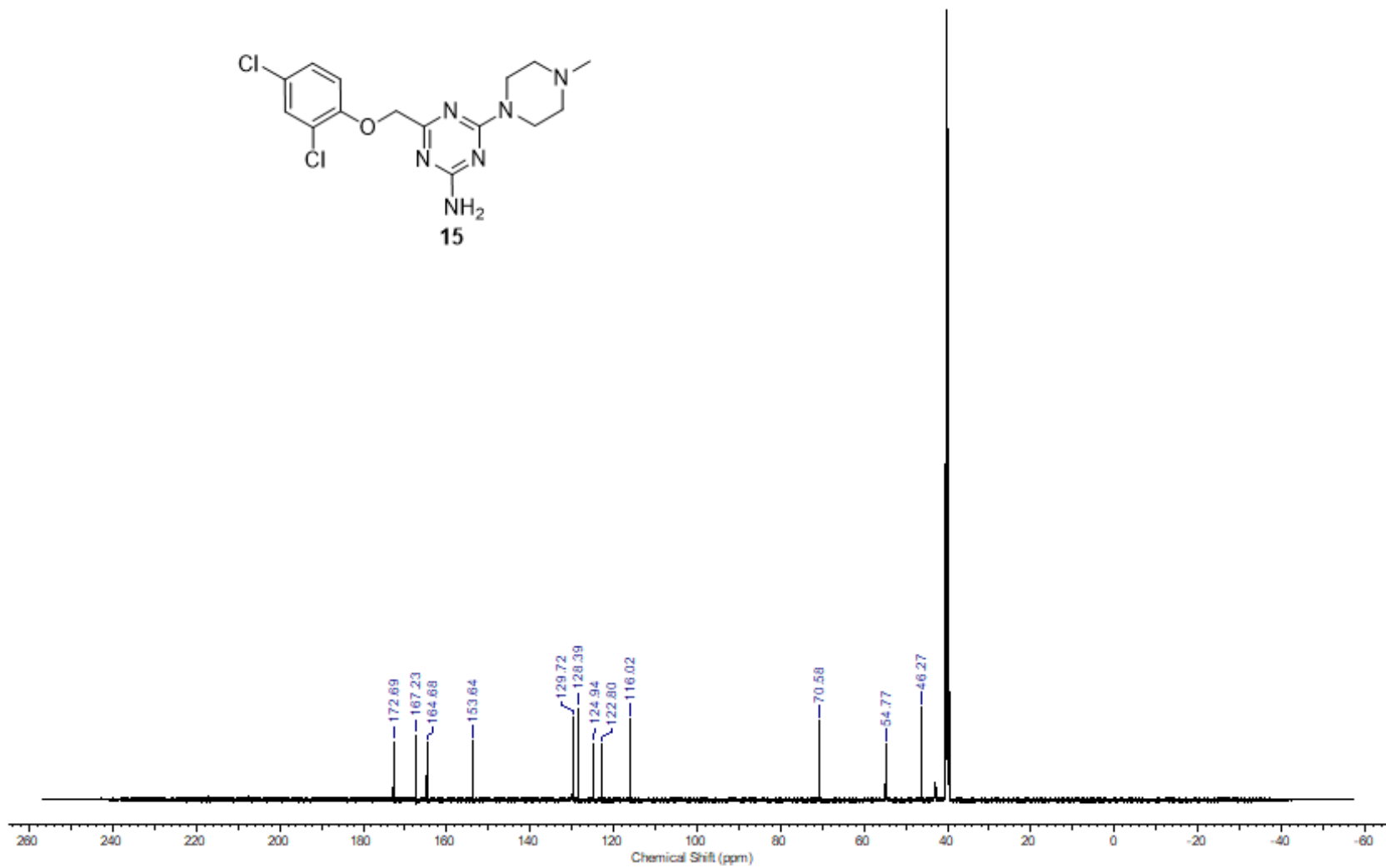
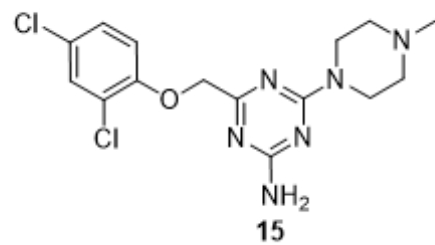


4-((2,4-Dichlorophenoxy)methyl)-6-(4-methylpiperazin-1-yl)-1,3,5-triazin-2-amine (**15**)

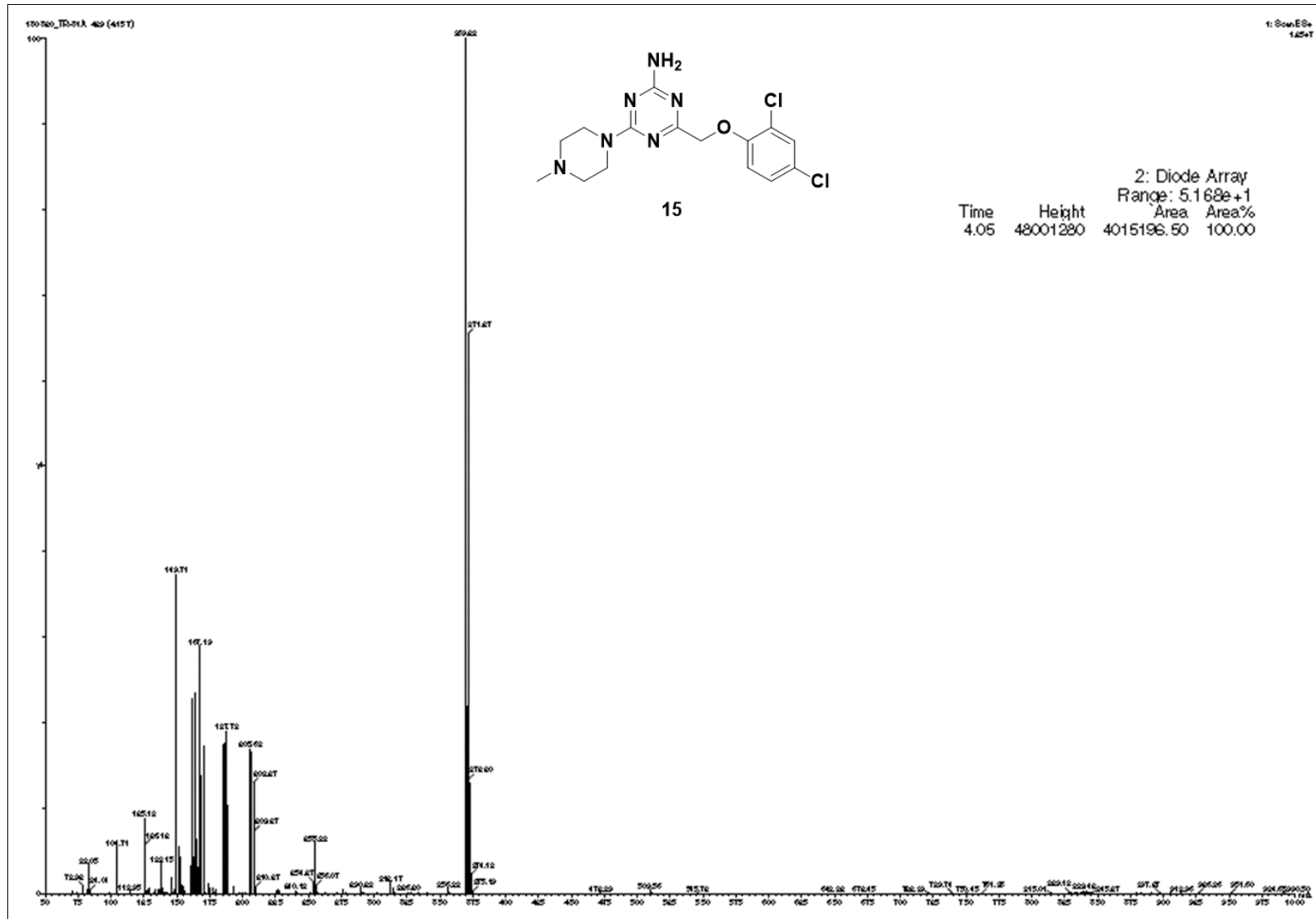
Compound **15** - ^1H NMR, 300 MHz, DMSO



Compound **15** – ^{13}C NMR, 125 MHz, DMSO

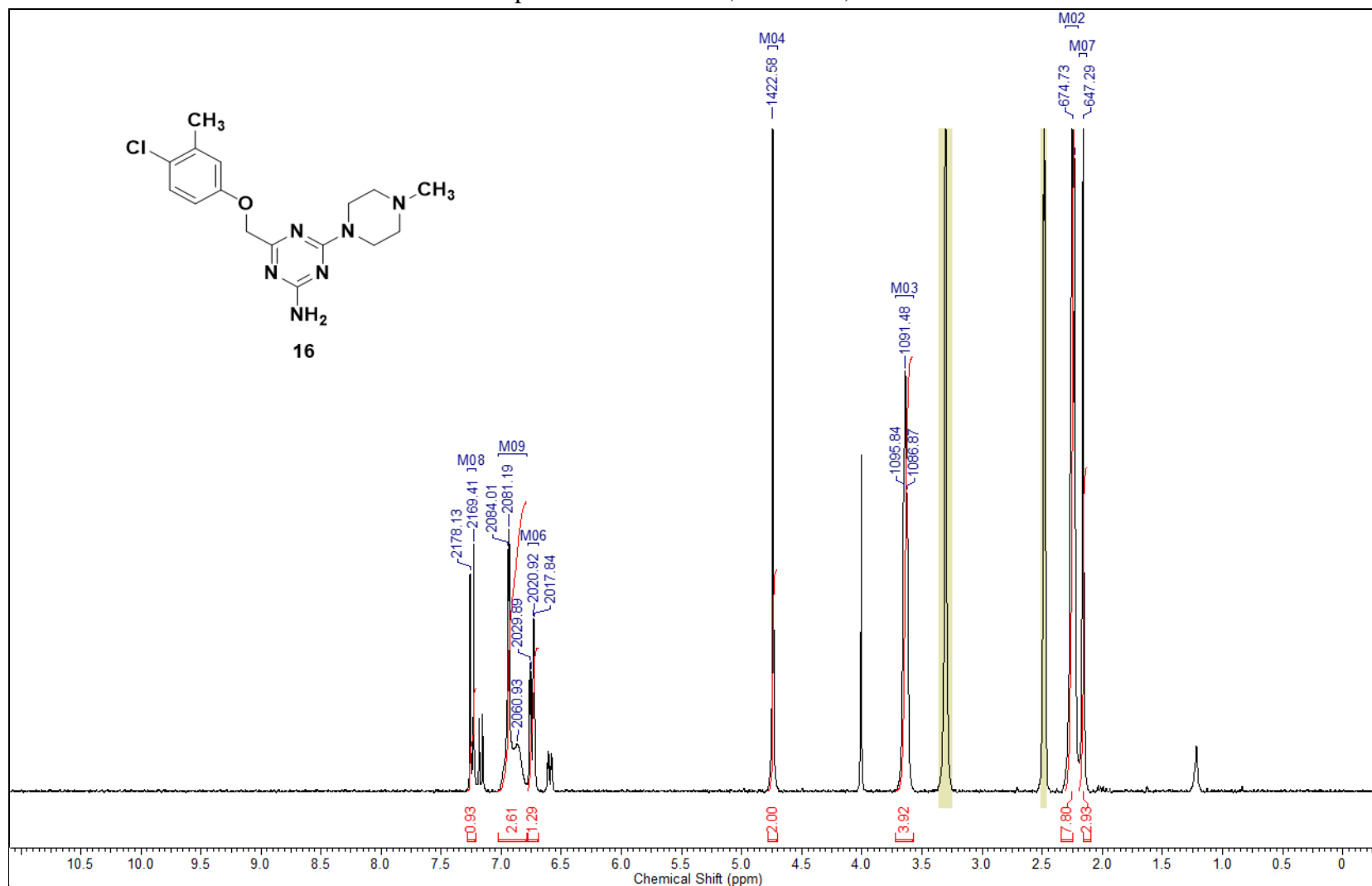


Compound 15 - LC/MS⁺

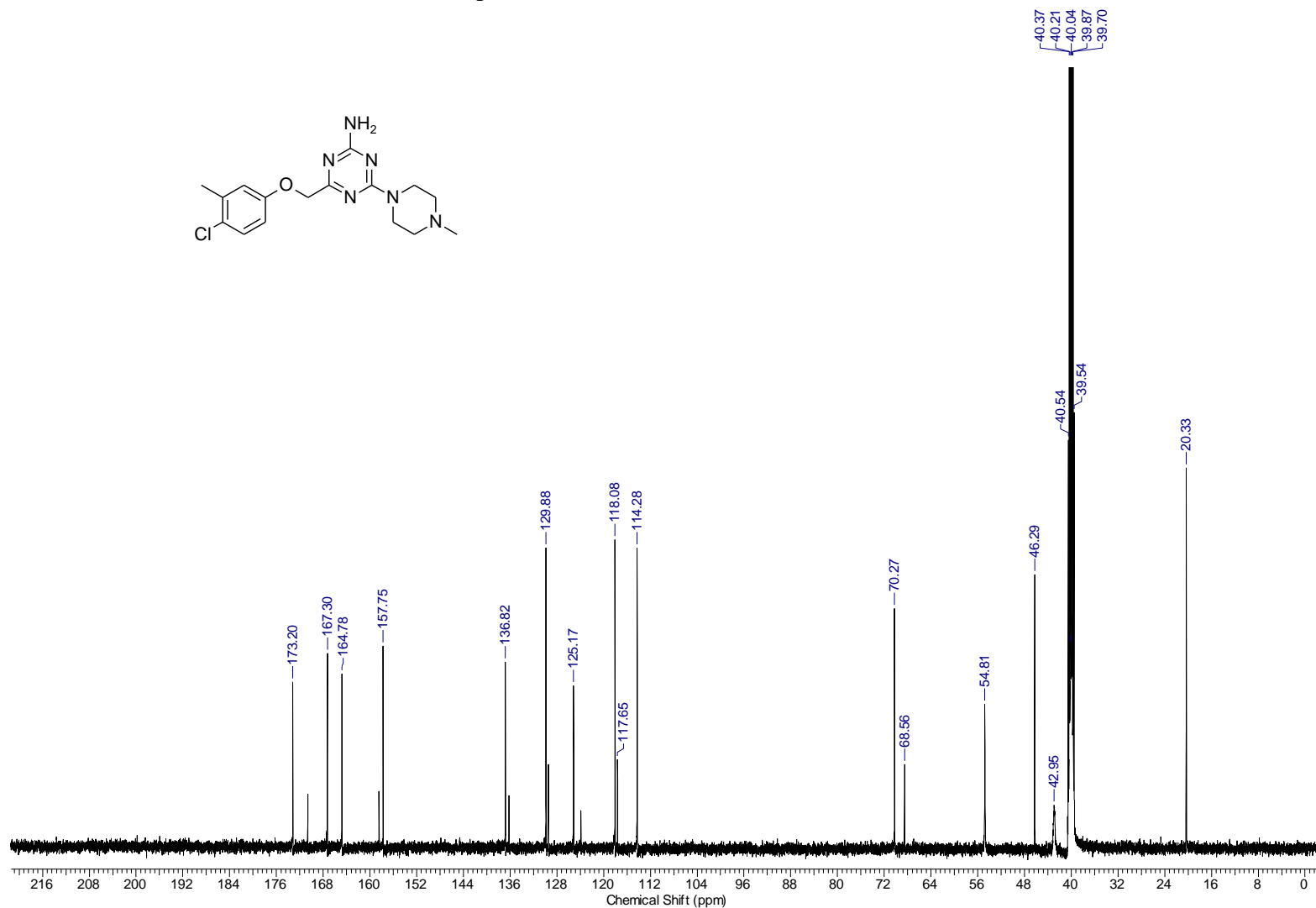
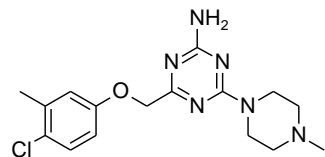


4-((4-Chloro-3-methylphenoxy)methyl)-6-(4-methylpiperazin-1-yl)-1,3,5-triazin-2-amine (**16**)

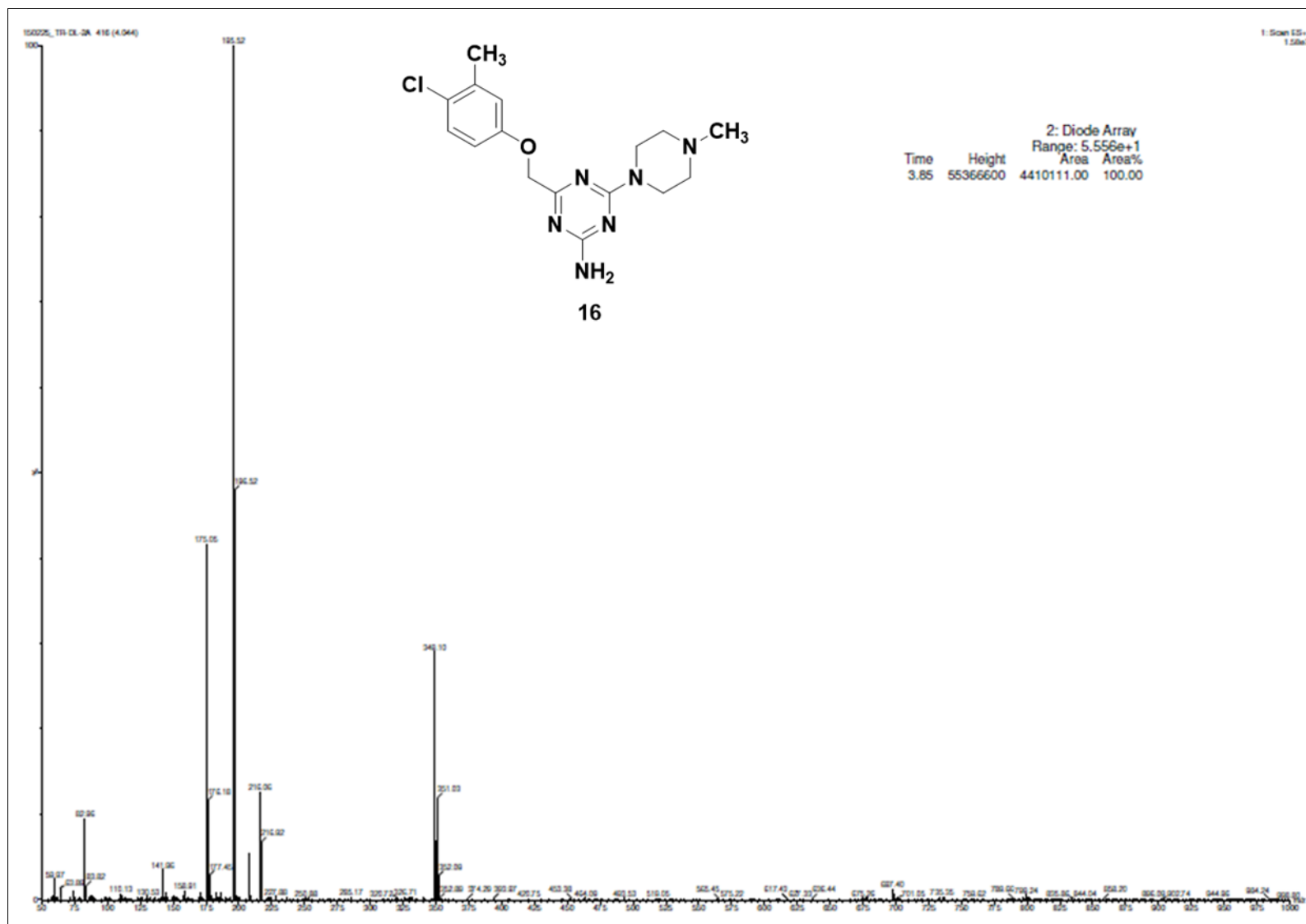
Compound **16** - ^1H NMR, 300 MHz, DMSO



Compound **16** – ^{13}C NMR, 125 MHz, DMSO

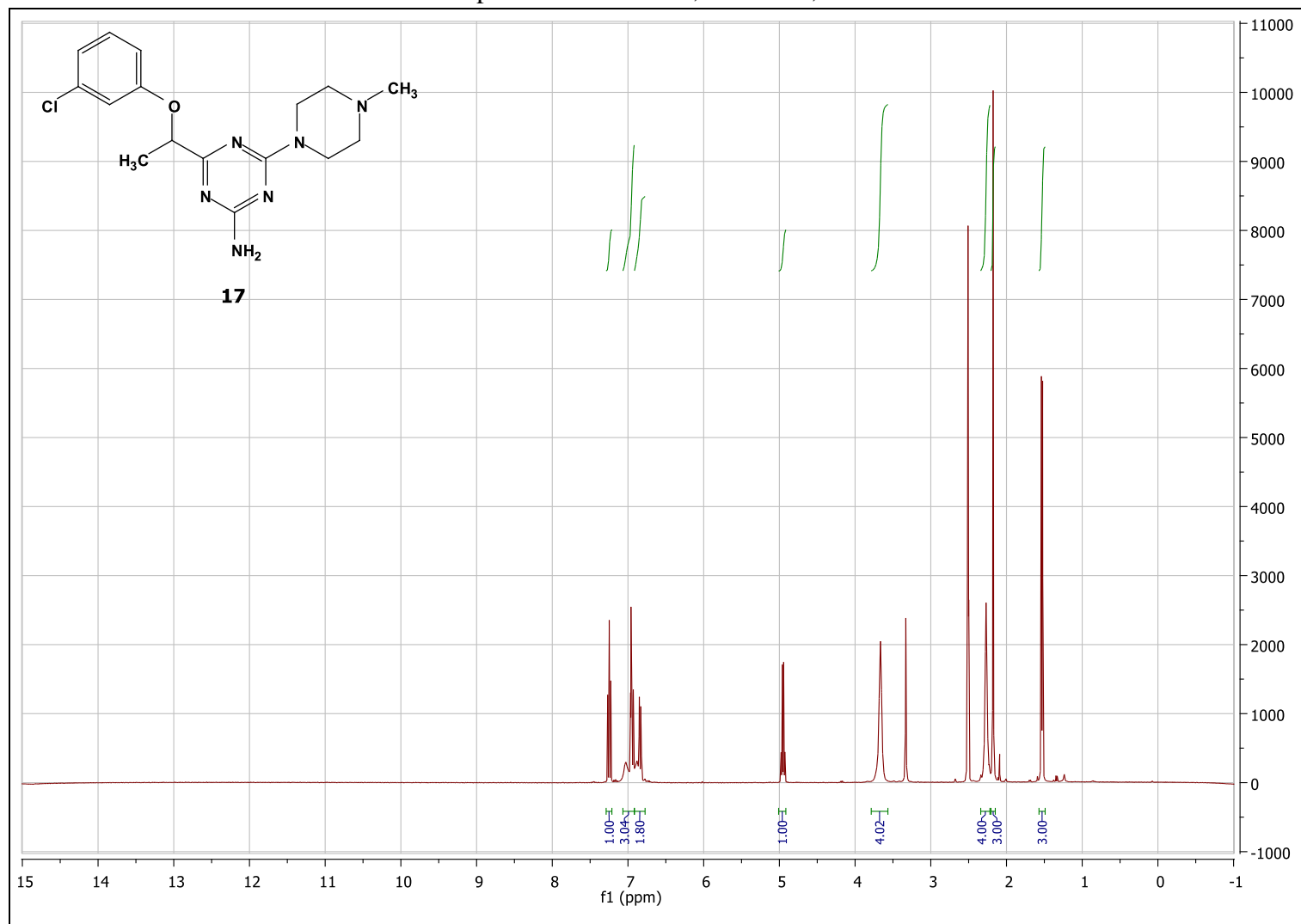


Compound 16 - LC/MS⁺

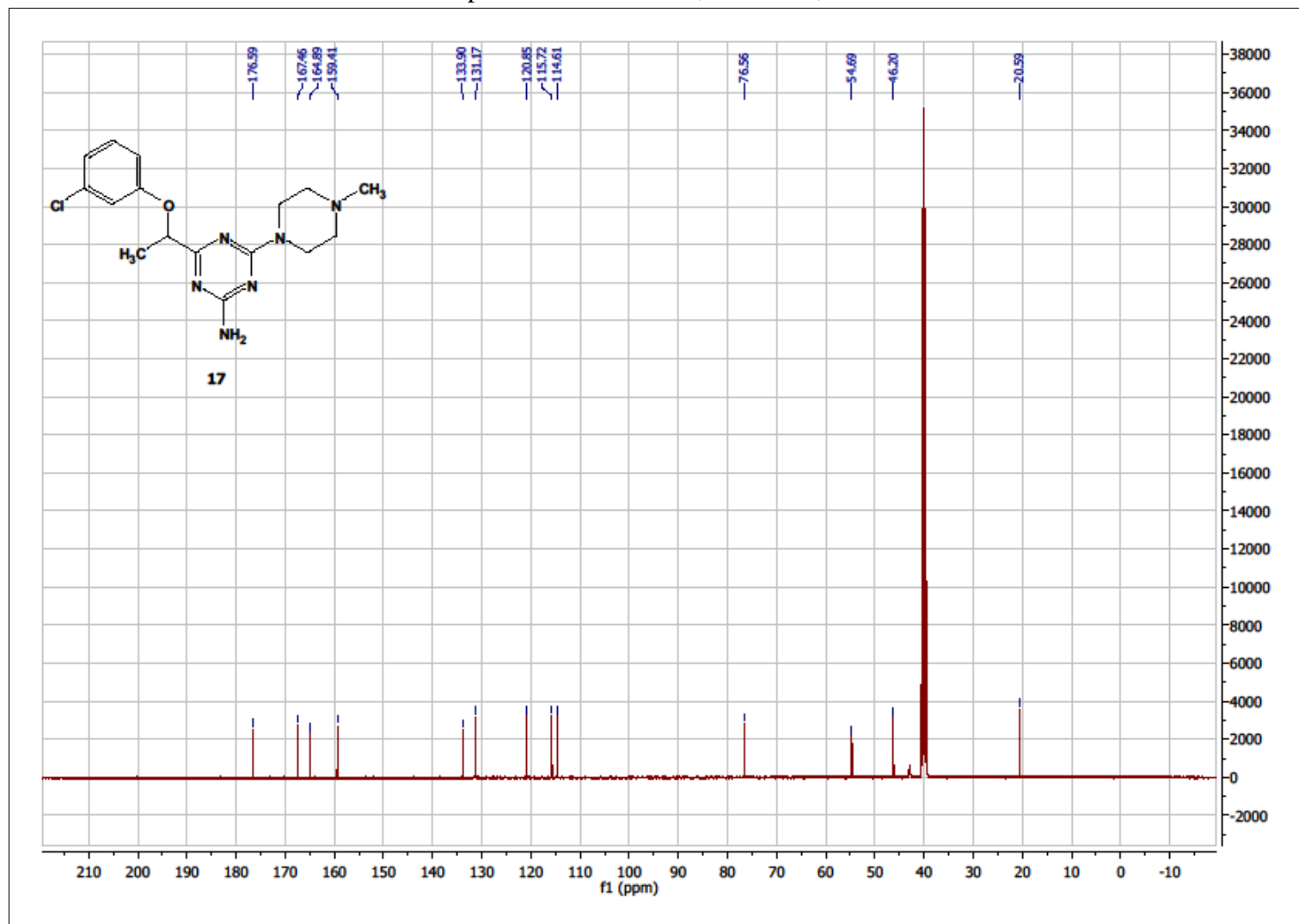


4-(1-(3-Chlorophenoxy)ethyl)-6-(4-methylpiperazin-1-yl)-1,3,5-triazin-2-amine (**17**)

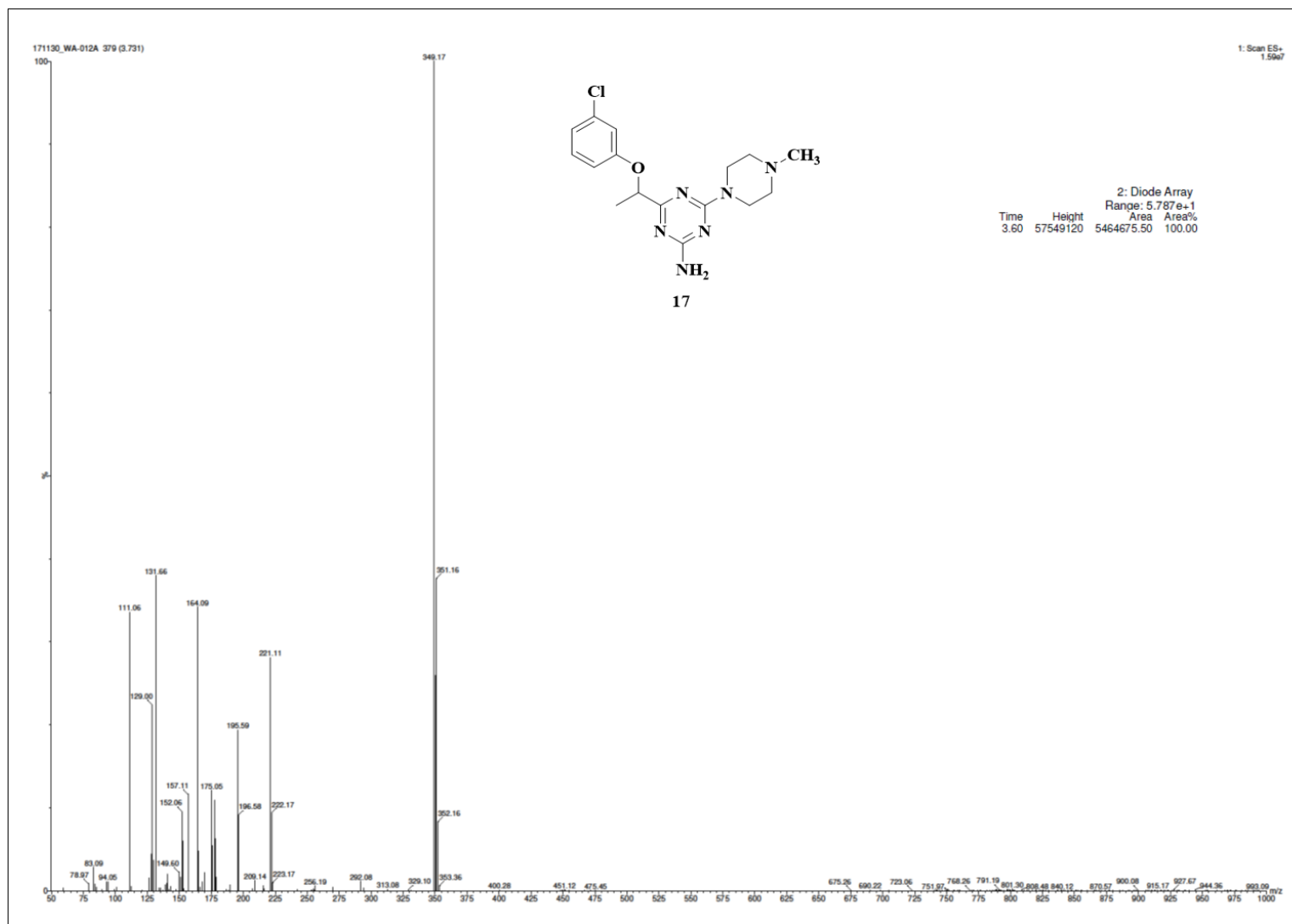
Compound **17**- ^1H NMR, 300 MHz, DMSO



Compound **17** - ^{13}C NMR, 300 MHz, DMSO

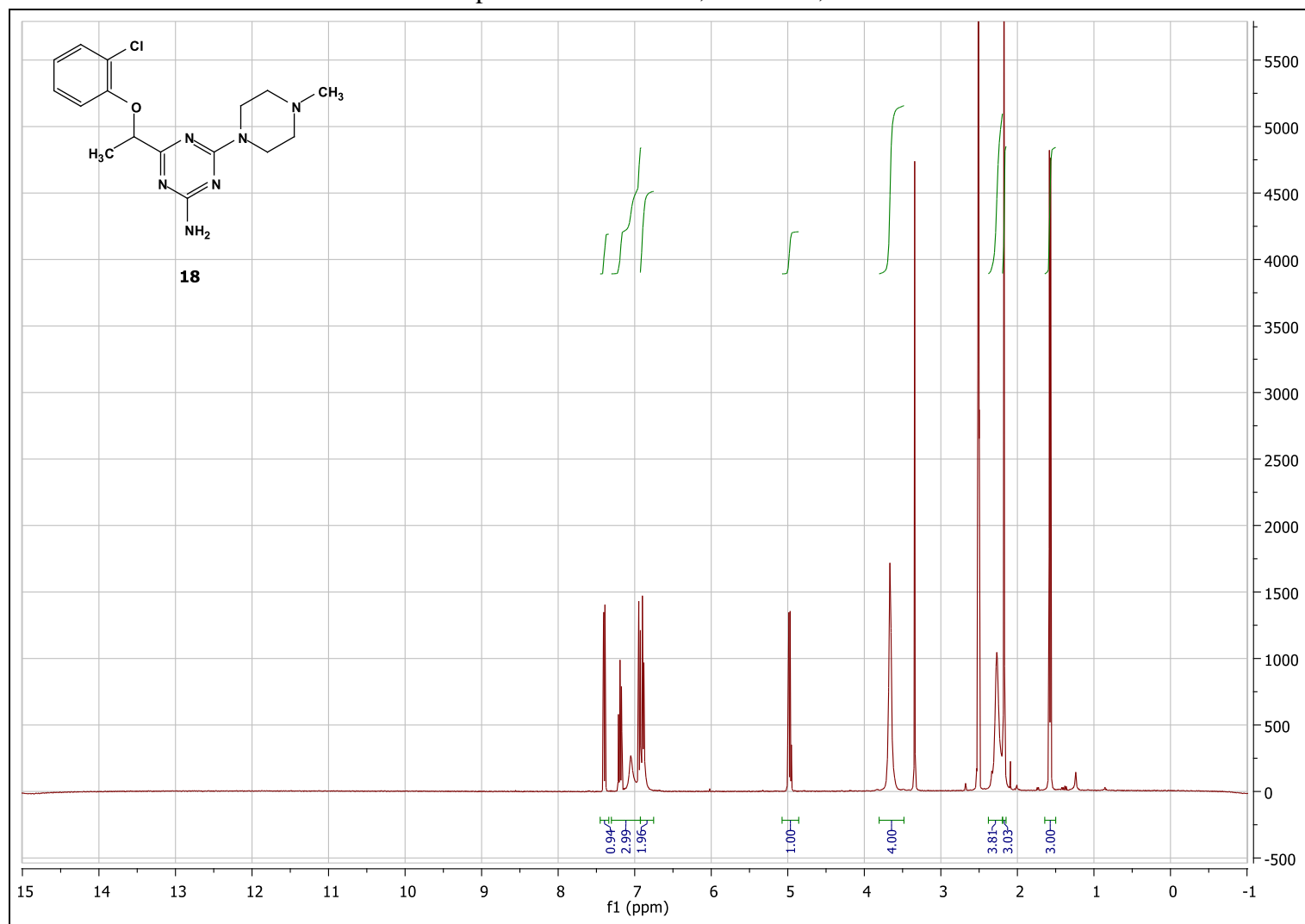


Compound 17 - LC/MS⁺

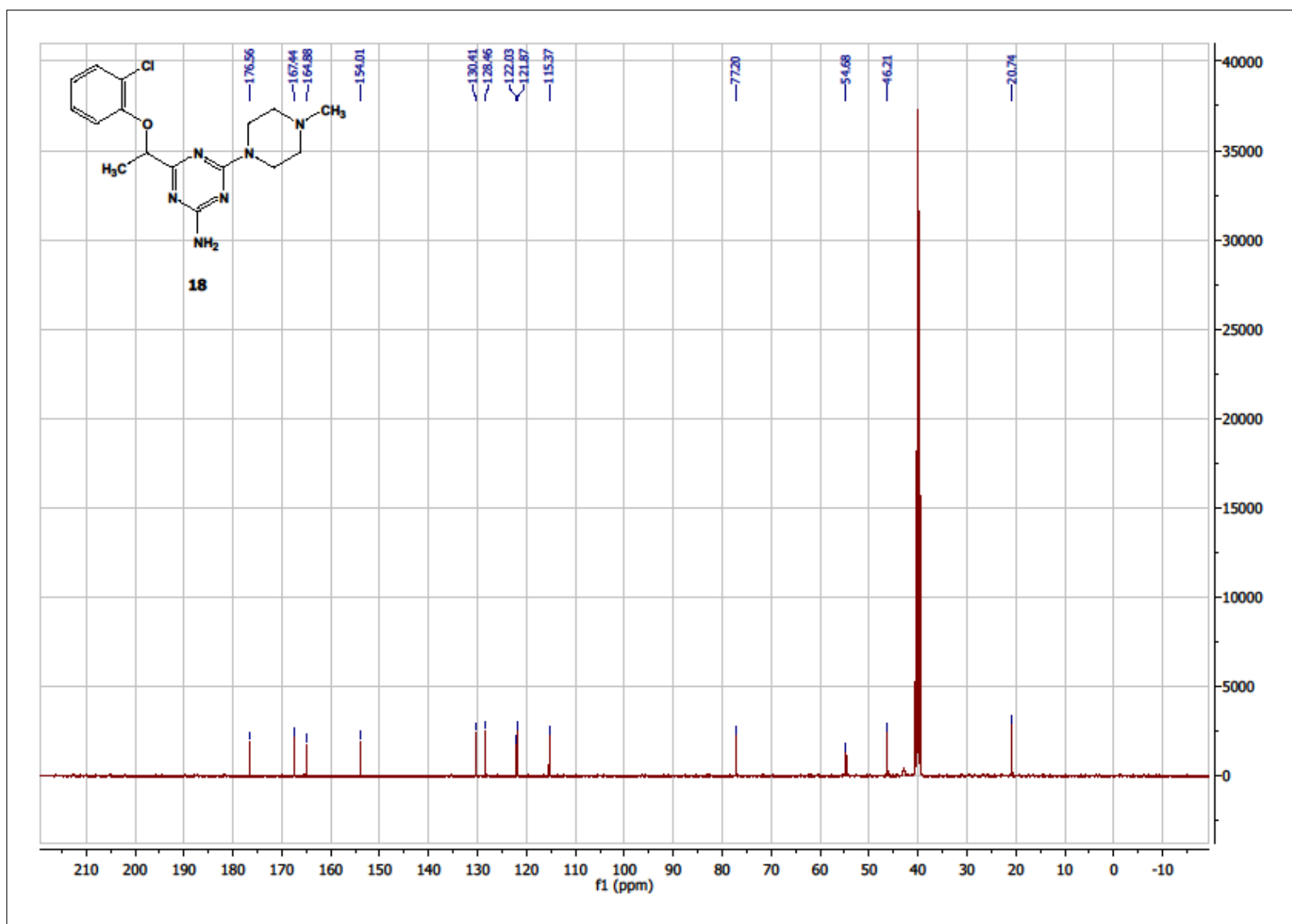


4-(1-(2-Chlorophenoxy)ethyl)-6-(4-methylpiperazin-1-yl)-1,3,5-triazin-2-amine (**18**)

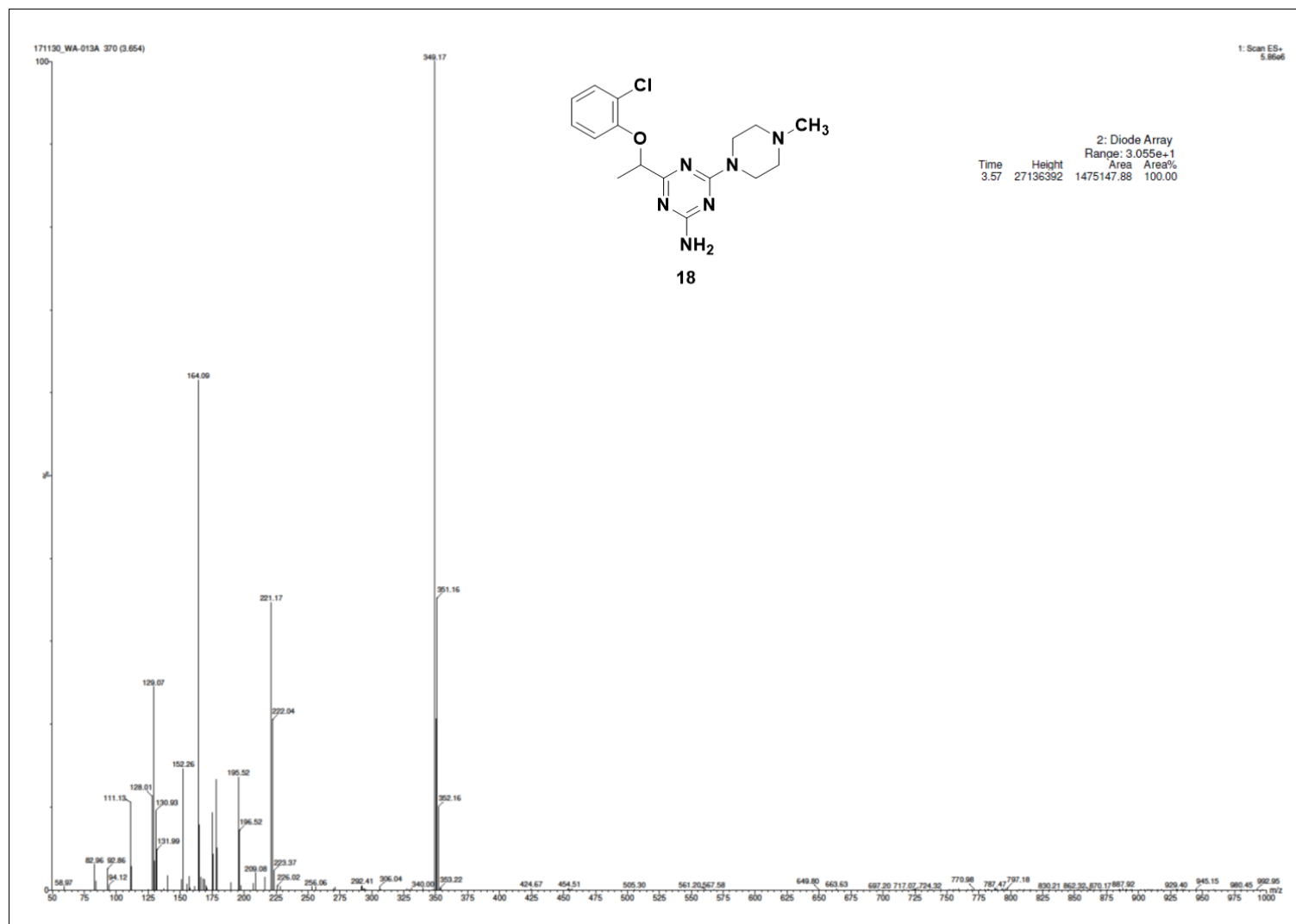
Compound **18** - ^1H NMR, 300 MHz, DMSO



Compound **18** - ^{13}C NMR, 300 MHz, DMSO

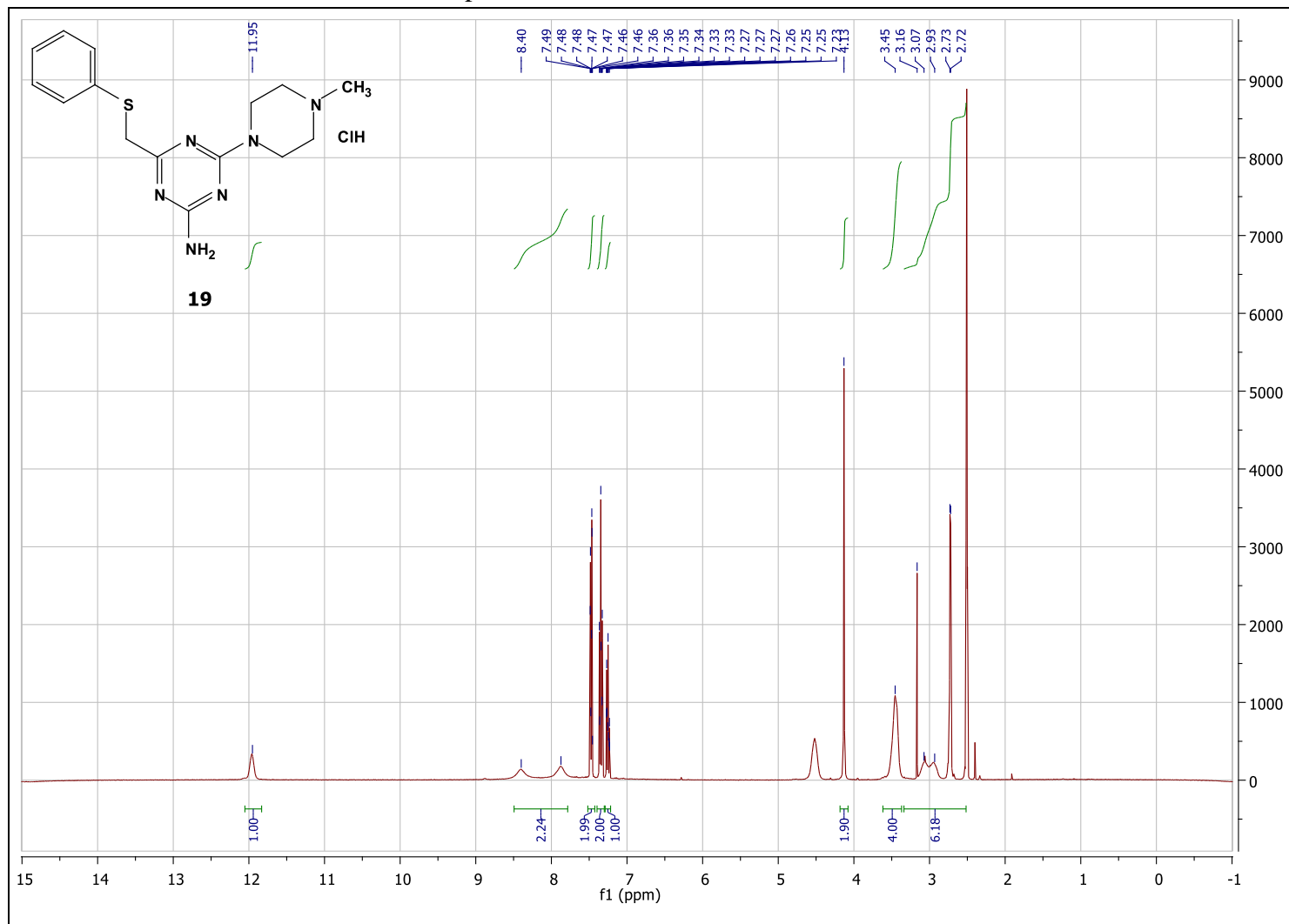


Compound 18 - LC/MS⁺

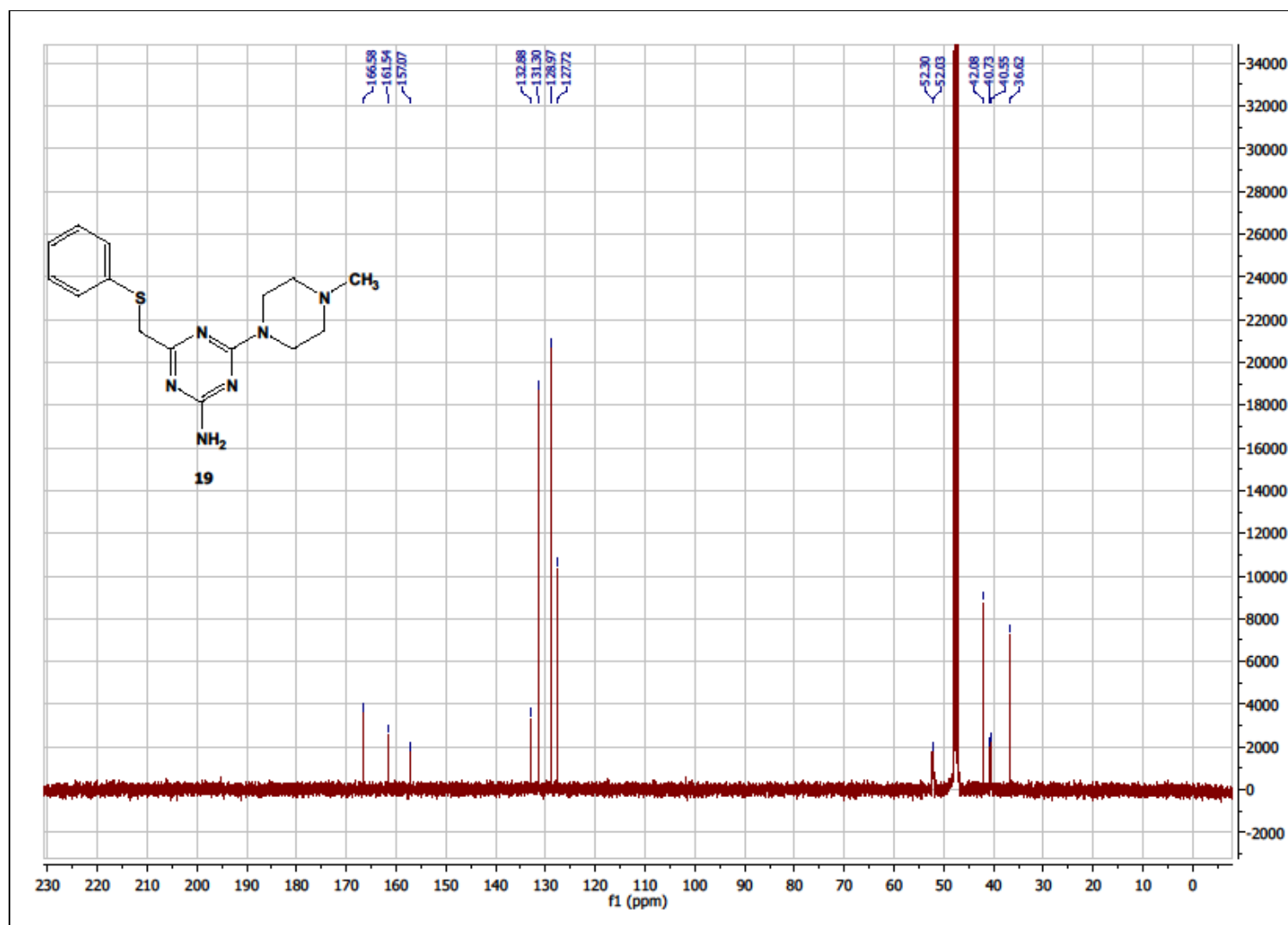


4-(4-Methylpiperazin-1-yl)-6-((phenylthio)methyl)-1,3,5-triazin-2-amine hydrochloride (**19**)

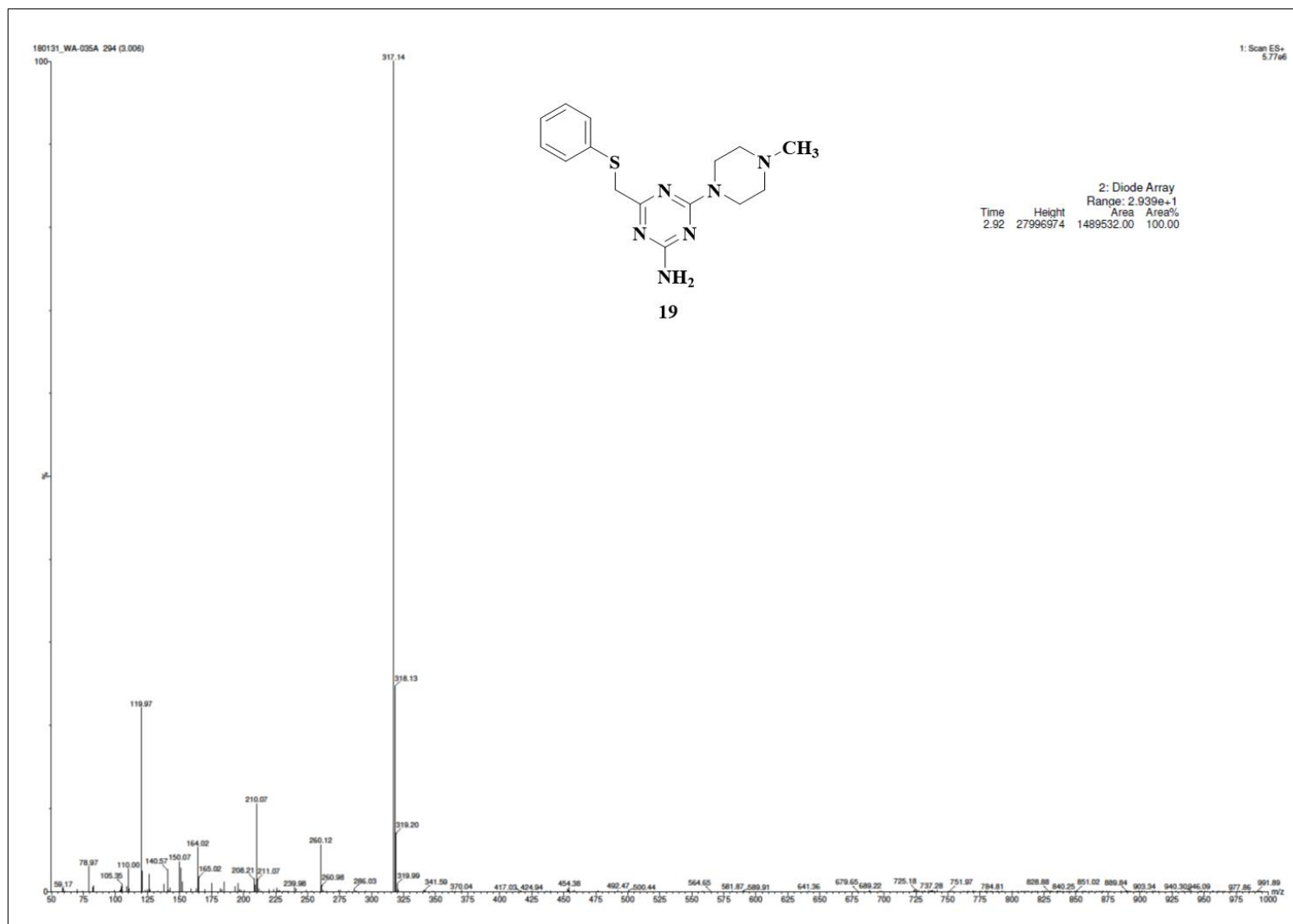
Compound **19** - ^1H NMR, 300 MHz, DMSO



Compound **19** - ^{13}C NMR, 300 MHz, MeOH

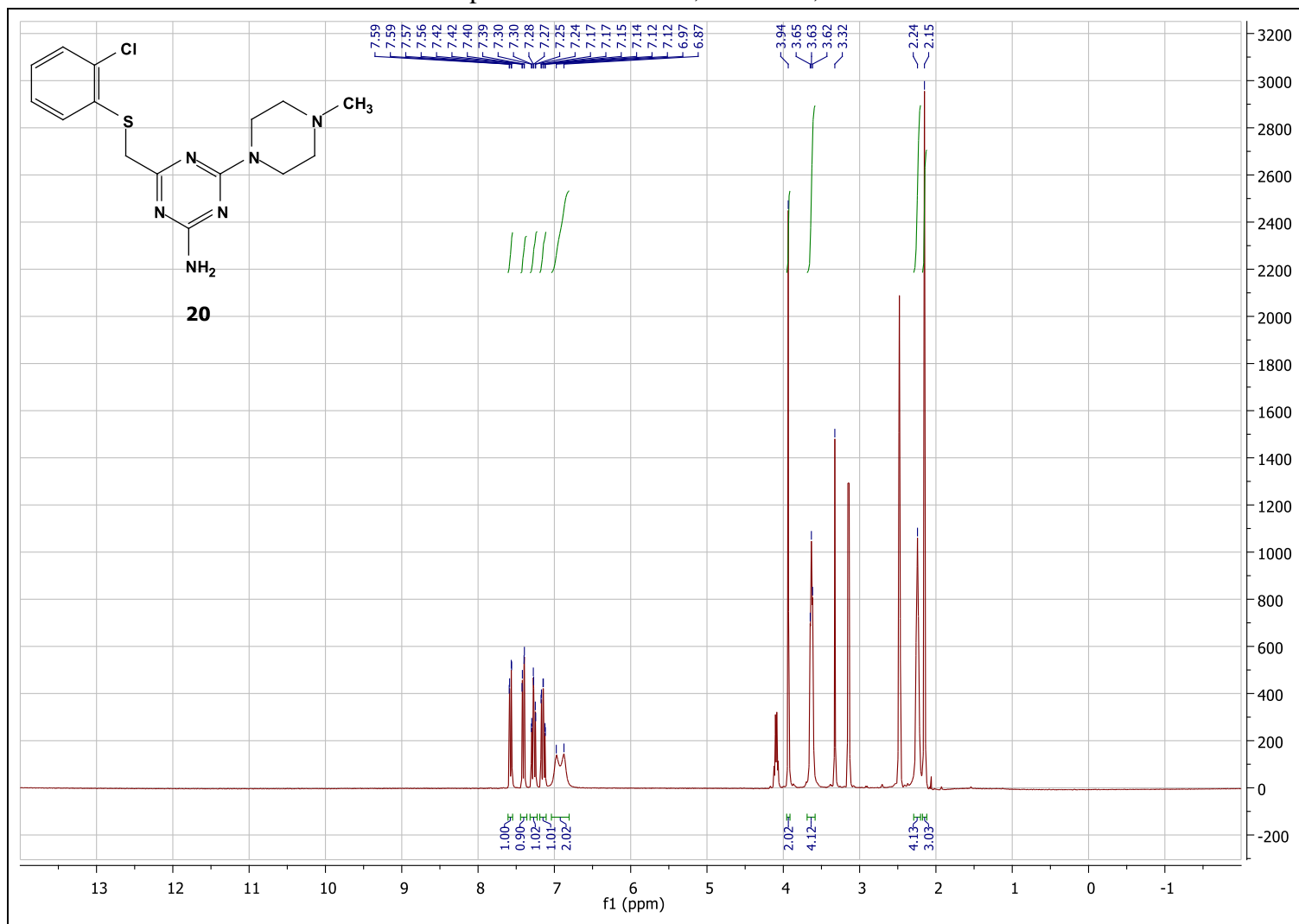


Compound 19 - LC/MS⁺

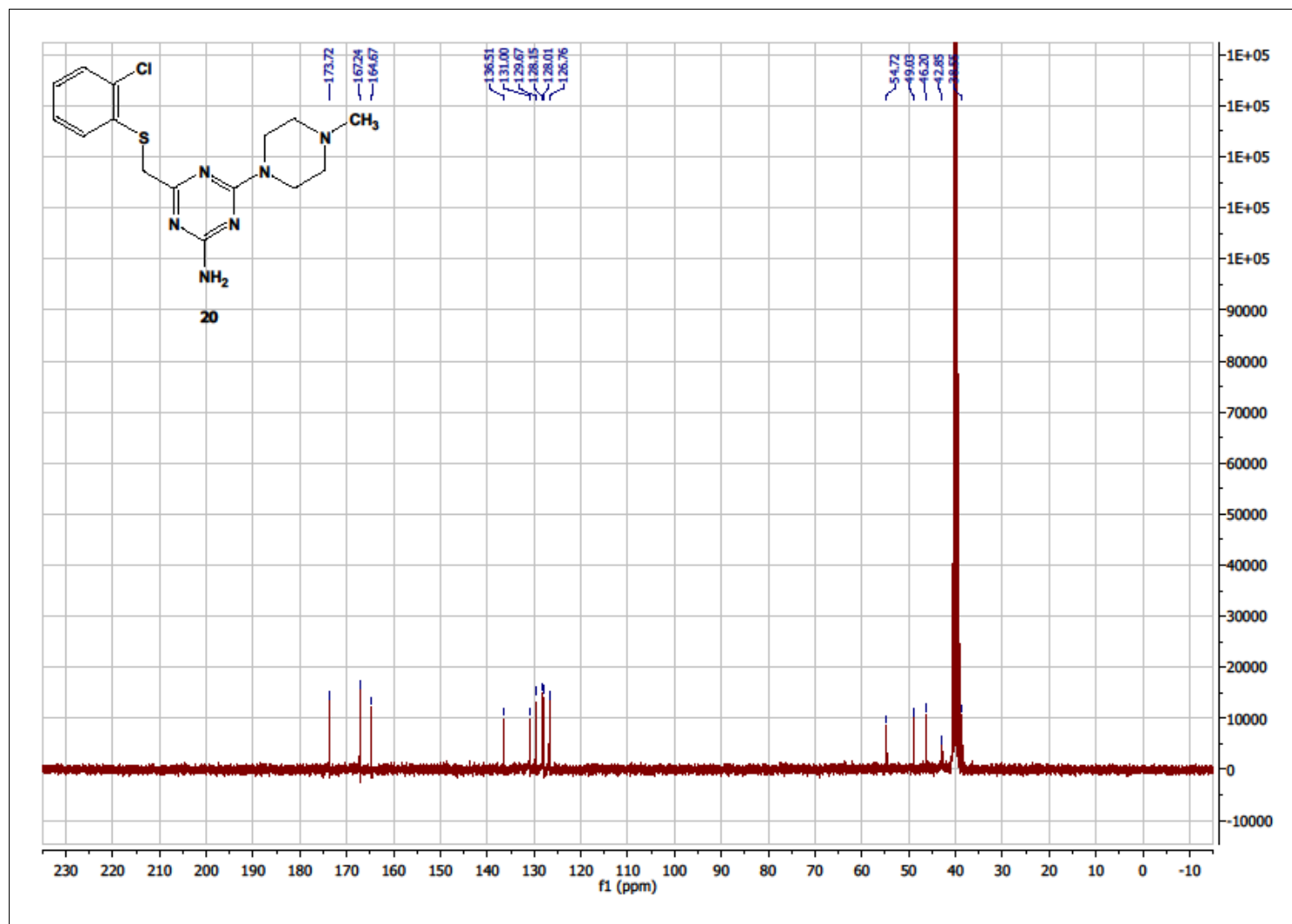


((2-Chlorophenyl)thio)methyl)-6-(4-methylpiperazin-1-yl)-1,3,5-triazin-2-amine (**20**)

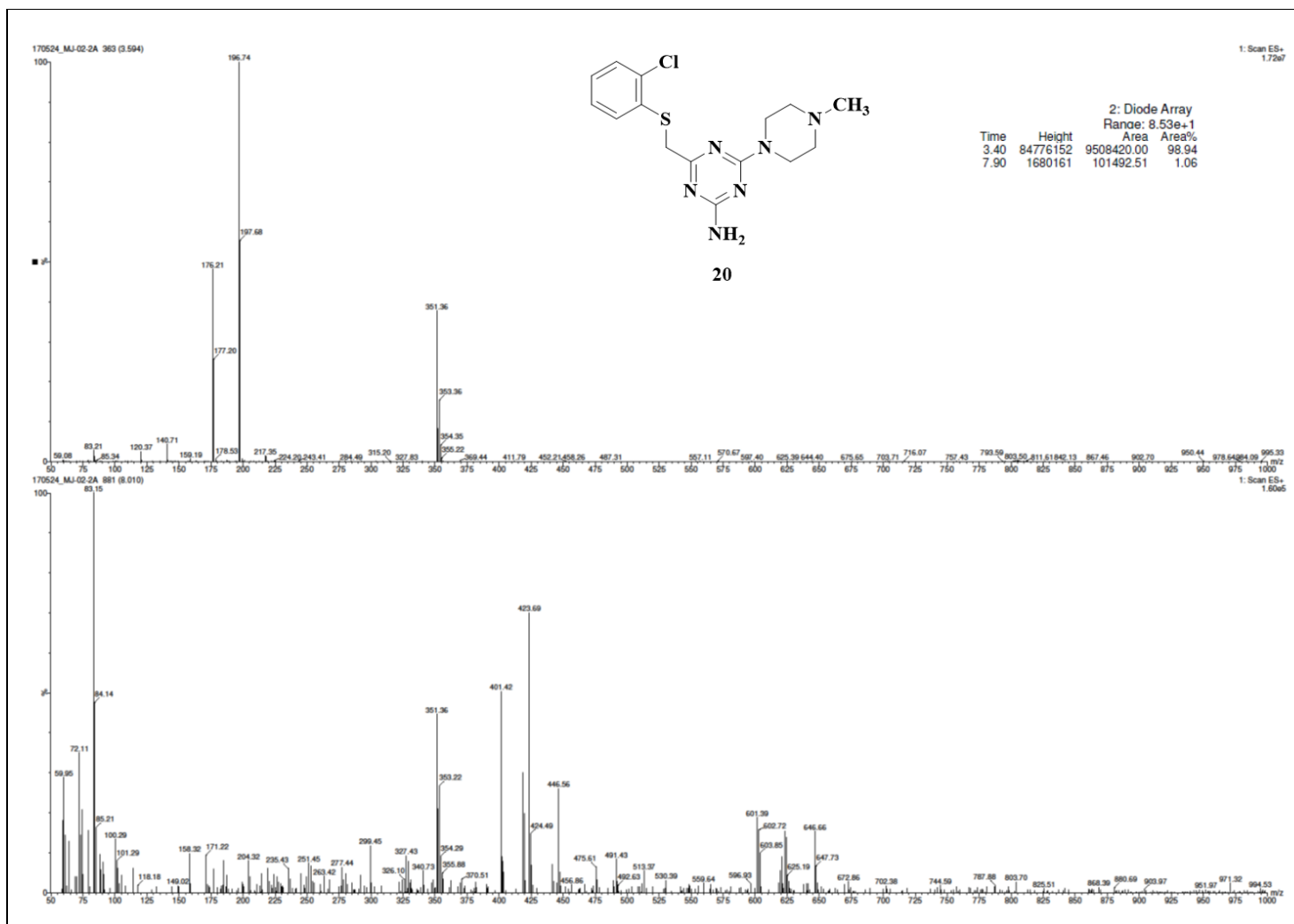
Compound **20** - ^1H NMR, 300 MHz, DMSO



Compound **20** - ^{13}C NMR, 300 MHz, DMSO

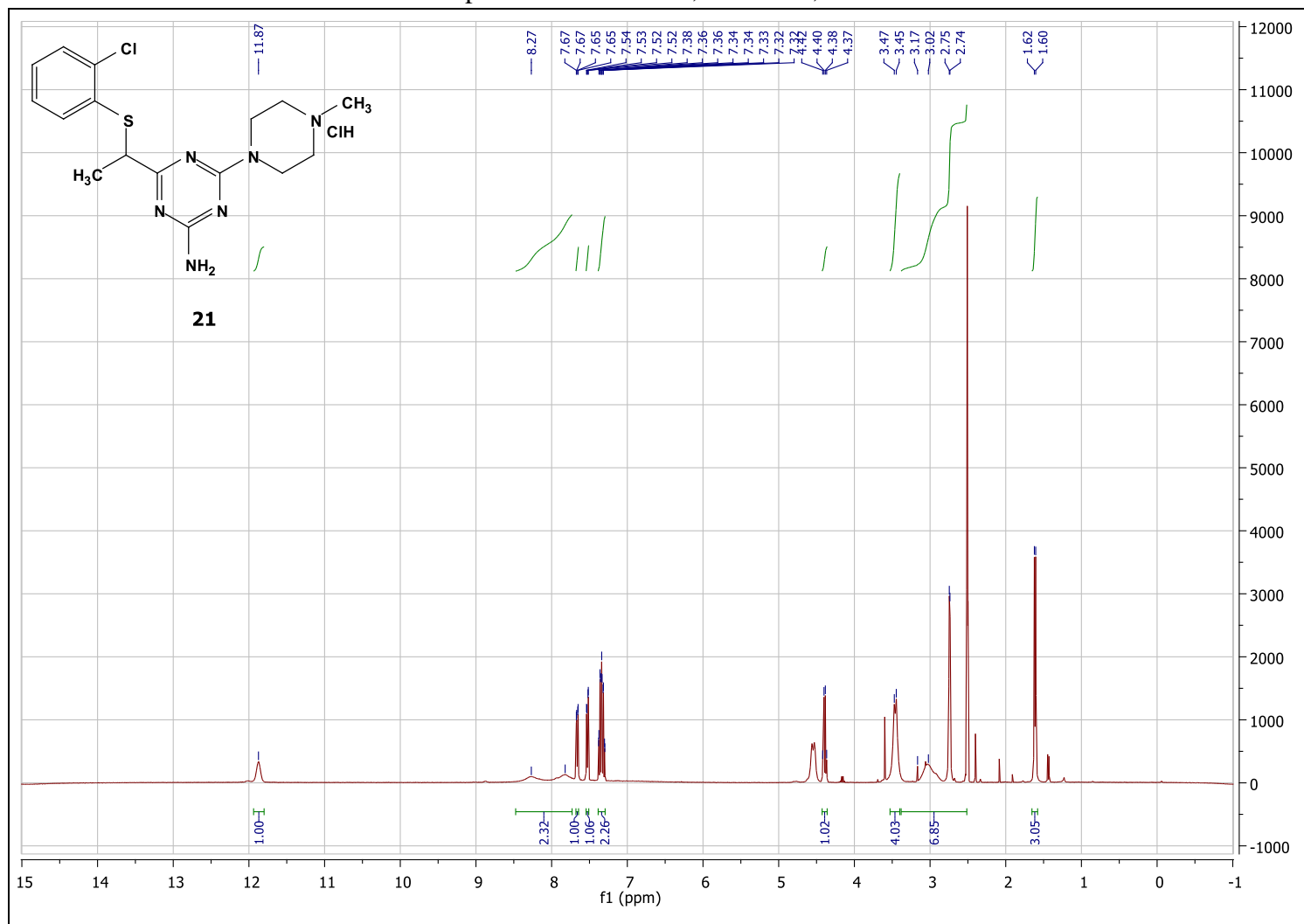


Compound 20 - LC/MS⁺

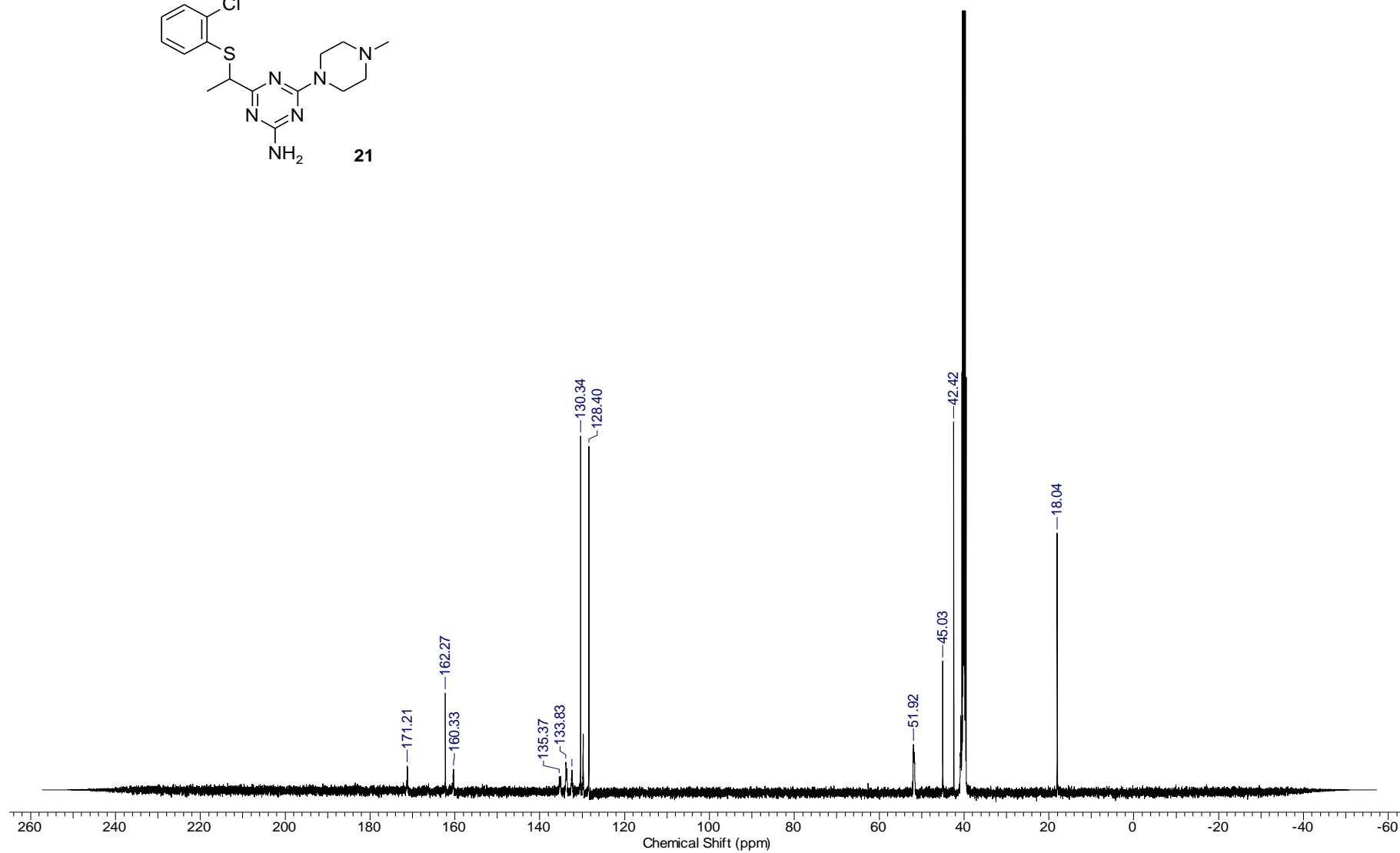
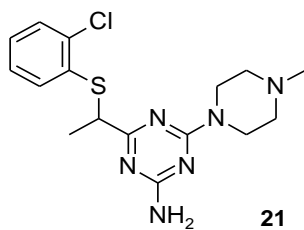


4-(1-((2-Chlorophenyl)thio)ethyl)-6-(4-methylpiperazin-1-yl)-1,3,5-triazin-2-amine hydrochloride (**21**)

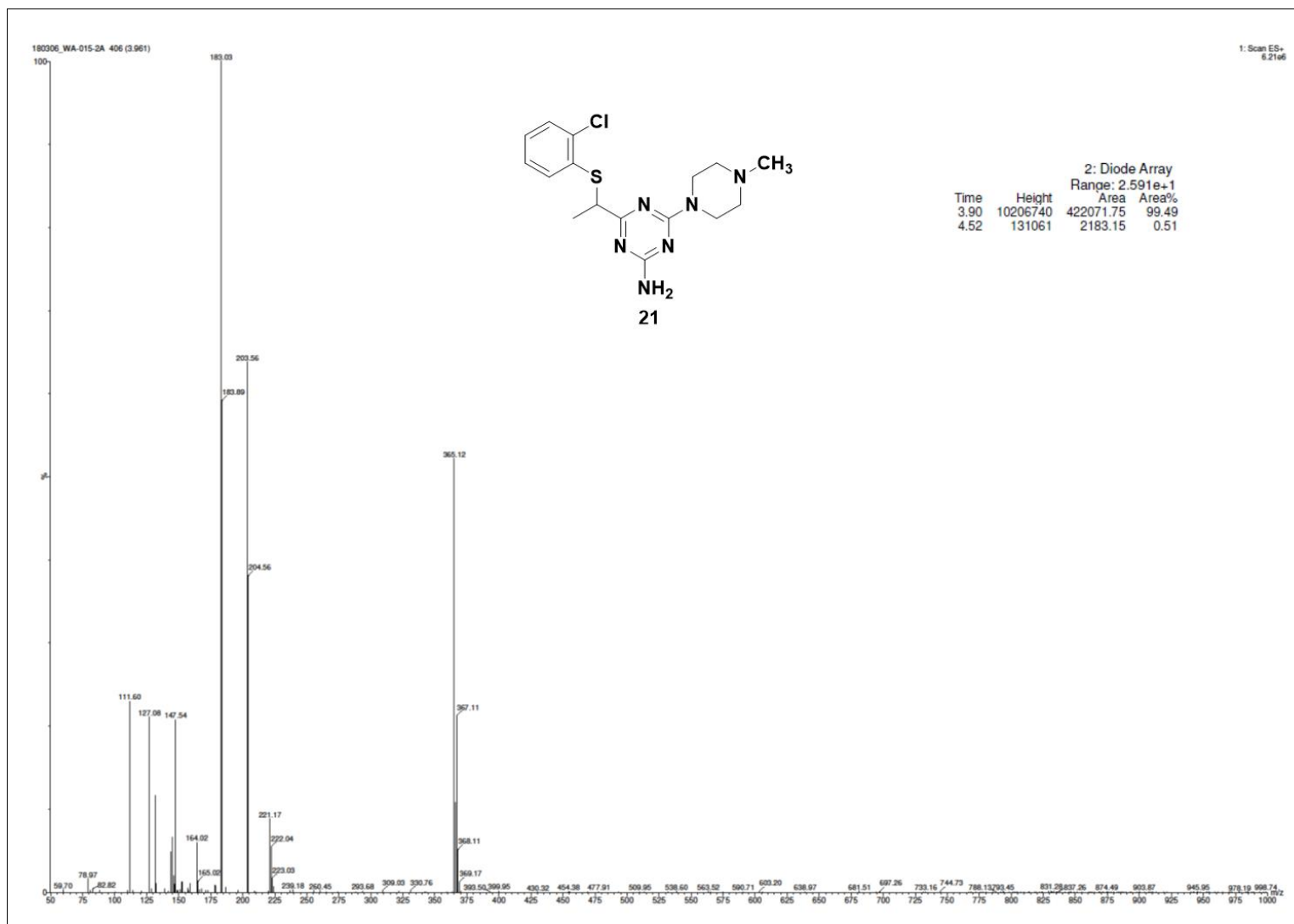
Compound **21** - ^1H NMR, 300 MHz, DMSO



Compound **21** - ^{13}C NMR, 125 MHz, DMSO

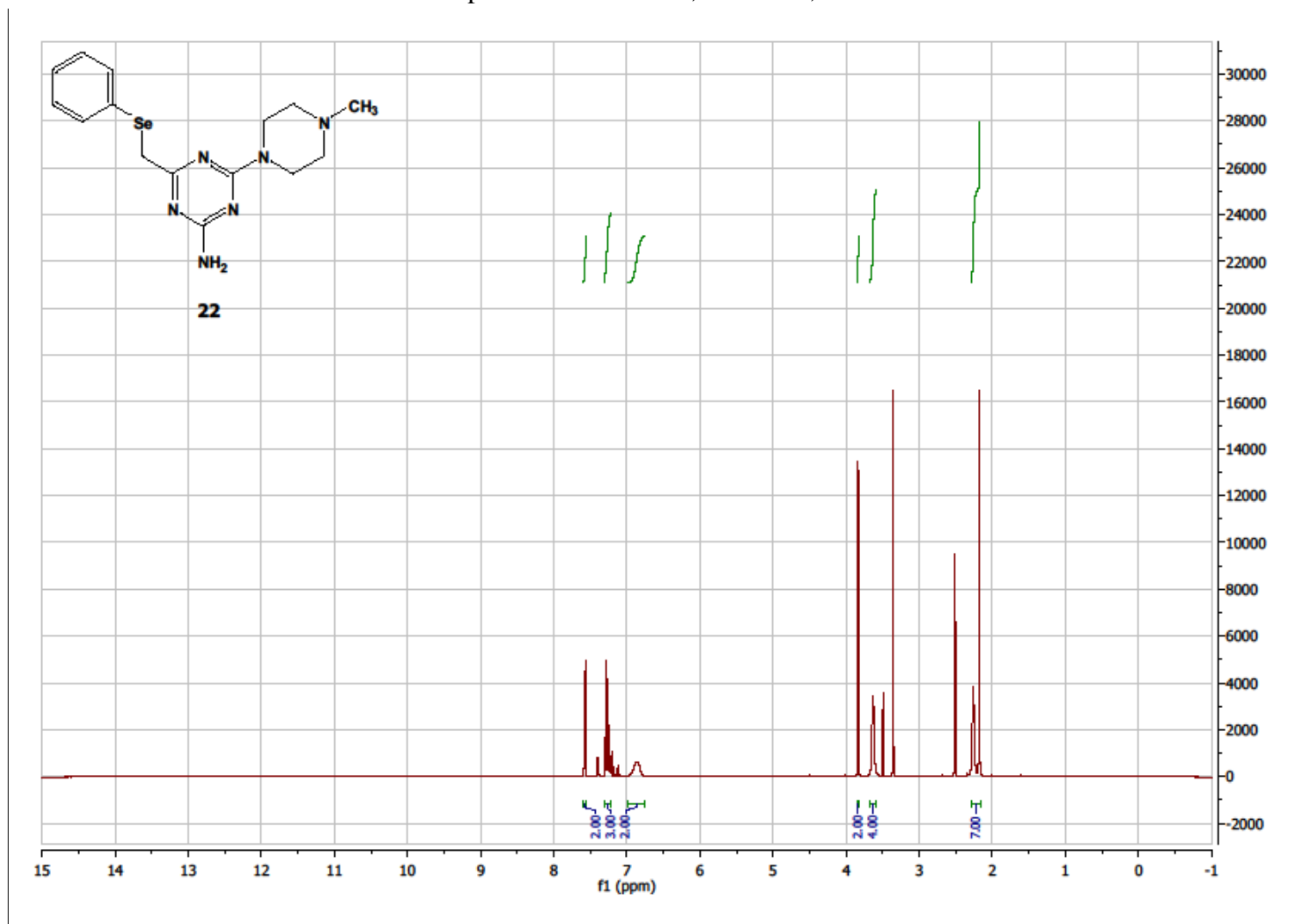


Compound **21** - LC/MS⁺

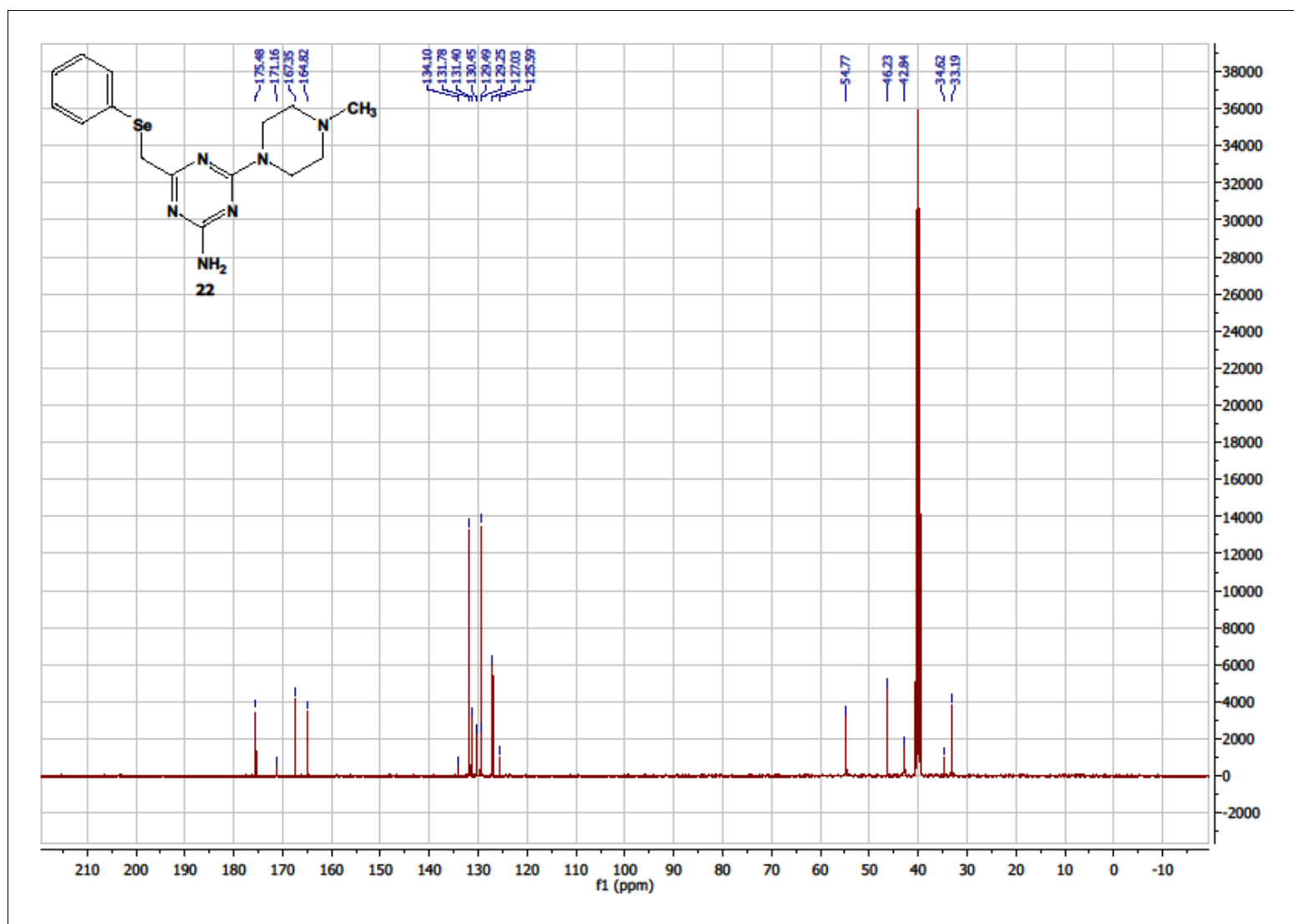


4-(4-Methylpiperazin-1-yl)-6-((phenylselanyl)methyl)-1,3,5-triazin-2-amine hydrochloride (**22**)

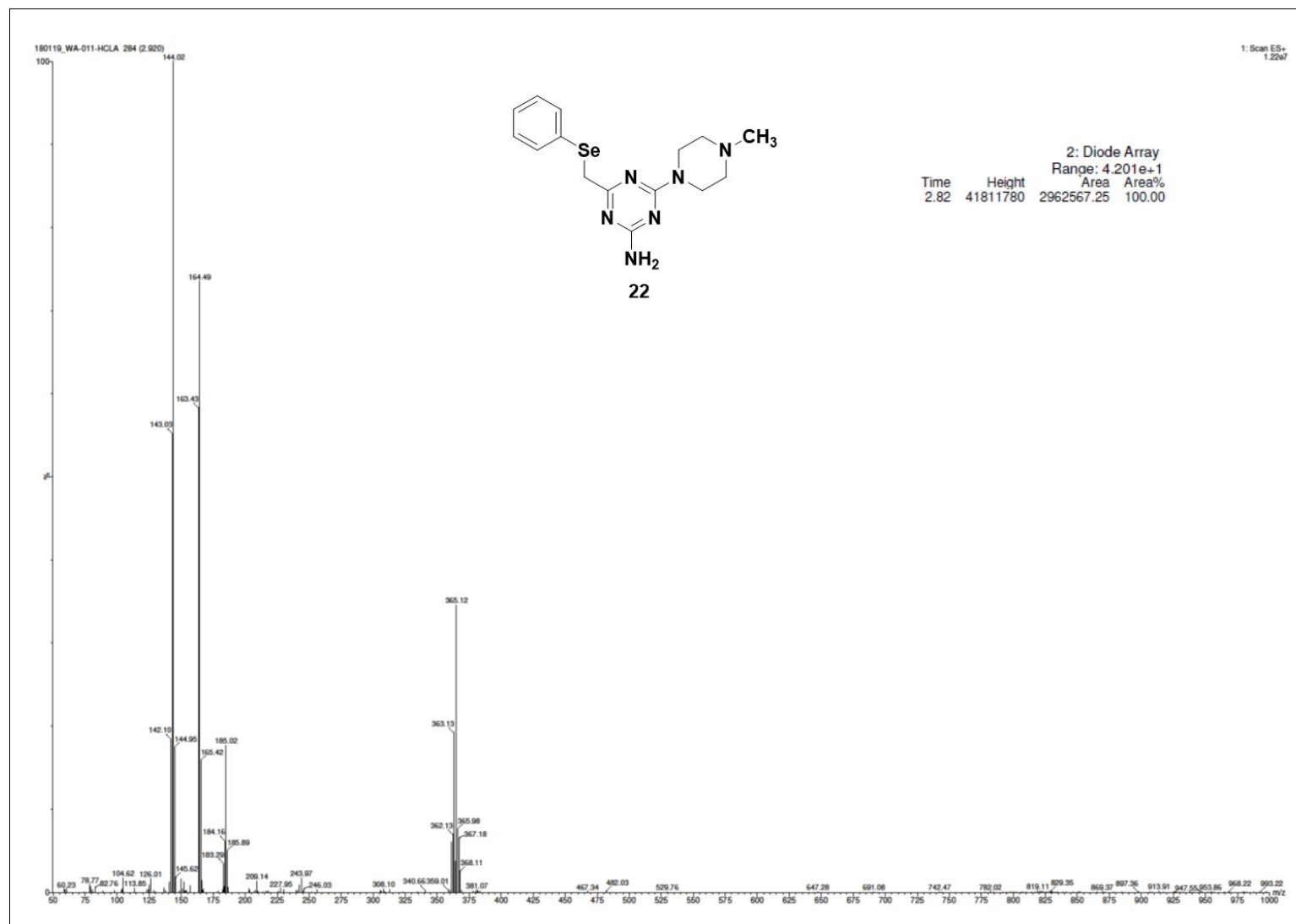
Compound **22** - ^1H NMR, 300 MHz, DMSO



Compound **22** - ^{13}C NMR, 300 MHz, DMSO

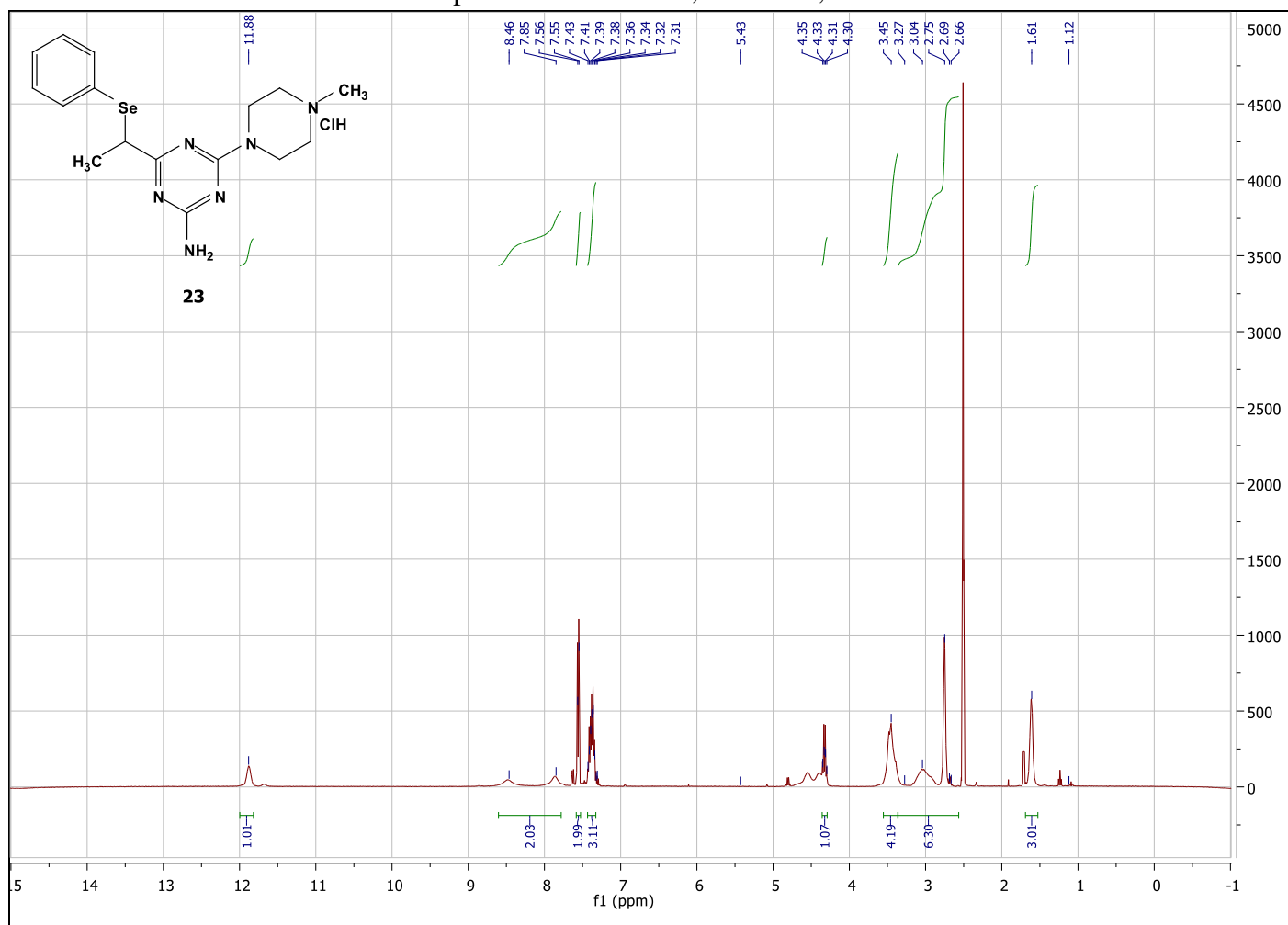


Compound 22 - LC/MS⁺

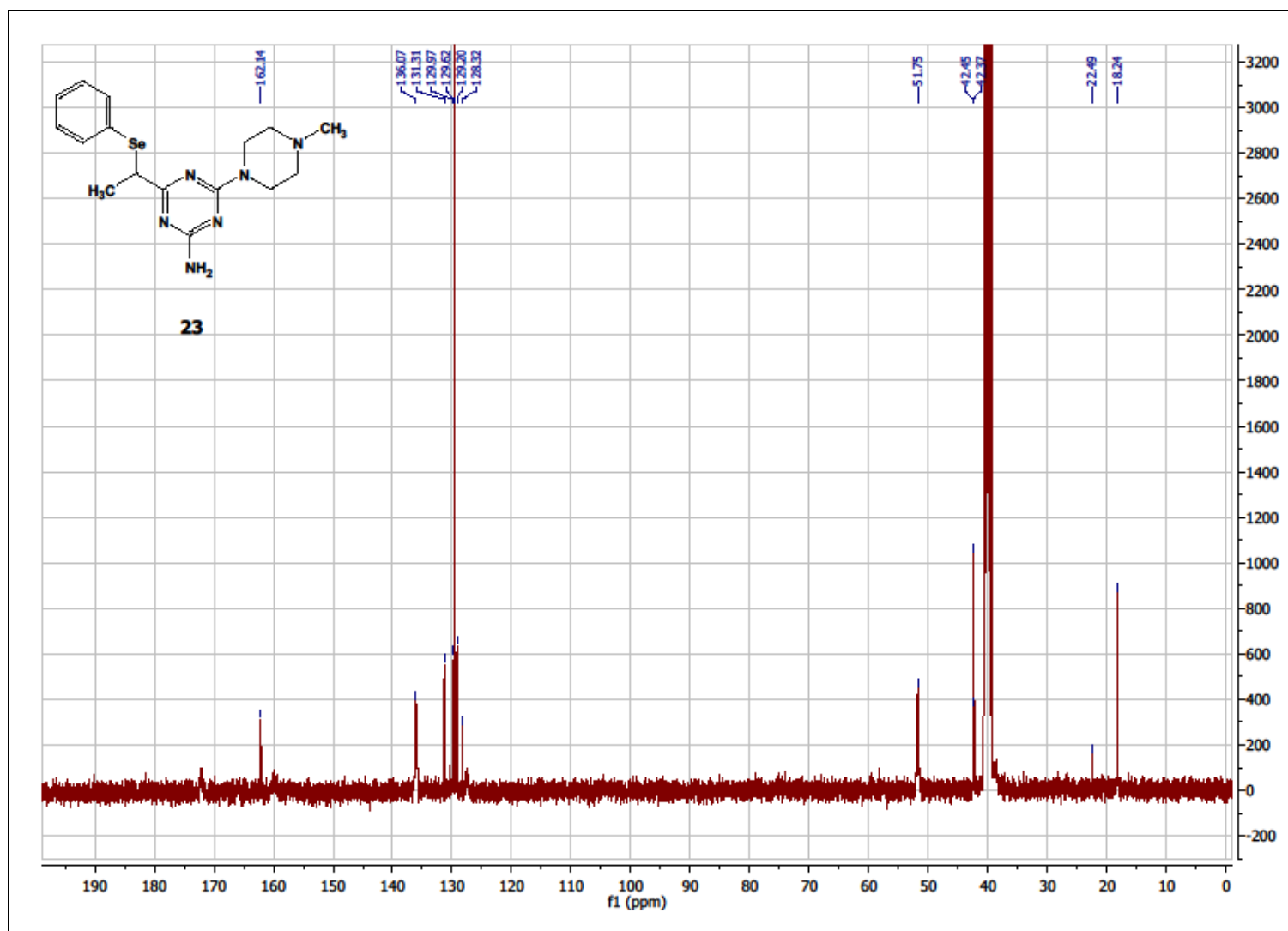


4-(4-Methylpiperazin-1-yl)-6-(1-(phenylselenyl)ethyl)-1,3,5-triazin-2-amine hydrochloride (**23**)

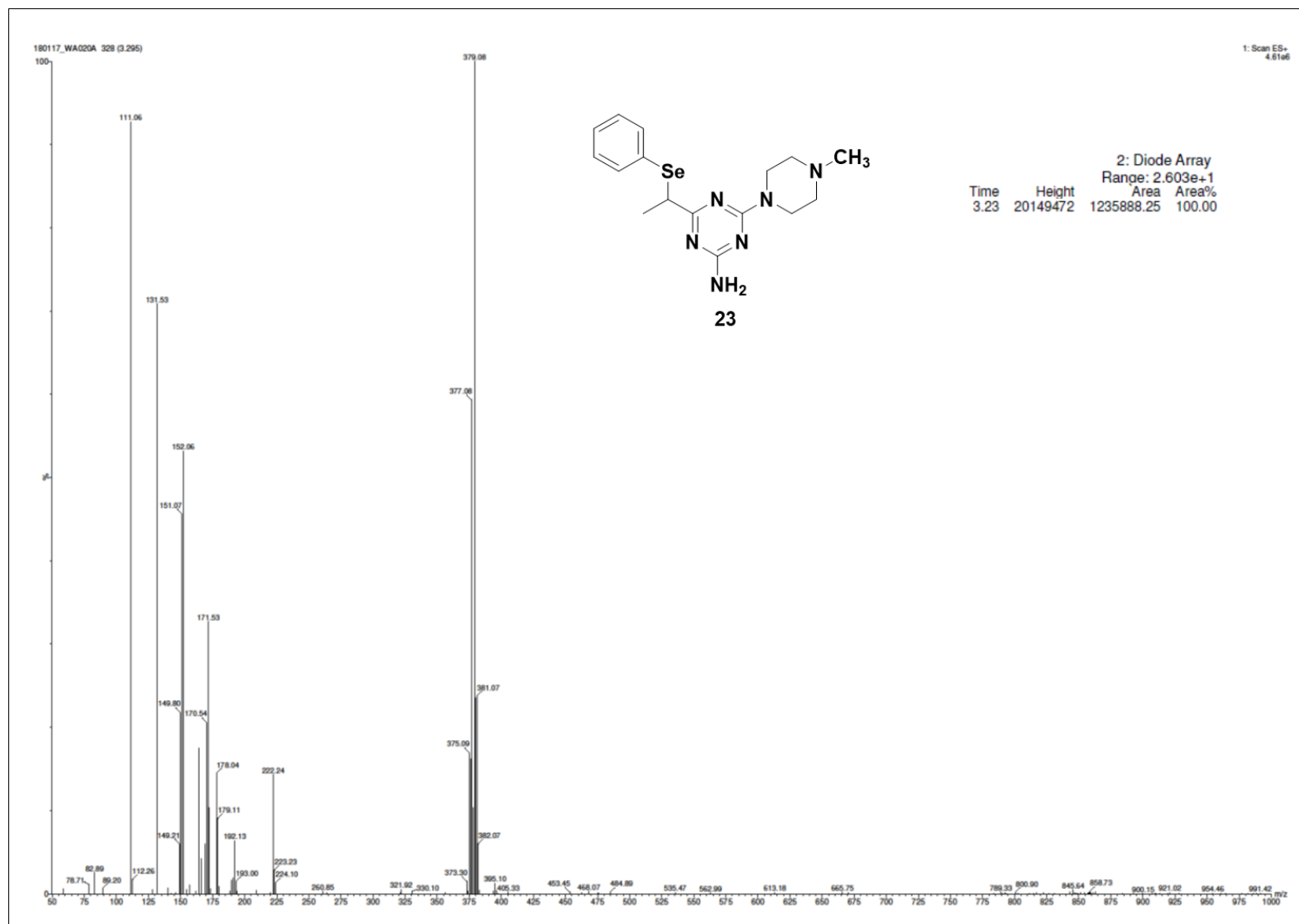
Compound **23** - ^1H NMR, 300 MHz, DMSO



Compound **23** - ^{13}C NMR, 300 MHz, DMSO

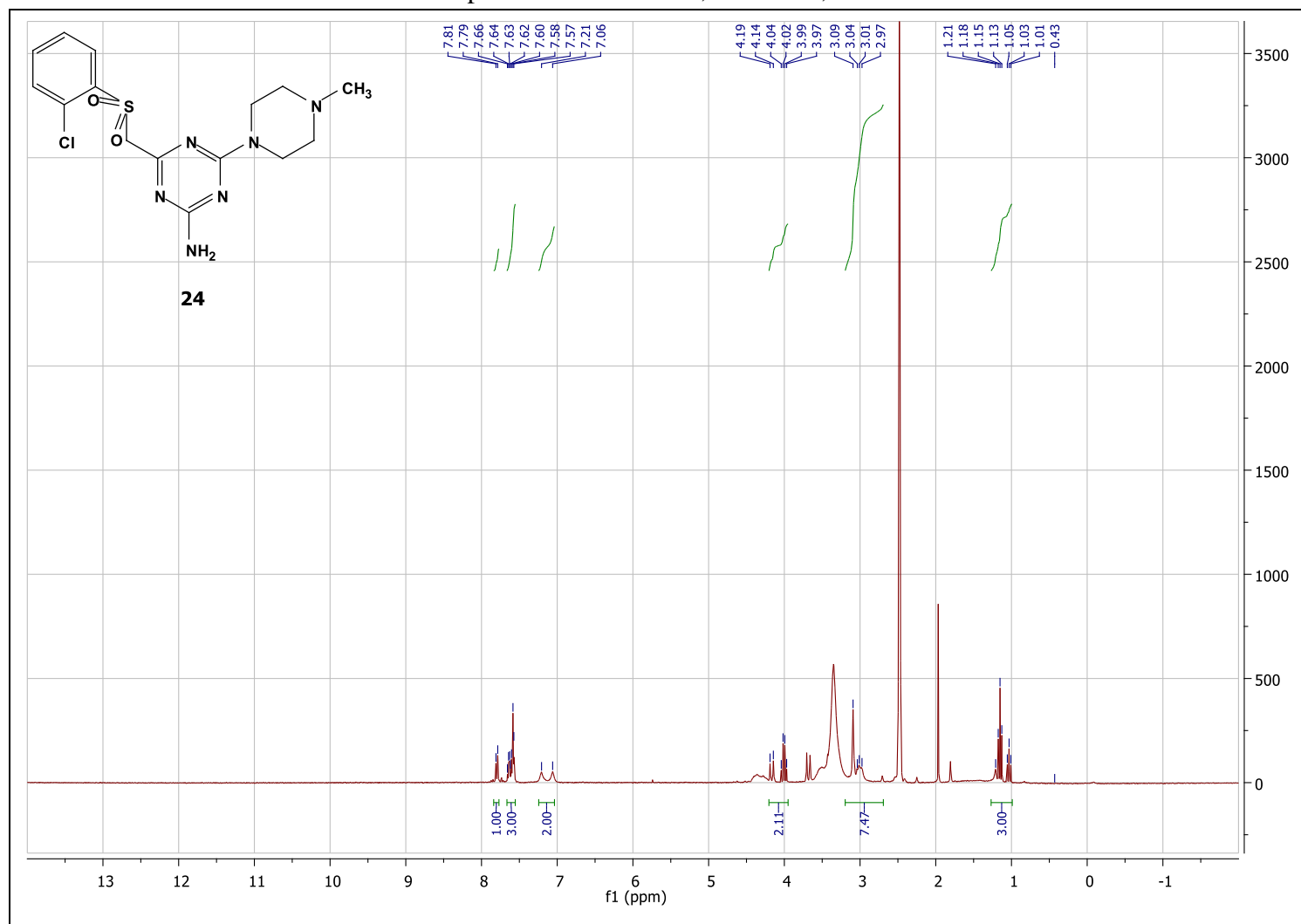


Compound 23 - LC/MS⁺

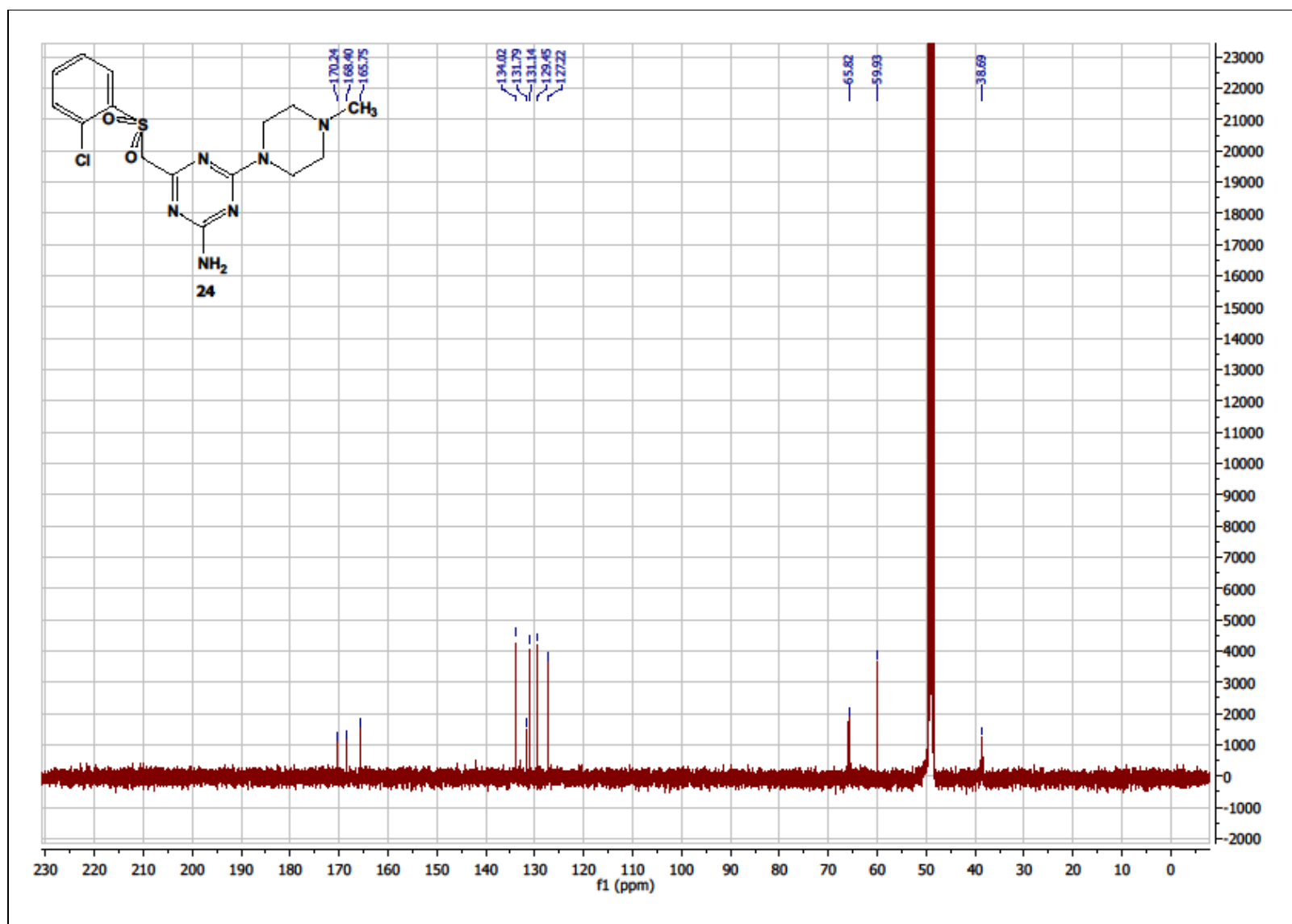


4-(((2-chlorophenyl)sulfonyl)methyl)-6-(4-methylpiperazin-1-yl)-1,3,5-triazin-2-amine (**24**)

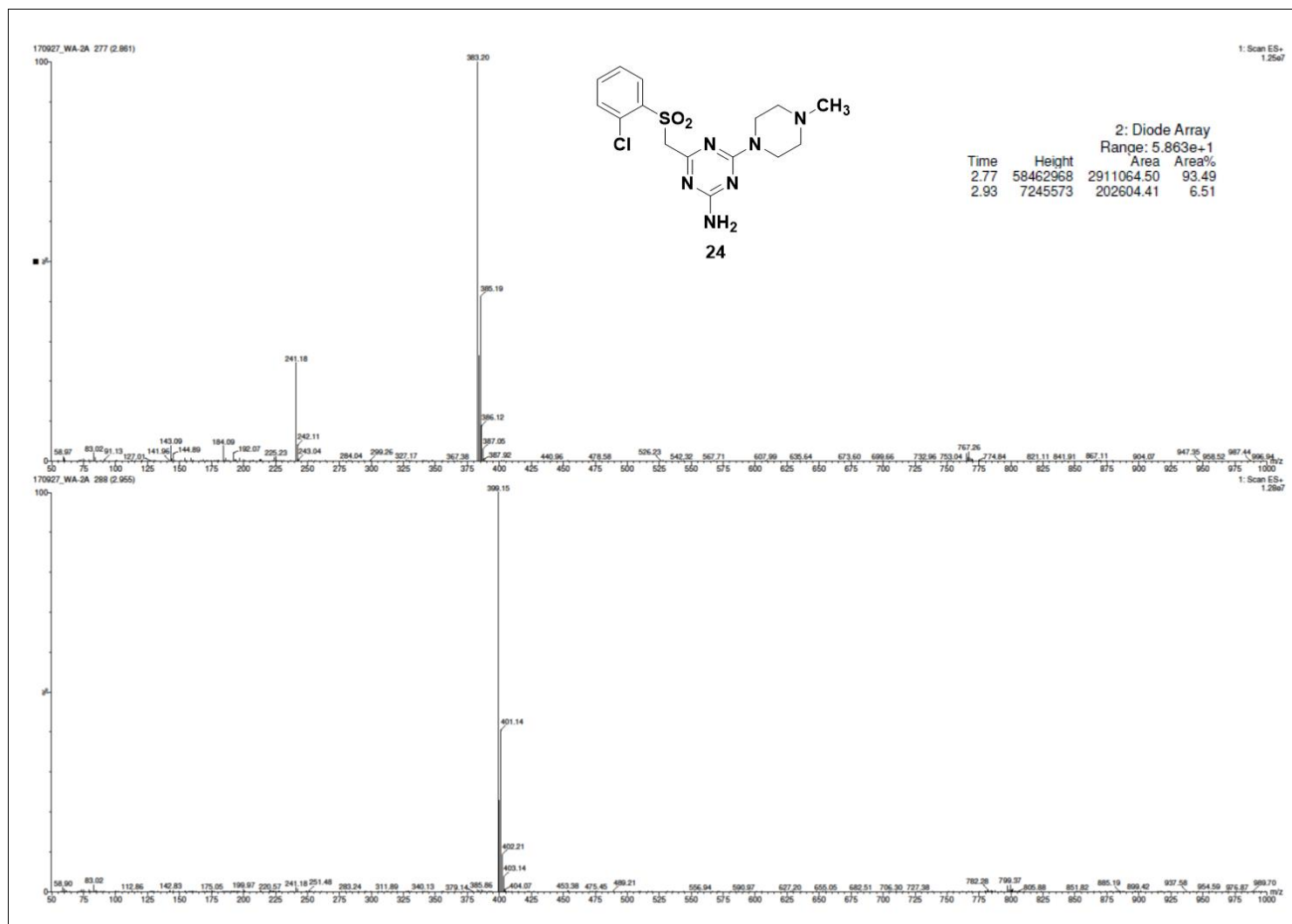
Compound **24** - ^1H NMR, 300 MHz, DMSO



Compound **24** - ^{13}C NMR, 300 MHz, MeOH



Compound 24 - LC/MS⁺



7.3. Supplementary material for Publication 3: Discovery of phenylselenoether-hydantoin hybrids as ABCB1 efflux pump modulating agents with cytotoxic and antiproliferative actions in resistant T-lymphoma.

Supplementary data

Discovery of phenylselenoether-hydantoin hybrids as ABCB1 efflux pump modulating agents with cytotoxic and antiproliferative actions in resistant T-lymphoma

Wesam Ali^{a,b}, Gabriella Spengler^c, Annamária Kincses^c, Márta Nové^c, Cecilia Battistelli^d, Gniewomir Latacz^a, Małgorzata Starek^e, Monika Dąbrowska^e, Ewelina Honkisz-Orzechowska^a, Annalisa Romanelli^f, Manuela Monica Rasile^f, Ewa Szymańska^a, Claus Jacob^{b*}, Clemens Zwergel,^{b,f,g*} Jadwiga Handzlik^{a*}

Procedures for preparation the compounds (21-30)

The intermediate compounds used in this work were either bought for compounds **22** and **24** or synthesized according to the literature in the case of compounds **21**, **23** and **25-30**. [1-5] Thus, we indicate their references, CAS numbers and ¹H NMR or their LC/MS⁺ spectra without further characterizing them.

General procedure for the compounds (21, 23, 25-26)

To a stirred solution of piperazine (10 mmol) in acetone (20 ml) and 20 mmol K₂CO₃, 1-bromo-3-chloropropane (20 mmol) was added slowly at 0°C. After the addition was completed the reaction mixture was stirred at room temperature for about 48 h.

The solvent was removed under reduced pressure and water was added to the residue. The resulting mixture was then extracted with CH₂Cl₂ (3*10 ml), dried by magnesium sulfate and evaporated to yield the desired product, which was used without further purification.

1-(3-chloropropyl)-4-phenylpiperazine (21)

CAS Number (**10599-17-4**). Light yellow liquid. Yield 91.50%. ¹H NMR (Chloroform-*d*) δ 7.25–7.22 (m, 2H, Ph), 6.91 (m, 2H, Ph), 6.86–6.82 (m, 1H, Ph), 3.22–3.19 (m, 4H, Pp-2,6-H), 2.70–2.65 (m, 2H, CH₂), 2.64–2.58 (m, 4H, Pp-3,5-H), 2.48–2.43 (m, 2H, CH₂), 1.85–1.70 (m, 2H, CH₂).

1-(3-chloropropyl)-4-(4-fluorophenyl)piperazine (23)[1]

CAS Number (**81514-10-5**). Light yellow liquid. Yield 93.5%, C₁₃H₁₈ClFN₂ (MW 256.11). LC/MS^{+/-}: purity: 78.13%, t_R=2.26, (ESI) *m/z* [M+H]⁺ 257.06.

1-(3-chloropropyl)-4-methylpiperazine (25) [2]

CAS Number (**104-16-5**). Colourless liquid. Yield 91.5%, C₈H₁₇ClN₂ (MW 176.11). LC/MS^{+/-}: purity: 80.52%, t_R=4.09, (ESI) *m/z* [M+H]⁺ 177.11.

ethyl 4-(3-chloropropyl)piperazine-1-carboxylate (26) [3]

CAS Number (**74571-66-7**). Colourless liquid. Yield 92%, C₁₀H₁₉ClO₂N₂ (MW 234.11). LC/MS^{+/-}: purity: 99.29%, t_R=6.20, (ESI) *m/z* [M+H]⁺ 230.87.

General procedure for the Se-alkylation (27-30)

As part of this general procedure, the appropriate diphenyl diselenide (9.5 mmol) dissolved in a 1:1 mixture of water and THF (50 mL) under protective nitrogen gas, sodiumborohydride (47.5 mmol) was added and the mixture was stirred for around 35 minutes while observing a decolorization in the first 1-3 minutes. Next, a solution of a methyl -2-bromo-acetate derivatives (19.37 mmol) in THF or DCM (5 mL) was added and the reaction was stirred at room temperature and monitored via thin layer chromatography (TLC). Upon consumption of the starting material usually occurring after 24-48 hours, the reaction mixture was diluted with 50 mL of a saturated aqueous solution of ammoniumchloride

and extracted with diethyl ether. The combined organic extracts dried over sodium sulfate, and the solvent was evaporated under reduced pressure to obtain the desired intermediate, which was used without further purification.

methyl 2-(phenylselanyl)acetate (27) [4]

CAS Number (68872-84-4). Colorless liquid. Yield 85%, C₉H₁₀O₂Se (MW 229.98). LC/MS⁺: purity: 99.29%, t_R=6.20, (ESI) *m/z* [M+H]⁺ 230.87.

methyl 2-(phenylselanyl)propanoate (28) [5]

CAS Number (65275-66-3). Light yellow liquid. Yield 87%, C₁₀H₁₂O₂Se (MW= 243.18). ¹H-NMR (Acetone) δ: 7.62–7.59 (m, 2H-Ph), 7.40–7.32 (m, 3H-Ph), 3.88 (q, *J* = 7.1 Hz, 1H-CH), 3.60 (s, 3H-CH₃), 1.50 (d, *J* = 7.1 Hz, 3H-CH₃).

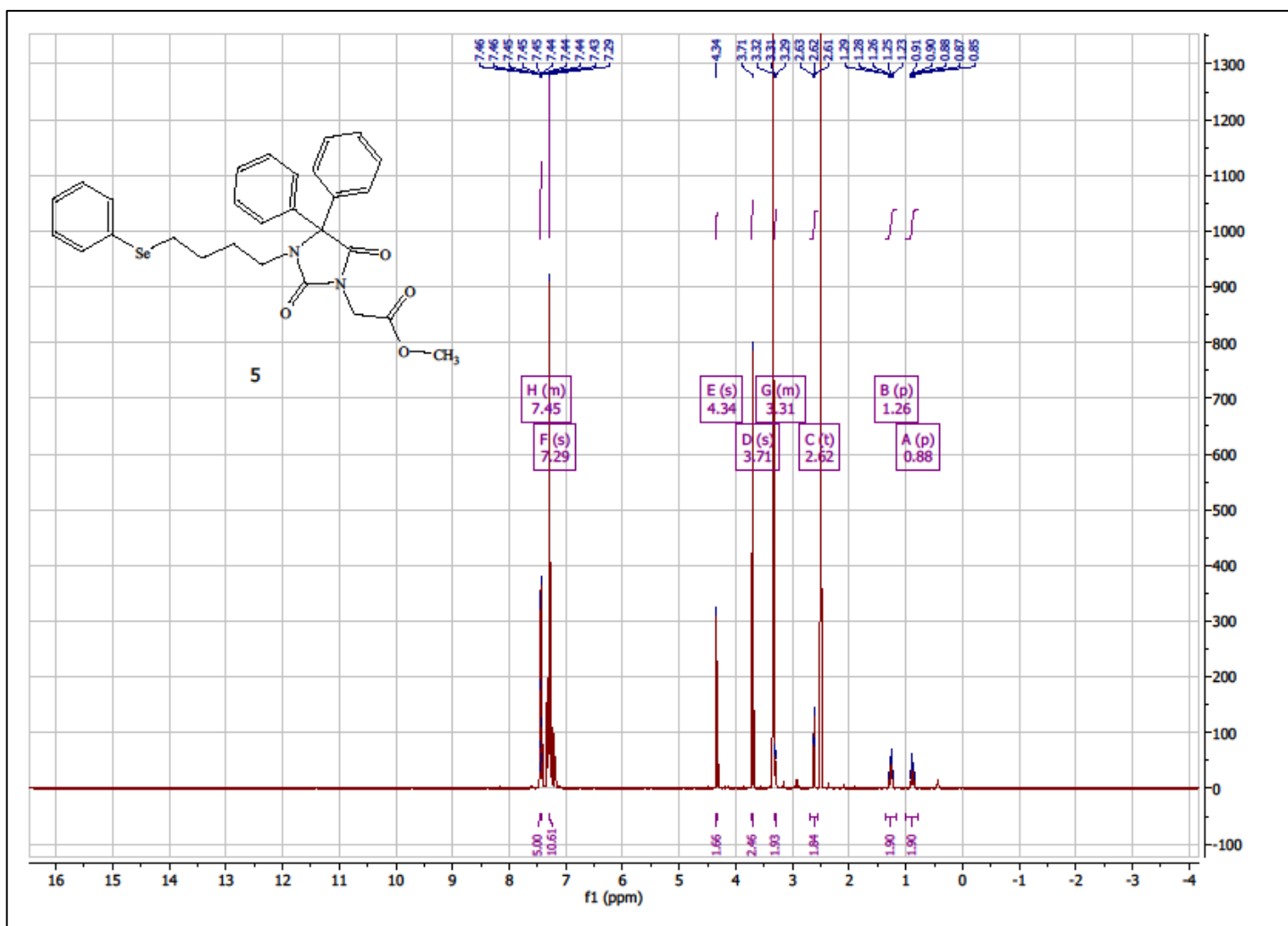
methyl 2-(phenylselanyl)butanoate (29) [6]

CAS number (946484-90-8). liquid, yellow. C₁₁H₁₄O₂Se (MW 258.02). ¹H NMR (DMSO) δ 7.55 – 7.51 (m, 2H), 7.37 – 7.30 (m, 3H), 3.71 (dd, *J* = 8.3, 6.7 Hz, 1H), 3.55 (s, 3H), 1.82–1.70 (m, 2H), 1.67 (ddd, *J* = 13.9, 7.3, 6.8 Hz, 1H), 0.90 (t, *J* = 7.3 Hz, 3H). ¹³C NMR (DMSO) δ 172.56, 134.83, 129.18, 128.38, 67.00, 51.79, 44.24, 25.11, 24.72, 12.29.

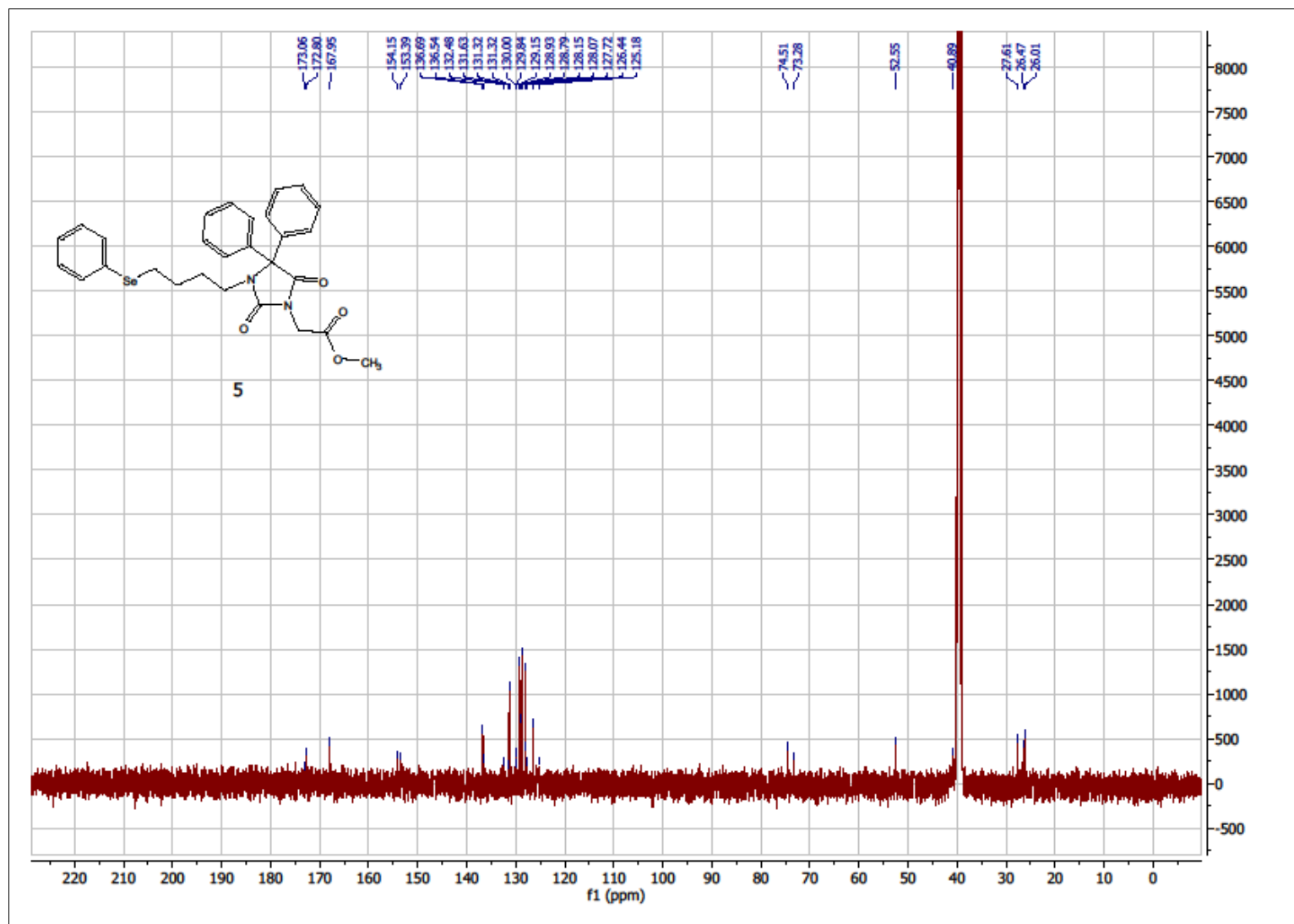
methyl 2-methyl-2-(phenylselanyl)propanoate (30) [7]

CAS number (59345-48-1). Dark yellow liquid. C₁₁H₁₄O₂Se (MW 258.02). ¹H NMR (DMSO-*d*₆) δ 7.56 (d, *J* = 1.3 Hz, 2H-Ph), 7.47 (s, 1H-Ph), 7.40–7.35 (m, 2H-Ph), 1.50 (s, 6H-2*CH₃), 1.09 (t, *J* = 7.1 Hz, 3H-CH₃). ¹³C NMR (DMSO) δ 173.48, 137.48, 129.38, 129.06, 128.95, 60.56, 45.15, 30.21, 25.87, 25.11, 13.78.

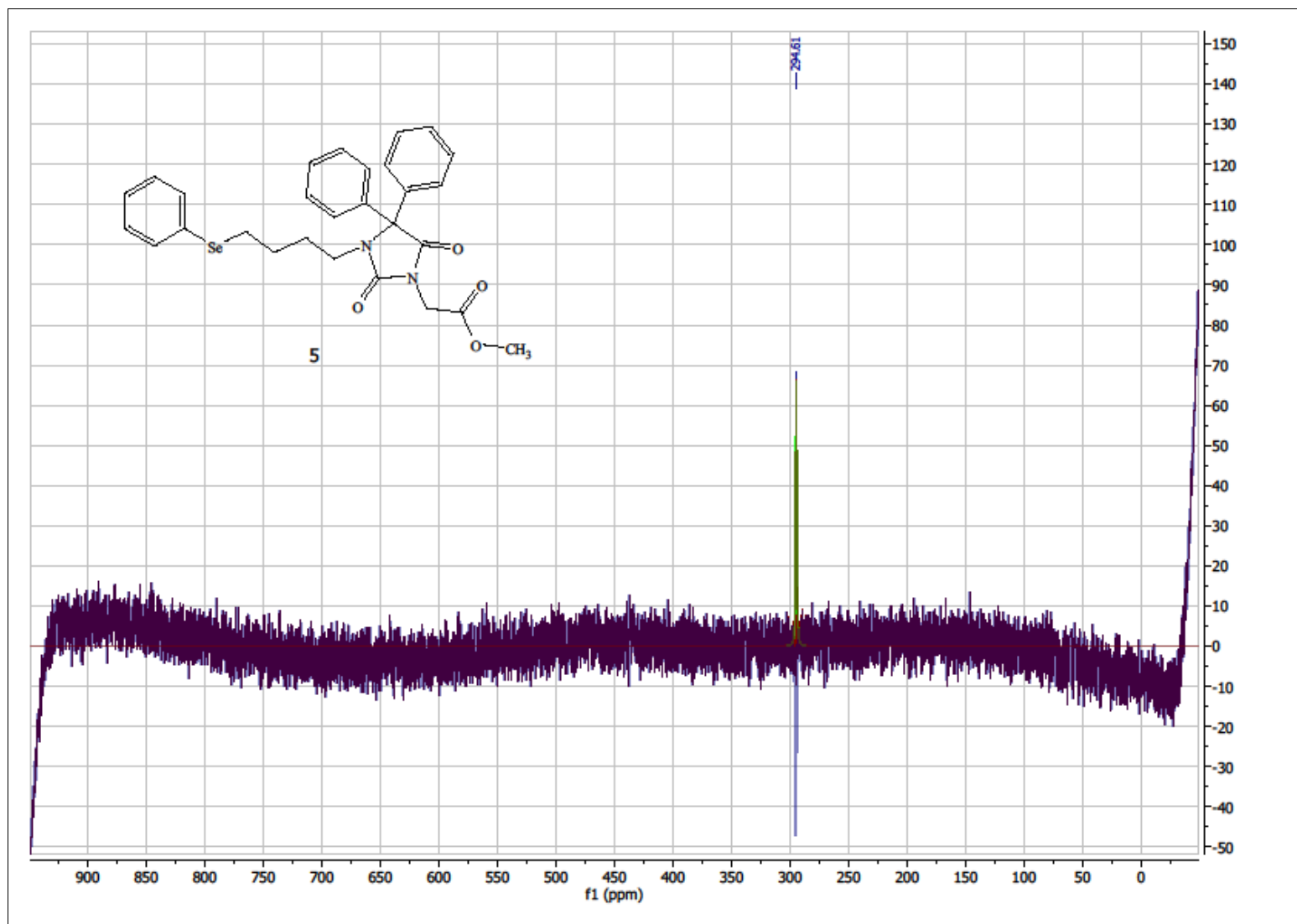
Methyl 2-(2,5-dioxo-4,4-diphenyl-3-(4-(phenylselanyl)butyl)imidazolidin-1-yl)acetate, compound (5), ^1H NMR (DMSO)



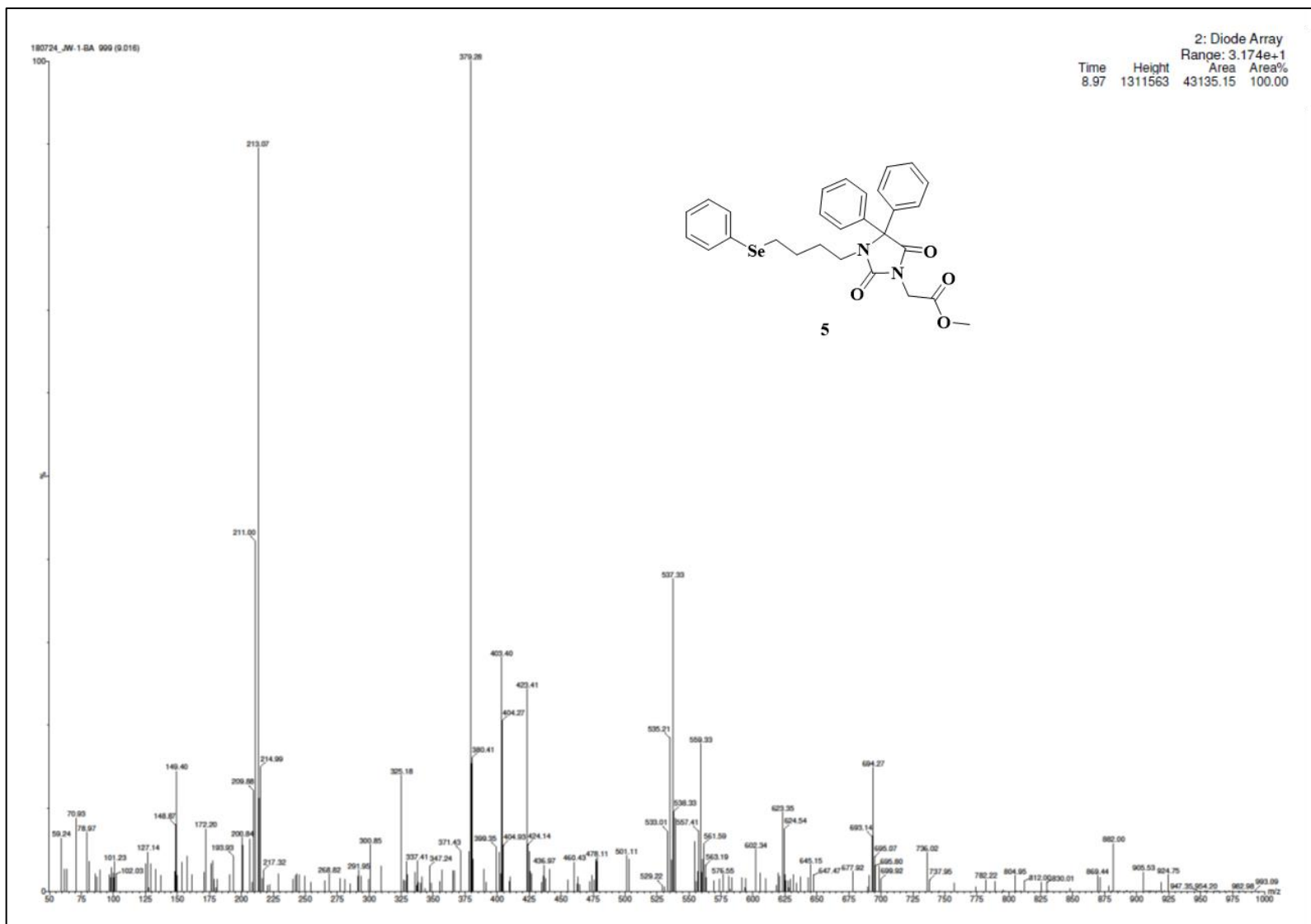
Compound 5, ^{13}C NMR (DMSO)



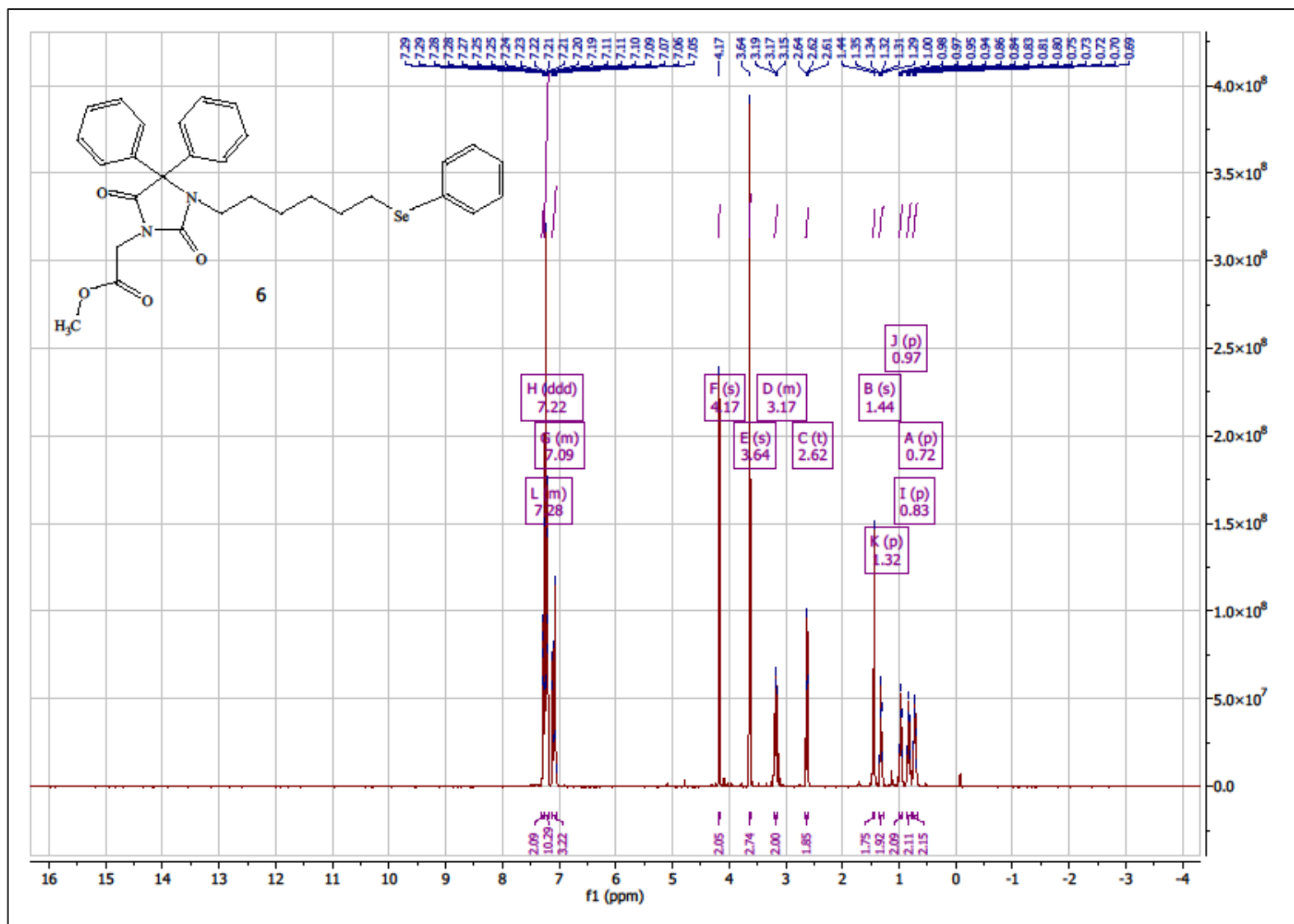
Compound **5**, ^{77}Se NMR (CDCl_3)



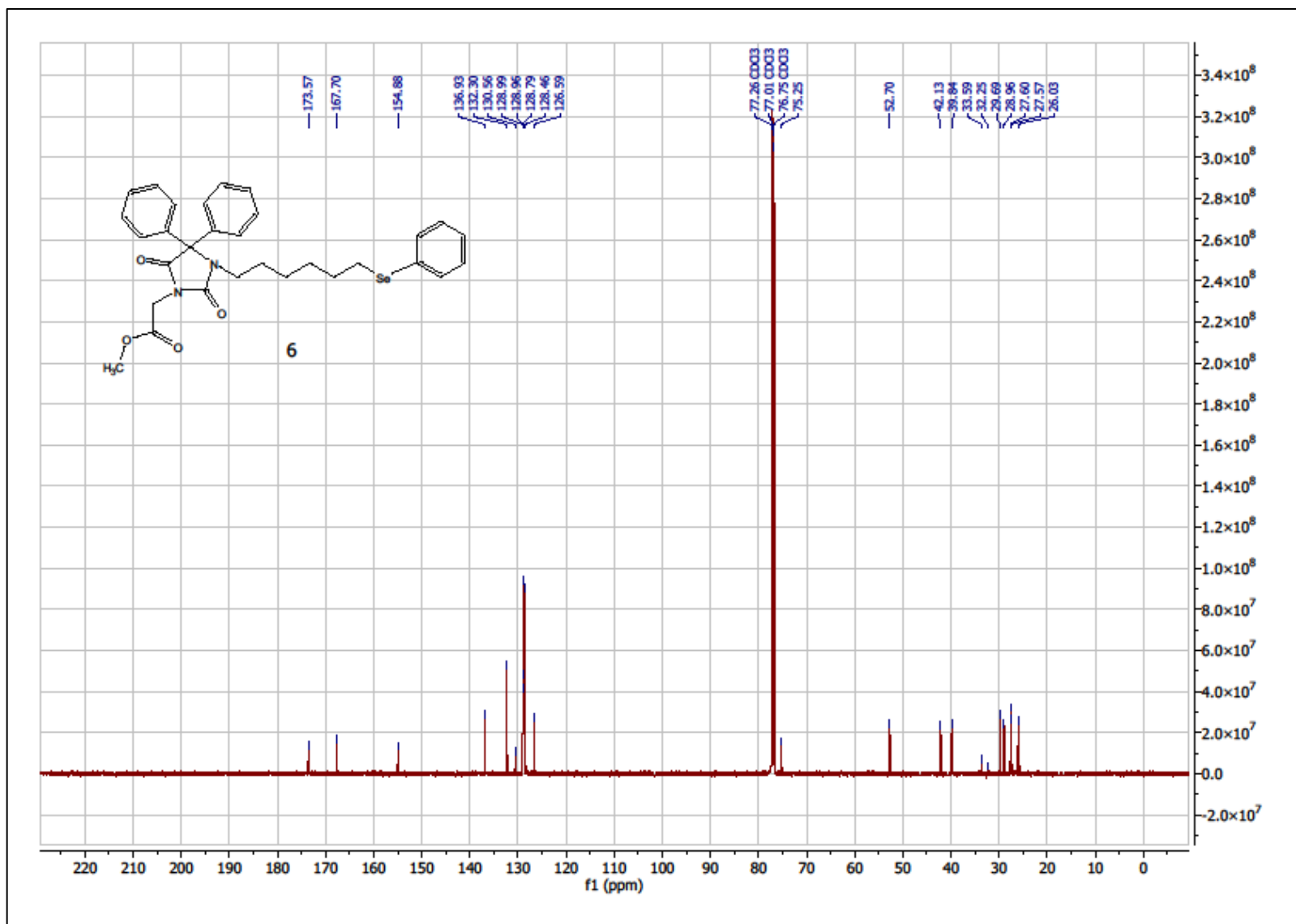
Compound 5, LC/MS⁺



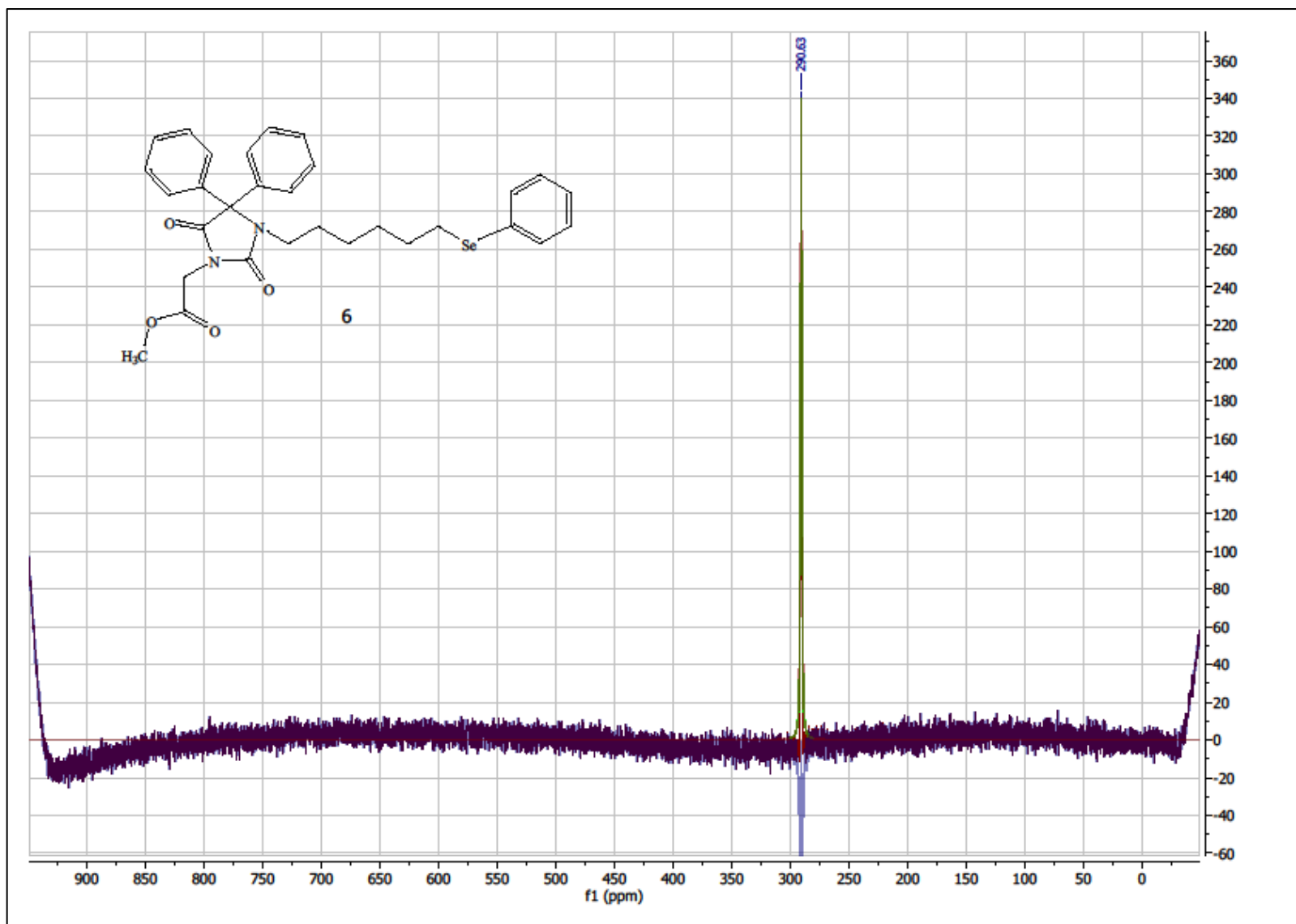
methyl 2-(2,5-dioxo-4,4-diphenyl-3-(6-(phenylselanyl)hexyl)imidazolidin-1-yl)acetate (**6**), ^1H NMR (CDCl_3)



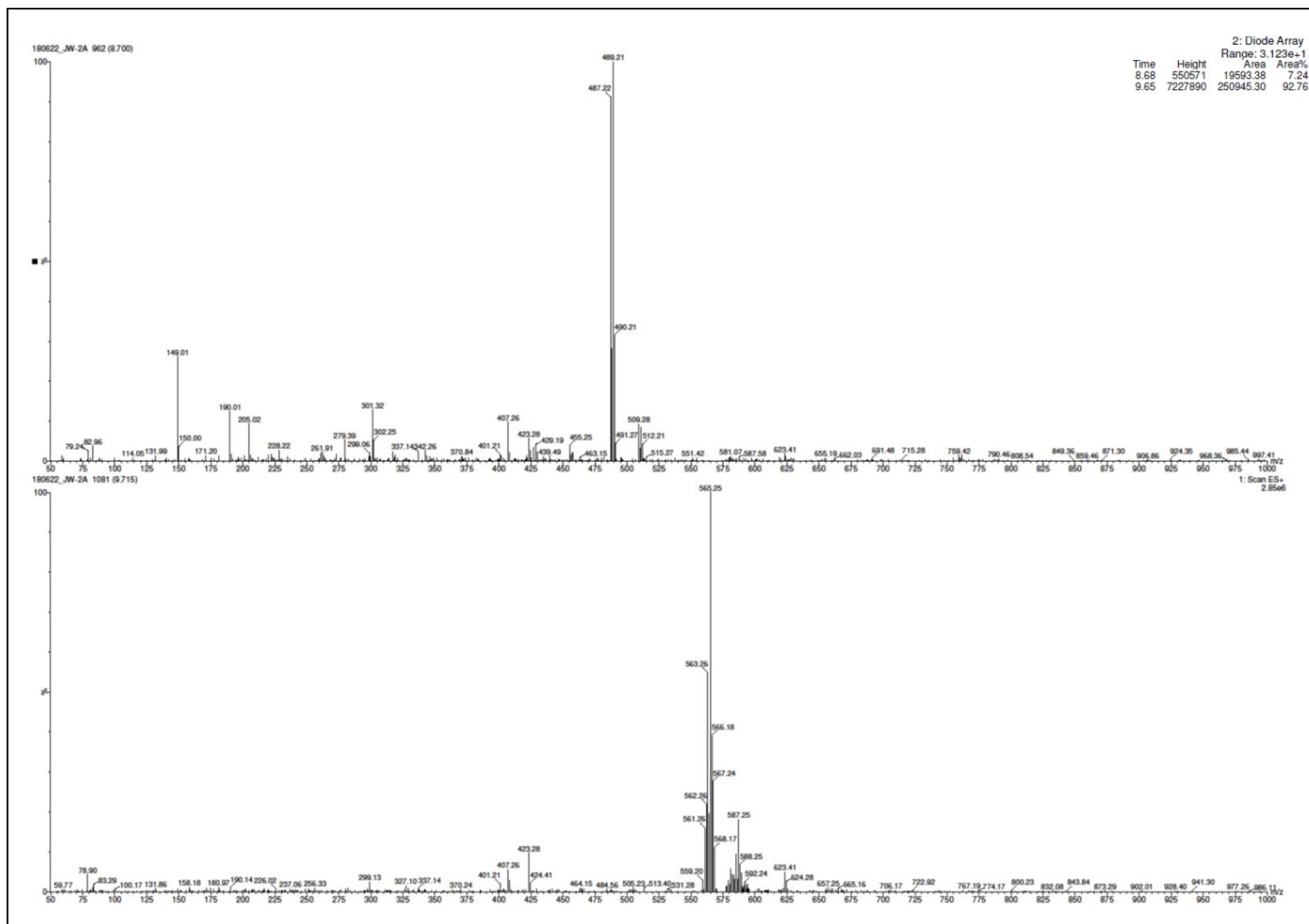
Compound 6, ^{13}C NMR (CDCl_3)



Compound **6**, ^{77}Se NMR (CDCl_3)

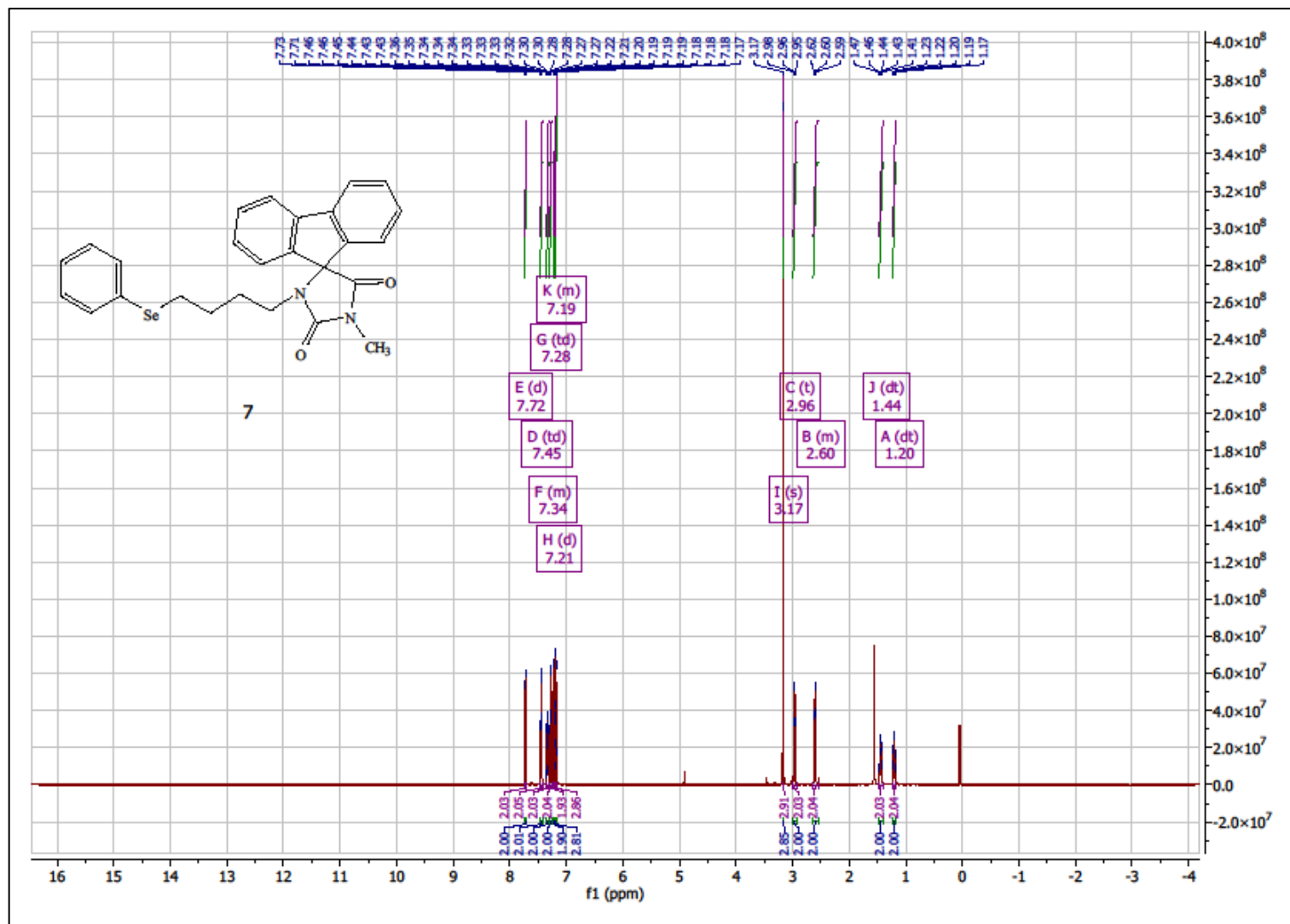


Compound 6, LC/MS⁺

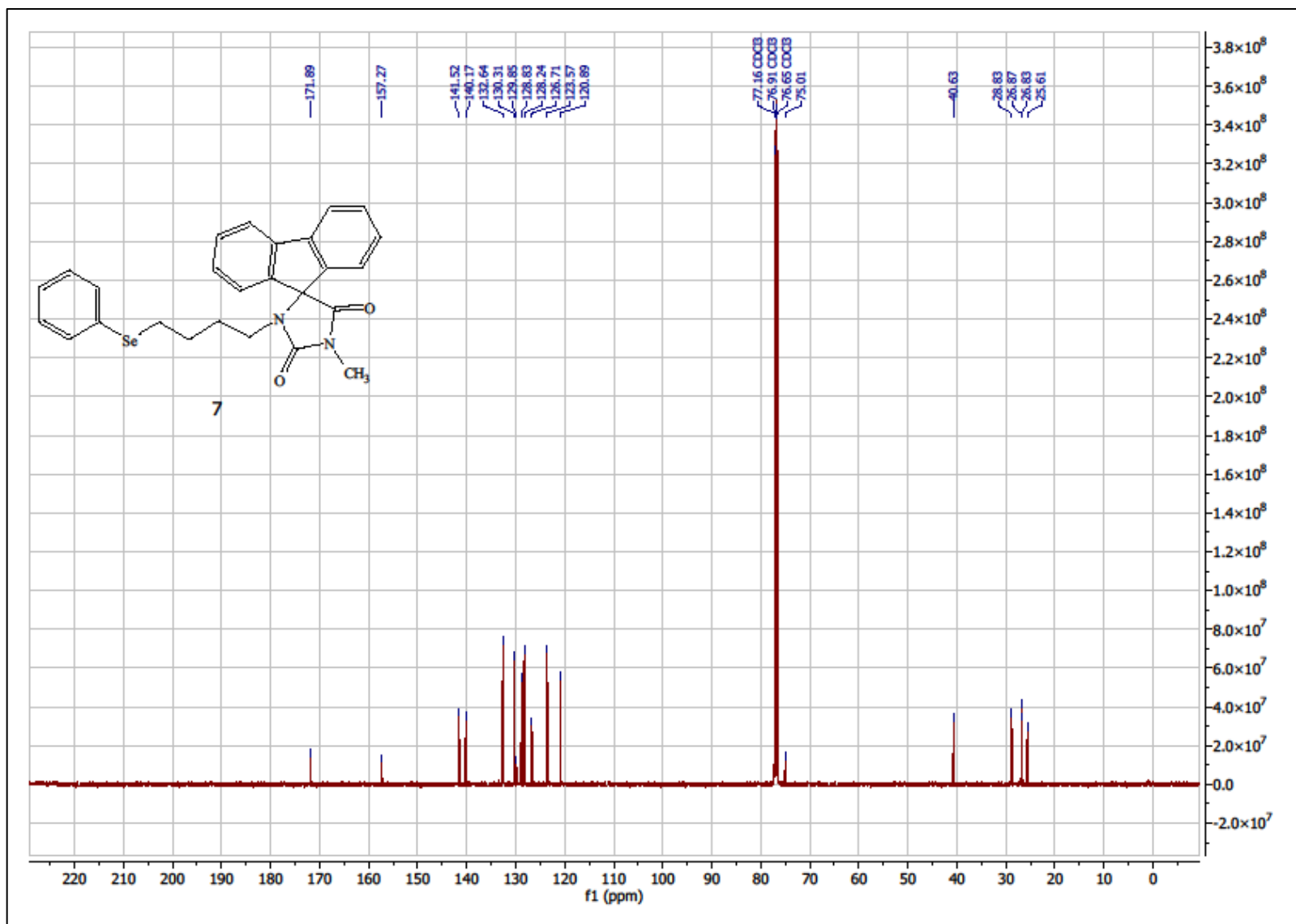


1'-methyl-3'-(4-(phenylselanyl)butyl)spiro[fluorene-9,4'-imidazolidine]-2',5'-dione (7)

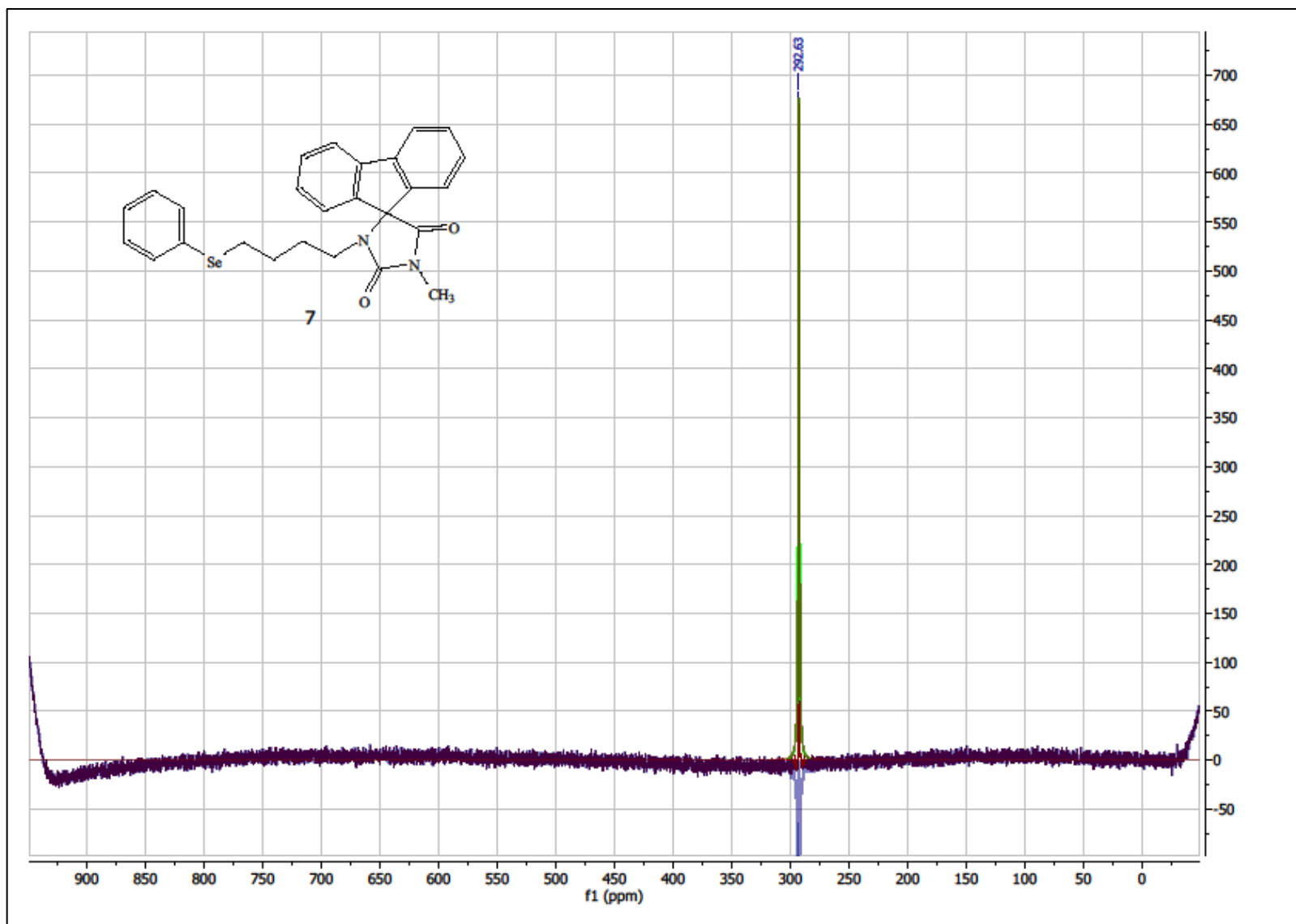
$^1\text{H NMR}$ (CDCl_3)



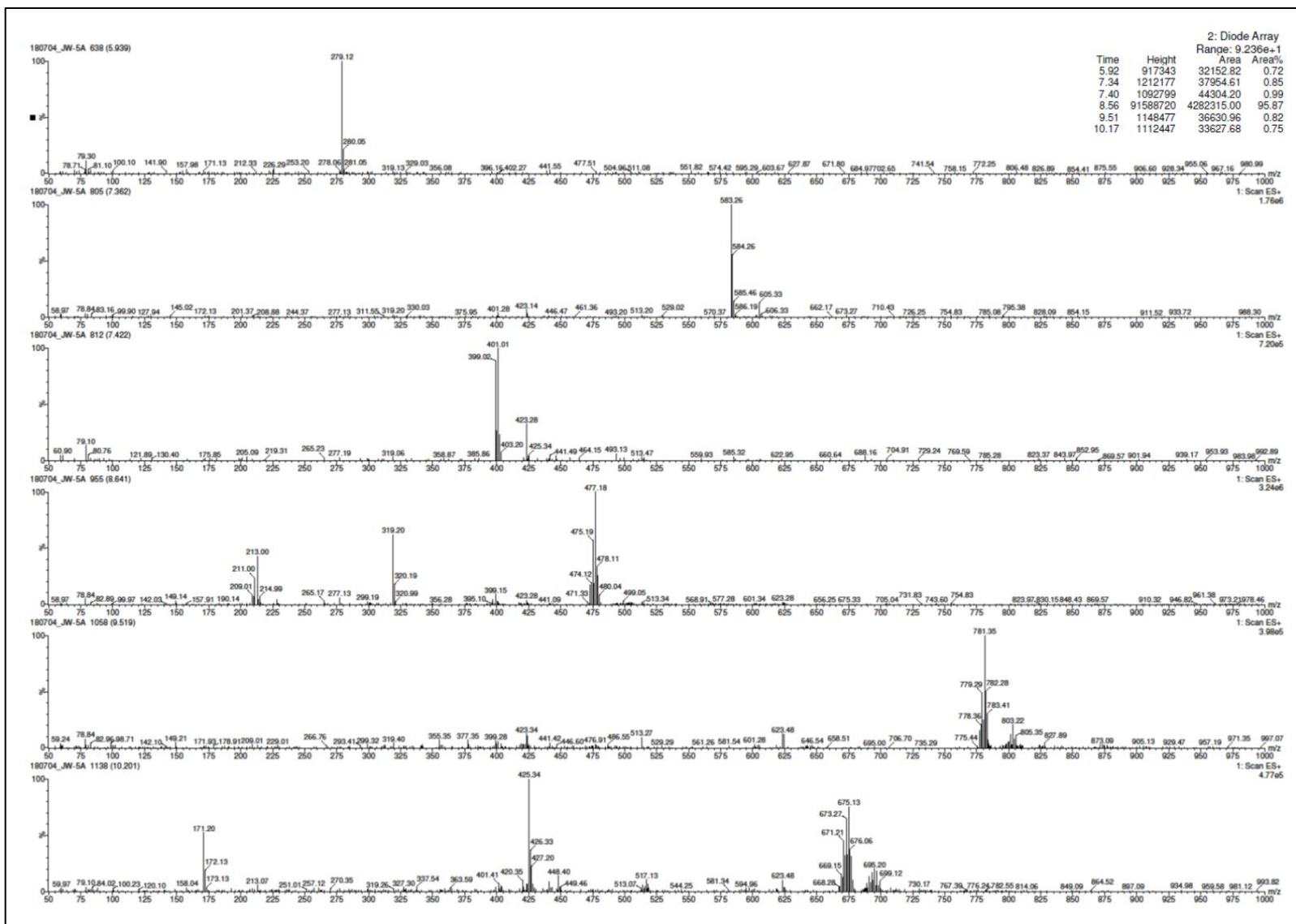
Compound 7, ^{13}C NMR (CDCl_3)



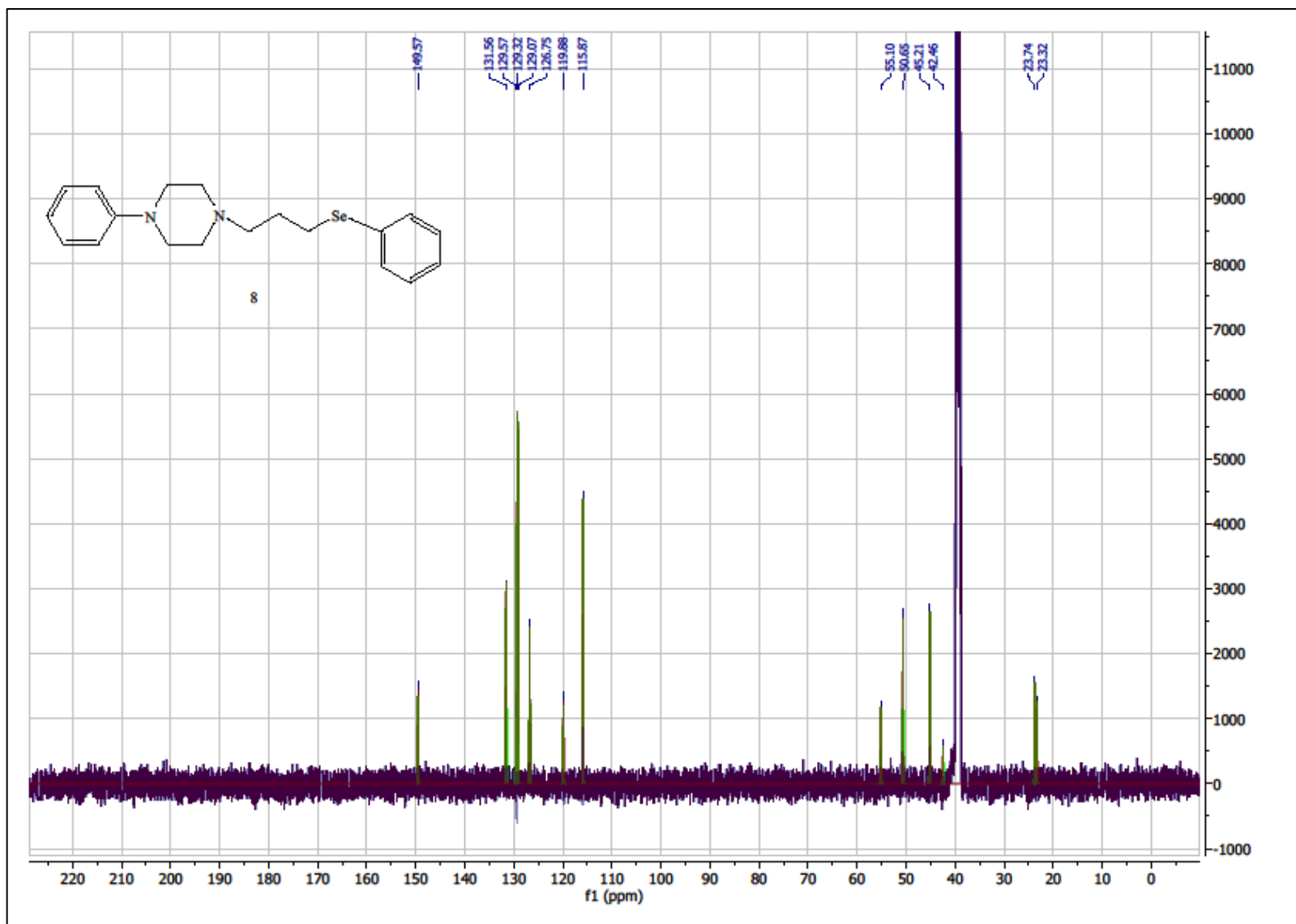
Compound 7, ^{77}Se NMR (CDCl_3)



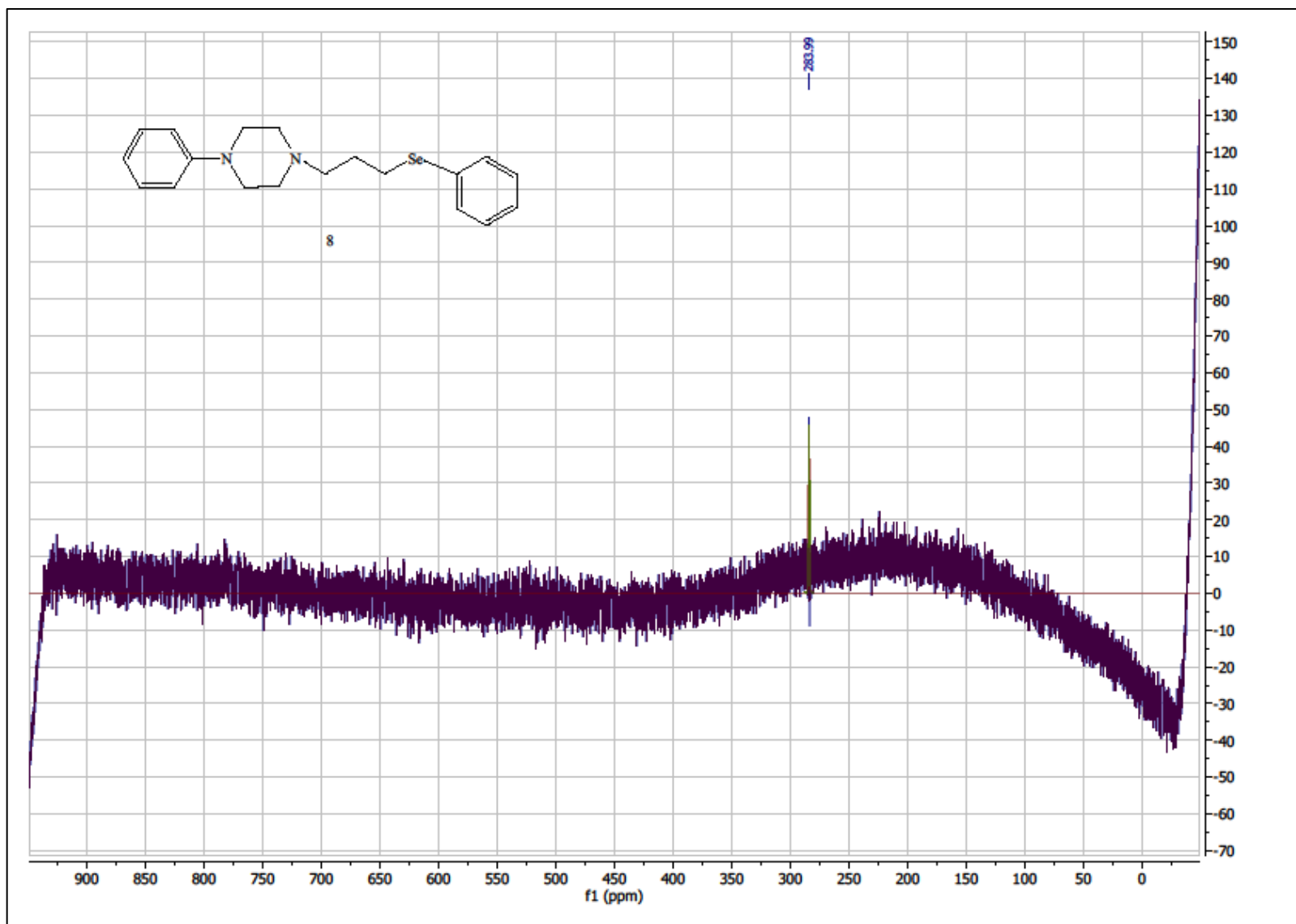
Compound 7, LC/MS⁺



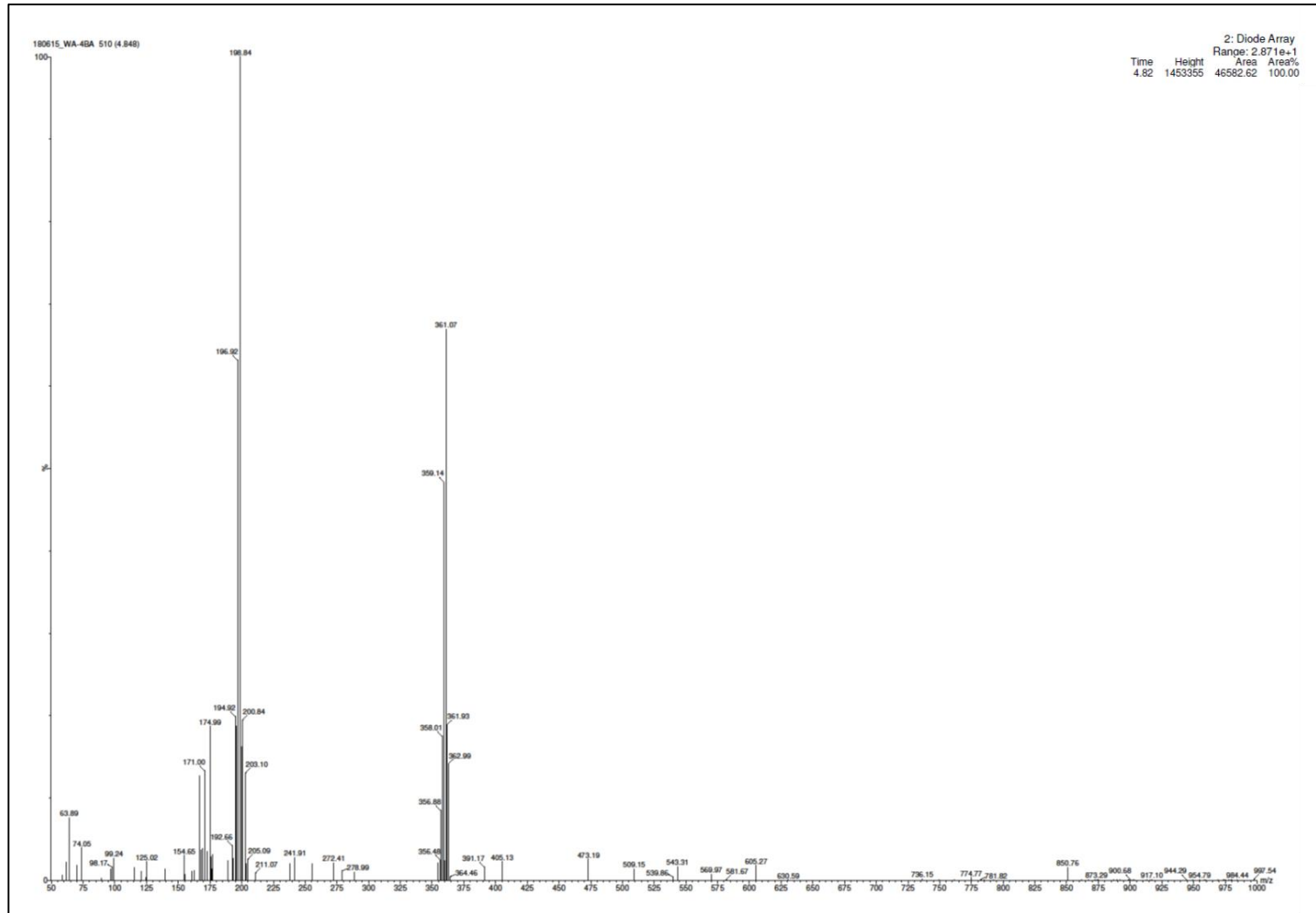
Compound **8**, ^{13}C NMR (DMSO)



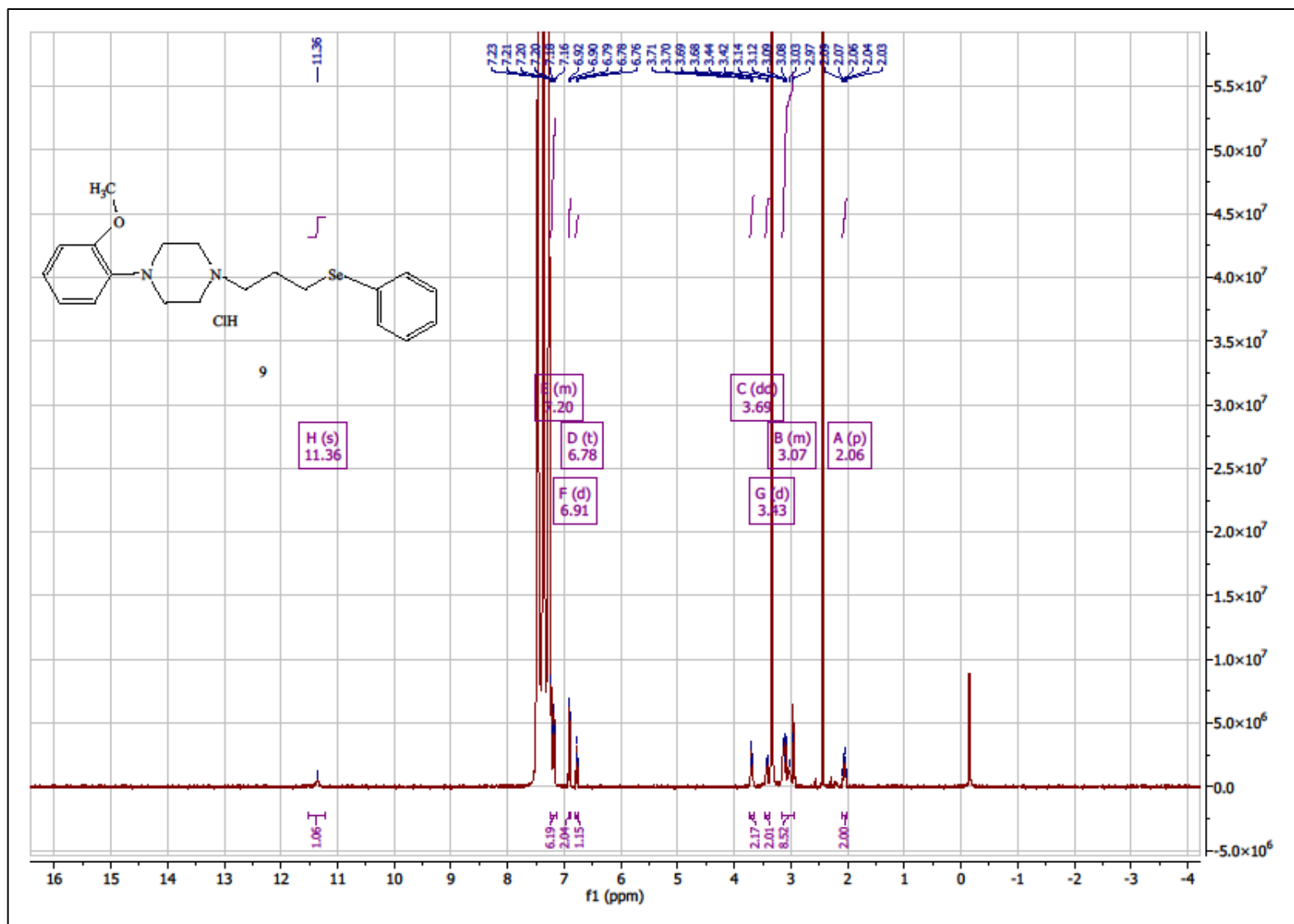
Compound **8**, ^{77}Se NMR (DMSO)



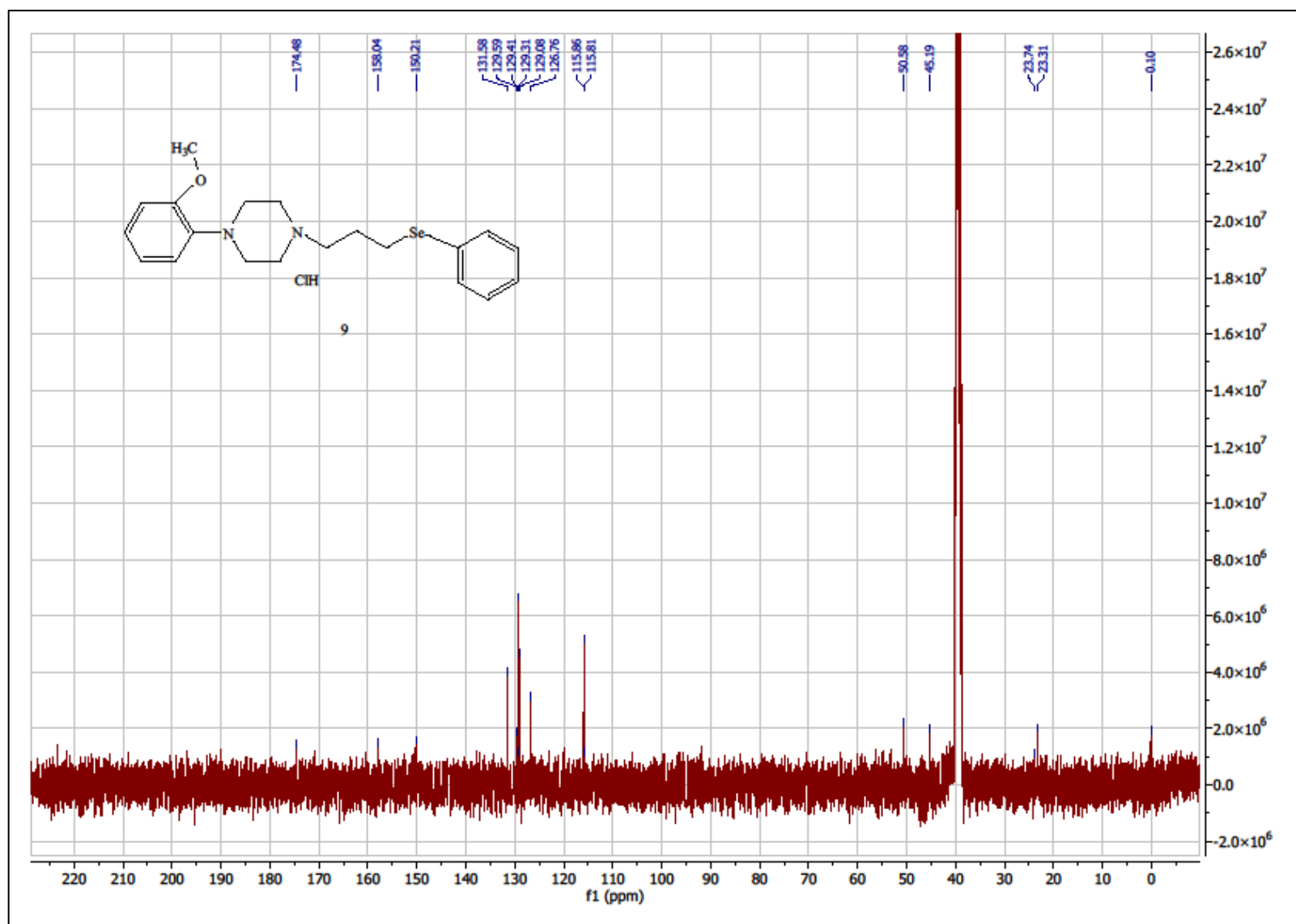
Compound 8, LC/MS⁺



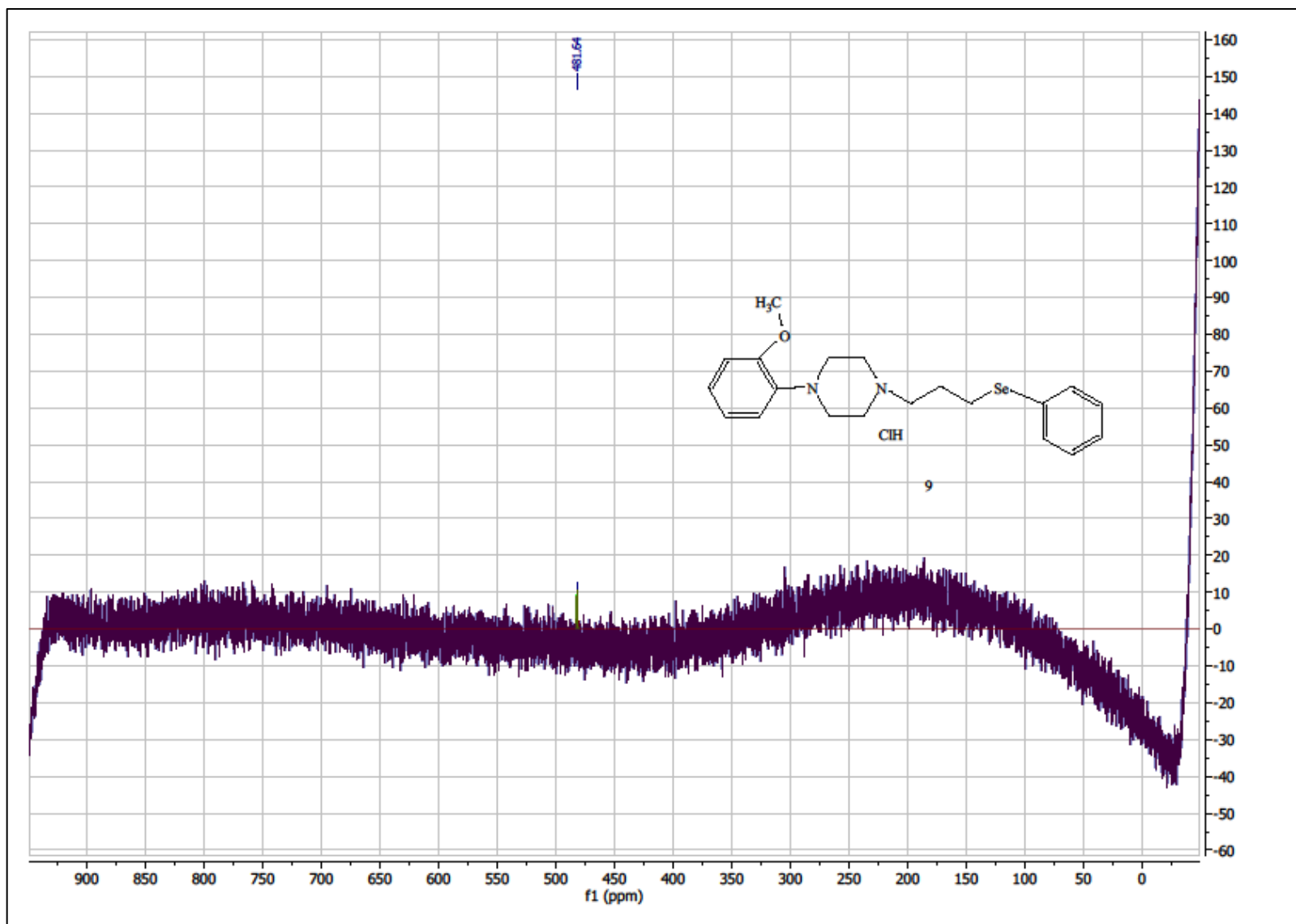
1-(2-methoxyphenyl)-4-(3-(phenylselanyl)propyl)piperazine hydrochloride(9), ¹H NMR (DMSO)



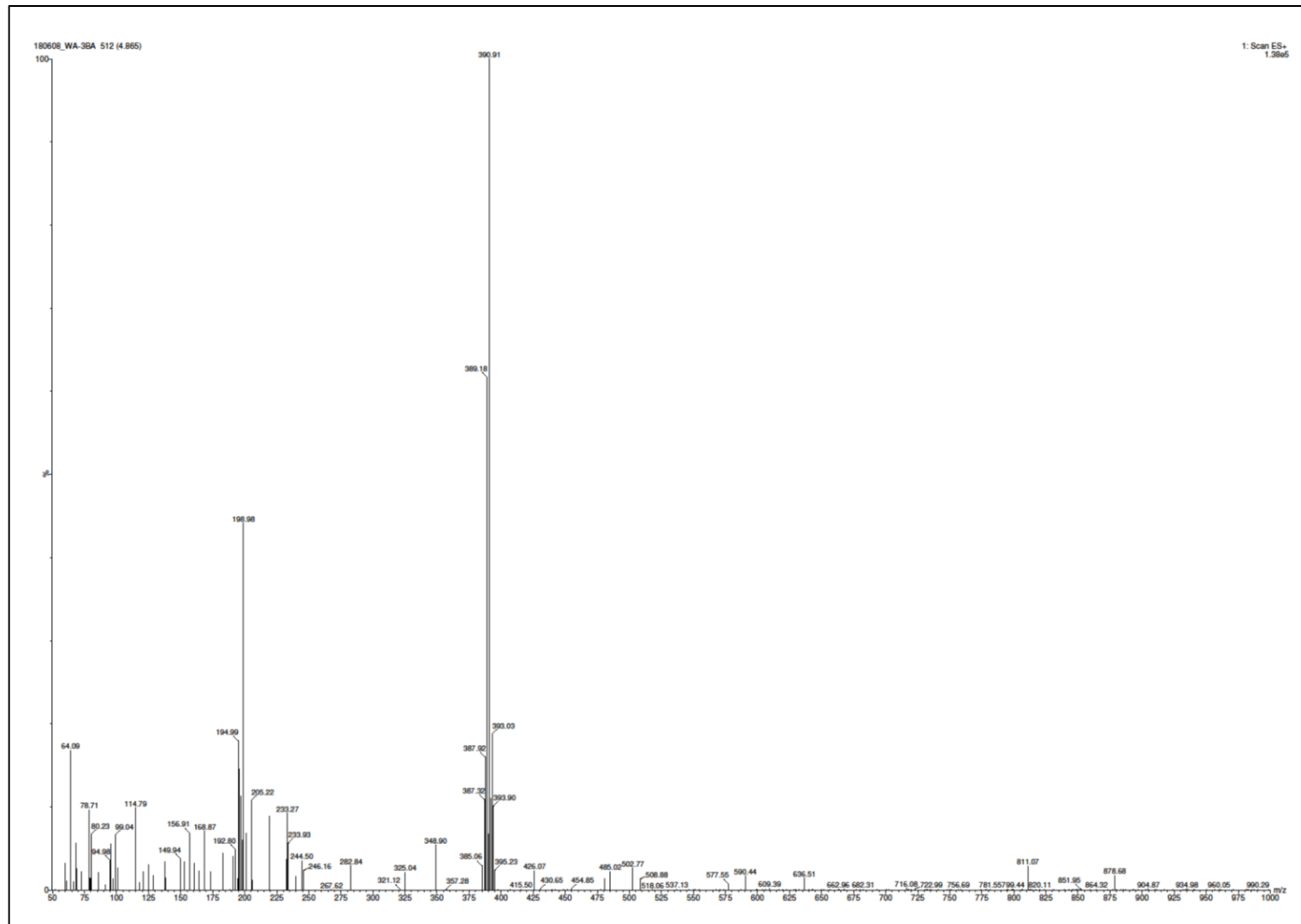
Compound 9, ^{13}C NMR (DMSO)



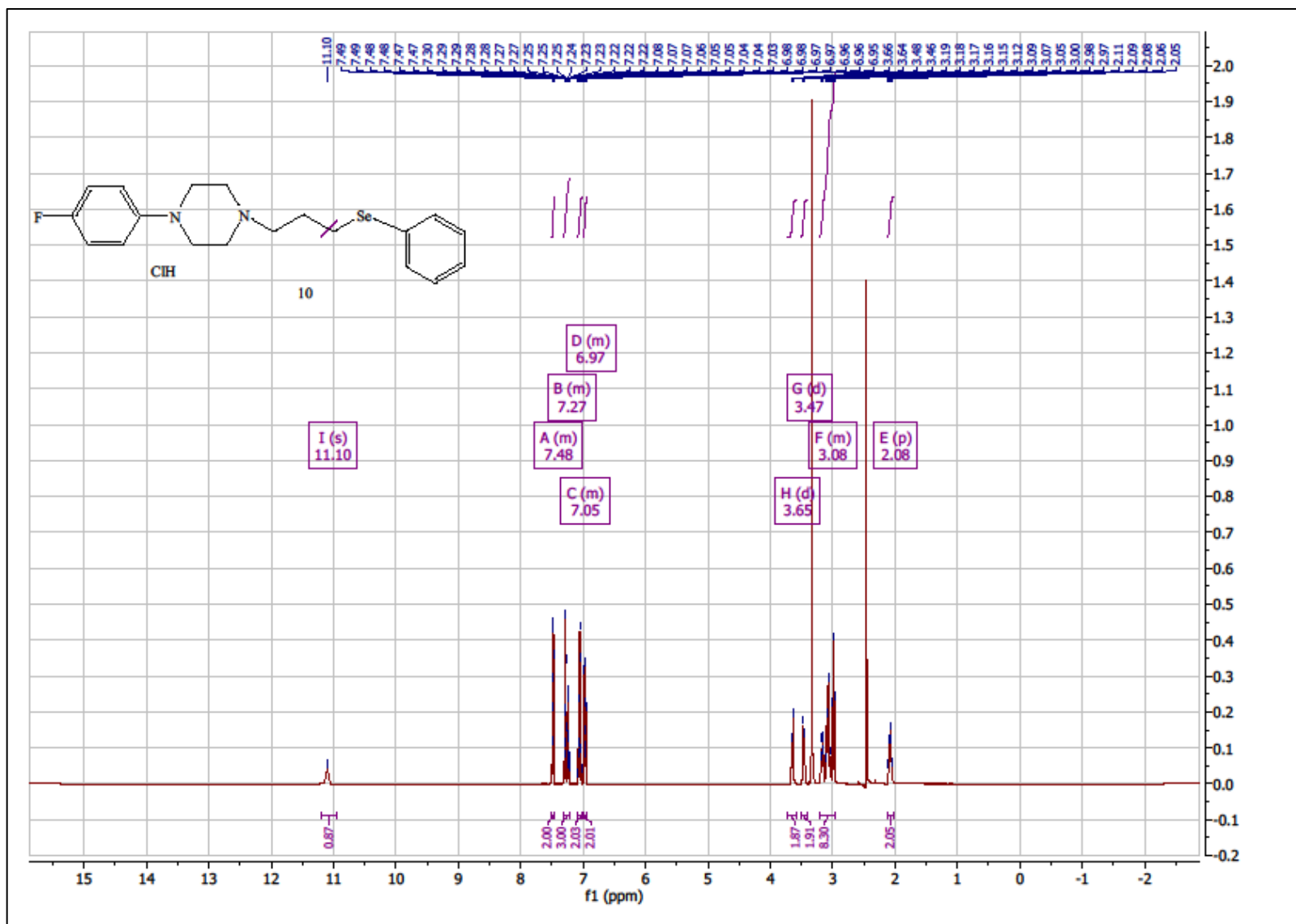
Compound 9, ^{77}Se NMR (DMSO)



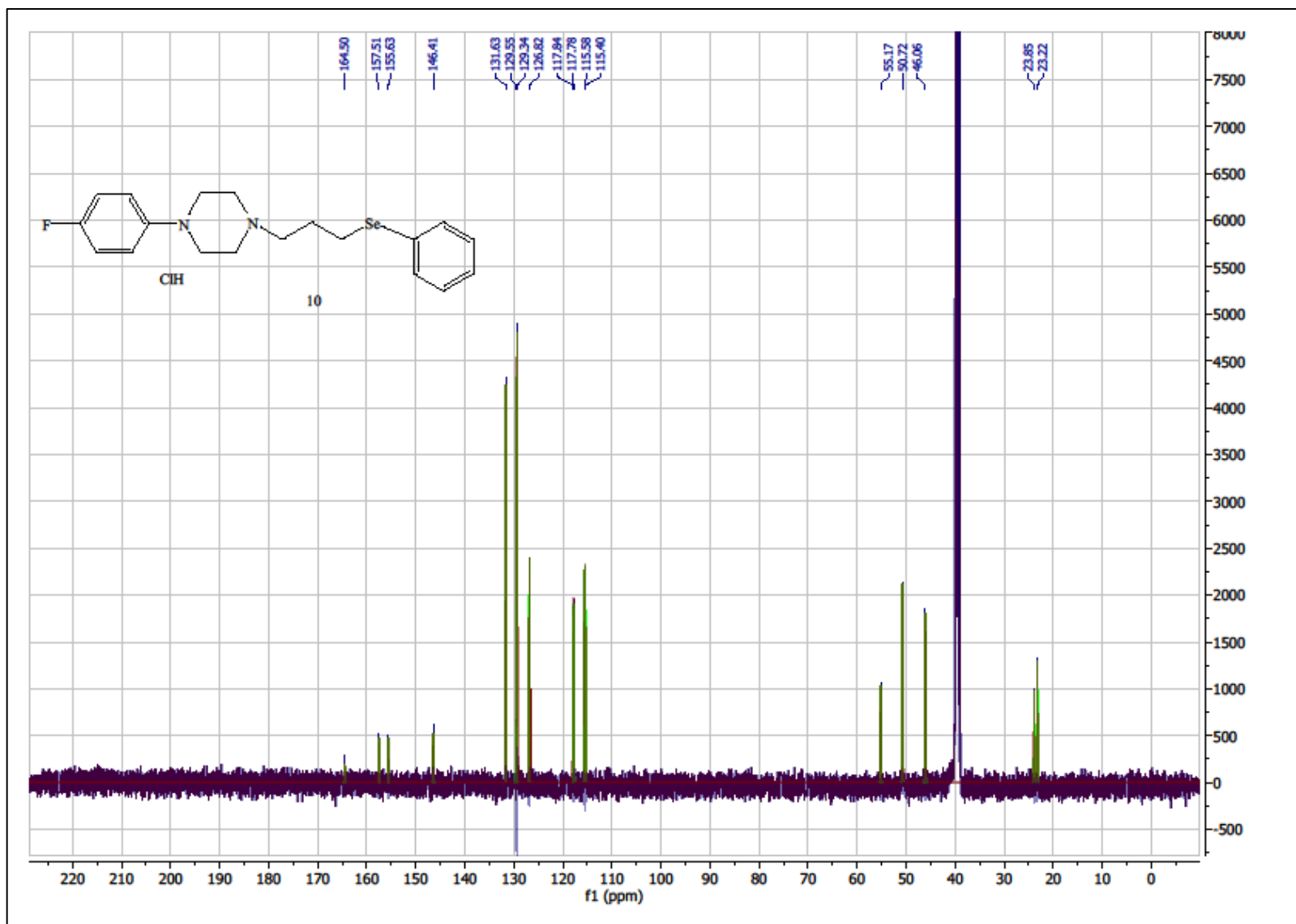
Compound 9, LC/MS⁺



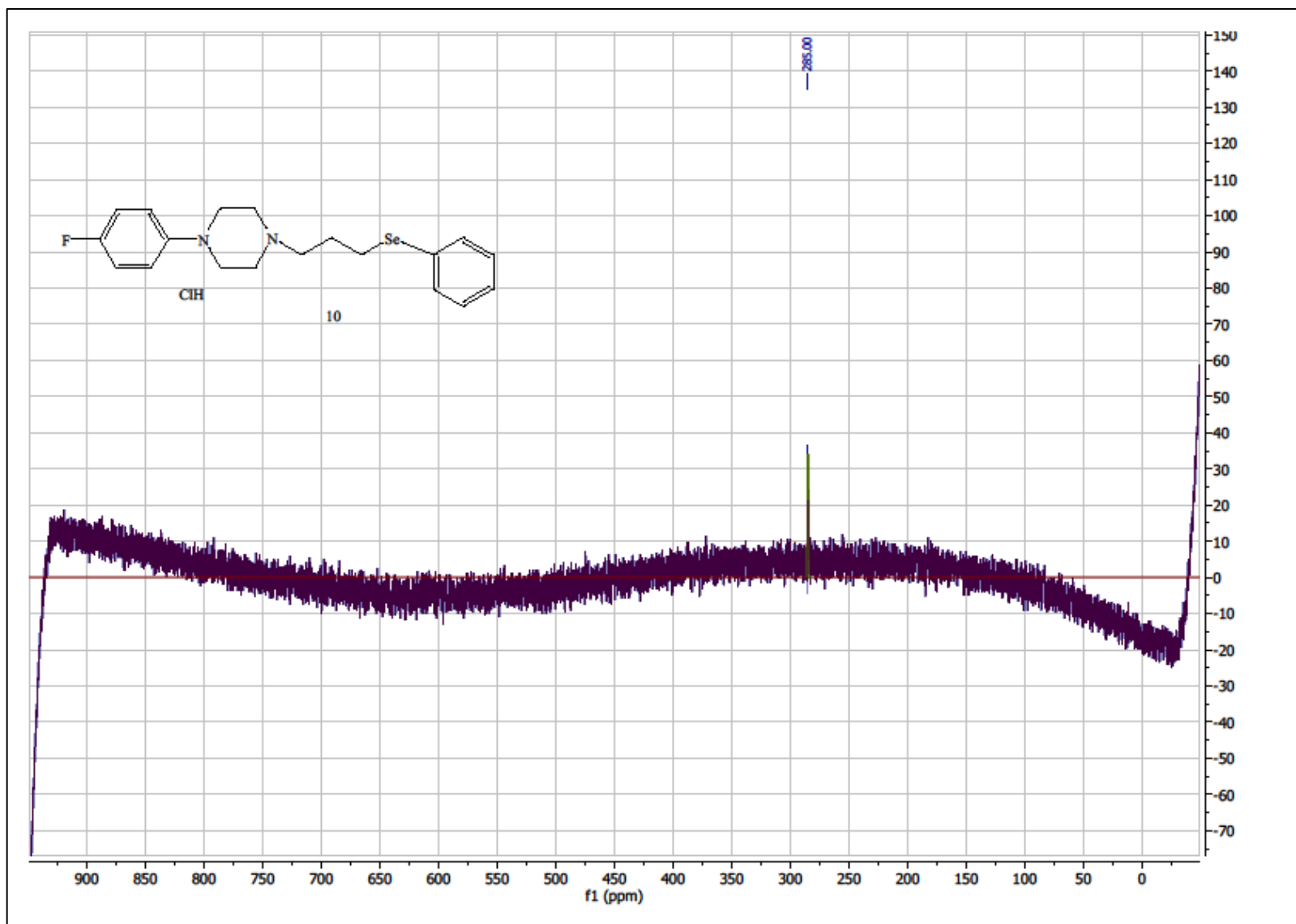
1-(4-fluorophenyl)-4-(3-(phenylselanyl)propyl)piperazine hydrochloride (**10**), ^1H NMR (DMSO)



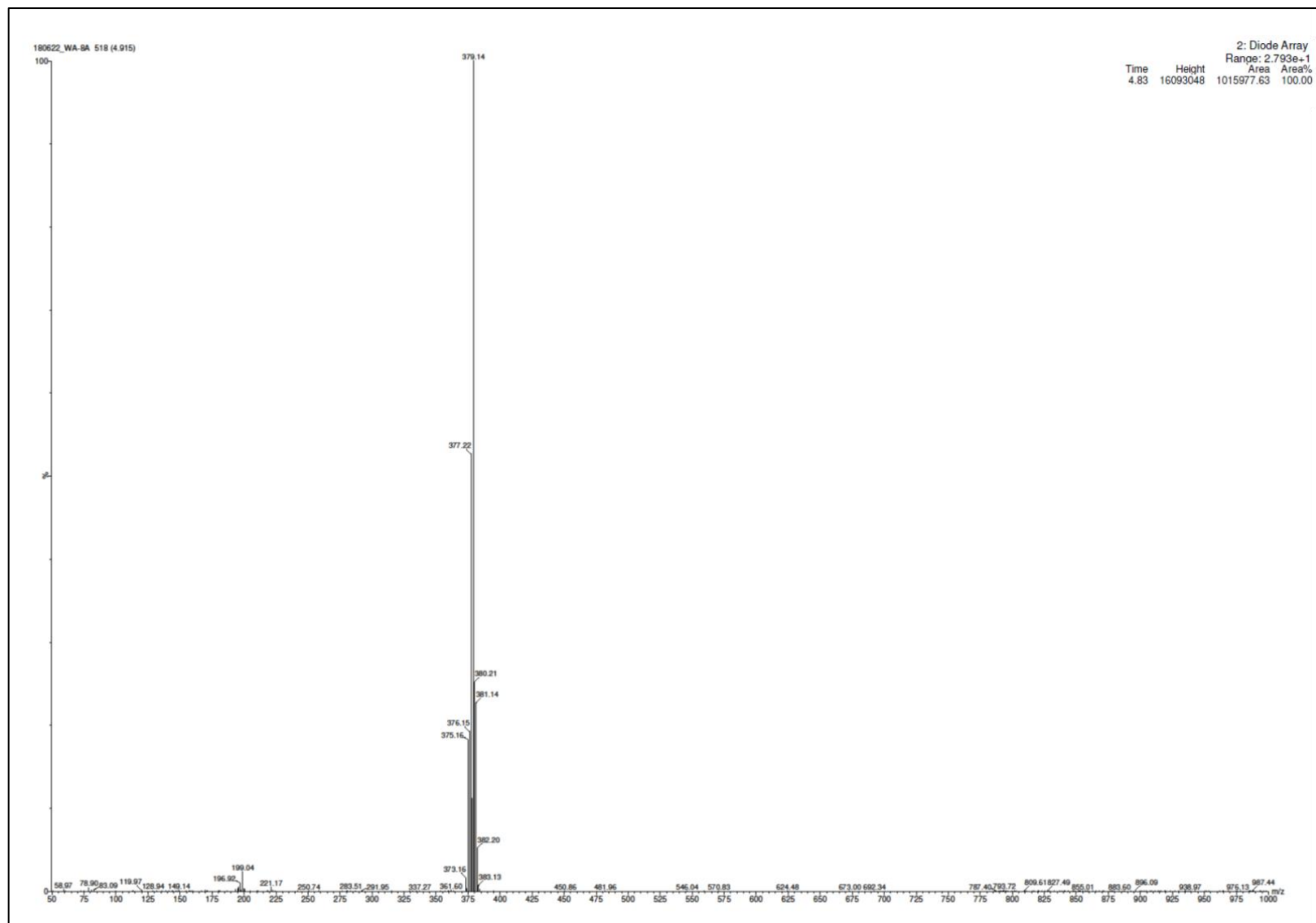
Compound **10**, ^{13}C NMR (DMSO)



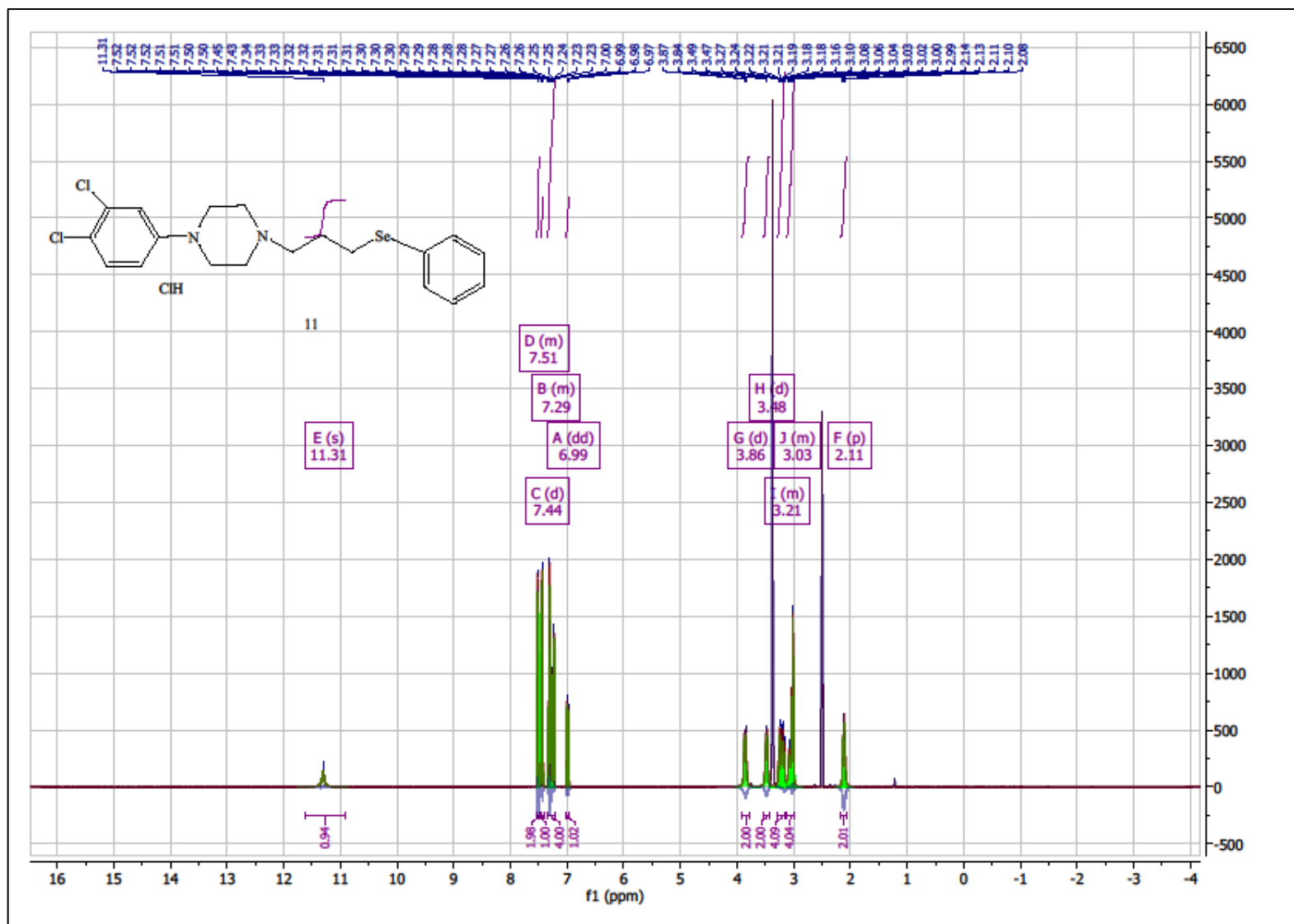
Compound **10**, ^{77}Se NMR (DMSO)



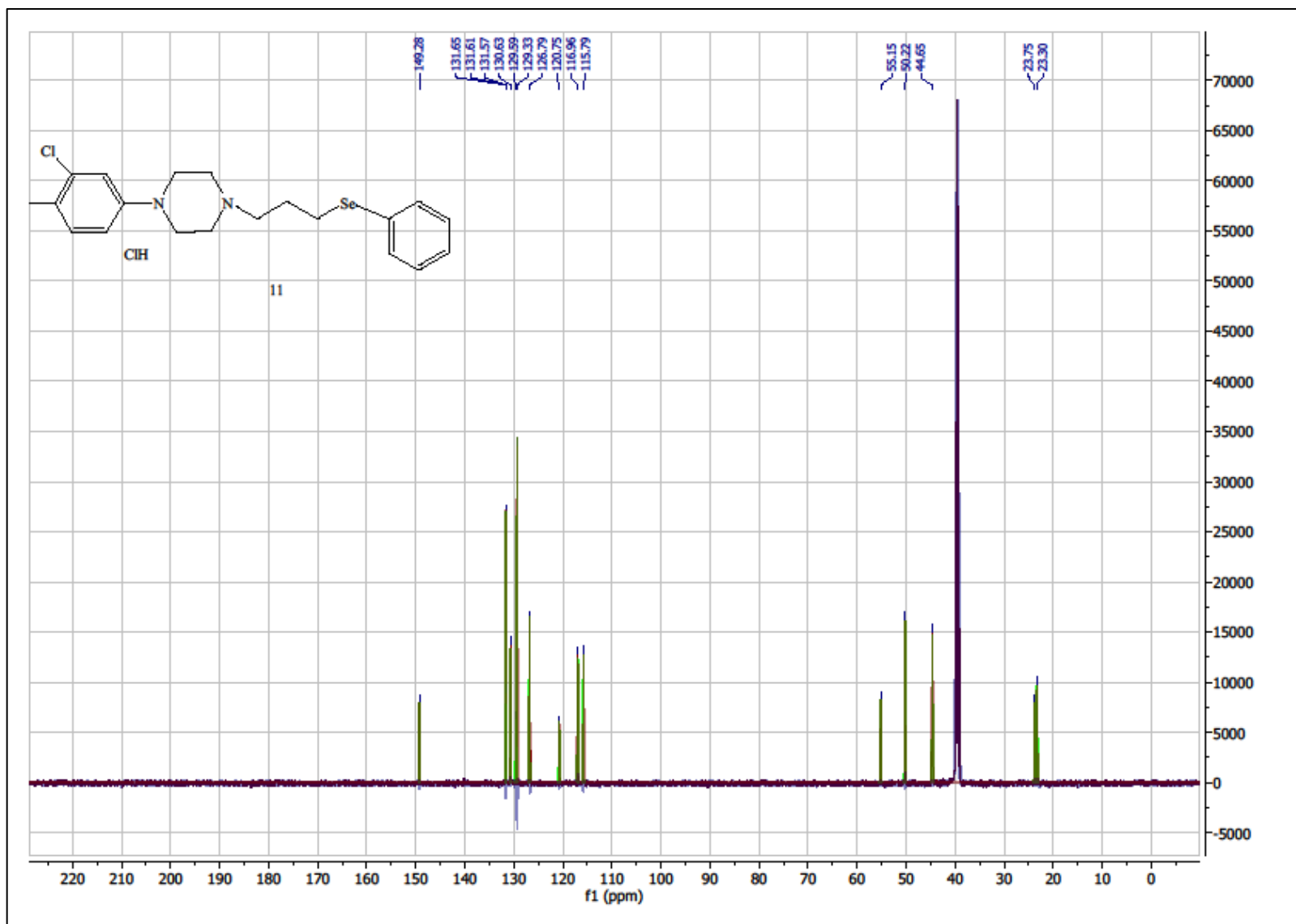
Compound 10, LC/MS⁺



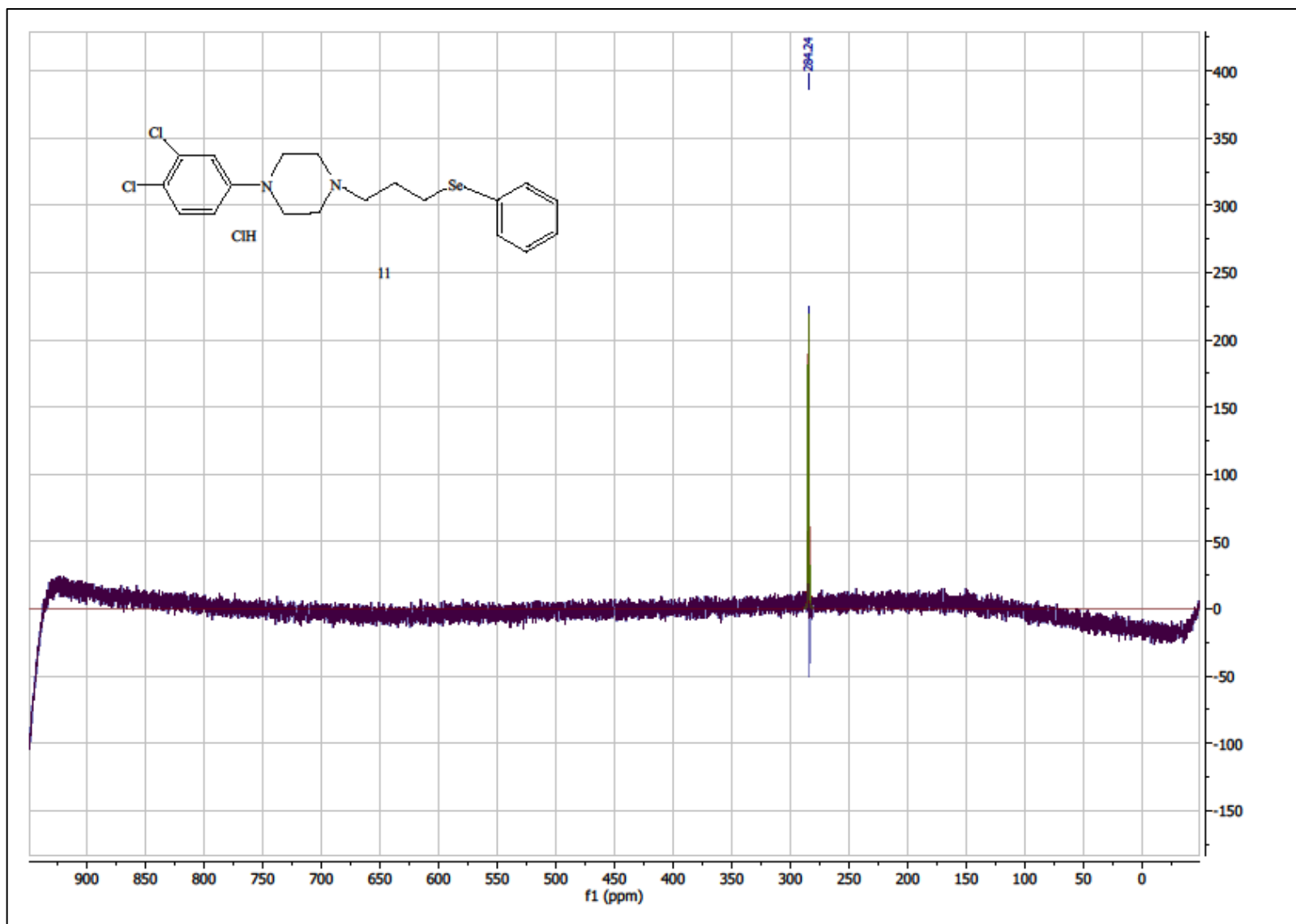
1-(3,4-dichlorophenyl)-4-(3-(phenylselanyl)propyl)piperazine hydrochloride (11), ¹H NMR (DMSO)



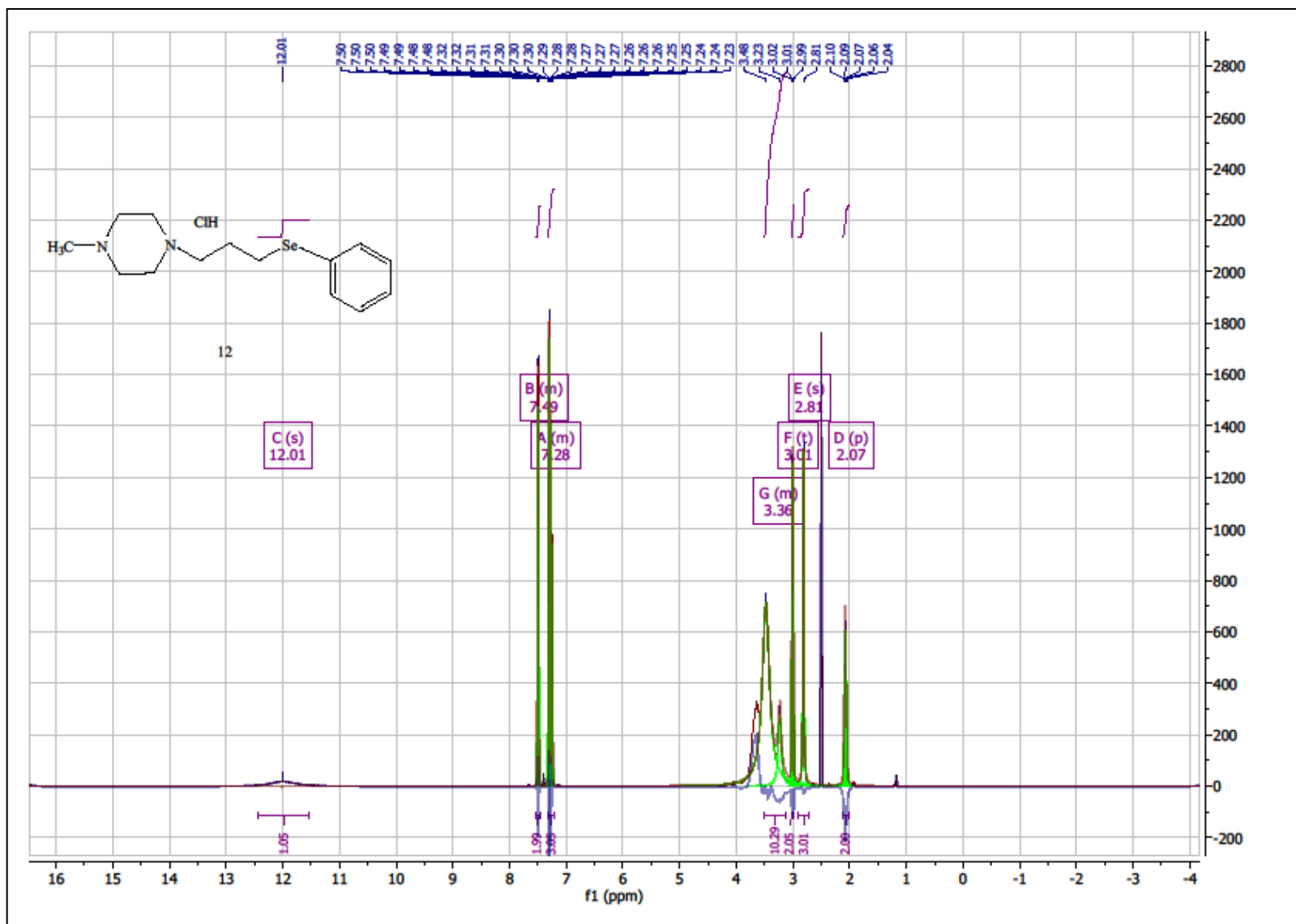
Compound **11**, ^{13}C NMR (DMSO)



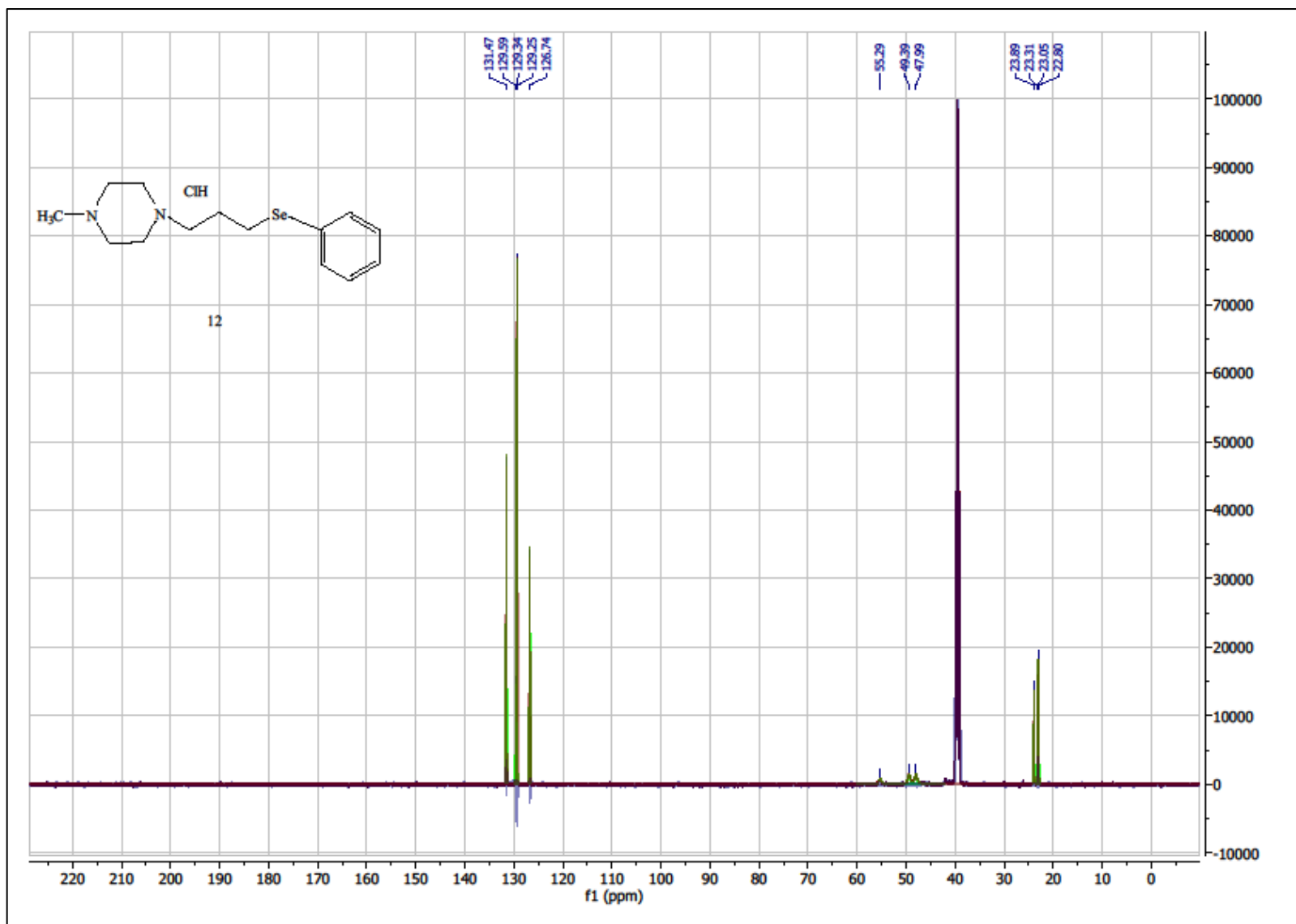
Compound **11**, ^{77}Se NMR (DMSO)



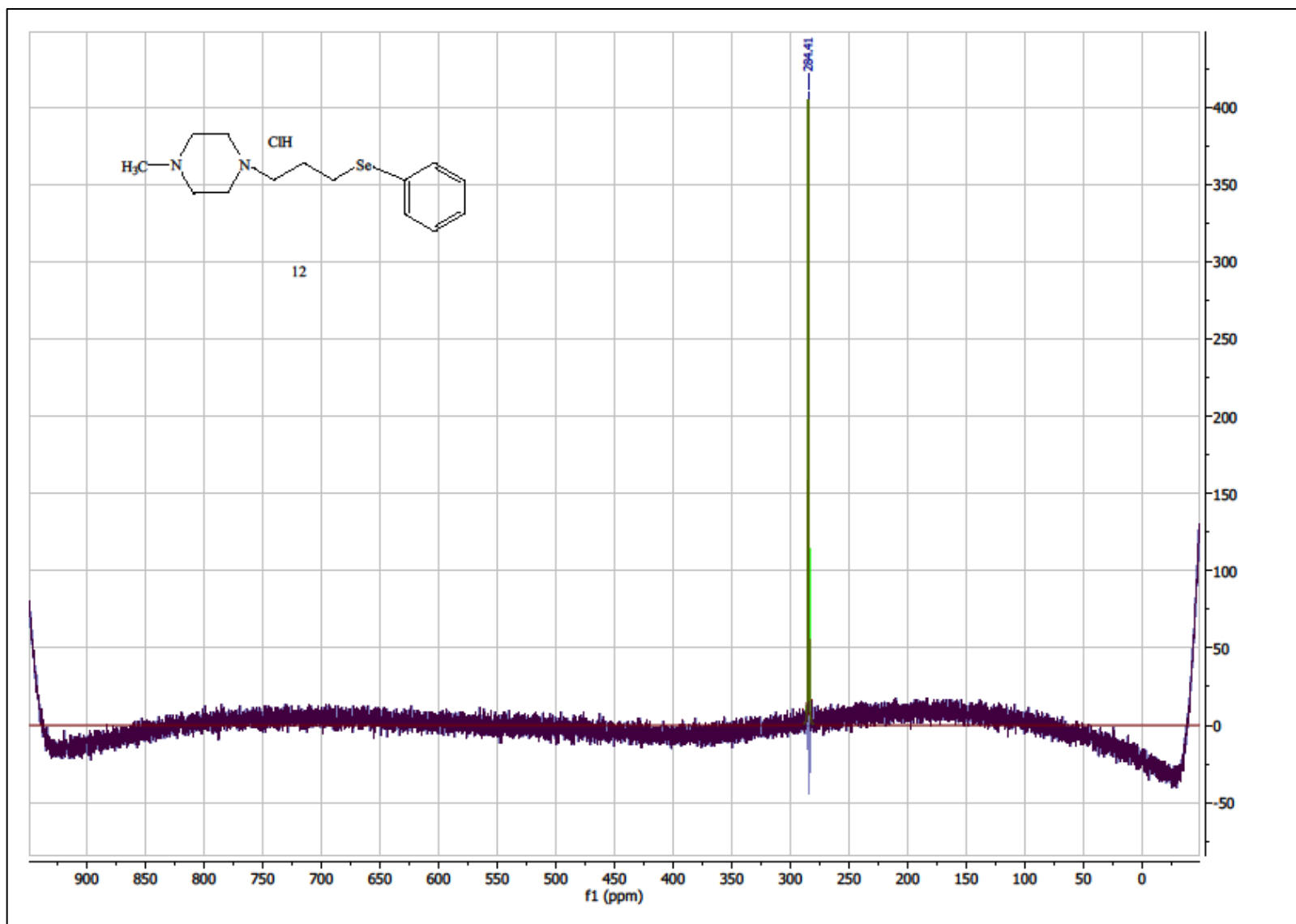
1-methyl-4-(3-(phenylselanyl)propyl)piperazine hydrochloride (12), ^1H NMR (DMSO)



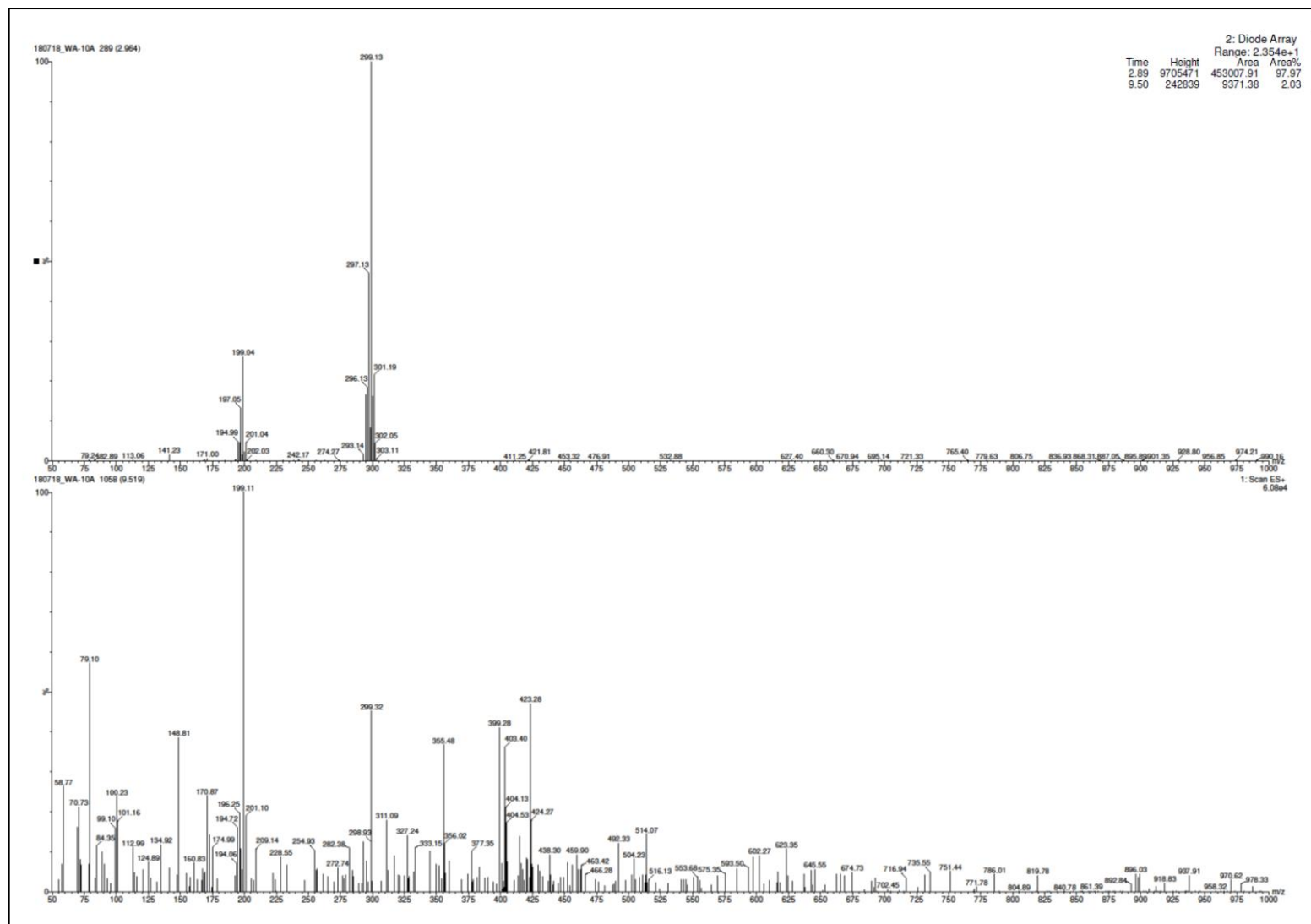
Compound 12, ^{13}C NMR (DMSO)



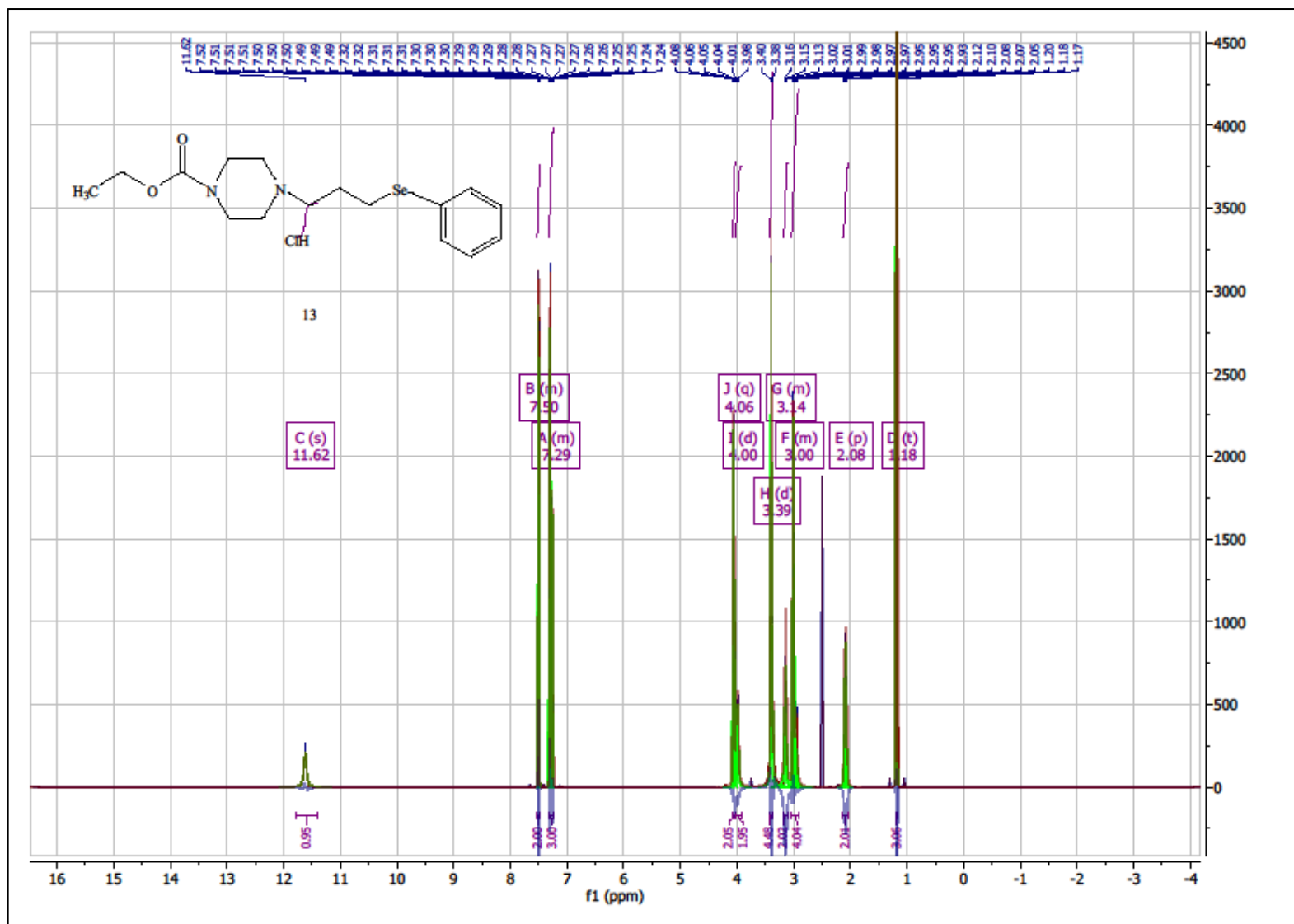
Compound **12**, ^{77}Se NMR (DMSO)



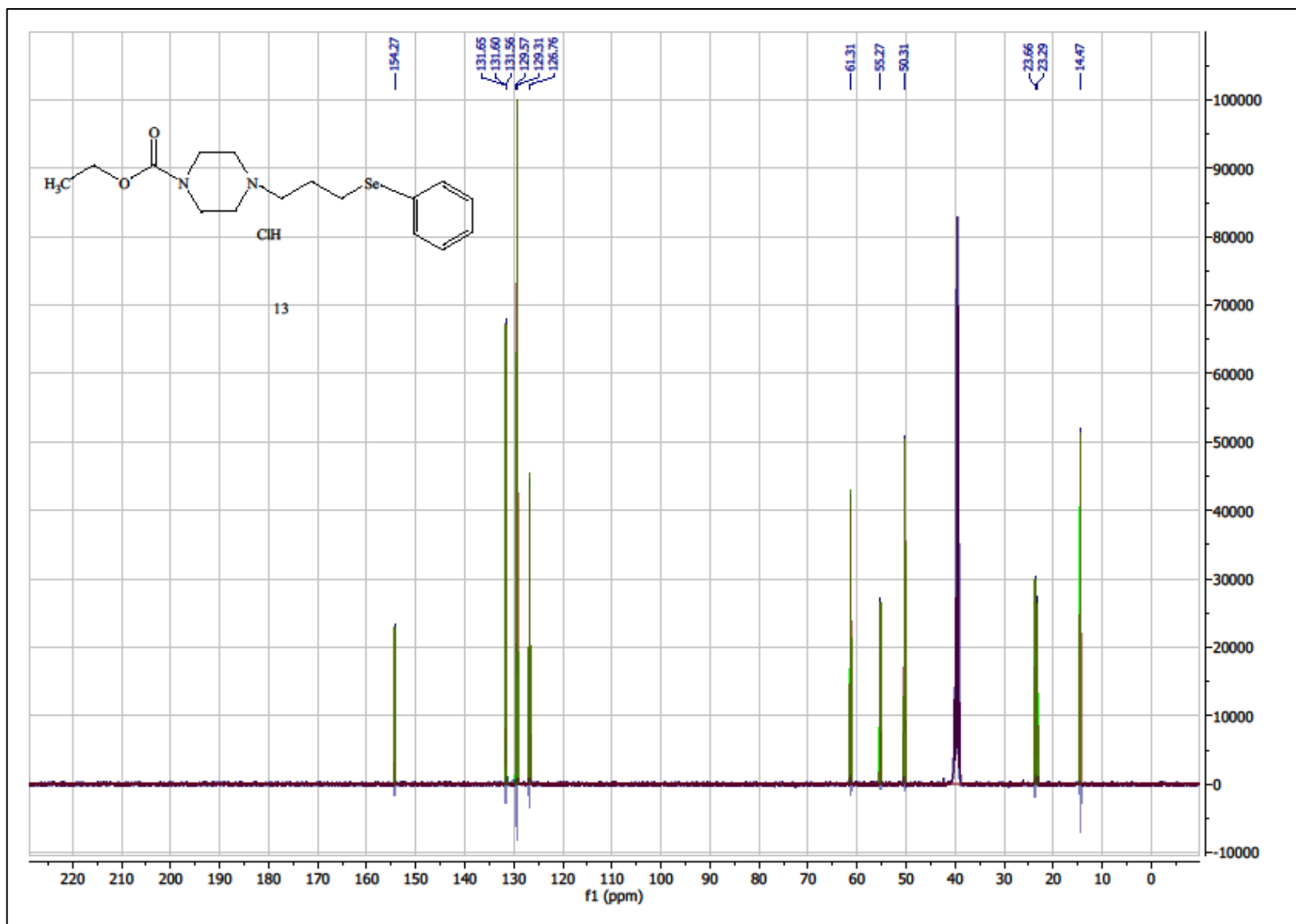
Compound 12, LC/MS+



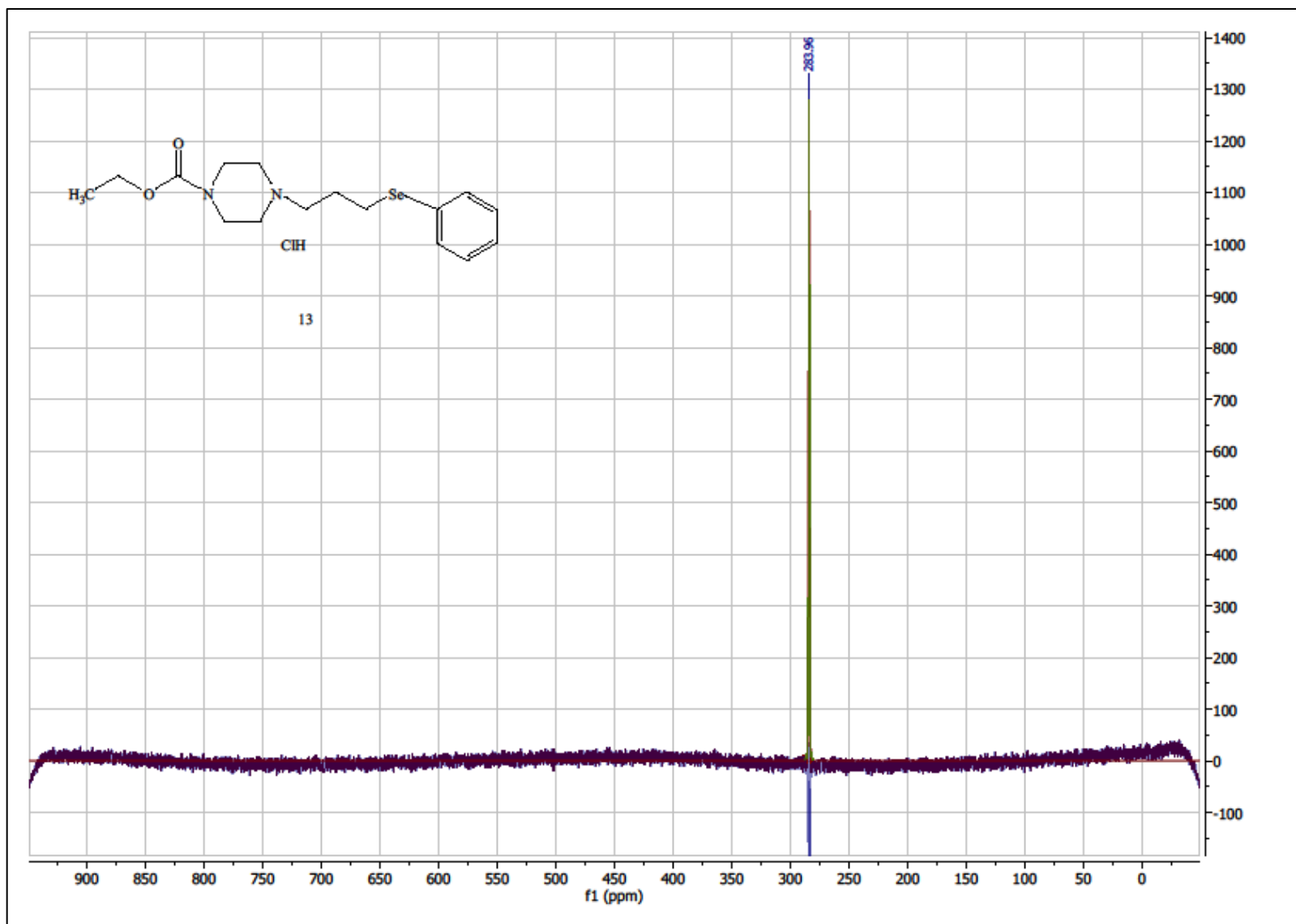
ethyl 4-(3-(phenylselanyl)propyl)piperazine-1-carboxylate hydrochloride (13), ¹H NMR (DMSO)



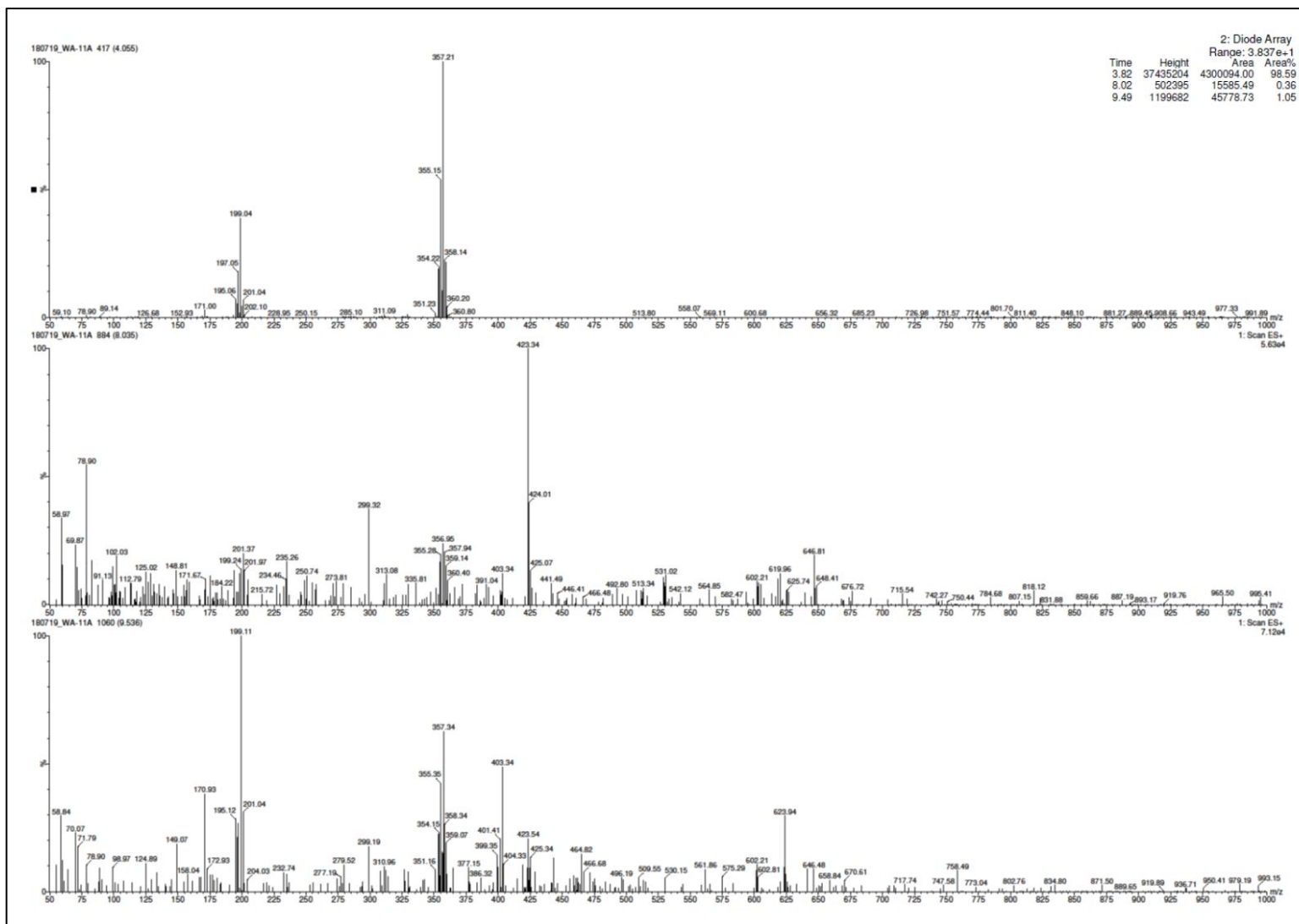
Compound **13**, ^{13}C NMR (DMSO)



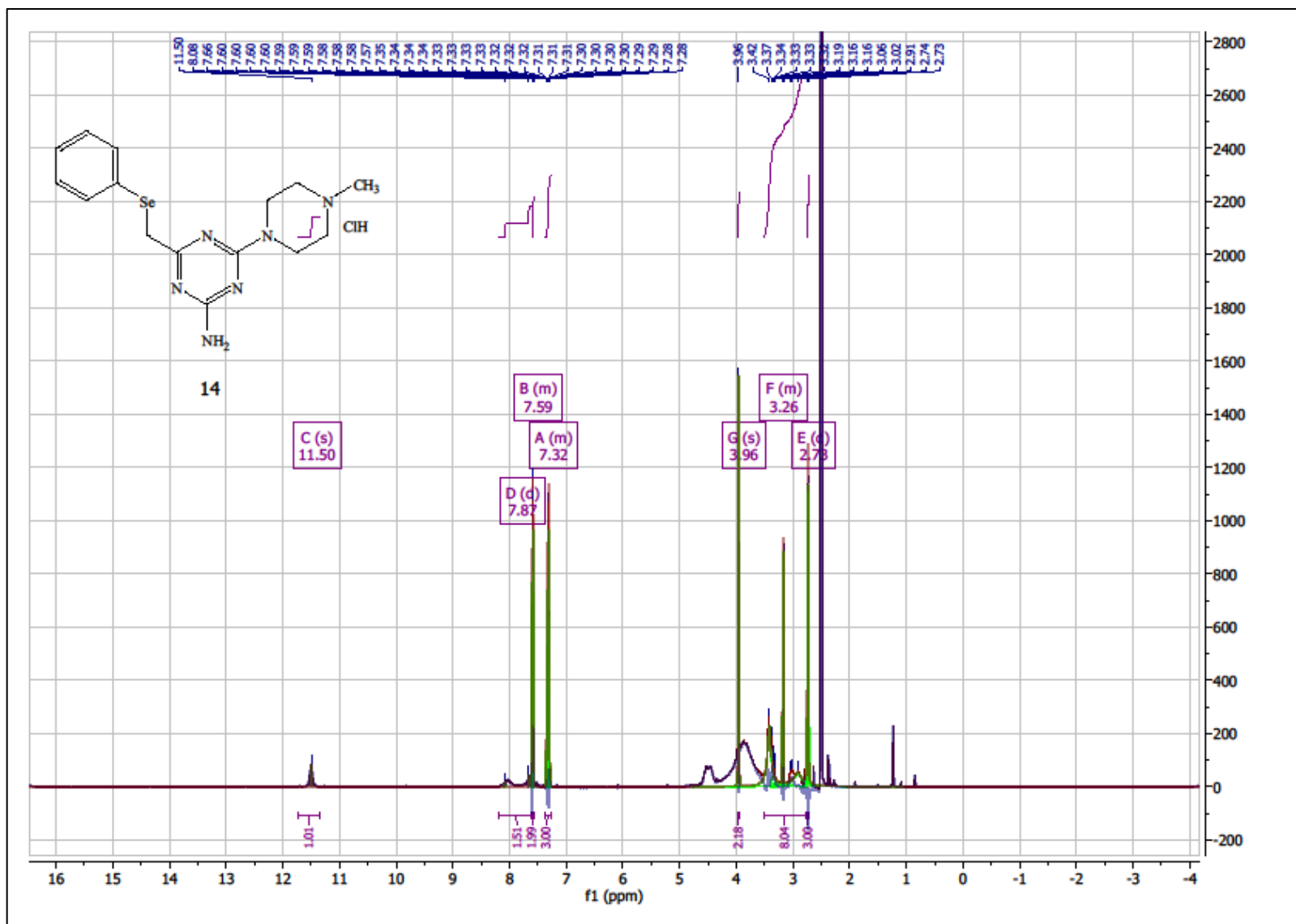
Compound **13**, ^{77}Se NMR (DMSO)



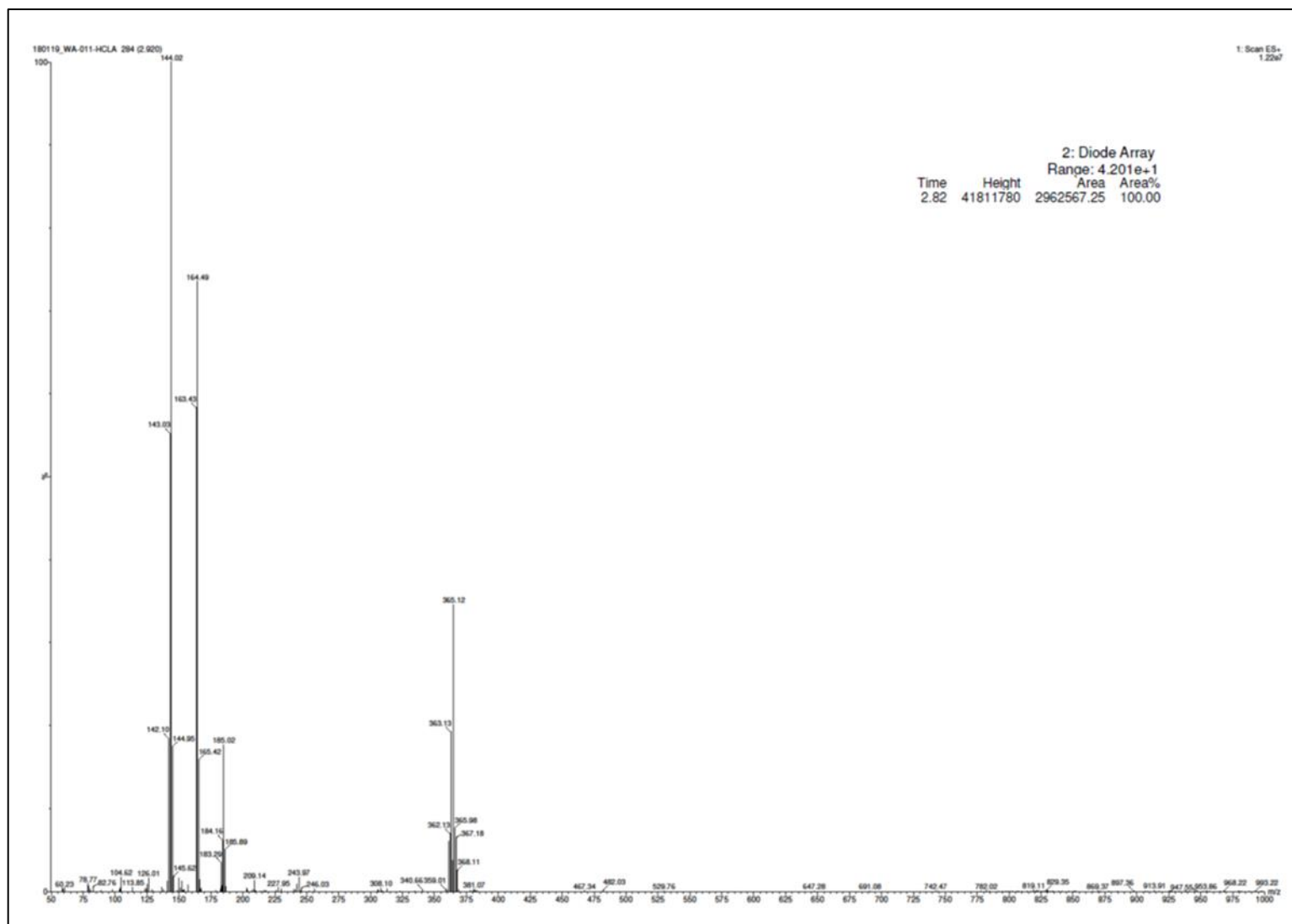
Compound 13, LC/MS+



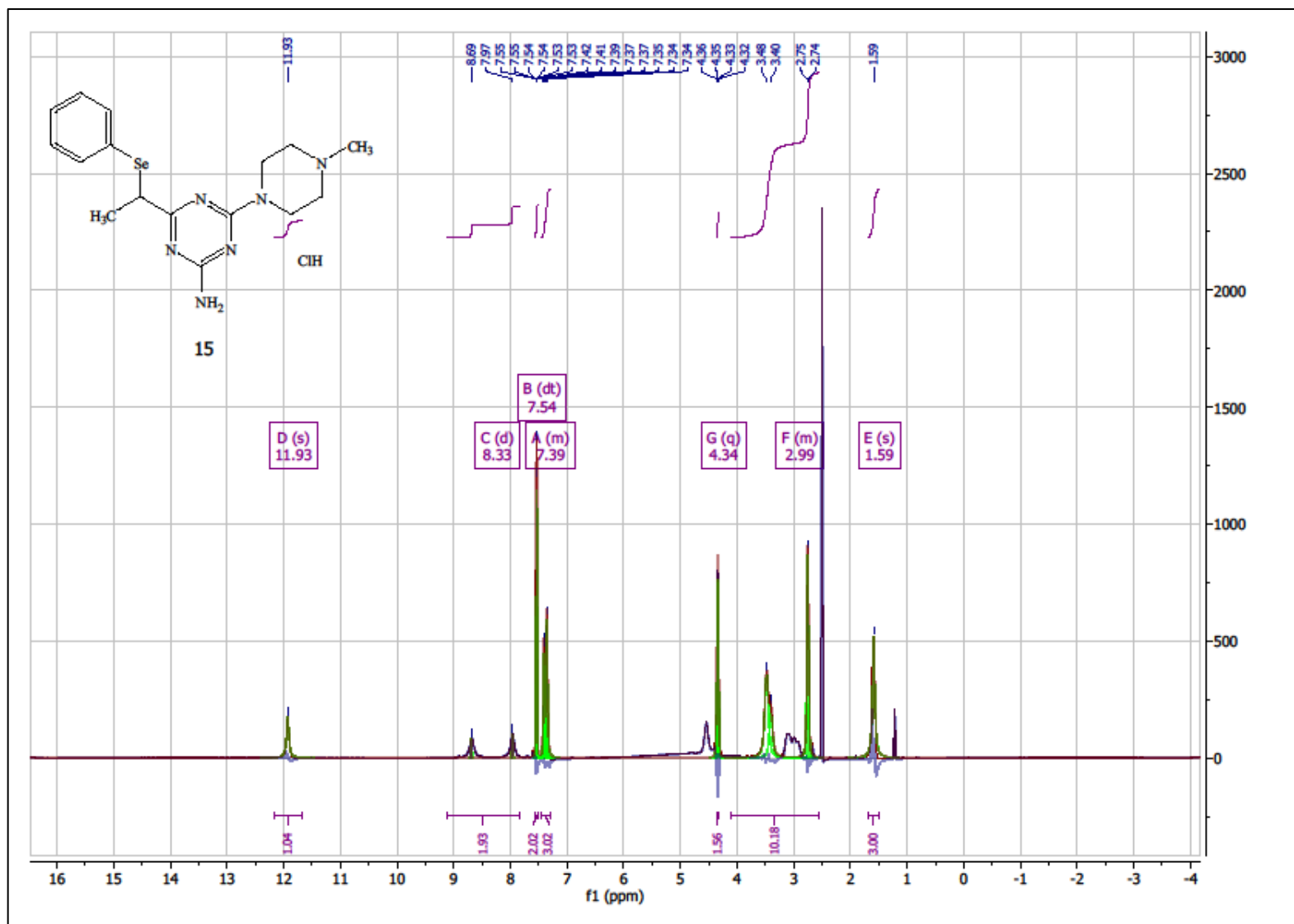
. 4-(4-methylpiperazin-1-yl)-6-((phenylselanyl)methyl)-1,3,5-triazin-2-amine hydrochloride (**14**), ¹H-NMR (DMSO)



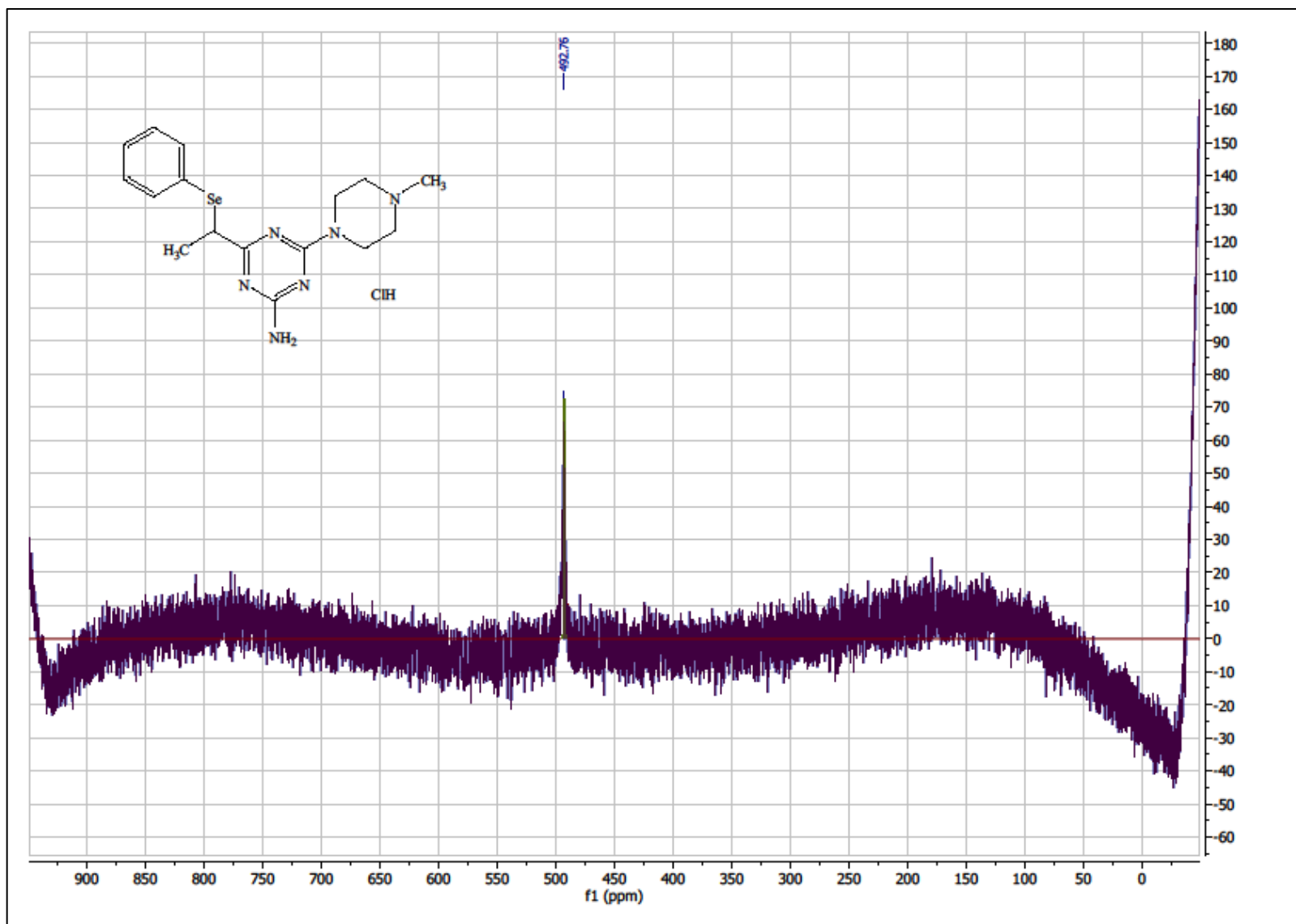
Compound 14, LC/MS⁺



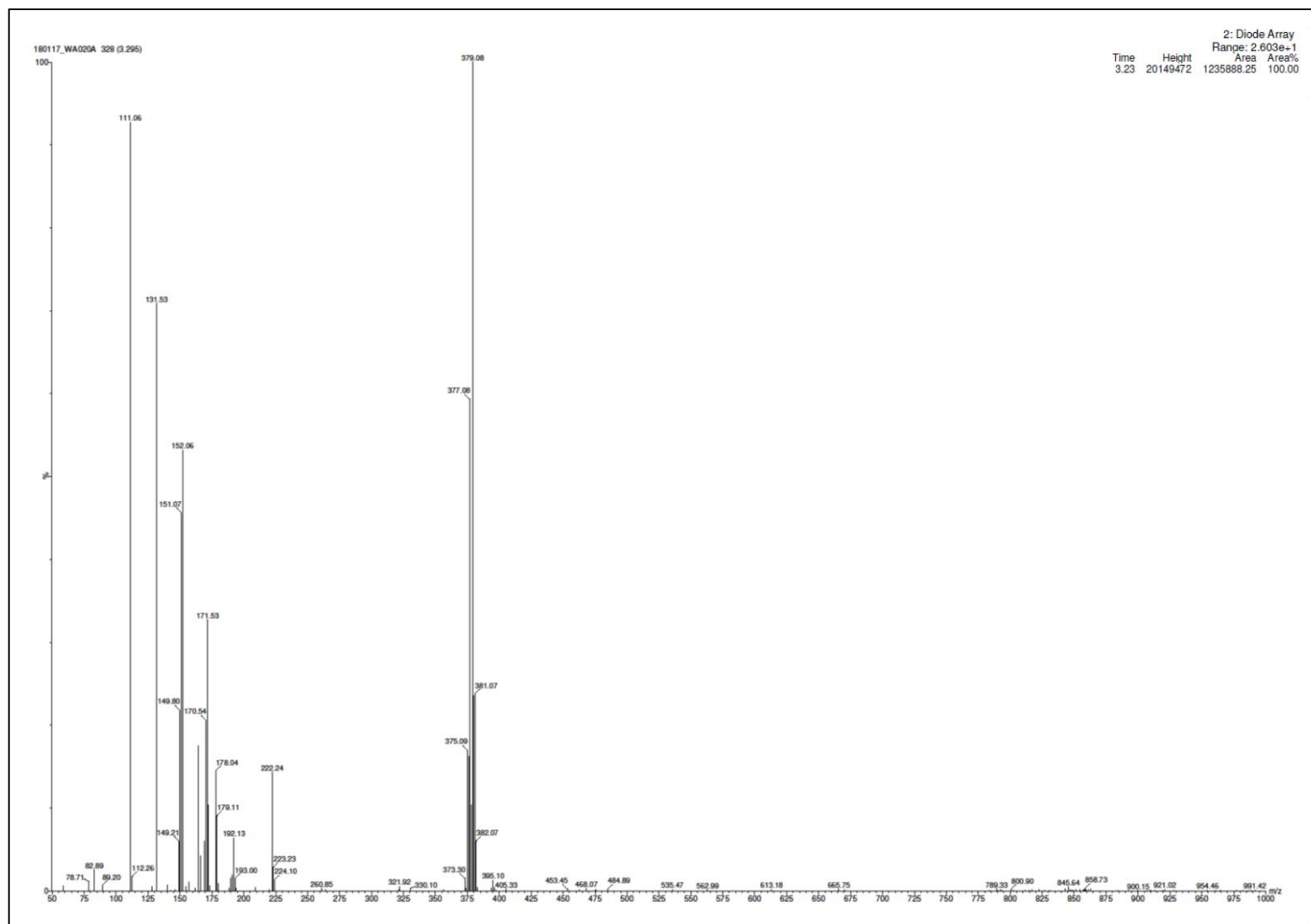
. 4-(4-methylpiperazin-1-yl)-6-(1-(phenylselanyl)ethyl)-1,3,5-triazin-2-amine hydrochloride (**15**), ¹H-NMR (DMSO)



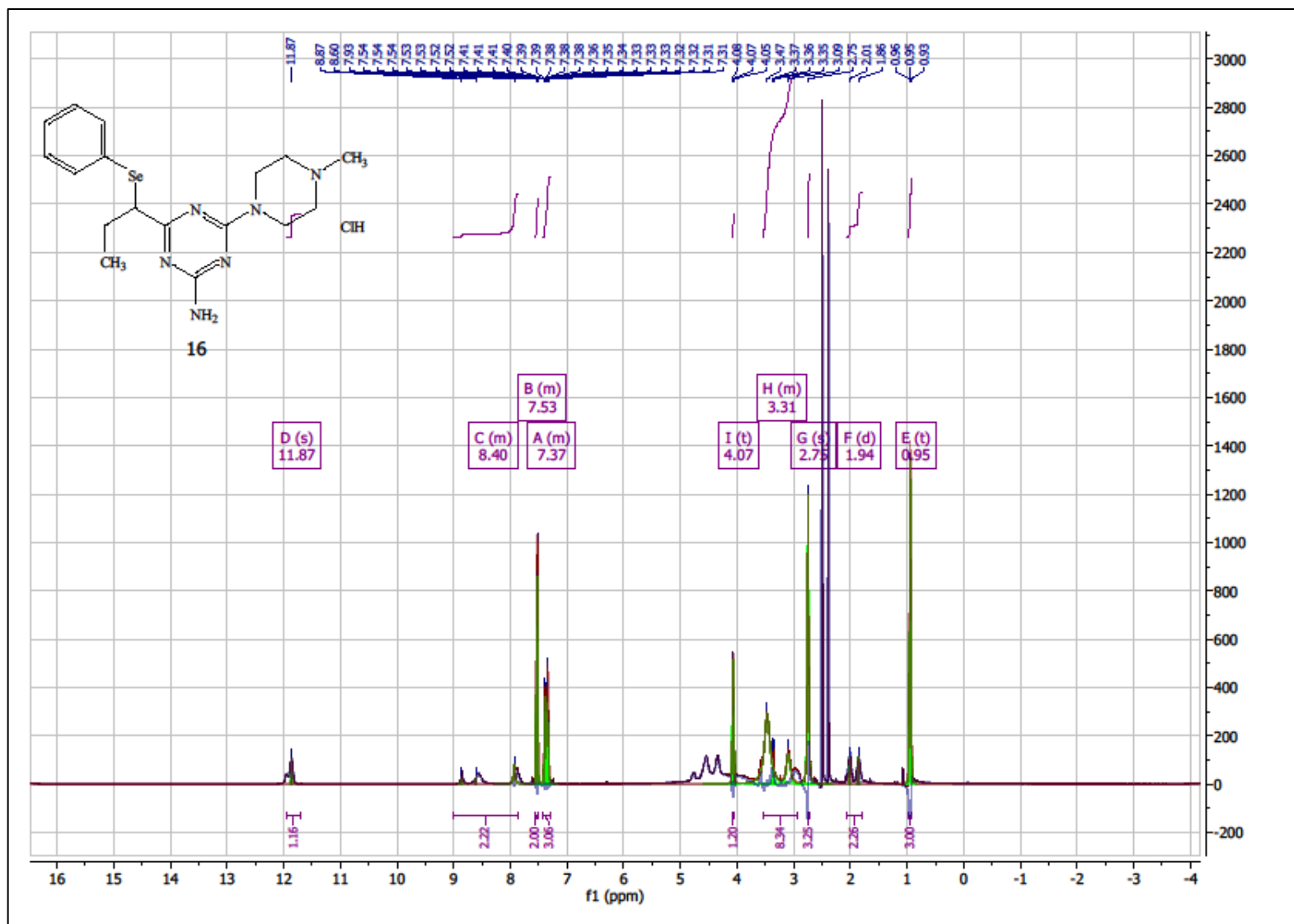
Compound 15, ^{77}Se -NMR (DMSO)



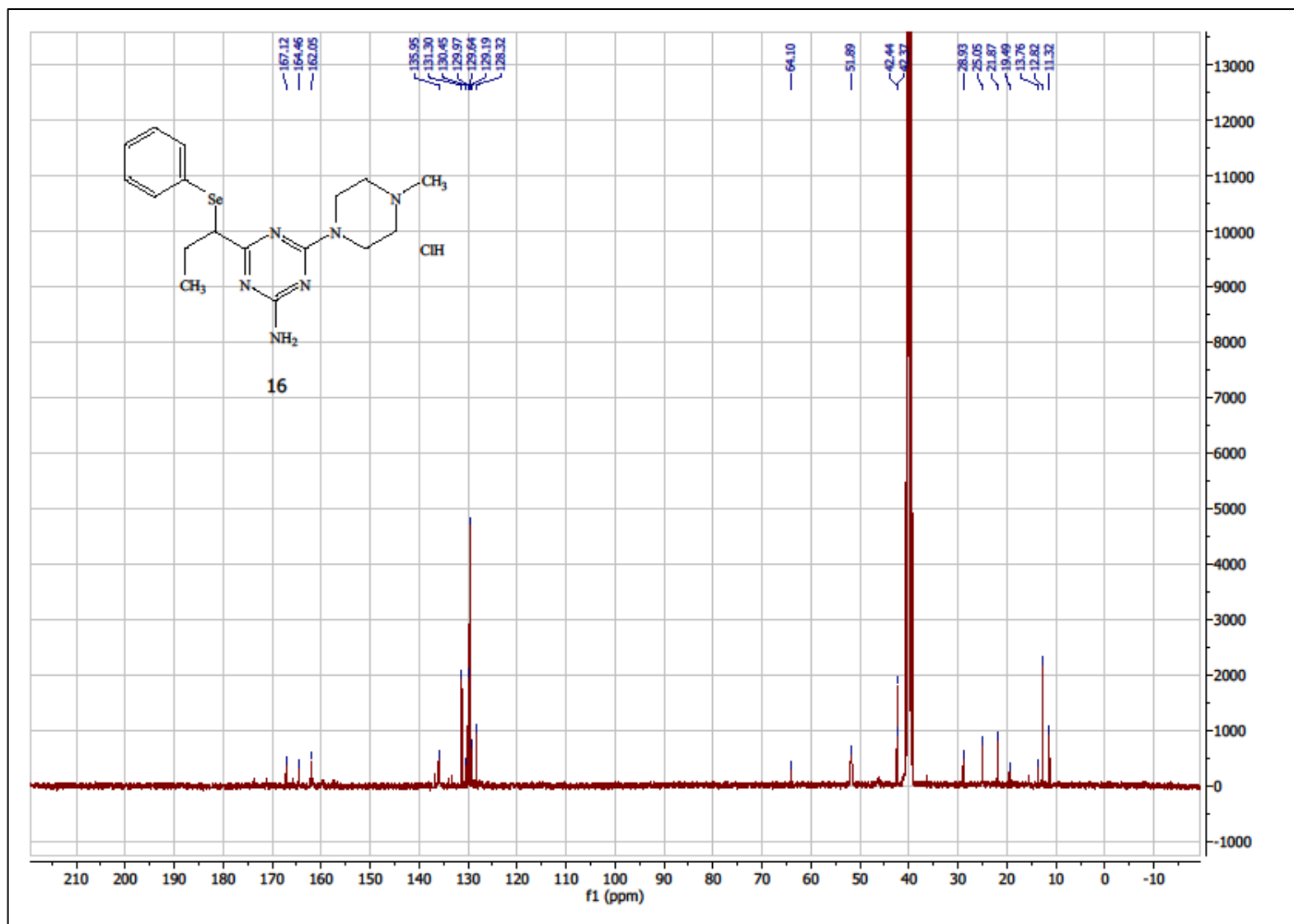
Compound 15, LC/MS⁺



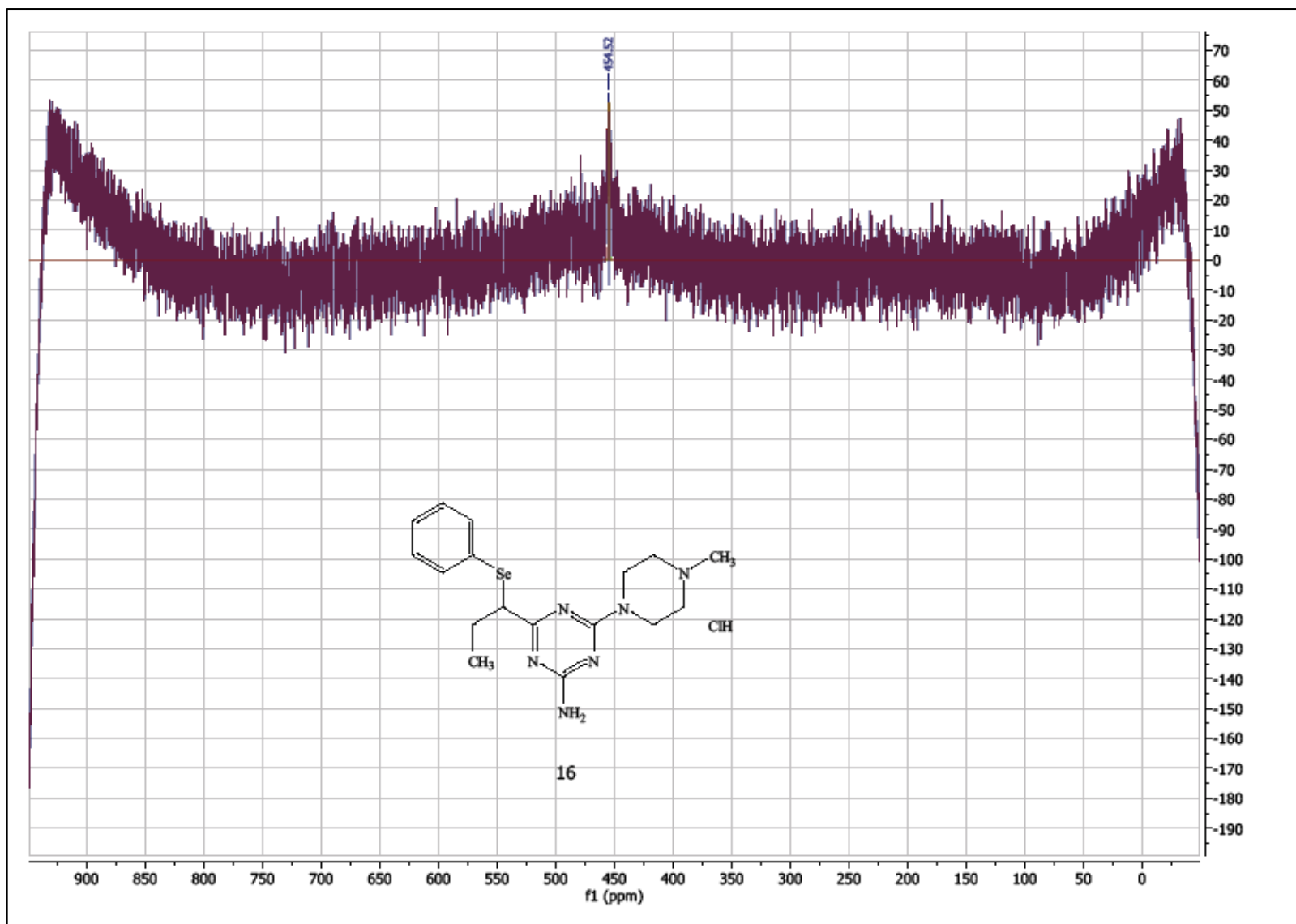
4-(4-methylpiperazin-1-yl)-6-(1-(phenylselanyl)propyl)-1,3,5-triazin-2-amine hydrochloride (**16**), ^1H NMR (DMSO- d_6)



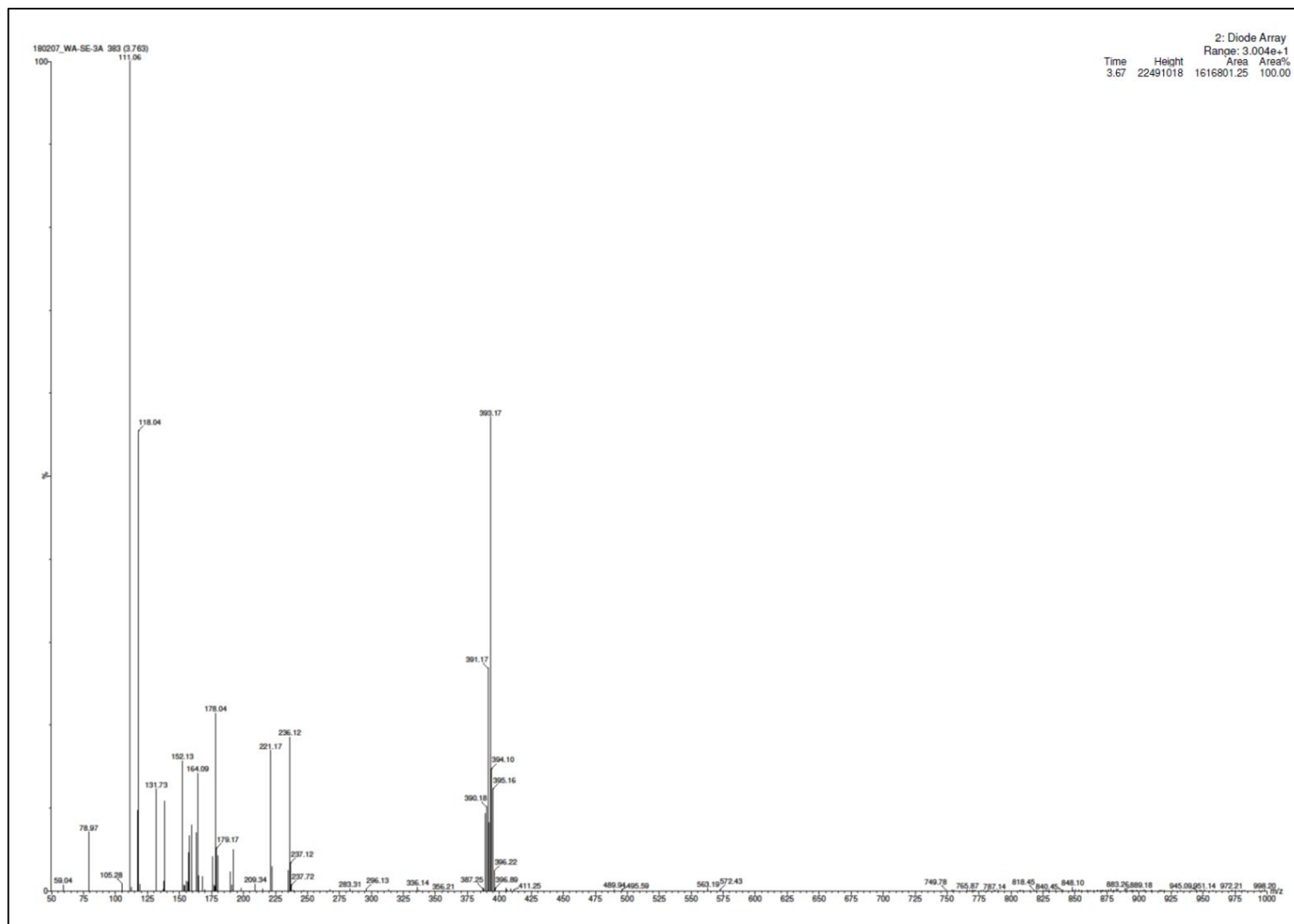
Compound 16, ^{13}C NMR (DMSO)



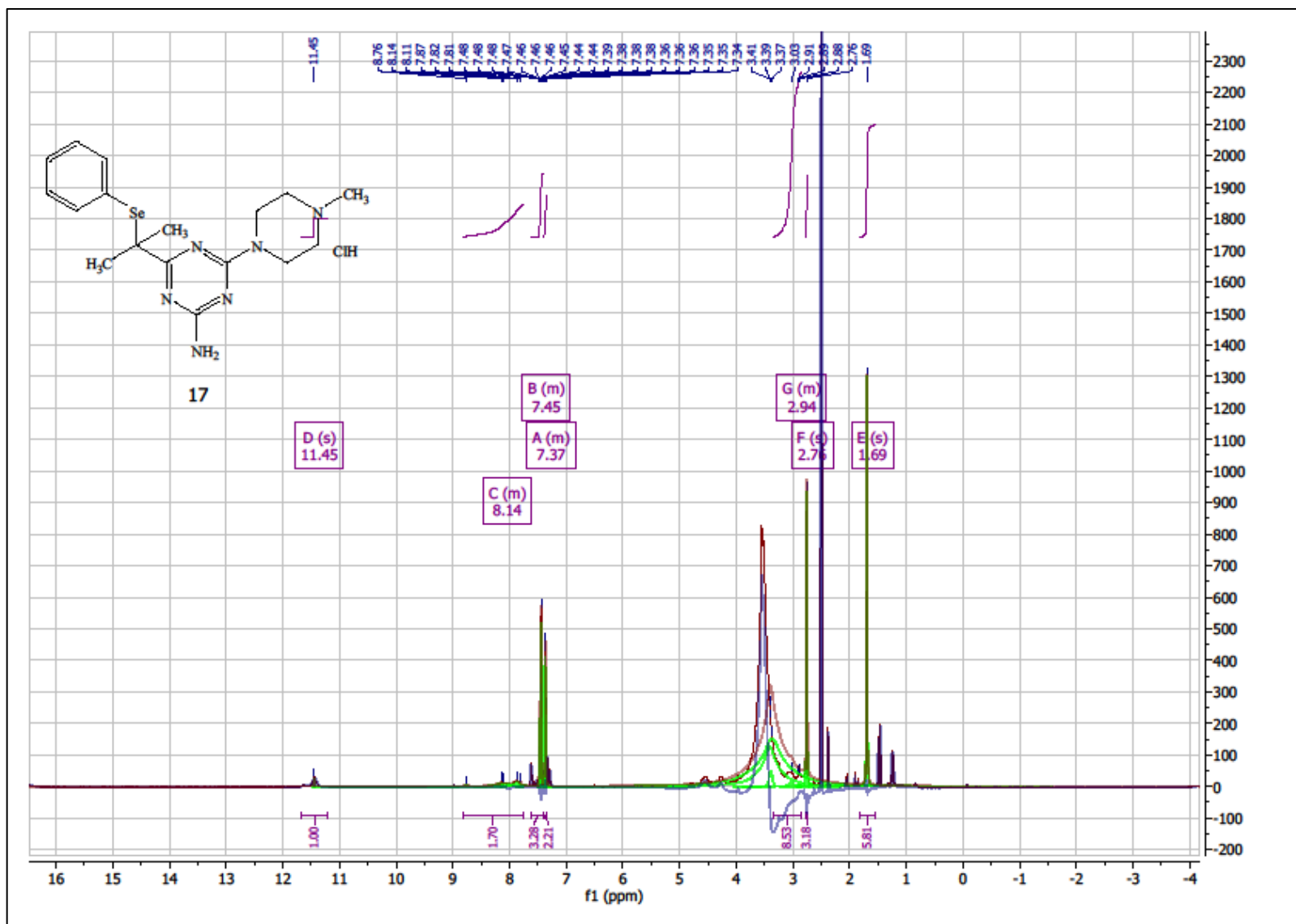
Compound **16**, ^{77}Se NMR (DMSO)



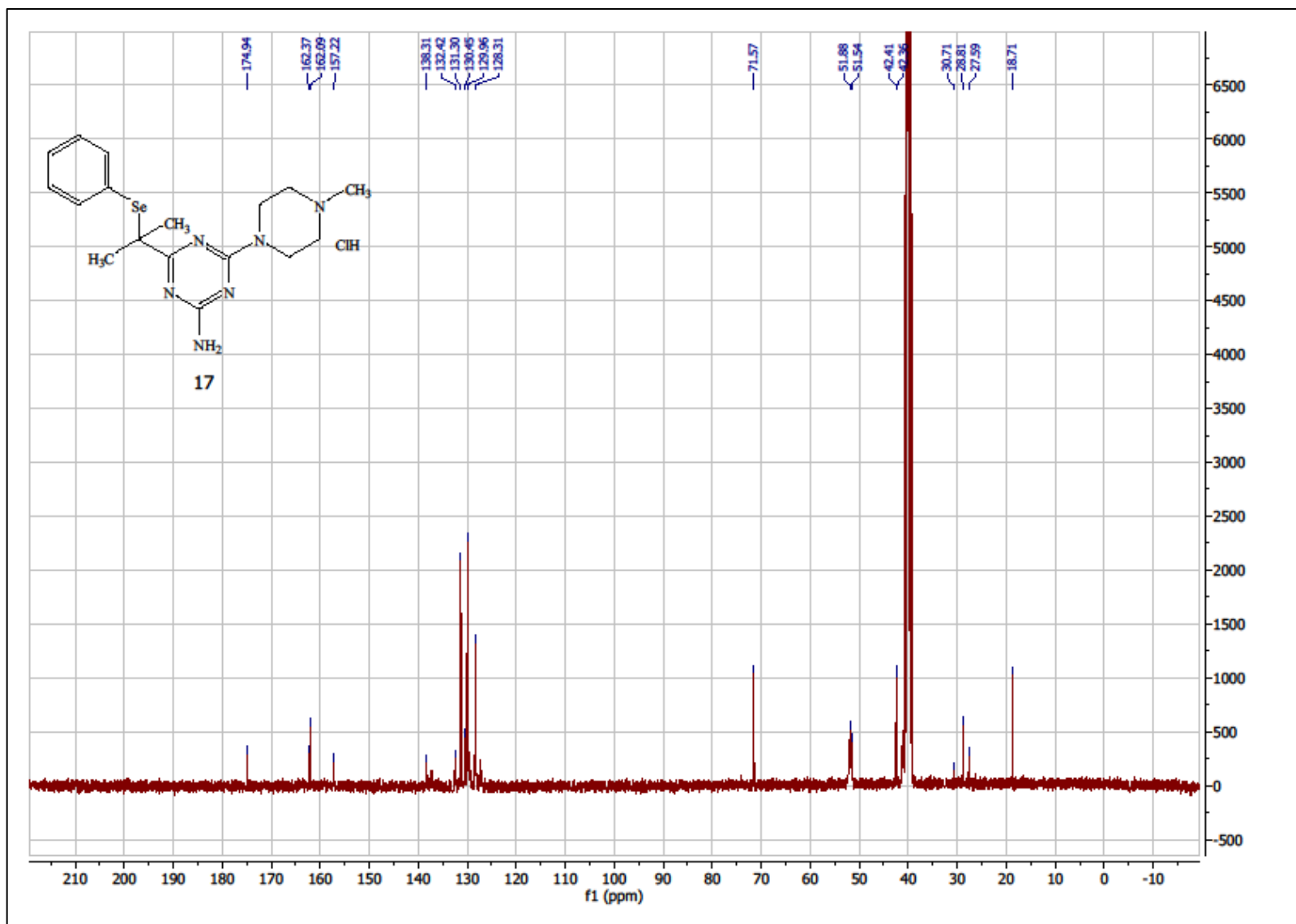
Compound 16, LC/MS⁺



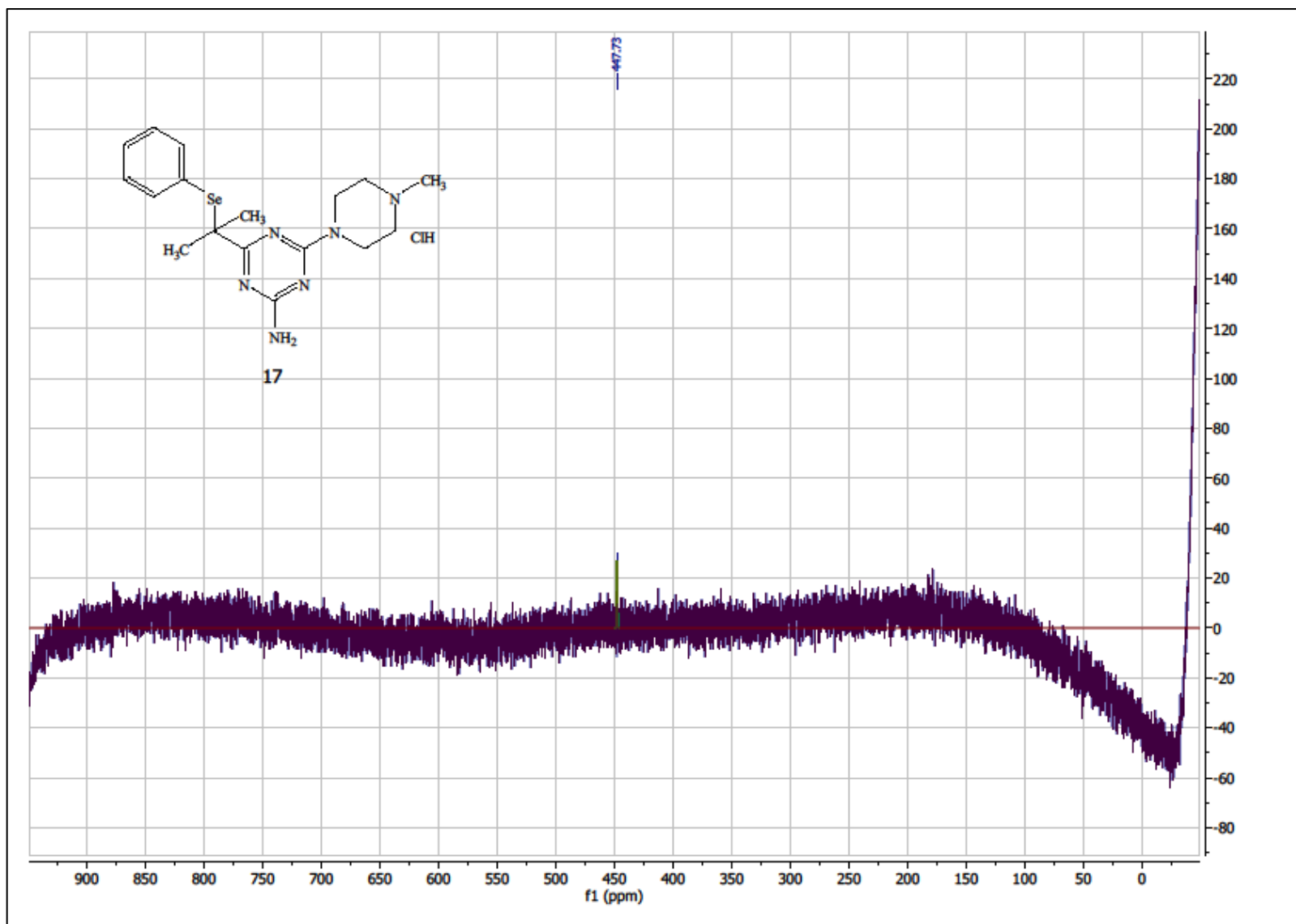
4-(4-methylpiperazin-1-yl)-6-(2-(phenylselanyl)propan-2-yl)-1,3,5-triazin-2-amine hydrochloride (**17**), ^1H NMR (DMSO)



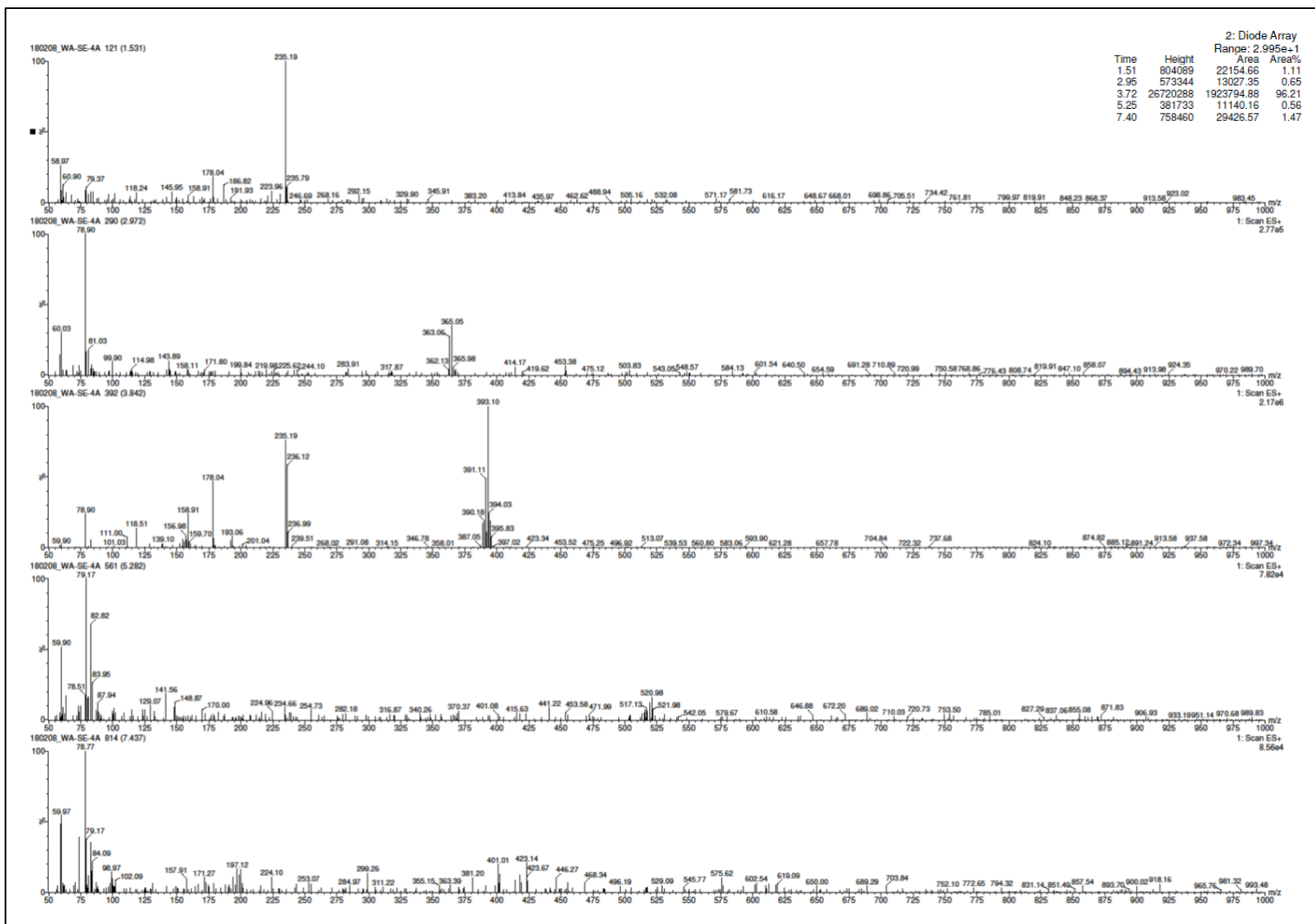
Compound 17, ^{13}C NMR (DMSO)



Compound 17, ^{77}Se NMR (DMSO)



Compound 17, LC/MS⁺



Lipophilicity

Lipophilicity of compounds (**5-17**) was estimated using standard RP-TLC method (Table S1).

Table S1: Lipophilicity data for the compounds **5- 17**

Compound	a	Sa	b=RM0	Sb	r2	Se	F
5	-4,1800	0,3096	4,2540	0,2487	0,9838	0,0490	182,3
6	-3,2600	0,3105	6,0540	0,2494	0,9927	0,0491	406,5
7	-3,6767	0,1588	3,8281	0,1088	0,9880	0,0592	578,4
8*	-2.3000	0.4254	2.7950	0.3226	0.9360	0.0951	29.23
9	-2.1600	0.1433	2,3853	0.1020	0.9701	0.0555	227.22
10	-2,5309	0,1386	2,5306	0,0927	0,9737	0,0727	333,3
11	-2,4727	0,0858	2,6218	0,0574	0,9893	0,0450	830,7
12	-0.7582	0.0337	1,0137	0.0225	0.9825	0.0177	506.31
13	-0.8660	0.0828	0,7903	0.0537	0.9398	0.9398	109.21
14	-2.1857	0.4085	2,6821	0.2998	0.8267	0.0017	28.63
15	-2.4200	0.3245	2,7421	0.2171	0.8607	0.1702	55.62
16	-1.4455	0.1108	1,7614	0.0741	0.9498	0.0581	170.13
17	-2.6509	0.2061	2,7467	0.1379	0.9484	0.1081	165.42

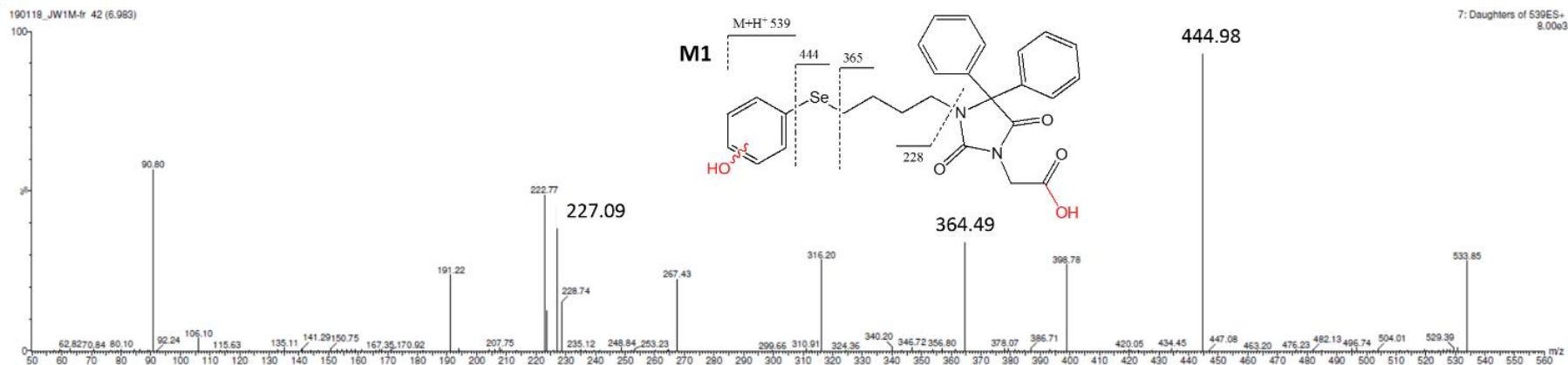
*Compound **8** tested in basic form, compounds **9-17** tested as hydrochlorides, compounds **5-7** do not have protonable centres

Retention parameters for the compounds were designated and analysed. Stationary phase RP-18 and mixtures of water/methanol in the variable proportions of organic modifier (from 40 to 90%) as a mobile phase were used. In all cases, calculated values of R_F corresponding to particular substances increased with increases in the percentage of the organic modifier in the mobile phase. The highest R_F values were obtained in water/methanol mobile phases (1:9, v/v) for all compounds. Substances **5** and **6** (at methanol concentration from 40 to 65%) and substance **7** (at methanol up to 45%) were retained at the start line; this could be explained by the highest affinity to the stationary phase and lower solubility in water solutions.

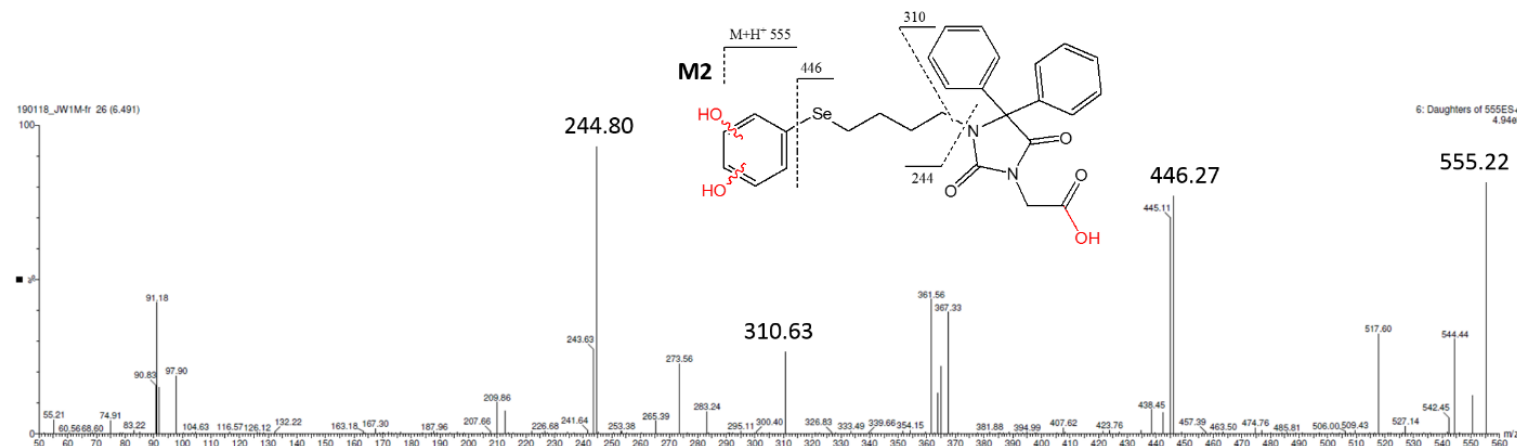
R_M values were calculated from the obtained R_F data. It was found that the R_M parameters decreased linearly with increasing amounts of the organic modifier (methanol) in the tested mobile phases. The determined regression coefficients (r^2) for all compounds were higher than 0.97. On the basis of the linear relationship between R_M values and the volume fraction of methanol, values of R_{M0} in the analysed systems corresponding to 100% of water were obtained by extrapolation.

Metabolic stability

A



B



C

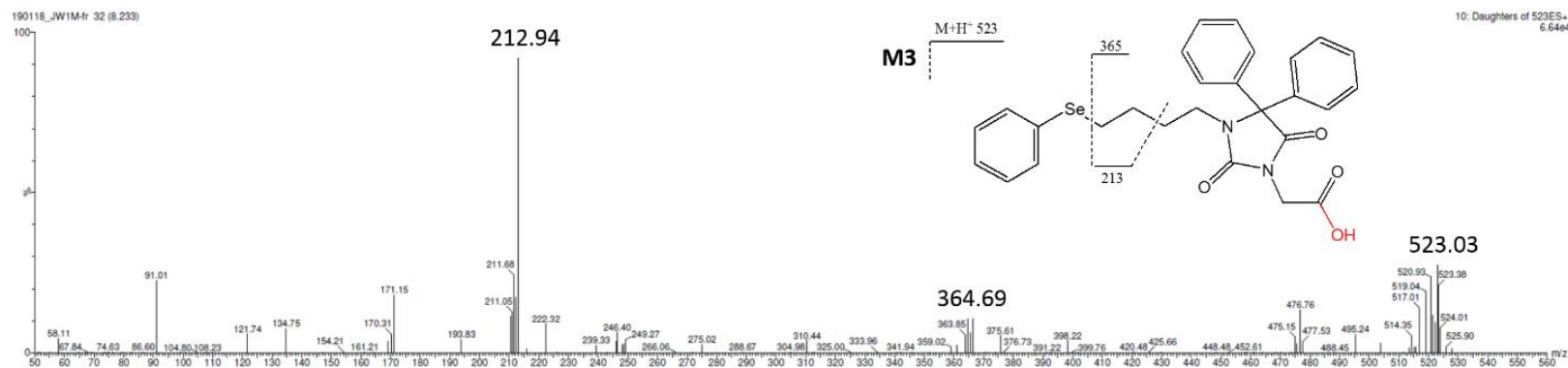
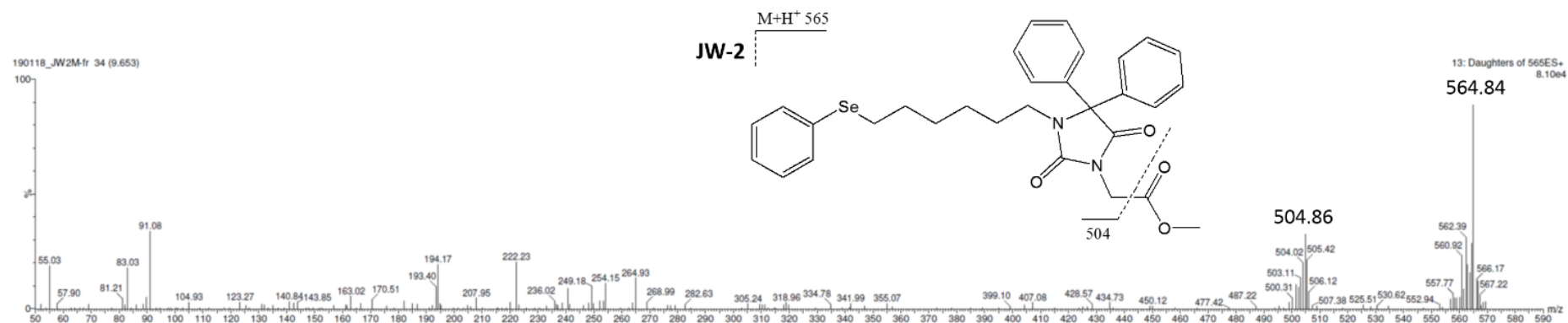
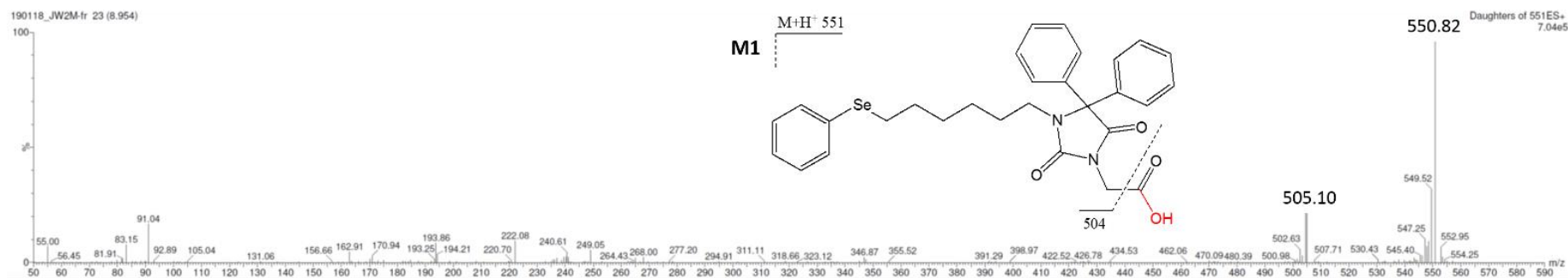
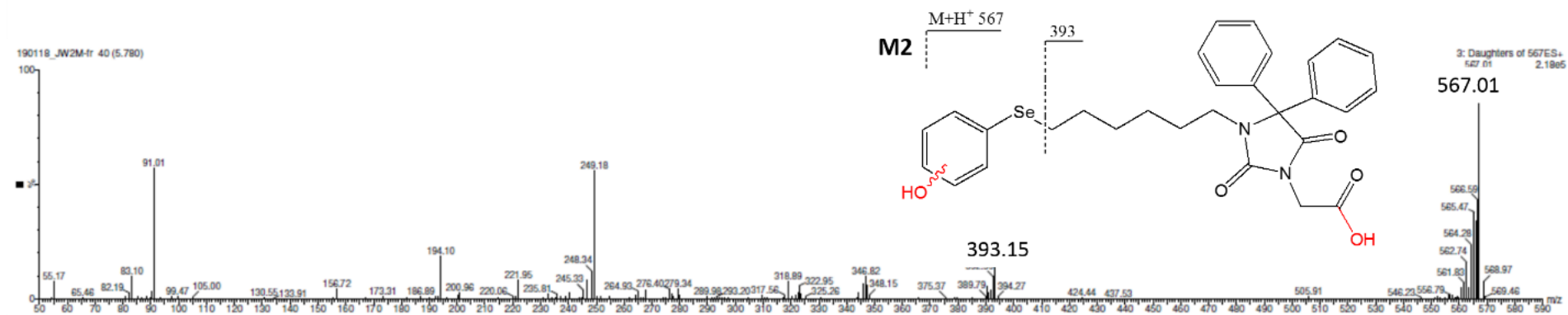


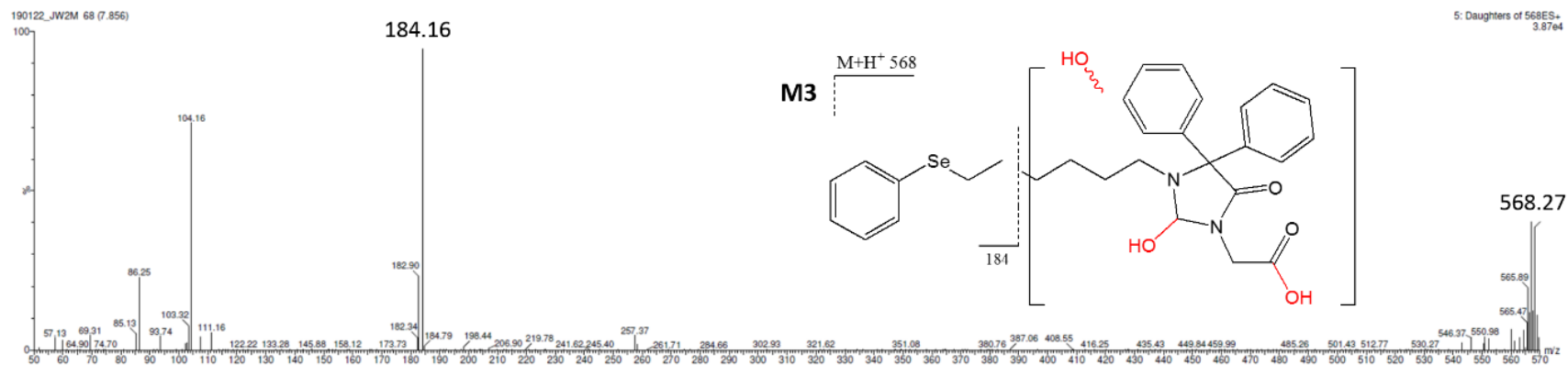
Figure S1 Ion fragment analyses and the most probable structures of compound's **5** metabolites M1 (A), M2 (B) and M3 (C).

A



B**C**

D



E

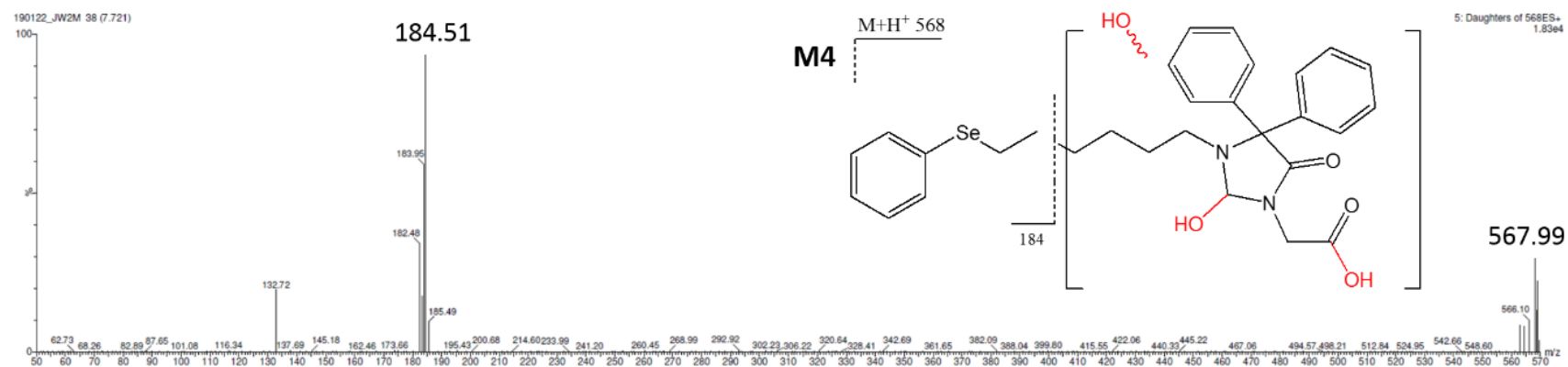
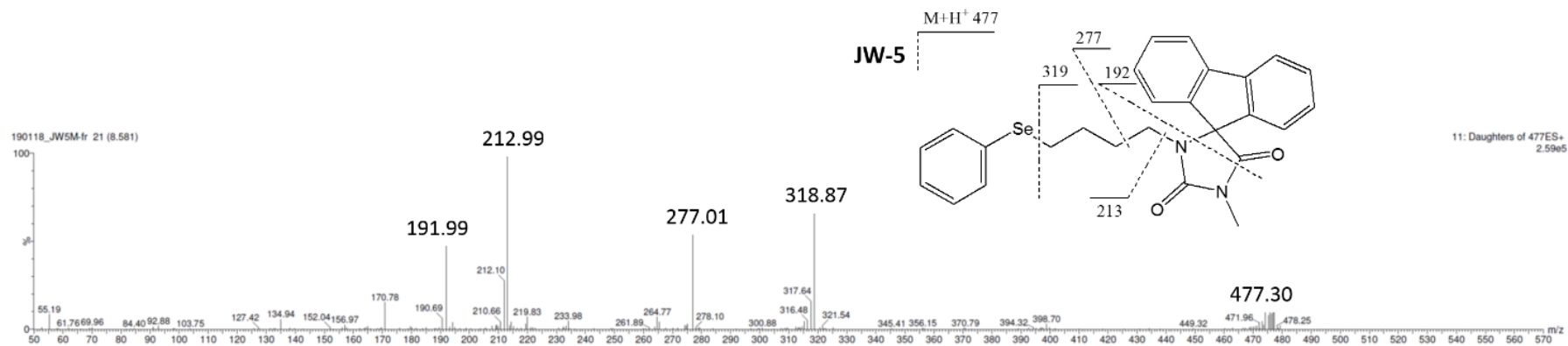
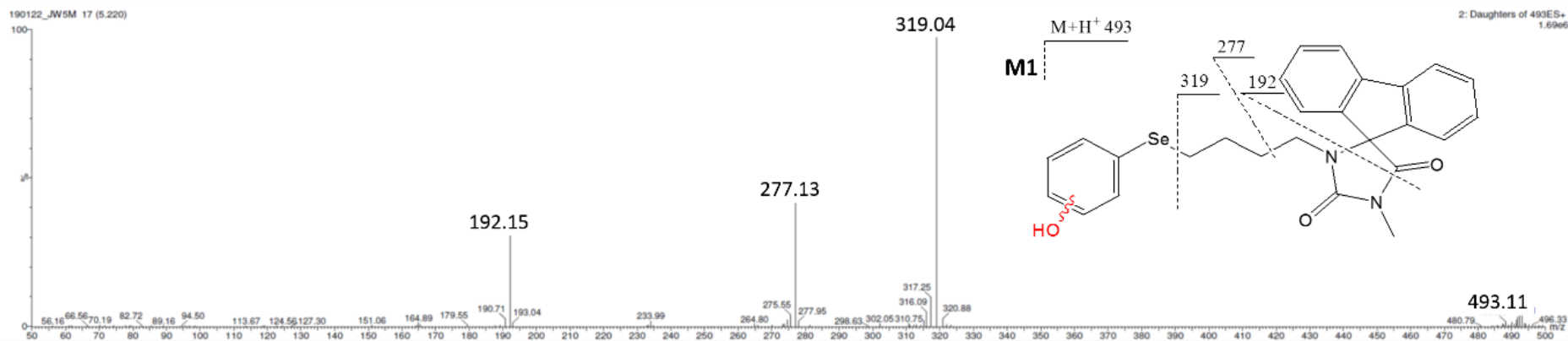


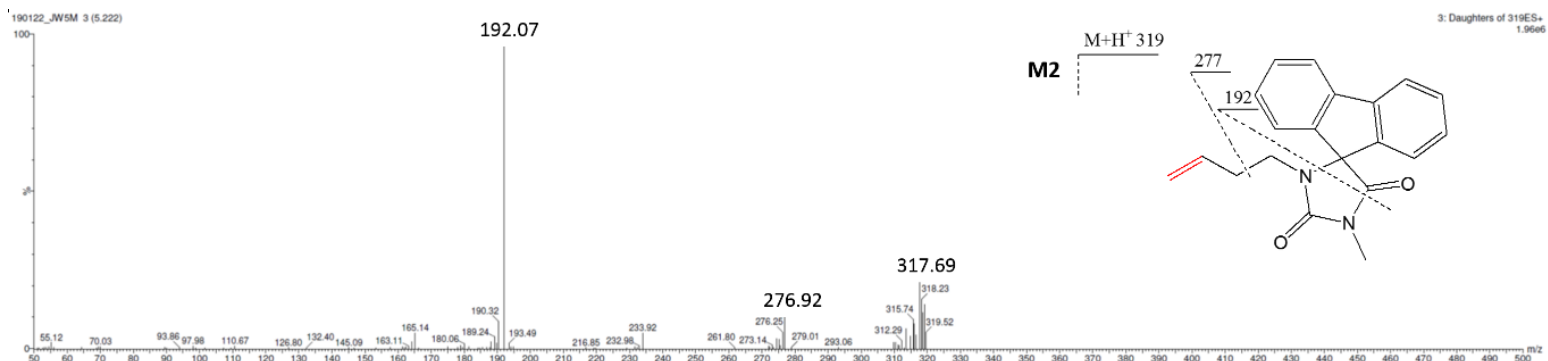
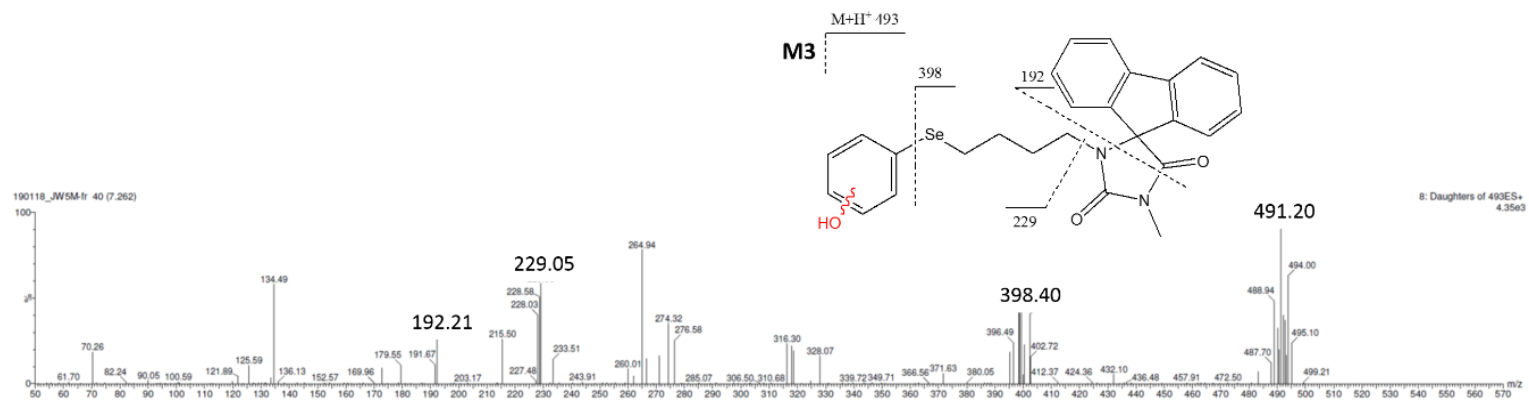
Figure S2 Ion fragment analyses of compound **6** (A) and its metabolites M1 (B), M2 (C) and M3 (D).

A

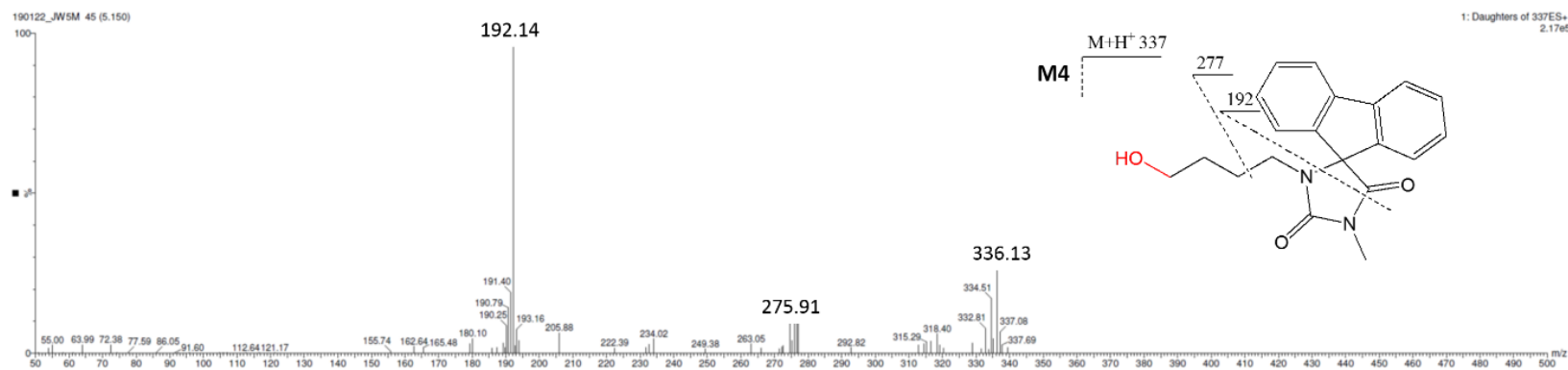


B



C**D**

E



F

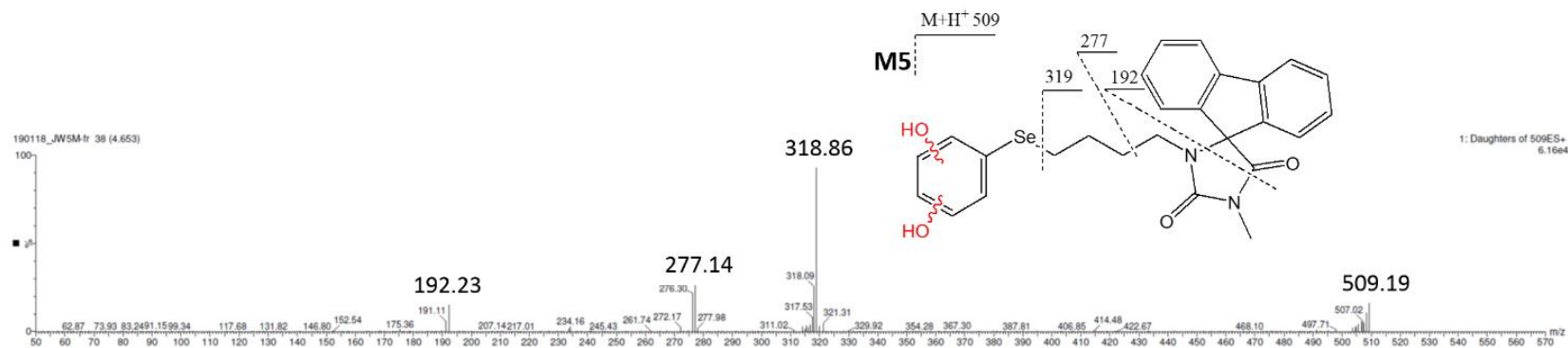


Figure S3 Ion fragment analyses of compound **7** (A) and its metabolites M1 (B), M2 (C), M3 (D), M4 (E) and M5 (F)

References:

- [1] S. Paudel, S. Acharya, K.M. Kim, S.H. Cheon, Design, synthesis, and biological evaluation of arylpiperazine-benzylpiperidines with dual serotonin and norepinephrine reuptake inhibitory activities, *Bioorg Med Chem*, 24 (2016) 2137-2145.
- [2] S.-J. Zhu, H.-Z. Ying, Y. Wu, N. Qiu, T. Liu, B. Yang, X.-W. Dong, Y.-Z. Hu, Design, synthesis and biological evaluation of novel podophyllotoxin derivatives bearing 4 β -disulfide/trisulfide bond as cytotoxic agents, *RSC Advances*, 5 (2015) 103172-103183.
- [3] P. Bernardelli, A. Denis, E. Lorthiois, H. Jacobelli, F. Vergne, D. Serradeil, F. Rousseau, A. Cronin, M. Kemp, Preparation of substituted phenols as histamine H3 ligands, in, Warner-Lambert Company LLC, USA . 2005, pp. 126 pp.
- [4] S. Torii, T. Inokuchi, G. Asanuma, N. Sayo, H. Tanaka, A Direct Phenylselenenylation of Alkyl Halides, Alkenyl Sulfonates, and Epoxides by an Electroreduction of Diphenyl Diselenide, *Chemistry Letters*, 9 (1980) 867-868.
- [5] F. Malihi, D.L. Clive, C.C. Chang, Minaruzzaman, Synthetic studies on CP-225,917 and CP-263,114: access to advanced tetracyclic systems by intramolecular conjugate displacement and [2,3]-Wittig rearrangement, *J Org Chem*, 78 (2013) 996-1013.
- [6] D.L. Clive, Z. Li, M. Yu, Intramolecular conjugate displacement: a general route to hexahydroquinolizines, hexahydroindolizines, and related [m,n,0]-bicyclic structures with nitrogen at a bridgehead, *J Org Chem*, 72 (2007) 5608-5617.
- [7] Z. Janousek, S. Piettre, F. Gorissen-Hervens, H.G. Viehe, Capto-dative substituent effects, *Journal of Organometallic Chemistry*, 250 (1983) 197-202.

8. List of conferences and workshop:

- XII COPERNICAN INTERNATIONAL YOUNG SCIENTISTS CONFERENCE, Toruń, Poland, June 2018 Searching for Potent and Selective 5-HT₆ Serotonin Receptor Ligands Among Aromatic Derivatives of 1,3,5-triazine with Thio-, Seleno- or Simple Ether Motives. **Wesam Ali**, Dorota Łażewska, Małgorzata Więcek, Grzegorz Satała, Muhammad Jawad Nasim, Katarzyna Kieć-Kononowicz, Claus Jacob, Jadwiga.

- VIII Meeting of the Paul Ehrlich Euro-PhD Network, Porto, Portugal, July 2018 Design, synthesis and biological evaluation of new chalcogen derivatives of 1,3,5-triazine with both antibacterial and serotonin 5-HT₆ receptor activity.

W. Ali, G. Satała, J. Czekajewska, P. Nowak, K. Witek, E. Karczewska, K. Kieć-Kononowicz, C. Jacob, J. Handzlik.

- VIII Meeting of the Paul Ehrlich Euro-PhD Network, Porto, Portugal, July 2018. Multicyclic aromatic compounds with 1,3,5-triazine core as a new grateful family of 5-HT₆ serotonin receptor agents. (Poster).

W. Ali, R. Kurczab, D. Łażewska, M. Więcek, G. Satała, M.J. Nasim, A. Partyka, M. Usyk, K. Półchłopek, A. Nowakowska, K. Kieć-Kononowicz, C. Jacob and J. Handzlik.

- G16 – ABWET conference, Napoli, Italy, December 2018 Biological evaluation of easy to handle, ready to use and bio-available chalcogen nanoparticles.

W. Ali, S. Griffin, M. Sarfraz, S. F. Hartmann, S. R. Pinnapireddy, M. J. Nasim, U. Bakowsky, C. M. Keck, and C. Jacob.

- 8th workshop of the multidisciplinary group SeS Redox & cataysis – (WSeS8), Perugia, Italy, May 2019 Discovery of novel modulators for ABCB1 cancer MDR efflux pump, among aryl-heterocyclic selenoethers.

Wesam Ali, Gabriela Spengler, Annamaria Kinsces, Annamaria Lubelska, Gniewomir Latacz, Małgorzata Starek, Monika Dąbrowska, Katarzyna Kieć-Kononowicz, Claudio Santi, Claus Jacob, Jadwiga Handzlik.

- 14th International Conference on the Chemistry of Selenium and Tellurium ICCST-14 (3rd-7th June 2019), Cagliari, Italy Phenyl Chalcogenides with Potential Anticancer Activity.

Wesam Ali, Gabriela Spengler, Annamaria Kinsces, Claus Jacob, Claudio Santi.